GEOLOGICAL SURVEY OF CANADA
COMMISSION GÉOLOGIQUE DU CANADA

PAPER 77-1B

This document was produced
by scanning the original publication.

Ce document est le produit d'une
numérisation par balayage
de la publication originale.

REPORT OF ACTIVITIES
PART B

Energy, Mines and Resources Canada
Énergie, Mines et Ressources Canada

1977

Technical editing and compilation
R.G. Blackadar
P.J. Griffin
H. Dumych
E.J.W. Irish

Production editing and layout
Michael J. Kiel
Lorna A. Frith
Leona R. Mahoney

Typed and checked by
Angelica F.V. Koops
Debby Busby
Janet Gilliland
Sharon Parnham

GEOLOGICAL SURVEY
PAPER 77-1B

REPORT OF ACTIVITIES
PART B

GEOLOGICAL INFORMATION
DIVISION

JUN 23 1977
JUIN

DIVISION DE L'INFORMATION
GÉOLOGIQUE

1977

Minister of Supply and Services Canada 1977

Printing and Publishing
Supply and Services Canada,
Ottawa, Canada K1A 0S9,

from the Geological Survey of Canada
601 Booth St., Ottawa, K1A 0E8

or through your bookseller.

Catalogue No. M44-77-1B
ISBN - 0-660-00825-4

Price: Canada: $6.00
Other Countries: $7.20

Price subject to change without notice

TABLE OF CONTENTS

Page

ANALYTICAL CHEMISTRY

S. ABBEY: Studies in "Standard Samples" for the analysis of silicate rocks and minerals 107

APPALACHIAN GEOLOGY

W.E. TRZCIENSKI, JR.: Petrology and tectonics of the Cambro-Ordovician sequence in the Quebec Appalachians 77

CORDILLERAN GEOLOGY

D. CRAW: Geology of the Southern Park Ranges, British Columbia 145

G.H. EISBACHER and S.L. HOPKINS: Mid-Cenozoic paleogeomorphology and tectonic setting of the St. Elias Mountains, Yukon Territory 319

GEOCHEMISTRY

W.D. GOODFELLOW and I.R. JONASSON: Geochemical distribution of uranium, tungsten, and molybdenum in the Tombstone Mountain batholith, Yukon 37

GEOPHYSICS

A.P. ANNAN: Time-domain reflectometry – air-gap problem in a coaxial line 55

A.P. ANNAN: Time-domain reflectometry – air-gap problem for parallel wire transmission lines 59

A.P. ANNAN and J.L. DAVIS: Impulse radar applied to ice thickness measurements and freshwater bathymetry 63

A.P. ANNAN and J.L. DAVIS: Impulse radar and time-domain reflectometry experiments in permafrost terrain during 1976 67

A.P. ANNAN and J.L. DAVIS: Radar range analysis for geological materials 117

B.W. CHARBONNEAU: Radioelement distribution patterns in the Frontenac Axis, Ontario 337

J.L. DAVIS: Omnidirectional communications antenna 69

J.L. DAVIS and A.P. ANNAN: Electrical properties of Saskatchewan potash ore in situ 75

J.L. DAVIS, G.C. TOPP, and A.P. ANNAN: Measuring soil water content in situ using time-domain reflectometry techniques 33

R.L. GRASTY: Calibration for total count gamma-ray surveys 81

T.J. KATSUBE: Electrical parameter conversion Table II 293

E.J. SCHWARZ: Remanent magnetism of an ultramafic flow from Munro Township, Ontario 197

Page

MARINE GEOSCIENCE

C.L. AMOS: An hypothesis on the evolution of the tides in the Bay of Fundy 47

D.L. BARRETT, D.E. HEFFLER, and C.E. KEEN: Ocean bottom seismometer developments 129

B.D. BORNHOLD: Echo sounding and subbottom profiling in Douglas Channel and Kitimat Arm, British Columbia 265

R.K.H. FALCONER: Marine geophysical and geological research in Baffin Bay and the Labrador Sea, **CSS Hudson** 1976 255

B.F.N. LONG: Determination of sediment transport rate in the Minas Basin, Nova Scotia: Preliminary results of the first tracer experiment using radioisotopes 85

B. MacLEAN and R.K.H. FALCONER: Baffin Island Shelf – Shallow corehole drilling, 1976 125

G.E. REINSON: Examination of bedforms in shallow water using side-scan sonar, Miramichi Estuary, New Brunswick 99

D.C. UMPLEBY and I.A. HARDY: Field work in the Nûgssuaq Embayment, West Greenland 93

F.J.E. WAGNER: Mollusc distribution, Bay of Fundy area, New Brunswick and Nova Scotia 97

MINERAL DEPOSITS

K.R. DAWSON: The Delphi forecasting technique 133

H.E. DUNSMORE: A new genetic model for uranium-copper mineralization, Permo-Carboniferous basin, northern Nova Scotia 247

H.E. DUNSMORE: Uranium resources of the Permo-Carboniferous basin, Atlantic Canada 341

D.J. FINDLAY and L.D. AYRES: Lang Lake – an early Precambrian porphyry copper-molybdenum deposit in northwestern Ontario 25

I.R. JONASSON, B.W. CHARBONNEAU, and K.L. FORD: On the nature and formation of radioactive hydrocarbons from the Ordovician rocks of the Ottawa area 109

W.S. MITCHELL, M. ZENTILLI, and K.A. TAYLOR: Distribution of uranium in an active geothermal area in the Azores 137

N. PRASAD: URE-3 (Uranium resource evaluation file) – A data base for uranium resource evaluation 199

M. ZENTILLI, W.S. MITCHELL, K.A. TAYLOR, and P.F. TAYLOR: Studies of distribution of uranium in selected ore environments using nuclear track techniques 141

MINERALOGY

G.J. PRINGLE and A.R. MILLER: A study of Cu-S-Se minerals: Electron microprobe analysis and X-ray powder data 113

J. RIMSAITE: Mineral assemblages at the Rabbit Lake uranium deposit, Saskatchewan: A preliminary report 235

Page

PALEONTOLOGY

M.J. COPELAND and J.M. BERDAN: Silurian and Early Devonian beyrichiacean ostracode provincialism in northeastern North America 15

M.J. COPELAND and T.E. BOLTON: Additional paleontological observations bearing on the age of the Lourdes Formation (Ordovician), Port au Port Peninsula, western Newfoundland 1

A.E.H. PEDDER and G. KLAPPER: Fauna and correlation of the type section of the Cranswick Formation (Devonian), Mackenzie Mountains, Yukon Territory 227

A.E.H. PEDDER: Systematics and biostratigraphic importance of the Lower Devonian rugose coral genus **exilifrons** 173

R.A. RAHMANI and W.S. HOPKINS, JR.: Geological palynological interpretation of Eureka Sound Formation on Sabine Peninsula, northern Melville Island, District of Franklin 185

B.G.T. van HELDEN: Correlation of microplankton assemblages with ammonite faunas from the Jurassic Wilkie Point Formation, Prince Patrick Island, District of Franklin 163

PRECAMBRIAN GEOLOGY

M.E. CHUTE and L.D. AYRES: Missi Island volcanic centre, Saskatchewan 29

N. RAST: Preliminary report on the geology of a part of the Pokiok Pluton and its surrounding metasediments, south-central New Brunswick 49

QUATERNARY GEOLOGY:
ENVIRONMENTAL AND ENGINEERING GEOLOGY STUDIES

P. FRANSHAM and D. BATTRUM: Pore pressure measurements in sensitive clay slopes, eastern Canada 295

P.J. KURFURST: Acoustic properties of frozen soils..... 277

QUATERNARY GEOLOGY:
INVENTORY MAPPING AND STRATIGRAPHIC STUDIES

R.W. BARENDREGT, J.H. FOSTER, and A. MacS. STALKER: Paleomagnetic remanence characteristics of surface tills found in the Pakowki-Pinhorn area of southern Alberta 271

C.M. CUNNINGHAM and W.W. SHILTS: Surficial geology of the Baker Lake area, District of Keewatin..... 311

R.D. THOMAS: A brief description of the surficial materials of north-central Keewatin, Northwest Territories 315

QUATERNARY GEOLOGY:
PALEOECOLOGY AND GEOCHRONOLOGY

W. BLAKE, JR.: Iceberg concentrations as indicators of submarine moraines, eastern Queen Elizabeth Islands, District of Franklin 281

S. LICHTI-FEDEROVICH: Fossil record of **Ceratophyllum demersum** L., **Elatine triandra** var. **americana** (Pursh) Fassett, and **Leersia oryzoides** (L.) Swartz from the Missinaibi Formation, northern Ontario..... 287

QUATERNARY SEDIMENTOLOGY AND GEOMORPHOLOGY

J. ROSS MACKAY: Changes in the active layer from 1968 to 1976 as a result of the Inuvik fire, District of Mackenzie 273

W.W. SHILTS and C.M. CUNNINGHAM: Anomalous uranium concentrations in till north of Baker Lake, District of Keewatin 291

D. SWAN and R. LINDEN: Plotting subroutines for the presentation of Geological Data 269

STRATIGRAPHY AND STRUCTURAL GEOLOGY

H.R. BALKWILL, W.S. HOPKINS, JR., and J.H. WALL: Lougheed Island and neighbouring small islands, District of Franklin 181

R.L. CHRISTIE: Stratigraphic reconnaissance of Lower Paleozoic rocks, Eastern Devon Island, Arctic Archipelago 217

P.S. GRAHAM, P.R. GUNTHER, and D.W. GIBSON: Geological investigations of the coal-bearing Kootenay Formation in the subsurface of the Upper Elk River Valley, British Columbia 203

T. JERZYKIEWICZ and J.R. McLEAN: Bedded volcanic chert near Coalspur, Central Foothills, Alberta 149

R.A. RAHMANI: Fault control on sedimentation of Isachsen Formation in Sverdrup Basin 157

J.W. SEARS and R.A. PRICE: Structural geology of the Albert Peak area, southeastern British Columbia 261

G.K. WILLIAMS: Some observations on the Horn Plateau, District of Mackenzie 191

G.K. WILLIAMS: The Celibeta structure compared with other basement structures on the flanks of the Tathlina High, District of Mackenzie 301

T.T. UYENO: Summary of conodont biostratigraphy of the Read Bay Formation at its type sections and adjacent areas, eastern Cornwallis Island, District of Franklin 211

INTRODUCTION

Most of the work undertaken by the Geological Survey is designed to contribute to the three main programs of the Department of Energy, Mines and Resources–the Minerals Program, the Energy Program and especially the Earth Science Service Program.

The ***Minerals Program*** *is designed to ensure adequate supply and effective use of the mineral resources of Canada through timely mineral information, technology and expertise derived from field, office and laboratory geological, geophysical and geochemical studies. The information that results from such studies contributes to:*

- *planning for increased regional economic development.*
- *developing a rational basis for improving our balance of trade position.*
- *increasing Canada's ability to be more self-reliant in mineral requirements.*
- *increasing our security of supply.*
- *better management of the mineral resources available to Canada.*

The ***Energy Program*** *is designed to ensure the availability of Canada's energy resources and to promote their effective use. The geological studies carried out in support of this program provide indications of the probable location of areas favourable to the occurrence of oil, natural gas, coal and other energy resources. Such studies enable estimates to be made of the quantity, quality, and probable distribution of the resources and provide integrated descriptions of the habitats in which energy resources may be found.*

The Energy Program obviously contributes significantly to planning for the expansion of primary and secondary industry and thus to increased regional economic development. It is the basis for plans for increasing Canada's ability to become more self-reliant in energy needs and for ensuring security of supply.

About 70 per cent of the work of the Geological Survey contributes to the ***Earth Science Service Program*** *which has the objective of ensuring the availability of the earth-science information needed for effective management of the Canadian landmass, including the continental shelves and adjacent ocean floors. This includes management of resources for land use, regional and urban development, and transportation.*

Bedrock and surficial surveys, regional analyses and syntheses, environmental and engineering geology studies, studies of standards, correlations and processes and studies of sedimentary and geomorphic processes are some of the Geological Survey's activities that contribute to this program.

The uses of the program are widespread and include:

- *more efficient and effective search for Canada's mineral and energy resources.*
- *better understanding of the geological evolution of Canada.*
- *more secure resource base.*
- *developing a basis for evaluating the impact of man's activities on the physical environment.*
- *land use planning including an evaluation of surficial material resources and terrain hazards.*

The 63 reports that comprise this publication all contribute to one or more of these programs.

As part of its evaluation of Canada's uranium and thorium resources the Geological Survey carries out investigations of the nature and distribution of uranium deposits both in Canada and abroad. Such studies aid in determining the metallogenic processes that govern uranium occurrence and thus help to establish guidelines that can be used in the search for new deposits. Reports 28, 29, 39, 45, and 63 are concerned with this subject. Reports 45 and 63 are of particular interest because they provide information on previously unreported uranium occurrences in the Permo-Carboniferous basin of Atlantic Canada and also a model that will assist in the search for similar occurrences. Other studies carried out as part of the Minerals Program are described in reports 3 and 27. The latter report describes a bibliography that was developed during an evaluation of the Delphi Forecasting Technique, a possible method for predicting future supplies of heavy metals and gives a brief review of the technique. Studies in mineralogy also support the Minerals Program and report 44 gives specialized data on the mineral assemblages found at the Rabbit Lake uranium deposit in Saskatchewan. An example of how samples of drift can be used in the search for mineral deposits is outlined in report 55.

A variety of geophysical studies are carried out in support of all three programs. Many of these are concerned with the development of techniques. Reports 5, 9, 11, 12, 13, 16, and 24 describe studies that range from using geophysical techniques to measure the thickness of sea ice to the development of a better antenna for use in the field.

Studies in marine geoscience are becoming increasingly important especially in the light of possible exploitation of offshore oil and natural gas resources. In this publication all but one of the reports devoted to marine geoscience are concerned with the East Coast. The exception, report 48 describes bottom studies in Douglas Channel, British Columbia. Reports 7, 17, 19, and 20 give information on past and present geological processes in coastal and marine areas. Reports 18, 25 and 46 describe regional reconnaissance work carried out on parts of the Atlantic Continental Shelf.

With the increasing use that is being made of the relatively sensitive land in the arctic, terrain studies are becoming more and more important in order to prevent major damage to the surface of the land. Reports 59 and 60 give results of inventory mapping in two areas west of Hudson Bay, areas that could be the site of major activity should the proposed pipeline from the Arctic Islands follow a route west of the Bay. Some deposits along the Ottawa and St. Lawrence valleys are unusually sensitive to stress and under extreme conditions liquify thereby causing collapse of any structures that are built on them. Report 57 gives results of one aspect of the continuing study of this problem.

Understanding the stratigraphy of rock sequences in sedimentary basins is essential if hydrocarbon potential is to be evaluated. The more information there is the more precisely can the estimates be made. Reports 35, 37, 40, and 42 give results from four areas within the Interior Plains. Structural studies, also important in unravelling the geological history of an area, are reported on in reports 32, 47, and 58. Stratigraphic correlation is very dependent on fossil identification and the Geological Survey maintains on-going paleontological studies. Reports 1, 2, 33, 34, 36, and 43 give some of the results of these studies.

R.G. Blackadar
Chief Scientific Editor

The Geological Survey of Canada

D.J. McLAREN, Director General

J.O. WHEELER, Deputy Director General

E. HALL, Scientific Executive Officer

M.J. KEEN, Director, Atlantic Geoscience Centre, Dartmouth, Nova Scotia

J.A. MAXWELL, Director, Central Laboratories and Administrative Services Division

PETER HARKER, Director, Geological Information Division

D.F. STOTT, Director, Institute of Sedimentary and Petroleum Geology, Calgary, Alberta

J.E. REESOR, Director, Regional and Economic Geology Division

A.G. DARNLEY, Director, Resource Geophysics and Geochemistry Division

J.S. SCOTT, Director, Terrain Sciences Division

Reprints

A limited number of reprints of the papers that appear in this volume are available by direct request to the individual authors. The addresses of the Geological Survey of Canada offices follow:

601 Booth Street,
OTTAWA, Ontario
K1A 0E8

Institute of Sedimentary and Petroleum Geology,
3303-33rd St. N.W.,
CALGARY, Alberta
T2L 2A7

British Columbia Office,
100 West Pender Street,
VANCOUVER, B.C.
V6B 1R8

Atlantic Geoscience Centre,
Bedford Institute of Oceanography,
P.O. Box 1006,
DARTMOUTH, N.S.
B2Y 4A2

When no location accompanies an author's name in the title of a paper, the Ottawa address should be used.

1. ADDITIONAL PALEONTOLOGICAL OBSERVATIONS BEARING ON THE AGE OF THE LOURDES FORMATION (ORDOVICIAN), PORT AU PORT PENINSULA, WESTERN NEWFOUNDLAND

Projects 720072 and 740084

M.J. Copeland[1] and Thomas E. Bolton[2]

Introduction

Early Paleozoic rocks of Port au Port Peninsula have been studied by Murray and Howley (1881), Schuchert and Dunbar (1934), Riley (1962), Rodgers (1965), Cumming (1967), Fåhraeus (1973, 1974), and Kay (1969; in Bergström et al., 1974). Fossils from these rocks have been discussed in those reports as well as by Cooper (1956), Bolton (1965) and Fritz (1966), and have been the subject of several theses at Memorial University of Newfoundland. The limestone and shale included in the Lourdes Formation, Long Point Group, by Kay (in Bergström et al., 1974) have been assigned to either the Middle Ordovician Mohawkian/Caradocian Wilderness Stage or lowest Trentonian Barneveld Stage (Schuchert and Dunbar, 1934, p. 72; Cooper, 1956, p. 13; Rodgers, 1965, p. 91; Bolton, 1965, p. 23; Cumming, 1967, p. 14; Whittington and Kindle, 1969, p. 655) or the older Middle Ordovician Valcourian-Ashbyan and Porterfieldian-Bolarian Stages by Kay (1969, p. 667, 668; 1974, in, Bergström et al., p. 1629). The discovery during the 1976 field season of an ostracode fauna within the shale unit at the base of member III of the Lourdes Formation (Kay, in Bergström et al., 1974) typical of the late Wilderness-early Barneveld Decorah Formation of Iowa and Minnesota reaffirms the late Wildernessian-Rocklandian assignment of most of the Lourdes Formation. This fauna and some of the corals and bryozoans characteristic of the adjacent limestone units are the basis for this discussion.

Table 1.1

Lourdes Formation, Long Point Group
(Modified from Kay, in Bergström et al., 1974)

Member III:	Limestone, alternating nodular calcisiltite, platy calcarenite with shaly partings, fossils abundant on few surfaces, 90 feet (27 m). Shale and interbedded thin quartz sandstone and calcarenite, fossils in basal beds, 28-34 feet (9-10 m).
Member II:	Bedded, rather massive-ledged calcarenite and calcisiltite, **Labyrinthites** reefs rising through ten feet of beds, upper contact a corrasion surface, 80 feet (24 m). Shale with nodular lensing calcarenite, 20 feet (6 m).
Member I:	Alternations of beds of quartz sandstone with some cross-bedding and limestone, particularly calcilutite, 60 feet (18 m).

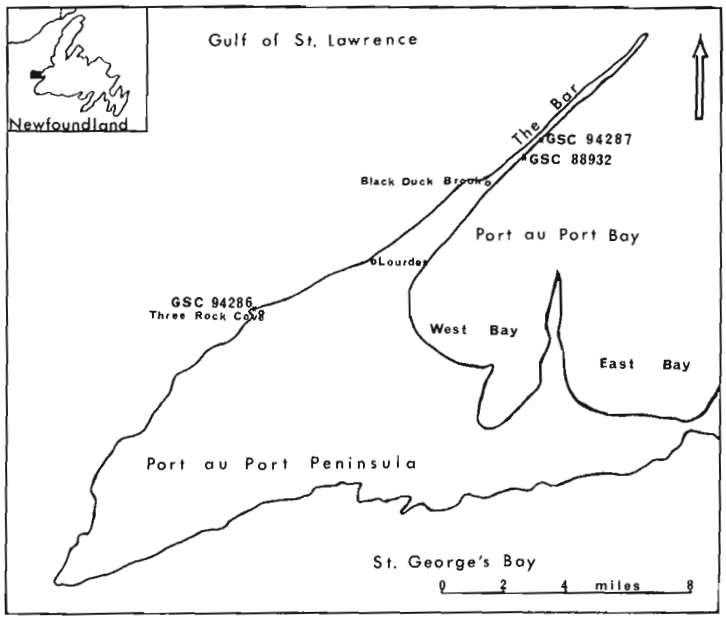

Figure 1.1. Locality map, Port au Port Peninsula, western Newfoundland.

Stratigraphy

As established by Kay (in Bergström et al., 1974) the Lourdes Formation, unconformably underlain by shaly argillite of the allochthonous Humber Arm Group and conformably overlain by clastic rocks of the Winterhouse Formation, can be subdivided into three informal members in its type locality along the eastern shore of the northern extension (The Bar) of Port au Port Peninsula.

This past field season, fossils were collected from exposures near the contact of members II and III on the west shore of Port au Port Peninsula in the Salmon Cove-Three Rock Cove area and on the east shore of The Bar near Black Duck Brook settlement (Fig. 1.1). The ostracode fauna was discovered only in the basal shale of member III of the latter section (loc. 94287); this unit is not exposed at Salmon Cove-Three Rock Cove (loc. 94286).

Microfauna (Ostracoda) (Plate 1.1, figures 9-25)

Samples of the lower shale unit of member III at GSC locality 94287 contain a sparse ostracode fauna represented by relatively few specimens, indeterminate bryozoans, crinoid remains and the brachiopod **Ptychopleurella** sp. (Pl. 1.1, figs. 7, 8). Species of the nine genera recognized and their occurrence elsewhere in North America are shown in Table 1.3.

[1] Regional and Economic Geology Division

[2] Special Projects, Office of the Director General

From: Report of Activities, Part B; Geol. Surv. Can., Paper 77-1B (1977)

Figure 1.2. Rocks of the Lourdes Formation, southeast coast of Long Point, locality 94287. **Labyrinthites** bioherm of upper member II in foreground, shale unit of lower member III exposed near lobster traps, overlying beds of member III in background (203106).

Table 1.2

Collecting localities, Port au Port Peninsula, western Newfoundland.

GSC locality	84824: Shore section Salmon Cove, Three Rock Cove area (48°37'30"N, 59°05'30"W); **Labyrinthites**-bearing upper beds of member II; collector W.T. Dean, 1969.
GSC locality	88932: On coast 1.35 to 1.5 miles (2.2-2.4 km) northeast of Winterhouse road junction at Black Duck Brook (48°42'N, 58°53'30"W); **Labyrinthites**-bearing upper beds of member II; collectors L.M. Cumming and H. Corkin, 1964, 1966, 1968.
GSC locality	94286: Shore section Salmon Cove and Three Rock Point (48°37'30"N, 59°05'30"W); **Labyrinthites**-bearing upper 20 feet of member II and **Diplotrypa**-bearing lower beds (20-30 feet above base) of member III; collector M.J. Copeland, 1976 (same as GSC locality 84824).
GSC locality	94287: Shore section 2.2 miles (3.5 km) northeast of Black Duck Brook corner (48°42'30"N, 58°53'W); members II (upper 20 feet) and III (lower 35 feet); collector M.J. Copeland, 1976 (Figs. 1.2, 1.3).

They are representative of the widespread North American ostracode assemblage described by Kay (1934; 1940), Harris (1957) and Copeland (1965; 1974; in Bolton et al., in press) from strata of Wilderness and early Barneveld age. This North American assemblage is divisible into southern and northern faunal provinces based on the more common occurrence of 'European' elements in the latter. In addition, these northern elements become more numerous and diverse in the later, Barneveldian, part of the assemblage range. The lack of known 'European' ostracodes in the present collection might therefore suggest its inclusion within the southern faunal province and/or its pre-Barneveldian age; however, the sample is too small to justify an unequivocal statement at this time.

This is the first documented report of a North American province Ordovician ostracode fauna from Newfoundland. Billings (1865, p. 299, 300), Schuchert and Dunbar (1934, p. 64) and Berdan (in Whittington and Kindle, 1963, p. 747) mention ostracodes from the Table Head Formation of western Newfoundland that are now considered earliest Middle Ordovician, Whiterockian. Schuchert and Dunbar (1934, p. 69) list a leperditicopid ostracode from the Long Point Series and Kay (in Bergström et al., 1974, p. 1629) likewise records three ostracode species from the Lourdes Formation, Port au Port Peninsula: **Ctenobolbina parroquettensis** Twenhofel and Whiting, **Aparchites** sp. and **"Leperditia"** sp. Identification of **C. parroquettensis** from the upper part of unit III of the Lourdes Formation has not been verified and it

Figure 1.3. Corallum of **Labyrinthites (Labyrinthites) chidlensis** Lambe, upper beds of member II, Lourdes Formation, locality 94287. Hammer handle is 13 inches (33 cm) long (203106-A).

may be in doubt as this species was previously reported (Twenhofel, 1938, p. 66) only from strata of the older, Chazyan, Mingan Formation. This, therefore, is the most easterly known occurrence of the widespread late Middle Ordovician North American ostracode assemblage and extends our knowledge of its distribution more than 500 miles (800 km) from its previous easterly limit in St. Lawrence Lowland.

Subclass Ostracoda Latreille, 1806
Order Palaeocopida Henningsmoen, 1953
Superfamily Hollinacea Swartz, 1936
Family Tetradellidae Swartz, 1936
Tetradella? newfoundlandensis Copeland n. sp.

Plate 1.1, figures 9-13

Description. Quadrilobate, lobes undivided and inclined posterodorsally, L1 and L3 overhanging dorsum, L1 and L4 joined ventrally, L2 and L3 slightly restricted ventrally, L2 constricted near mid-length. Trisulcate, S1 long, narrow, joined dorsally with prominent, broad S2, S3 long, narrow.

Ventral field lowly rounded, nearly planar, surmounted by indistinct, thread-like carina, here termed histium, extending along the distal edge of the histial lobe from beneath L1 to posterior cardinal area. Heteromorph with histial ridge extending anteriorly to posterior edge of circumlocular crest. Both dimorphs with histial ridge marking the posteroventral angle of L4, descending abruptly at posterodorsal edge of L4 to near valve margin and terminating at or near posterior cardinal angle. No tecnomorphic velar ridge observed; heteromorph with fine, thread-like (discontinuous?) velar ridge extending in a curve from mid posterior margin to posterior edge of circumlocular crest. Marginal ridge low, indistinct.

Dimorphic, heteromorph with three anteroventral loculi. Loculi with circumlocular crests closely appressed, apparently without connecting locular crests or lines of division.

Holotype, heteromorphic left valve, 1.10 mm long, 0.80 mm high; paratypes, three tecnomorphic valves, 0.85-0.90 mm long, 0.60 mm high.

Number of specimens studied, 6.

Types. Holotype, GSC 48848; paratypes GSC 48845-48847.

Occurrence. Shale unit at base of member III, GSC locality 94287.

Discussion. Within the Palaeocopida, abvelar locular dimorphism is typically expressed by genera of the Tetradellidae. **T.? newfoundlandensis** possesses such dimorphism and is quadrilobite but is not otherwise a typical species of **Tetradella** in that L1 and L3 are undivided lobes, the histium is not prominently crested and the velum is reduced to a thread-like ridge on the near-planar sub-histial field. The presence of greatly reduced histial and velar ridges is suggestive of species of **Dilobella** which, however are typically bilobate. Of presently known dilobellids, only **D. marginata** Teichert (a species of questionable tetradellid affinity) from Cape Calhoun, northern Greenland, may prove to be quadrilobate and thus bear some resemblance to **T.? newfoundlandensis.**

Megafauna (Anthozoa, Stromatoporoidea, Bryozoa)

The megafossils examined during the present study include representatives of the corals **Labyrinthites (Labyrinthites chidlensis** Lambe (Pl. 1.3, figs. 1-7) and **Billingsaria parvituba** (Troedsson) (Pl. 1.4, figs. 1, 4-7) collected from the **Labyrinthites**-bearing upper beds of member II. Both these species have been described recently in association either with the limited ranging cephalopod **Gonioceras** or late Mohawkian ostracodes in the Bad Cache Rapids Formation of Melville Peninsula, District of Franklin (Bolton et al., in press); they have also been reported from the Gonioceras Bay-lower Cape Calhoun formations of northwestern Greenland (Troedsson, 1929). A late Wilderness-Barneveld Middle Ordovician age was advocated for these rocks rather than the late Ordovician age accepted for many years. In the Lourdes Formation, **L. (L.) chidlensis** is most abundant in member II in association with **Gonioceras** and **B. parvituba** [**B. parva** (Billings) of Kay], middle Mohawkian ostracodes are present in the basal shale unit of member III, and a similar trilobite (W.T. Dean, pers. comm.) and brachiopod fauna apparently occurs throughout the two members (Schuchert and Dunbar, 1934, p. 70, 71; Cooper, 1956, p. 12, 13; Kay, in Bergström et al., 1974, p. 1629, Table 1). On the basis of these megafossils, therefore, a late Wildernessian-Rocklandian age is suggested for the major, fossiliferous part of the Lourdes Formation.

Laminar expansions of the stromatoporoid **Labechia** sp. (Pl. 1.2, figs. 4, 5, 7), anastomosing branches of the bifoliate cryptostomate bryozoan **Stictoporella** sp. aff. **S. fenestrata** Hall (Pl. 1.1, figs. 1, 2, 4-6), and massive hat-shaped zoaria of the trepostomate bryozoan **Diplotrypa schucherti** Fritz also were recognized within the bioherms of Port au Port Peninsula. Limestone above the basal shale unit of member III contained similar but consistently larger colonies of the trepostomate bryozoan (Pl. 1.2, figs. 1-3, 6, 8) and a cyclostomate bryozoan **Ceramopora** sp. (Pl. 1.1, fig. 3).

ANTHOZOA

Labyrinthites (Labyrinthites) chidlensis Lambe
Plate 1.3, figures 1-7

1965 **Labyrinthites (Labyrinthites) chidlensis** Lambe. BOLTON, p. 23 (for previous synonymy).

1965 **Labyrinthites chidlensis** Lambe. RODGERS, p. 87.

1966 **Labyrinthites chidlensis** Lambe. FRITZ, p. 1335.

1973 **Labyrinthites chidlensis** Lambe. FÅHRAEUS, p. 1827.

1974 **Labyrinthites chidlensis** Lambe. KAY, in Bergström et al., p. 1629.

Description. Discoidal (120 mm wide and 30 mm thick) to domed fasciculate coralla ranging in size from 65 mm wide and 50 mm thick to 300+ mm and 190+ mm (hypotypes, GSC 48868, 48872), with some colonies reported as much as 3 feet (0.9 m) in diameter and 2 feet (0.6 m) high; in transverse section, corallites phaceloid, oval to polygonal, 0.2 to 0.35 mm in diameter; individuals usually touching at corners or directly connected through short, hollow tubes, thus forming a chain-like network;

Table 1.3

Ostracodes of the shale unit, lower member III, Lourdes formation, GSC locality 94287 and their occurrence elsewhere in North America.

	1	2 a	2 b	2 c	3	4	5 a	5 b
'Aparchites' fimbriatus (Ulrich)	X	X	X	X		X		
Cryptophyllus spp.	X	X	X	X	X	X	X	X
Euprimitia linepunctata (Kay)	X		X	X	X			
Eurychilina sp. cf. **E. ventrosa** Ulrich	X	X		X	X		X	X
Punctaparchites rugosus (Jones)	X		X	X	X	X	X	X
Saccelatia arrecta (Ulrich)				X	X			
Schmidtella umbonata Ulrich				X	X			
Tetradella? newfoundlandensis Copeland n. sp.								
Winchellatia sp. aff. **W. minnesotensis** Kay				X				

1 - Bucke Formation, Lake Timiskaming, Ontario
2 - Decorah Formation, Iowa and Minnesota, a - Spechts Ferry Member,,b - Guttenberg Member, c - Ion Member
3 - Kirkfield Formation, Healey Falls, and Braeside beds, Ottawa Valley, Ontario
4 - Lower shale unit, Silliman's Fossil Mount, Baffin Island
5 - Simpson Group, Oklahoma, a - Tulip Creek Formation, b - Bromide Formation

corallites occasionally coalesce and have a common wall (Pl. 1.3, fig. 2), in the extreme development cerioid; in longitudinal section, corallites slightly sinuous, constant diameter, increasing laterally (Pl. 1.3, fig. 1); tabulae thin, complete, flat to slightly concave, 2 to 3 per 2 mm; horizontal tubes 0.1 mm in diameter, up to 0.3 mm apart, walls continuous between connecting tubes (Pl. 1.3, fig. 7).

Types. Hypotypes, GSC 15307-15310, 48867-48872.

Occurrences. Upper beds of member II, GSC localities 88932, 94286, 94287.

Discussion. The age and regional distribution in North America of **Labyrinthites** has been discussed in Bolton (1965) and Bolton et al. (in press). The hemispheric colonies abundant in the Long Point beds have been assigned to a coral of the Black River **Tetradium**-type (Billings, in Murray and Howley, 1881, p. 342, 394), the bryozoan **Monotrypa** (**M. magna** Ulrich) (Schuchert and Dunbar, 1934, p. 70; Sullivan, in Riley, 1962, p. 69), and more recently to the tabulate coral **L. (L.) chidlensis**, as listed in the synonymy.

Billingsaria parvituba (Troedsson)
Plate 1.4, figures 1, 4-7

1974 **Billingsaria parva** (Billings). KAY, in Bergström et al., p. 1629.
In press **Billingsaria parvituba** (Troedsson). BOLTON et al. (for complete synonymy).

Description. Coralla massive expansions up to 150 mm wide and 35 mm thick, cerioid; in transverse section, corallites 4- to 6-sided, 1.0 to 1.3 mm in diameter, walls thick; 8 straight thick major septa extend nearly to centre of a corallite in best preserved forms, some tips bulbous, and 8 very short minor septa; columella 0.1 mm in diameter; in longitudinal section, tabulae close, complete, flat, 2 to 3 per corallite diameter; central cylindrical columella continuous between 2 or 3 tabulae.

Types. Hypotypes, GSC 48873-48875.

Occurrences. Upper beds of member II, GSC localities 94287, 84824.

Discussion. **Billingsaria parva** (Billings) from the Chazyan Mingan Formation of Mingan Islands, Quebec, differs from **B. parvituba** in that the corallites are consistently smaller, 0.6 to 0.7 mm in apart, 1 per corallite diameter (Pl. 1.4, figs. 2, 3). The Lourdes Formation specimens closely resemble those described from the Bad Cache Rapids Formation of Melville Peninsula, District of Franklin.

BRYOZOA

Diplotrypa schucherti Fritz
Plate 1.2, figures 1-3, 6, 8

1966 **Diplotrypa schucherti** FRITZ, p. 1335.

Description. Zoaria massive, ranging from balls 70 mm in diameter to mounds 130 mm diameter and 60 mm thick, surfaces with low broad monticules; in tangential section, zooecia hexagonal to rounded depending on the presence of mesopores, 0.4 to 0.5 mm in diameter to a maximum of 0.8 mm in maculae, 3.5 to 4 zooecia in 2 mm, walls thin and essentially amalgamate with only rare integrate preservation, single mesopores at corners, rarely paired in maculae, triangular to rectangular, never abundant, no acanthopores; in longitudinal section, zooecial walls uniformly thin, diaphragms complete varying from flat to slightly concave or convex, normally 4+ in 2 mm averaging 0.5 mm apart, in crowded zones 5 to 7 in 2 mm and 0.2 to 0.3 mm apart, few beaded mesopores with no apparent zoning.

Types. Holotype, Peabody Museum (YPM) 4656/34; paratypes, GSC 20681, 20682; hypotypes, GSC 48861-48864.

Occurrences. GSC localities 94286, 94287, 88932.

Discussion. In zooecial diameter, these specimens resemble **Diplotrypa bassleri** (Troedsson) from the Bad Cache Rapids Formation of Melville Peninsula, District of Franklin, and Cape Calhoun Formation of northwestern Greenland. The diaphragms, however, are more widely spaced in **D. bassleri,** 2 to 3 per 2 mm.

References

Bergström, S.M., Riva, J., and Kay, M.
1974: Significance of conodonts, graptolites, and shelly faunas from the Ordovician of western and north-central Newfoundland; Can. J. Earth Sci., v. 11, no. 12, p. 1625-1660.

Billings, E.
1865: New species of fossils from the Quebec Group in the northern part of Newfoundland; Geol. Surv. Can., Paleozoic Fossils, v. I, p. 207-338.

Bolton, T.E.
1965: Ordovician and Silurian tabulate corals **Labyrinthites, Arcturia, Troedssonites, Multisolenia,** and **Boreaster**; Geol. Surv. Can., Bull. 134, p. 17-33.

Bolton, T.E., Sanford, B.V., Copeland, M.J., Barnes, C.R., and Rigby, J.K.
Geology of Ordovician rocks, Melville Peninsula and region, southeastern District of Franklin; Geol. Surv. Can., Bull. 269. (in press)

Cooper, G.A.
1956: Chazyan and related brachiopods; Smithson. Misc. Coll., v. 127, pts. 1 and 2.

Copeland, M.J.
1965: Ordovician Ostracoda from Lake Timiskaming, Ontario; Geol. Surv. Can., Bull. 127.

1974: Middle Ordovician Ostracoda from southwestern District of Mackenzie; Geol. Surv. Can., Bull. 244.

Cumming, L.M.
1967: Platform and klippe tectonics of western Newfoundland: a review; R. Soc. Can., Sp. Publ. 10, p. 10-17.

Fåhraeus, L.E.
1973: Depositional environments and conodont-based correlation of the Long Point Formation (Middle Ordovician), western Newfoundland; Can. J. Earth Sci., v. 10, no. 12, p. 1822-1833.

1974: Fossils and sedimentology of the Paleozoic strata of Port au Port Peninsula; in Lower Paleozoic Stratigraphy of the Port au Port area, Newfoundland, Geol. Assoc. Can.-Mineral. Assoc. Can. 74, Fieldtrip Manual B-4.

Fritz, M.A.
1966: **Diplotrypa schucherti,** a new bryozoan species from the Long Point Formation (Ordovician), western Newfoundland; J. Paleontol., v. 40, no. 6, p. 1335-1337.

Harris, R.W.
1957: Ostracoda of the Simpson Group; Okla. Geol. Surv., Bull. 75.

Kay, G.M.
1934: Mohawkian Ostracoda: species common to Trenton faunules from the Hull and Decorah Formations; J. Paleontol., v. 8, no. 3, p. 328-343.

1940: Ordovician Mohawkian Ostracoda: Lower Trenton Decorah Fauna; J. Paleontol., v. 14, no. 3, p. 234-269.

1969: Thrust sheets and gravity slides of western Newfoundland; Am. Assoc. Pet. Geol., Mem. 12, p. 665-669.

Murray, A. and Howley, J.P.
1881: Geological Survey of Newfoundland.

Riley, G.C.
1962: Stephenville map-area, Newfoundland; Geol. Surv. Can., Mem. 323.

Rodgers, J.
1965: Long Point and Clam Bank Formations, western Newfoundland; Proc. Geol. Assoc. Can., v. 16, p. 83-94.

Schuchert, C. and Dunbar, C.O.
1934: Stratigraphy of western Newfoundland; Geol. Soc. Am., Mem. 1, p. 69-73.

Troedsson, G.T.
1929: On the Middle and Upper Ordovician faunas of northern Greenland; Part II; Medd. om Grønland, v. 72, pt. 1, no. 1, 1928.

Twenhofel, W.H.
1938: Geology and paleontology of the Mingan Islands, Quebec; Geol. Soc. Am., Sp. Paper No. 11.

Whittington, H.B. and Kindle, C.H.
1963: Middle Ordovician Table Head Formation, western Newfoundland;Geol. Soc. Am., Bull., v. 74, p. 745-758.

1969: Cambrian and Ordovician stratigraphy of western Newfoundland; Am. Assoc. Pet. Geol., Mem. 12, p. 655-664.

PLATE 1.1

BRYOZOA

Figures 1, 2, 4-6. **Stictopora** sp. aff. **S. fenestrata** Hall

1, 5, 6. Portion of a shallow tangential section, X 20, illustrating single and double rows of acanthopores between zooecial apertures; longitudinal section, X 40, lacking hemisepta; and transverse section, X 20, illustrating median tubuli in mesotheca and rectangular zooecial sections near the mesotheca, GSC loc. 94287 (member II), GSC 48839.

2. Portion of a transverse section of a zoarium, X 20, illustrating median tubuli in mesotheca, absence of hemisepta, and thin zooecial walls, GSC loc. 94287 (member II), GSC 48840.

4. Portion of a colony, X 1, GSC loc. 88932 (member II), GSC 48841.

Figure 3. **Ceramopora** sp. Longitudinal section, X 10, illustrating numerous connecting pores in zooecial walls, GSC loc. 94286 (member III), GSC 48842.

BRACHIOPODA

Figures 7, 8. **Ptychopleurella** sp. Brachial and pedicle views, X 20 and X 10, GSC loc. 94287 (shale unit base of member III), GSC 48843, 48844.

OSTRACODA

(All specimens from shale unit base of member III, GSC loc. 94287, X 40, except Figures 21 and 23, X 20 and reconstruction, Figure 13, X 80)

Figures 9-13. **Tetradella**? **newfoundlandensis** Copeland n. sp.

9-11. Right and left lateral views of three tecnomorphic valves, paratypes, GSC 48845-48847.

12, 13. Left lateral view of heteromorphic valve and ventral reconstruction, holotype, GSC 48848.

Figure 14. **Saccelatia arrecta** (Ulrich), lateral view of a left valve, GSC 48849.

Figures 15, 17. **Schmidtella umbonata** Ulrich, right and left lateral views of two specimens, GSC 48850, 48852.

Figure 16. **Cryptophyllus** sp., lateral view of a left valve, GSC 48851.

Figures 18-20. **Winchellatia** sp. aff. **W. minnesotensis** Kay, left and right lateral views of three valves, GSC 48853-48855.

Figure 21. **'Aparchites' fimbriatus** (Ulrich), left lateral view of a carapace, GSC 48856.

Figure 22. **Euprimitia linepunctata** (Kay), right lateral view of a carapace, GSC 48857.

Figure 23. **Eurychilina** sp. cf. **E. ventrosa** Ulrich, left lateral view of an incomplete heteromorphic valve, GSC 48858.

Figures 24, 25. **Punctaparchites rugosus** (Jones), right and left lateral views of two specimens, GSC 48859, 48860.

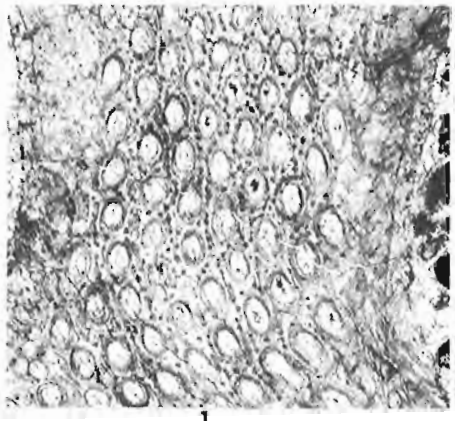

1

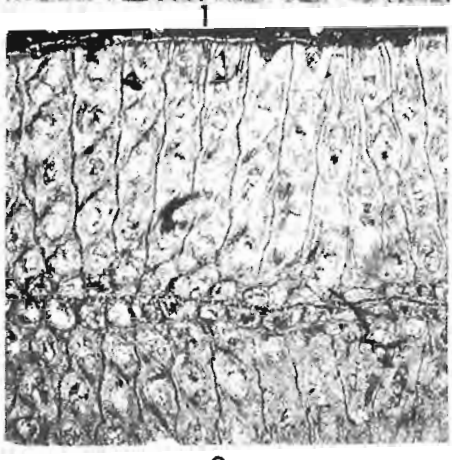

2

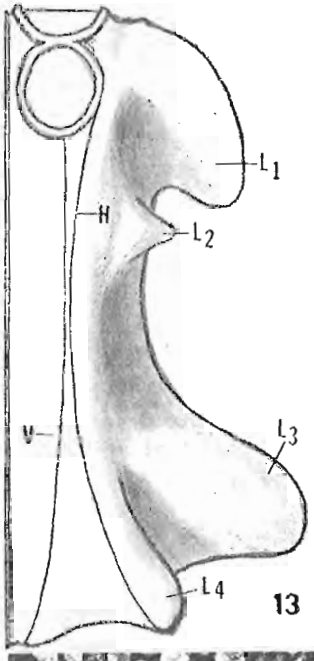

13

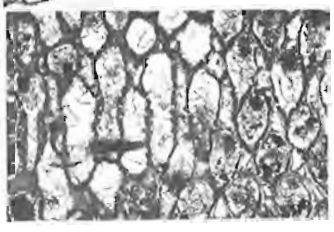

3

4

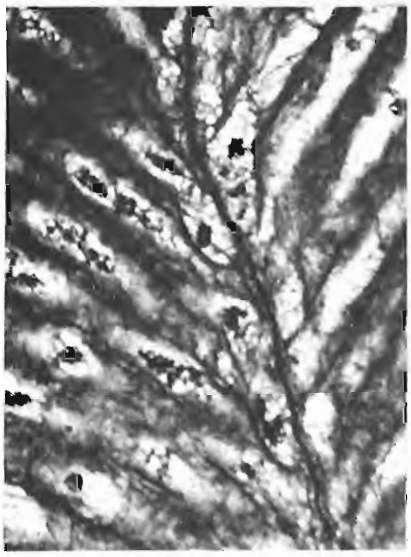

5

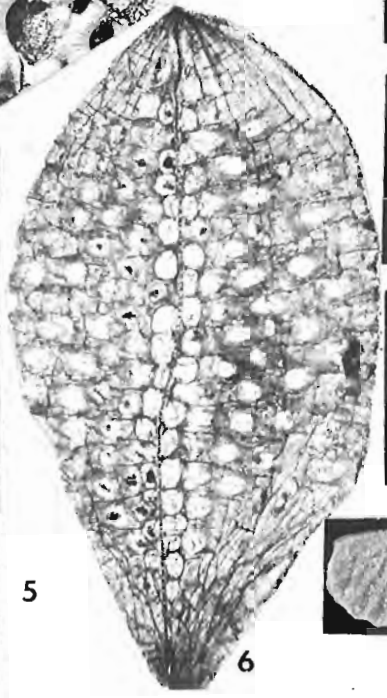

6

9

10

11

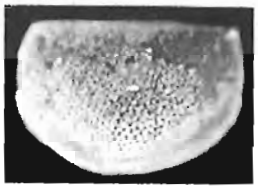

14

12

15

16

18

17

21

19

20

22

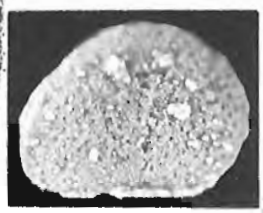

24

23

7

8

25

PLATE 1.2

BRYOZOA

Figures 1-3, 6, 8. **Diplotrypa schucherti** Fritz

1. Tangential section, X 20, illustrating monticule zooecia and few small angular mesopores, GSC loc. 94286 (member III), GSC 48861.

2, 3. Longitudinal sections, X 20, illustrating variation in beaded mesopore abundance and a rejuvenation surface, GSC locs. 94287 (member III), 94286 (member III), GSC 48862, 48863.

6, 8. Tangential section, X 20 and X 40, illustrating normal zooecia and mesopores, and amalgamate zooecial walls, GSC loc. 94286 (member III), GSC 48864.

STROMATOPOROIDEA

Figures 4, 5, 7. **Labechia** sp. Longitudinal sections of two specimens, X 6, X 6, X 10, illustrating variation in sizes of cysts and scattered pillars, GSC loc. 94287 (member II), GSC 48865, 48866 (fig. 7).

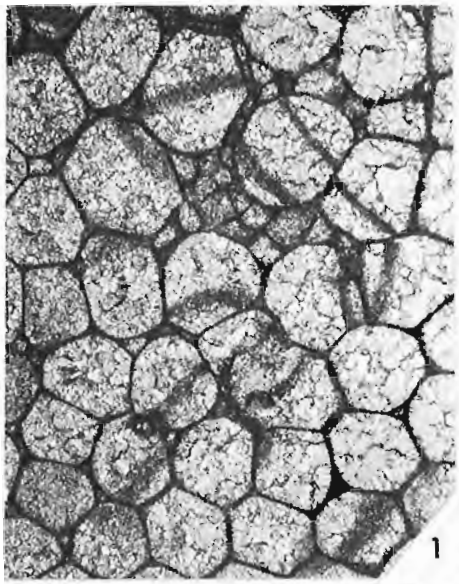

1

2

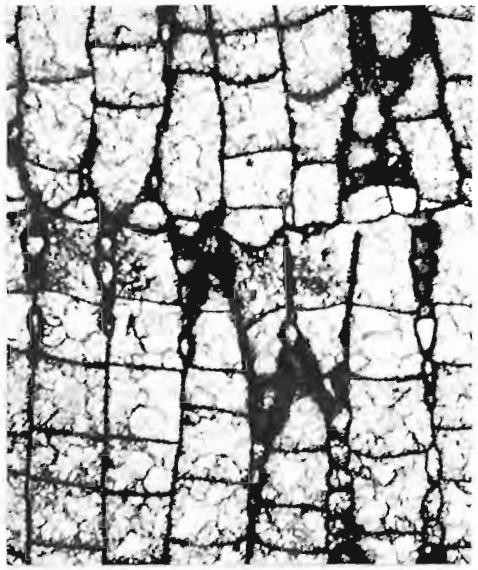

3

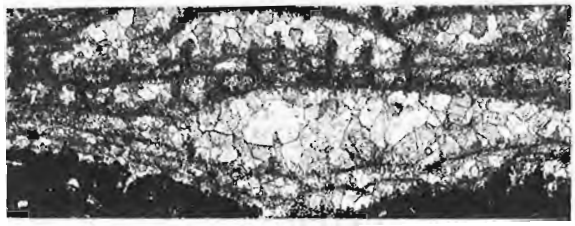

4

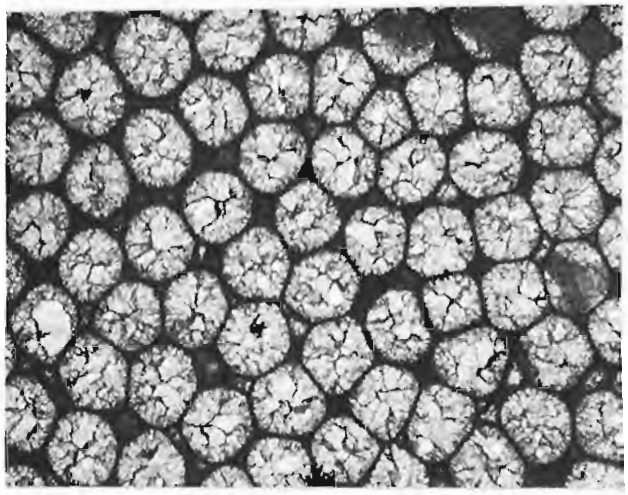

6

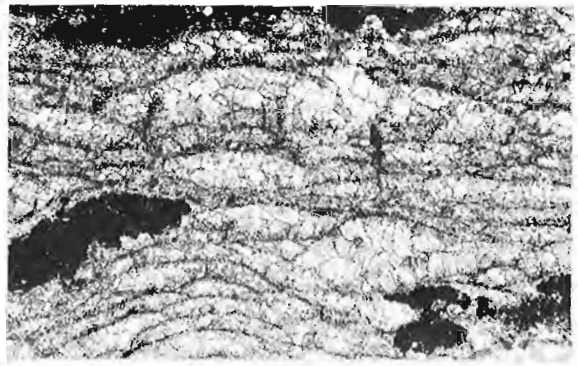

5

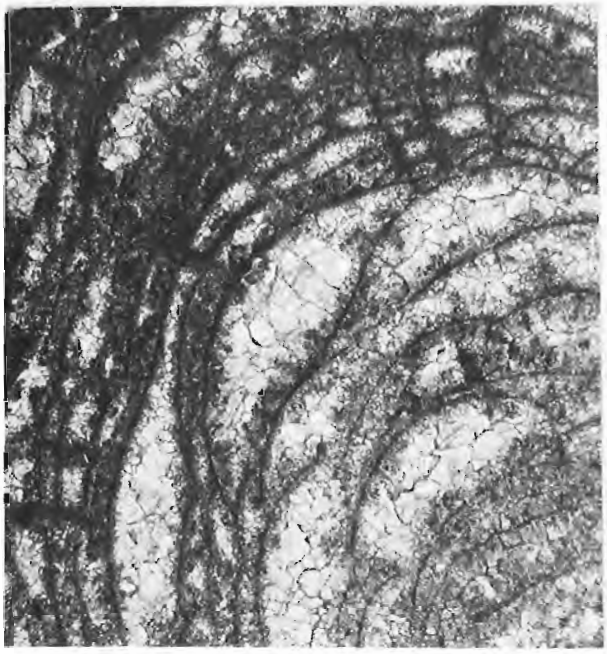

7

8

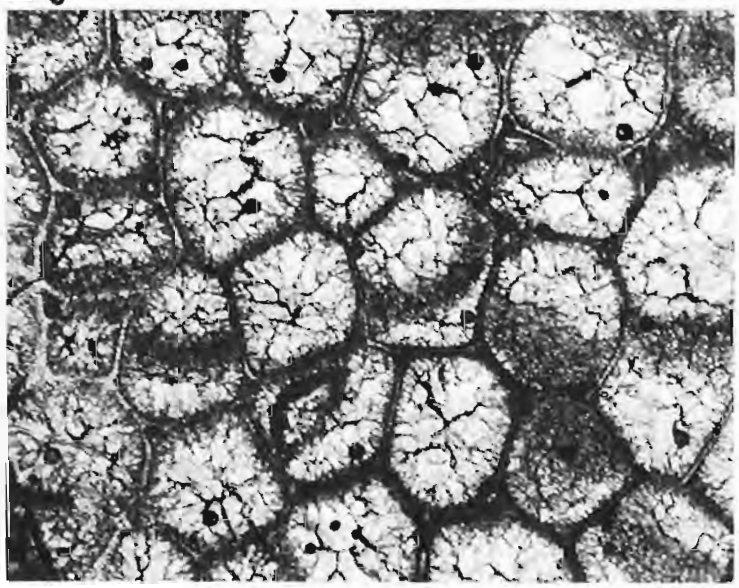

PLATE 1.3

ANTHOZOA

Figures 1-7. **Labyrinthites (Labyrinthites) chidlensis** Lambe

1. Longitudinal section, X 10, illustrating lateral increase of corallites, GSC loc. 94286 (member II), GSC 48867.

2, 4. Transverse sections, X 10, illustrating closely spaced isolated oval to cerioid corallites, GSC locs. 94287 (member II), 94286 (member II), GSC 48868, 48869.

3. Transverse section, X 10, with more angular corallites, GSC loc. 88932 (member II), GSC 15307b.

5, 7. Transverse and longitudinal sections, X 20, cutting numerous horizontal connecting tubes, GSC loc. 94287 (member II), GSC 48870.

6. Longitudinal section, X 40, illustrating connecting tubes and common walled corallites, GSC loc. 94287 (member II), GSC 48871.

1

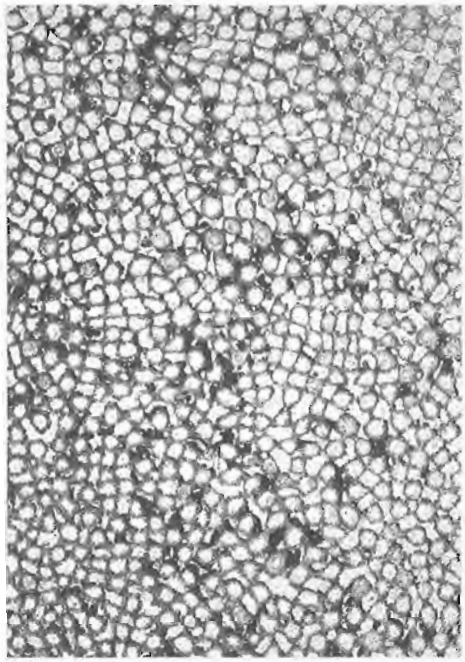

2

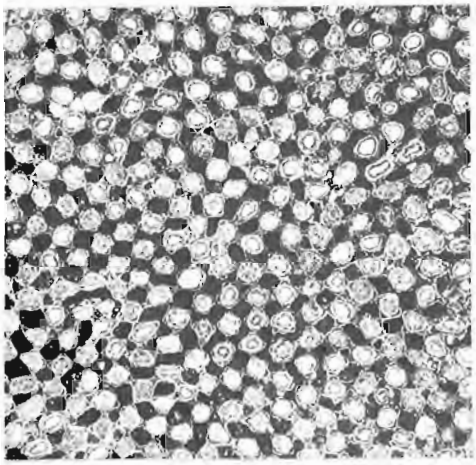

3

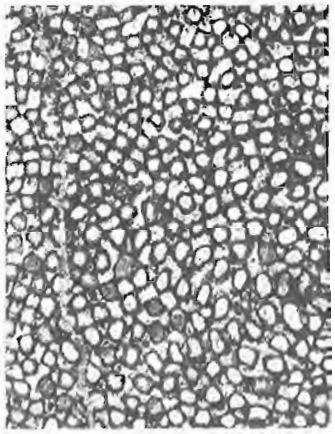

4

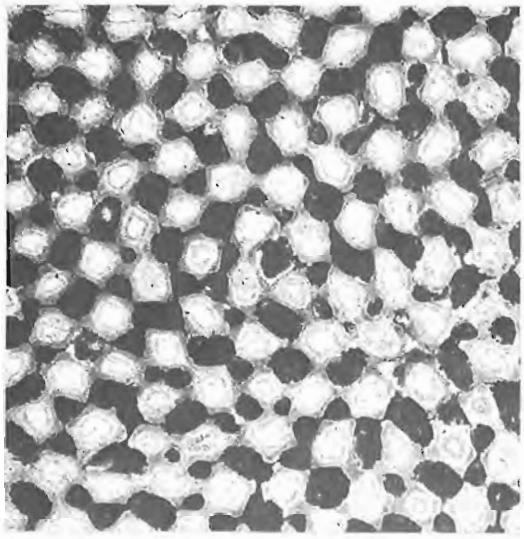

5

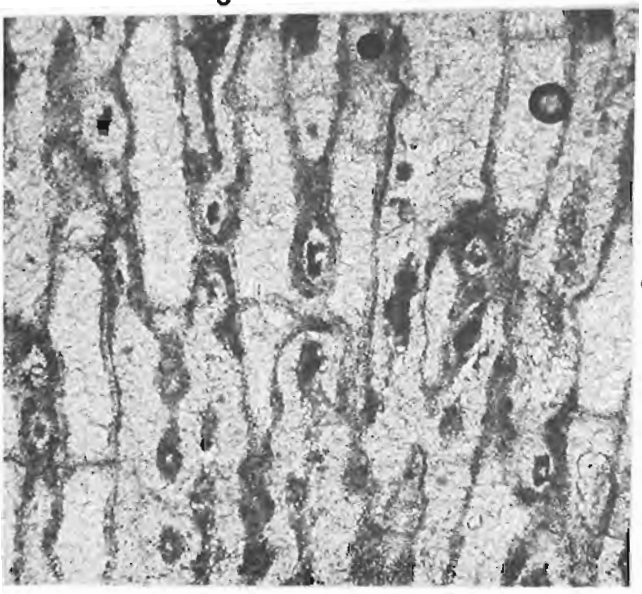

6

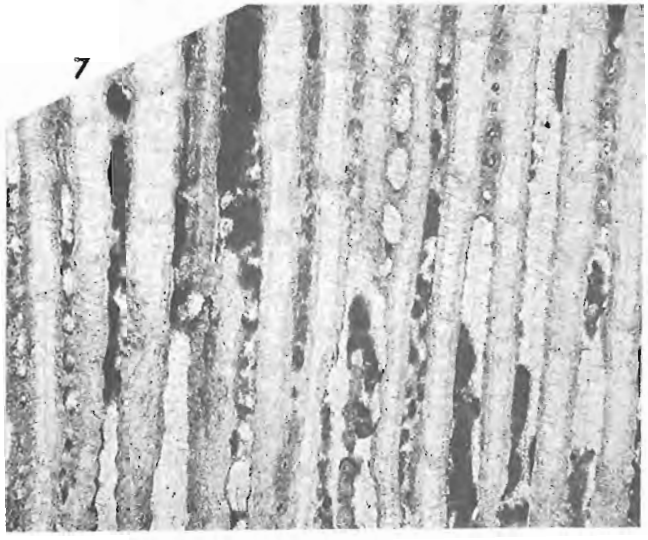

7

PLATE 1.4

ANTHOZOA

Figures 1,4-7. **Billingsaria parvituba** (Troedsson)

1, 4, 5. Transverse and longitudinal sections, X 10, X 10, X 4, with well preserved septa, GSC loc. 94287 (member II), GSC 48873.

6, 7. Transverse and longitudinal sections, X 10, illustrating the variation in preservation of primary (some bulbous tips) and secondary septa within different parts of the colony, and thin-walled **Nyctopora**-like corallites, GSC loc. 94287 (member II), GSC 48874.

Figures 2, 3. **Billingsaria parva** (Billings). Transverse and longitudinal sections, X 10, illustrating thick walls, 8 stubby septa, and widely spaced tabulae, Mingan Formation, Mingan Islands, Quebec, syntype, GSC 1003.

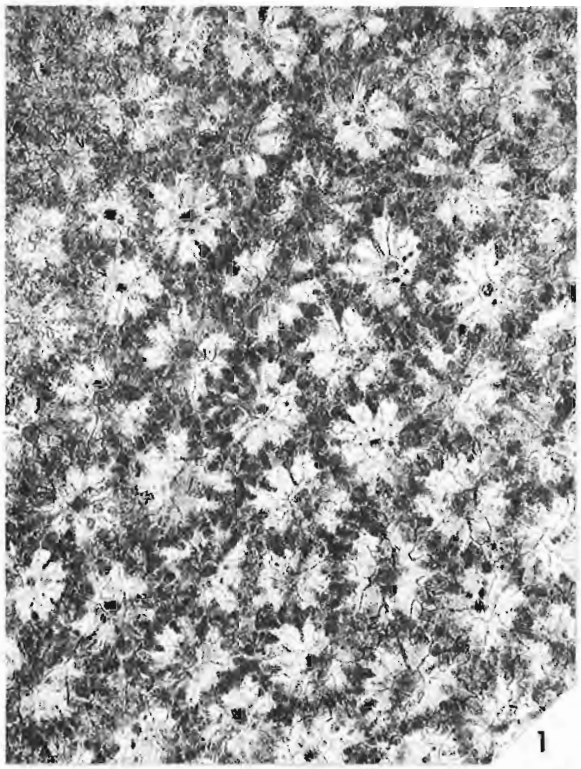

1

2

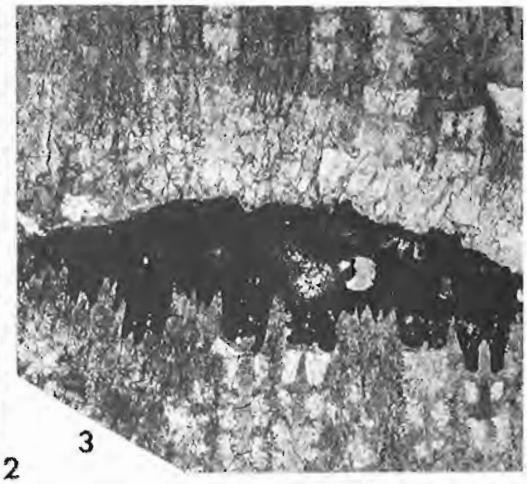

3

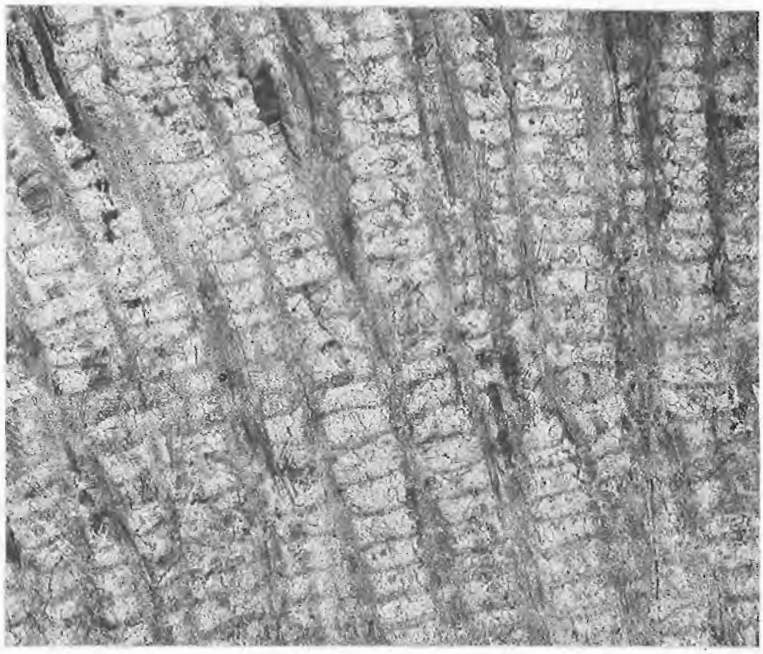

4

5

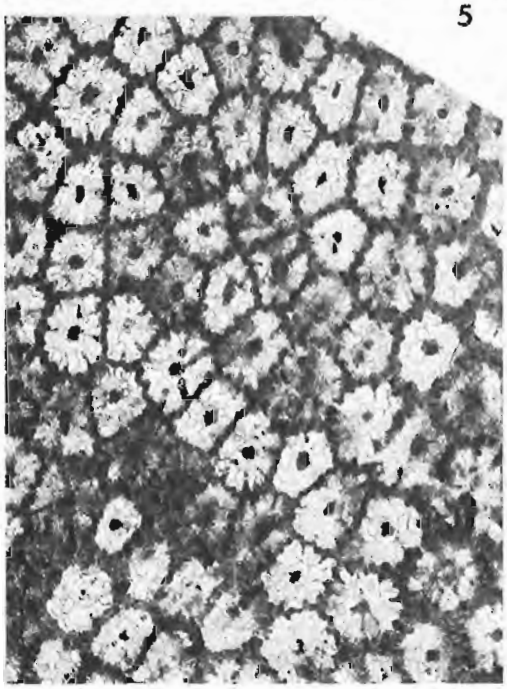

6

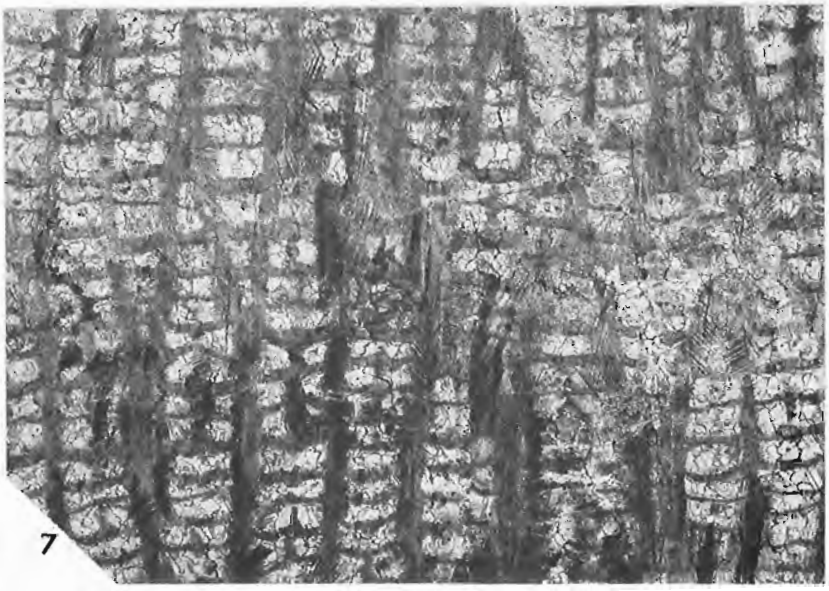

7

SILURIAN AND EARLY DEVONIAN BEYRICHIACEAN OSTRACODE PROVINCIALISM IN NORTHEASTERN NORTH AMERICA

Project 720072

M.J. Copeland and Jean M. Berdan[1]
Regional and Economic Geology Division

Studies of Silurian and Early Devonian ostracodes in northeastern North America demonstrate that a diagnostic North American faunal succession exists in the Appalachian Province (Appohimchi Subprovince of Boucot, 1974) from westernmost Virginia to Gaspé, and that an equally distinctive north European succession is present in the Arisaig-Eastport region of Maritime Canada and New England (Fig. 2.1). The most conspicuous ostracodes in both areas are large beyrichiaceans, which, on the bases of physical and faunal evidence, inhabited a shallow-water environment. Those of the Appalachian Province were endemic to North America, whereas those of the Arisaig-Eastport region are closely allied with cosmopolitan species from the Baltic area and Great Britain. The beyrichiaceans of the Appalachian Province are found both in platform sedimentary rocks (i.e., Silurian limestone suite of Berry and Boucot, 1970) and in areas that were tectonically active at the time of deposition. The beyrichiaceans of the Arisaig-Eastport region are from a tectonically active area, but their close allies from the Baltic are in platform deposits. Therefore, it seems unlikely that the dissimilarity of the two ostracode faunas is due to differences in environment, but rather that there must have been some sort of physical barrier between them.

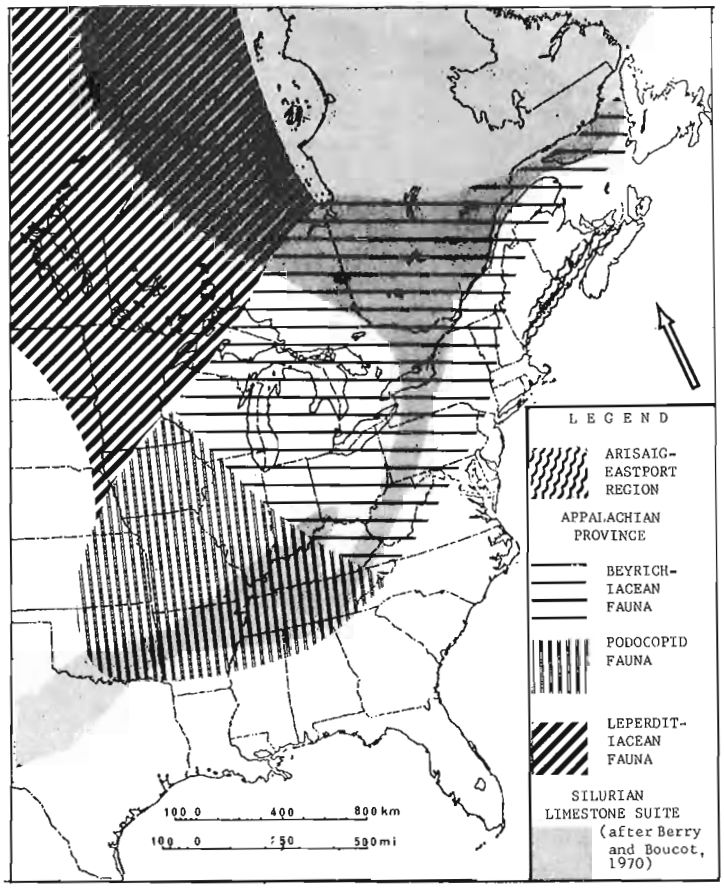

Figure 2.1. Distribution of Silurian and Early Devonian ostracode faunas in eastern North America. Leperditiacean fauna discussed by Copeland (1976).

Ostracode Zonation

Appalachian Province

The Appalachian Province is characterized by the appearance of zygobolbine beyrichiids during the middle part of the Niagaran Series (Rickard, 1975), the oldest of which are the primitive zygobolbine genera **Zygocosta** and **Zygobursa** described by Copeland (1970). These are associated in rocks of the lower Clinton Group (Copeland, 1974) with species of the brachiopod **Virgiana** and are considered by Berry and Boucot (1970) as Llandoverian B1-B3. The origin of the zygobolbine stock is not certainly known, but a North American eurychilinid or European piretellid ancestry has been postulated for beyrichiaceans in general (see Martinsson, 1962, p. 114-116 for summary). The zygobolbines diversified throughout the Niagaran and became a conspicuous element of the fauna.

The presence of this zygobolbine fauna enabled Ulrich and Bassler (1923) to establish a Niagaran ostracode zonation in the north-central Appalachian Province that has become the faunal standard for most Clinton rocks of eastern North America (Berdan, in Berry and Boucot, 1970). Ulrich and Bassler (1923, p. 349-352) proposed nine zygobolbine zones (for zonal nomenclature see captions of Plate 2.1, Plate 2.2, figs. 1-9), of which Gillette (1947, p. 22) recognized four in the Clinton Group of central New York (zones 2, 3, 5, 8). In addition, Gillette (1947, p. 22-24) proposed the aechminid **Paraechmina spinosa** Zone, which he considered to be the equivalent of the youngest, **Drepanellina clarki** Zone of Ulrich and Bassler (their zone 9). We agree with the suggestion of Swartz (1934, p. 121) that the **Drepanellina clarki** Zone (herein, zone 10) is younger than the **Paraechmina spinosa** Zone (zone 9), and thus indicate ten zones on Plates 2.1 and 2.2, which show ostracodes typical of each of the Appalachian Province zones and the ranges of important genera. Because Ulrich and Bassler (1923, p. 350, 351) themselves considered their oldest zone, that of **Zygobolba erecta**, to be restricted and of doubtful utility, we have replaced this zone with the zone of **Zygocosta** and **Zygobursa** (zone 1). Other modifications of the ostracode zonal succession may be required as studies continue, especially with respect to the validity of the **Zygosella postica** and **Bonnemaia rudis** Zones (Ulrich and Bassler, 1923, p. 350, 351; zones 6, 7).

[1]U.S. Geological Survey, Washington, D.C.

From: Report of Activities, Part B;
Geol. Surv. Can., Paper 77-1B (1977)

PLATE 2.1

EARLY SILURIAN OSTRACODE FAUNAS OF THE APPALACHIAN PROVINCE

1 (A_1). Zone of **Zygocosta** and **Zygobursa** (figs. 1-3).

1, 2. **Zygocosta williamsi** (Ulrich and Bassler)
Right tecnomorphic and left heteromorphic views, x20, north shore of bay west of Rocky Bay, Bruce Peninsula, Ontario, Dyer Bay Formation, hypotypes, GSC 24399, 24404.

3. **Zygobursa praecursor** Copeland
Left heteromorphic view, x20, road cut, north bank of Jupiter River AT Twenty-four Mile Lodge, Anticosti Island, Quebec, upper Becscie Formation, paratype, GSC 24396.

2 (A_2). Zone of **Zygobolba anticostiensis** (figs. 4-6)

4. **Zygobolba anticostiensis** Ulrich and Bassler
Left tecnomorphic view, x16, shore section 2.75 miles (4.5 km) east of Ottawa, Anticosti Island, Quebec, Jupiter Formation, hypotype, GSC 33123.

5, 6. **Zygobolba robusta** Ulrich and Bassler
Left tecnomorphic and right heteromorphic views, x17, same locality as fig. 4, Jupiter Formation, hypotypes, GSC 33118, 33117.

3 (A_3). Zone of **Zygobolba decora** (figs. 7 , 8)

7, 8. **Zygobolba decora** (Billings)
Right heteromorphic and left tecnomorphic views, x20 and x15, Southwest Point Road, 3.5 miles (5.6 km) south of Jupiter River Firetower, Anticosti Island, Quebec, Jupiter Formation, hypotypes, GSC 33128, 33133.

4. Zone of **Zygobolbina emaciata** (figs. 9, 10)

9, 10. **Zygobolbina emaciata** Ulrich and Bassler
Left heteromorphic and tecnomorphic views of latex squeezes of external impressions, x15, near toll-gate, Cove Gap, Tuscarora Mt., 4.5 miles (7 km) northwest of Mercersburg, Pennsylvania, syntypes, USNM 63526.

5. Zone of **Mastigobolbina lata** (fig. 11)

11. **Mastigobolbina lata** (Hall)
Right tecnomorphic view of latex squeeze of external impression, x15, New Hartford, New York, Kirkland Formation, hypotype, USNM 63520.

6. Zone of **Zygosella postica** (fig. 12)

12. **Zygosella postica** Ulrich and Bassler
Right tecnomorphic view of latex squeeze of external impression, x15, along Western Maryland Railway tracks, east end of the gorge cut by Wills Creek through Wills Mt. west of Cumberland, Maryland, Rose Hill Formation, paratype, USNM 63502a.

7. Zone of **Bonnemaia rudis** (fig. 13)

13. **Bonnemaia rudis** Ulrich and Bassler
Right heteromorphic view of latex squeeze of external impression, x15, Mulberry Gap, Powell Mt., 5 miles (8 km) northwest of Sneedville, Tennessee, Rose Hill Formation, cotype, USNM 63551.

8. Zone of **Mastigobolbina typa** Ulrich and Bassler (figs. 14-23)

All specimens from north side of US Highways 22 and 322 along Juniata River, midway between Millerstown and Thompsontown, Pennsylvania, Rose Hill Formation.

14, 15. **Mastigobolbina typa** Ulrich and Bassler
Right and ventral hetermorphic views, x10, hypotypes, USNM 243439 and 243440.

16, 17. **Mastigobolbina triplicata** (Foerste)
Right and ventral (anterior to right) heteromorphic views, x10, hypotype, USNM 243441.

18. **Bonnemaia crassa** Ulrich and Bassler
Right tecnomorphic view, x10, hypotype, USNM 243442.

19, 20. **Zygosella vallata** Ulrich and Bassler
Right and ventral heteromorphic views, x10, hypotype, USNM 243443.

21, 22. **Bonnemaia celsa** Ulrich and Bassler
Left and ventral (anterior to left) heteromorphic views, x10, hypotype, USNM 243444.

23. **Plethobolbina typicalis** Ulrich and Bassler
Right tecnomorphic view, x10, hypotype, USNM 243445.

(A_1 = upper Becscie Formation, A_2 = lower Jupiter Formation, A_3 = upper Jupiter Formation, Anticosti Island, Quebec)
(O_1 = Rochester Shale, Ontario and western New York)

NIAGARAN
CLINTON
9
8
7
6
5
4
3
2
1
Paraechmina
spinosa
Zygocosta
Zygobursa
Zygobolba
Zygobolbina
Mastigobolbina
Zygosella
Plethobolbina
Bonnemaia
O1
A3
A2
A1
1
2
3
4
5
6
7
8
9
10
11
12
13
14
15
16
17
18
19
20
21
22
23

PLATE 2.2

MIDDLE SILURIAN – EARLY DEVONIAN OSTRACODE FAUNAS
OF THE APPALACHIAN PROVINCE

9 (O_1). Zone of **Paraechmina spinosa** (figs. 1-4)

1. **Paraechmina postica** Ulrich and Bassler
Left view, x15, DeCew Falls, Ontario, 20-25 feet (6-7.5 m) above base of Rochester Shale, hypotype, GSC 15191.

2, 3. **Paraechmina spinosa** (Hall)
Left and right views, x15, DeCew Falls and Niagara River, Ontario, 30-35 feet (9-10.5 m) and 28-30 feet (8.5-9.0 m) above base of Rochester Shale, hypotypes, GSC 15192a, b.

4. **Paraechmina abnormis** (Ulrich)
Left view, x15, DeCew Falls, Ontario, 15-30 feet (4.5-9.0 m) above base of Rochester Shale, hypotype, GSC 15193c.

10 (O_2). Zone of **Drepanellina clarki** (figs. 5-9)

5, 6. **Drepanellina clarki** Ulrich and Bassler
Right heteromorphic and tecnomorphic views, x15, Baltimore and Ohio Railroad tracks between Pinto and McKenzie, Maryland, 'Rochester' Shale, hypotypes, USNM 145237, 145239.

7-9. **Cornikloedenia ventralis** (Ulrich and Bassler)
Right tecnomorphic and heteromorphic views, x15, Rose Hill, Cumberland, Maryland, 'Rochester' Shale, cotypes, USNM 83479 (figs. 7, 9), topotype, USNM 243446 (fig. 8).

McKenzie Formation (G_1) (figs. 10, 11)

10, 11. **Pintopsis tricornis** (Ulrich and Bassler)
Left hetermorphic and right tecnomorphic views, x16, same locality as figs. 5, 6, 85 feet (25 m) horizontally below top of McKenzie Formation, hypotypes, USNM 142248, 142250.

Wills Creek Formation (fig. 12)

12. **'Kloedenia' normalis** Ulrich and Bassler
Left heteromorphic view, x15, east bank of Flintstone Creek, north of Flintstone, Maryland, 182 feet (55 m) above base of Wills Creek Formation, lectotype, USNM 162287.

Tonoloway Limestone (figs. 13, 14)

13, 14. **Welleria obliqua** Ulrich and Bassler
Right heteromorphic and right tecnomorphic views, x15, Keyser, West Virginia, syntypes, USNM 82966.

Cobleskill Limestone (figs. 15, 16)

15, 16. **Kloedeniopsis hartnageli** Berdan
Left tecnomorphic and right heteromorphic views of latex squeezes of external impressions, x15, south side of Spring Street, Schoharie, New York, holotype and paratype, USNM 162285, 162286c.

St. Alban Formation, Roncelles Member (G_2) (fig. 17)

17. **Kloedeniopsis eufimbriata** Swartz and Whitmore
Left tecnomorphic view, x20, Cap des Rosiers Cove, Gaspé, Quebec, 82-87 feet (33-35 m) above base of St. Alban Formation, hypotype, GSC 48734.

Chapman Sandstone (figs. 18, 19)

18, 19. **Zygobeyrichia** sp. aff. **Z. apicalis** Ulrich
Left heteromorphic and right tecnomorphic views of latex casts, x15, south branch of Presque Isle stream, Chapman township, Aroostook County, Maine, topotypes, USNM 243447, 243448.

Coeymans Limestone (figs. 20, 21)

20, 21. **Lophokloedenia granulata** (Hall)
Left tecnomorphic and left heteromorphic views, x15, 0.1 mile (0.15 km) north of Cullen, New York, and 17-19 feet (5-6 m) below top of Judds Falls, north-northeast of Cherry Valley, New York, hypotypes, USNM 243449, 243450.

(O_1, O_2 = Eramosa Formation, Ontario)

(G_1 = Sayabec Formation, G_2 = St. Alban Formation, G_3 = basal Cap Bon Ami Formation, Gaspé, Quebec).

NIAGARAN
CAYUGAN
E. DEVONIAN
COEYMANS Ls.
KEYSER Ls.
TONOLOWAY Ls.
WILLS CREEK Fm.
McKENZIE Fm.
10
9
Paraechmina spinosa
Drepanellina
Welleria
Zygobevrichia
Pintopsis
Kloedeniopsis
Cornikloedenia
Lophokloedenia
G3
G2
?
G1
G2
O1
?
1
2
3
4
5
6
7
8
9
10
11
12
13
14
15
16
17
18
19
20
21

PLATE 2.3

LATE SILURIAN OSTRACODE FAUNAS OF THE ARISAIG-EASTPORT REGION

1-18. Fauna of the type section of the Stonehouse Formation, Arisaig, Nova Scotia.

1-4. **Londinia arisaigensis** Copeland
Right tecnomorphic views and ventral and lateral heteromorphic views, x15 and x17, hypotypes, GSC 14564c, e, 14563a, b.

5. **Kloedenia wilckensiana** (Jones)
Right tecnomorphic view, x17, hypotype, GSC 14514.

6-8. **Frostiella** sp. cf. **F. plicata** (Jones)
Left, dorsal and ventral heteromorphic views, x9 and x15, hypotype, GSC 14513.

9, 10. **Hemsiella maccoyiana sulcata** (Reuter)
Left and right heteromorphic views, x17, hypotypes, GSC 14511, 14512.

11. **Hemsiella maccoyiana mclearni** Copeland
Left heteromorphic view, x15, paratype, GSC 14561.

12, 14, 15. **Nodibeyrichia pustulosa** (Hall)
Left tecnomorphic views, x9 and x16, right heteromorphic view, x16, hypotypes, GSC 14500, 14504, 14503.

13. **Sleia kochi** (Boll)
Left tecnomorphic view, x17, hypotype, GSC 14507.

16. **Hemsiella** sp. cf. **H. maccoyiana** (Jones)
Right tecnomorphic view, x17, hypotype, GSC 14508.

17, 18. **Macrypsilon salterianum** (Jones)
Right tecnomorphic and heteromorphic views, x16, hypotypes, GSC 14566, a.

19-27. Fauna of the Leighton Gray Shale Member, Pembroke Formation, Eastport and Pembroke quadrangles, Maine.

19. **Frostiella** sp. cf. **F. groenvalliana** Martinsson
Right tecnomorphic view of a latex cast, x15, southeast end of Leighton Neck, Eastport and Pembroke quadrangles, hypotype, USNM 244733.

20. **Londinia** sp. cf. **L. arisaigensis** Copeland
Left tecnomorphic view of a latex cast, x15, same locality as figure 19, hypotype, USNM 244734.

21-23. **Sleia** sp.
Ventral heteromorphic view and right heteromorphic and tecnomorphic views of latex casts, x15, same locality as figure 19, figured specimens USNM 244735-244737.

24, 25. **Hemsiella** sp.
Right tecnomorphic and left heteromorphic views of latex casts, x15, north side of Leighton Cove, first point east of island, 5 feet (1.5 m) above sandy layer, Eastport and Pembroke quadrangles, figured specimens USNM 244738, 244739.

26. **Lophoctenella** sp.
Left tecnomorphic view of a latex cast, x15, northeast side of Leighton Neck, east of small point southwest of Wilson Ledges, Eastport quadrangle, figured specimen, USNM 244740.

27. **Macrypsilon** sp.
Left tecnomorphic view of a latex cast, x15, same locality as figure 24, figured specimen USNM 244741.

28-34. Fauna of the Hersey Red Shale Member, Pembroke Formation, Pembroke quadrangle, Maine.

28. **Beyrichia** sp.
Right tecnomorphic view of exfoliated specimen, x15, head of Sipps Bay, 0.3 mile (0.5 km) southeast of bridge over Sipps Brook, figured specimen USNM 244742.

29-32. **Nodibeyrichia** sp.
Right tecnomorphic and left heteromorphic views of partly and completely exfoliated specimens, x15, same locality as figure 28, figured specimens USNM 244743-244746.

33. **Nodibeyrichia** sp.
Right tecnomorphic view, x15, east point at head of Sipps Bay, 3500 feet (1050 m) south-southeast of junction of US Highway 1 bypass and old US Highway 1, figured specimen USNM 244747.

34. **Carinokloedenia**? sp.
Right tecnomorphic view, x15, same locality as figure 33, figured specimen USNM 244748.

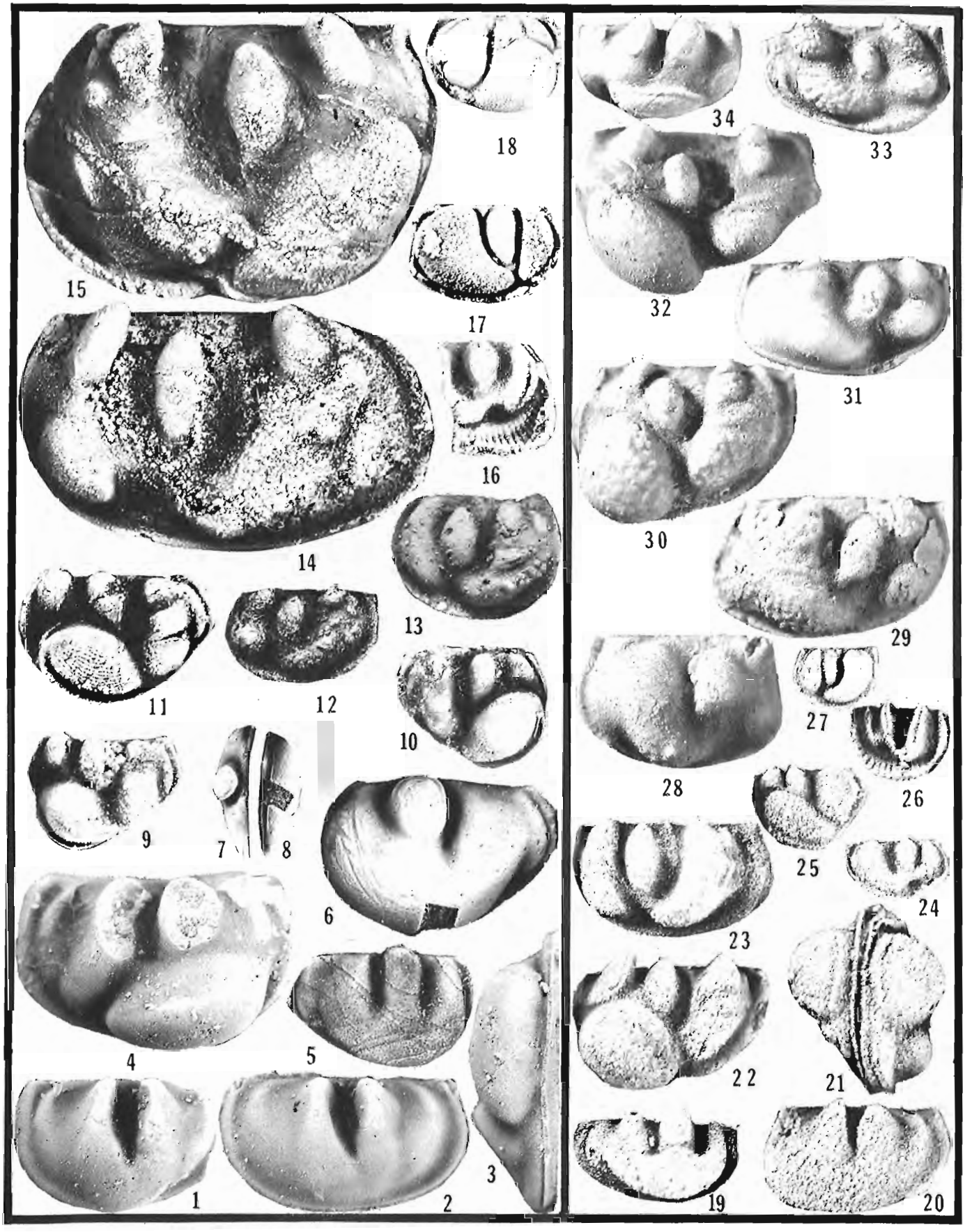
1
2
3
4
5
6
7
8
9
10
11
12
13
14
15
16
17
18
19
20
21
22
23
24
25
26
27
28
29
30
31
32
33
34

In general, all or part of this succession may be applied to Niagaran ostracode faunas throughout an area including the northern Gulf of St. Lawrence, southern James Bay, western Great Lakes and westernmost Virginia (Fig. 2.1). In Canada, faunas of only the three oldest zones (1-3) and the two youngest zones (9, 10) have been recognized, but faunas of zones 2-10 occur throughout much of the Appalachian region of the northeastern United States, and some as far west as Lake Superior (Plate 2.1, figs. 1-23; Plate 2.2, figs. 1-9). This predominantly zygobolbine zonation has limited application except in the northern Appalachian Province, because only two zygobolbine genera are known to occur elsewhere in the world (Martinsson, 1962). The early occurrence and primitive dimorphism demonstrated by this group suggest that the group may represent the stock from which some of the later beyrichiid faunas evolved. This may be inferred from Martinsson's (1962, fig. 39, and p. 357) morphological study of Silurian beyrichiacean faunas of Gotland. On the basis of the occurrence of, or the method used to close, the dolonoid space of the heteromorphic crumina (brood pouch), two groups of beyrichiaceans are distinguished -- one composed of the Treposellinae, Craspedobolbininae and Amphitoxotidinae, and the other, the Zygobolbinae and Beyrichiinae. To this second group, here termed the beyrichiid fauna, we add the Kloedeniinae, a subfamily unknown from Gotland but well represented within the European Beyrichienkalk fauna.

The Zygobolbinae existed only during the Niagaran Series; their last representative, **Drepanellina**, occurs in the **Drepanellina clarki** Zone of the 'Rochester' Shale (lower part of the McKenzie Formation) of Maryland and adjacent States (Ulrich and Bassler, 1923), in the "Herkimer Sandstone" of New York (Berdan and Zenger, 1965) and in the Eramosa Member of the Amabel (Lockport) Formation of southern Ontario (Berry and Boucot, 1970, p. 115). The zygobolbines were replaced in the Cayugan Series by other large beyrichiids, formerly known, erroneously, as '**Kloedenia**' in North America. This group includes such genera as **Cornikloedenia, Pintopsis, Welleria, Kloedeniopsis, Lophokloedenia, Zygobeyrichia** and others as yet unrevised (Plate 2.2, figs. 7-21). Species of these genera, mostly endemic to the Appalachian Province, are associated with Cayugan-Helderbergian smaller beyrichiaceans, kloedenellaceans, thlipsuraceans, and primitiopsaceans (Swartz and Whitmore, 1956; Berdan, in Boucot, 1961; Copeland, 1962; Berdan, 1972). No formal system of zonation is here proposed for these ostracodes, but some genera have fairly short ranges, which are shown on Plate 2.2

Arisaig-Eastport Region

Although rocks of Early Silurian age (Llandoverian) occur in the Arisaig-Eastport region, no ostracodes have been found in them. One occurrence of possible Wenlockian ostracodes (Bastin and Williams, 1914) in the Eastport area in Maine is in a silty shale block that may be incorporated in a diatreme (Olcott Gates, pers. comm., 1974) and cannot be placed stratigraphically. The earliest datable ostracodes in this province are beyrichiaceans (Plate 2.3), typical of those from Ludlovian rocks of Gotland, the Beyrichienkalk of the Baltic area and the Downtonian of Great Britain (Berdan, in Pecora, 1966; Martinsson, 1967; Martinsson, in Berry and Boucot, 1970). Species of **Frostiella** (Plate 2.3, figs. 6-8) and true **Kloedenia** (Plate 2.3, fig. 5) occur in the type section of the Stonehouse Formation of northeastern Nova Scotia, **Londinia arisaigensis** (Plate 2.3, figs. 1-4) only occurring in the lower 100 feet (30 m) and **Nodibeyrichia pustulosa** (Plate 2.3, figs. 12, 14, 15) only in the upper 570 feet (175 m), as shown by Copeland (1960, 1964). Similar species of **Londinia** are found in the Jones Creek Formation of southern New Brunswick, and species of **Londinia** (Plate 2.3, fig. 20) and **Frostiella** (Plate 2.3, fig. 19) occur in the Leighton Gray Shale Member of the Pembroke Formation in the Eastport and Pembroke quadrangles, Maine, suggesting correlation with the lower part of the Stonehouse sequence (Berdan, 1971). A species of **Nodibeyrichia** (Plate 2.3, figs. 29-33) from the overlying Hersey Red Shale Member of the Pembroke Formation may equate with that in the upper part of the Stonehouse Formation (Martinsson, in Berry and Boucot, 1970). The youngest marine rocks in this area of southeastern Maine, the Eastport Formation, are thought to be Gedinnian because their ostracodes, although new and undescribed, most closely resemble Early Devonian forms from Podolia and Germany (Berdan, 1971).

Biogeographic Considerations

It seems unlikely that beyrichiacean ostracodes arose independently at the same time in two relatively remote unconnected depositional provinces such as the middle Niagaran of North America and the late Llandoverian-early Wenlockian of Europe. The complicated morphology of such highly dimorphic ostracodes would seem to dictate against this. Beyrichiaceans were for the most part large benthonic animals, distinguished from other dimorphic ostracodes by the presence of a crumina or 'brood pouch' (Henningsmoen, 1965) in which the eggs were retained, hatched, and probably brooded (Martinsson, 1962). The necessity of a free-swimming pelagic larval stage could thus be obviated or greatly restricted. The development of cruminae or intracarapace brood chambers for protection of the young may have been a response to a rigorous shallow-water environment, and the larvae were not subject to wide dispersal. This may account, in part, for the localization of beyrichiacean faunas within the Appalachian Province. For example, Lundin (1971) found that beyrichiacean species represent only 2 per cent of the Silurian and Devonian Henryhouse-Haragan ostracode fauna of Oklahoma, whereas nearly 55 per cent of the ostracodes listed by Swartz and Whitmore for the Silurian and Devonian Manlius and Decker formations are beyrichiaceans. This latter figure may be substantiated by ostracode studies presently underway in Gaspé, Quebec. This difference is believed to be caused by environmental factors; possibly somewhat deeper water conditions prevailed in western Tennessee and Oklahoma (Fig. 2.1).

Some faunal connection is evident between the northern Appalachian and European Provinces during the Late Ordovician. This is demonstrated by the similarity of certain Late Ordovician hollinaceans, particularly tetradellids, from Anticosti Island, Quebec and from the Baltic (Copeland, 1973), and by their common extinction at the close of the Ordovician. Some cataclysmic event, possibly a glacial regime, as postulated by Berry and Boucot (1973, and many others) all but eradicated Ostracoda from Early Silurian faunas of North America. If sea level was lowered because of glacio eustatic conditions, a very shallow water connection may have formed, by which the Late Ordovician or Early Silurian ancestral beyrichiacean stock could have migrated. The direction of this migration is speculative, but the

consequent primitive zygobolbine beyrichiid assemblage appears earlier and is more widely distributed in shallow-water, platform-type sedimentary rocks of northeastern North America than in Europe. When water depths again became greater during the later Llandoverian or early Wenlockian, this migration route would have been severed, and independent beyrichiid evolution could have taken place along the margins of each continental segment. By Ludlovian-Pridolian time, the more westerly North American 'false **Kloedenia**' assemblage had evolved throughout the northern Appalachian Province, and the Beyrichienkalk fauna or true **Kloedenia** assemblage had become established in the more easterly Arisaig-Eastport region and in the Baltic-British area.

These distinctive shallow-water faunas were effectively separated by a barrier, either of land as suggested by Boucot (1975, p. 272) for the Early Devonian, a deep water trough, as proposed by McKerrow and Ziegler (1971) for the Early Silurian, or both in sequence (Poole, 1976). The thick succession of turbidites containing some monograptid graptolites that extends through central New Brunswick and Maine suggests that some combination incorporating a deep water barrier was necessary. Deposition of marine sediments ceased earlier in the Arisaig-Eastport region than in the Appalachian Province, and there is no evidence of a post-early Gedinnian ostracode fauna in the former region. However, marine sedimentation continued through the Early Devonian in the Appalachian Province, and the well-developed North American 'false **Kloedenia**' assemblage is found in rocks of this age. Some indications are that by Siegenian time the barrier was less effective, as Abushik (1971) has described the typically Appalachian Province genus **Zygobeyrichia** from the upper Ivane horizon in Podolia, Ukrainian SSR.

Significantly, the endemism of beyrichiid ostracodes in the Appalachian Province parallels that of two other benthonic groups of fossils, the brachiopods (Boucot, Johnson, and Talent, 1969) and the corals (Oliver, 1976), although the beyrichiids apparently were effectively isolated earlier (middle Niagaran, Llandoverian) than the other groups.

References

Abushik, A.F.
1971: Ostrakod'i opornogo razreza silura-nizhnego devonia Podolii; in Paleozoiskie ostrakod'i iz oporn'ikh razrezov Evropeiskoi chasti SSSR, Izdatel'stvo "Nauka", Moscow, USSR.

Bastin, E.S. and Williams, H.S.
1914: Eastport Folio, Maine; U.S. Geol. Surv., Geol. Atlas Folio 192.

Berdan, J.M.
1971: Silurian to Early Devonian ostracodes of European aspect from the Eastport quadrangle, Maine; Geol. Soc. Am., Abstr., v. 3, no. 1, p. 18.

1972: Brachiopoda and Ostracoda of the Cobleskill Limestone (Upper Silurian) of central New York; U.S. Geol. Surv., Prof. Paper 730.

Berdan, J.M. and Zenger, D.H.
1965: Presence of the ostracode **Drepanellina clarki** in the type Clinton (Middle Silurian) in New York State; U.S. Geol. Surv., Prof. Paper 525-C, p. C96-C100.

Berry, W.B.N. and Boucot, A.J.
1970: Correlation of the North American Silurian rocks; Geol. Soc. Am., Spec. Paper 102.

1973: Glacio-eustatic control of Late Ordovician-Early Silurian platform sedimentation and faunal changes; Geol. Soc. Am., Bull. 84, no. 1, p. 275-283.

Boucot, A.J.
1961: Stratigraphy of the Moose River Synclinorium, Maine; U.S. Geol. Surv., Bull. 1111-E, p. 153-188.

1974: Silurian and Devonian biogeography; in C.A. Ross, ed., Paleogeographic Provinces and Provinciality; Soc. Econ. Mineral Paleontol., Spec. Publ. 21, p. 165-176.

1975: Evolution and extinction rate controls; Developments in Palaeontology and Stratigraphy, 1, Elsevier Scientific Publishing Company, Amsterdam, Oxford, New York.

Boucot, A.J., Johnson, J.G., and Talent, J.A.
1969: Early Devonian brachiopod zoogeography; Geol. Soc. Am., Spec. Paper 119, 113 p.

Copeland, M.J.
1960: Ostracoda from the Upper Silurian Stonehouse Formation, Arisaig, Nova Scotia, Canada; Palaeontology, v. 3, pt. 1, p. 93-103.

1962: Ostracoda from the Lower Devonian Dalhousie Beds, northern New Brunswick; Geol. Surv. Can., Bull. 91, p. 18-51.

1964: Stratigraphic distribution of Upper Silurian Ostracoda, Stonehouse Formation, Nova Scotia; Geol. Surv. Can., Bull. 117, p. 1-13.

1970: Two new genera of beyrichiid Ostracoda from the Niagaran (Middle Silurian) of eastern Canada; Geol. Surv. Can., Bull. 187, p. 1-7.

1973: Ostracoda from the Ellis Bay Formation (Ordovician), Anticosti Island, Quebec; Geol. Surv. Can., Paper 72-43.

1974: Silurian Ostracoda from Anticosti Island, Quebec; Geol. Surv. Can., Bull. 241.

1976: Leperditicopid ostracodes as Silurian biostratigraphic indices; in Report of Activities, Part B, Geol. Surv. Can., Paper 76-1B, p. 83-87.

Gillette, T.
1947: The Clinton of western and central New York; N.Y. State Mus., Bull. no. 341.

Henningsmoen, G.
1965: On certain features of palaeocope ostracodes; Geol. Foeren. Stockh. Foerh., v. 86, p. 329-394.

Lundin, R.F.
1971: Possible paleoecological significance of Silurian and Early Devonian ostracode faunas from midcontinental and northeastern North America; Bull. Centre Rech. Pau-SNPA, 5 suppl., p. 853-868.

Martinsson, A.
1962: Ostracodes of the Family Beyrichiidae from the Silurian of Gotland; Univ. Uppsala Pal. Inst., Publ. 41.

1967: The succession and correlation of ostracode faunas in the Silurian of Gotland; Geol. Foeren. Stockh. Foerh., v. 89, p. 350-386.

McKerrow, W.S. and Ziegler, A.M.
1971: The Lower Silurian paleogeography of New Brunswick and adjacent areas; J. Geol., v. 79, no. 6, p. 635-646.

Oliver, W.A., Jr.
1976: Biogeography of Devonian rugose corals; J. Paleontol., v. 50, no. 3, p. 365-373.

Pecora, W.T.
1966: Geological Survey research 1966; U.S. Geol. Surv., Prof. Paper 550-A.

Poole, W.H.
1976: Plate tectonic evolution of the Canadian Appalachian Region; in Report of Activities, Part B, Geol. Surv. Can., Paper 76-1B, p. 113-126.

Rickard, L.V.
1975: Correlation of the Silurian and Devonian rocks in New York State; New York State Mus. and Sci. Serv., Geol. Survey, Map and Chart Ser. No. 24.

Swartz, F.M.
1934: Silurian sections near Mount Union, Central Pennsylvania; Geol. Soc. Am., Bull., v. 45, p. 81-134.

Swartz, F.M. and Whitmore, F.C., Jr.
1956: Ostracoda of the Silurian Decker and Manlius Limestone in New Jersey and eastern New York; J. Paleontol., v. 30, no. 5, p. 1029-1091.

Ulrich, E.O. and Bassler, R.S.
1923: Paleozoic Ostracoda: Their morphology, classification and occurrence; Maryland Geol. Surv., Silurian, p. 271-391.

3. LANG LAKE – AN EARLY PRECAMBRIAN PORPHYRY COPPER-MOLYBDENUM IN NORTHWESTERN ONTARIO

E.M.R. Research Agreement 1135-D13-4-111/76

D.J. Findlay[1] and L.D. Ayres[1]
Regional and Economic Geology Division

Introduction

Until recently, Precambrian porphyry copper-molybdenum deposits were virtually unknown. However, during the past five years numerous deposits have been discovered which have affinities for Mesozoic and Cenozoic porphyry deposits (Kirkham, 1972; Riley et al., 1971), particularly those of British Columbia, South America, and the southwest Pacific. These Precambrian deposits are typically large, low grade mineralized zones with alteration halos associated with porphyritic plutons in metavolcanic sequences. As yet, all known deposits are below ore grade, with the possible exception of the copper-bearing envelope around the McIntyre Copper Mine near Timmins, Ontario which may be a porphyry deposit (Pyke and Middleton, 1971).

The volcanic sequences containing the deposits are generally isoclinally folded and metamorphosed to low to medium rank. The porphyritic plutons and associated mineralization and alteration are also commonly deformed and metamorphosed although the extent of the deformation and metamorphism is largely undocumented.

In order to properly explore and exploit Precambrian porphyry deposits,more knowledge is needed about the nature of the mineralization and alteration and especially the effects of deformation and metamorphism. For example, if the porphyry plutonism and mineralization are genetically related to the volcanism, as is suggested in many deposits, then the deposit will be folded along with the enclosing sequence. Consequently, when the enclosing strata are subvertical, which is the common attitude in many greenstone belts, the erosion surface through the deposit will represent a vertical rather than a horizontal section. In such a vertical section, zoning of alteration and mineralization may show a different pattern than that documented in more recent, less deformed deposits where the exposed section is more or less horizontal. Furthermore, if the original horizontal dimensions of the mineralized zone were greater than its thickness, then, in the presently exposed section, a larger proportion of the mineralization may be inaccessible to open-pit mining. On the other hand, if the plutonism occurred during or after much of the deformation, then the exposed section through the deposit will range from inclined to horizontal depending on the amount of postplutonism deformation.

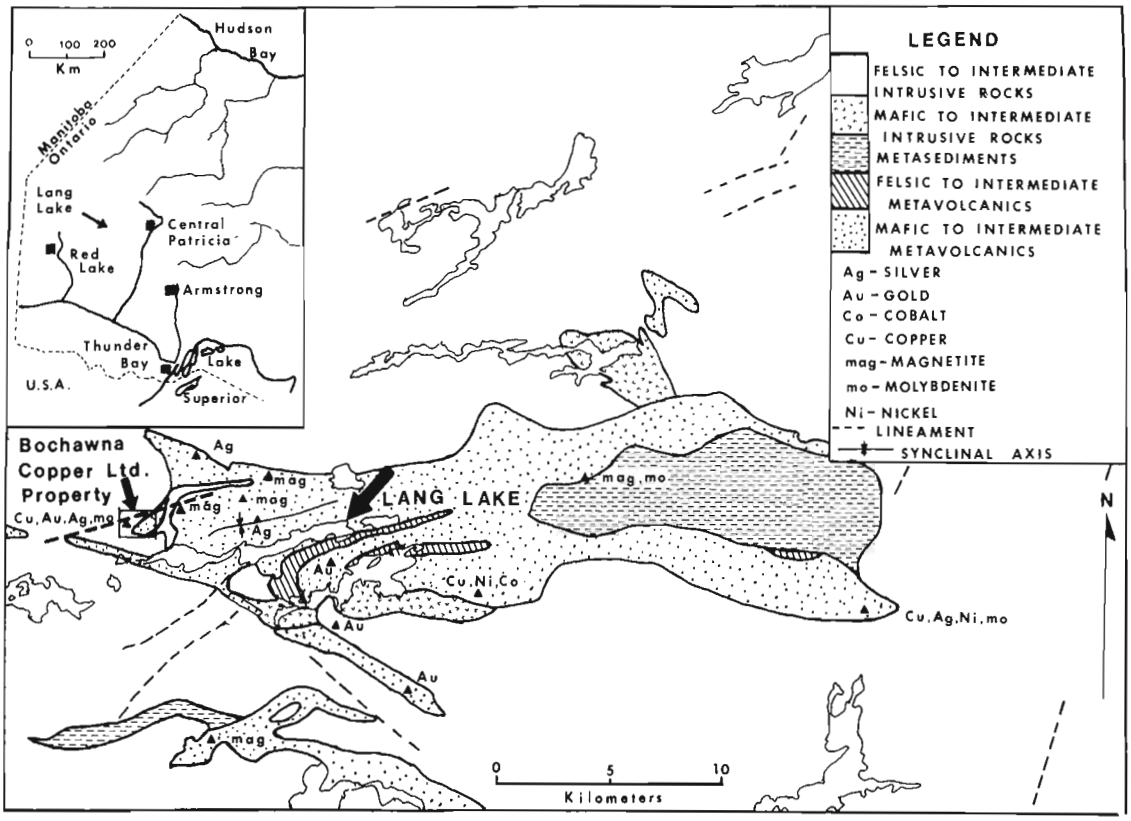

Figure 3.1. Regional setting of the Bochawna Copper Mines Ltd. property (modified from Fenwick, 1969).

[1] Department of Earth Sciences, University of Manitoba, Winnipeg, Manitoba R3T 2N2

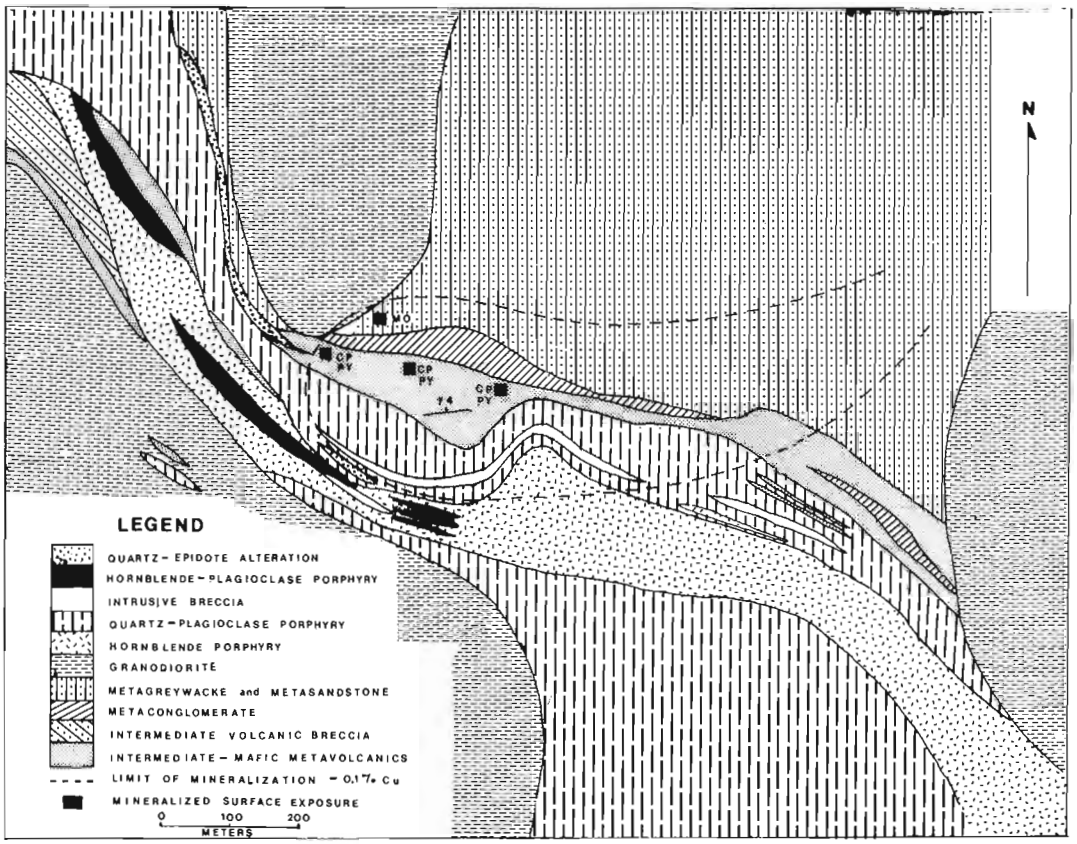

Figure 3.2. Geological map of the main mineralized area, Bochawna Copper Mines Ltd., based on surface outcrops and diamond drill core.

In Mesozoic and Cenozoic porphyry deposits, the degree of alteration is related to the grade of mineralization, and documentation of alteration can be used to outline exploration targets (Carson and Jambor, 1974; Lowell and Guilbert, 1970). Most alteration mineral assemblages, however, will be strongly affected by subsequent metamorphism. Thus, in order to use alteration as an exploration guide in metamorphosed Precambrian porphyry deposits, alteration assemblages must be better documented and the effects of metamorphism evaluated. In particular, the relationship between the present metamorphosed alteration assemblages, and the premetamorphism assemblages should be determined.

The objectives of the Lang Lake study are to document the nature of the mineralization and associated alteration; to determine the relationship between mineralization, and the associated plutonic and volcanic rocks; and to study the effects of deformation and metamorphism.

Geological Setting

During 1976, field work, augmenting 1975 field information (Findlay, 1976), was carried out on the Lang Lake property of Bochawna Copper Mines Ltd., 160 km east of Red Lake, northwestern Ontario (51°35'N; 91°32'W) (Fig. 3.1). Much of the time was spent examining the extensive (6135 m) drill core on the property because outcrop exposure is less than 10 per cent.

The property is at the western end of the Lang-Cannon Lakes metavolcanic-metasedimentary belt (Fenwick, 1969; Riley, 1969) (Fig. 3.1). At the property, a steeply dipping north-facing metavolcanic-metasedimentary sequence has been intruded by equigranular granodiorite stocks and by a complex sequence of porphyritic to locally aphyric dykes that commonly contain one or more of quartz, plagioclase, and hornblende phenocrysts (Fig. 3.2). To date, ten dyke phases have been identified from textural and mineralogical variations and cross-cutting relations. In order of decreasing age these are an older hornblende porphyry, seven quartz-plagioclase porphyry phases including an intrusive breccia, and two younger mafic porphyry phases.

The metavolcanic-metasedimentary sequence and the dyke suite have been regionally metamorphosed to upper greenschist facies. Local alteration, closely associated with the copper mineralization, is also present.

The older hornblende porphyry forms a broadly concordant southeast-trending zone up to 110 m wide (Fig. 3.2). Alteration and deformation mask petrographic variations within the unit but some textural variations are present and suggest that the unit is composed of a series of dykes or sills up to 10 m wide rather than a single intrusion. When unaltered, the hornblende porphyry is characterized by 30 to 35 per cent medium to coarse grained, euhedral, randomly oriented hornblende phenocrysts in a grey-brown aphanitic groundmass.

Quartz-plagioclase porphyry forms two southeast-trending units (Fig. 3.2), each of which is a multiple intrusion comprising at least six different types of quartz-plagioclase porphyry. The widths of individual dykes range from less than 1 m to 60 m and appear to parallel the boundaries of the unit. Both units have relatively sharp, broadly concordant contacts with the older hornblende porphyry and the metavolcanic-metasedimentary sequence although narrow quartz-plagioclase porphyry dykes up to 2 m wide occur in country rocks adjacent to the dyke unit. Country rock septa and xenoliths are rare in the dyke units.

Individual phases of the quartz-plagioclase porphyry can be distinguished by the relative abundance of quartz and plagioclase phenocrysts, the relative sizes, shapes, distribution, and colour of the phenocrysts, and the colour of the fine grained to aphanitic groundmass. Phenocryst content ranges from 5 to 35 per cent plagioclase ($An_0 - An_{30}$) and 5 to 20 per cent quartz. The three most abundant phases are very similar in composition and texture; they contain 12 to 18 per cent medium to coarse grained plagioclase phenocrysts and 4 to 7 per cent fine to medium grained quartz phenocrysts in an aphanitic groundmass of quartz, plagioclase, potassium feldspar, and biotite.

Intrusive breccia dykes up to 6 m wide intruded both the hornblende and quartz-feldspar porphyry units. They contain 15 to 20 per cent medium to coarse grained plagioclase phenocrysts and up to 30 per cent angular to subangular clasts that range in size from less than 1 cm to more than 10 cm. Clast texture varies from medium to coarse grained equigranular to fine grained porphyritic.

The two younger, mafic porphyry phases are volumetrically minor and the age relationship between them is uncertain. Two of these phases form dykes up to 10 m wide with sharp chilled contacts within quartz-feldspar porphyry. The more abundant of these two phases has 20 per cent medium to coarse grained, euhedral to subhedral hornblende phenocrysts and 10 to 15 per cent medium to coarse grained, euhedral to subhedral plagioclase phenocrysts in an aphanitic groundmass. The dykes parallel the older quartz-plagioclase porphyry dykes and are concentrated in zones up to 40 m wide (Fig. 3.2). The second phase has 15 to 20 per cent medium to coarse grained, subhedral hornblende phenocrysts and 10 per cent medium grained biotite phenocrysts in a grey-green, aphanitic groundmass; this type is not shown on Figure 3.2.

The granodiorite is equigranular and medium to coarse grained with a homogenous to locally aggregated mineral distribution. Based on the relative abundances of biotite, hornblende, and quartz, two phases have been distinguished, the petrographic work may define other phases. The granodiorite and porphyry phases are not in contact with each other and exact age relationships between them are uncertain. However, at one locality a quartz-plagioclase porphyry dyke contains clasts of granodiorite, suggesting that the granodiorite is older.

Sulphide mineralization extends over an east-trending zone 700 m long and up to 300 m wide (Fig. 3.2). Pyrite, pyrrhotite, chalcopyrite, and molybdenite are the main sulphide minerals and they occur disseminated or locally concentrated in stringers and veins in shear zones and fractures. Silver and gold are present in trace amounts. In the western half of the mineralized zone, the average copper grade is between 0.25 and 0.35 per cent but the average molybdenum content is less than 0.005 per cent. Copper values greater than 1 per cent are locally present but are restricted to zones less than 5 m wide; values greater than 0.5 per cent are restricted to zones less than 10 m wide.

The mineralized zone has an easterly trend, slightly discordant to the trend of the porphyry units (Fig. 3.2). Mineralization is rare in the granodiorite but occurs in the various porphyry phases and in country rocks. The mineralized zone is asymmetric to the porphyry plutons with most of the mineralization on the north side, or stratigraphic top of the plutons. The highest copper values are actually in pyroclastic and autoclastic breccias and sedimentary rocks above, but close to the northernmost quartz-plagioclase porphyry pluton. The higher porosity of the clastic rocks apparently favoured sulphide deposition because interlayered massive flow units contain less mineralization than the breccias. The discordant trend of the mineralized zone may represent an old fracture system. It is coincident with a linear structure that extends through the mineralized zone (Fig. 3.1).

Alteration of mineralized and unmineralized rocks is ubiquitous, but only preliminary petrographic work has been completed on the alteration. Epidote, quartz, chlorite, carbonate, sericite, albite, sphene, and clay minerals are common alteration products. A large zone of epidote-quartz alteration occurs in the quartz-plagioclase porphyry (Fig. 3.2). It has diffuse borders and contains fine grained epidote and quartz with epidote predominating.

Synthesis

The porphyritic nature, fine grained to aphanitic groundmass, chilled contacts, and complexity of the porphyritic units supports a high-level subvolcanic origin. The spatially associated granodiorite stocks, on the other hand, are medium to coarse grained and equigranular suggesting a deeper level of emplacement although still in the epizone. This difference in emplacement level probably reflects an age difference between the two plutonic events, even though the granodiorite and quartz-plagioclase porphyry are generally similar in composition. Poorly documented age relations suggest that the granodiorite is older than the porphyry phases.

The occurrence of the porphyritic units in a volcanic sequence would normally be interpreted as indicating a close temporal association between volcanism and porphyry plutonism. The age and depth relations discussed above, however, appear to indicate that the porphyry plutonism is younger than the volcanism. Possibly they are a marginal dyke phase of granitic batholiths that occur several kilometres northeast of the property (Fig. 3.1). These postulated relationships can be tested by petrographic work. If the porphyry plutons are related to the batholiths they should have a lower metamorphic grade than adjacent units. If, on the other hand, they are older than the batholiths, they should have the same general metamorphic grade as adjacent units.

The complexity of the quartz-plagioclase porphyry dyke units, the general similarity of phases within the units, the lack of country rock septa, and the relatively sharp contacts of the units show that the units are not dyke swarms. Rather they are the loci of porphyry intrusion that may represent the progressive expansion of two sill-like subvolcanic magma chambers by successive pulses of magma from a larger fractionating granodiorite reservoir. The older hornblende porphyry is distinctly different from the quartz-plagioclase porphyry phases but is also sill-like. It may represent a less fractionated pulse of magma.

The occurrence of mineralization within the quartz-plagioclase porphyry but its concentration above the porphyry supports a temporal and genetic relationship between porphyry plutonism and mineralization. The presence of both high porosity country rocks and a possible discordant fracture system may have been the major controls for localizing mineralization. The effect, if any, of the older granodiorite on the mineralization has not yet been determined.

A major unresolved problem is the precise relationship between volcanism, the various plutonic events, mineralization and alteration, deformation, and metamorphism. Some general comments about these relationships were made above, but more detailed statements must await completion of comprehensive petrographic work now in progress.

References

Carson, D.J.T. and Jambor, J.L.
1974: Mineralogy, zonal relationships and economic significance of hydrothermal alteration at porphyry copper deposits, Babine Lake area, British Columbia; Can. Min. Metall. Bull., v. 67, p. 110-133.

Fenwick, K.G.
1969: Lang-Cannon Lakes area (west half); Ont. Dep. Mines, Prel. Map P. 581.

Findlay, D.J.
1976: Lang Lake, an Archean porphyry copper-molybdenum deposit; Centr. Prec. Stud., Univ. Manitoba, 1975 Ann. Rept., p. 103-107.

Kirkham, R.V.
1972: Geology of copper and molybdenum deposits; in Report of Activities, Part A, Geol. Surv. Can., Paper 72-1A, p. 82-87.

Lowell, J.D. and Guilbert, J.M.
1970: Lateral and vertical alteration-mineralization zoning in porphyry ore deposits; Econ. Geol., v. 65, p. 373-408.

Pyke, D.R. and Middleton, R.S.
1971: Distribution and characteristics of the sulfide ores of the Timmins area; Can. Inst. Min. Met., Trans., v. 74, p. 157-168.

Riley, R.A.
1969: Bochawna Copper Mines Limited; Ont. Dep. Mines, Misc. Paper 23, p. 8-9.

Riley, R.A., King, H.L., and Kustra, C.R.
1971: Mineral exploration targets in northwestern Ontario; Ont. Dep. Mines Northern Affairs, Misc. Paper 47, 72 p.

MISSI ISLAND VOLCANIC CENTRE, SASKATCHEWAN

E.M.R. Research Agreement 1135-D13-4-111/76

M.E. Chute[1] and L.D. Ayres[1]
Regional and Economic Geology Division

Introduction

The metallogenic relationship between modern island arcs and porphyry-type copper and/or molybdenum mineralization led Kirkham (1974) to suggest that ancient island arcs could host this type of mineralization. Ayres and Findlay (1976) further suggested that known Precambrian porphyry deposits are more closely related to porphyry deposits in Cenozoic island arcs, where mineralized plutons appear to be an integral part of the volcanism and occupy the lower parts of volcanic vents, than to Cenozoic and Mesozoic porphyry deposits of the southwestern United States where plutons emplaced in much older Precambrian and Paleozoic sedimentary and metasedimentary rocks are the locus of mineralization. A possible example of this type of Precambrian deposit is Missi Island in Amisk Lake, east-central Saskatchewan (54°40'N; 102°15'W) about 25 km west-southwest of Flin Flon. Here pyrite, chalcopyrite, and minor molybdenite mineralization is associated with a porphyritic dyke suite that may represent an eroded vent complex (Kirkham, 1974) with the dykes being the intrusive equivalent of overlying felsic to intermediate metavolcanic formations (Fig. 4.1).

Investigation of the Missi Island volcanic centre began in 1975 (Ayres and Findlay, 1976). Objectives of the project are determination of the form and structure of the vent complex, relationships between the vent complex and associated mineralization, character and distribution of the alteration and mineralization, effects of metamorphism on the alteration assemblages, and the relationship between the porphyritic dyke suite and younger altered trondhjemite plutons. J.S. Fox (pers. comm.) of the Saskatchewan Research Council is investigating the overlying metavolcanic formations to the west.

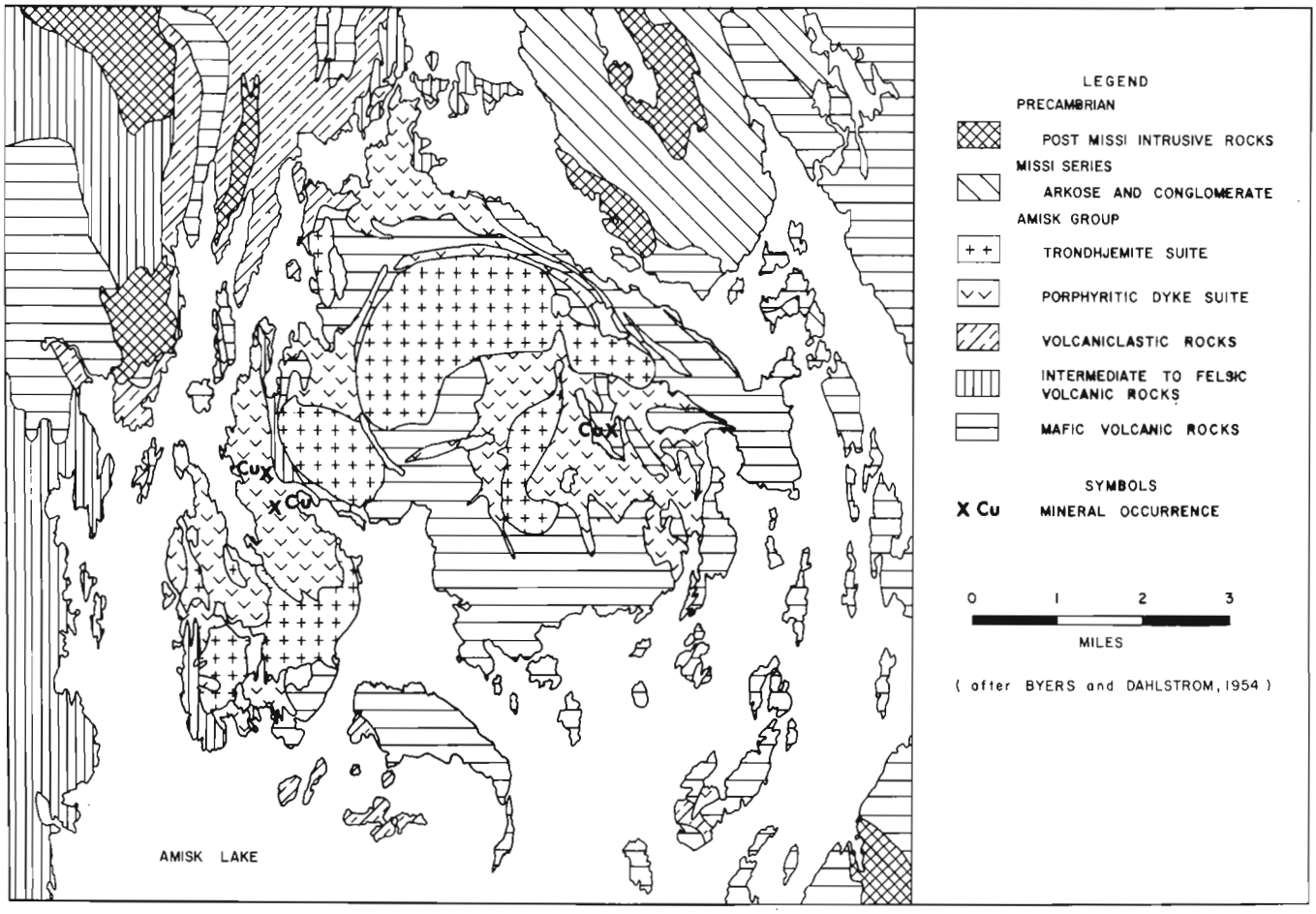

Figure 4.1. Geologic map of Missi Island and vicinity, Amisk Lake, Saskatchewan (modified after Byers and Dahlstrom (1954)).

[1] Department of Earth Sciences, University of Manitoba, Winnipeg, Manitoba R3T 2N2

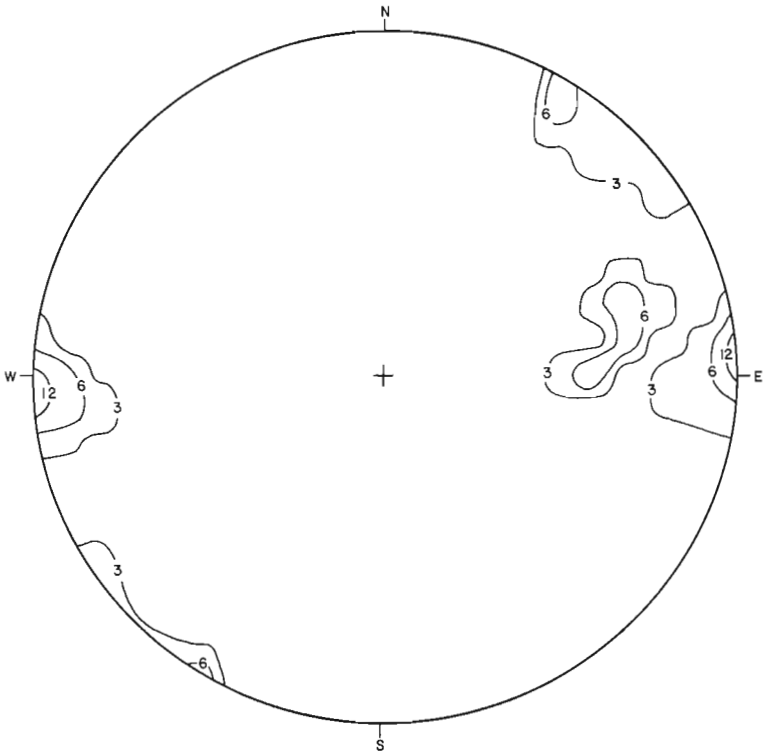

Figure 4.2. Equal-area plot of poles to 70 porphyritic dykes with contours at 3, 6, and 12 per cent.

Preliminary Field Results

The Amisk Group is of Aphebian age and, near Flin Flon, is a thick, complex assemblage of metamorphosed basaltic to rhyolitic flows, pyroclastic rocks, and associated volcaniclastic units. It was apparently erupted from several centres, one of which is thought to be at Missi Island. The Amisk Group has been interpreted as an island arc assemblage (Bailes, 1971).

At Missi Island, which has an area of 75 km^2, metamorphosed mafic flows and minor pyroclastic rocks are intruded by two subvolcanic suites: (1) an older porphyritic dyke suite and (2) younger discrete stocks of altered trondhjemite (Fig. 4.1; Byers and Dahlstrom, 1954). Investigations during the 1976 field season were confined to the west and southwest parts of Missi Island where the porphyritic dyke suite occurs in a transitional zone between steeply dipping, west-facing mafic flows and overlying intermediate to felsic flows and fragmental rocks. This area represents a near-vertical section through part of the vent complex. Metamorphic grade is greenschist facies.

The porphyritic dyke suite varies in composition and texture from coarse grained, equigranular metagabbro to medium and fine grained, quartz-feldspar porphyries of quartz monzonite composition. Groundmass textures are invariably aphanitic to fine grained. Based on phenocryst populations, groundmass textures, composition, and colour, numerous dyke types have been identified. The most common type in the area examined is a mesocratic, fine to medium grained, quartz-feldspar porphyry of quartz diorite composition. Correlation between dyke types in widely separated outcrops is tenuous because of the similarity of many dyke types and the effects of hydrothermal alteration and metamorphism. No consistent areal distribution of dyke types has been recognized within the study area.

The sequence of magmatic evolution shown by intrusive relationships between dyke types is complex and has not been completely deciphered. Intrusive relationships observed in one outcrop are difficult to correlate with intrusive relationships observed in other outcrops because of the problems of dyke correlation. Furthermore, deduced age relationships are conflicting, suggesting that there was more than one episode of emplacement of some dyke types. In individual outcrops where intrusive relationships were observed, the more highly altered dykes are invariably intruded by dykes that have lower degrees of pervasive hydrothermal alteration.

The widths of dykes range from 1 cm to 20 m. No consistent relationship was observed between dyke type, thickness, or areal distribution. Seventy poles to dykes are plotted on an equal area diagram in Figure 4.2, the attitudes indicating that the dykes have a north-northwest preferred orientation with a steep to vertical dip. Dyke attitude is independent of dyke type. The dykes are roughly parallel to the enclosing volcanic strata.

The dyke suite is restricted largely to Missi Island where it underlies 25 per cent of the island. Dykes are concentrated in definite zones or areas up to 500 m wide (Fig. 4.1) within which dykes make up 100 per cent of the rocks. Away from these areas there is a relatively rapid progression across zones several hundred metres wide from 100 per cent dykes to less than 10 per cent dykes. In the western part of the island, the generally concordant nature of both individual dykes and dyke zones, and the lack of country rock septa in the dyke zones show that the porphyritic suite is not a dyke swarm. Instead, each area of dykes appears to represent a locus of dyke or sill emplacement that was gradually expanded by successive pulses of dyke injection. Each of these dyke-rich areas is termed a "sill complex". A similar model is envisaged for porphyry dyke emplacement at Lang Lake, northwestern Ontario (Findlay and Ayres, 1977). In some "sill complexes" the oldest dyke phase is relatively abundant and may represent a larger sill-like pluton subsequently intruded by numerous younger dykes.

No relationship has yet been identified between the type of dyke and the type or degree of alteration and mineralization. Two types of alteration have been recognized: pervasive and veinlets. Pervasive hydrothermal alteration affects both dykes and country rocks and is characterized by textural destruction, silicification, and sericitization. Alteration veinlets of quartz, carbonate, chlorite, epidote, hematite, or pyrite are widespread and do not appear to be related to any specific dyke type or degree of pervasive hydrothermal alteration. Alteration veinlets are commonly cut by younger dykes.

Disseminations and veinlets of pyrite are common in the dykes and the volcanic country rocks and the abundance of pyrite is directly related to the degree of pervasive alteration. Chalcopyrite is restricted in its distribution but three major chalcopyrite-bearing zones have been explored on Missi Island (Fig. 4.1). These zones are all associated with the porphyritic dyke suite, generally at or near contacts with mafic metavolcanic country rocks. Minor molybdenite and arsenopyrite have been observed.

Dykes which are texturally and compositionally similar to the younger discrete stocks of altered trondhjemite were intimately injected into the porphyritic dyke suite adjacent to the stocks. These stocks have not yet been examined.

Conclusions

Several features of the intrusive rocks on Missi Island suggest that the plutons are subvolcanic and may represent an eroded vent complex. These include the general restriction of the two plutonic suites to the immediate vicinity of Missi Island, the porphyritic nature and fine groundmass grain size of the dyke suite, the concentration of dykes in distinct "sill complexes" comprising 100 per cent dykes, thinness of dykes, chilled contacts, general concordant nature of dykes in the western part of the island, absence of pegmatite in the younger trondhjemite plutons, and pervasive hydrothermal alteration within and associated with the plutonic rocks.

Two models for the development of the Missi Island volcanic centre, as exposed on the western side of Missi Island, are currently being considered. In one model, the highly altered, older porphyritic phase in the "sill complexes" represents large concordant, pod-like, epizonal plutons that were intimately intruded by younger porphyritic dykes. In the other model, the older porphyritic phase simply represents the earliest intrusion of thin dykes that were successively intruded by younger porphyritic dykes. Additional data on the distribution of younger porphyritic phases may indicate that small plugs or stocks of these phases are present within the centre. In both models, all of the porphyritic phases are related to the overlying intermediate to felsic volcanic units.

If the porphyritic "sill complexes" are related to overlying volcanic units, the position of the various "sill complexes" within the vent may have been controlled by lithostatic load. Accordingly, progressively younger complexes should be displaced upward (westward) in the vent to compensate for lithostatic load increases due to a growing volcanic edifice. "Sill complexes" in the central and eastern part of the island, should thus represent either older parts of the vent intrusion, or exhibit textural and compositional differences related to simultaneous emplacement at deeper crustal levels. These "sill complexes" and the younger trondhjemite stocks will be investigated in 1977.

References

Ayres, L.D. and Findlay, D.J.
1976: Precambrian porphyry copper and molybdenum deposits in Ontario and Saskatchewan; in Report of Activities, Part B, Geol. Surv. Can., Paper 76-1B, p. 39-41.

Bailes, A.H.
1971: Preliminary compilation of the geology of the Snow Lake – Flin Flon – Sherridon area; Manit. Dep. Mines Natural Resour., Mines Branch Geol., Paper 1-71, 27 p.

Byers, A.R. and Dahlstrom, C.D.A.
1954: Geology and mineral deposits of the Amisk-Wildnest Lakes area; Sask. Dep. Min. Resour., Rep. 14, 177 p.

Findlay, D.J. and Ayres, L.D.
1977: Lang Lake – an Early Precambrian porphyry copper-molybdenum deposit; in Report of Activities, Part B, Geol. Surv. Can., Paper 77-1B, rep. 3.

Kirkham, R.V.
1974: Geology of copper and molybdenum deposits in Canada; in Report of Activities, Part A, Geol. Surv. Can., Paper 74-1A, p. 377-379.

5.

MEASURING SOIL WATER CONTENT IN SITU USING TIME-DOMAIN REFLECTOMETRY TECHNIQUES

Project 750028

J.L. Davies, G.C. Topp[1], and A.P. Annan
Resource Geophysics and Geochemistry Division

Introduction

The need for improved methods of measuring soil water content accurately and over extensive areas is increasing as crop yield optimization and conservation of natural resources become increasingly necessary. At present the common technique for determining soil water content is to remove a soil specimen and measure its weight before and after drying. The neutron probe is an indirect measurement that is slowly gaining acceptance but the method is unsuitable for rapid reconnaissance. Various other indirect methods, contacting and non-contacting, exist but none is totally satisfactory (Barringer, 1973, 1975).

The complex dielectric constant in the frequency band of 1MHz to 1GHz holds promise of being a remotely detectable soil physical property which is primarily dependent on water content (Nikodem, 1966, Hoekstra and Delaney, 1974, Cihlar and Ulaby, 1974, and Davis and Annan, in press). Unfortunately, there is a scarcity of reliable data on the electrical properties of wet soils in this frequency range. This report summarizes recent experimental results obtained using time-domain reflectometry (TDR) techniques. The experiments were carried out

(a) to determine the relationship between the dielectric constant, in the frequency band of 1MHz to 1GHz, and soil water content;

(b) to determine if TDR techniques provide a practical method for measuring soil water content in situ.

Experimental Work

The TDR technique is discussed in general terms by Fellner-Feldegg (1969). Davis and Chudobiak (1975) and Davis and Annan (in press) discuss the technique as applied to the measurement of the electrical properties of wet soils. Briefly, with the TDR technique, the propagation velocity of a fast rise-time step is determined by measuring the time required for the step signal to travel in a known length of transmission line. The electromagnetic wave velocity in this line is the same as that in the material surrounding the line. If the propagation velocity is known then the dielectric constant of the material can be estimated. The magnetic properties of virtually all bulk geological materials do not vary significantly from the magnetic properties in free space. TDR techniques have not revealed any change of the propagation velocity associated with soil type or loss properties (Davis and Annan, in press).

[1]Soil Research Institute, Agriculture Canada

Thus

$$V = \frac{c}{(K_a)^{1/2}} \qquad (1)$$

where V = the propagation velocity in the line
c = velocity of an electromagnetic wave in vacuum, 3×10^8 m/s and
K_a = apparent dielectric constant.

$$K_a = \left(K'^2 + \left(K'' + \frac{\sigma_{dc}}{\omega \varepsilon_o} \right)^2 \right)^{1/2} \qquad (2)$$

where K' = the real dielectric constant,
K'' = the imaginary dielectric constant or the dielectric loss,
σ_{dc} = the zero frequency conductivity,
ω = the angular frequency, $2\pi f$, and
ε_o = the free space permitivity, 8.854×10^{-12} F/m.

If the electric loss is small compared to the real dielectric constant, i.e.

$$\left(K'' + \frac{\sigma_{dc}}{\omega \varepsilon_o} \right) \ll K', \qquad (3)$$

then $K_a \approx K'$.

The apparent dielectric constant can be estimated knowing the travel time, t, and transmission line length, L, from

$$K_a = \left[\frac{ct}{L} \right]^2 \approx K' \qquad (4)$$

A step function with a rise time of 0.1 ns has a continuous energy spectrum from DC to 10^{10} Hz. The frequencies are limited by the transmission line dimensions and any impedance matching transformers in the circuit. In these experiments the maximum frequency range is from 10^6 to 10^9 Hz. The electrical properties of the soil in the line also reduce the frequency range.

Laboratory Measurements

To determine the relationship between the apparent dielectric constant and volumetric soil water content (θ_v) the travel time of the TDR signal in a one metre long coaxial transmission line was measured. The inside diameter of the shield is 5 cm and the volume of soil in the tube is 1844 cm^3. The line is filled with a soil and the water content is varied by pumping a known amount of water through porous ceramic discs along two sides of the line. Standard laboratory burettes are used to measure the amount of water put in or taken out of the soil. The temperature for experiments reported here was kept at +20.3°C. A Tektronix 7S12 TDR unit is used for the

From: Report of Activities, Part B; Geol. Surv. Can., Paper 77-1B (1977)

Table 5.1

Soil Type, Bulk Density and Particle Size Distribution

Soil (Depth)	Bulk Density gm cm^{-3}	%(0.002mm) (clay)	%(0.002-0.05mm) (silt)	%(0.05-2.0mm) (sand)	Textural Class
Rubicon (0-20cm)	1.42	8.9	25.9	65.2	sandy loam
Caldwell (0-20cm)	1.23	31.6	31.3	33.1	clay loam
Caldwell (40-50cm)	1.04	35.7	42.4	21.9	clay loam
Caldwell (90-110cm)	1.14	65.6	31.1	3.3	heavy clay

laboratory measurements. The data are recorded on Polaroid film for preliminary analysis and on analogue magnetic tape for future computer analysis.

Field Measurements

To determine if the TDR method provides a practical technique for measuring soil water content in the field, the velocity of the TDR signal is determined for a parallel wire transmission placed vertically in the soil. The line is constructed of 6 mm diameter rods, 20 cm long, kept separated by a PVC block at one end. The travel time of the TDR signal is measured using a portable cable tester (Tektronix 1502). Soil samples were taken from within the transmission line for gravimetric water content measurements. In this way the apparent dielectric constant and the water content are determined for the same soil.

Results and Discussion

Figure 5.1 shows the results, to date, of the dielectric measurements versus volumetric soil water content made on four different soils whose characteristics are listed in Table 5.1. The soils range in texture from a sandy loam to a heavy clay. In general the spread of data points is comparable to the measurement precision but there is some indication, though small, of differences associated with soil type and/or density.

No experiments have been done to show the relationship between K_a and bulk density for the different soils. From these experiments, which cover a reasonable range of densities, as is shown in Table 5.1, it is expected that K_a is only weakly dependent on density. Water having a dielectric constant of as much as sixteen times that of dry soil is expected to mask the density differences at water contents above 10 per cent. The temperature dependance of the dielectric constant has been found to be of little practical significance for field applications. (Davis, 1975, and Davis and Annan, in press.)

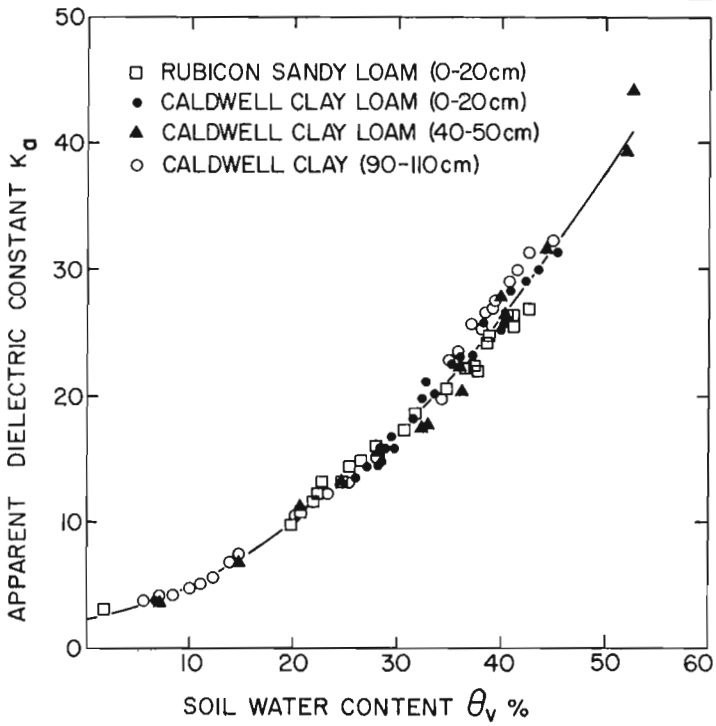

Figure 5.1. Experimental results of K_a versus soil water content for four different soils.

From the data in Figure 5.1 an empirical relationship between apparent dielectric constant and soil water content, θ_v, is found to be

$$K_a = 2.26 + 0.176\theta_v + 0.0106\theta_v^2 \qquad (5)$$

Figure 5.2 shows the above relationship with the area of uncertainty indicated. The scatter of points is not a normal distribution and thus we set the limits of uncertainty by eye to encompass 95 per cent of the data points. The uncertainty in determining θ_v from the dielectric constant will not be reduced by more and better experimental precision of dielectric constant unless other soil variables contributing to the uncertainty are taken into account (Davis and Annan, in press).

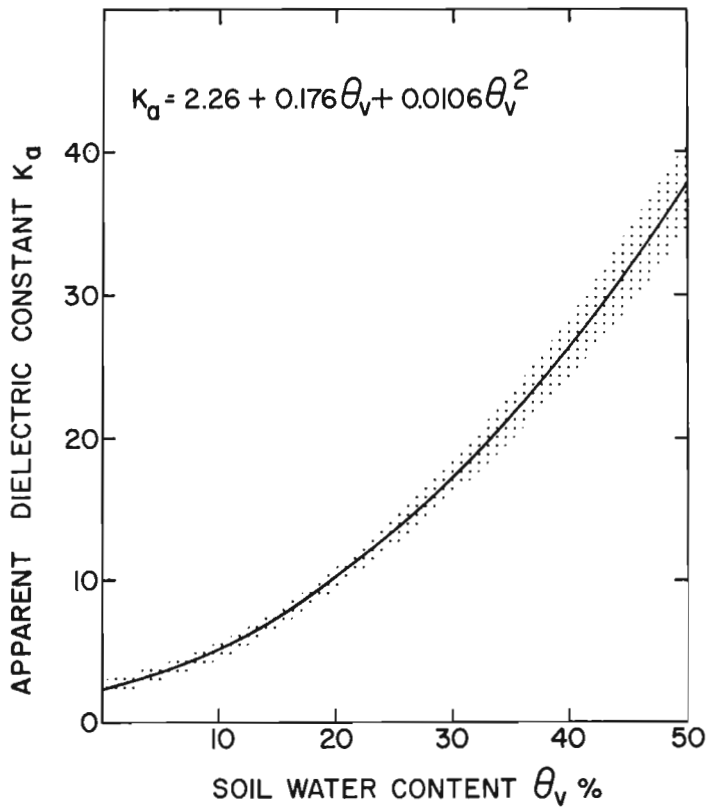

Figure 5.2. Area of uncertainty on the variation of K_a versus soil water content.

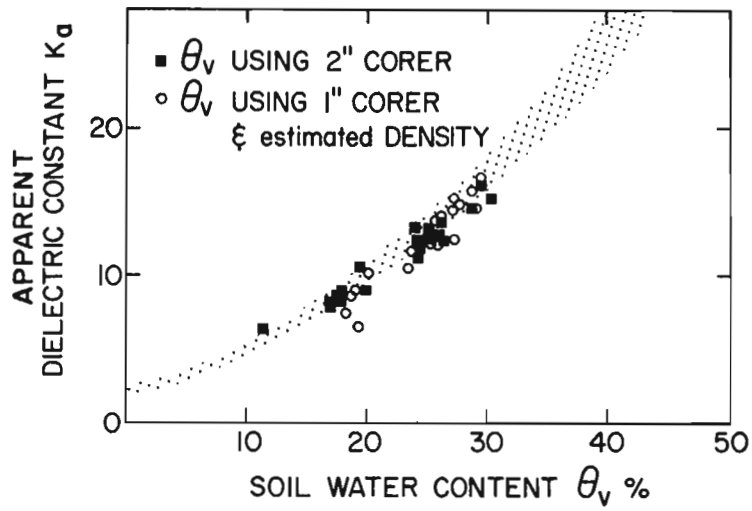

Figure 5.3. Field results of K_a versus soil water content in the surface 20 cm of a Caldwell clay loam. The area of uncertainty of K_a versus θ_v from the laboratory experiments is also shown.

Field Measurements

Figure 5.3 shows the dielectric constant data versus volumetric water content from all measurements obtained in the surface 20 cm during the past summer. The shadowed area is that which is derived from the laboratory experiments. The volumetric water content for data points depicted (■) was derived from gravimetric water content and density measurements for samples taken with a 5 cm diameter corer. For data points indicated by (○), the volumetric water content was inferred from the gravimetric water contents of 2.5 cm diameter sample, combined with bulk densities obtained from independent measurements taken nearby. The dielectric constant measurements were obtained using a 20 cm long parallel-wire transmission line with a wire separation of 5 cm.

A TDR measurement takes about two minutes to obtain plus about another three minutes for interpretation and calculations. A gravimetric measurement takes about 24 hours for drying and further time is necessary for cooling, weighing and calculations.

The slope of the field measurements agrees well with that of laboratory measurements but they are in general at a lower dielectric constant. This decrease of dielectric constant is because of a small air gap formed around the transmission line as it is inserted by hand into the soil (Annan, 1977). The design of the transmission line will be modified to minimize errors which are generated by air gaps.

Conclusions

The results of the work to date indicate the following:

(a) The real dielectric constant, in the frequency band from 10^7 to 10^9 Hz, depends strongly on soil water content and weakly on other soil properties such as soil type, density and temperature.

(b) From qualitative variations observed on the TDR records the dielectric loss appears to vary a great deal with soil type, water content and temperature. The losses increase as 1) the grain size decreases, 2) the water content increases, and 3) the temperature increases. The TDR travel times have not been measurably altered by any of the loss properties of the soils in these experiments; thus the apparent dielectric constant is approximately equal to the real dielectric constant.

(c) From the laboratory measurements on the four soils an empirical relationship $K_a = 2.26 + 0.176\theta_v + 0.0106\theta_v^2$ can be derived. More laboratory measurements and simultaneous dielectric and soil water content field measurements are required to establish the reliability of this relationship.

(d) K_a is a sensitive indicator of soil water content with a precision of better than ±3 per cent overall. Greater precision may result if other soil variables are considered.

(e) The TDR technique provides a practical method of measuring the soil water content in the field. Improved probe design will increase the measurement precision. A microprocessor based system is being built which will allow a direct readout of soil moisture in the field.

The TDR technique is a significant advance for measuring soil water content rapidly. The technique will provide the ground truth necessary for the development of further more rapid, soil-water-content sensors.

References

Annan, A.P.
1977: Time-domain reflectometry-air-gap problem for the parallel wire transmission lines; in Report of Activities, Part B, Geol. Surv. Can., Paper 77-1B, rep. 10.

Barringer, A.R.
1973: Assessment of the use of radio frequencies for the remote sensing of soil moisture. Report prepared for The Canada Centre for Remote Sensing by Barringer Research Ltd., Rexdale, Canada.

1975: Final report on remote sensing of soil moisture. Report prepared for the Canada Centre for Remote Sensing by Barringer Research Ltd., Rexdale, Canada.

Cihlar, J. and Ulaby, F.T.
1974: Dielectric properties of soils as a function of moisture content: RSL Technical Report 177-47, The University of Kansas Centre for Research, Inc., Lawrence, Kansas, 66044.

Davis, J.L.
1975: Relative permittivity measurements of a sand and clay soil in situ; in Report of Activities, Part C, Geol. Surv. Can., Paper 75-1C, p. 361-365.

Davis, J.L. and Annan, A.P.
1977: Electromagnetic detection of soil moisture: Progress Report 1; Submitted to Can. J. of Remote Sensing. (in press)

Davis, J.L. and Chudobiak, W.J.
1975: In situ meter for measuring relative permittivity of soils; in Report of Activities, Part A, Geol. Surv. Can., Paper 75-1A, p. 75-79.

Hoekstra, P. and Delaney, A.
1974: Dielectric properties of soils at UHF and microwave frequencies; J. Geophys. Res., v. 79, p. 1699-1708.

Fellner-Feldegg, H.
1969: The measurement of dielectrics in the time domain; J. Phys. Chem., v. 73, no. 3, p. 616-623.

Nikodem, H.J.
1966: Effects of soil layering on the use of VHF radio waves for remote terrain analysis; Proceedings of the 4th Symposium on Remote Sensing of Environment, University of Michigan, Ann Arbor, Mich., p. 691-703.

6. GEOCHEMICAL DISTRIBUTION OF URANIUM, TUNGSTEN, AND MOLYBDENUM IN THE TOMBSTONE MOUNTAINS BATHOLITH, YUKON

Project 750051: Uranium Reconnaissance Program

W.D. Goodfellow and I.R. Jonasson
Resource Geophysics and Geochemistry Division

Introduction

The exploration for uranium has been a recent development for the Yukon Territory. Initially, stream sediment sampling was carried out by exploration and mining companies in areas underlain by Proterozoic (Helikian ?) sedimentary and volcanic rocks where several uranium occurrences are associated with intrusive and extrusive breccias. Recently, however, increasing emphasis has been placed on alkaline multi-phase intrusive rocks as not only a source but a host for the 'porphyry uranium' (Armstrong, 1974) type of deposit. Uranium deposits of this type occurring elsewhere in the world include the Bokan Mountain deposits of Alaska (Mackevett,1963), the Rossing deposit of South West Africa (Berning et al., 1976) and the Crocker Well deposit of South Australia (Campana and King, 1958).

During the summer of 1976, 28 490 km^2 of the central Yukon were surveyed at a density of one sample in five square miles in an effort to evaluate the uranium potential of a range of geologically favourable environments (Goodfellow et al., 1976). Detailed studies of selected areas were carried out in conjunction with the reconnaissance survey with the objective of providing additional information on the various chemical and mechanical processes affecting the supply, transport and deposition of elements in the stream system. Samples of stream sediments and water were collected at a density of four samples per line of stream. Rock samples representing the different lithologies were also collected.

One area investigated in greater detail is the Tombstone Mountain area (Detail Area No. 7, Jonasson and Goodfellow, 1976) of the west central Yukon (Fig. 6.1) which is underlain by Cretaceous alkaline plutons that intrude older sedimentary rocks. This area is of particular interest in light of the occurrence of uranium in veins intersecting the pseudoleucite tinguaite phase of the Tombstone batholith.

Geology and Petrography

The Tombstone Mountains are characterized by jagged spires, some of which are bounded by fault-controlled vertical sides, which are intersected by deeply incised streams. Below approximately 1500 m, the stream valleys are filled primarily with glacial and alluvial material, much of which is indigenous.

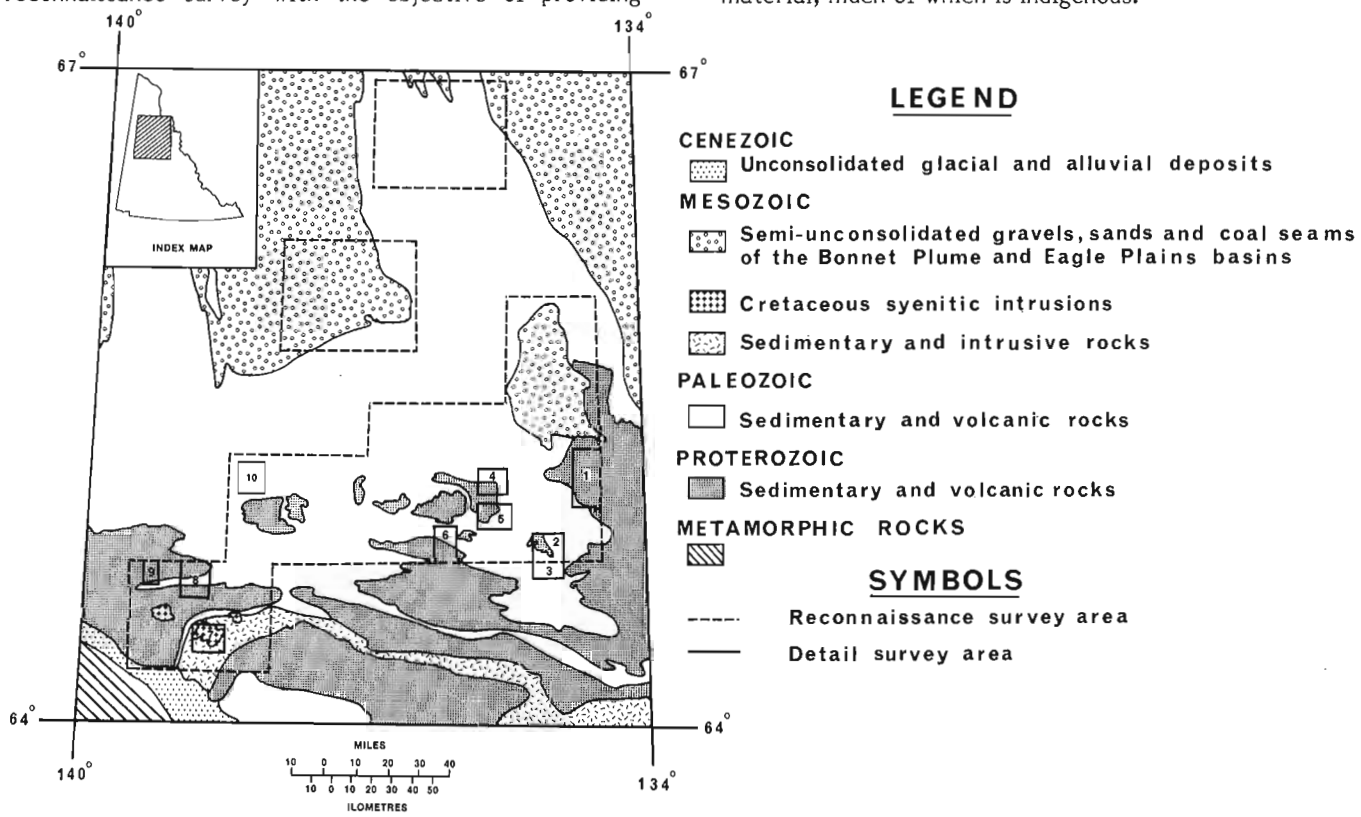

Figure 6.1. General geology of the central Yukon with the outline of the reconnaissance and detailed survey areas (the Tombstone batholith is located in detail area No. 7).

From: Report of Activities, Part B;
Geol. Surv. Can., Paper 77-1B (1977)

The geology of the Tombstone Mountains of the west-central Yukon Territory has been mapped most recently by Green (1972) and by Tempelman-Kluit (1970). The area that was surveyed geochemically (Fig. 6.2) is underlain by an alkaline batholith of Cretaceous age which intrudes Cretaceous Keno Hill Quartzite, diorite and gabbro, and Jurassic sedimentary rocks. The petrography of the Tombstone batholith was examined most recently by Tempelman-Kluit (1968) and the following descriptions are taken from that account. The core of the batholith is composed of alkali syenite which is enclosed by monzonite, quartz monzonite and diorite towards the margins. The syenite which makes up the bulk of the intrusion is composed of phenocrysts of orthoclase set in a medium grained allotriomorphic groundmass of microperthitic orthoclase, andesine, aegerine-augite, amphibole, biotite and minor quartz. The accessory minerals are sphene, zircon, apatite and opaques.

Pseudoleucite tinguaite occurs in two areas within the Tombstone batholith. In the first area, pseudoleucite tinguaite is located along the southern margin of the batholith where it occurs in sharp contact with monzonite and Keno Hill Quartzite. The second area is located near the centre of the batholith where pseudoleucite tinguaite is in gradational contact with the enclosing syenite.

Pseudoleucite tinguaite is composed of phenocrysts of pseudoleucite, an intergrowth of potash feldspar and nepheline, set in a groundmass of potash feldspar, nepheline, biotite, fluorite and minor cancrinite. The pseudoleucite phenocrysts show excellent trapezohedral crystal form and contain cancrinite, calcite, plagioclase, biotite and melanite in addition to orthoclase and nepheline. Narrow veins of fluorite and galena cut the rock locally and many pseudoleucite crystals are altered in part to clay minerals and sericite.

Geochemistry

The analytical results for stream sediment and water are presented in Table 6.1. Stream sediments were sieved to minus 80-mesh and analyzed by Chemex Laboratories for Au, Pb, Zn, Co, Ni, Ag, Mn, Fe, Ba, Mo (AAS) and W (colorimetry). Stream waters were collected unfiltered and analyzed by Barringer Research Laboratories, Whitehorse, for U (fluorimetric), F (specific ion electrode) and pH. The water samples were then shipped acidified to the Geological Survey laboratories where they were subsequently analyzed for Au and Pb (flameless AAS).

Most of the sediment in streams draining the Tombstone batholith has been derived by the mechanical breakdown of rock-forming minerals which have been transported as particulates during the heavy spring run-off. Stream sediments range in size from fine silt to boulders, with only minor organic matter present. The low Mn concentrations in stream sediments (Table 6.1), which are in general comparable in Mn levels in the underlying rock (Table 6.2), demonstrate the absence of

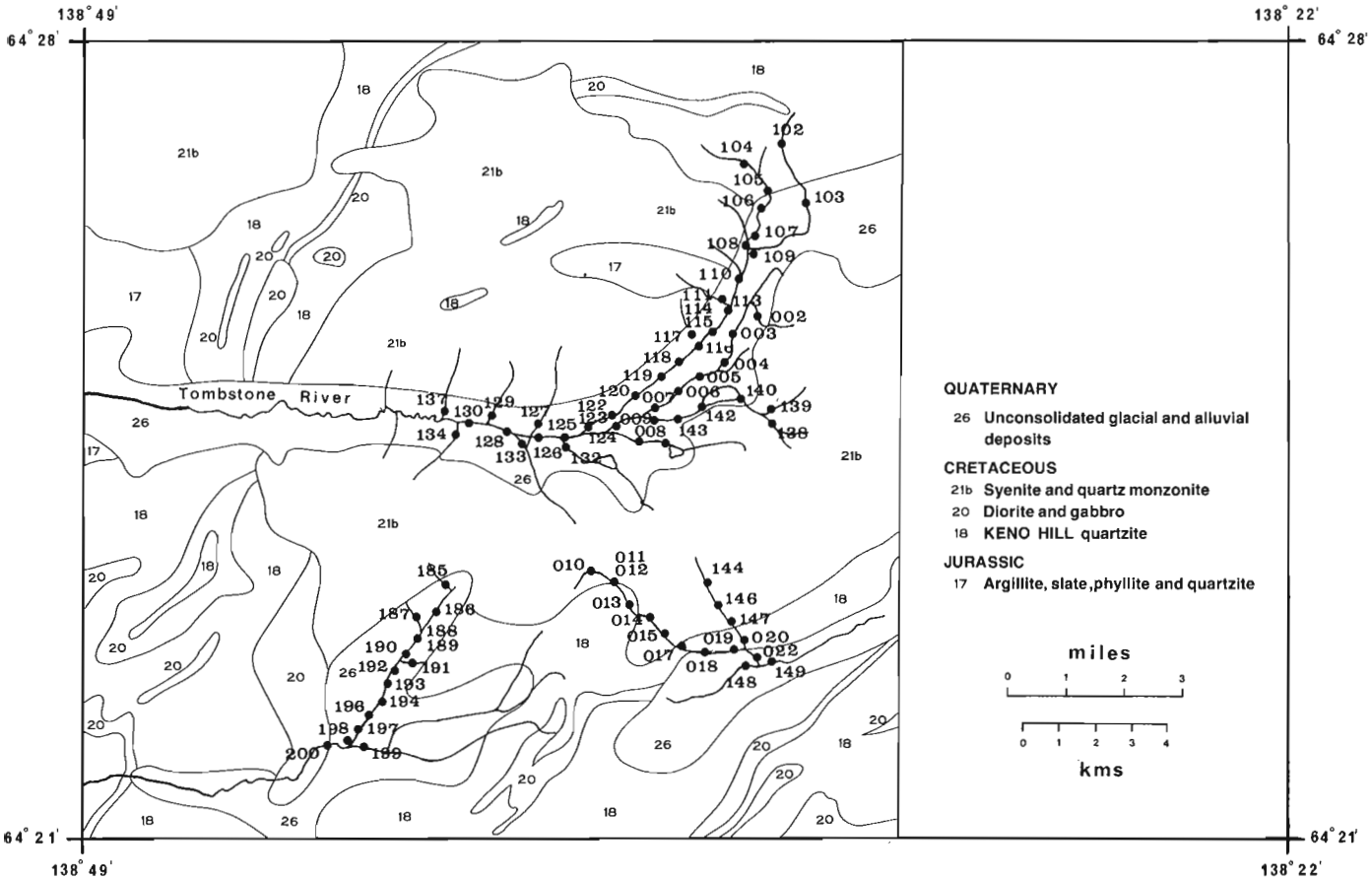

Figure 6.2. Sample number (116B763 series) locations for stream sediments and waters (geology after Green, 1972).

Table 6.1

Chemical Analyses of Stream Sediments and Waters from the Tombstone Mountains

	STREAM SEDIMENT												STREAM WATER				
SAMPLE NO	Zn	Cu	Pb	Ni	Co	Ag	Mn	Fe	Ba	Mo	W	U	U	F	Cu	Pb	pH
116B 763002	103	55	31	15	8	0.1	325	1.90	1130	10	20	48.1	0.08	290	4.2	0.8	7.4
03	94	37	31	11	4	0.0	220	1.90	1230	9	20	60.1	0.22	300	1.2	0.8	7.3
04	91	35	26	21	8	0.1	380	2.25	1200	10	8	28.3	0.08	300	1.1	0.8	7.3
05	63	21	21	12	5	0.1	280	1.90	1160	13	45	31.8	0.08	380	0.7	<0.5	7.4
06	63	20	20	12	5	0.1	140	1.55	1140	9	20	26.5	0.04	400	2.2	2.5	7.3
07	88	26	26	16	7	0.1	425	2.15	1230	11	15	41.5	0.10	410	1.4	1.6	7.3
08	65	19	28	8	5	0.1	255	1.90	1150	8	100	157.5	0.14	340	1.6	1.7	7.2
09	105	25	29	14	6	0.1	560	2.15	1170	14	50	133.0	0.12	400	0.8	0.7	7.3
10	270	57	200	14	8	0.1	450	2.30	830	3	15	29.0	0.12	310	0.8	1.0	7.3
11	220	70	136	26	15	0.1	755	3.30	1060	14	15	99.6	0.60	370	3.5	3.3	7.1
12	225	71	124	24	15	0.1	475	3.30	1080	11	20	115.4	0.06	390	1.7	1.2	7.2
13	182	70	172	39	25	0.1	500	4.90	700	47	20	14.9	0.04	210	0.8	0.7	7.1
14	166	34	110	18	11	0.2	680	2.50	800	9	8	55.5	0.06	400	<0.5	<0.5	7.3
15	164	33	103	20	11	0.2	640	2.40	880	7	5	74.4	0.10	450	1.2	<0.5	7.4
17	120	90	74	11	5	0.1	495	1.75	920	2	10	44.8	0.12	490	<0.5	<0.5	7.3
18	98	17	62	9	5	0.1	510	1.70	860	2	2	54.7	0.10	550	<0.5	0.5	7.5
19	106	25	68	11	6	0.1	465	1.70	800	2	2	51.4	0.12	570	<0.5	<0.5	7.4
20	130	31	74	14	8	0.1	570	2.10	960	1	2	66.3	0.08	500	<0.5	0.7	7.1
22	91	22	50	11	5	0.1	385	1.60	880	1	2	50.8	0.06	560	1.5	<0.5	7.4
116B 763102	104	200	21	42	22	0.1	310	5.10	870	8	6	12.0	0.02	26	1.6	<0.5	6.5
103	74	92	16	34	26	0.1	520	2.80	1270	4	2	11.6	0.02	24	0.6	<0.5	6.2
104	149	275	60	59	35	0.2	270	4.30	820	7	2	33.2	0.04	30	2.5	<0.5	6.6
105	178	390	62	83	136	0.6	3000	5.85	700	27	6	71.6	0.02	36	1.7	<0.5	6.8
106	54	30	17	16	12	0.1	250	2.05	770	5	2	11.2	0.18	42	1.0	<0.5	6.9
107	104	82	32	32	12	0.1	495	2.75	980	3	6	17.3	0.02	48	1.0	<0.5	6.9
108	102	75	36	23	20	0.1	720	2.65	970	4	6	29.7	0.08	68	1.3	<0.5	7.0
109	72	67	26	29	15	0.1	245	2.10	970	4	20	23.1	0.02	66	0.8	<0.5	7.0
110	95	37	25	18	10	0.1	350	2.05	1350	4	15	21.1	0.04	92	1.0	<0.5	7.0
111	150	116	35	30	17	0.1	440	3.50	1280	8	6	22.8	0.02	132	2.7	<0.5	7.0
113	110	73	25	19	18	0.1	540	2.35	1480	4	10	19.4	0.74	100	1.3	<0.5	6.8
114	106	44	21	20	17	0.1	525	2.10	1480	4	20	25.9	0.04	142	1.9	<0.5	7.1
115	98	41	19	19	14	0.1	425	2.10	1360	3	10	26.9	0.04	144	1.9	<0.5	7.1
116	80	37	17	16	11	0.1	340	1.70	1380	2	6	20.6	0.04	144	1.1	<0.5	7.1
117	135	86	29	20	16	0.1	515	2.70	1440	11	6	45.6	0.04	300	1.0	<0.5	7.1
118	86	38	18	17	12	0.1	375	1.90	1390	2	6	24.8	0.02	172	0.7	<0.5	7.1
119	89	40	19	18	12	0.1	345	1.90	1480	4	2	22.4	0.02	156	2.7	<0.5	7.1
120	55	27	16	12	7	0.1	270	1.40	1370	1	2	13.2	0.02	184	1.6	<0.5	7.2
122	61	26	16	13	9	0.1	285	1.40	1480	2	6	19.1	0.02	210	1.5	<0.5	7.3
123	57	25	14	12	7	0.1	275	1.40	1360	2	20	19.5	0.04	210	1.1	<0.5	7.2
124	60	27	15	13	8	0.1	280	1.35	1530	2	6	16.5	0.02	220	2.2	<0.5	7.2
125	67	28	17	14	10	0.1	330	1.50	1500	2	6	20.8	0.09	360	1.4	<0.5	7.3
126	66	28	16	13	9	0.1	305	1.50	1440	2	2	19.1	0.10	370	4.5	4.0	7.3
127	77	38	21	13	6	0.1	295	2.10	1130	3	6	20.8	0.02	152	1.0	<0.5	7.0
128	74	29	17	14	9	0.1	365	1.60	1500	2	10	0.6	0.08	360	0.8	<0.5	7.2
129	90	32	20	16	9	0.1	420	2.00	1070	2	2	24.9	0.04	240	0.8	<0.5	7.2
130	58	24	17	11	7	0.1	300	1.50	1380	3	15	29.5	0.06	360	1.5	<0.5	7.2
131	112	43	70	13	14	0.1	1520	2.60	970	87	60	578.5	0.46	300	2.1	2.5	6.9
132	97	25	18	13	7	0.1	495	2.25	1130	12	30	76.7	0.06	350	1.0	<0.5	7.0
133	76	24	31	7	6	0.1	660	1.80	1480	5	6	48.3	0.20	280	1.0	0.7	7.1
134	47	11	15	6	5	0.1	350	1.35	1500	4	10	27.5	0.40	410	1.0	0.9	7.3
135	90	27	21	22	11	0.1	950	2.70	1000	60	200	90.4	0.64	310	0.5	<0.5	6.7
137	71	23	36	11	7	0.1	300	2.40	1100	5	2	23.0	0.02	168	0.5	<0.5	6.9
138	48	8	32	2	2	0.1	275	1.10	1500	1	8	61.8	1.00	176	0.8	0.6	7.0
139													0.92	280	1.1	0.8	7.1
140	79	21	28	8	5	0.1	225	1.60	1070	12	50	223.1	0.56	330	0.7	<0.5	7.2
142													0.24	300	0.9	<0.5	7.0
143	87	24	31	10	5	0.1	255	1.75	1040	15	75	218.4	0.26	330	0.7	<0.5	7.0
144													0.04	400	1.0	0.9	6.6
146													0.20	440	0.5	<0.5	7.0
147	160	36	80	28	10	0.1	660	2.70		1	2	51.6	0.10	460	0.5	<0.5	6.7
148	79	31	36	19	7	0.1	400	1.80	1140	1	2	6.2	0.02	72	0.8	<0.5	7.6
149													0.06	500	1.1	0.8	7.4
185	175	53	145	14	10	0.1	755	2.60	880	4	2	15.6	0.02	220	0.9	1.3	7.3
186	115	29	83	11	6	0.1	380	2.30	1080	2	5	14.5	0.02	220	3.2	3.5	7.2
187	180	32	109	11	7	0.1	665	2.25	1040	2	60	23.0	0.02	84	1.1	1.4	7.4
188	220	40	144	10	12	0.1	940	3.60		1	2	20.6	0.02	260	1.5	<0.5	7.3
189	180	41	114	13	10	0.6	795	2.60	940	3	2	28.7	0.02		1.0	3.8	
190	200	37	148	11	10	0.2	800	2.90	1010	2	2	31.4	0.02	280	1.0	12.0	7.3
191	140	18	138	14	9	0.4	500	1.65	780	1	2	11.0	0.10	126	1.0	1.0	7.8
192	155	30	107	12	9	0.2	585	2.20	1000	2	2	28.2	0.02	240	2.2	2.4	7.4
193	285	41	630	11	8	1.8	855	2.75	1000	2	2	21.8	0.02	240	2.2	2.1	7.5
194	325	49	1040	11	9	1.8	1020	2.95	990	4	10	20.1	0.02	240	1.0	1.4	7.5
196	215	38	495	9	7	1.8	695	2.55	1090	1	2	23.3	0.02	230	2.0	16.0	7.5
197	180	38	350	12	8	1.4	555	2.50	1050	2	2	17.5	0.02	240	2.6	13.0	7.5
198	210	45	430	17	10	1.6	660	2.55	960	2	2	18.2	0.02	240	1.5	1.0	7.4
199	88	24	23	21	8	0.1	310	1.95	1040	1	2	3.6	0.02	60	2.1	7.0	7.9
116 763200													0.02	56	3.0	16.0	7.6

Stream Sediment: Fe in %, other elements in ppm Stream Water: All elements in ppb

Table 6.2

Chemical analyses of rocks from the Tombstone Mountains

Sample No.	Cu	Pb	Zn	Co	Ni	Mn	Fe	U^1	U^2	Ag	W	Mo	Ba	Rock Type
116B765002	9	40	16	2	2	133	0.88	9.4	16.4	0.2	2	7.9	540	Monzonite
03	2	40	68	2	2	77	0.66	13.6	22.2	0.2	2	3.8	330	"
04	3	17	36	2	2	319	2.42	34.0	60.0	0.2	2	2.5	210	"
05	4	32	47	5	2	365	1.32	3.6	5.1	0.2	4	2.5	1880	Syenite
06	4	17	16	2	2	139	0.70	2.4	3.0	0.2	4	3.8	1860	"
07	5	48	68	7	2	460	2.75	5.2	10.0	0.2	4	7.2	1840	"
08	4	64	54	2	2	494	2.00	20.0	31.3	0.2	4	11.6	470	Monzonite
09	3	80	88	5	2	674	2.27	16.8	26.1	0.2	2	3.8	1560	Syenite
10	4	48	91	2	2	572	2.00	14.4	24.7	0.2	2	4.4	230	Pseudoleucite tinguaite

Notes: all elements in ppm except Fe which is in %

[1] uranium determined fluorimetrically

[2] uranium determined by delayed neutron activation

inorganic matter as a scavenger of trace and minor elements. The mechanical derivation of most sediments is attested to by the overall similarity in major element chemistry between the stream sediments and rocks from the Tombstone batholith. Because of the large difference in Ba between the syenite and monzonite of the Tombstone batholith (Table 6.2), the distribution of Ba in stream sediments is particularly effective in differentiating the syenitic core from the monzonitic margins of the batholith.

The high Cu and Ni in the minus 80-mesh fraction of stream sediment compared to their concentrations in the underlying rocks undoubtedly results from their hydromorphic dispersion and sorption onto the surfaces of fine particulate material. The Cu concentration of stream water certainly supports this interpretation.

The high Zn, Ni and to a lesser extent, Cu and Pb in sediments (763102-763117) from streams draining the northeastern contact of the batholith reflect the Jurassic shales which have been mapped in this area. The low pH of streams draining these pyritic shales is important in the dissolution of metals from the underlying Jurassic shales.

The distribution of U in stream sediments (Fig. 6.3) outlines two areas of high U potential within the Tombstone batholith. The first area has U concentrations ranging up to 115 ppm (Table 6.1) in sediments from streams draining the southern contact of the batholith where U mineralization in the form of pitchblende occurs in veins intersecting pseudoleucite tinguaite. The second area contains U concentrations ranging up to 576 ppm in sediments from three tributaries of the Tombstone River which intersect the centre of the batholith where syenite has been mapped. At their confluences with the Tombstone River, the U content of stream sediments decreases rapidly to background levels, presumably due to an overwhelming dilution effect.

The concentrations of U in stream sediments most likely resulted from a combination of mechanical and chemical processes. From Table 6.2 it is clear that approximately 50 per cent of the U is present in the rock in a readily leachable form, possibly associated with fluorite and apatite, or occurring as pitchblende; the remainder is tied up in minerals such as zircon and sphene which are relatively resistant to decomposition. Consequently, it is not surprising that the U anomalies in the coarse fraction (-20 + 80 mesh) of stream sediments are coincident with U anomalies in the fine fraction (-80 mesh).

The distribution of U in stream water (Fig. 6.4) is very similar to the U pattern in stream sediments. In general, two areas are outlined within the Tombstone batholith that have U concentrations ranging up to 1 ppb. The high concentrations of U and F (Fig. 6.5) further suggest that a portion of the U may be associated with fluorite or apatite, both of which are accessory minerals in the pseudoleucite tinguaite (Tempelman-Kluit, 1968). The high F associated with U in tributaries of the Tombstone River draining from the centre of the batholith suggests that this area should be investigated for additional occurrences of tinguaite which is considered to be the host for U along the southern contact.

The presence of galena veinlets intersecting the pseudoleucite tinguaite (Tempelman-Kluit, 1968) undoubtedly explains the association of high Pb (Fig. 6.5) with U and F in streams draining the southern contact. The presence of galena and sphalerite in this area is indicated further by the high Pb (200 ppm) and Zn (270 ppm) in stream sediments. The abnormally high Pb (16 ppb) in waters and Ag, Pb and Zn in sediments from streams draining the southwestern contact reflect the presence of Ag-Pb-Zn (Spotted Fawn Property) mineralization known to occur in veins intersecting the Keno Hill Quartzite (Cockfield, 1919). The concentration of Pb in stream waters is well within the solubility limits of $PbCO_3$ for the neutral to slightly alkaline pH conditions of streams draining the Tombstone batholith.

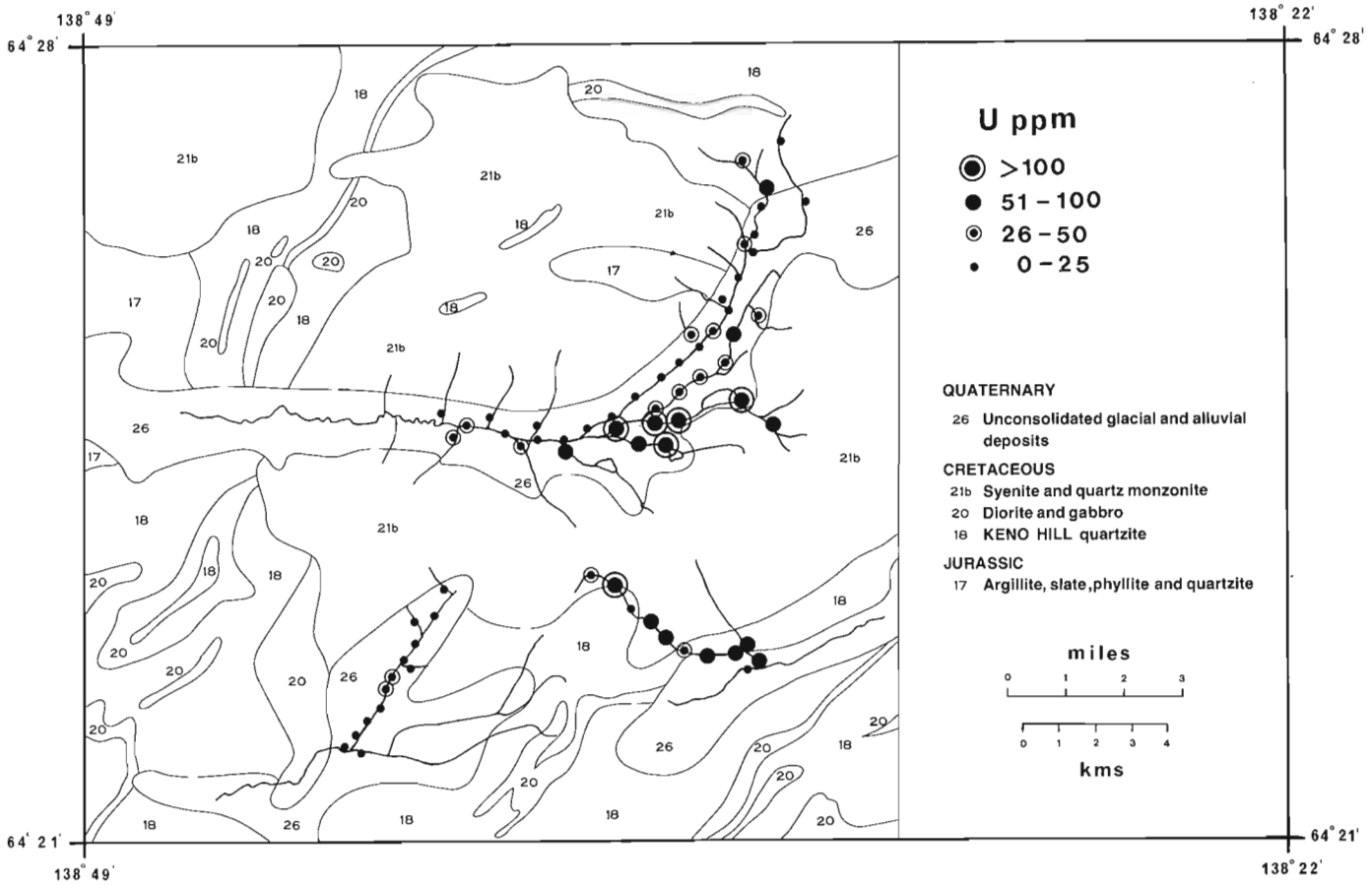

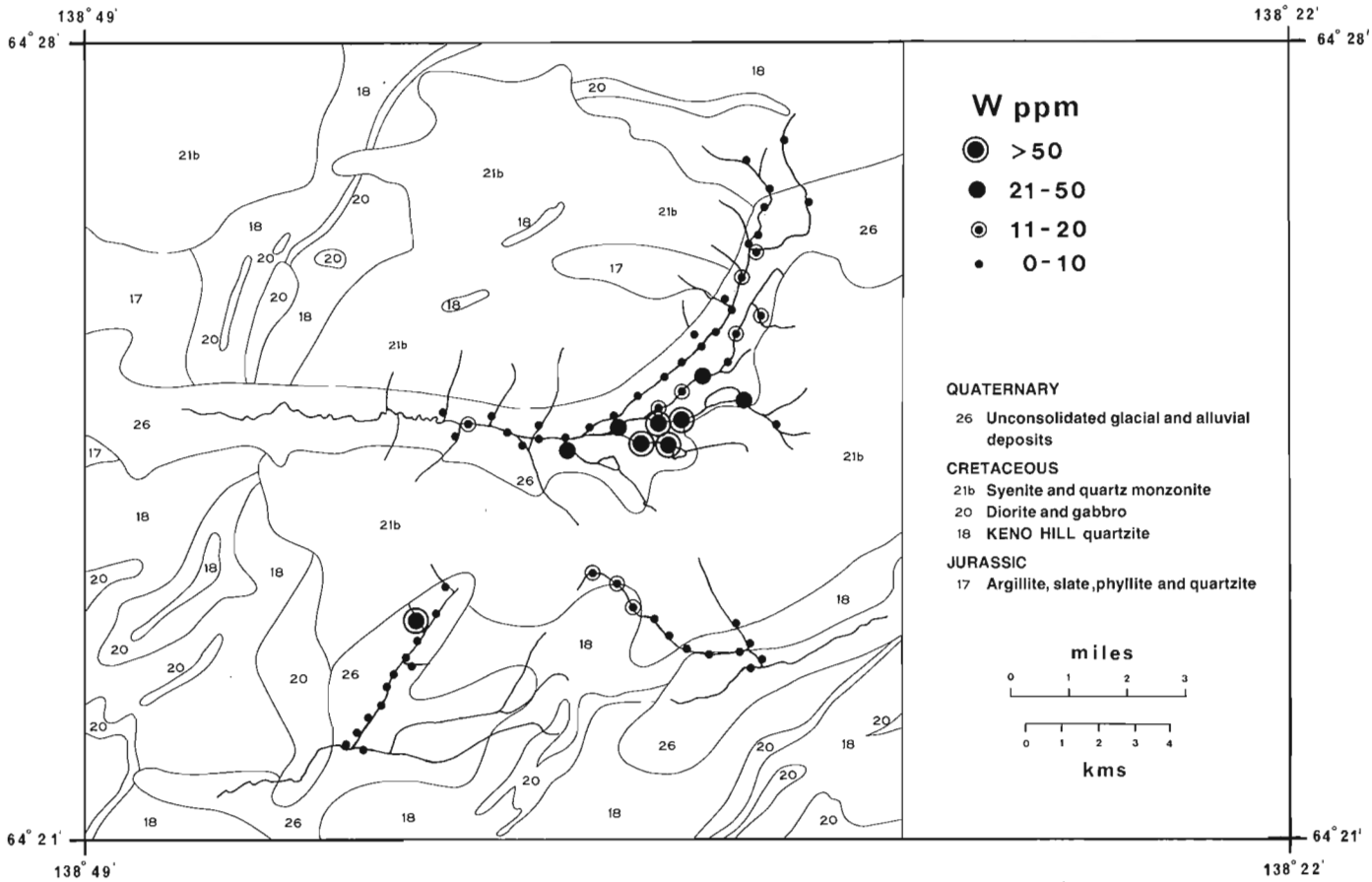

Figure 6.3. Distribution of U and W in sediments (minus 80-mesh fraction) from streams draining the Tombstone batholith.

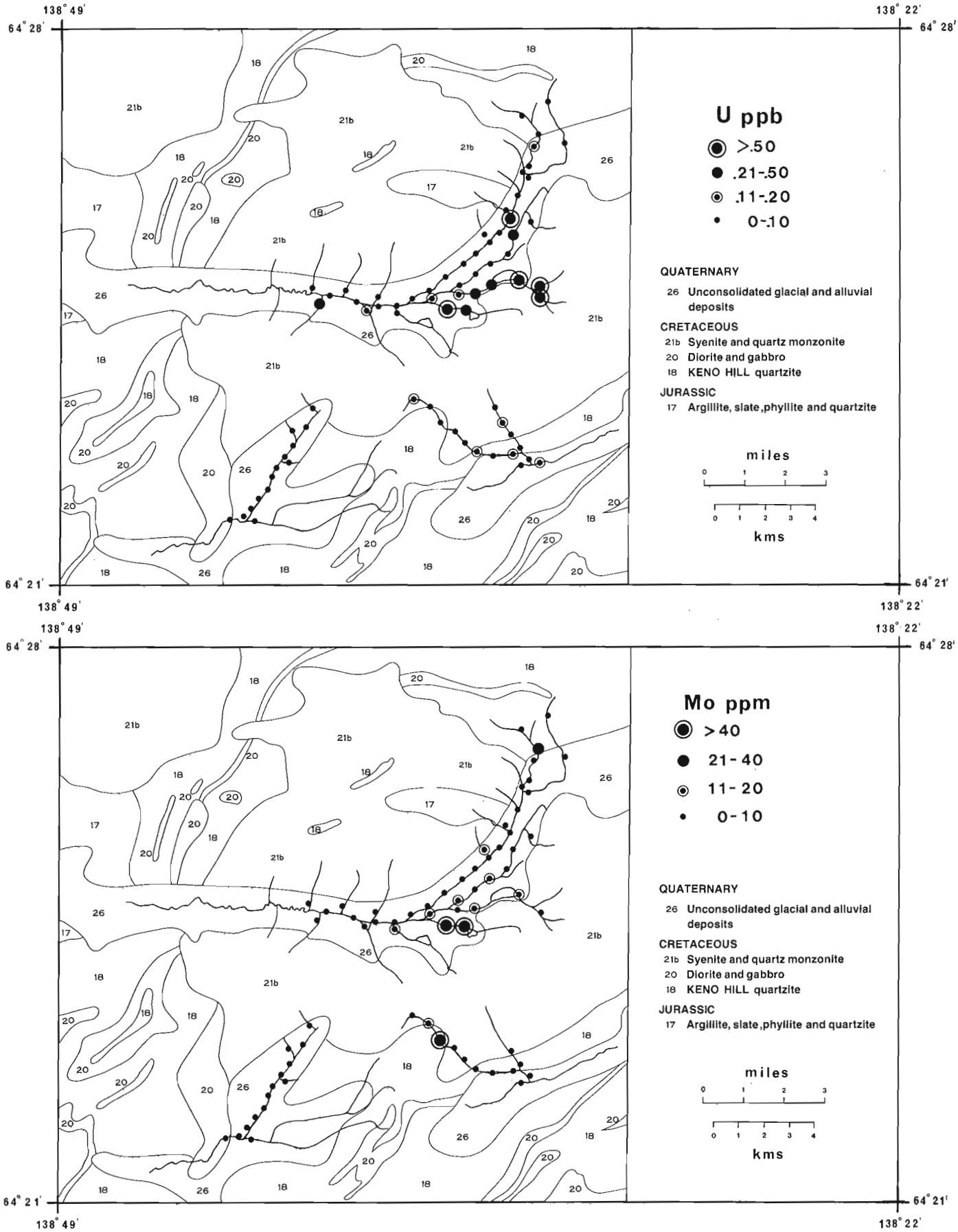

Figure 6.4. Distribution of U in waters and Mo in sediments (minus 80-mesh fraction) from streams draining the Tombstone batholith.

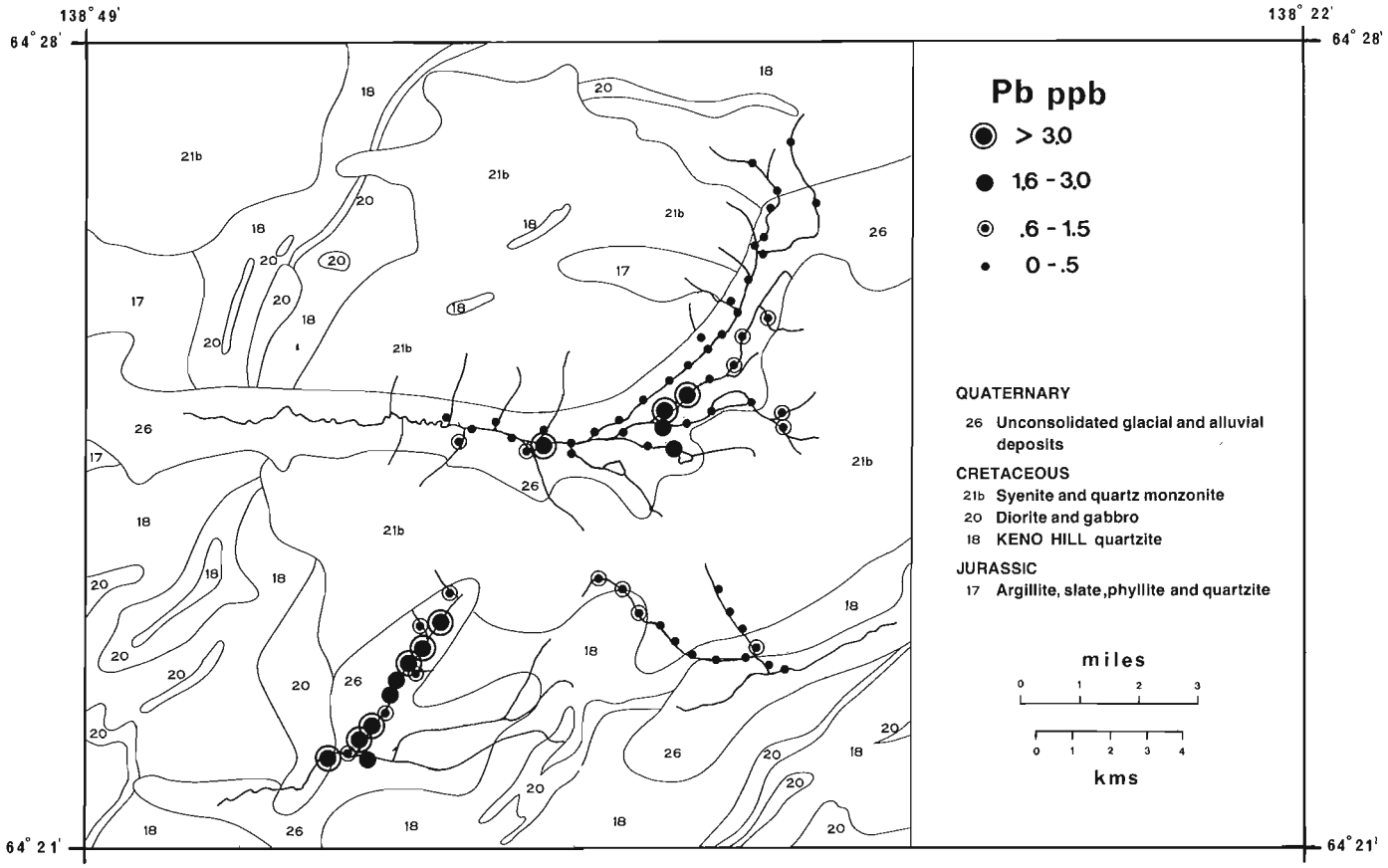

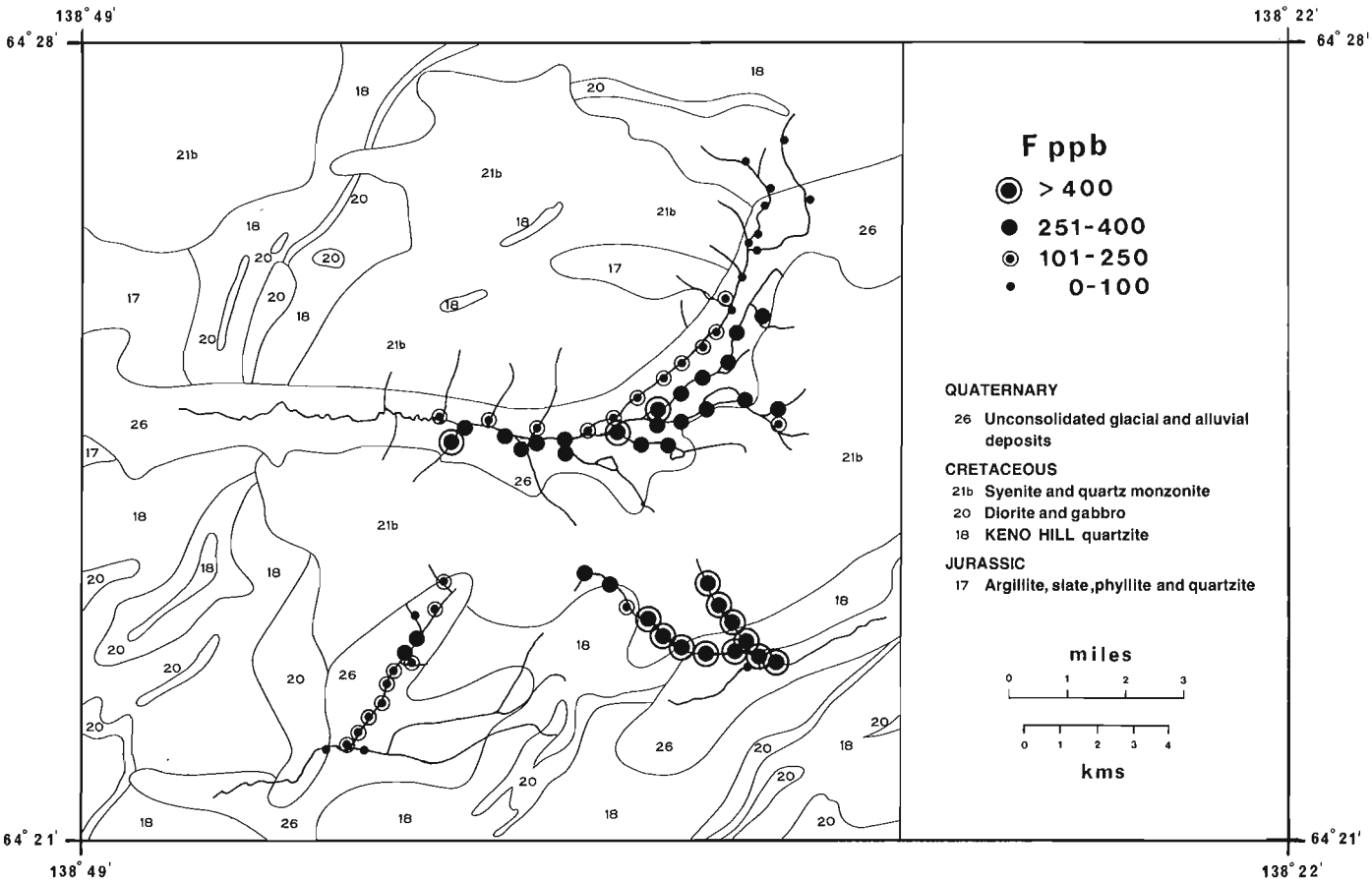

Figure 6.5. Distribution of Pb and F in waters from streams draining the Tombstone batholith.

The high Pb in stream waters from tributaries of the Tombstone River draining the central sections of the batholith is spatially associated with the U anomaly in this area. However, the stream sediments, unlike those draining the southern contact, contain background levels of Pb, Zn and Ag suggesting that the mineral associations in these sections of the batholith are different.

For all streams intersecting the Tombstone batholith, there is close spatial association of high W (Fig. 6.3), Mo (Fig. 6.4) and U in the stream sediments. Certainly, a U – Mo association is not unusual but W is less commonly associated with U in similar geological environments described elsewhere (Mackevett, 1963; Semenov, 1974). By examining their distribution in the underlying rocks (Table 6.2), it is apparent that although the U – Mo association is present, there is no clear association of W with U. One possible explanation for what appears to be contradictory evidence of the W – U association in stream sediments and rocks is that W is not directly associated with the U mineralization but spatially zoned about it. One possible mode of occurrence would be in scheelite veins similar to W showings present in acid plutons from the Keno Hill area.

Discussion

The Tombstone batholith represents a multiphase intrusion which is zoned from syenite at the core to pseudoleucite tinguaite at the southern contact where it intrudes monzonite and quartzite (Tempelman-Kluit, 1968). The tinguaite, which may represent the end product of an oversaturated differentiation series, contains abnormally high concentrations of U, likely associated with fluorite. Under processes of fractional crystallization in a closed system, U would be retained in a halogen-rich and carbonate residual magma as a complex ion (Bohse et al., 1974).

Uranium deposits associated with differentiated plutonic rocks would be expected to occur where the residual halogen-rich magma concentrated at the apical area of the magma chamber, or was intruded into the enclosing rocks. Sørenson et al. (1974) have demonstrated that the Kavenfjeld U deposit of South Greenland formed by the partitioning of U into a halogen-rich residual magma which later solidified. Other U deposits which are considered to have formed under similar processes include the Rössing of South Africa (Backström, 1970) and the Ross Adams of Alaska (Mackevett, 1963), both of which contain U associated with fluorite veins which intersect a highly differentiated igneous complex.

In terms of exploration, the principal criterion of a "uranium porphyry" type of deposit would be a highly differentiated complex that formed under a closed system, thus retaining the volatiles. Miarolitic granitic rocks indicate that at least some of the volatiles escaped, perhaps due to a decrease in pressure, sometime during the crystallization process. Consequently, the U would be expected to be dispersed into cavities throughout the rock and would therefore be unlikely to form U concentrations, at least initially. Massive plutonic rocks, however, indicate that the volatiles were retained and the U may be expected to be concentrated in the residual magma.

This interpretation of the origin of U in the Tombstone batholith is supported by the geochemistry of stream sediments and waters, and rocks. The association of U with F is supported by the presence of fluorite veins which intersect pseudoleucite tinguaite along the southern contact where U in the form of veins occurs. This area of U mineralization is outlined by high U, Mo, W, Pb and Zn in stream sediments and U, F and Pb in stream waters. A second area near the centre of the batholith is also outlined by similar element associations in tributaries of the Tombstone River where no tinguaite has yet been mapped. However, in light of the geochemical response, it must be considered an area of high U and W potential.

References

Armstrong, F.C.
1974: Uranium resource of the future-'porphyry' uranium deposits; Proc. Symp. Form. Uran. Ore Dep., Int. Atomic Energy Agency, Vienna, p. 625-634.

Berning, J., Cook, R., Hiemstra, S.A., and Hoffman, U.
1976: The Rössing uranium deposit, South West Africa; Econ. Geol., v. 71, p. 351-368.

Bohse, H., Rose-Hansen, J., Sørensen, H., Steenfelt, A., Løvborg, L., and Kunzendorf, H.
1974: On the behavior of uranium during crystallization of magmas – with special emphasis on alkaline magmas; Proc. Symp. Form. Uran. Ore Dep., Int. Atomic Energy Agency, Vienna, p. 49-60.

Campana, B. and King, D.
1958: Regional geology and mineral resources of the Olary Province; South Australia Dept. Mines. Bull., v. 34, 133 p.

Cockfield, W.E.
1919: Silver-lead deposits of the Twelvemile area, Yukon; Geol. Surv. Can., Summ. Rept. 1918, Pt. b, p. 15-17; reprinted in Geol. Surv. Can., Mem. 284, 1957, p. 477-480.

Goodfellow, W.D., Jonasson, I.R., and Lund, N.G.
1976: Geochemical orientation and reconnaissance surveys for uranium in central Yukon; in Report of Activities, Part C, Geol. Surv. Can., Paper 76-1C, p. 237-240.

Green, L.H.
1972: Geology of Nash Creek, Larsen Creek and Dawson map-areas, Yukon Territory; Geol. Surv. Can., Mem. 364, 157 p.

Jonasson, I.R. and Goodfellow, W.D.
1976: Uranium reconnaissance program: Orientation studies in uranium exploration in the Yukon; Geol. Surv. Can. Open File 388, 97 p.

Mackevett, E.M., Jr.
1963: Geology and ore deposits of the Bokan Mountain uranium thorium area, southeastern Alaska; U.S. Geol. Surv., Bull. 1154, 125 p.

Semenov, E.I.
1974: Economic mineralogy of alkaline rocks; in The Alkaline Rocks (ed. H. Sørensen), Wiley-Interscience, p. 543-544.

Sørensen, H., Rose-Hansen, J., Nielsen, B.L., Løvborg, L., Sørensen, E., and Lungaard, T.
1974: The uranium deposit at Kvanefjeld, the Ilimaussag intrusion, South Greenland; Geology, reserves, benefication, Greenlands Geol. Unders., Rapp. 60.

Tempelman-Kluit, D.J.
1968: A re-examination of pseduoleucite from Spotted Fawn Creek, west-central Yukon; Can. J. Earth Sci., v. 6, p. 55-62.

Tempelman-Kluit, D.J. (cont.)
1970: Stratigraphy and structure of the "Keno Hill Quartzite" in Tombstone River – Upper Klondike River map-areas, Yukon Territory; Geol. Surv. Can., Bull. 180, 102 p.

von Backström, J.W.
1970: The Rössing uranium deposit near Swakopmund, South West Africa; in Uranium Exploration Geology. Int. Atomic Energy Agency, Vienna, Austria, p. 143-150.

Project 740012

Carl L. Amos
Atlantic Geoscience Centre, Dartmouth

Introduction

There is evidence to suggest that the extreme tidal range (up to 16.3 m) presently occurring in the Bay of Fundy, has been in existence for only a short period of time. Grant (1970), working with cores from the Minas Basin margins, indicated that prior to 4000-5000 years B.P. the tides of the Bay of Fundy were insignificant but may have commenced developing 6000 years B.P. Grant also suggested that the changes in tidal range may have been complicated by a progressive postglacial submergence of the region.

During the summer of 1976, a series of vibrocores were taken through the top 4 m of surficial sediment in the subtidal regions of the Minas Basin system and Minas Channel. The aims were to document any sedimentological evidence of submergence and to detect any changes in the magnitude of tidal current activity, as it is considered that such evidence is best preserved in the subtidal sediments: Recognizable sedimentological horizons were then dated by the ^{14}C method (total carbon), to provide a more complete postglacial history of the region; core location and stratigraphy are illustrated in Figure 7.1.

Vibrocore Results

It was found that each of the vibrocores showed a similar stratigraphic sequence: The lower 3-4 m of the cores were silts and clays containing open marine, inner shelf foraminifera (**Trochammina inflata, Elphidium excavatum clavatum,** etc.) and mulluscs (**Nucula proxima, Spisula polynyma,** etc.) and overlay the hummocky reflector which is thought to represent a compacted surface of the Pleistocene sediments (dated at 14 000 and 37 000 years B.P.). These watery, fine grained sediments thicken towards the centre of the basin indicating that they were deposited in a fashion typical of quiet water embayment sedimentation. The included microfauna are normally found in water depths less than 10-15 m, but are now within sediments more than 30 m below present mean sea level. It thus appears that there has been a progressive deepening of the region by at least 15 m since the time of deposition of these sediments. Six horizons throughout the muddy unit have been dated by radiocarbon analysis and an accretion rate of 0.1 cm/year has been calculated for this unit. Using the accretion rate, the top of this fine grained unit may be dated at 5300 years B.P., while the oldest dated sediments were deposited 8665 years B.P.

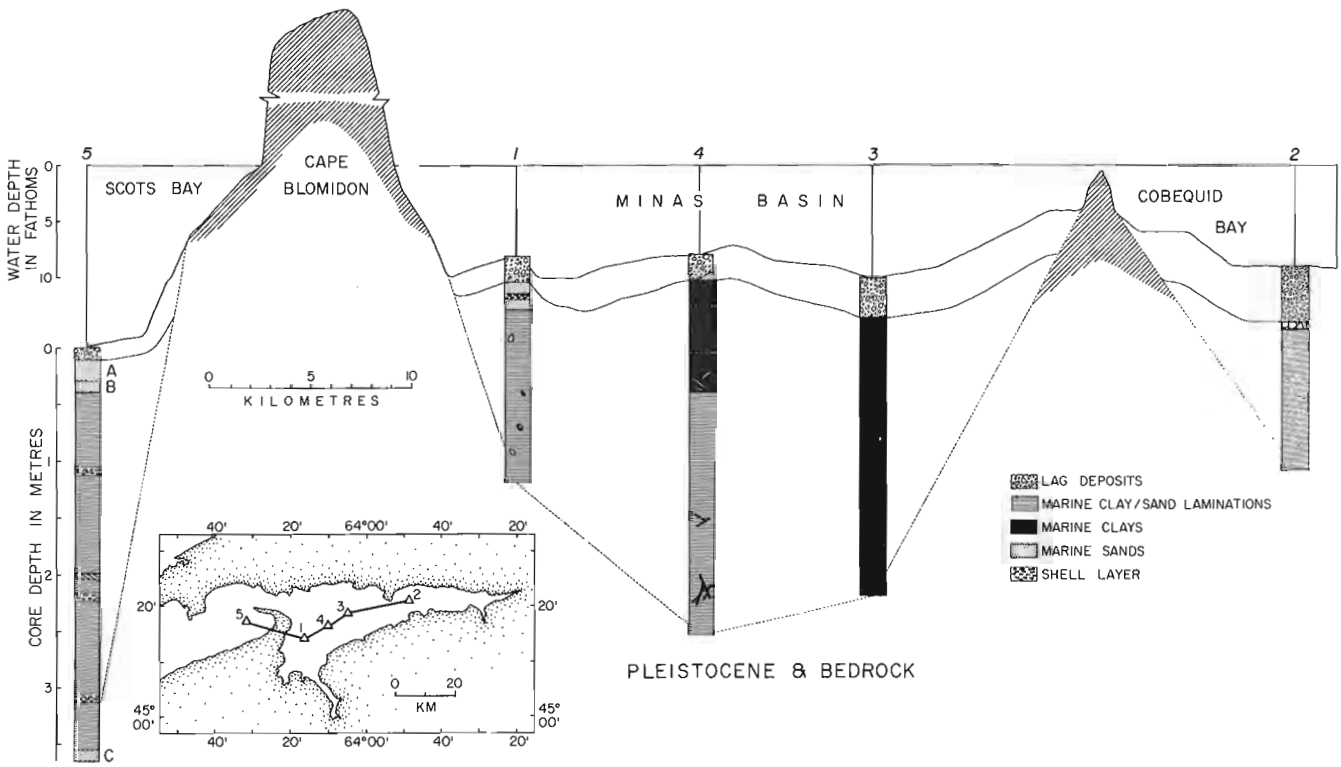

Figure 7.1. The location of depth of five vibrocores taken in the Bay of Fundy/Minas Basin system during May 1976; the interpreted stratigraphy is also indicated.

From: Report of Activities, Part B;
Geol. Surv. Can., Paper 77-1B (1977)

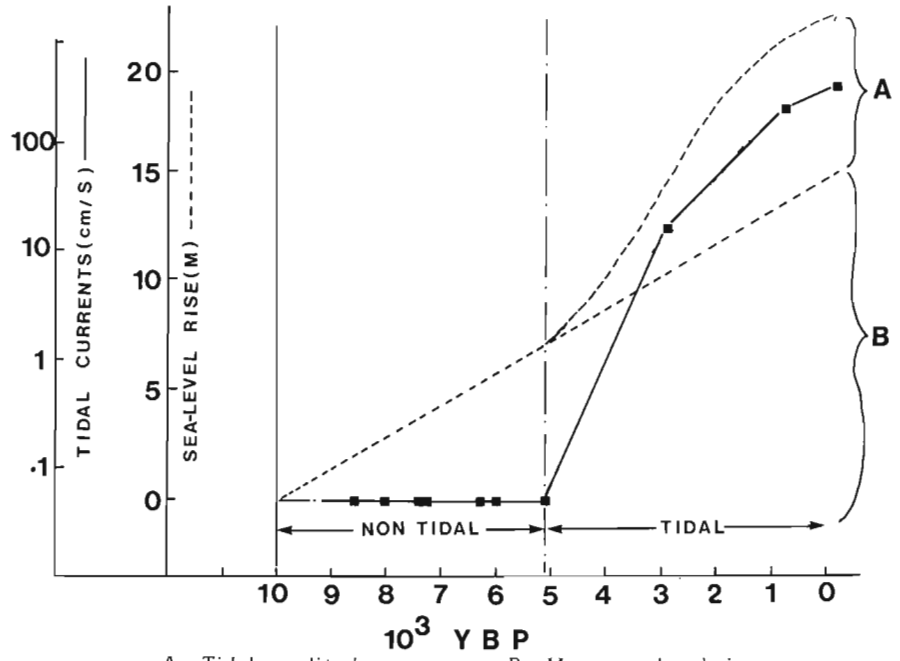

A. Tidal amplitude; B. Mean sea-level rise.

Figure 7.2. The solid line represents the maximum tidal currents considered to have been active in the Minas Basin, plotted relative to time. The dashed line represents the progressive rise in mean sea-level, superimposed by the increase in tidal amplitude over the last 5000 years.

A medium/coarse sand unit, (0-30 thick) overlies the fine grained sediments. The mineralogical composition of the sands shows them to be derived from two sources: 1) from the degradation and reworking of glacial outwash sands marginal to the basin; and 2) from cliff line erosion of the Triassic sandstones. The minimum current required to transport these sands would be approximately 5-15 cm/s (Hjulstrom, 1939). This current speed is thought to approximate the velocity of tidal currents considered to have been operating at the time of deposition. Radiocarbon dating of the overlying and underlying sediments indicates that the sands were deposited between 5300 and 1000 years B.P. and have an average age of 3000 years B.P. Radiocarbon dating of the included shell detritus shows them to be 7300 years old. These shells may, therefore, have been derived from glacial deposits having grown in situ and subsequently mixed with more recent forms, or from early Holocene marginal material with a bivalve infauna.

Overlying the sand unit is a unit which is coarser still, comprising admixtures of sand, granules, pebbles, cobbles and shell debris. The textural and mineralogical immaturity of this sediment, and the presence of intact shells suggests that these sediments were deposited from ice-rafting of material derived from the shoreline of the basin and have not been transported along the bed. The unit contains shells of Macoma balthica, (an intertidal clam), which have been dated at 1000 years B.P. The sediments which now comprise this ice-rafted unit may well be the lag deposit left after winnowing of finer material by tidal current action. The modal class of the sediment size comprising this deposit will not suffer transport by currents slower than 150 cm/s. As these deposits appear to be in situ it is considered that the tidal currents operating during the time of formation of this unit were marginally less than 150 cm/s. Consequently, there must have been a marked increase in current activity subsequent to the period during which the underlying sands were being laid down, i.e. from 3000 to 1000 B.P. It is considered that the mechanism necessary to lift and transport shore ice and its included sediments to the sites of deposition requires a significant tidal range as exemplified by the tidal currents invoked.

The present surficial deposits of the basin, which are also considered to be ice-rafted, overlie the ice-rafted unit, and are generally composed of pebbles and cobbles. These deposits are found over a large region of the subtidal zone. Current measurements made in the vicinity of the core sites have recorded mean velocities of up to 300 cm/s, occurring in conjunction with 16-m tides.

The inferred tidal currents quoted above have been plotted against time in Figure 7.2. The figure indicates that prior to 5000 years B.P. tidal current activity was insignificant but has been increasing steadily since that time (indicated by the solid line). The dotted lines in the figure show the simplified, inferred ranges of increase in mean sea level estimated from the microfaunal evidence. The increase in tidal range and progressive sea-level rise combine to produce a relative increase in the height of high tide of the region of 23 m during postglacial times. The results are generally in keeping with Grant (1970), who appears not to have found marginal intertidal sediments older than 3000 to 4000 years.

Identification of the benthonic fossils and interpretation of the paleo-environments were carried out by Drs. Vilks, Schafer and Wagner and by Mrs. Cole.

References

Grant, D.R.
1970: Recent coastal submergence of the Maritime provinces, Canada., Can. J. Earth Sci., v. 7, p. 676-679.

Hjulstrom, F.
1939: Transporation of detritus by moving water; in Recent Marine Sediments, (Ed.) Trask, P.D. publ. Dover Publ. Inc., p. 5-31.

8. PRELIMINARY REPORT ON THE GEOLOGY OF A PART OF THE POKIOK PLUTON AND ITS SURROUNDING METASEDIMENTS, SOUTH-CENTRAL NEW BRUNSWICK

E.M.R. Research Agreement 1135-D13-4-156/76

N. Rast[1]
Regional and Economic Geology Division

Introduction

The Pokiok pluton is a large granitic body situated in the axial belt of the Acadian Orogen of New Brunswick. In a general sense it has a northeast-southwest trend, subparallel to regional strike, but in detail it is discordant (Fig. 8.1). The body has a maximum length of about 100 km and a maximum width of 25 km. The Trans-Canada Highway (Fig. 8.2) crosses the pluton west of Fredericton, affording reasonable exposures in roadcuts, but in general exposure is poor. The most detailed previous work on the granite, by Patterson (1957), was incorporated into Woodstock-Fredericton sheet (Geol. Surv. Can. Map 37-1959), compiled by Anderson and Poole. Martin (1970) and Poole (1972) discussed some of the isotopic age dating work carried out on the Pokiok pluton, which suggests an age of 350-390 m.y., or fairly late Devonian. Martin (1970) pointed out the relatively large chemical variation within the pluton. On the basis of comparison of feldspars with other New Brunswick granites of a similar age, he suggested a relatively deep emplacement of the body.

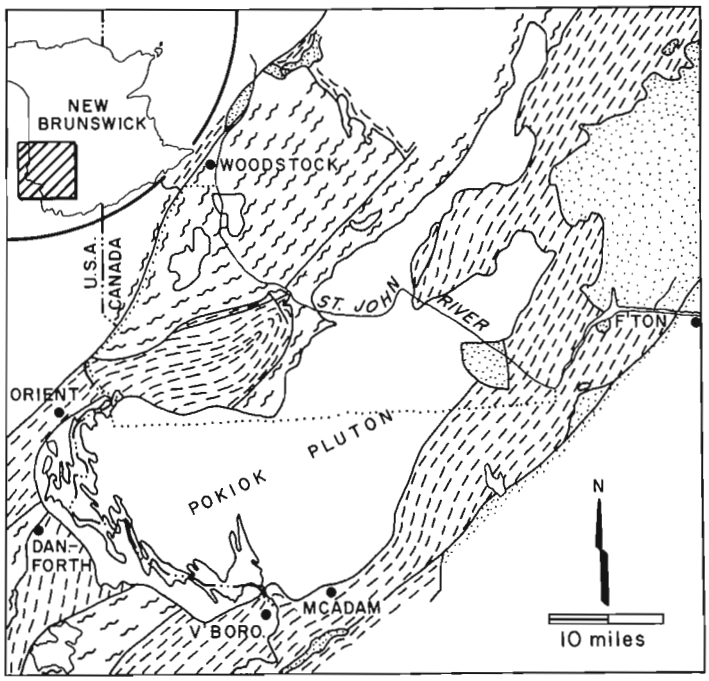

Figure 8.1. The setting of the Pokiok pluton. Dotted line and the Saint John River outline the map shown in Figure 8.2. Carboniferous is dotted, Siluro-Devonian sediments are dashed and pre-Silurian rocks are shown in zigzag.

The present study commenced in 1973. The early work was assisted by Mr. A. Hickinbotham. In 1976 the author began systematic research on the granitic rocks and Silurian sediments to the east of the pluton, while Mr. B. O'Brien mapped the older sedimentary and volcanic formations to the west.

Stratigraphy of the Country Rocks

At present, no completely substantiated stratigraphic column can be established in the country rocks. The stratigraphic sequence can only be recognized on the basis of lithologies which are dated by analogy with nearby recognizable stratigraphic units. East of the granite fairly uniform greywacke, sandstones and siltstones, rhythmically interbedded with shales, show pronounced flute and load clasts, which indicate a general current direction from northeast to southwest. The rocks are folded subisoclinally, with steep or vertical axial planes and therefore no regional direction of facing can be recognized. These rocks, sometimes informally referred to as "Fredericton greywacke", have been dated as Wenlock to Ludlow on the basis of graptolites (Gordon and Cumming, 1966). In general the eastern, fossiliferous, parts of this unit are more pelitic than the western parts that form the margin of the Pokiok pluton. The more massive and gritty western portion can be compared to the so-called "Taxis River Grits", which, at least in part, may be Llandoverian. Near McAdam an angular unconformity which occurs within the succession of apparently Silurian strata, may represent a discordance between Silurian and Ordovician sediments.

On the western margin of the pluton four different varieties of sediments have been found.

(a) A series of phyllitic, graded sandstones, and greywackes contains thin shales with quartzitic laminations. Very near the granite body these rocks show well developed retrogressed porphyroblasts which originally were almost certainly andalusite. O'Brien (pers. comm.) also suspects the presence of cordierite.

These strongly schistose, polydeformed quartzose rocks occur only at the edge of the granite and are quite unlike any other sedimentary rocks in the immediate vicinity. On the Woodstock-Fredericton sheet they are shown as an aureole to the granite, but lithologically and metamorphically, they resemble the Cambrian(?) Grand Pitch Formation of Maine (Neuman, 1967). These rocks are also very similar to quartzites mapped by Poole (1958), some thirty miles to the north.

(b) Strongly deformed, dark, partly graphitic shales and sandstones contain very well graded greywacke units up to 30 cm thick. The dark shales characteristically contain chert. This is undoubtedly a turbidite sequence.

[1] Department of Geology, The University of New Brunswick, P.O. Box 4400, Fredericton, N.B. E3B 5A3.

From: Report of Activities, Part B, Geol. Surv. Can., Paper 77-1B (1977)

These rocks are lithologically identical to those mapped by Anderson (1968) as Ordovician on the basis of some fossil evidence. Common presence of chert is diagnostic of these rocks but they include minor conglomerates and carbonates which can hardly be distinguished from Siluro-Devonian lithotypes except by more pronounced deformation in the presumed Ordovician rocks. Along the Eel River south and southeast of Meductic (Fig. 8.2) there are pillow lavas and sub-acid lapilli tuffs and rhyolites within the assumed Ordovician rocks. Near Monument Brook on the American border, variolitic basalts occur. The Ordovician basic rocks, in particular, are much denser and finer grained than the assumed Siluro-Devonian volcanics.

(c) Dark, chloritic, and reddish shales cannot be distinguished from the manganese shales and siltstone of the Woodstock area (Hamilton-Smith, 1972) north of the ground mapped. Outcrops of these rocks occur normally close to type (d) to be described below. These rocks are at present correlated with similar beds near Woodstock and with the bottom of the Smirna Mills Formation of Maine (Pavlides, 1972). Thus they are presumed to be basal Silurian. Conglomerates associated with this horizon may represent the basal Silurian conglomerates, although the evidence is, at present, inconclusive. Hamilton-Smith (1972) suggested that similar rocks to the west of Woodstock represent the lower member of Smirna Mills Formation.

(d) Schistose conglomerates, limestones (partly or entirely marmorized), calcareous phyllites and limestone conglomerates outcrop in the vicinity of Canterbury (Fig. 8.2). The sequence involves a substantial amount of volcanics, and minor intrusives, of basaltic type with abundant amygdules. Limited observations suggest that these basaltic rocks are younger than the adjacent conglomerates. Limited fossil information, e.g. recovery of coarse strophomenid brachiopods, implies that the calcareous rocks are Silurian or even younger. Quartzose siltstones to the southwest of the Canterbury exposures, which appear to have been generally least metamorphosed and deformed, probably form the top of this sequence.

East of Ritchie near the Saint John River a particularly large metasedimentary xenolith of garnetiferous schists and gneisses occurs within the granitic body. These rocks cannot be related to any others in the vicinity and may be older than any so far observed.

The proposed sedimentary succession west of the Pokiok pluton is shown in Table 8.1.

Although at present just a working hypothesis, the succession accords reasonably well with the regional succession both in Maine and New Brunswick.

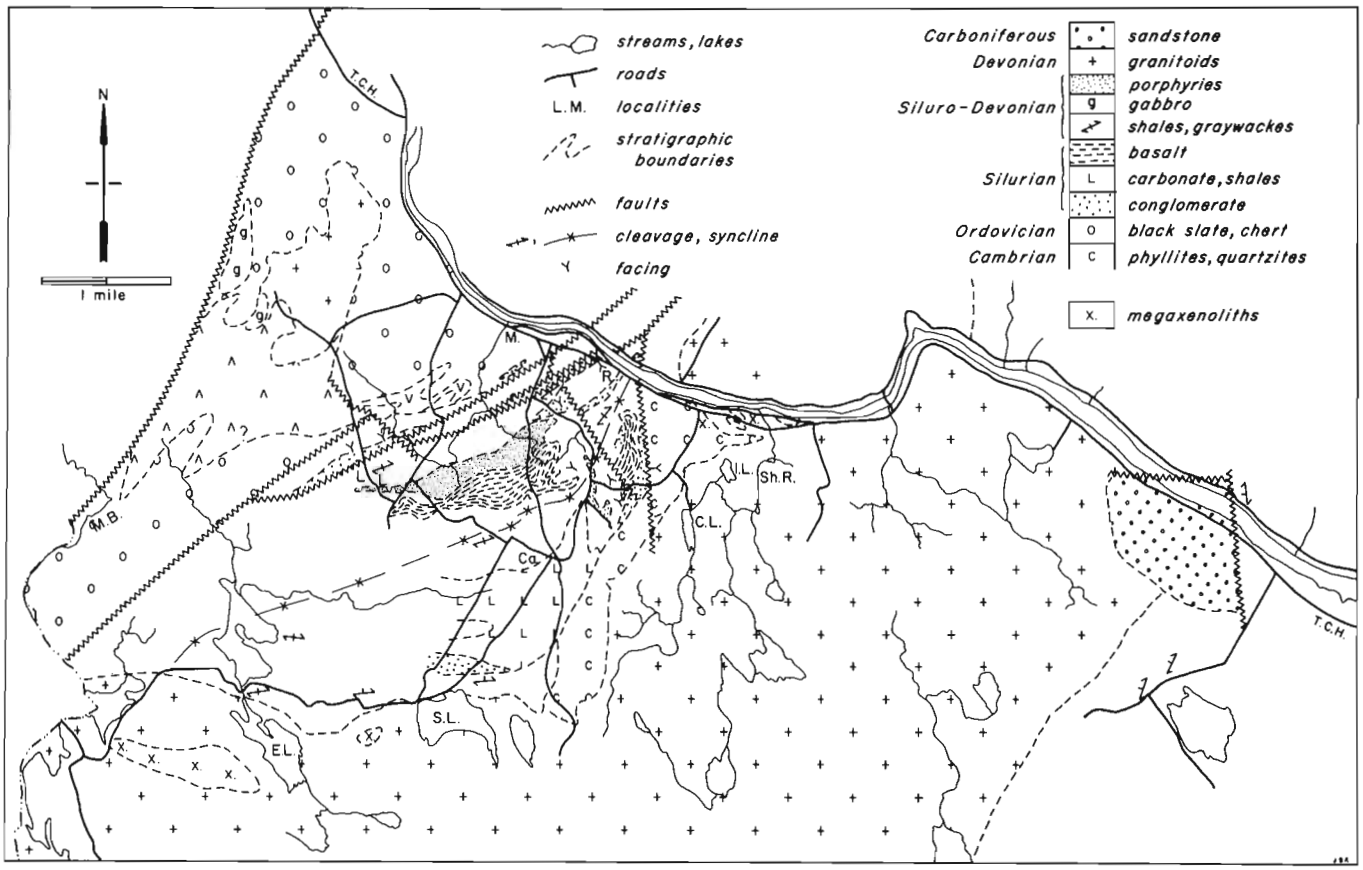

Ca – Canterbury
C.L. – Charlie Lake
E.L. – Eel Lake
I.L. – Ingraham Lake
M. – Meductic
M.B. – Monument Brook
R. – Ritchie
Sh.R. – Shogomac River
S.L. – Skiff Lake
T.C.H. – Trans-Canada Highway

Figure 8.2. Stratigraphic detail on either side of the Pokiok pluton.

Table 8.1

Tentative Stratigraphic Succession
West of the Pokiok Pluton

red sandstone	Carboniferous
— Unconformity —	
d – Calcareous phyllites, conglomerates and basalts	Siluro-Devonian
c – dark and reddish manganiferous slates	Llandovery
— Possible unconformity —	
b – dark schistose pyritic slates, pillow lavas	Ordovician
a – graded quartzites and phyllites resting on gneisses in part included in the Pokiok intrusion	Cambrian?

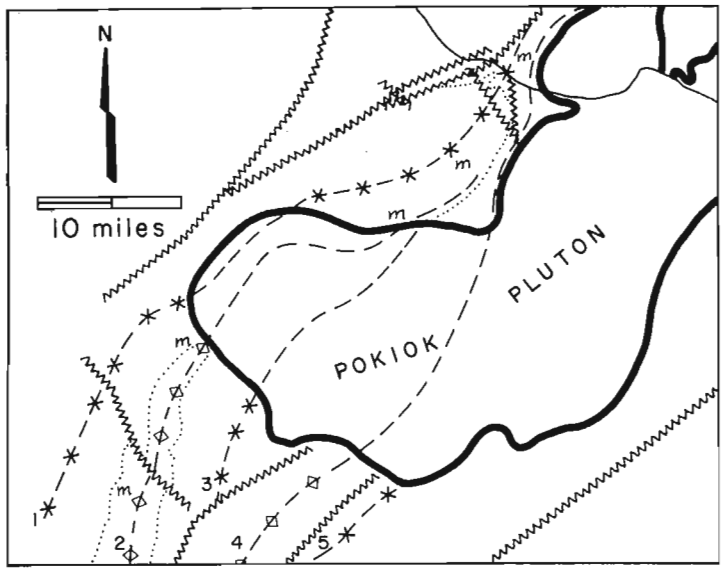

Figure 8.3. The outline of regional tectonics and metamorphism. The pluton is outlined by a heavy line. Traces of synclines and anticlines (1-5) shown (⊀ and ⊕) and numbers as in text, faults in zigzag, stratigraphic boundaries as in Figure 8.1, dotted. Letters (m) indicate belt of regional metamorphism.

Pokiok Pluton

The rocks of the Pokiok pluton vary in composition from granite through adamellite to granodiorite and tonalite, although the main rock type is porphyritic biotite adamellite with microcline perthite megacrysts reaching 10 cm in long dimension. An extensive zone of marginal breccia and zenoliths occurs along the western margin of the pluton from Eel Lake to Charlie Lake associated with pegmatitic and aplitic dykes and a coarsening in grain size in the adamellite. Along the eastern margin of the intrusive the contacts are clean and discordant with rare granite dykes.

The brecciated contact rocks do not show signs of cataclasis and the fragments are cemented by massive granite. Under the microscope, abundant randomly oriented biotite characterizes the hornfelsed xenoliths, which show varying degrees of assimilation, and some develop porphyritic feldspars within them. The breccias are interpreted as due to intrusive, rather than tectonic, action.

Towards Ritchie and Saint John River the pluton is composite and exhibits three different facies.

(a) The coarse porphyritic adamellite with large microcline feldspars forms the largest part of the pluton. In addition to microcline, the rock consists of strongly zoned plagioclase, quartz and biotite. Hornblende-bearing phases are rare. In places, signs of cataclasis are present with quartz developing undulose extinction and biotite being partly retrogressed to chlorite.

(b) Medium grained, dark, granodiorite occurs at the margin of the main Pokiok intrusion. It consists of an oligoclase-quartz-amphibole assemblage, the last being often partly or completely chloritized. The rock has a pronounced foliation generally dipping about 40 degrees. In places the rock is replete with semi-assimilated xenoliths of schists whose schistosity parallels the foliation in the granodiorite, thus indicating a common tectonic origin. The close association of this rock with large fragments of paragneiss and biotite schist suggests an original relationship. The tectonic foliation and more mafic composition imply that it is older than the undeformed porphyritic adamellite.

(c) Dark, flow-banded tonalite, a relatively fine grained rock, occurs in dykes, of which the best example occurs north of Ingraham Lake at the confluence of Shogomac River and the Saint John (Fig. 8.2). Within a fine grained plagioclase-quartz rock containing small amounts of biotite, elongated laths of twinned hornblende crudely outline a flow pattern. At Shogomac River the tonalite cross-cuts and includes foliated granodiorite. The detailed parallelism of marginal banding with the jagged edges of the granodiorite indicates that it is of flow rather than tectonic origin.

At Ingraham Lake the foliation of granodiorite strikes at 80 degrees to the contact with adamellite. Despite the absence of an exposed contact, the adamellite clearly cross-cuts the granodiorite. The flow-banded tonalite is completely undeformed and its relation to the main adamellite is not obvious. Dykes of similar, though somewhat more basic, material outcrop some distance away from the pluton and their relations to the main body of the pluton are obscure.

The foliated granodiorite and xenoliths within it are cut by a dyke system of aplites, pegmatites and aplopegmatites, all consisting of quartz, feldspar, muscovite and chloritized biotite. The prevalent direction of these dykes varies from 040 – 068 degrees, although minor cross-connecting veins trend east-west. The dip of all these dykes is generally steep and they are emplaced within joints or faults. In one case an aplite vein is emplaced along a small strike-slip feature (040° strike) which displaces the xenoliths by a distance of 5 cm in a right-lateral sense. The vertical dykes cut foliation of much gentler dip and are therefore essentially post-tectonic. It is proposed that the dykes were derived from the

porphyritic adamellite and are genetically related to it. Such dykes are effectively absent from the eastern margin of the Pokiok intrusive.

The coarser grain size of the western margin of the adamellite and the presence of dykes of pegmatite and aplite indicate that the western margin represents a deeper section of the granite and adjacent rocks than the eastern margin. An essentially horizontal outlier of Pennsylvanian red sandstones (Fig. 8.2) overlaps the eastern margin of the pluton indicating that the implied tilt from west to east took place prior to Pennsylvanian time. The Middle-Upper Devonian age of intrusion of the porphyritic adamellite is well known from isotope dating. On the other hand the ages of other intrusive phases are completely unknown. The tonalite is post-tectonic, but the foliated granodiorite is pre-tectonic and associated with strongly deformed sediments with a common principal schistosity. If this schistosity is Acadian then the granodiorite is at least pre-Acadian.

Minor Structure and Metamorphism of the Aureole

The regional trend of the rocks both to the east and west of the Pokiok pluton is approximately 20 degrees east of north, but there is an arcuate deflection around the western edge of the Pokiok pluton (Fig. 8.2). The cleavage makes a similar deflection, though not so pronounced. The pluton is cross-cutting in detail, and therefore this deflection undoubtedly developed prior to the emplacement of the pluton. Cleavage-bedding intersections suggest that folds plunge sub-horizontally to the east of the pluton but plunge to the southwest and west to the west of it.

An essentially single episode of interpenetrative deformation affected all Silurian rocks. The so-called "stretching lineation", marked by elongated flakes of chlorite and mica, has a steep plunge and there is no obvious refolding. East of the pluton, apart from the margin of the granite, the grade of regional metamorphism is low. To the west, the Silurian rocks are affected by a regional metamorphism reaching high greenschist or amphibolite facies. This belt of regional metamorphism stretches subparallel to the granite body with an approximately north-south orientation (Fig. 8.3). Patterson (1957) confused it with the thermal aureole of the granite, but thin sections show that the regionally metamorphosed rocks have been overprinted by later biotite and andalusite produced in the thermal aureole. Thus the high grade metamorphic belt is related to a regional dynamothermal effect. The occasional amphibolites and very schistose diorites found amongst the metasedimentary rocks support this contention. The rocks of the metamorphic belt were invaded first by granodiorites and diorites, now foliated, and subsequently intrusions of non-schistose aspect, including the porphyritic adamellite.

Within the "high grade" metamorphic belt one can recognize calcareous and conglomeratic members. These have elsewhere yielded Silurian fossils, as well as phyllitic and schistose metapelites and quartzites showing abundant evidence of polyphase deformation. The latter are overturned eastward, whereas Silurian strata are folded either symmetrically or show overturning to the west or northwest. In hand specimens of rhyolites one can demonstrate three sets of minor structures a) S_1 schistosity (cleavage) forms at a small angle to bedding and often appears subparallel, b) S_2 schistosity (cleavage), not entirely interpenetrative, is axial planar to very compressed minor folds. Over much of the ground S_1 and S_2 are so close to each other that an average plane of foliation referred to here as a "mean foliation" is produced. c) S_3 schistosity, a steep crenulation, usually strikes 45 – 65 degrees and dips down the plane of mean foliation. S_3 is rarely associated with strong cleavage, although in places it has been observed within kink bands.

The structure referred to as S_2 is coeval with the main cleavage in Silurian rocks and kinks associated with S_3 also affect Silurian strata. However, S_1 is restricted to the metapelite-quartzite sequence and therefore is, in all probability, pre-Silurian. Since both pre-Silurian and Silurian strata enter into the high grade zone of metamorphism, it is proposed that this regional metamorphism is Silurian or younger.

In thin sections the rocks of Grand Pitch aspect show signs of over-printing of the regional metamorphism by two later thermal events. The first produced decussate biotite and andalusite(?). The second produced decussate chlorite, muscovite and ores and converted the earlier andalusite into coarse shimmer aggregate. The same events can be deduced from thin sections of Silurian metasediments from the American side of the border. The regional metamorphism was coeval with the main schistosity indicating that it was at least partly syntectonic with Acadian deformation.

Regional Structure and Relationships

Large scale folds are difficult to recognize in this ground on the basis of dip and strike measurement since virtually all metasediments to the west and south of the pluton are steeply inclined and sub-isoclinally folded. However, Larrabee et al. (1965) have delineated a stratigraphic succession in Maine to which one can refer all the lithostratigraphic units of the ground to northwest of the granite. The folds identified by Larrabee et al. (1965) can be provisionally traced into New Brunswick. The following sequence of fold traces is recognized between Orient and Vanceboro (Fig. 8.3): (1) North Bancroft Syncline, (2) Danforth anticline, (3) broken Flagstaff Mountain Syncline, (4) broken Baskahegan Lake anticline and (5) broken Todds Farm Syncline. All these folds, with corresponding lithologic successions, can be recognized in New Brunswick (Fig. 8.3). The "high grade" belt of metamorphism roughly parallels the fold traces but in detail is transgressive. Although not specifically mentioned, it can be recognized in Maine by localities with high grade minerals including almandine garnet and pyrrhotite (Larrabee et al., 1965, p. 27).

In Maine the edge of the pluton cuts abruptly across the Devonian cores of the successive synclinal folds implying that the intrusion has remained essentially untilted since the time of its emplacement. In New Brunswick however the eastern edge of the pluton appears to expose higher levels of the pluton than the western edge. Bi-Sb mineralization occurs exclusively along the eastern edge.

The metasedimentary rocks in New Brunswick are affected by late faulting and a fairly extensive local brecciation. The date of these brittle events is unknown but must be Carboniferous or later since Carboniferous outliers in the vicinity are affected. Two major directions of intra-Carboniferous or post-Carboniferous faulting are recognized – namely northeast-southwest and north-northwest – south-southeast.

Conclusion

The Pokiok pluton, which according to previous investigations, was emplaced between 348 and 387 m.y., appears to be a multiphase intrusion. The geological data adduced here demonstrates several petrographic phases, but their separation in time, and the role played by differential cooling owing to a post-intrusive tilt remain uncertain.

References

Anderson, F.D.
1968: Woodstock, Millville, and Coldstream map-areas, Carleton and York Counties, New Brunswick; Geol. Surv. Can., Mem. 353.

Gordon, A.J. and Cumming, L.M.
1966: Mactaquac-Woodstock section of the Saint John River: New Brunswick Dep. Nat. Res., Min. Res. Br.; Unpubl. Rep. 11 p.

Hamilton-Smith, T.
1972: Stratigraphy and structure of Silurian rocks of the McKenzie Corner area: New Brunswick Dep. Nat. Res., Min. Res. Br.; Rep. Invest. no. 15, 36 p.

Larrabee, D.M., Spencer, C.W., and Swift, D.J.P.
1965: Bedrock geology of the Grand Lake area, Aroostook, Hancock, Penobscot, and Washington Counties, Maine; U.S. Geol. Surv., Bull. 120 1-E, 38 p.

Martin, R.F.
1970: Petrogenetic and tectonic implications of two contrasting Devonian batholithic associations in New Brunswick, Canada; Am. J. Sci., v. 268, p. 309-321.

Neuman, R.B.
1967: Bedrock geology of the Shin Pond and Stacyville quadrangles, Penobscot County, Maine; U.S. Geol. Surv., Prof. Paper 524-1.

Patterson, J.M.
1957: Geology of the Canterbury map area (West Half); Unpubl. M.Sc. thesis, Univ. New Brunswick, Fredericton, N.B.

Pavlides, Louis.
1972: Geological map of the Smyrna Mills quadrangle, Aroostook County, Maine; U.S. Geol. Surv., Map GQ-1024.

Poole, W.H.
1958: Napadogan, York County, New Brunswick; Geol. Surv. Can., Map 11-1958.

1972: p. 70 in: Wanless, R.K., Stevens, R.D., Lachance, G.R. and Delabro, R.N., Age Determinations and geological studies, K-Ar Isotopic Ages; Geol. Surv. Can., Paper 71-2, 96 p.

9. TIME-DOMAIN REFLECTOMETRY – AIR-GAP PROBLEM IN A COAXIAL LINE

Project 750037

A.P. Annan

Resource Geophysics and Geochemistry Division

Introduction

The electrical properties of soils in situ have been determined by using time-domain reflectometry techniques (Davis, 1975, and Davis and Chudobiak, 1975), with a coaxial transmission line. The coaxial line is inserted into the soil in such a manner that the soil fills the space between the inner and outer conductor. Compaction of soil and wiggle of the probe on insertion can generate air spaces around the conductors forming the coaxial line. After analysis of the problem of air gaps around parallel wire transmission lines also used for these measurements, it was felt that air gaps in the coaxial line might introduce significant measurement error. This air gap could be the source of discrepancies observed in data obtained on the two types of transmission lines. In the following, a brief derivation of error due to air gaps concentric to the cylindrical conductors forming the coaxial line is presented. The air gap effect is compared with that previously derived for the parallel wire transmission line.

Basic Theory

The basic theory of transmission lines operating with only TEM (transverse electromagnetic modes) is extensively discussed by Ramo, et al. (1965), Jordan and Balmain (1968) and others. For continuity the basic equations and theory are briefly presented in order to clarify later discussions.

An electrical transient propagates along a transmission line as a wave. The voltage, V, between and the current, I, in the conductors forming the line satisfy the wave equation

$$\frac{\partial^2 V}{\partial z^2} = \frac{1}{U^2}\frac{\partial^2 V}{\partial t^2} \qquad (1)$$

$$\frac{\partial^2 I}{\partial z^2} = \frac{1}{U^2}\frac{\partial^2 I}{\partial t^2} \qquad (2)$$

where z is the distance along the line, t is time, and U is the electromagnetic wave velocity of the line. For first order analysis of soil electrical properties, losses are neglected and only a bulk dielectric constant is considered. For most applications this assumption is quite valid since the soil loss tangests are considerably less than unity. Neglecting losses, the velocity along the line is determined by the insulating material between the conducting lines. The velocity is expressed by

$$U = \frac{1}{(LC)^{1/2}} \qquad (3)$$

where L and C are the line inductance and capacitance per unit length. The L and C of the line are determined by magnetic and electrical properties of the material surrounding the conductor. For TEM mode propagation, L and C are the same as the electrostatic inductance and capacitance.

Coaxial Transmission Line

In a coaxial line, a circular cylinder of radius r_1 is placed concentrically in a circular space of radius r_4 formed inside a second conductor. This is illustrated in Figure 9.1. If the material between the inner and outer conductor is homogeneous with permeability μ and permittivity ϵ, the inductance and capacitance per unit length are

$$L = \frac{\mu}{2\pi} \ln\left(\frac{r_4}{r_1}\right) \qquad (4)$$

$$C = \frac{2\pi\epsilon}{\ln\left(\frac{r_4}{r_1}\right)} \qquad (5)$$

These expressions yield

$$U = \frac{1}{(\mu\epsilon)^{1/2}} \qquad (6)$$

which is the electromagnetic wave velocity of the material between the conductors.

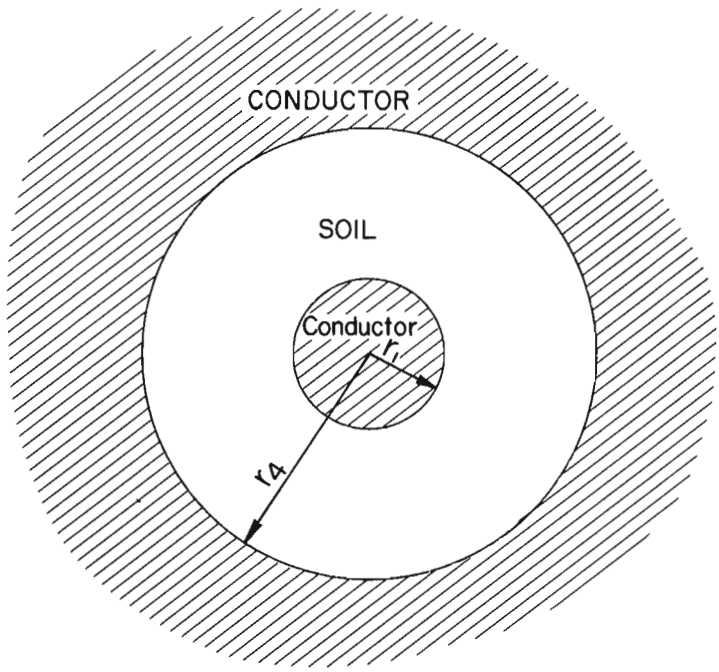

Figure 9.1. Coaxial line used for measurement of the electrical properties of soil.

From: Report of Activities, Part B; Geol. Surv. Can., Paper 77-1B (1977)

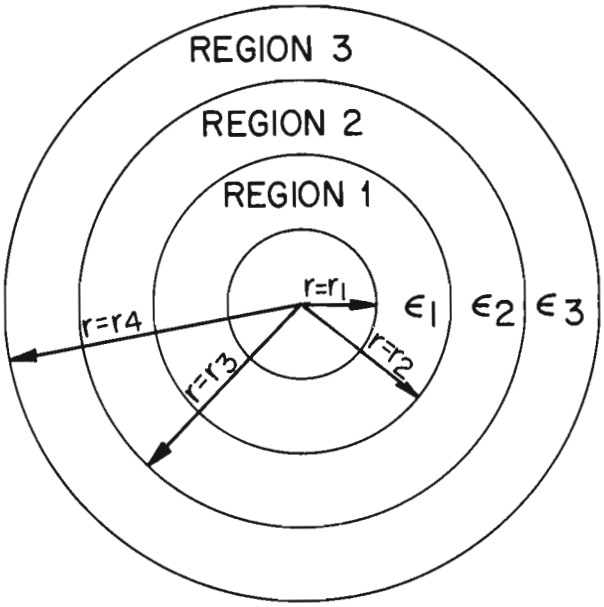

Figure 9.2. Geometry for coaxial line with air gaps.

Coaxial Line with Air Gap

The practical use of a coaxial line for electrical property measurements of soils in situ requires insertion of the line into the soil. Since this insertion process is sometimes difficult to achieve without probe wobble, an air gap can form around the inner conductor and near the outer conductor. To obtain an estimate of the error associated with this air gap, the idealized model shown in Figure 9.2 has been analyzed to determine the air-gap effect. Since the permeability of soil varies little from that of air, the inductance L is unchanged. To analyze the air-gap effect, it is necessary to examine the line capacitance as a function of the size of these air spaces.

The capacitance of the line with a gap, C_g, is the same as the electrostatic capacitance of the line with the geometry of Figure 9.2. The capacitance is determined by solving for the electric potential between the lines when they are held at a potential difference V. This is a straight forward boundary value problem.

The solution to this boundary value problem is given by the author (Annan, 1976; Air-Gap problem for coaxial transmission lines, Int. Rep.). The capacitance of the line with gaps is

$$C_g = \frac{2\pi K_1 \varepsilon_o}{D} \qquad (7)$$

where

$$D = \ln\left(\frac{r_2}{r_1}\right) + \frac{K_1}{K_2} \ln\left(\frac{r_3}{r_2}\right) + \frac{K_1}{K_3} \ln\left(\frac{r_4}{r_3}\right) \qquad (8)$$

The parameters in 7 and 8 are

ε_o – freespace permittivity – 8.85×10^{-12} F/m

K_i – dielectric constant of region i.

Effect of Air Gap in Dielectric Constant Estimates

The dielectric constant of a material is defined as

$$K = \frac{\varepsilon}{\varepsilon_o} \qquad (9)$$

For TDR interpretations, the velocity of wave propagation on the line in soil is used to determine an apparent bulk soil dielectric constant K_A defined as

$$K_A = \left(\frac{U_o}{U}\right)^2 \qquad (10)$$

where U_o is the electromagnetic wave velocity in free space, 3×10^8 m/s. For a line with no air gap,

$$K_A = K_2 \qquad (11)$$

With the air gap present

$$K_A = FK_2 \qquad (12)$$

where

$$F = \frac{\frac{K_1}{K_2} \ln\left(\frac{r_4}{r_1}\right)}{\ln\left(\frac{r_2}{r_1}\right) + \frac{K_1}{K_2} \ln\left(\frac{r_2}{r_3}\right) + \frac{K_1}{K_3} \ln\left(\frac{r_4}{r_3}\right)} \qquad (13)$$

The effect of various air gaps and water filled gaps are illustrated by displaying K_A versus K_2 for coaxial line dimensions employed in the field and in the laboratory.

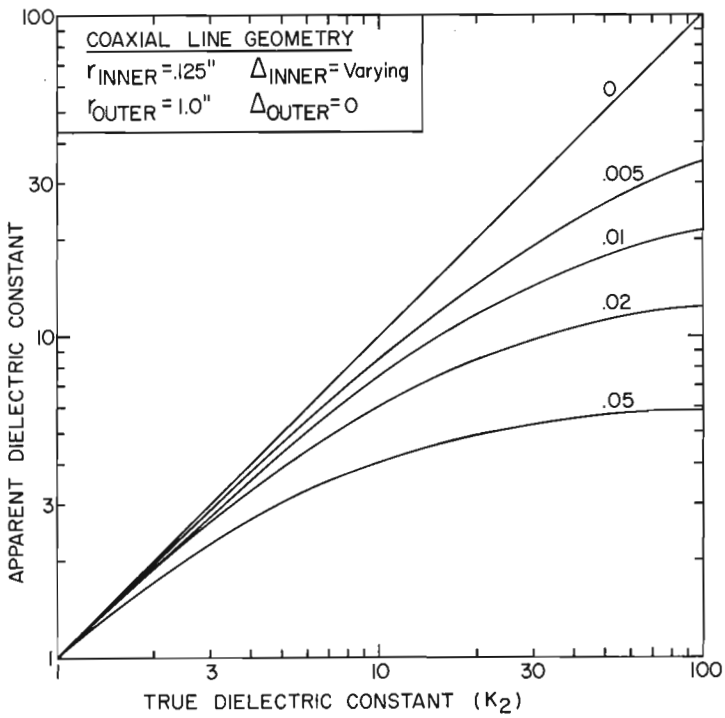

Figure 9.3. Apparent dielectric constant versus true dielectric constant for a coaxial line with an air gap around the inner conductor only.

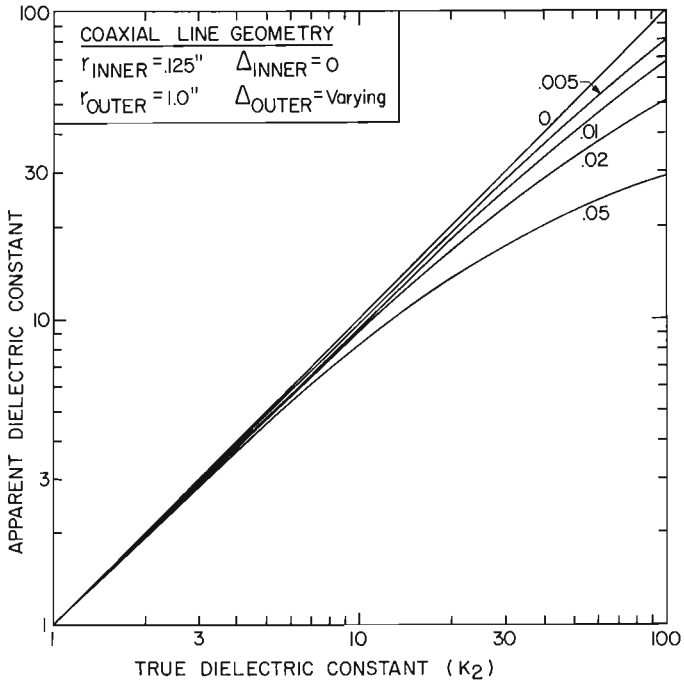

Figure 9.4. Apparent dielectric constant versus true dielectric constant for a coaxial line with an air gap at the outer conductor only.

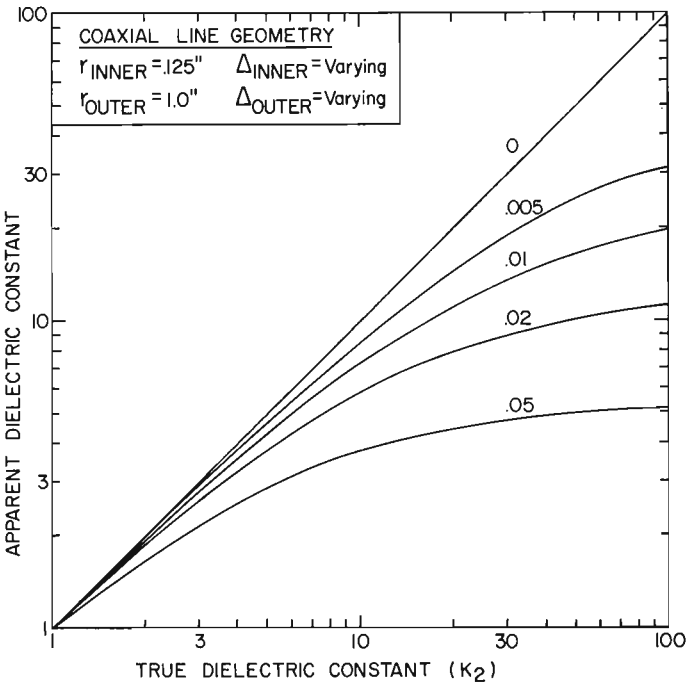

Figure 9.5. Apparent dielectric constant versus true dielectric constant for a coaxial line with air gaps at the inner and outer conductor.

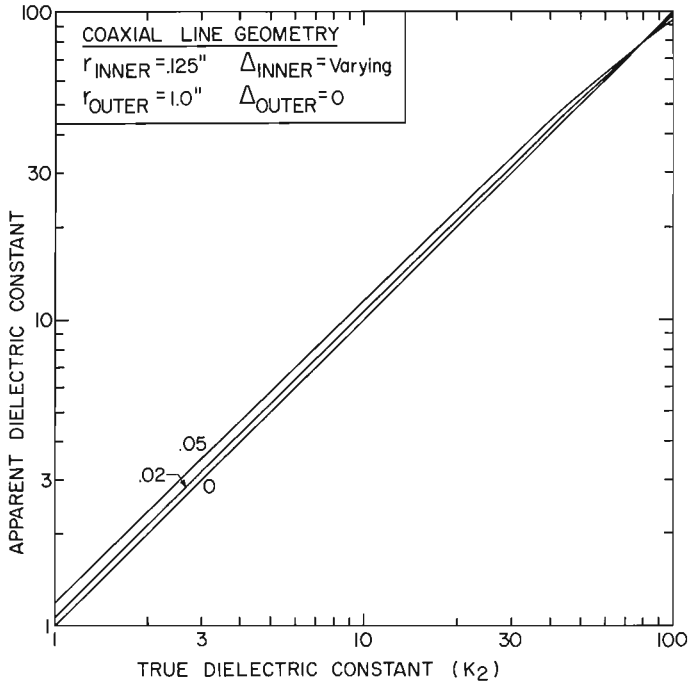

Figure 9.6. Apparent dielectric constant versus true dielectric constant for a coaxial line with a water filled gap around the inner conductor.

Computed Results

The coaxial lines in use consist of an inner conductor of radius 0.125 inch and an outer conductor of radius 1.0 inch. To study the air gap effect at the inner and outer conductor separately, the individual gaps were alternatively set to zero while the other was varied. Figure 9.3 shows the effect of an air gap at the inner conductor only. The gap at the inner conductor, $\Delta_{inner} = (r_2 - r_1)$, was set to 0, 0.005, 0.01, 0.02 and 0.05 inch. The dielectric constant, K_1, was set to unity. The gap has the effect of reducing the apparent dielectric constant K_A. As the soil dielectric constant increases, K_A approaches a maximum value asymptotically. The error associated with the gap increases as the gap size increases and as the soil dielectric constant K_2 increases.

The effect of the air gap at the outer conductor, $\Delta_{outer} = (r_4 - r_3)$ is similar to that of the gap at the inner conductor. The apparent dielectric constant versus true dielectric constant response for the outer gap dimension varying is shown in Figure 9.4. Here $K_3 = 1$ and $\Delta_{outer} = 0$, 0.005, 0.01, 0.02 and 0.05 inch. The error associated with the outer gap is much smaller than the error for the inner gap of the same size. The error increases as gap size and soil dielectric constant increase.

The effect of having air gaps at the inner and outer conductor is shown in Figure 9.5. The inner and outer gaps have the same size and run through the same values as used for the independent variation of the gap sizes. The response is dominated by the inner gap.

Since the inner gap has the most effect on erroneous determinations of the bulk dielectric constant, the effect of a water filled inner gap was analyzed. These results

are shown in Figure 9.6. Here $K_1 = 81$ and Δ_{inner} was set to 0.02 and 0.05 inch. The apparent dielectric constant is greater than the true dielectric constant, K_2, for $K_2 < 81$ and less than K_2 for $K_2 > 81$. The error associated with water filled gap is small compared to the same size air gap.

Summary and Conclusions

The presence of air gaps in the coaxial transmission line used for determination of the dielectric constant of soils can introduce a large error. The air gap around the inner conductor is much more critical than the air gap at the outer conductor. The presence of a water filled gap is not a serious problem. For the typical range of dielectric constants observed in soils, namely, 2 to 50, the air gap at the inner conductor should be less than 0.05 inch for the line geometry used here.

The air gap effect for the coaxial line has the same type of behaviour exhibited as the air gap for the parallel wire transmission line (Annan, 1977). The presence of an air gap in both systems causes the apparent dielectric constant to be lower than the true soil dielectric constant. As the soil dielectric increases, the apparent dielectric constant increases to asymptotically approach a maximum value which is a function of the line geometry and air gap size.

References

Annan, A.P.
1977: Time-domain reflectometry – air-gap problem for parallel wire transmission lines; in Report of Activities, Part B, Geol. Surv. Can., Paper 77-1B, rep. 10.

Davis, J.L.
1975: Relative permittivity measurements of a sand and clay soil in situ; in Report of Activities, Part C, Geol. Surv. Can., Paper 75-1C, p. 361-365.

Davis, J.L. and Chudobiak, W.J.
1975: In situ meter for measuring relative permittivity of soils; in Report of Activities, Part A, Geol. Surv. Can., Paper 75-1A, p. 75-79.

Jordan, E.C. and Balmain, K.G.
1968: Electromagnetic Waves and Radiating Systems, Prentice-Hall Inc., Englewood Cliffs, N.J., 753 p.

Ramo, S., Whinnery, J.R., and Van Duzer, T.
1965: Fields and Waves in Communication Electronics; John Wiley and Sons, Inc., New York, 751 p.

TIME-DOMAIN REFLECTOMETRY – AIR-GAP PROBLEM FOR PARALLEL WIRE TRANSMISSION LINES

Project 750037

A.P. Annan
Resource Geophysics and Geochemistry Division

Introduction

Time-domain reflectometry (TDR) methods for the determination of the electrical properties of soil in situ are discussed by Davis (1975), Davis and Chudobiak (1975). The method most frequently used in the field involves insertion of a pair of rods into the ground to form a parallel wire transmission line. An electromagnetic transient is transmitted along the line and the velocity of the guided wave is determined by measuring the travel time for a known length of line. The measured velocity is used to infer a dielectric constant for the soil. The general theory of transmission lines is given by Jordan and Balmain (1968), and Ramo et al. (1965).

A problem associated with insertion of rods into the ground is that a small air gap is frequently present around the rods. In the following analysis, the effect of this gap on field observations is examined. The results show that a serious underestimate of soil dielectric can occur.

The propagation of an electromagnetic transient along a transmission line occurs in the transverse electromagnetic mode as long as the physical dimensions of the line are small compared to the wavelength. For first order calculations, the electrical loss is neglected for our velocity analysis. The analysis of loss properties will be discussed in a later article. The voltage and current along the line satisfy the wave equation

$$\frac{\partial^2 V}{\partial z^2} = \frac{1}{U^2}\frac{\partial^2 V}{\partial t^2} \qquad (1)$$

$$\frac{\partial^2 I}{\partial z^2} = \frac{1}{U^2}\frac{\partial^2 I}{\partial t^2} \qquad (2)$$

where V and I are the voltage between and current along the two elements forming the transmission line, U is the velocity of the wave, z is distance along the line and t is time. The velocity along the line is expressed in terms of the line geometry and associated electrical properties by

$$U = \frac{1}{(LC)^{1/2}} \qquad (3)$$

where L and C are the line inductance and capacitance per unit length. For TEM wave propagation, L and C are the same as the electrostatic inductance and capacitance. For a parallel wire transmission line made of circular wires of radius b and separation 2a embedded in a homogeneous material of permittivity ε and permeability μ

$$L = \frac{\mu}{\pi}\cosh^{-1}\left(\frac{a}{b}\right) \qquad (4)$$

$$C = \frac{\pi\varepsilon}{\cosh^{-1}\left(\frac{a}{b}\right)} \qquad (5)$$

The problem we wish to analyze is the situation where the medium is magnetically homogeneous but not electrically homogeneous. The line is separated from the surrounding soil by an air gap. Since the permittivity of the air differs from that of the soil, the problem to be solved reduces to finding the new line capacitance C_g when the gap is present.

In order to find C_g it is necessary to solve the problem of finding the electric field between the two wires when one wire is held at a voltage V with respect to the other. Since C_g is the static field capacitance, the problem reduces to solving for the electric potential ϕ, (Jordan and Balmain, 1968; Jackson, 1962; Morse and Feshback, 1953). In a homogeneous material ϕ satisfies the Laplace equation

$$\frac{\partial^2 \phi}{\partial x^2} + \frac{\partial^2 \phi}{\partial y^2} = 0 \qquad (6)$$

x and y are the cartesian co-ordinates in a plane perpendicular to the transmission line.

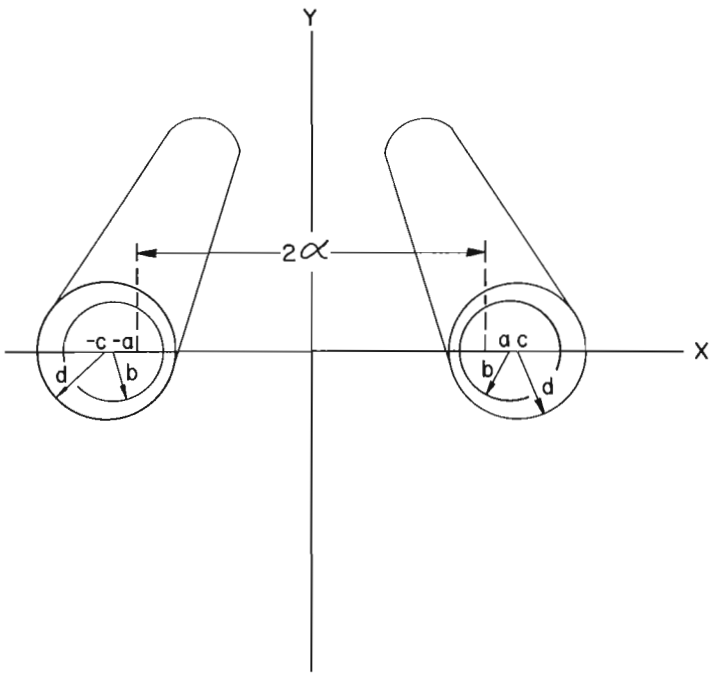

Figure 10.1. View of the two conductive cylinders with eccentric gaps.

From: Report of Activities, Part B; Geol. Surv. Can., Paper 77-1B (1977)

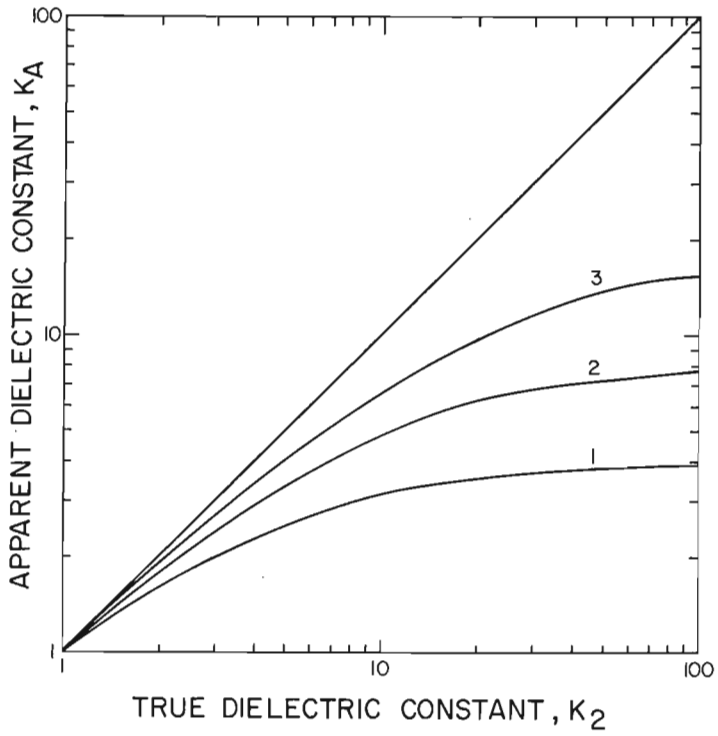

Figure 10.2. Apparent dielectric constant versus true soil dielectric constant for models 1, 2 and 3 (see Table 10.1).

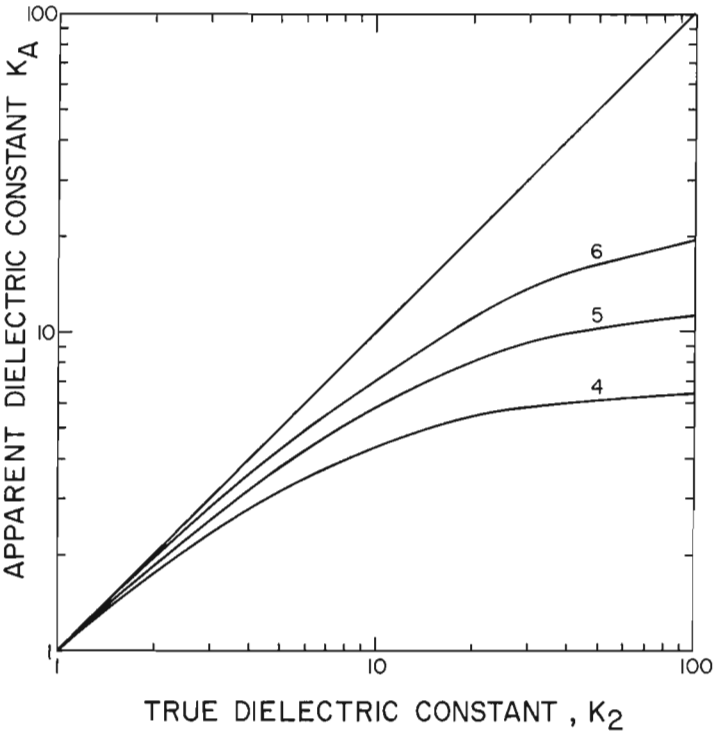

Figure 10.3. Apparent dielectric constant versus true soil dielectric constant for models 4, 5 and 6 (see Table 10.1).

Boundary Value Problem

The geometrical model of the air gap and line has to be specified in order to solve for ϕ and to determine C_g. The simplest model consists of two circular cylinders surrounded by a concentric, circular air gap. Unfortunately, this geometry is not amenable to a simple analytical solution of the Laplace equation. In order to yield a relatively easily solved problem, the centre of the air gap cylinder is slightly offset from the centre of the wire cylinder. By correctly adjusting the offset, the circular surfaces of the gap and wire can be made to conform to a bipolar co-ordinate system (Morse and Feshback, 1953). In such a geometry the Laplace equation (6) can be solved analytically and a simple expression for C_g derived.

The idealized transmission line is shown in Figure 10.1. The circular metallic wires forming the line have centres at ($x = \pm a$, $y = 0$) and radius b. The circular air gaps have centres at ($x = \pm c$, $y = 0$) and radius d.

The capacitance of the line with the air gap has been evaluated by Annan (Air gap problem for parallel wire transmission lines; Int. Rep. 1976). The resulting capacitance is

$$C_g = \frac{\pi K_1 K_2 \varepsilon_o}{K_1 \xi_1 + K_2 (\xi_o - \xi_1)} \qquad (7)$$

where the variables are

K_1 — dielectric constant of the material in the gap

K_2 — dielectric constant of the soil between the lines

ε_o — free space permittivity — 8.85×10^{-12} F/m

ξ_1 — $\cosh^{-1}(\frac{c}{d})$

ξ_o — $\cosh^{-1}(\frac{a}{b})$

The idealization of the transmission line and gap to conform to a bipolar co-ordinate system yields a non-uniform thickness to the air gap. For most applications, the air gap is small and an average gap value is most easily specified. Defining the average gap size as Δ, c/d can be expressed in terms of a, b, and Δ. The result is

$$\frac{c}{d} = \frac{\left[\left(\frac{a}{b}\right)^2 + 2n + n^2\right]^{1/2}}{1 + n} \qquad (8)$$

where

$$n = \frac{\Delta}{b} \qquad (9)$$

Effect on Field TDR Observations

The effect of the air gap in TDR measurements of soil dielectric properties can be expressed using 5 and 7. In the field, the electromagnetic wave velocity on the parallel wire transmission is measured and used to infer

the dielectric constant of the soil. From expression 3, the velocity for a line embedded in soil compared to the velocity of the line in free space is

$$\frac{U_{soil}}{U_o} = \frac{1}{(K_{soil})^{1/2}}$$

U_0 is the free space velocity and equals 3×10^8 m/s. Thus, field measurements of U_{soil} yield an estimate of the dielectric constant of the soil, K_{soil}. In practice, the observed soil velocity U_{obs}, may be contaminated by an air gap or other uncontrollable variables. As a result, a velocity measurement for the soil yields an apparent dielectric constant defined as

$$K_A = \left(\frac{U_o}{U_{obs}}\right)^2 \qquad (10)$$

If the difference between U_{obs} and U_{soil} is generated by the presence of an air gap,

$$K_A = K_{soil} \cdot F \qquad (11)$$

where

$$F = \frac{C_g}{C} = \frac{K_1 \xi_o}{K_2(\xi_o - \xi_1) + K_1 \xi_1} \qquad (12)$$

is the ratio of the line capacitance with and without a gap.

Computed Results

The effect of air gaps on lines used in the field is demonstrated in Figures 10.2, 10.3. Several line configurations which have been used for field measurements were taken for study here. The air gap effect is displayed on graphs of apparent dielectric constant as inferred from the TDR measurement versus true soil dielectric constant. In all cases, the apparent dielectric constant is lower than the true dielectric constant. In addition, as the true dielectric constant gets large, the apparent dielectric constant approaches a constant limit (which is determined by line geometry) asymptotically. The bigger the gap, the lower this limit. The line geometries considered here are summarized in Table 10.1.

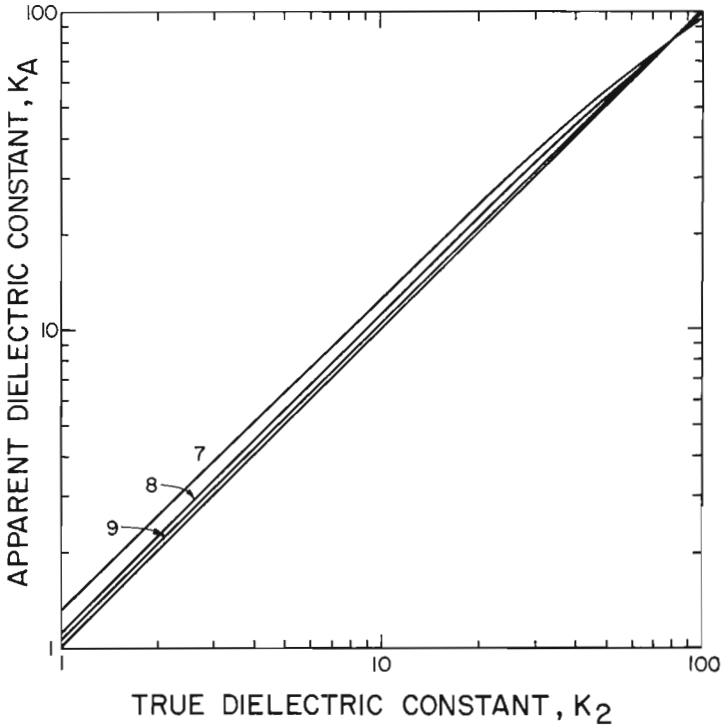

Figure 10.4. Apparent dielectric constant versus true soil dielectric constant for models 7, 8 and 9 (see Table 10.1). The gap in these models is assumed to be filled with water.

Table 10.1

Line Model Parameters

Model	a	b	Δ	K_1	K_2
1	1	.125	.125	1	varying
2	1	.1875	.0625	1	varying
3	1	.25	.03125	1	varying
4	1	.125	.0625	1	varying
5	1	.125	.03125	1	varying
6	1	.125	.015625	1	varying
7	1	.125	.125	81	varying
8	1	.1875	.0625	81	varying
9	1	.25	.03125	81	varying

Figure 10.4 shows another situation in which the air gap of geometries 1, 2, and 3 is filled with water (K_1 assumed to be 81). In this case, the apparent dielectric constant is higher than that of the soil for $K_2 < 81$. For $K_2 > 81$ the response is similar to the air gap situation for $K_2 > 1$.

Summary and Conclusions

The air gap (and water-filled gap) problem encountered in determination of the dielectric constant of soils in situ using TDR methods on parallel wire transmission lines has been analyzed theoretically. While the theoretical model is somewhat idealized when compared to the real situation, it provides quantitative estimates of the type of error which can appear with indiscriminate field measurements.

A number of conclusions have been drawn from this study. First of all, the air gap poses a serious problem if not eliminated or accounted for. The apparent dielectric constant can be grossly in error if the soil dielectric constant is large.

If the line geometry is known, the air gap error can be removed from the data. Unfortunately, the apparent dielectric constant is insensitive to the soil dielectric constant when the latter is large. As a result, a small measurement error in the apparent dielectric constant can produce gross errors in the estimate of the true dielectric constant.

The effect of a water-filled gap poses a much less serious problem. The presence of the water yields an apparent dielectric constant greater than the true dielectric constant (soils have $K_2 < 80$ for frequencies of interest here); however, this error is not nearly as large as that associated with an air gap.

References

Davis, J.L.
1975: Relative permittivity measurements of a sand and clay soil in situ: in Report of Activities, Part C, Geol. Surv. Can., Paper 75-1C, p. 361-365.

Davis, J.L. and Chudobiak, W.J.
1975: In situ meter for measuring relative permittivity of soils; in Report of Activities, Part A, Geol. Surv. Can., Paper 75-1A, p. 75-79.

Jackson, J.D.
1962: Classical Electrodynamics; John Wiley and Sons, Inc., p. 641.

Jordan, E.C. and Balmain, K.G.
1968: Electromagnetic Waves and Radiating Systems; Prentice-Hall Inc., Englewood Cliffs, N.J., 753 p.

Morse, P.M. and Feshbach, H.
1953: Methods of Theoretical Physics; McGraw-Hill, p. 1939.

Ramo, S., Whinnery, J.R., and Van Duzer, T.
1965: Fields and waves in communication electronics; John Wiley and Sons, Inc., New York, 751 p.

11. IMPULSE RADAR APPLIED TO ICE THICKNESS MEASUREMENTS AND FRESHWATER BATHYMETRY

Project 750037

A.P. Annan and J.L. Davis
Resource Geophysics and Geochemistry Division

Introduction

Knowledge of ice thickness on frozen lakes and rivers has obvious applications. In the North, frozen rivers are frequently used as roads and bridges. The water depth at these locations is also of interest. If the water is only a fraction of a metre deep, failure of an ice bridge is not catastrophic. If the water is several metres deep, lives and valuable equipment can be lost if the ice fails. Water depth information also has navigational and environmental uses. Impulse radar is a technique that can provide ice thickness and water depth rapidly and reliably. In this report, the utility of the radar technique is demonstrated.

Field Site and Radar

An ice bridge crosses the Yukon River at Dawson City, Y.T. This bridge is used annually and replaces a ferry which is used in the summer. An extensive drilling program has been carried out in the area of the bridge with the objective of determining the thickness of gravel on the river bottom. A radar sounding survey was carried out on the river ice in early April, 1976. The survey had three objectives; namely, to measure ice thickness, water depth, and gravel thickness to bedrock. The work was experimental since there was no a priori knowledge of whether the available radar equipment could probe wet materials to the depth necessary to see bedrock in the area. Furthermore, there was no way to ascertain whether the gravel-bedrock interface would be a good electrical reflector.

The radar system employed was a Geophysical Survey Systems Inc. ice thickness system which was modified for our field program. Discussions of this impulse radar can be found in Morey (1974), and Annan and Davis (1976). Two impulse antenna systems were available. A pair of 2ns impulse antennas were used to provide high resolution information from shallow depths; 10ns impulse antennas were used for low resolution probing to greater depths. The radar reflections from the subsurface are displayed on a variable-grey-scale graphic recorder. In addition, the data was recorded on an instrumentation tape recorder for further digital data enhancement processing.

Sample Field Results and Interpretation

Figure 11.1 shows a radar record obtained by traversing the ice bridge with the 2ns antennas. The first event on the record, indicated by the number 1, is the direct transmit-receive signal combined with reflections from the air-ice interface. Event number 2 is the reflection from the ice-water interface. Events 3 and 4 are multiple reflections of the ice-water return; the pulse bounces back and forth in the ice as it suffers partial reflection at the ice-air boundary and the ice-water boundary. Other features on the record which are not discussed in detail here are associated with inhomogeneities in the ice such as rocks and puddles of water on the surface. The river bottom is visible in the original data at some locations. Unfortunately, it is a very weak event and does not show up when the data is rephotographed.

The traverse across the ice bridge was repeated using the 10ns antenna system. The radar section obtained is shown in Figure 11.2. The time scale for this record is just less than three times that in Figure 11.1. The record is very different from the section in Figure 11.1. Event 1 is the direct transmitter to receiver signal plus surface reflection returns. Event 2 is the ice-water reflection and event 3 is the river-bottom reflection. The shape of the river bottom is obvious from the record. Some subbottom features are visible but there is no distinct, continuous reflector which might be identified as the bedrock interface. This is probably because of the following:

(a) much of the incident signal is reflected at the ice-water and river-bottom interfaces and thus very little signal enters the gravel;

(b) the high attenuation of the radar signal in the wet gravel; and

(c) the slow transition from gravel to weathered bedrock which would act as a very poor reflector to the radar signal.

Two other very peculiar features are observed on the radar section and are indicated by event numbers 4 and 5. Where the river bottom shows that shoals are present there appears to be a dipping reflector. While there is no definite explanation for these events, there is a good probability that they are associated with frazil ice stuck to the bottom of the surface ice. Frazil ice is the term applied to small ice crystals which form in stretches of fast-moving open water. This poorly understood form of ice frequently accumulates under down-stream ice (Osterkamp, 1976). Since there was considerable open water up-stream from the test areas, the frazil ice is a consistent hypothesis.

The interpretation of the radar records to given interface depths was accomplished by assuming a velocity of 0.167 m/ns for ice and 0.033 m/ns for water. These velocities are inferred from the commonly accepted dielectric constants for ice and water, namely, 3.2 and 81. The interpreted section is displayed in Figure 11.3.

Summary and Conclusions

The impulse radar appears to be a quick, reliable technique for measuring freshwater ice thickness and shallow water depths. About three minutes were required

From: Report of Activities, Part B;
Geol. Surv. Can., Paper 77-1B (1977)

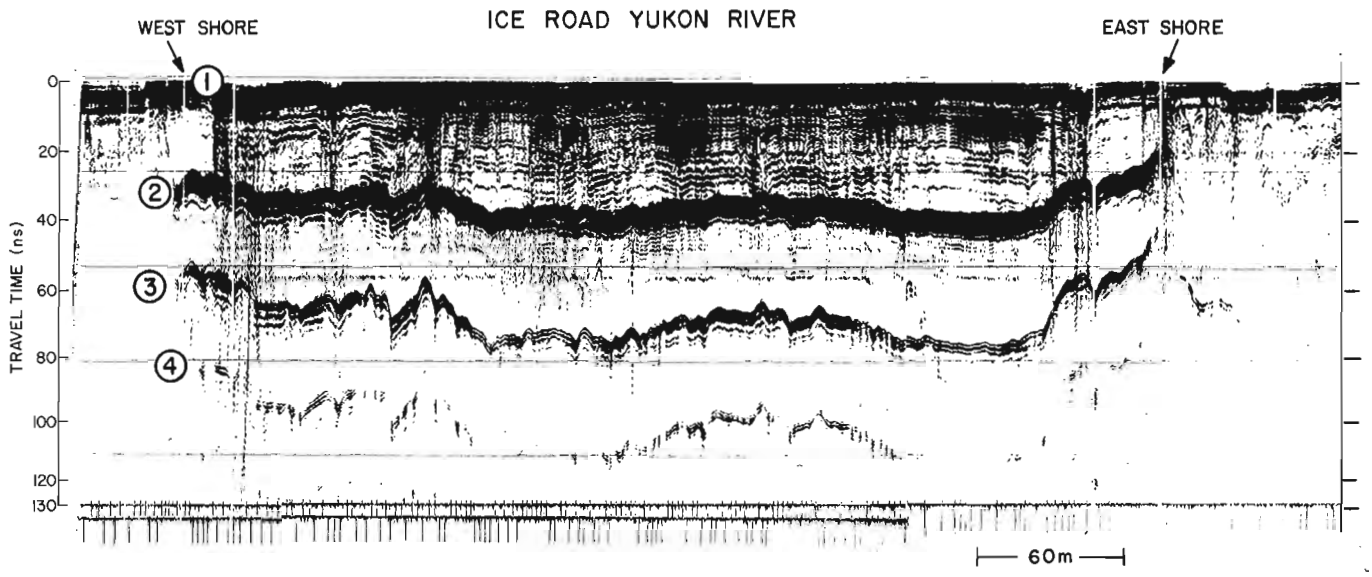

Figure 11.1. Radar section of the ice bridge across the Yukon River obtained with the 2ns impulse antennas.

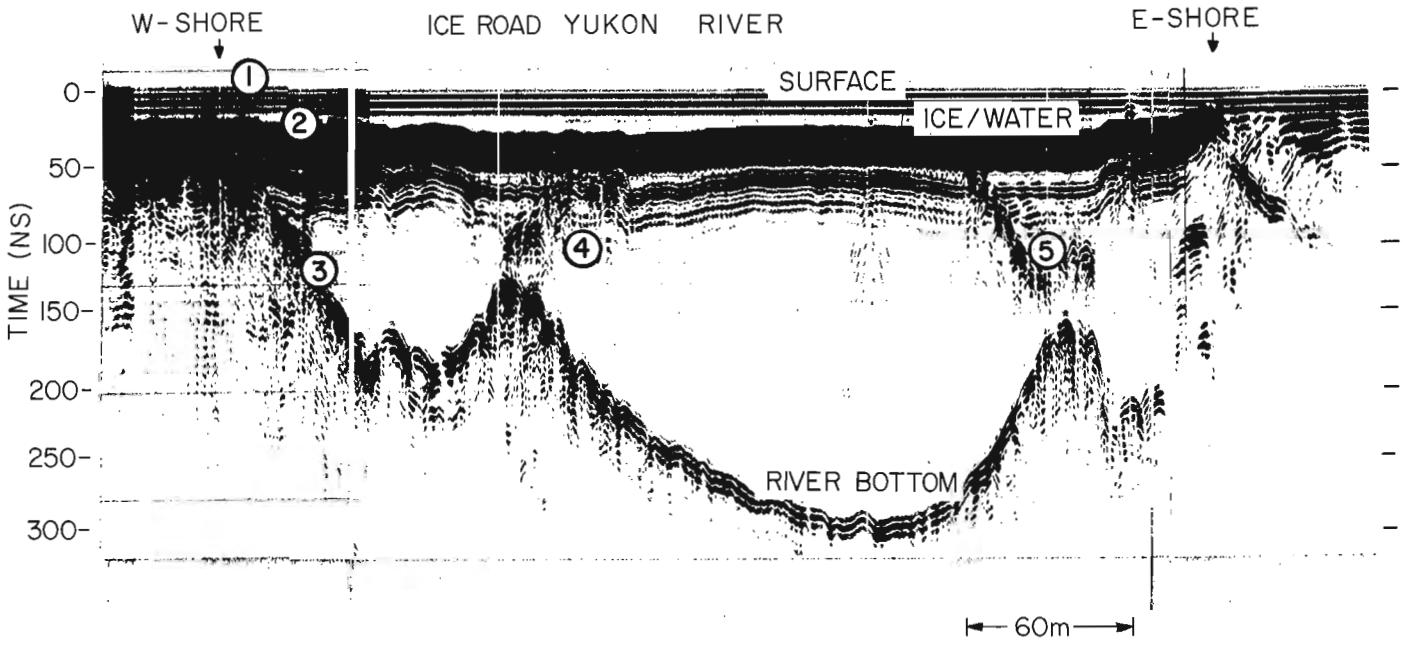

Figure 11.2. Radar section of the ice bridge across the Yukon River obtained with the ions impulse antennas.

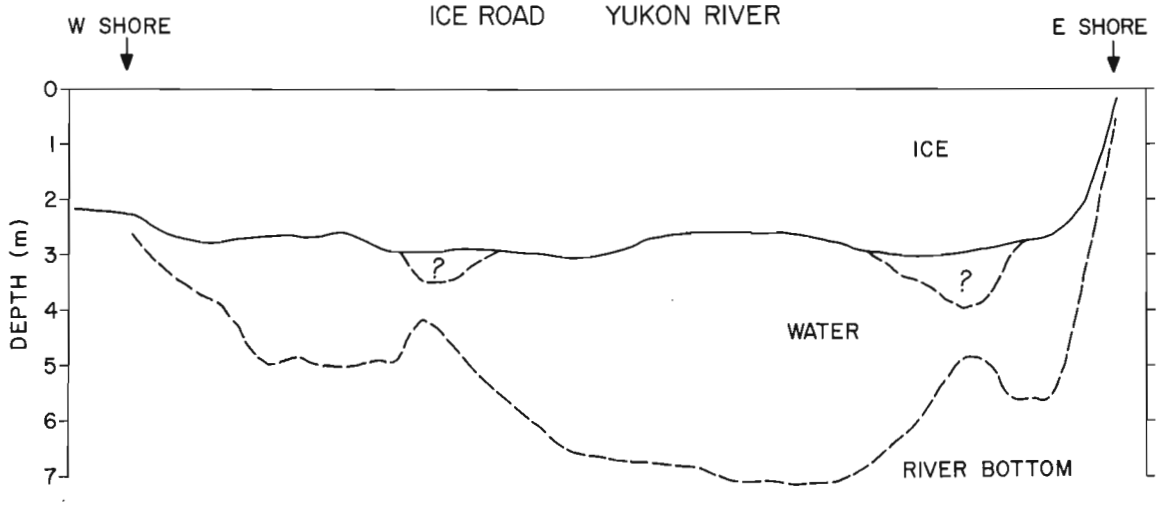

Figure 11.3. Interpretation of the radar sections in Figures 11.1 and 11.2.

to traverse the 360 m bridge and the data were immediately available. The data displayed here demonstrate the value of differing frequency-impulse duration systems. The 2ns antenna data give high resolution information about ice thickness. The 10ns antenna data yield information about much deeper structure at the expense of resolution.

The water depths have been confirmed by drilling data (J. McKinney, pers. comm.). A detailed report on the whole Yukon River survey is in the final stages of preparation and the water depths are found to be consistent with drilling and water flow information.

The suggestion that the radar can detect and delineate the extent of frazil ice is a subject which requires further research. Frazil ice is a serious problem for hydroelectric engineering projects such as those along the St. Lawrence Seaway.

References

Annan, A.P. and Davis, J.L.
1976: Impulse radar sounding in permafrost; Radio Science, v. 11, no. 4, p. 383-394.

Morey, R.M.
1974: Continuous subsurface profiling by impulse radar; Proceedings of Engineering Foundation Conference on Subsurface Exploration for Underground Excavation and Heavy Construction, Hennicker, N.H., U.S.A., p. 213-232.

Osterkamp, T.E.
1976: Frazil ice nucleation by mass exchange processes at the air-water interface; Proceedings of the Symposium on Applied Glaciology, 12-17 September, Cambridge, England; J. of Glacial., v. 19, no. 81.

12. IMPULSE RADAR AND TIME-DOMAIN REFLECTOMETRY EXPERIMENTS IN PERMAFROST TERRAIN DURING 1976

Project 750037

A.P. Annan and J.L. Davis
Resource Geophysics and Geochemistry Division

Radar sounding and time-domain reflectometry (TDR) are two new techniques for studying the high frequency electrical properties of permafrost. The Geological Survey is carrying out an extensive test program to assess these new methods which may provide valuable geotechnical information for future engineering projects in permafrost terrain. Both the radar and the TDR operate in the frequency range 1 to 1000 MHz. Frozen geological materials exhibit relatively low electrical loss in this frequency range. Both techniques provide spatial resolutions of the order of 10 cm. TDR is best suited for monitoring changes of electrical properties at fixed locations while radar is most gainfully used for laterally extrapolating information from drilling or fixed monitoring sites.

An extensive field program was conducted during the spring field season of 1976. Experimental work was carried out around Inuvik, Tuktoyaktuk, Rea Point and Norman Wells, District of Mackenzie, and Dawson City, Yukon Territory.

The work at Inuvik was based at the Inuvik Research Laboratory. Experimental surveys were conducted on the ice road to Tuktoyaktuk and on two thermally insulated sections of the Mackenzie Highway south of Inuvik. Thirty-five miles of the proposed highway route from Inuvik to Tuktoyaktuk were also surveyed.

The experiments at Tuktoyaktuk were made from the Polar Continental Shelf Project base. Further experiments, using higher frequencies, and shorter pulse length antennas, than those carried out the previous year, were conducted at the Involuted Hill test site (Annan et al., 1975a), Davis et al., 1976 and Annan and Davis 1976. The Tuktoyaktuk runway was also resurveyed.

At Norman Wells several tests were carried out on a variety of terrains. The Norman Wells runway was extensively profiled. An eight-mile section of the proposed Mackenzie Highway route was surveyed. The ice thickness and water depth were measured across two ice bridges which spanned the Mackenzie River.

Dawson City provided a relatively different geologic setting. During a brief period, ice thickness and water depth were measured on a grid on the Yukon River. Two miles of line were profiled in Hunker Creek Valley. The primary aim of this survey was to detect the gravel-bedrock interface. Unfortunately, this boundary was not detected but a strong echo from the frozen to unfrozen soil boundary was mapped. Geologic control was kindly provided by Anglo American on the Yukon River and by Du Pont Exploration at Hunker Creek. The Dawson City runway was also profiled.

At Rea Point extensive surveys were carried out on Consett River. Upstream, the Hecla sandstone formation was virtually transparent to the radar signal. Using wide angle reflection and refraction sounding (Annan et al., 1975) the propagation velocity of the radar signal in the sandstone was calculated and it was determined that subsurface structure was detected to depths greater than 30 m. Near the coast, no deep reflectors were observed. This could be caused by higher loss in the sandstone or the absence of deep reflectors. Geologic control was obtained by drilling 30 holes, 20 m deep. Test work was also performed on Frustration River north of Rea Point. Logistic support was provided during this time by Panarctic Oils Ltd. at Rea Point and Polar Continental Shelf Project at Resolute Bay. An attempt to do experimental sounding on the South Melville icecap had to be abandoned after several days of bad weather prevented flying to the icecap.

Briefly, some conclusions to date are as follows: 1) Radar can be used to map lithology in coarse grained soils; interfaces at depths exceeding 30 m have been mapped; 2) Fine grained soils exhibit significantly higher electrical loss; in clay covered areas, penetration of radar signals was less than 3 m; 3) Ice thickness on freshwater lakes and rivers can be mapped quickly and routinely; 4) Water depths of shallow lakes and rivers can be mapped from an ice covered surface; river and lake bottoms have been mapped to depths of 7 m; 5) The electromagnetic wave velocities of frozen soil and ice are so similar that ice content cannot be inferred from velocity measurements alone; and 6) Subsurface freeze-thaw boundaries can be mapped from surface observations and monitored against time.

References

Annan, A.P. and Davis, J.L.
1976: Impulse radar sounding in permafrost; Radio Science, v. 11, p. 383-394.

Annan, A.P., Davis, J.L., and Scott, W.J.
1975a: Impulse radar profiling in permafrost; in Report of Activities, Part C, Geol. Surv. Can., Paper 75-1C, p. 343-351.

1975b: Impulse radar wide angle reflection and refraction sounding in permafrost; in Report of Activities, Part C, Geol. Surv. Can., Paper 75-1C, p. 335-341.

Davis, J.L., Scott, W.J., Morey, R.M., and Annan, A.P.
1976: Impulse radar experiments on permafrost near Tuktoyaktuk, Northwest Territories; Can. J. Earth Sci., v. 13, p. 1584-1590.

From Report of Activities, Part B;
Geol. Surv. Can., Paper 77-1B (1977)

Project 750028

J.L. Davis
Resource Geophysics and Geochemistry Division

Introduction

In the field reliable communications between field personnel and base camp are necessary for safe and efficient working conditions. A walk or drive of several hours over rough terrain from camp to the work area is common for field parties each day. The difference between a minor accident or a major personal injury or the success or failure of a program may depend on the ability to communicate reliably from the area of work to the base camp. Realizing this need, an antenna with the following specifications was designed.

The antenna must be:

a) compatible with the Motorola PT-300 series transceivers;
b) omnidirectional;
c) capable of a range of at least 2 km and up to 15 km depending on local topography;
d) light-weight;
e) robust;
f) easy to assemble; and
g) easy to install.

Some reasons for these specifications are outlined below.

a) The Motorola PT-300 series transceivers are, in the author's opinion, the most reliable, short-range transceivers presently available from the Department of Energy, Mines and Resources, Technical Field Support Services. These transceivers operate at a frequency of 150 MHz and have a rated power output of five watts. The lower frequency-transceivers available from TFSS are not robust enough for field operations and they often suffer from interference from "CB'ers".

b) Field personnel may be working at many locations scattered around the base camp; thus an omnidirectional antenna is necessary.

c) A range of at least 2 km is necessary under most conditions for the antenna to be competitive with the antenna supplied with the PT-300. Normally the range will be significantly greater than the above minimum range if properly installed. The topography between stations is the major factor affecting the range. The propagation characteristics at this frequency are similar to those of VHF television.

d) Many field camps are transported by aircraft or manhauled and thus a light, robust antenna is necessary.

e) Field personnel are not usually electronic technicians and thus the antenna must be simple to assemble and use. 'Gerry-rigging' is likely to be the rule rather than the exception and the antenna must be amenable to this.

Antenna Design and Implementation Specifications

The simplest omnidirectional antenna that is likely to meet the above specifications is the vertical antenna. The vertical antenna is a short driven element, about 0.25 wavelength (λ) long, placed on the ground. This limits the choices of location and also does not permit the antenna to be raised above local obstructions. To make the antenna practical a simulated ground can be used. This

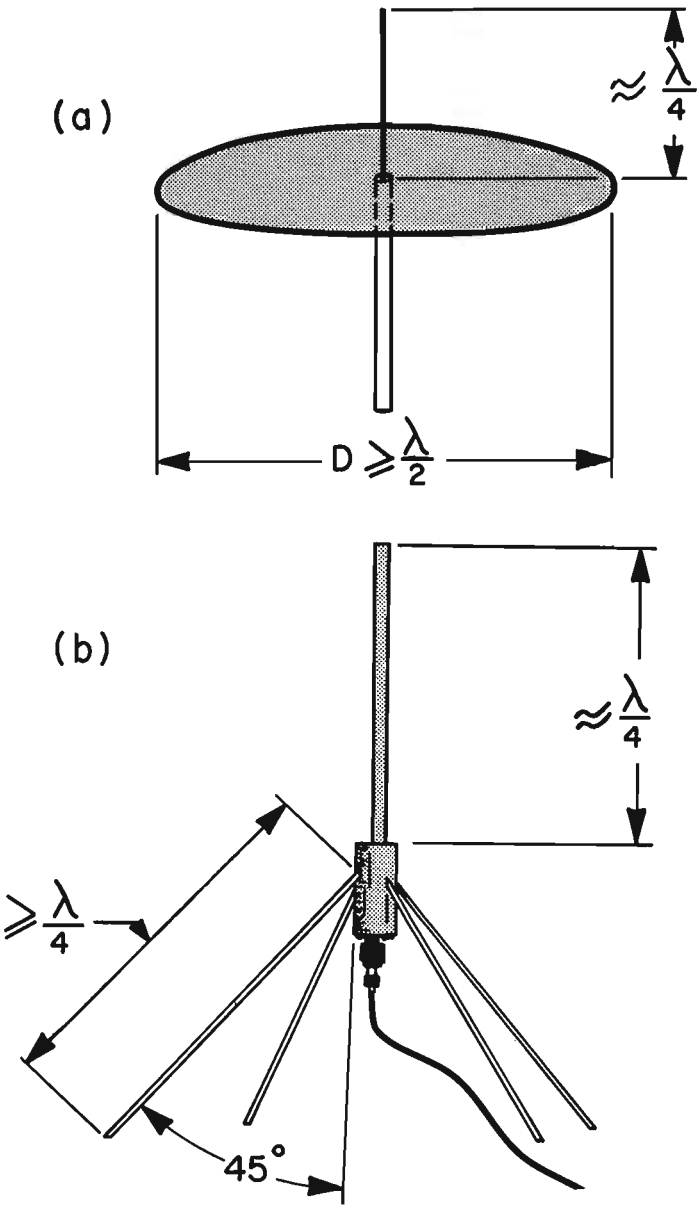

Figure 13.1. a) Ground-plane antenna
b) Ground-plane antenna with sloping radials.

From: Report of Activities, Part B; Geol. Surv. Can., Paper 77-1B (1977)

Table 13.1

Free space transmission ranges

Antenna type	G_T dB	E_T dB	G_r dB	E_r dB	Maximum Range, km $\alpha_1 = 0$	$\alpha_1 = 3$dB
Gnd. plane to gnd. plane	2	-3	2	-3	50	
Gnd. plane to gnd. plane	2	-3	2	-3		32
PT-300 to PT-300	0	-10	0	-10	6	
Gnd. plane to PT-300	2	-3	0	-10	18	
Gnd. plane to PT-300	2	-3	0	-10		13

type of radiator is known as a ground-plane antenna (Kraus, 1950; Williams, 1950, and the A.R.R.L. Antenna Book, 1960) and is shown in Figure 13.1a. A 0.25λ vertical radiator is located in the centre of a large sheet metal circular ground plane at least 0.5λ in diameter. The efficiency of the antenna increases as the dimensions of the ground plane increase.

To reduce the size and weight, the solid sheet ground plane may be replaced by radial conductors; however, the efficiency is proportional to the proximity of the radial conductors. Reduction of the number of conductors leads to a decrease in antenna efficiency.

There are a number of practical problems with the ground-plane antenna described. One is that most of the power is radiated at a high vertical angle which is wasteful, and the other problem is the low input impedance (about 20Ω) to the antenna. This low impedance makes it difficult to couple the power from the transceiver to the antenna. One change which helps reduce both these problems is to slope the radial elements downwards as is shown in Figure 13.1b. In fact, a 45 degree slope on the radials increases the input impedance to about 50Ω. This allows the antenna to be connected directly to the transceiver via commercially available 50Ω coaxial cable. A further advantage is that the angle of maximum radiation in the vertical plane is brought closer to the horizontal plane.

The ground-plane antenna potentially solves most of the specification requirements such as being omnidirectional and lightweight. The approximate dimensions of the vertical radiator is 0.25λ. In air

$$\lambda = \frac{c}{f}$$

where c = propagation velocity in free space,
3×10^8 m/s, and
f = frequency;

Thus

$$\lambda = \frac{3 \times 10^8}{1.5 \times 10^8} = 2 \text{ m},$$

and therefore the vertical element will be about 50 cm long. The radius of the ground-plane elements must be ≥λ/4 or ≥50 cm. These dimensions appear to be practical for a field antenna. The antenna can be easily elevated and thus the range should exceed the required minimum of 2 km as is discussed in Appendices 13.1 and 13.2.

The maximum free-space range between two transceivers can be estimated by using a modified radar range equation. Appendix 13.1 gives the necessary calculations. Table 13.1 shows the free-space transmission ranges between PT-300's with the existing PT-300 antennas, the ground-plane antennas, and a ground-plane antenna to a PT-300 antenna. The maximum separation between two antennas at known heights is discussed in Appendix 13.2. Figure 13.2 shows the maximum range between PT-300's with the different antenna combinations at known heights. Figure 13.2 shows a number of interesting situations which are:

1) increasing the height of the PT-300 antennas above 2 m will not increase the range because the range is limited by the transceiver's system performance,

2) there is little advantage in having a ground-plane antenna higher than 10 m when communicating with a PT-300 antenna, and

3) if the maximum practical height for the ground-plane antennas, in the field, is arbitrarily chosen to be 15 m then the range is not limited by transceiver system performance. Keep in mind that maximum ranges shown in Figure 13.2 assume a smooth earth, such as that found at sea, and does not account for hills, trees or other obstructions. Normally the ranges will be significantly less than those shown. The way to optimise the range and reliability in practical situations is to have the antennas as high as possible.

The antenna must be connected to the transceiver by a transmission line. Some of the signal is attenuated in any transmission line. Transmission lines with air dielectrics have the lowest attenuation but they are very expensive and not very robust (ARRL Antenna Book, 1960). Table 13.2 shows the attenuation, nominal diameter, and weight per length of two reasonably priced transmission lines. The RG-8/U cable is bulky and weighs four times more than an equal length of RG-58/U cable. The attenuation in the RG-58/U cable is 2.3 times greater than that of the RG-8U cable. A compromise must be

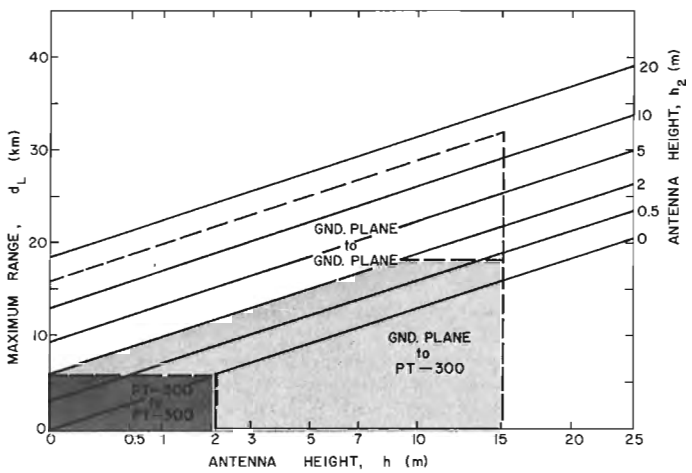

Figure 13.2. The maximum range between PT-300's with different antenna combinations at different heights.

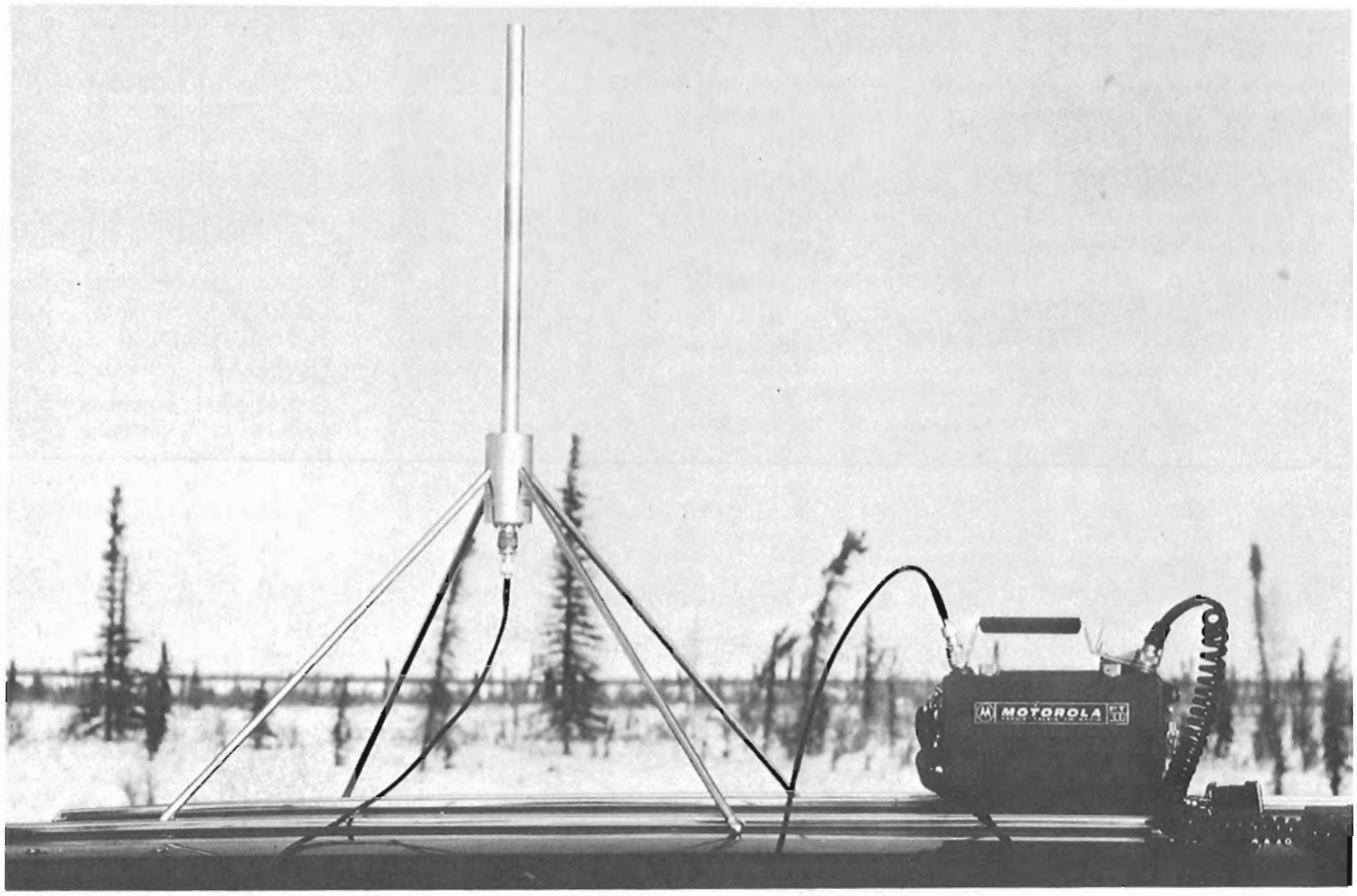

Figure 13.3. Ground-plane antenna and a Motorola PT-300 transceiver.

Table 13.2

Two standard coaxial transmission lines

Type	Impedance Ω	Diameter mm	Weight kg/m	Attenuation dB/m
RG-8/U	52	10.3	0.16	0.08
RG-58/U	53.5	5.0	0.04	0.19

made between antenna height, transmission line loss and cable weight. Note, the maximum free-space range between a ground-plane antenna with 16 m of RG-58/U and a PT-300 is reduced from about 18 km with no transmission line loss to 13 km as is shown in Table 13.1. The range with a similar length of RG-8/U is 17.7 km.

Practical Antenna Design

The practical design of the ground-plane antenna met the specifications in the following order or priority: robust, easy to assemble, simple to install and light-weight.

Figure 13.3 shows a ground-plane antenna and a PT-300. Detailed drawings may be obtained from the author. The materials are aluminum. The radials (4) are constructed of 9.5 mm diameter solid rod for robustness, and are screwed into the centre support. The vertical element is made of 19.1 mm tubing with 1.6 mm wall thickness both for robustness and to help increase the frequency band width of the antenna (Kraus, 1950). The slight increase in band width will make the antenna less sensitive to undesired impedance mismatch effects due to nearby objects. This element is also screwed into the centre support. The centre support, which holds the radials, connects the transmission line efficiently to the antenna and should be used to attach the antenna to the supporting tower. This part of the antenna is at ground potential and therefore may be connected directly to a grounded metal tower if so desired. The weight of the antenna as shown is 4 kg.

Field Trials

The antenna was set up about 3 m above ground away from any obstructions. A Buntoon Impedance Meter was used to check the impedance versus frequency characteristics of the antenna. The vertical stub was trimmed to 42.5 cm, and the impedance was measured to be 50Ω purely resistive at 150 MHz. The impedance mismatch remained less than 50 per cent over a frequency range of 148 to 152 MHz. This band width should ensure that the impedance characteristics are not severely affected by less than optimum installations. No measurements were carried out on the radiation pattern of the antenna.

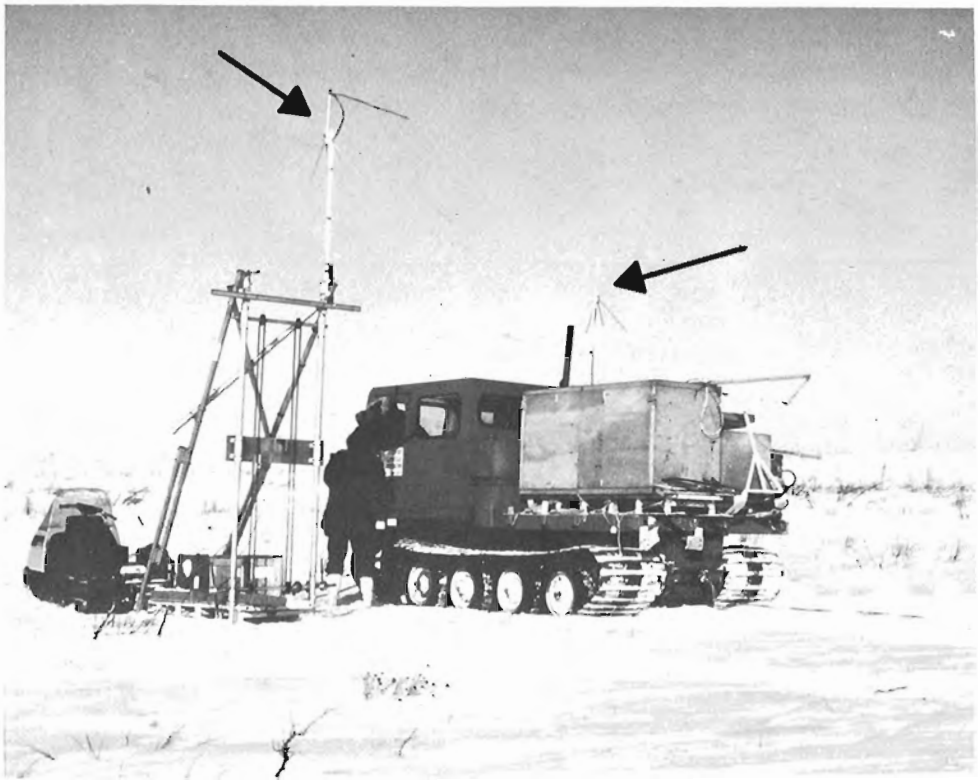

Figure 13.4

Ground-plane antennas mounted on a portable drill rig and a Nodwell.

The antenna has been used in the field in a number of environments. Figure 13.4 shows the antenna mounted on a Nodwell FN 60 and on a portable drill rig. The antennas travelled over tundra a distance of about 100 km mounted like this. The only malfunction occurred when one of the radials came loose and fell off the antenna which was mounted on the Nodwell. (The field personnel have never been quite the same since that journey either.)

A maximum range of 10 km in hilly terrain was achieved between two ground-plane antennas, one at 15 m high and the other 2 m high. At the Involuted Hill test site, reliable communications have been achieved between a ground-plane antenna at 7 m height and PT-300 antennas at ground level over ranges of 6 km, even with 30 m high hills between the antennas. An example where the ground-plane antenna showed significant superiority to the standard PT-300 antennas was when two PT-300's at a range of about 1 km and near line-of-sight could not communicate with each other. Both PT-300's could communicate with base camp behind a hill about 4 km away which had a ground-plane antenna.

Conclusions

The ground-plane antenna described here significantly increases the reliability of communications between field personnel. The antenna is lightweight, robust and easy to assemble and install. The antenna should be located as high as possible, connected with low-loss transmission line and, of course, the batteries should be at full charge for maximum range and reliability.

References

A.R.R.L. Antenna Book
1960: The American Radio Relay League, Inc., West Hartford, Conn., U.S.A., 320 p.

Glazier, E.J.D. and Lamont, H.R.L.
1958: Transmission and Propagation; The Services Textbook of Radio Vol. 5; Her Majesty's Stationary Office, London, 500 p.

Kraus, J.D.
1950: Antennas; McGraw-Hill Book Co., Inc., New York, 553 p.

Ridenour, L.N.
1947: Radar System Engineering; McGraw-Hill Book Co. Inc., New York, 748 p.

Williams, H.P.
1950: Antenna Theory and Design; Sir Isaac Pitman & Sons, Ltd., London, 522 p.

Appendix 13.1

The maximum free-space range can be found by using the radar equation without the target parameters. The equation is

$$\frac{P_r}{P_t} = \frac{G_t E_t G_r E_r \lambda^2 \alpha_1}{16\pi^2 R^2} \qquad (1\text{-}1)$$

where $\frac{P_r}{P_t}$ is the system performance (the ratio of the receiver sensisivity to the transmitted power),

G_t is the gain of the transmitter antenna,

E_t is the efficiency of the transmitter antenna,

G_r is the gain of the receiver antenna,

E_r is the efficiency of the receiver antenna,

λ is the wavelength,

R is the range between transmitter and receiver, and

α_1 is the transmission line attenuation.

Note, the attenuation in air is assumed to be negligible. The equation may be rearranged such that the range

$$R = \log^{-1}\left\{\frac{1}{20}\left[P_t - P_r + \alpha_1 + G_t + E_t + G_r + E_r + 20\log(\lambda) - 10\log(16\pi^2)\right]\right\} \qquad (1\text{-}2)$$

where P_t, P_r, α_1, G_t, E_t, G_r, and E_r are expressed in dB. For a PT-300 the receiver sensitivity is assumed to be 40 μv into a 50Ω load (P_r = -105dB) and the transmitter output power is 5W (P_t = +7dB).

Therefore $P_t - P_r$ = 112dB. Frequency of the PT-300 is 150 MHz and using Eq. (1) λ = 2 m. The estimated gains and efficiencies of the different antennas are given in Table 13.2 along with the calculated maximum free-space range.

Appendix 13.2

The solution of the maximum line-of-site range between two antennas at known heights can be found in textbooks on radio propagation or radar, such as Glazier et al. (1958) and Ridenour (1947). Simply the optical horizon distance

$$d_o = \left[h(2r+h)\right]^{1/2} \qquad (2\text{-}1)$$

where h is the antenna height, and r is the radius of the earth. Since h is small compared to r

$$d_o \approx (2rh)^{1/2}$$

Close to the earth's surface the dielectric constant of the atmosphere is slightly greater than one, and this decreases to unity at altitudes where the density approaches zero (Glazier et al., 1958). This gradient of dielectric constant causes a slight bending of the ray and has the effect of appearing to increase the earth's radius r to r'. The value of r' varies with atmospheric conditions, but its average value, for what is known as the 'standard atmosphere' is usually taken as 1.25 r. The earth's radius is 6370 km, and thus the standard value of r' is about 8500 km.

The corrected expression for the horizon distance for VHF radio waves is

$$d_o \approx (2r'h)^{1/2} \qquad (2\text{-}2)$$

If a wave is to propagate between two antennas at heights h_1 and h_2 without interception by the curvature of the earth then the maximum separation d_L between them occurs when the direct ray is just tangential to the surface, that is:

$$d_L = (2r'h_1)^{1/2} + (2r'h_2)^{1/2} \qquad (2\text{-}3)$$

Project 750028

J.L. Davis and A.P. Annan
Resource Geophysics and Geochemistry Division

Introduction

Since dry salt is an excellent electrical insulator, radio waves can propagate through great thicknesses of salt with little attenuation. This relatively unique property has made massive salt structures in geologic environments amenable to radar probing (Holser et al., 1972; Stewart and Unterberger, 1976). Most measurements of the electrical properties of salt have been made in the laboratory (Breckenridge, 1948; Cook, 1975). Furthermore, the studies have been primarily concerned with the properties of halite (NaCl), the more common variety of naturally occurring salt. The information on the properties of sylvite, KCl, the primary potash mineral mined in Saskatchewan, is extremely limited. In order to assess the utility of impulse radar techniques in the Saskatchewan potash mines, it is essential to know the electrical properties of sylvite in the frequency range 10 to 1000 MHz. This report briefly summarizes measurements of the bulk electrical properties of potash ore in situ.

Experimental Technique

The electrical properties of the salt were measured using time-domain reflectometry techniques (Fellner-Feldegg, 1969; Davis and Chudobiak, 1975). Two rods, 1.3 cm in diameter and at lengths of either 16 or 32 cm were inserted into 1.3 cm diameter holes 32 cm long drilled 5 cm apart in the tunnel wall. The two rods form a parallel wire transmission-line. Measurements of the propagation characteristics of electrical transients along the transmission-line yield estimates of the local electrical properties. More specifically, a) the propagation velocity in the line gives a measure of the real dielectric constant, K', assuming that the magnitude of the losses are small (i.e., tan δ is ($<<1$)), and b) the difference in the amplitude of the reflection from the open circuit on the short line compared to the long line gives an estimate of the attenuation of the transient in the medium. (Note: the average value of tan δ for the worst case, the clay seam, is 0.1 and thus the estimate of K' to a first order is satisfactory.)

Measurement Sites and Results

Holes were drilled in four locations with differing mineralogy in the Central Canada Potash mine. These sites as shown in Figure 14.1 are denoted 1, 2, 3 and 4. Site 1 was a sylvite rich zone; site 2 was a lower sylvite content zone; site 3 was a clay seam with both rods inserted in the plane of the seam; site 4 was at the same clay seam with rods inserted parallel to the clay seam but located in the salt above and below the seam.

The results of the experimental measurements plus other available information on the electrical properties of salts are listed in Table 14.1. There are significant variations of the dielectric constant from the various sites. The attenuation measurements are much less precise than the dielectric measurements; they should be viewed as order of magnitude estimates. The responses in the salt and clay were distinctly different.

Table 14.1

Site No.	Real Dielectric Constant K'	Attenuation, α dB/m Ave. Freq. 10-1000 MHz	Remarks
1	5.5	1.2	sylvite rich
2	4.7	1.6	lower sylvite content than in Site No. 1
3	6.4	3.0	in clay rich seam
4	5.2	2.0	across clay rich seam
Pure salt (NaCl)	5.9	0.004	Breckenridge (1948) lab. meas.
Cote Blanch Salt Dome	6.8	0.015 @400 MHz	Stewart and Unterberger (1976)
Sylvite rich (little clay visible)	5.2	0.4 @100 MHz	Laboratory measurement; Katsube (pers. comm.)

From: Report of Activities, Part B; Geol. Surv. Can., Paper 77-1B (1977)

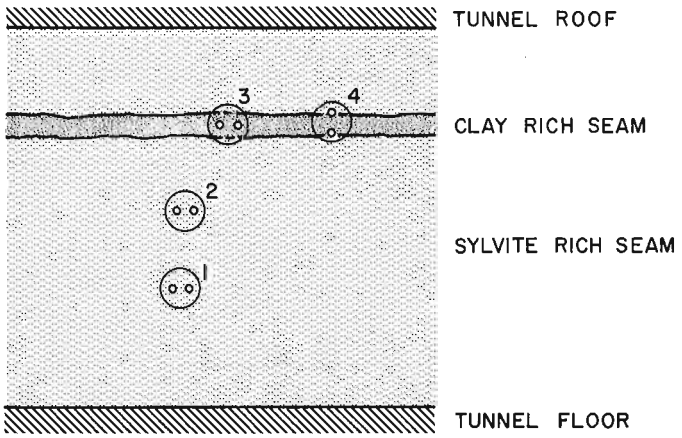

Figure 14.1. Location of TDR test sites in potash tunnel wall.

Summary and Conclusions

The Saskatchewan potash ore exhibits significantly higher electrical loss than has been reported for other massive salt occurrences. The electrical loss appears to be associated with the clay content of the salt. Sites 1 and 2 had visible amounts of clay mixed with the salt which probably accounts for the relatively high loss (compared to pure salt) observed at these sites.

The observed attenuations limit the penetration of any available radar system to much less than 100 m. Unless areas of lower clay content are encountered, radar probing should be probably limited to targets at ranges less than 50 m.

In order to obtain conclusive evidence that the clay is the primary source of electrical loss, a controlled program of measurements at sites of known mineralogy must be carried out. In addition, such measurements would indicate whether or not there are significant variations in the electrical properties of the ore as the sylvite content changes.

References

Breckenridge, R.G.J.
1948: Low frequency dispersion in ionic crystals; J. Chem. Phys., v. 16, p. 959-967.

Davis, J.L. and Chudobiak, W.J.
1975: In situ meter for measuring relative permittivity of soils; in Report of Activities, Part A, Geol. Surv. Can., Paper 75-1A, p. 75-79.

Cook, J.C.
1975: Radar transparencies of mine and tunnel rocks; Geophysics, v. 40, p. 865-885.

Fellner-Feldegg, H.
1969: The measurement of dielectrics in the time-domain; J. Phys. Chem., v. 73, p. 616-623.

Holser, W.T., Brown, R.J.S., Roberts, F.A., Fredriksson, O.A., and Unterberger, R.R.
1972: Radar logging of a salt dome; Geophysics, v. 37, p. 889-906.

Stewart, R.D. and Unterberger, R.D.
1976: Seeing through rock salt with radar; Geophysics, v. 41, p. 123-132.

15. PETROLOGY AND TECTONICS OF THE CAMBRO-ORDOVICIAN SEQUENCE IN THE QUEBEC APPALACHIANS

E.M.R. Research Agreement 1135-D13-4-173/76

W.E. Trzcienski, Jr.[1]
Regional and Economic Geology Division

This note is a preliminary report of an ongoing petrologic study in the Cambro-Ordovician sequence in the Quebec Appalachians. Its goal is the synthesis of petrologic and tectonic data in order to present a plate tectonic model for this region that incorporates the petrologic observations.

The Quebec ultramafic belt is probably a remnant of early Paleozoic oceanic crust (St. Julien and Hubert, 1975; Laurent, 1975). Tectono-stratigraphic evidence (St. Julien and Hubert, 1975) suggests that this ultramafic belt as well as the surrounding rocks were caught up as allochthonous masses. According to plate tectonic models a zone of obduction (St. Julien and Hubert, 1975) or subduction (Poole, 1976) should have been located somewhere in the neighbourhood of the ultramafic belt. In either case, providing that a later event did not destroy it, the rocks involved should show the rather unique features associated with convergent plate boundaries, that is, relatively high pressure metamorphism as well as calc-alkaline to alkaline igneous activity.

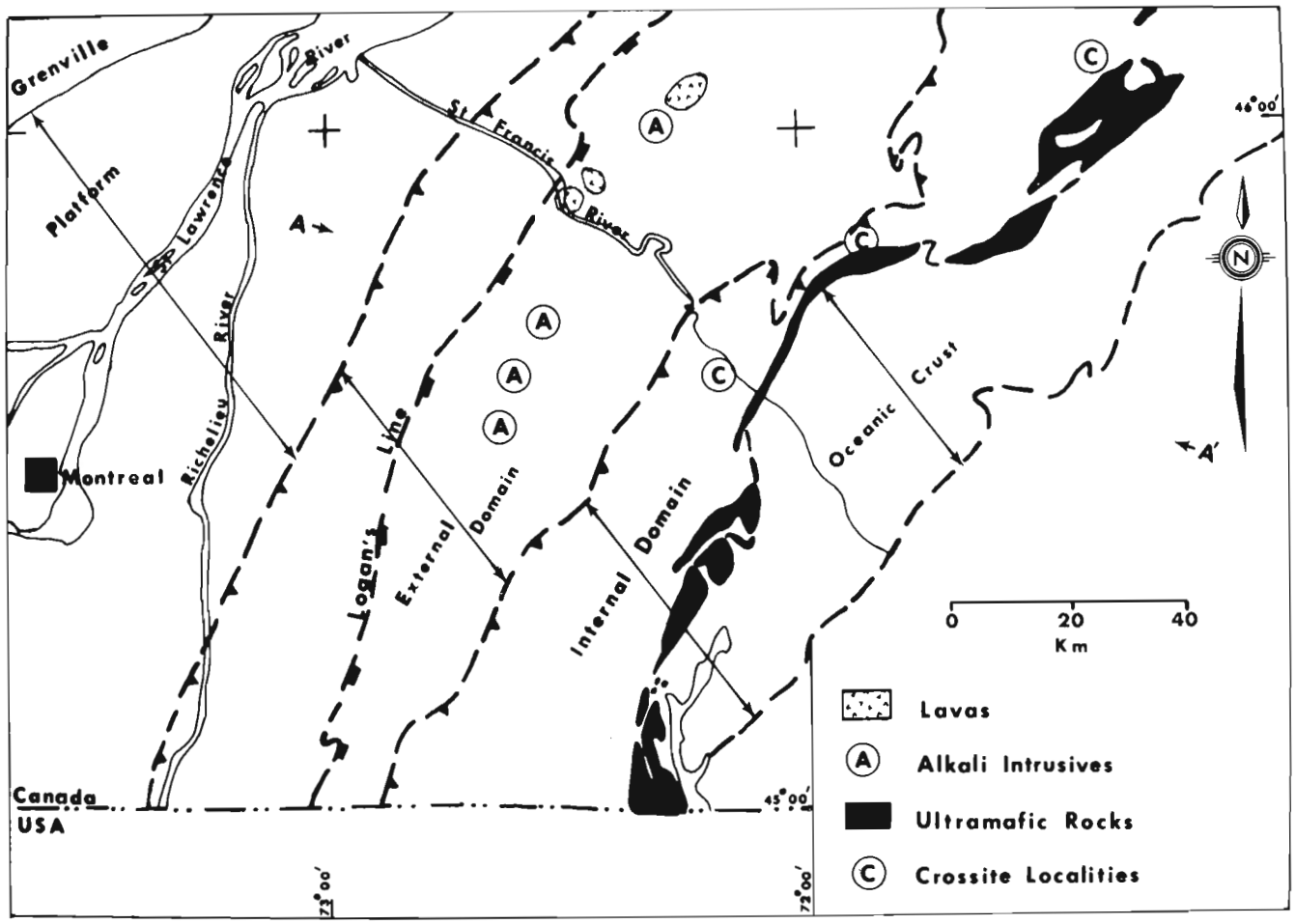

Figure 15.1. Simplified geologic map of the Cambro-Ordovician sequence of southeastern Quebec. The tectonic divisions are after St. Julien and Hubert (1975) to whom the reader is referred for details. The location of the lavas and alkali intrusives is based upon the maps of Lesperance (1963) and Clark (1964). AA' is a hypothetical cross-section shown in Figure 15.4.

[1]Département de Génie minéral, Ecole Polytechnique, Université de Montréal, Montréal, Québec H3C 3A7.

From: Report of Activities, Part B;
Geol. Surv. Can., Paper 77-1B (1977)

Figure 15.2. Pillow lavas exposed in the trap-rock quarry at St. Wencelas, Quebec.

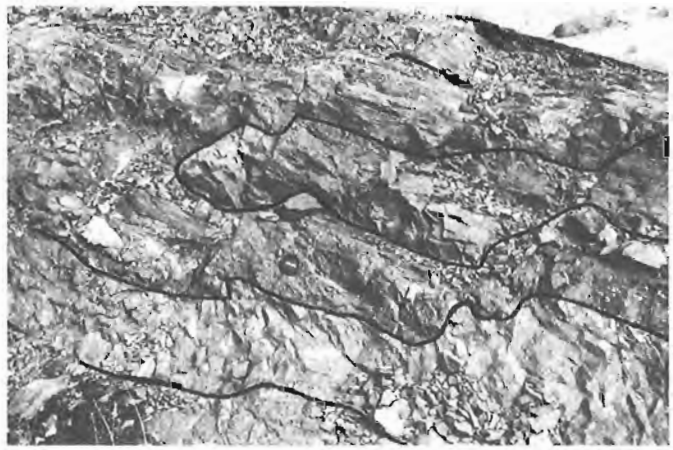

Figure 15.3. Interlayering of igneous and metasedimentary rocks in the alkali intrusive north of Chicoines, Quebec. The light coloured rock is syenite. The lens cap is resting on a band of metasediment.

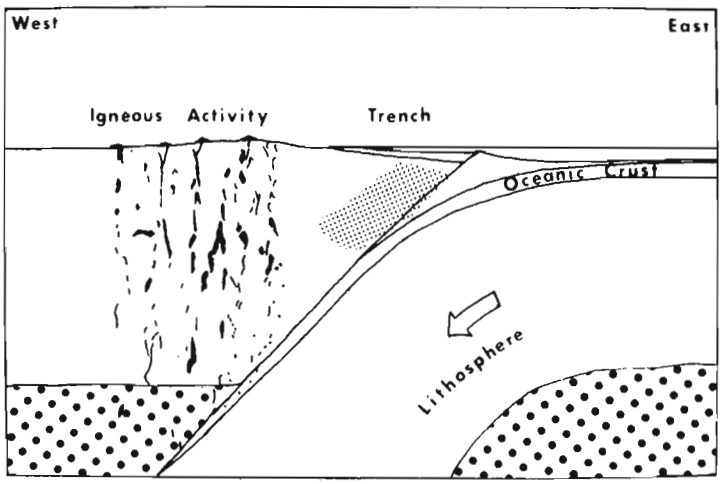

Figure 15.4.

Hypothetical Ordovician cross-section (AA' of Figure 15.1) of southeastern Quebec. The area of igneous activity corresponds to the belt of lavas and intrusives in the external domain. The finely stippled region (trench) corresponds to the crossite-bearing rocks indicative of relatively high-pressure, low-temperature metamorphism. The oceanic crust includes the ophiolite sequences of the Eastern Townships. The arrow indicates the direction of the subducting lithospheric slab. Large stipples represent the asthenosphere. (Figure adapted from Ernst, 1967.)

Crossitic amphibole suggestive of moderately high metamorphic pressures has been identified west of the ultramafic belt (Trzcienski, 1976). This type of amphibole has now been recognized in the Ham-Nord area, northeast of Asbestos, Quebec, (Trzcienski, unpubl. data) and just north of Thetford Mines (Birkett, 1976, pers. comm.). All three localities (Fig. 15.1) are on the west side of the ultramafic belt. The texture of the crossite, commonly in unoriented crystals, is suggestive of a non-penetrative deformation and deep burial of the host rocks.

About 40 km west of the crossite localities (Fig. 15.1), in the external domain of St. Julien and Hubert (1975), are a series of lava flows and alkali igneous intrusives. The lavas vary in form from flow breccias to pillow basalts (Fig. 15.2). The degree of alteration is highly variable but many of the rocks retain much of their original igneous mineralogy and texture. The better preserved rocks are commonly ophitic with plagioclase laths (commonly albitized) enclosing groundmass pyroxene – a diopside augite (Wo_{43} En_{44} Fs_{13}) with up to 1.50% TiO_2. Some of the lavas have undergone low-grade metamorphism producing prehnite and/or pumpellyite and chlorite in addition to the original igneous minerals. The best outcrops of these lavas occur in the river at Drummondville and at the trap-rock quarries in Drummondville, St. Cyrille and St. Wencelas.

Occurring in the same belt as the lavas are a series of igneous intrusions, commonly found interfingering with the country rock (Fig. 15.3). These field relations suggest that only the topmost parts of the intrusions are exposed. The country rock found in contact with the igneous rock is only slightly deformed and shows an incipient spotted hornfels texture. The southernmost intrusive near Roxton Pond is more than 1 km in diameter. The southern part of the intrusive is a mica peridotite containing olivine (Fo_{82}) enclosed in poikilitic diopside augite ($Wo_{43}En_{47}$ Fs_{10}), poikilitic kaersutite (Mg/(Mg+Fe) = 0.76) or, less commonly, poikilitic biotite (Mg/(Mg+Fe) = 0.79). Some serpentinization of the olivine has taken place. The only other primary mineral is magnetite occurring in isolated octahedra. The northern part of the intrusive is a syenite composed of titaniferous augite, kaersutite, biotite,

plagioclase, K-feldspar and minor amounts of apatite, sphene and ilmenite. Associated with these rocks are various amounts of sulphides.

North of Roxton Pond are numerous isolated outcrops of syenite along with three other rather large (2 km diameter) bodies: one at Acton Vale, one north of Chicoines and one at Notre Dame de Bon Conseil. The mineralogy of all these rocks is essentially the same as that near Roxton Pond. Two differences at Notre Dame de Bon Conseil should be noted, however. Analcime has been tentatively identified and the pyroxenes are strongly zoned (Wo_{56} En_{37} Fs_{7} to Wo_{47} En_{12} Fs_{41}). There is little doubt that all these intrusives are consanguinous but demonstration of the consanguinity between the intrusive and extrusive rocks awaits further chemical data. The spatial distribution does suggest a common parentage, but no direct links have been found between intrusive and extrusive rocks.

Doig and Barton (1968) have dated biotite by K-Ar methods in the Notre Dame de Bon Conseil intrusive at 428 m.y. This age near the Ordovician-Silurian boundary correlates well with the postulated age of deformation in this area (St. Julien and Hubert, 1975).

Although all the data have not been assembled and any model is always subject to change it is interesting to compare petrologic observations described above with current plate tectonic models from an idealized cross-section of a consuming plate margin (Fig. 15.4) the sequence proceeding from the ocean toward the continent is: oceanic crust, a zone of subduction with high P and low to moderate T metamorphism, and finally a zone of igneous activity (intrusive and extrusive). From southeast to northwest in southern Quebec one observes: (1) the ophiolites of the ultramafic belt, (2) moderately high pressure metamorphism as evidenced by crossite-bearing rocks, and (3) igneous activity, both intrusive and extrusive. One can easily fit into the ideal plate tectonic model (Fig. 15.4) the three distinct petrologic regions of southeastern Quebec. If this model is relevant, the Eastern Townships of Quebec represent the remnants of an Ordovician, westward dipping subduction zone. The model remains subject to change as new data are acquired.

References

Clark, T.H.
1964: Yamaska-Aston area; Que. Dep. Nat. Resourc., Geol. Rep. 102, 192 p.

Doig, R. and Barton, J.M., Jr.
1968: Ages of carbonatites and other alkaline rocks in Quebec; Can. J. Earth Sci., v. 5, p. 1401-1407.

Ernst, W.G.
1976: Petrologic phase equilibria; W.H. Freeman and Company, San Francisco, 333 p.

Laurent, R.
1975: Occurrence and origin of the ophiolites in southern Quebec, Northern Appalachians; Can. J. Earth Sci., v. 12, p. 443-455.

Lesperance, P.J.
1963: Acton area; Que. Dep. Nat. Resourc., Prel. Rep. 496, 9 p.

Poole, W.H.
1976: Plate tectonic evolution of the Canadian Appalachian region; in Report of Activities, Part B, Geol. Surv. Can., Paper 76-1B, p. 113-126.

St. Julien, P. and Hubert, C.
1975: Evolution of the Taconian orogen in the Quebec Appalachians; Am. J. Sci., 275A, p. 337-362.

Trzcienski, W.E., Jr.
1976: Crossitic amphibole and its possible tectonic significance in the Richmond area, southeastern Quebec; Can. J. Earth Sci., v. 13, p. 711-714.

Project 720084

R.L. Grasty
Resource Geophysics and Geochemistry Division

In 1975 the Federal-Provincial Uranium Reconnaissance Program (URP) commenced with airborne radioactivity surveys in Manitoba, Saskatchewan, and Ontario utilizing the Geological Survey of Canada high sensitivity gamma-ray spectrometer system. In 1976 three additional aircraft under contract to the Federal Government were involved in the program. With the vast amount of gamma-ray data becoming available it was considered highly desirable that the results from all four systems should have some common basis for comparison. In the case of the three radioelements and their ratios this can be readily achieved through the conversion of count rates in the respective windows, after appropriate correction, to equivalent ground concentrations of potassium, uranium and thorium, based on flights over the Breckenridge calibration strip (Grasty, 1976). The radioelement data would then not depend on the particular system flown, e.g. its sensitivity, flying height or sampling period. This calibration procedure was adopted for the presentation of the contour maps of potassium, uranium and thorium and for their respective ratios for all 1975 Uranium Reconnaissance Program surveys.

The calibration and standardization of total count measurements, however, is a more complex problem. In 1974 and 1975, the International Atomic Energy Agency (IAEA) convened two meetings to consider and recommend uniform measurement units for radioactivity surveys (IAEA, 1976). As a result of the discussions, it was decided that the most practical solution to the calibration of total count measurements was to use uranium as a standard and define a new unit called a 'Unit of Radioelement Concentration', abbreviated 'ur'. This new unit is defined in the following way: 'A geological source of one unit of radioelement concentration produces the same instrument response as a source containing 1 ppm of uranium in radioactive equilibrium'. Although it could be argued that this new unit is synonomous with 'equivalent uranium' the new terminology avoids any implication that the observed radioactivity originates entirely from uranium. This paper explains the procedures adopted by the Geological Survey in following the IAEA recommendations in reporting total count measurements in terms of the new 'ur' unit.

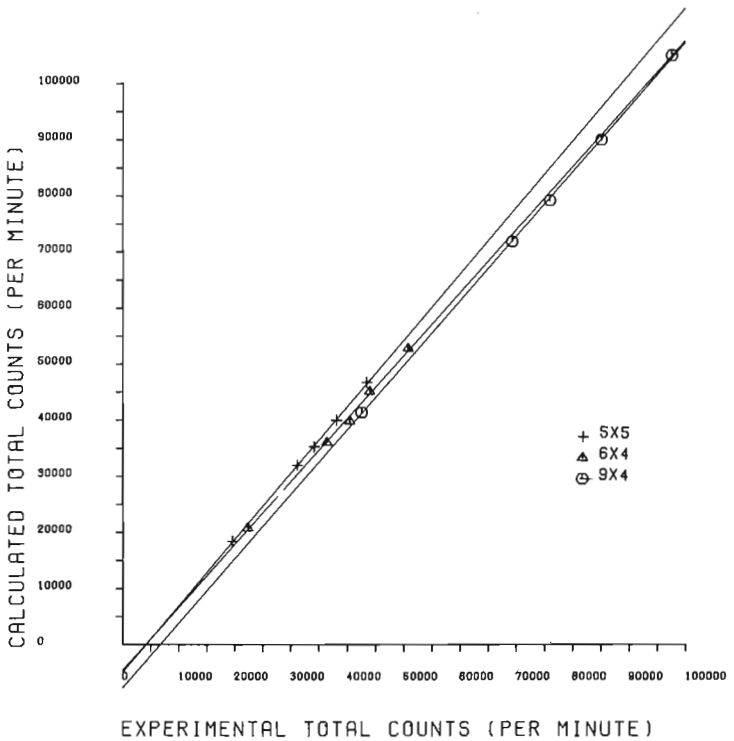

Figure 16.1. Comparison of experimental and calculated total count rate.

Through the use of sophisticated computational technique considerable information has recently become available on the energy distribution of the natural gamma-radiation field and its variation with elevation above the ground (Beck, 1972; Lovborg and Kirkegaard, 1975). By combining the information of the gamma-radiation field with the calculated detector response, it is possible to calculate the total count rates that would be observed over uniformly radioactive sources for cylindrical detectors of different sizes.

To verify the theoretical calculations, experiments were carried out in the summer of 1976, using three large cylindrical NaI(Tl) detectors commonly used in airborne surveys to compare calculated and measured total count rates on the five calibration pads at Uplands airport, Ottawa (Grasty and Darnley, 1971). The crystals, a 12.7 x 12.7 cm (5 x 5 inch), 15.2 x 10.2 cm (6 x 4 inch) and a 22.9 x 10.2 cm (9 x 4 inch), were placed at the centre of each pad, approximately 2 cm above the surface, and the output from the photomultipliers fed into a multi-channel analyzer interfaced to a Texas Instrument 960 A mini-computer. Details of the instrumentation have been described by Bristow (1975). Programs stored in the computer were then utilized to compute the counts recorded in the standard total count window from 0.41 to 2.81 MeV.

Table 16.1

Calculated Total Count (0.41-2.81 MeV)
Per Unit Concentration of the Radioelements
(At Ground Level)

Crystal Size	Total Count (c/s)		
Centimetres	Potassium (%)	Uranium (ppm)	Thorium (ppm)
12.7x12.7	71.9	27.7	13.2
15.2x10.2	60.7	22.3	10.7
22.9x10.2	162.0	62.3	29.6

From: Report of Activities, Part B;
Geol. Surv. Can., Paper 77-1B (1977)

Table 16.2

Analyses of the Uplands Test Pads

	Pad 1	Pad 2	Pad 3	Pad 4	Pad 5
K (%)	1.70	2.27	2.21	2.21	2.33
eU (ppm)	2.4	7.3	3.0	2.9	11.7
eTh (ppm)	8.9	12.6	26.1	40.8	13.2

Table 16.1 shows the predicted total count rate for each of the three crystals per unit concentration of the radioelements, as calculated by L. Lovborg of the Danish Atomic Energy Commission (Lovborg et al., in press). Utilizing the results of core sample analyses from the five pads, shown in Table 16.2 (Grasty and Darnley, 1971), the expected total count rates were then calculated for each crystal over all five pads. These results are presented graphically in Figure 16.1. Using a least squares technique, a straight line was fitted to the data for the three crystals and gave values of the slope of 1.18 ± 0.01 for the 5 x 5-inch crystal, 1.12 ± 0.03 for the 6 x 4-inch crystal and 1.15 ± 0.01 for the 9 x 4-inch crystal. The computed least squares line is shown in Figure 16.1. The fact that the slope (the ratio of the calculated to observed total count rate) has a value slightly higher than unity can be explained by the lack of downward scattered lower energy radiation due to the finite size of the calibration pads and also by the detector covering which absorbs some radiation. The intercept on the experimental axis arises from background radiation due to cosmic radiation, atmospheric radioactivity as well as the radioactivity of the equipment.

Calculated and measured total count rates were also compared for the Geological Survey Skyvan system utilizing twelve 22.9 x 10.2 cm crystals flying over the Breckenridge calibration strip. The experimental values were obtained at 125 m and were compared to values calculated at 150 m. The extra 25 m used in the calculations compensates for scattering and absorption in the aircraft structure and detector housing beneath the crystals, which is equivalent to approximately 25 m of air. Based on the mean concentration of the test strip, the calculated total count rate of 2046 c/s compared favourably to the experimental value of 1990 c/s. Both the ground and airborne experiments demonstrate that the total count rate can be calculated quite accurately for a variety of crystal sizes over sources of different radioelement composition.

One difficulty in comparing total count systems arises from the difference in the potassium, uranium and thorium gamma-ray spectra. The thorium daughters ^{212}Pb and ^{228}Ac and the uranium daughter ^{214}Pb have strong emission lines between 0.16 and 0.4 MeV and consequently the detector total count response to thorium and uranium shows large fluctuations when the lower level discriminator setting varies between these energy limits. This is illustrated in Table 16.3 which shows the uranium equivalent of potassium and thorium as a function of the energy of the lower level discriminator, for a portable instrument (IAEA, 1976). The table shows that with a lower energy threshold of 0.15 MeV, a source with a concentration of 1% potassium will give the same total count rate as a source containing only 1.33 ppm uranium.

Table 16.3

The Uranium Equivalent of Potassium and Thorium, in 'ur' as a Function of the Energy of the Lower Level Discriminator for a 3.81 cm x 2.54 cm NaI(Tl) Detector (IAEA, 1976)

MeV	1% K	1 ppm eTh
0.15	1.33	0.44
0.20	1.58	0.45
0.30	1.91	0.43
0.40	2.35	0.49
0.50	2.45	0.47

Table 16.4

The Uranium Equivalent of Potassium and Thorium, in 'ur' for some NaI(Tl) Detectors at Ground Level (Lower Level Discriminator Set at 0.41 MeV)

Crystal Size Diam. x Height inches	1% K	1 ppm eTh
4x4	2.59	0.477
5x5	2.60	0.477
6x4	2.60	0.477
9x4	2.61	0.477
11 1/2x4	2.61	0.477

These results are in close agreement with those presented graphically by Lovborg et al. (1976). Since the relative efficiency of two detectors can vary with the energy of the incident gamma-ray photons, two total count systems calibrated in 'ur', over a pure uranium source may not indicate the same ur value over the same geological source even if their lower level discriminator settings are the same. However, Lovborg et al. (in press), have shown that for ground measurements of radioactivity, provided the total count window has a lower energy threshold of about 0.41 MeV, then the uranium equivalent of potassium and thorium are almost independent of the detector used. Table 16.4 shows the calculated uranium equivalent of 1 ppm thorium and 1% potassium for five such crystals at ground level. The table shows that for all five detectors, 1 ppm thorium will give the same total count rate as 0.477 ppm uranium. Similarly, 1% potassium has a uranium equivalent of 2.60 ppm uranium.

Another important consideration is the effect of altitude on the total count response to the three radioelements. Table 16.5 shows the calculated uranium equivalent of potassium and thorium at an altitude of 150 m for the same five crystals compared previously. It can be seen that the uranium equivalent of thorium and potassium is the same for all five crystals, however, the values are different to those at ground level (Table 16.4).

Table 16.5

The Uranium Equivalent of Potassium and Thorium, in 'ur' for some NaI(Tl) Detectors at 150 m (Lower Level Discriminator Set at 0.41 MeV)

Crystal Size	1% K	1 ppm eTh
4x4	3.01	0.497
5x5	3.01	0.497
6x4	3.00	0.497
9x4	3.00	0.496
11 1/2x4	3.00	0.496

This is because the gamma-ray spectrum for each radioelement varies appreciably with elevation above the ground due to the build-up of lower energy Compton scattered radiation. There is also a considerable attenuation of the strong low energy emission lines. The results show that a system calibrated at ground level over a pure uranium source will indicate 0.477 units of radioelement concentration at ground level over a pure thorium source of 1 ppm. However a system calibrated at 150 m and flown at the same altitude over the same thorium source will indicate 0.497 units of radioelement concentration. Similarly, a 1% potassium source will indicate 2.60 ur at ground level and 3.00 at 150 m. The variation is greater for potassium since it has only one gamma-ray emission line at 1.46 MeV whereas the thorium and uranium decay series have many gamma-ray emission lines. It should be emphasized that these results presented in Tables 16.4 and 16.5 are only valid for detectors with their lower energy thresholds set at 0.41 MeV, and in general are not valid for systems with significantly different thresholds. The total count window for the Geological Survey system has this particular threshold. Because of this altitude effect it is theoretically only possible to compare total count systems flown and calibrated at similar altitudes. However, in practice, problems will only arise from a comparison of systems calibrated at different altitudes when they are flown over sources which are relatively pure in one or other of the radioelements. Even in the worst possible case, the errors will amount to a maximum of 14%, which is comparable to other uncertainties in the airborne measurements, i.e. soil moisture etc. In the Federal-Provincial Uranium Reconnaissance Program all systems are flown at a nominal survey altitude of 125 m and provided they are correctly calibrated at this altitude, the problem does not arise.

Ideally, the procedure to follow in calibrating an airborne total count system would be to fly over a pure uranium source of known concentration in order to convert the total count measurements to units of radioelement concentration. However such ideal sources of sufficient size and uniformity of radioactivity are difficult, if not impossible, to find, and an alternative procedure has to be devised. At first sight an obvious solution would be to carry out a ground survey of an airborne calibration strip using a calibrated total count instrument, enabling the ur value of the strip to be determined. Because of the variation, with survey height, of the spectra from the three radioelements, this has been shown to lead to some error. Since we have shown for a variety of crystals that the total count can be reliably calculated over sources of varying radioelement composition, a theoretical approach appeared to be warranted.

Table 16.6

The Uranium Equivalent (Units of Radioelement Concentration) of the Breckenridge Calibration Strip for some NaI(Tl) Detectors

Crystal Size Diam. x Height (inches)	Units of Radioelement Concentration (ur)
4x4	10.9
5x5	10.9
6x6	10.8
9x4	10.8
11 1/2x4	10.8

The Breckenridge test strip has a mean concentration of 2.03 % potassium, 0.92 ppm equivalent uranium and 7.70 ppm equivalent thorium (Grasty, 1976). Based on these results, the uranium concentration in ppm that would give the same total count rate at an altitude of 150 m was calculated from the data presented in Table 16.5 for the five different crystals. This uranium concentration in ppm is then by definition the ur value of the calibration strip. The results are presented in Table 16.6 and as expected are similar for all crystals, suggesting that the results are independent of the crystal size, provided the lower energy threshold is set at 0.41 MeV.

The spectrometer systems operated by the contractors for the Uranium Reconnaissance Program utilize 4 x 4 x 16 inch, square prismatic crystals which are combined in three groups of four to give compact detector volumes of approximately 1000 cubic inches. Because of the lack of symmetry about the vertical axes for these particular crystals it is an extremely complex problem to calculate their expected total count rate. In order to calibrate these particular systems it is assumed that their total count responses to the three radioelements are similar to those of the large cylindrical detectors and that for all systems at an altitude of 125 m the Breckenridge calibration strip has 10.8 units of radioelement concentration.

The experimental procedure in calibrating the total count rate of each system consists of flying at different altitudes over the test strip. From these flights, a mean total count rate can be found for each system at the nominal survey altitude of 125 m. This is achieved by fitting an exponential to the variation of total count rate with survey altitude. This procedure is more accurate than flying only once at an altitude of 125 m. The relationship of mean count rate and the radioactive concentration of the strip can then be utilized to convert all total count rates to the new units of radioelement concentration. This calibration procedure, because of its theoretical nature is far from ideal, but is at least

superior to the present practice of reporting total counts as counts per sampling interval, which gives no basis for comparing systems.

References

Beck, H.L.
1972: The physics of environmental gamma radiation fields; in the Natural Radiation Environment II, Springfield, ERDA, v. 1.

Bristow, Q.
1975: Gamma-ray spectrometry instrumentation; in Report of Activities, Part C, Geol. Surv. Can., Paper 75-1C.

Grasty, R.L.
1976: A calibration procedure for an airborne gamma-ray spectrometer; Geol. Surv. Can., Paper 76-16.

Grasty, R.L. and Darnley, A.G.
1971: The calibration of gamma-ray spectrometers for ground and airborne use; Geol. Surv. Can., Paper 71-17.

International Atomic Energy Agency
1976: Radiometric reporting methods and calibration in uranium exploration; Tech. Rep. Series 174, IAEA, Vienna.

Lovborg, L., Grasty, R.L., and Kirkegaard, P.
Aerial techniques for environmental monitoring; Proceedings of American Nuclear Society Symposium, Las Vegas, March, 1977. (in press).

Lovborg, L. and Kirkegaard, P.
1975: Numerical evaluation of the natural gamma radiation field at aerial survey heights; Danish Atomic Energy Commission, Riso Report 317.

Lovborg, L., Kirkegaard, P., and Mose Christiansen, E.
1976: Exploration for uranium ore deposits; IAEA, Vienna.

17. DETERMINATION OF SEDIMENT TRANSPORT RATE IN THE MINAS BASIN, NOVA SCOTIA: PRELIMINARY RESULTS OF THE FIRST TRACER EXPERIMENT USING RADIOISOTOPES

Project 740012

Bernard F.N. Long
Atlantic Geoscience Centre, Dartmouth

Introduction

Sediment tracer experiments, using radioisotopes, constitute one aspect of the research currently in progress to determine sediment transport rates and directions in the Minas Basin. The overall aim of the research is to obtain a fuller understanding of the nature and movement of the unconsolidated sediments of the Minas Basin, and to develop a sedimentary budget for the system. The site selected for the first experiment (Fig. 17.1), which took place from October 27 to November 17, 1976, was the large intertidal sand bar at Economy Point (described by Klein, 1970) and is illustrated in Figure 17.2. The natural radioactivity was low in this area; the mean on the experimental site was 30 Cps.

The sediment tracer experiments are concerned with the movement of the sand fraction in the intertidal zone. The purpose is to establish rates of sediment transport by direct experimental observation using a small sample of artificial sand, tagged with a short lived radioisotope. This technique thus supplements indirect extrapolations from hydrodynamic observations.

The experimental design used for determining the movement of transported sandy material was established by Crickmore and Lean (1962, 1963), Courtois and Hours (1965), Courtois and Sauzay (1966), and Sauzay (1968).

One kilogram of glass sand which has the same dynamic characteristics as the natural sediment was released at the study site and its dispersion by wave and current processes was monitored on a regular basis. The glass contained 0.5% gold which was made radioactive to the level of 2 curies. Specifically, the monitoring procedure establishes the movement of the tracer material by locating the position of the centre of gravity of the dispersed sample. From this information it is possible to calculate the bedload transport of sand through the study site.

Material and Equipment

The tracer

The tracer used was ^{198}Au encased in 1 kg of non-reactive glass fragments. The glass composition was:

SiO_2	50.0%
Al_2O_3	20.0%
CaO	18.0%
MgO	6.0%
TiO_2	5.0%
Au	0.5%

The tracer material was released at low tide at 11:30 h on October 27, 1976.

Only the γ radiation, which is 30% of the total radiation was measured during the monitoring procedure. The half life of this isotope is 2.7 days.

Detector and Probes

The detection equipment was a Saphimo-Stel marine probe (gamma probe detector, type: SGRS 54 1, with an NaI crystal of 1x1.5") and a Saphimo-Stel detector (type IPP4). The main specifications of this equipment are:

Sensitivity over 8 ranges

0 — 15 Cps	0 — 1 500 Cps
0 — 50 Cps	0 — 5 000 Cps
0 — 150 Cps	0 — 15 000 Cps
0 — 500 Cps	0 — 50 000 Cps

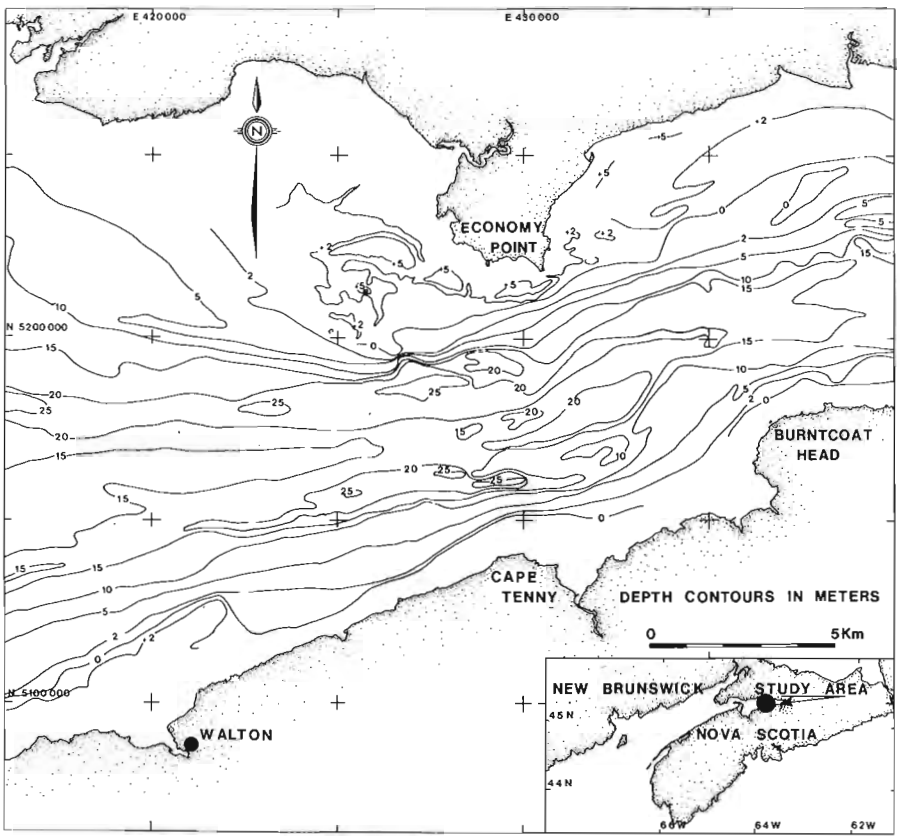

Figure 17.1. Bathymetry of study area in Minas Basin.

From: Report of Activities, Part B; Geol. Surv. Can., Paper 77-1B (1977)

Table 17.1

Position and Rate of Movement of the Centre of Gravity (CG) as a Function of Time

Interval between the detection No.	Interval in days between two detections	Position of CG in metres to East of the release point	U_{mo}
1- 2	1	24	12.0
2- 3	1	32	10.67
3- 4	1	29	7.25
4- 5	1	28	5.60
5- 6	1	53	8.83
6- 7	1	23	3.29
7- 8	5	48	4.00
8- 9	1	62	4.77
9-10	3	67	4.19

o = Current meter x = Immersion point

Figure 17.2. Immersion site.

Table 17.2

Evolution of the Activity as a Function to Time on the Surface

Time (Days)	Activity deter.[1] (Cps)	Activity Cor.[2] (Cps)	Activity A_o[3] (Cps)	Activity A_o mCi	A_o-N_o	N_o/A_o
2	13 562 000	13 562 000	22 603 333	753	1269	0.372
3	8 260 375	8 260 375	18 989 367	632	1390	0.313
4	11 196 725	11 196 725	33 923 059	1114	908	0.551
5	5 317 125	6 283 875	22 850 454	714	1308	0.353
6	3 623 750	4 710 875	22 221 102	740	1282	0.366
7	4 680 625	6 084 812	38 030 075	1188	834	0.588
12	412 900	536 770	11 182 708	349	1673	0.173
13	219 150	284 895	9 496 500	296	1726	0.146
16	30 350	43 838	2 435 493	76	1945	0.038

[1]Activity deter.: Activity Reading on the sand bar
[2]Activity cor.: Activity corrected by the ratio: Activity of Calibration/Activity measured on the detection day
[3]Activity A_o: Activity adjusted as if there were no decay

Dissemination of energy over 12 ranges

50 keV	250 keV	800 keV
100 keV	300 keV	1000 keV
150 keV	400 keV	1500 keV
200 keV	600 keV	2000 keV

Two laboratory calibrations of the probe were carried out prior to the experiment (Sauzay, 1968), which included a threshold energy calibration and a geometric calibration expressed as the number of counts per second per unit of activity per surface area (1 $\mu Ci/m^2$) for a source buried at the depth 20 cm.

The resulting calibration function was:

$$f = f_o e^{-\alpha z}$$

where: f_o and α are specific coefficients of the probe relating to the geometry and the threshold and z is the mean depth of burial (in centimetres). For this probe and for the threshold of 50 keV a calibration was tested before and after the experiment (f_o = 30 and α = 0.10).

Field Monitoring Procedure

During the experiment, each day at low tide (during the time when the sand bar was accessible from the shoreline) the operators detected the cloud of radioactive sand. Using the probe and integrator, one person surveyed the radioactive area, following parallel lines 10 m apart and taking note of the activity detected. Two men, in radio communication, obtained the exact position of the person carrying out the survey by sextant readings.

The monitoring schedule was as follows:

Nature	Day	Hours
Natural radioactivity	26/10	09.00-11.00
Release	27/10	11.30
1st Detection Survey	28/10	11.00-13.00
2nd Detection Survey	29/10	12.00-14.30
3rd Detection Survey	30/10	13.00-15.30
4th Detection Survey	31/10	14.00-16.30
5th Detection Survey	1/11	15.00-16.30
6th Detection Survey	2/11	15.30-17.30
7th Detection Survey	3/11	16.30-18.00
8th Detection Survey	8/11	08.00-09.00
9th Detection Survey	9/11	08.30-09.30
10th Detection Survey	12/11	09.30-11.30

Sediment cores were taken from the sand bar in the vicinity of the dispersed material at the end of the experiment. The cores were obtained to determine the distribution of the activity as a function of the depth of burial of the tracer (Fig. 17.2).

Results

For each monitoring survey three plots of data were constructed which included contoured activity diagrams (Fig. 17.3), transport diagrams and cumulative transport diagrams (Fig. 17.4).

For each survey, the lines of isoactivity were plotted (Fig. 17.3). The activity of the contour lines were the limits of the different instrumental scales: 50 000; 15 000; 5000; 1500; 500; 150; 50 counts per second (1 μCi = 37 000 counts per second. For all these lines the threshold is 50 keV).

Table 17.3

Calculation of the Position of Centre of Gravity and Depth of Burial during the Experiment

Time (1) (day)	Activity A_o (2) 10 Cps	Centre of (3) Gravity metres	Activity A_o (4) Cor. in 10 Cps.	Position of (5) Centre of Grav. Cor. metres	$K = \frac{1}{f_o}\frac{N}{A}$ (6)	$\frac{\alpha}{\beta} K$ (7)	$z_{in\ cm}$ (8)
2	22.60	21	24.2	24	.40	0.038	12.2
3	19.04	26	22.3	32	.37	0.35	14.0
4	33.42	23	38.2	29	.63	.0603	3.0
5	22.8	16	27.9	28	.54	.0516	5.8
6	22.2	49	27.5	53	.547	.0520	5.5
7	38.0	15	48.9	23	.20	.0190	32.0
12	11.2	14	37.5	48	.30	.0287	21.8
13	9.5	29	41.0	62	.325	.0310	17.0
16	2.43	21	36.0	67	.41	.0390	11.5

(1) Time after the release day
(2) Activity A_o reading in Table 17.2
(3) Centre of Gravity determined from the transport diagram (Fig. 17.3)
(4) Activity A_o cor.: Activity A_o(2) corrected for threshold effect
(5) Position of Centre of Gravity of Activity A_o cor. (4)
(6) $K = \frac{1}{f_o}\frac{N}{A}$ Calculation of the ratio; activity in the sand bar/activity reading
(7) $\frac{\alpha}{\beta}$ K is the value of the coefficient of equation (6) during the experiment

$$y_1 = \frac{1}{\beta}\frac{\alpha}{f_o}\frac{N}{A} z$$

(8) z depth of burial of radioactive tracer in centimetres.

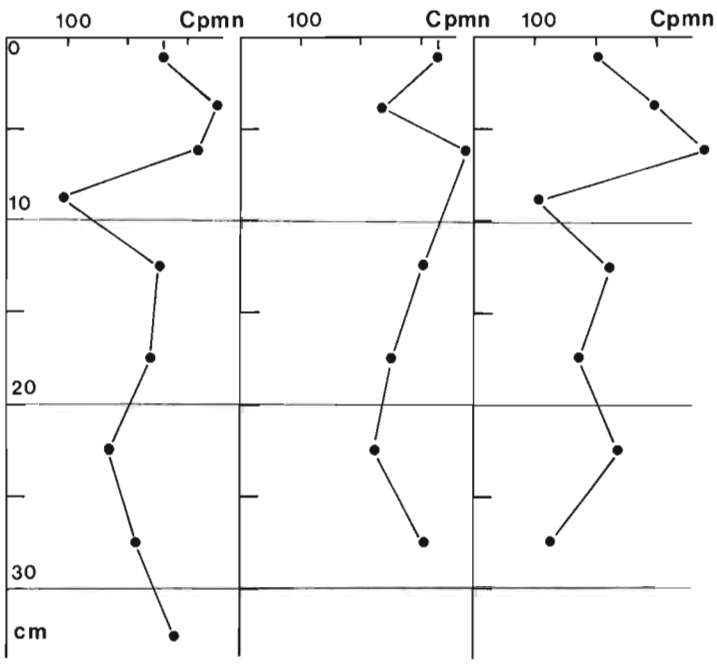

#1 Immersion Point
#2 20 Metres East of Immersion Point
#3 40 Metres East of Immersion Point

From the map of isoactivity a plot of the distribution of activity along north-south lines was made (Fig. 17.4) and the total activity along each line was integrated using a planimeter. With this information, the distribution of activity along an east-west line may be deduced. The centre of gravity was then determined by reading the 50th percentile of the cumulative distribution.

For the rational interpretation of the different measures the following parameters were calculated and have been defined by Crickmore and Lean (1962, 1963), Courtois (1964), Courtois and Sauzay (1966), and Sauzay (1968):

a) The rate of movement of the centre of gravity on the surface;

b) The balance of count rate (ratio between the activity on the surface and the total activity);

c) The depth of burial of the tracer;

d) The bedload sediment movement.

Figure 17.3.

Distribution of radioactivity with depth in three cores (the activity is in count per minute).

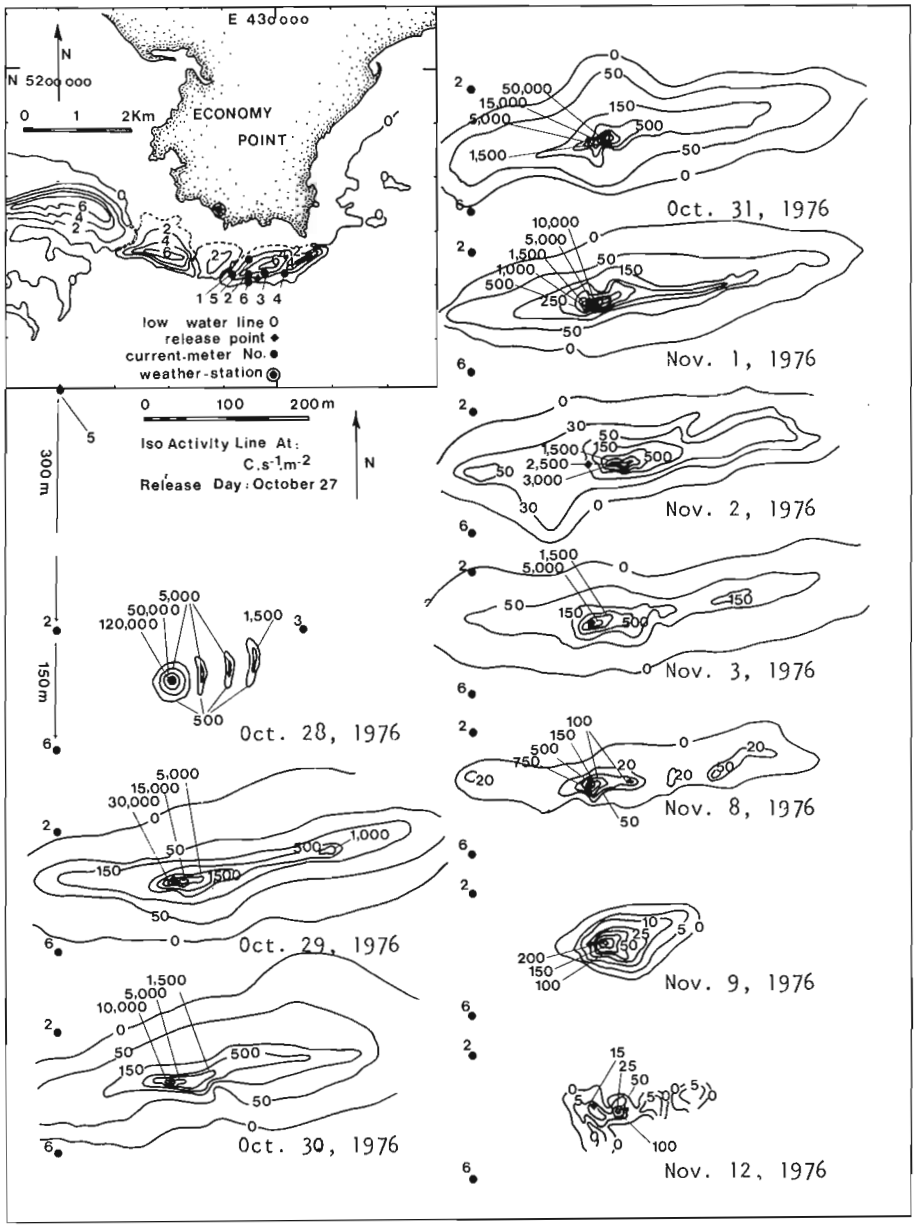

Figure 17.4. Evolution of isoactivity lines during the experiment.

The position of the centre of gravity was determined from the cumulative transport diagrams (Fig. 17.3), corrected for the threshold effect (Courtois, 1967). These results are tabulated in Table 17.3. For each monitoring survey, the distance between the release point (IP) and the centre of gravity (CG) is the mean length of transport (L_m). The mean rate of movement between the first day and the day of the survey is U_{mo}.

Thus:

$$U_{mo} = \frac{L_m(d) - L_m(o)}{t(d) - t(o)} \qquad (1)$$

The results of U_{mo} are tabulated in Table 17.1. The average movement of the centre of gravity (U_{G16}) over the period of the experiment (16 days) 4.19m/day; the mean speed of the centre of gravity (U_{Gm}) was 6.73m/day.

In order to determine the depth of burial of the tracer the balance of count rate (R) was employed where:

$$R = \frac{N_o}{A_o} \qquad (2)$$

and N is the total activity detected during the survey (in Cps/m^2) and $N_o = \frac{N}{e\text{-}0693 \frac{t}{\bar{T}_{1/2}}}$

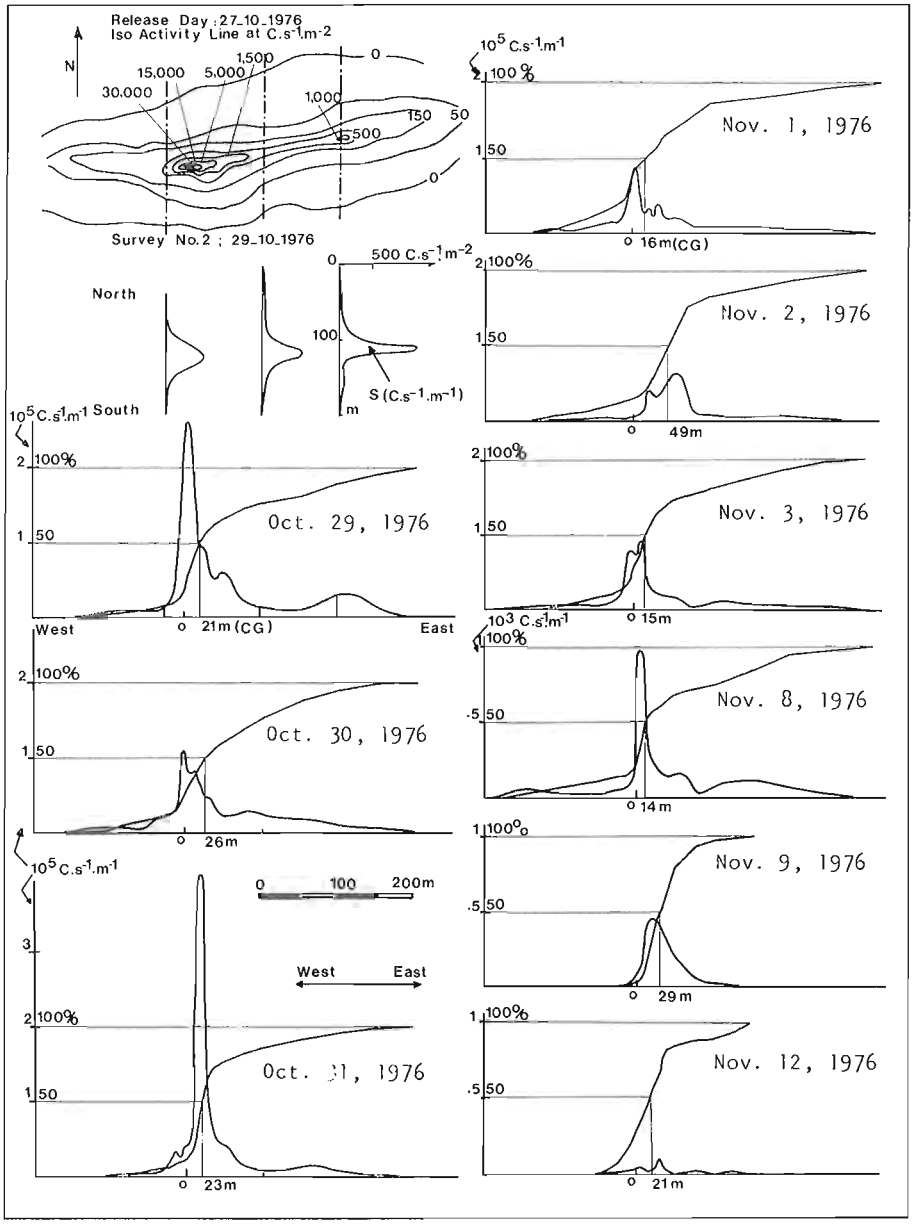

Figure 17.5. Evolution of transport during the experiment and determination of Centre of Gravity.

and A is the total activity on the day of the survey.

$$A = A_o e^{-0.693 \frac{t}{T\,1/2}} \qquad (3)$$

where A_o = initial activity on the day of release
(m curies, with 1 μCi — 37 000 Cps)
t = time in days (d)
T 1/2 = half life of isotope (2.7 days)
0.693 mev is an emission characteristic of the ^{198}Au

The total activity detected during the survey was given by:

$$N = \iint n\,ds \qquad (4)$$

where n is the total activity per unit of surface area; ds is a unit of surface area.

Taking into account the geometric function of the problem $f = f_o e^{-\alpha z}$, (defined previously) we have the relation between N and z:

$$\frac{1}{\beta} \cdot \frac{\alpha}{f_o} \cdot \frac{N}{A} z = 1 - e^{-\alpha z} \qquad (5)$$

which is the intersection of two functions of z

$$y_1 = \frac{1}{\beta} \frac{\alpha}{f_o} \frac{N}{A} z \quad \text{(for a linear solution)} \qquad (6)$$

$$y_2 = 1 - e^{-\alpha z} \quad \text{(for an exponential solution)}$$

where β is a function of the depth and distribution of the tracer. Generally the value of β is between 1.05 and 1.15, (see Sauzay, 1968; Jenneau et al., 1973).

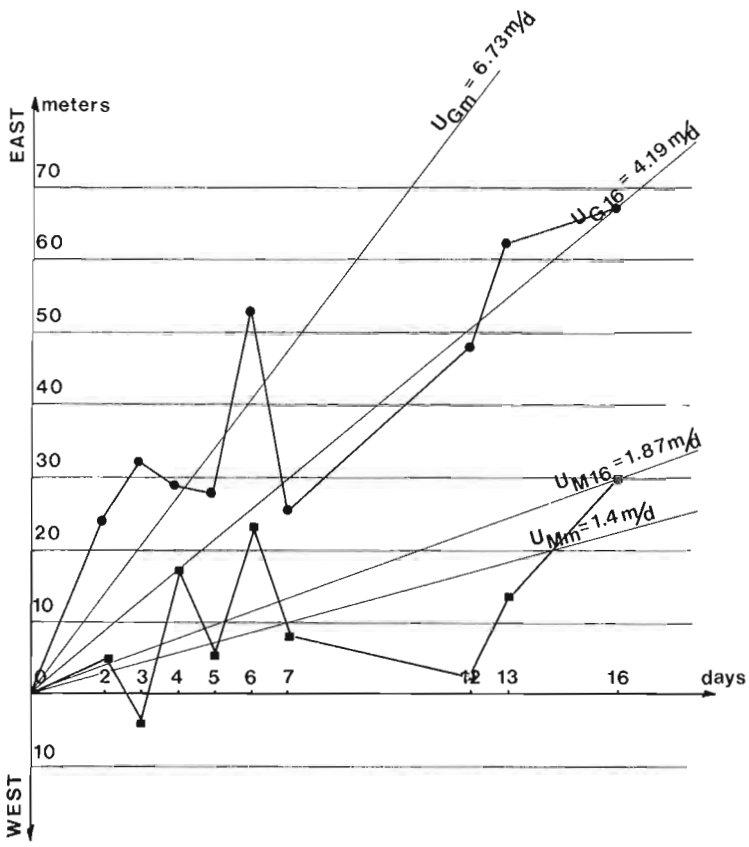

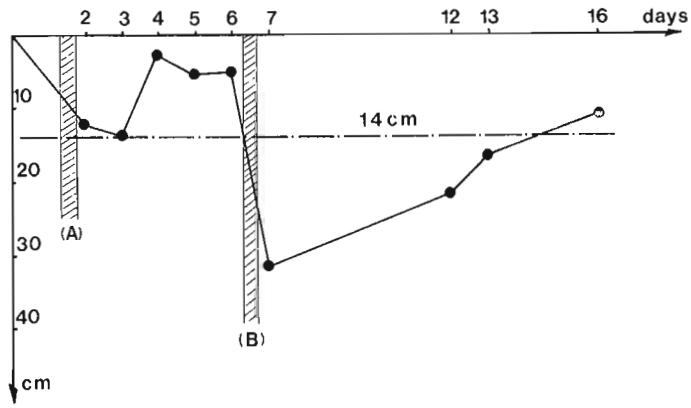

Figure 17.6

Evolution of Maximum Activity and Centre of Gravity as a function of time. Relationship between the thickness of bedload transport and the time during the experiment. The depth is in centimetres; (A) and (B) illustrate the burying of the radioactive tracer when the sand waves pass over the initial radioactive cloud.

U_{Gm} – mean speed of the Centre of Gravity

$U_{G_{16}}$ – speed of the Centre of Gravity between the release day and the last survey

$U_{M_{16}}$ – speed of the maximum of activity between the release day and the last survey

M_{Mm} – mean speed of maximum activity

Values of z were obtained using a graphical solution. For all the calculations we used the same exponential relationship and only the slope of the linear equation changes, because the balance of count rate $(\overline{N})$ is different for each survey (see Tables 17.2 and 17.3). $(\overline{A})$

The bedload sediment movement (D) expressed in tonnes per day is determined as follows:

$D = \rho \cdot w \cdot U_m \cdot z$

ρ = density of the sediment ($2.2 t/m^3$)

w = unit of width (1 m)

U_m = mean rate of movement of the centre of gravity (6.73 m/d)

z = mean thickness of movement (0.14 m)

$D = 2.2 \times 1 \times 6.73 \times .14 = 2.07$ t/d (or 1 m^3/d)

The total transport of sediment was thus 2 tonnes per linear metre in the eastern direction.

Conclusion

In scientific terms the experiment was successful in providing an indication of the direction (eastern) and quantity of sediment (2 tonnes) moving on the East Sand Bar at Economy Point. But the presence of active bedforms on the sand bar obscures, to some degree, the quantitative estimations of sediment transport. No observations of bedform migration were made during the experiment, however, this omission will be rectified in any new experiments. The precision of the surveys decreased

throughout the experiment because of the very short half life of the radioactive tracer and because the time available for each survey (one hour at low tide) was insufficient.

Further Work

Two experiments are planned for 1977 at the following sites:-

1) The northern part of the East Sand Bar at Economy Point;

2) The subtidal area, 1 km south of East Sand Bar at Economy Point.

For these experiments an isotope with a medium half life of the order of 10 days would be the best solution. This will permit detection over a period of four to six weeks, and the errors due to radioactive decay during the first two weeks will be reduced considerably.

References

Courtois, G.
1964: The possible use of a limited number of radioactive grains in the quantitative study of sedimentary shifts; Int. J. Appl. Radiat. Isotopes, v. 15, p. 655-663.

1967: Isotopes in sedimentology; Isotopes in Hydrology, Int. Atomic Energy Agency, p. 117-165, Vienna, 1967.

Courtois, G. and Hours, R.
1965: Propositions concernant les conditions particulières d'emplois des radioisotopes pour étudier les mouvements des sédiments; Eurisotop. Cah. Inf. 8, Rept. 29, p. 441-480.

Courtois, G. and Sauzay, G.
1966: Count rate balance methods using radioactive tracers for measuring sediment mass flow; La Houille Blanche, v. 3, p. 279-290.

Crickmore, M.J. and Lean, G.H.
1962: The measurement of sand transport by the time integration method with radioactive tracer; R. Soc. Lond., Proc. A270: 1340, p. 27-47.

1963: Methods for measuring sand transport using radioactive tracers; Radioisotopes in Hydrology Symposium, Tokyo, 1963.

Jeanneau, B., Sauzay, G., Barusseau, J.P., and Long, B.F.
1973: Compte-rendu des études de déplacement sédimentaires le long de l'Ile de RE par emploi de traceurs radioactifs; Report C.E.A. No. DR/TAAR/AR.S.73-16.

Klein, G. DeV.
1970: Depositional and dispersal dynamics of intertidal sand bars; J. Sed. Petrol., v. 40, p. 1095-1127.

Sauzay, G.
1968: Méthode du bilan des taux de comptage d'indicateurs radioactifs pour la détermination du débit de charriage des lits sableux; Thèse doc. Ing., Toulouse.

Project 750036

D.C. Umpleby and I.A. Hardy
Atlantic Geoscience Centre, Dartmouth

During the 1976 field season, the authors participated in one month's field work in central West Greenland between 70° and 72°N. The project was undertaken in conjunction with geologists of the Geological Survey of Greenland. From a base camp at Marrait kidlît on southwest Nûgssuaq Peninsula (Fig. 18.1), coastal sections were reached by the **M/V Steenstrup,** a vessel owned by the Geological Survey of Greenland. Remote and inland areas were visited by chartered helicopter. A total of 19 sections were investigated (Fig. 18.1). Lithologic and palynological analysis of the sample material collected at these sites will be conducted to confirm postulated ages of earlier workers and permit correlation with offshore areas of Eastern Canada.

All sites visited are in the Nûgssuaq Embayment, the site of a Cretaceous to Paleocene delta. The delta complex is between the Greenland landmass to the east and a central, north-trending basement high to the west (Fig. 18.1). An excellent evaluation of the Nûgssuaq Embayment and a description of its sedimentary facies, has recently been published by staff members of the Greenland Geological Survey (Henderson et al., 1976). Sediments within the embayment are mostly nonmarine and have been deposited in fluviatile and deltaic environments from a southern source (Table 18.1). The facies' belts trend east to west. Rare marine tongues are found as far south as south-central Nûgssuaq Peninsula, while on its north coast prodelta marine muds having a predominantly marine aspect occur. Scattered Cretaceous outcrops to the north, on the east coast of Svartenhuk Halvø, appear to have had local sediment sources, and were deposited in fault-generated depocentres not related to the deltaic complex.

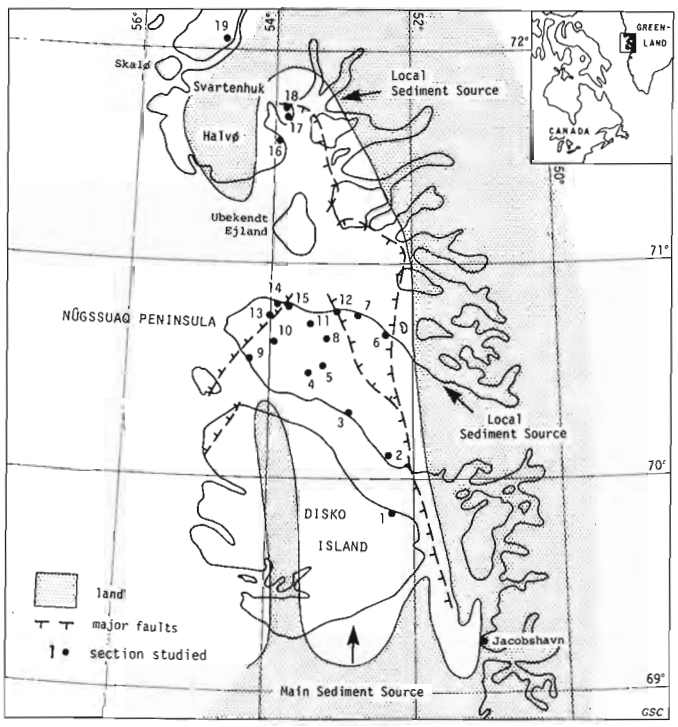

Figure 18.1. Paleogeographic map showing the localities investigated and sediment transport directions of the Cretaceous-Tertiary rocks of the Nûgssuaq Embayment, modified after Henderson et al., 1976.

Table 18.1

Generalized stratigraphy, Nûgssuaq Embayment.

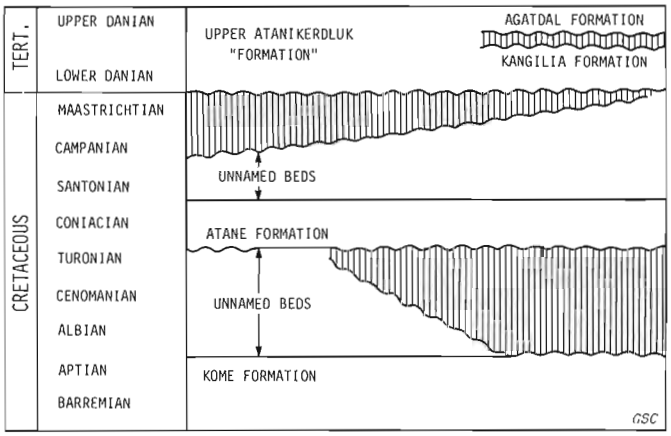

Late Cretaceous to lowermost Tertiary sand and shale sections were measured on the northeast coast of Disko Island, and on the south coast of Nûgssuaq Peninsula. Farther north, scattered outcrops of poorly-exposed sediments of Lower Cretaceous to possibly Eocene age were visited. The so-called "burning shales", at a classic locality near Niaqornat on the north coast of Nûgssuaq were sampled extensively (locality 15, Fig. 18.1).

Sediments of the embayment are covered by very thick (5 km) basalts, which onlap the adjacent Precambrian terrane. The basalts consist of several discrete units. The lower breccia unit, locally up to 1 km thick, was extruded from the west and deposited in shallow lagoons of the delta complex during the early Paleocene. This was followed by a period of appreciable tectonic activity. Overlying units consist of subaerially-extruded varieties of olivine to feldspar-phyric basalts which locally contain interbasaltic nonmarine sediments. Final stages of volcanism are marked by diverse extrusives including, locally, acid lavas and pyroclastics.

Exposures are generally poor for several reasons, such as: the friable nature of the various sand units; the incompetence of the shales; post-extrusive faulting causing extensive large scale slumping of overlying brecciated basalts – a feature aggravated by undercutting due to recent marine erosion; and the severe erosion by continental glaciers during the Pleistocene. The problem

From: Report of Activities, Part B;
Geol. Surv. Can., Paper 77-1B (1977)

of poor exposures, coupled with the similar nature of the predominantly nonmarine shale sequences, has led to doubtful correlations between exposures. It is expected that proposed palynological work to be performed at the Atlantic Geoscience Centre, will make future correlations more reliable.

Localities within the Nûgssuaq Embayment investigated during the 1976 field season (Fig. 18.1) are:

A. Disko Island

1. Nûgârssuk, west of Pingo 69°49'N 52°12'W — Atane Formation (Upper Cretaceous): massive current-bedded sandstones with coaly streaks, pebble bands, concretions, petrified tree trunks and coalified wood.

B. Nûgssuaq Peninsula

2. (i) Atanikerdluk 70°04'N 52°18'W — Atane Formation (Upper Turonian-Coniacian): massive fluvial sandstones with interbedded fossiliferous shale and thin coal beds.

   (ii) Atanikerdluk 70°05'N 52°21'W — Upper Atanikerdluk Formation (Early Tertiary (Upper Danian)) consisting of four members: (i) Quikavsak Member – "estuarine" sandstone and shales; (ii) Naujât Member – marine shales; (iii) Umiussat Member – quartz sandstone with interbedded siltstone and shale; (iv) Aussivik Member – black, bituminous shale, overlain by coarse sandstone.

3. Atâ 70°19'N 52°57'W — Atane Formation (Upper Turonian-Coniacian) and the Kangilia Formation (Danian): dark shale overlain by Quikavsak Member.

4. Auvfarssuaq Valley 70°27'N 53°28'W — Maastrichtian-Santonian alternating shales and fluvial sandstones overlain by Danian shales.

5. Auvfarssuaq Valley 70°27'N 53°27'W — Upper Cretaceous-Danian contact and unconformity between the Upper and Lower Danian sandstone/shale sequence.

6. Kûk 70°39'N 52°22'W — Rhyolites (including aquagene tuffs), laterite and ferric paleosols overlying a basal conglomerate of quartzite pebbles (equivalent to the basal Kome Formation).

7. Qaersut 70°45'N 52°45'W — Basal sandstone with plant remains, overlying deeply weathered basement.

8. Agatdalen 70°35'N 53°08'W — Kangilia and Agatdal formations (Upper and Lower Danian): See Rosenkrantz's (1970) classical marine sequence. A thick (5 m) conglomerate overlain by Upper Danian marine black shale, of the Agatdal Formation. The concretions are derived from Maastrichtian age sediments, within a Danian matrix and in turn is overlain by Danian.

9. Marrait kidlît 70°32'N 54°13'W — Upper Danian – fossiliferous limestone-volcanic breccia. The limestone has been injected upward into extruded pillow lavas. Similar breccias occur in the Triassic Karmutsen Formation of the Queen Charlotte Islands (Sutherland Brown 1968).

10. Itivdle Valley 70°36'N 54°03'W — Highly weathered Danian shales riddled by Tertiary dykes.

11. Tunorssuaq 70°43'N 53°28'W — A Lower Danian lithostrome consisting of Upper Danian-Eocene(?) reworked shales, containing massive fragments of volcanic breccia and conglomerate.

12. Ikorfat 70°46'N 53°03'W — Kome Formation (Lower Cretaceous (Aptian)): unconformably overlain by Albian/Cenomanian Atane Formation.

13. Kûp qûororssua 70°46'N 54°03'W — Ifsorisok Formation (Early Tertiary): interbasaltic sediments with light spotted shales and cleaved basalts, and some coaly material.

14. Nûluk 70°49'N 54°03'W — Ifsorisok Formation (Early Tertiary): interbasaltic sediments composed of volcaniclastic sediments plus alternating tuffs containing rootlets and coal seams.

15. Niaquornat 70°48'N 53°43'W — Late Cretaceous "burning shales" that are the result of surface oxidation of black shales, producing a sulphurous odor and reddish tinge on the sediments.

C. Svartenhuk Halvo Peninsula

16. Niagornakavsak 71°35'N 53°53'W — Cretaceous marine shales, overlying Precambrian basement.

17.	Southern Itsako Peninsula 71°38'N 53°48'W	An exposed basement high, found to have basalt flows with chilled margins and overlain by Tertiary basalts.
18.	Northern Itsako Peninsula 71°44'N 53°47'W	A Cretaceous sandstone unconformably overlain by shales.
19.	Painivik 71°58'N 55°00'W	A granule-sized Tertiary(?) grit overlain by columnar basalts.

References

Sutherland Brown, A.
1968: Geology of the Queen Charlotte Islands, British Columbia; in B.C. Dept. Mines and Petrol. Resources, Bull., no. 54, 226 p.

Henderson, G., Rosenkrantz, A., and Schiener, E.J.
1976: Cretaceous-Tertiary sedimentary rocks of West Greenland; in Geology of Greenland, p. 341-362.

Rosenkrantz, A.
1970: Marine Upper Cretaceous and lowermost Tertiary deposits in West Greenland; Med. dansk. geol. Foren., v. 19, p. 406-453.

19. MOLLUSC DISTRIBUTION, BAY OF FUNDY AREA, NEW BRUNSWICK AND NOVA SCOTIA

Project 750038

F.J.E. Wagner
Atlantic Geoscience Centre, Dartmouth

Nine grab samples were obtained from the approaches to and the outer part of St. Marys Bay (Stations 113-121 inclusive) and from 29 stations in Bay of Fundy during the cruise of **CSS Dawson** in 1975 (Fig. 19.1). Water depths at the collecting sites range between 31 and 73 m in St. Marys Bay and approaches and between 27 and 199 m in Bay of Fundy.

The molluscan fauna comprises 98 species (45 gastropods, 52 pelecypods and one scaphopod). Presence/absence species data were analyzed using a Q-mode cluster analysis (Bonham-Carter, 1967) to determine similarities between samples. Nine major groupings are indicated at the 0.2 level of similarity (Fig. 19.2). Areal distribution of these biotopes is shown in Figure 19.3.

Biotope 1 is present on both sides of Bay of Fundy (Stations 114, 115 and 117 along the western shore of Nova Scotia and Stations 140 and 148 on the New Brunswick side). Twelve of the 39 species identified from Biotope 1 are common to both areas. Most common species are **Cerastoderma pinnulatum** (Conrad) and **Pandora gouldiana** Dall. Biotope 2 is most widely distributed areally. Three stations, 120, 121 and 122 are located in the approaches to Bay of Fundy, whereas the remaining 11 stations are located in the upper reaches of the bay. About one-third of the 61 species identified are present in both areas. **Cerastoderma pinnulatum** (Conrad), **Hiatella arctica** (Linné), **Modiolus modiolus** (Linné) and **Cyclocardia borealis** (Conrad) are the dominant species in this biotope. Five of the six species of Biotope 3 occur also in Biotope 2, but Biotope 3 is singled out because of the absence of certain species as compared with Biotope 2. Since the sixth species is represented only by a single valve and is, therefore, not diagnostic although the species is unique to this biotope, Biotope 3 can be included in Biotope 2. Biotope 4 occurs in widely separated areas of the bay and is characterized by only seven species. The index species for this biotope is **Astarte undata** Gould. Except for one station (Station 135; depth 60 m), Biotope 5 is confined to the basin (115-199 m) east of Grand Manan Island. Three of the 30 species recorded in Biotope 5, namely **Astarte subaequilatera** Sowerby, **Nucula tenuis** (Montagu) and **Nuculana pernula** (Müller), may be regarded as index species for this biotope. Biotope 6 adjoins Biotope 5 to the west and partly overlaps it in depth range (29-133 m). **Nuculana pernula** is a key species for this biotope also, but in this case it is associated with **Periploma fragile** (Totten). Biotope 7, like Biotope 1, exhibits a split distribution with two stations off the southwestern New Brunswick coast and two stations in St. Marys Bay, Nova Scotia. Eleven species are associated

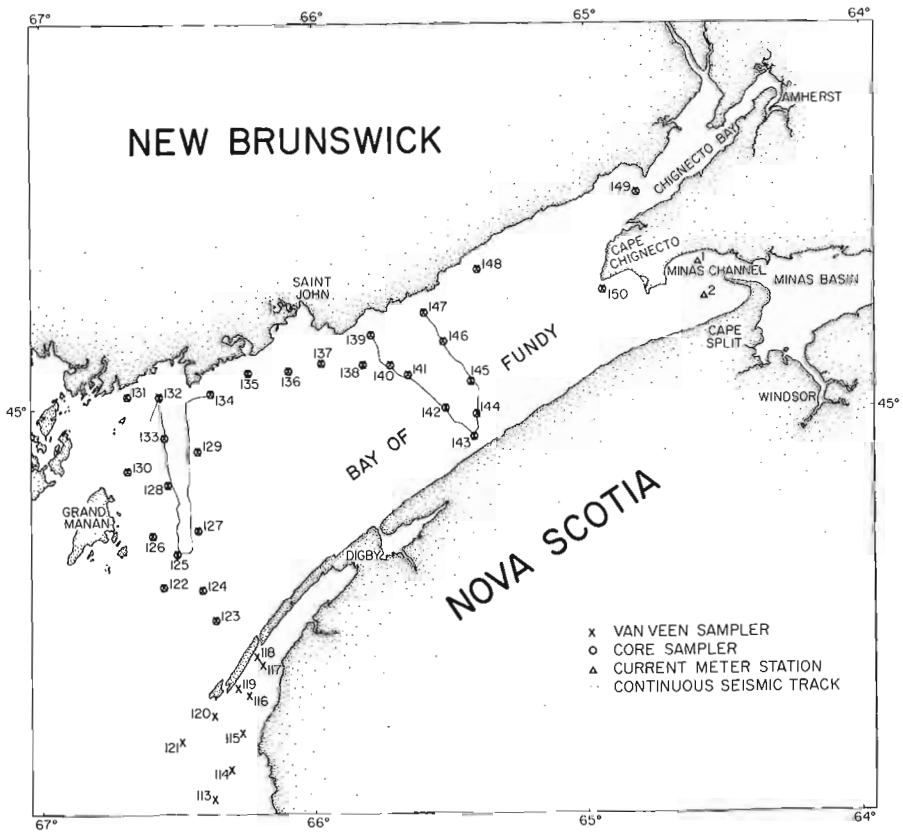

Figure 19.1. Index map showing location of sampling stations.

From: Report of Activities, Part B; Geol. Surv. Can., Paper 77-1B (1977)

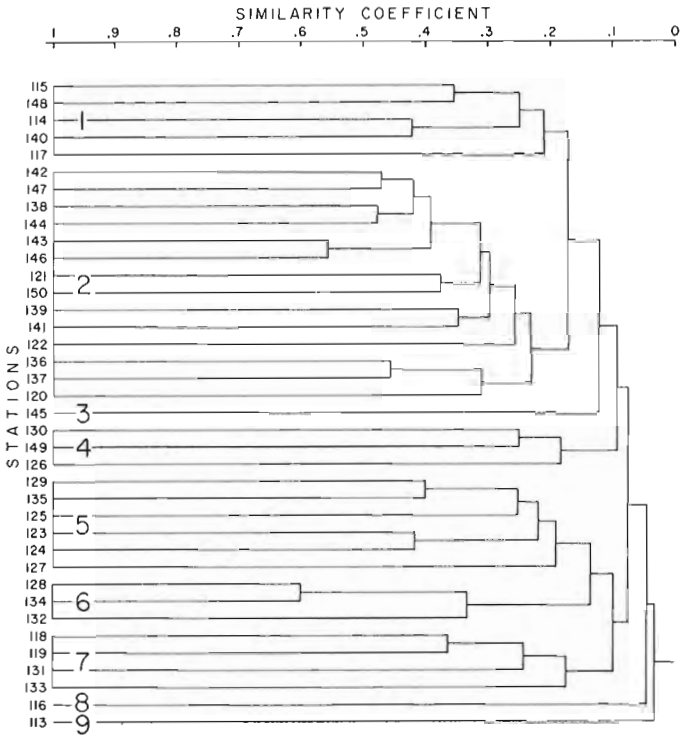

Figure 19.2. Dendogram showing similarity of samples and the nine clusters used to identify biotopes in St. Marys Bay and Bay of Fundy. Samples were compared using the Jaccards coefficient and clustered using the unweighted pair-group method (see: Sokal and Sneath, 1963).

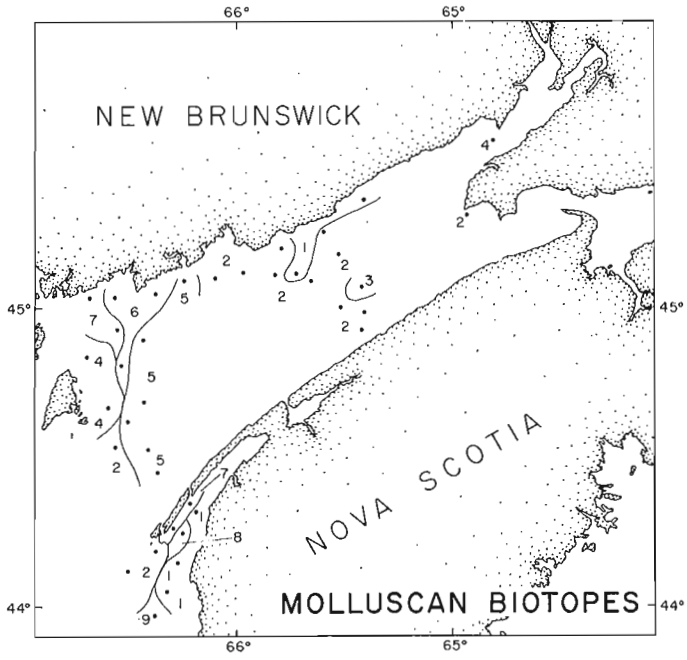

Figure 19.3. Distribution of the molluscan assemblages in St. Marys Bay and Bay of Fundy in November 1975.

with this biotope and the assemblages are dominated by **Arctica islandica** (Linné), **Lunatia triseriata** (Say) and **Yoldia myalis** (Couthouy). Biotopes 8 and 9, both represented by one station only, are in the St. Marys Bay area. Index species for Biotope 8 are **Lyonsia hyalina** (Conrad) and **Solariella obscura** (Couthouy), and for Biotope 9 it is **Skeneopsis planorbis** (Fabricius). In spite of some species in each of Biotopes 7, 8 and 9 occurring also in the adjacent Biotope 1, the assemblages in each case are sufficiently different as to characterize discrete biotopes.

Physical characteristics of the biotopes are as follows: Biotope 1, depth range 31-79 m, sandy or muddy bottom with coarser grained material (pebbles and/or cobbles) locally; Biotope 2, depth range 27-84 m (one station at 166 m), bottom predominantly sand with pebbles; Biotope 3, depth 71 m, sandy bottom; Biotope 4, depth range 125-139 m (one station at 33 m), bottom mainly silt and sand; Biotope 5, depth range 115-139 m (one station at 60 m), mainly muddy bottom, but with two stations with sand and pebbles also in the channel between Nova Scotia and Grand Manan Island, New Brunswick; Biotope 6, depth range 29-133 m, muddy bottom; Biotope 7, depth range 33-79 m, muddy bottom; Biotope 8, depth 33 m, sandy bottom and Biotope 9, depth 66 m, cobbles. Although the index species are not restricted to the depth ranges of the biotopes they characterize, they are related to the type of bottom sediment recorded for the biotopes in which they are found.

A comparison of assemblages from the mid-Wisconsinan deposits of the southwestern coastal area of Nova Scotia (Wagner, 1977) with the biotopes described for adjacent waters shows a marked similarity between the Pleistocene and Recent faunas in the area. The Pleistocene assemblages show greatest similarity with those of Biotope 1. The deduced depth of 10-25 m for the Pleistocene assemblages (Wagner, 1977), based on the literature, is slightly less than the depth range of 31-35 m for the stations for Biotope 1 in the St. Marys Bay area.

References

Bonham-Carter, G.F.
1967: Fortran IV program for Q-mode data cluster analysis of nonquantitative data using IBM 7090/7094 computers; Univ. Kansas, Computer Contrib. 17, 13 p.

Sokal, R.R. and Sneath, P.H.
1963: Principles of numerical taxonomy; W.H. Freeman and Co., San Francisco.

Wagner, F.J.E.
1977: Palaeoecology of marine Pleistocene Mollusca, Nova Scotia; Can. Jour. Earth Sciences. (in press)

EXAMINATION OF BEDFORMS IN SHALLOW WATER USING SIDE-SCAN SONAR, MIRAMICHI ESTUARY, NEW BRUNSWICK

Project 750047

G.E. Reinson
Atlantic Geoscience Centre, Dartmouth

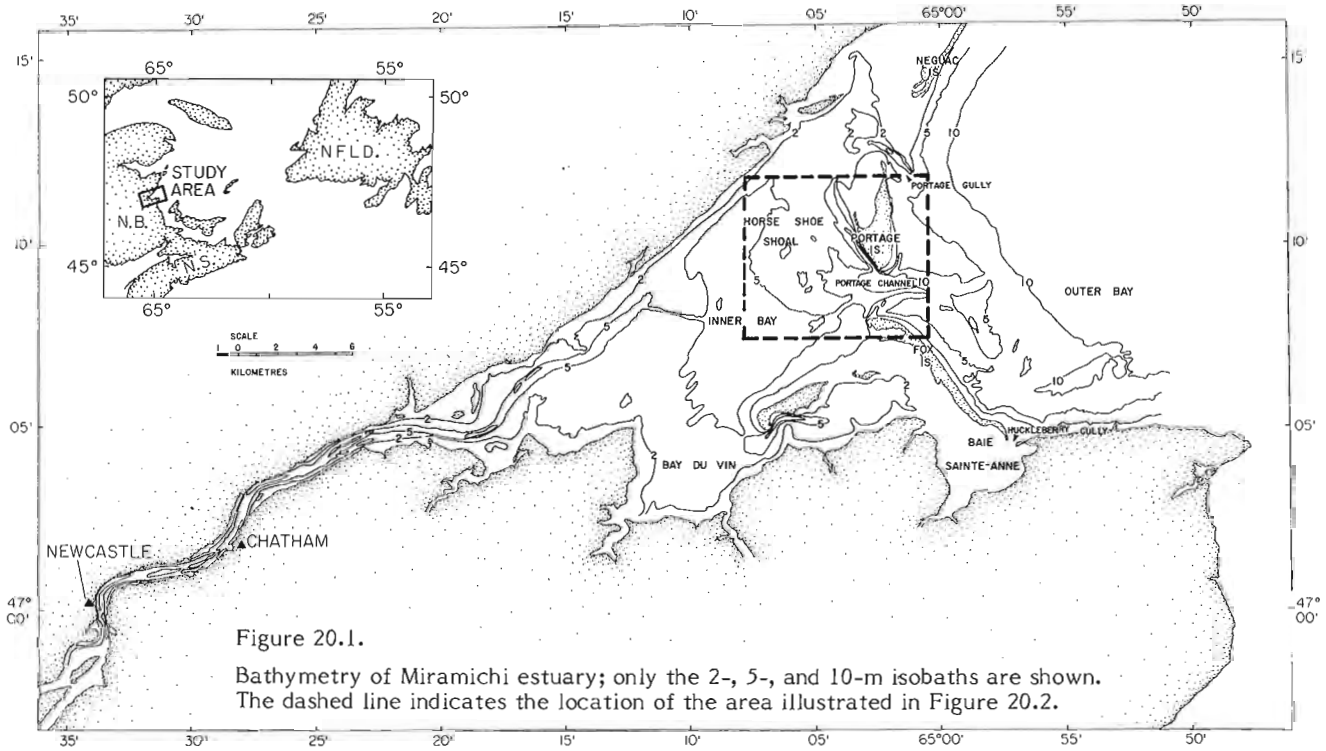

Figure 20.1.

Bathymetry of Miramichi estuary; only the 2-, 5-, and 10-m isobaths are shown. The dashed line indicates the location of the area illustrated in Figure 20.2.

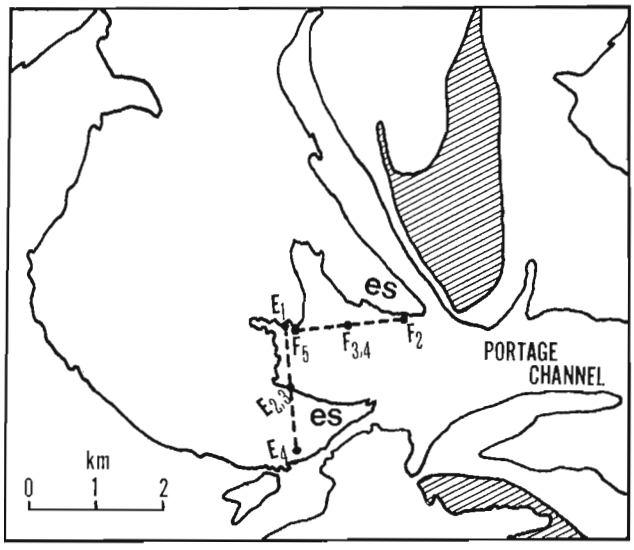

Figure 20.2. Flood-tidal delta as delineated by the 5-m isobath. The locations of the sonograms in Figures 20.3 to 20.6 are shown as dashed lines. The ebb spits (es) are situated at the sides of the flood-ramp.

Introduction

The submarine morphology at the mouth of the Miramichi estuary, northeastern New Brunswick (Fig. 20.1), is typical of a large tidal-delta system (Reinson, 1976a, b). The flood-tidal delta adjacent to the main inlet includes a horseshoe-shaped shoal (Fig. 20.2), part of which is covered by an extensive sand-wave field. The shape of the shoal probably reflects a segregation of dominant flow paths of flood and ebb currents. During flood, dominant currents are directed westward in a relatively unconfined manner through the centre of the shoal, creating a flood-ramp; the name proposed by Hayes (1975) for the seaward-facing slope on the flood-tidal delta over which the main force of the flood current is directed. According to Hayes a flood-ramp is always covered with flood-oriented sand waves. During ebb, currents flow around the perimeter of the shoal forming channels. This segregation of flood and ebb flow favours the formation of sand spits by ebb-tidal current at the perimeter of the shoal. These spits taper-off in a seaward direction, and then abruptly disappear where the peripheral channels merge with the main inlet channel (Fig. 20.2).

From: Report of Activities, Part B; Geol. Surv. Can., Paper 77-1B (1977)

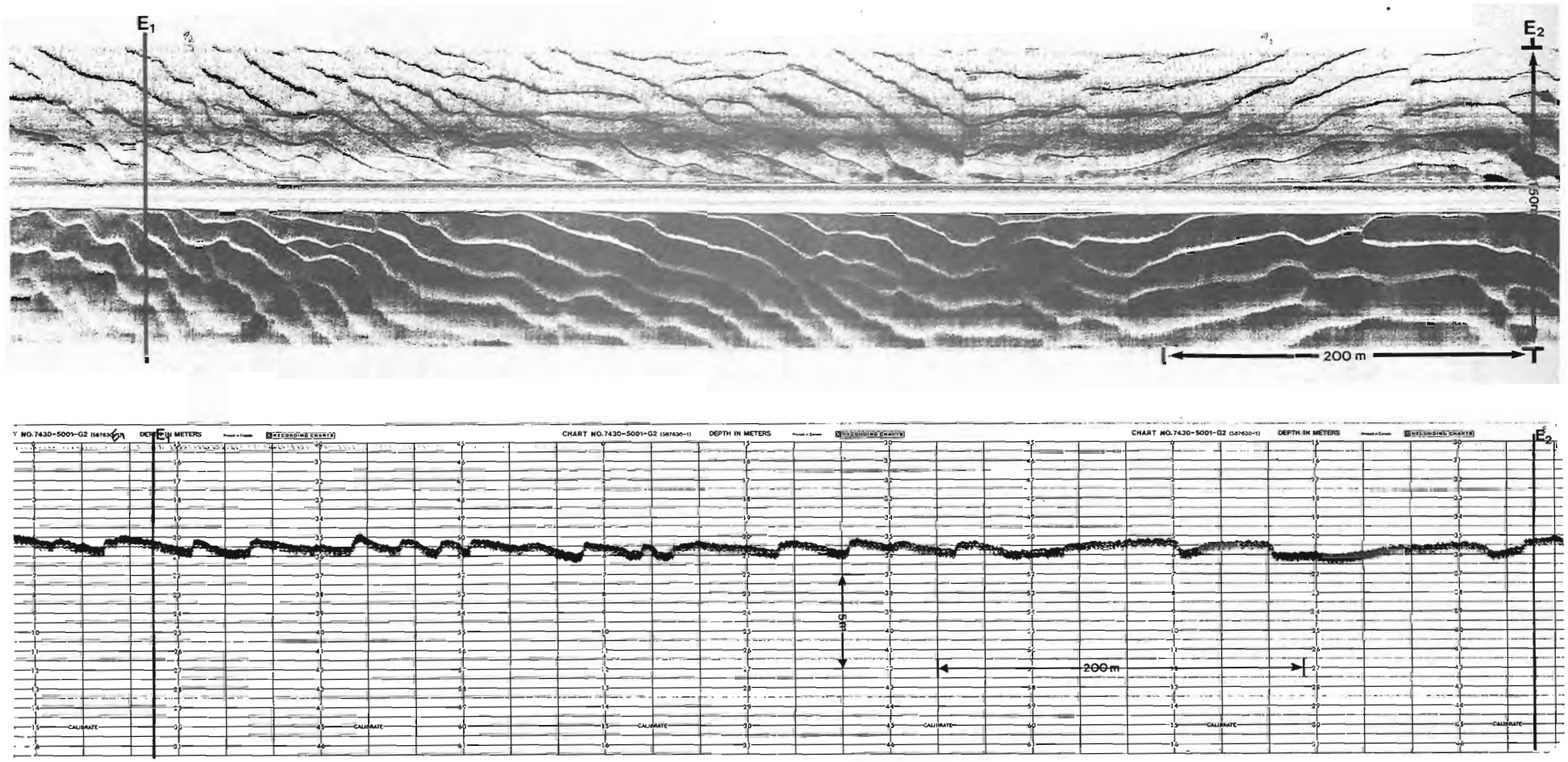

Figure 20.3. Side-scan sonogram and corresponding echogram across the innermost portion of the flood-ramp. Flood-oriented sand waves completely cover the surveyed area.

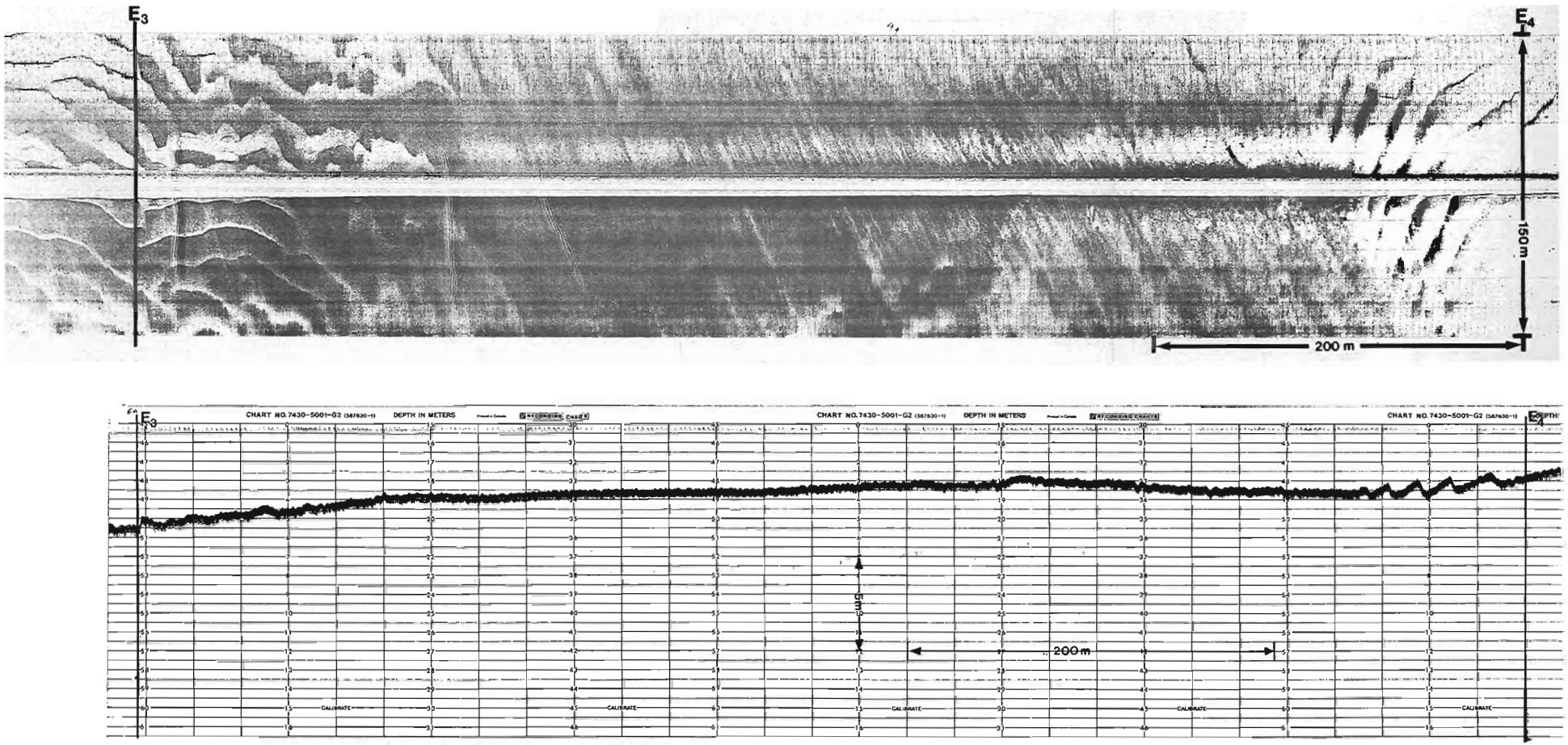

Figure 20.4. Side-scan sonogram and corresponding echogram across the inner part of the southern ebb spit. Note the large area, devoid of sand waves, in the middle of the sonogram.

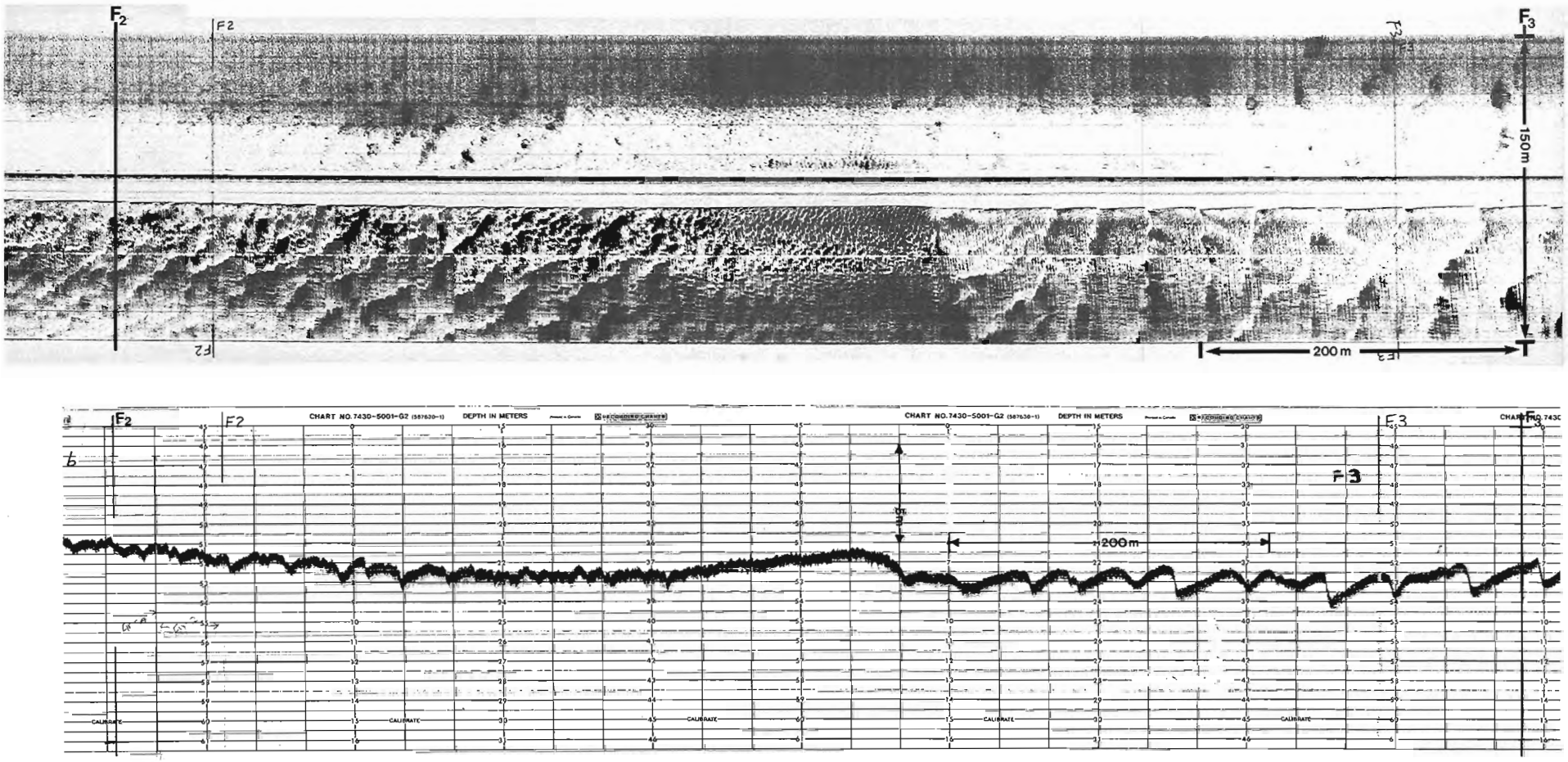

Figure 20.5. Side-scan sonogram and corresponding echogram across the northern flank of the flood-ramp. On the left a transitional bedform field is evident consisting of flood-oriented sand waves which are highly modified by flood-oriented megaripples. In the centre, a well-defined flood-oriented megaripple field is present. A sharp boundary is evident between this megaripple field and the large flood-oriented sand-wave field situated on the right side of the survey records.

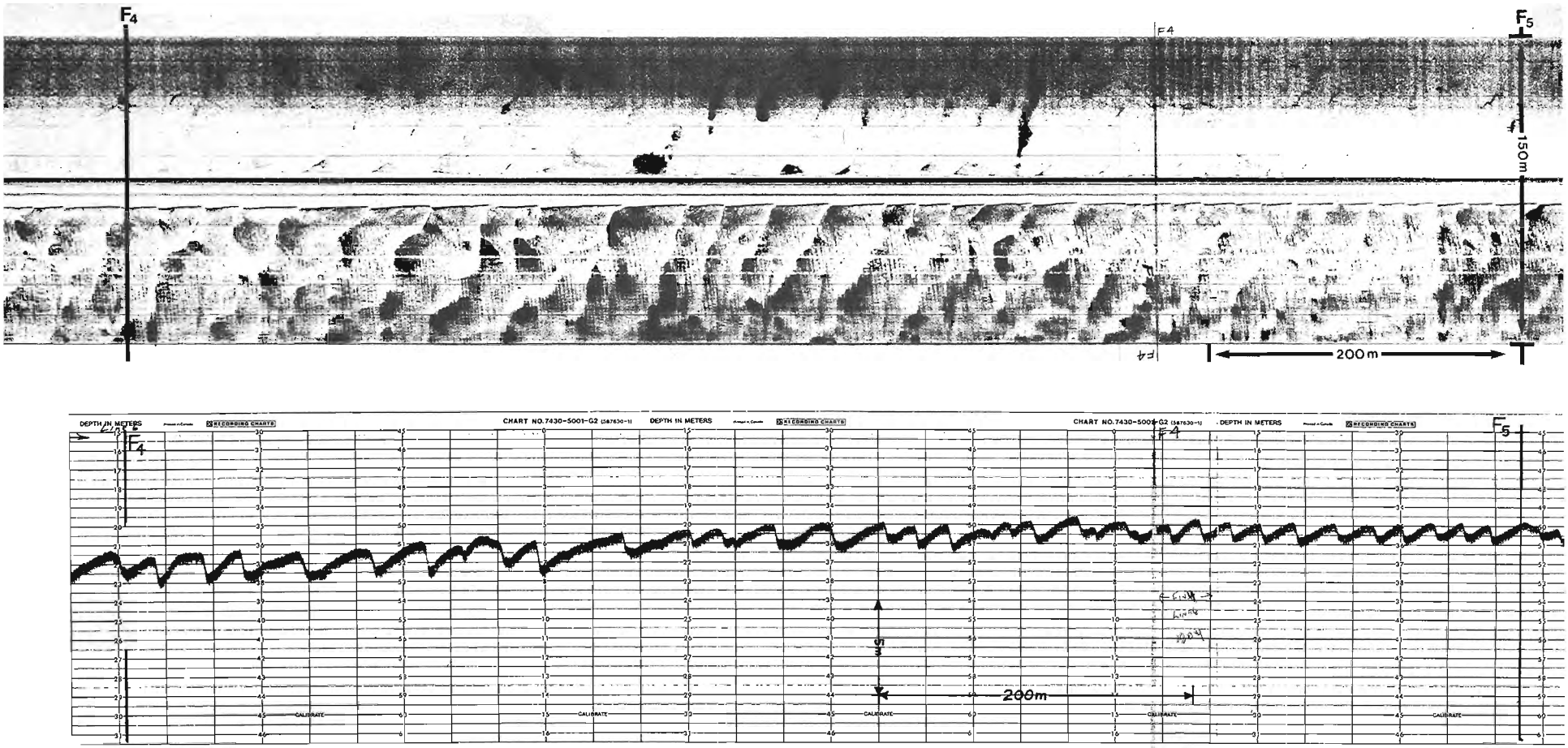

Figure 20.6. Side-scan sonogram and corresponding echogram across the flood-ramp. This survey line runs normal to the one illustrated in Figure 20.3. Note the well-defined flood-oriented sand waves, which become smaller in wave length and height, as water depth decreases.

The flood-tidal delta was surveyed recently, using side-scan sonar in conjunction with a conventional echo-sounder, in order to investigate the bedforms in detail. This paper presents preliminary results from the survey, and contributes to the findings of a continuing project on the sediment dynamics and morphology of tidal inlets of the Miramichi barrier-island system.

Bedform Morphology

The terms "sand waves" and "megaripples", as used here, are defined respectively as "asymmetrical bedforms with wave lengths greater than 6 m" and "asymmetrical bedforms with wave lengths greater than 60 cm but less than 6 m" (Hayes, 1975). The side-scan and echo-sounding records illustrated in Figures 20.3 to 20.6 were selected to show the variation in bottom morphology on the flood-tidal delta, and to demonstrate the value of three-dimensional records in conjunction with echo-sounding, for determining the true orientation of bedforms and hence dominant sediment transport directions. Survey line E-E was run at high water, and survey line F-F early in the succeeding ebb cycle (Fig. 20.2); both survey lines indicate the existence of an extensive sand-wave field on the flood-ramp of the delta (Figs. 20.3 to 20.6).

Figure 20.3 illustrates a portion of the survey line which crosses near the inner margin, and perpendicular to, the axis of the southern fork of the bifurcated flood-ramp. Figure 20.4 illustrates the continuation of the same survey line crossing the innermost part of the southern ebb spit. Low amplitude, highly asymmetrical sand waves cover the floor of the flood-ramp (Fig. 20.3). The slip-faces of the flood-oriented sand waves face westward indicating a direction of migration which is parallel to the axis of the inlet throat. Sand waves are not present over a large area of the southern ebb spit, which is characterized by parallel lineations (Fig. 20.4). Near the end of the survey line, sand waves again occur on the shallowest portion of the shoal, but with their slip-faces facing south.

Another survey line illustrated in Figures 20.5 and 20.6 was obtained over the flank of the northeastern ebb spit and traverses the flood-ramp, roughly normal to the E-E survey line (Fig. 20.2). Three bedform fields are evident: a flood-oriented sand-wave field with superimposed megaripples which have greatly modified the sand waves; a flood-oriented megaripple field (both these fields are located in shallow water near the flood-ramp margin); and an extensive field of unmodified asymmetrical flood-oriented sand waves flooring the flood-ramp. The sand waves on the flood-ramp range in wave length from 10 to 54 m, and in amplitude from 0.4 to 1.5 m. Both wave length and amplitude of the sand waves decrease with decreasing water depth.

Discussion

Sand waves are thought to form in response to relatively low flow velocities compared to megaripples, which form under much higher flow velocities (Boothroyd and Hubbard, 1975; Southard, 1975). Systematic studies of intertidal and subtidal bedforms (Boothroyd and Hubbard, 1975; Hayes et al., 1969) have shown that megaripples can be generated, irradicated, and then regenerated over a tidal cycle, and thus may migrate in both ebb and flood directions. Conversely, sand waves are modified relatively little over a tidal cycle; the direction of migration being controlled by the dominance of the opposing tidal currents.

The presence of flood-oriented sand waves over the entire flood-ramp indicates that dominant currents over this area (and therefore dominant sediment-transport directions) are landward during the flood-tidal stage. Echo-sounding over the same area around three quarter ebb to low water stage in the tidal cycle indicates that the flood-oriented direction of the sand waves is maintained even during ebb-flow, and does not respond significantly to reversal of tidal currents over the time scale of a tidal cycle. The flood-oriented megaripples and transitional bedforms at the northeastern margin of the flood-ramp (Fig. 20.5) delineate an area that is subjected to higher flood-current velocities than those which occur over most of the flood-ramp. Both flood and ebb transport of sand may occur in this region, and the relative instability of the bedforms present on the flank of the ebb spit may indicate that the flood-current deposited sediment is not shielded from the strong ebb-currents that flow around the periphery of the shoal. The zone on the southern ebb spit that is barren of sand waves (Fig. 20.4), presents some problems in interpretation at this time; further detailed examination of all the available side-scan and echo-sounding records is necessary to properly evaluate this morphological feature.

Work is continuing on the bedform morphology of the flood and ebb-tidal deltas. An effort will be made to map the bedform fields in relation to areal variations in bottom topography and tidal-current flow conditions. The feasibility of documenting the seasonal variations in bedform morphology is also being investigated. An attempt will be made this winter to obtain bottom profiling records through the ice, to document the effects of such an upper boundary layer on tidal-current flow patterns, and on morphology and magnitude of sand-wave forms.

It is noteworthy that side-scan sonar techniques can be usefully employed in very shallow-water environments, as indicated by the records presented in this paper. Usable sonographs were obtained in water depths as shallow as 2 m, under extremely calm sea conditions.

I am grateful to T. Corbett for his advice on the operation of side-scan sonar, and to M. Gorveatt and K. Robertson for their expert technical assistance in the field.

References

Boothroyd, J.C. and Hubbard, D.K.
1975: Genesis of bedforms in mesotidal estuaries; in Proceedings of the Second International Estuarine Research Conference, ed. L.E. Cronin; Academic Press, New York, v. 11, p. 217-234.

Hayes, M.O.
1975: Morphology of sand accumulation in estuaries; in Proceedings of the Second International Estuarine Research Conference, ed. L.E. Cronin; Academic Press, New York, v. 11, p. 3-22.

Hayes, M.O., Anan, F.S., and Bozeman, R.N.
1969: Sediment dispersal trends in the littoral zone - a problem in paleogeographic reconstruction; in "Coastal Environments: Northeast Massachusetts and New Hampshire"; Univ. Mass. Dept. Geol. Pub. Ser., Contrib. No. 1-CRG, p. 290-315.

Reinson, G.E.
1976a: Surficial sediment distribution in the Miramichi estuary, New Brunswick; in Report of Activities, Part C, Geol. Surv. Can., Paper 76-1C, p. 41-44.

Reinson, G.E. (cont'd.)
1976b: Channel and shoal morphology in the entrance to the Miramichi estuary, New Brunswick; in Report of Activities, Part C, Geol. Surv. Can., Paper 76-1C, p. 33-35.

Southard, J.B.
1975: Chapter 2: Bed configurations; in "Depositional Environments as Interpreted from Primary Sedimentary Structures and Stratification Sequences"; Soc. Econ. Paleontol. Mineral., SEPM Short Course no. 3, p. 5-44.

21. STUDIES IN "STANDARD SAMPLES" FOR THE ANALYSIS OF SILICATE ROCKS AND MINERALS

Project 690089

Sydney Abbey
Central Laboratories and Administrative Services Division

Work in this area proceeded along three lines: (1) compilation of data and upgrading of recommended values for three Canadian reference rocks (two Bancroft syenites bearing radioactive minerals and the Mount Royal gabbro); (2) updating of compilation of "usable values" and other information on available reference samples from all sources; and (3) promotion of worldwide co-operation in the preparation, categorization and application of reference materials for silicate rock analysis.

(1) A first report on the collaborative analysis of samples SY-2, SY-3 and MRG-1 (Abbey et al., 1975) appeared as a CANMET publication. Additional data (approximately 50 per cent more than before) received since the preparation of the first report have been embodied in a supplement. That supplement includes a number of new and improved recommended values for the concentrations of many of the components of the three samples.

(2) Much additional information has appeared in the literature since the publication of the "1974 edition of 'usable' values" (Abbey, 1975). A great deal of that information has been compiled into a new publication, in its last stages of preparation at this writing. The new publication will include values for a number of reference materials which are not rocks (e.g. clays, refractories, bauxites) but whose compositions make them useful in calibrating instruments for rock analysis. Completion of the work is awaiting results of a systematic replicate analysis of eight new samples from the U.S. Geological Survey, now underway in our laboratories.

(3) An invited Plenary Lecture, "Standard Samples: How standard are they?" was presented and a panel discussion on the same topic was conducted at the INTERAN '76 Conference on Analysis of Geological Materials, in Prague, Czechoslovakia. The Conference, and visits to Czechoslovak laboratories, provided useful contacts and much information about reference sample programs in Eastern Europe. Participation was initiated in the International Study Group on Reference Materials, whose headquarters are in South Africa, and in the editorial board of GEOSTANDARDS NEWSLETTER, a new international journal published in France. The text of the Plenary Lecture and a report on other "standards-oriented" activities at INTERAN '76 are to appear in the first issue of GEOSTANDARDS NEWSLETTER. Also expected in that issue is a brief report on three new reference rocks from the U.S.S.R., translated from the Russian, and with comments by the writer.

References

Abbey, Sydney
1975: Studies in "standard samples" of silicate rocks and minerals, Part 4, 1974 edition of "usable" values; Geol. Surv. Can., Paper 74-41.

SY-2, SY-3 and MRG-1, A report on the collaborative analysis of three Canadian rock samples for use as certified reference materials. Supplement 1, CANMET Report MRP/MSL 76-32. (in press)

1977: Overview of topics on geochemical reference samples during the INTERAN '76 Conference on analysis of geological materials; Geostandards Newsletter, vol. 1, p. 5-6.

1977: "Standard Samples: How standard are they?"; Geostandards Newsletter, vol. 1, p. 39-45.

Abbey, Sydney, Gillieson, A.H., and Perrault, Guy
1975: SY-2, SY-3 and MRG-1. A report on the collaborative analysis of three Canadian rock samples for use as certified reference materials; CANMET Report MRP/MSL 75-132 (TR).

Tauson, L.V., Lontsikh, S.V., Shafrinsky, Yu.S., and Kozlov, B.D.
1974: Geochemical standards of igneous rocks. 1974 Yearbook of the Institute of Geochemistry, Irkutsk, p. 370-375. Translation and comments by Sydney Abbey. Geostandards Newsletter, in press.

From: Report of Activities, Part B; Geol. Surv. Can., Paper 77-1B (1977)

22. ON THE NATURE AND FORMATION OF RADIOACTIVE HYDROCARBONS FROM THE ORDOVICIAN ROCKS OF THE OTTAWA AREA

Project 740081

I.R. Jonasson, B.W. Charbonneau and K.L. Ford
Resource Geophysics and Geochemistry Division

Introduction

Radioactive hydrocarbons such as those which will be discussed here were first described in detail by Steacy et al. (1973). They identified discrete radioactive grains associated with amorphous hydrocarbon materials, grains of chalcopyrite and some pyrite. The host rock for the samples described from the South March area was dolomitic sandstone of the Lower Ordovician March Formation. Charbonneau et al. (1975) described this and other"thucolite" occurrences from elsewhere in the South March and nearby Marchhurst areas. In places, hand specimens of mineralized sediments contained up to 4% chalcopyrite and 0.05% U_3O_8 in hydrocarbon. Other metals including Pb, Mo, Mn and Ag are commonly associated with U in the hydrocarbons, while trace Mo probably occurs in the chalcopyrite. Not all hydrocarbon occurrences are radioactive. Typical data are presented in Table 22.1 for some oxidized specimens in which the hydrocarbons survive essentially intact.

Ford (1975) and Ford et al. (1976 and unpublished work) have made some detailed studies of the mineralogy of these U-Cu showings. Chalcopyrite was observed to be the dominant sulphide phase near the surface, however downdip pyrite seemed to be the dominant sulphide. Occasionally sulphide grains were associated with hydrocarbon material and also encased by rinds of goethite containing up to 6% Cu, possibly a product of chalcopyrite oxidation. Pyrite and marcasite were also described. Pyrite was observed to occur either as a single phase or in close association with hydrocarbon, sometimes surrounding it, other times banded or interlayered.

Ford (1975) described the hydrocarbon material as containing up to 4.7% U_3O_8; ThO_2 was not present. Cu, Ca, Fe, Si and Ti were also found to be common impurities. Hydrocarbon occurs as irregular grains or seams on parting planes within the carbonate sediments and within interstices between quartz grains. Some bulk analyses (this work) of hydrocarbon grains separated from weathered bedrock from the Marchhurst occurrences were found to contain similar amounts of U.

Specimens of radioactive hydrocarbon have also been found in vertical fractures in the Oxford Formation in close proximity to U-Cu mineralization in underlying March Formation near South March. The samples were black and apparently amorphous. No discrete U or Th minerals were recognizable. Electron microprobe analyses, performed by A.G. Plant of the Geological Survey, revealed that the main mass of the sample was homogeneous hydrocarbon containing U, about 5% Ca and minor Cu, Fe, Ti, Si, Mg and S. Grains of pyrite, chalcopyrite and an Fe oxide, possibly goethite, were shown to be present within the hydrocarbon mass (Fig. 22.1).

The radioactive hydrocarbons found in both the March and Oxford formations are considered to be of epigenetic origin. The time of emplacement is in doubt, but possibilities include early deposition of fluids along bedding and in compaction or dewatering fractures during or shortly after diagenesis. In the case of the Oxford Formation occurrences, which lie in larger fractures, it is likely that the time of emplacement could be much later if the hydrocarbons have been remobilized from underlying March Formation. The regional distribution of these blanket-like Cu-U hydrocarbon occurrences as revealed by drilling results kindly provided by the Kerr Addison Company suggests that certain thin, rubbly intraformational strata are host to these minerals over a wide area. These horizons may represent ancient water tables or aquifers through which groundwaters once percolated.

Discussion

There is considerable indirect evidence that the amorphous hydrocarbons now present are relics of organic matter which was responsible for the

Table 22.1

Metal content of some hydrocarbon-rich carbonate rocks from the South March area, Ontario. Values are in ppm except where noted.

Sample	Fe%	U%	Zn	Cu	Pb	Ag	Mo	Mn
1.	3.61	0.02	66	3200	91	4	27	1850
2.	1.54	0.01	11	320	17	1	3	600
3.	1.25	0.01	13	420	50	5	40	650
4.	1.63	0.02	25	2300	330	5	120	1070
5.	2.77	0.01	47	1500	120	5	87	1230
6.	2.23	0.02	20	790	340	36	77	1460
7.	4.41	0.04	40	4900	720	44	110	2720

From: Report of Activities, Part B; Geol. Surv. Can., Paper 77-1B (1977)

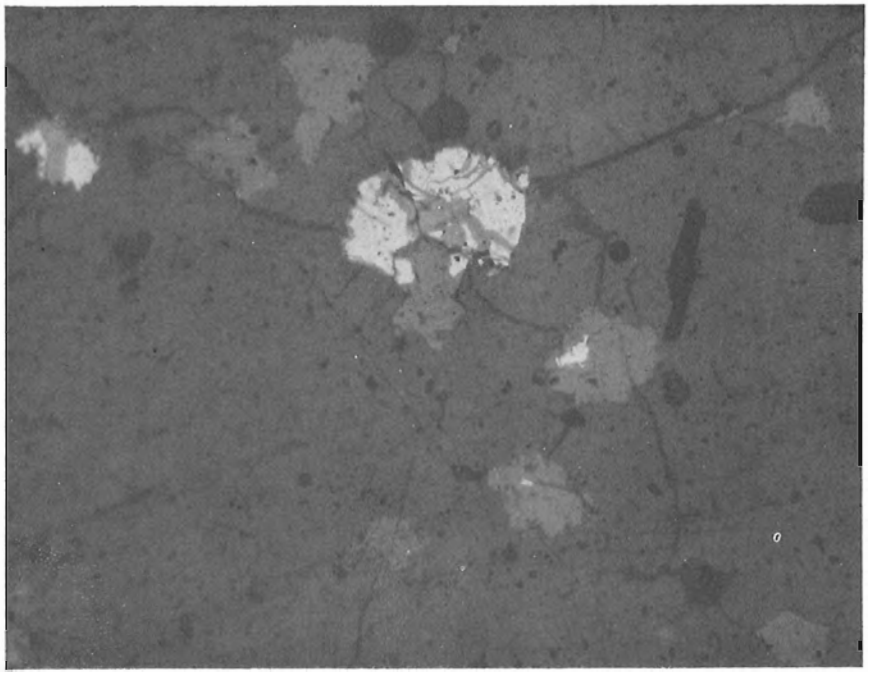

Figure 22.1. Radioactive hydrocarbon: Oxford Formation. Main mass is homogeneous hydrocarbon. Bright grains are mainly pyrite with some chalcopyrite. Light grey grains are iron oxide, probably goethite. Magnification: X350. Mineral identification by A.G. Plant.

transportation of U, Cu and other trace metals into the sediments. It is further postulated that this organic matter was likely some form of the polymeric, polyelectrolyte material known collectively as humic and fulvic acids.

According to Schnitzer and Khan (1972) the following ions form very stable strong complexes with fulvic acid: Fe^{3+}, Al^{3+}, Cu^{2+}, Pb^{2+}, Ca^{2+}; Zn^{2+}, Mn^{2+} and Mg^{2+} form weaker complexes. Roughly the same order of stability is followed for metal ion-humic acid complexes as well. It is generally considered that the strong complexes are true inner-sphere or chelate types whereas the weaker complexes are outer-sphere types. For example, van Dijk (1971) assigned the following order of increasing stability for divalent metal ion-humic acid complexes:

Ba, Ca, Mg, Mn, Co, Ni, Fe, Zn, Pb, Cu, (Fe III).

Little work has been done to date on UO_2^{++} complexes, however Pauli (1975) has conducted experiments which indicate that UO_2^{++} forms very strong soluble humic acid complexes, at least as strong as Cu^{2+}.

No work has been published on the complexes which might form between U^{4+} ions and soluble humic matter. It is likely that such complexes do form and are stable under the reducing conditions normally experienced in groundwaters. Kovalev and Generalova (1968) have reported that normally immobile species such as the hydrolyzate ions of Ti^{4+}, Zr^{4+} and Th^{4+} are readily stabilized in solution by the complexing action of humic and fulvic acids. U^{4+} is chemically a very similar ion to Th^{4+} and therefore might be expected to be similarly mobile in the presence of natural organic acids.

The strength of complexes formed and the related ability of humic and fulvic acids to dissolve silicate minerals are further illustrated by the work of Huang and Keller (1972) who found that fulvic acid can extract Al, Si, Fe and Mg from clays and other silicate minerals. Moreover, Fotiyev (1971) has demonstrated that "aqueous humus" from marsh waters contains considerable dissolved silica which forms a 1:2 complex with fulvic acid. Carbonates and sulphides are also readily solubilized by aqueous humic acids (Baker, 1973).

The presence of sulphide ion in the groundwater system does not appear to be a total deterrent to the migration of metal-humate complexes. Kovalev and Generalova (1974) investigated the effects of organic acids on the formation of Fe sulphides. They observed that the presence of organic acids, especially fulvic acid, suppressed the formation of pyrite. Pauli (1975) studied the system humic acids: metal ions, Cu, Zn, Pb, Ni, Cd: saturated H_2S. Although some 60 per cent of the metal humates were transformed into sulphides, some 30 per cent remained with acid precipitatable humus. Boulegue and Michard (1974) noted that polysulphide ions, species common in reducing groundwaters, serve as good acidity and redox buffers as well as strong complexers. Humic acid-polysulphide interactions result in the stabilization of the organics by incorporating polysulphide into their structure. The complexing ability of these addition complexes towards metal ions is also further strengthened. Other ions such as $S_2O_3^{=}$ (Listova, 1966) are commonly present in groundwaters and have been shown to form very stable complexes with ions such as Pb^{++} under weakly acid conditions.

Conclusions

The relevance of this work to the formation of Cu-U hydrocarbon residues in Paleozoic rocks can now be demonstrated. The ability of humic acids to transport UO_2^{++}, Cu^{++}, Pb^{++}, Ca^{++}, Fe^{++} and ions is undoubted. There is good evidence that reduced species, such as U^{4+} and ions normally considered to be immobile, Th^{4+}, Zr^{4+}, Ti^{4+}, Si^{4+}, Al^{3+}, are also rendered quite mobile by humic acids. Thus interactions between them either in solution or as coalescing gels become possible. Fotiyev (1971) has suggested that kaolin could form from the interaction of organic complexes of Si and Al; Huang and Keller (1972) consider that bauxite may form as a result of leaching and accumulation of Al-fulvate complexes. Similarly it can be suggested that uranotitanates, of which brannerite is an end member, could also form in this way, or coffinite could exsolve from a hydrocarbon-rich

solution containing both U and Si. Of course, other related mechanisms involving adsorption of U ions onto pre-existing hydrocarbon residues, titania or silica skeleta likely complicate the model. But in the absence of matching quantities of counter ions, uraninite itself may exsolve from a degrading hydrocarbon complex along with some sulphides of Cu and Fe. Given sufficient time this would likely occur spontaneously, but there is one further aspect which may be important to the formation of U-rich hydrocarbon residues and that relates to the well known ability of prolonged radiation (X-ray, gamma, UV) to promote dehydrogenation and polymerization and accelerate precipitation of organic compounds.

It is therefore proposed that the very even distribution of U, and certain other trace ions such as Ca^{++}, in the South March area hydrocarbons are the result of catalytic polymerization of soluble humic materials which have also contributed to the collection of these ions en route. Ions then become trapped at their complexation sites rather than migrating to crystallization loci as might happen in gel reactions. Ca^{++} is abundant in these hydrocarbons because of its ability to form strong humate complexes and most importantly, because of its easy availability in carbonate rocks. Its content may well represent the saturation complexing capacity of the original transporting organic acids.

This mechanism is proposed as a strong possibility for this particular environment. It does not exclude other adsorption-precipitation mechanisms or the involvement of other complexing agents in the mineralizing process.

References

Baker, W.E.
1973: The role of humic acids from Tasmanian Podzolic soils in mineral degradation and metal mobilization; Geochim. Cosmochim. Acta, v. 37, p. 269-281.

Boulegue, J. and Michard, G.
1974: Interactions between sulphur-polysulphide systems and organic material in reducing media; Acad. Sci. C.R., Ser. D, v. 279, no. 1, p. 13-15.

Charbonneau, B.W., Jonasson, I.R., and Ford, K.L.
1975: Cu-U mineralization in the March Formation Paleozoic rocks of the Ottawa-St. Lawrence Lowlands; in Report of Activities, Part A, Geol. Surv. Can., Paper 75-1A, p. 229-233.

van Dijk, H.
1971: Cation binding of humic acids; Geoderma, v. 5, p. 53-67.

Ford, K.L.
1975: Petrography, geochemistry and geophysics of a U-Cu occurrence, South March, Ontario; Unpubl. B.Sc. (Hons) thesis, Carleton Univ., Ottawa.

Ford, K.L., Charbonneau, B.W., and Watkinson, D.H.
1976: Mineralogy and geochemistry of the uranium-copper occurrence in dolomitic sandstone, South March, Ontario; Abstr., Ann. Meet. Geol. Assoc. Can., Edmonton, Alta. May 19-21, p. 44.

Fotiyev, A.V.
1971: Nature of aqueous humus; Dokl. Akad. Nauk. SSSR, v. 199, no. 1, p. 198-201.

Huang, W.H. and Keller, W.D.
1972: Organic acids as agents of chemical weathering of silicate minerals; Nature (London), Phys. Sci., v. 229, no. 96, p. 149-151.

Kovalev, V.A. and Generalova, V.A.
1968: Interaction of humic acids with element-hydrolyzates; Mater. Semin. Geochim. Gibergenezakory Vyvetrivaniya, Publ. 1969, Ed. Lukashev, K.I., Izd. Akad. Nauk Belorusskoi SSR Minsk, p. 91-99.

1974: Modelling of formation of sulphide from iron humate complexes; Geokhim., v. 11, no. 3, p. 425-433.

Listova, L.P.
1966: Experimental data on the solubility of lead sulphide under oxidizing conditions; Geokhim. (Akad. Nauk SSSR), no. 1, p. 60-69.

Pauli, F.W.
1975: Heavy metal humates and their behaviour against hydrogen sulphide; Soil Sci., v. 119, no. 1, p. 98-105.

Schnitzer, M. and Khan, S.U.
1972: Humic substances in the environment; Marcel Dekker Inc., New York, N.Y.

Steacy, H.R., Boyle, R.W., Charbonneau, B.W., and Grasty, R.L.
1973: Mineralogical notes on the uranium occurrences at South March and Eldorado, Ontario; in Report of Activities, Part B, Geol. Surv. Can., Paper 73-1B, p. 103-105.

23. A STUDY OF Cu-S-Se MINERALS: ELECTRON MICROPROBE ANALYSIS AND X-RAY POWDER DATA

Projects 620308, 750010

G.J. Pringle[1] and A.R. Miller[2]

Various Cu-Se and Cu-S-Se minerals have been documented by Earley (1950) and Harris et al. (1970a, 1970b). The present study involves the chemistry and X-ray diffraction characteristics of umangite (Cu_3Se_2), berzelianite ($Cu_{2-x}Se$) and athabascaite ($Cu_{5+1}Se_4$). This assemblage was encountered as fracture fillings in a highly carbonatized mafic intrusive rock from Christopher Island, Baker Lake, N.W.T. Hematite is the most abundant gangue mineral in the veins and occurs as anhedral aggregates and subhedral blades that are up to 0.3 mm in length. The other associated minerals are botryoidal pitchblende, calcite, Fe-rich chlorite, minor cerussite and minor clausthalite.

Berzelianite and athabascaite occur as intergrowths forming angular plates among the hematite blades in the coarser grained portions of the veins (Fig. 23.1). Umangite occurs in the finer grained portions of the veins where it is commonly mantled by the berzelianite and athabascaite mixture. Clausthalite (0.01-0.02 mm) is restricted to the finer grained areas and occurs both as inclusions in the selenides and as discrete peripheral grains.

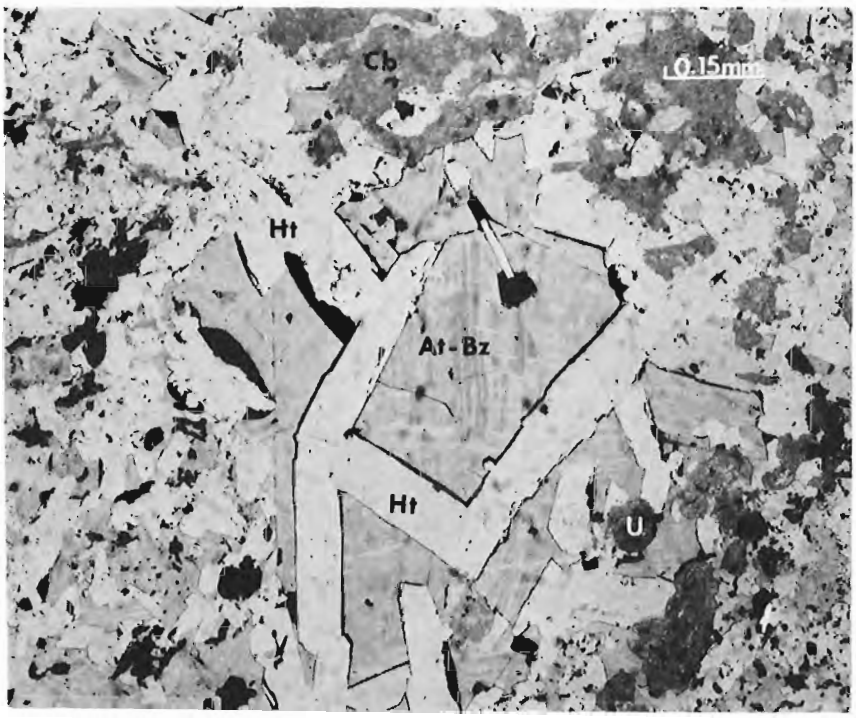

Figure 23.1. Photomicrograph of fine grained athabascaite-berzelianite intergrowth (At-Bz) associated with the assemblage: hematite (Ht) + carbonate (Cb) + botryoidal pitchblende (U), Baker Lake, N.W.T. (GSC 203179).

The selenide compositions were determined on a Materials Analysis Company (MAC) electron microprobe operated at 20Kv and a specimen current of about 0.03 micro-amperes. Corrections were applied to the data using the computer program ERPMAG, developed at CANMET by combining EMPADR VII (Rucklidge and Gasparrini, 1969) and MAGIC IV (Colby). The standards and X-ray lines used were: synthetic CuSe (Cu K_α, Se K_α), synthetic CuS (S K_α), chalcopyrite (Fe K_α), galena (Pb M_α) and halite (Cl K_α).

It proved difficult to obtain analyses that were not composites because of the nature of the fine grained athabascaite-berzelianite mixture. Analyses 3 to 6 (Table 23.1) are spots on what appear to be coarser blades of athabascaite under the microscope. Sulphur ranges from 3.3 to 3.6 wt per cent while Fe is as high as 1.5 wt per cent. Analysis 12 (Table 23.1) has the highest copper content and probably is close to the true berzelianite composition in the sample. Sulphur in the berzelianite approaches 3.0 wt per cent.

Umangite in the finer grained portions of the vein contains no sulphur and variable iron up to 2.1 wt per cent (Table 23.1). The umangite has minute grey inclusions that contribute minor concentrations of Pb, Cl and probably Fe. The low totals in the umangite analyses remain unexplained, however, it is possible that the finely dispersed inclusions also contain O, H_2O, OH or CO_3. The powder pattern from a mount including the umangite and some surrounding material is in excellent agreement with data from the J.C.P.D.S. file card 19-402 (Table 23.2).

It was not possible to prepare separate X-ray powder diffraction mounts of each of the selenide phases because of the fine intergrowth. The pattern presented in Table 23.3 is a mixture of athabascaite and berzelianite. Analysis 6 (Table 23.1) is the average of several spot analyses on the athabascaite blades in the material used to prepare this mount. Analysis 8 is a broad beam analysis of this same area including both athabascaite and berzelianite. The athabascaite pattern from this area compares favourably with that presented by Harris et al. (1970a).

The type specimens of athabascaite from Martin Lake, Lake Athabasca area, northern Saskatchewan, were obtained from the National Mineral Collection for comparison. The specimens were re-analysed (Analyses 1 and 2, Table 23.1) and X-ray powder mounts were prepared from both the high sulphur (2.6 wt per cent) and the low sulphur (0.3 wt per cent) varieties. Seven lines were

[1]Central Laboratories and Administrative Services Division

[2]Regional and Economic Geology Division

From: Report of Activities, Part B; Geol. Surv. Can., Paper 77-1B (1977)

Table 23.1

Microprobe Analyses of the Selenides

		Elements Wt. %							Formula (Se, S) = 4.00			
		Cu	Se	S	Fe	Pb	Cl	Total				
1	Sulphur-bearing Athabascaite, Martin Lake	52.1	44.0	2.6	0.3	-	-	99.0	$Cu_{5.13}$	$Fe_{.03}$	$Se_{3.49}$	$S_{.51}$
2	Athabascaite, Martin Lake	49.8	48.2	0.3	0.04	-	-	98.34	$Cu_{5.06}$	$Fe_{.01}$	$Se_{3.94}$	$S_{.06}$
3	Athabascaite	51.8	43.4	3.6	1.5	-	-	100.3	$Cu_{4.92}$	$Fe_{.16}$	$Se_{3.32}$	$S_{.68}$
4	Athabascaite	52.3	43.5	3.3	0.2	-	-	99.3	$Cu_{5.03}$	$Fe_{.02}$	$Se_{3.37}$	$S_{.63}$
5	Athabascaite	52.1	43.1	3.3	0.4	-	-	98.9	$Cu_{5.05}$	$Fe_{.04}$	$Se_{3.37}$	$S_{.63}$
6	Athabascaite	52.9	43.1	3.6	0.1	-	-	99.7	$Cu_{5.06}$	$Fe_{.01}$	$Se_{3.32}$	$S_{.68}$
7	Athabascaite + Berzelianite	55.0	42.5	3.1	0.4	-	-	101.0	$Cu_{5.46}$	$Fe_{.04}$	$Se_{3.39}$	$S_{.61}$
8	Athabascaite + Berzelianite	56.1	41.7	3.0	0.2	-	-	101.0	$Cu_{5.68}$	$Fe_{.02}$	$Se_{3.40}$	$S_{.60}$
9	Athabascaite + Berzelianite	57.2	40.0	3.4	0.1	-	-	100.7	$Cu_{5.87}$	$Fe_{.01}$	$Se_{3.31}$	$S_{.69}$
10	Berzelianite + Athabascaite	56.9	39.7	3.0	0.2	-	-	99.8	$Cu_{6.00}$	$Fe_{.03}$	$Se_{3.37}$	$S_{.63}$
11	Berzelianite + Athabascaite	58.2	38.3	3.0	0.2	-	-	99.7	$Cu_{6.33}$	$Fe_{.03}$	$Se_{3.35}$	$S_{.65}$
12	Berzelianite	60.0	37.2	2.9	0.3	-	-	100.4	$Cu_{6.73}$	$Fe_{.04}$	$Se_{3.36}$	$S_{.64}$
13	Umangite, Martin Lake	54.9	45.5	0.1	0.0	-	-	100.5	$Cu_{5.96}$	$Fe_{.00}$	$Se_{3.99}$	$S_{.01}$
14	Umangite	49.1	43.8	0.0	0.4	3.2	0.3	96.8	$Cu_{5.57}$	$Fe_{.05}$	$Se_{4.00}$	$S_{.00}$
15	Umangite	46.7	40.7	0.0	2.1	7.0	0.5	97.0	$Cu_{5.71}$	$Fe_{.30}$	$Se_{4.00}$	$S_{.00}$
16	Umangite	47.7	40.0	0.0	1.6	4.3	0.3	93.9	$Cu_{5.93}$	$Fe_{.23}$	$Se_{4.00}$	$S_{.00}$

Table 23.2

X-ray Powder Data for Umangite

G.S.C. Film no. 56047		Umangite JCPDS 19-402	
d	Iest	d	Iest
4.28	3	4.28	10
3.56	10	3.55	100
3.21	8*	3.20	50
3.11	8	3.11	60
2.867	2	2.865	12
2.565	2	2.564	16
2.380	1	2.380	8
2.266	8	2.264	45
2.141	3	2.140	25
2.024	7b	2.025	35
2.017	9**	2.002	20
1.940	1	1.934	20
1.911	4	1.910	40
1.832	9	1.831	80
1.780	8	1.780	60
1.718	2**	1.715	25
1.639	2	1.639	16
1.603	½	1.610	2
1.558	1	1.554	4
		1.508	2
1.457	½	1.459	2b
1.424	1	1.424	6b
1.365	1b	1.366	4b
		1.360	4b
		1.358	4b
1.286	½	1.281	4
1.278	½	1.278	4
1.258	½	1.255	6
1.233	1b	1.231	6
1.206	2	1.205	14
1.189	1	1.190	10
1.156	1b**	1.166	8
1.147	½	1.146	2b
1.133	½	1.132	2b
		1.113	2b
1.100	½	1.100	2b
1.051	½		
1.037	½		
.9420	½		

*includes athabascaite
**includes berzelianite
The mount is a mixture of umangite and some surrounding material.
Extra lines from hematite, athabascaite and berzelianite have been removed except where they overlap with umangite.
CuK_{α}. 114.7 mm camera.

Table 23.3

X-Ray Powder Data for the Athabascaite-Berzelianite Mixture

G.S.C. Film no. 56046		Athabascaite Harris et. al. (1970A)		Berzelianite Earley (1950)	
d	Iest	d	Iest	d	Iest
12.1	3	12.1	½		
6.01	½	6.00	½		
		4.11	½		
3.42	1	3.44	3		
		3.34	½		
3.29	4			3.33	9
3.23	10	3.235	10		
3.11	½*	3.112	1		
3.01	9	3.015	6		
2.87	2	2.870	2	2.88	1
2.75	1	2.744	2		
2.59	½*	2.606	½		
2.49	2*	2.490	2		
		2.391	½		
		2.200	½		
2.08	1*	2.105	2		
2.02	9			2.03	10
1.991	10	1.997	8		
1.892	5	1.893	5		
1.814	1	1.817	3		
1.719	2	1.720	½	1.729	8
1.694	1	1.694	2		
1.663	4	1.664	4		
1.426	1			1.434	3
1.371	2	1.374	3		
1.309	1			1.317	2
1.290	1	1.294	3		
1.211	1	1.205	2		
1.164	1			1.171	4
1.151	1	1.149	2		
1.130	1	1.132	2		
1.098	1			1.105	2
1.074	1	1.074	½		

*Lines from mixed cerussite have been removed except where they are superimposed.
CuK_{α}. 114.7 mm camera.

selected to produce refined cell parameters for both type materials and the material from Baker Lake. Since too few lines were used for maximum precision the results given in Table 23.4 can be used only in a relative sense to show the decrease in cell parameters with increasing sulphur content.

Table 23.4

Refined Cell Parameters for Athabascaite.
Orthorhombic cell (Å)

Sample	% S (Table 23.1)	a_o	b_o	c_o
Baker Lake	3.6	8.176	12.054	6.441
Martin Lake	2.6	8.231	12.101	6.461
Martin Lake	0.3	8.242	12.137	6.497

Table 23.5

Berzelianite Cell Edge with Composition
(Harris et al., 1970b)

Sample	Formula	Cell Edge (Å)
Martin Lake	$Cu_{1.751}Se$	5.740 ± .001
Synthetic 129	$Cu_{1.801}Se$	5.746 ± .001
W. Moravia	$Cu_{1.854}Se$	5.748 ± .002
Synthetic 155	$Cu_{1.806}Se_{.826}S_{.173}$	5.724 ± .002
Synthetic 159	$Cu_{1.799}Se_{.699}S_{.300}$	5.702 ± .001
Synthetic 157	$Cu_{1.680}Se_{.499}S_{.501}$	5.653 ± .002
Martin Lake	$Cu_{1.797}Se_{.683}S_{.317}$	5.696 ± .003
Anal. 12, Table 23.1	$Cu_{1.68}Fe_{.01}Se_{.84}S_{.16}$	5.705 ± .001

The diffraction pattern of berzelianite (Table 23.3) shows a consistently smaller d spacing than that of Earley (1950) and gives a refined cubic cell dimension of 5.705Å. The relationship between cell size and composition of sulphur-bearing berzelianites presented by Harris et al. (1970b) gives 27 atomic % S in the (Se:S) position for the Baker Lake specimen as compared to a measured value of 16 atomic %, (Table 23.1, analysis 12). Table 23.5 lists the data used by Harris with the addition of the berzelianite from Baker Lake. The three sulphur-free samples can be used to estimate the effect of the increased copper deficiency in the Baker Lake sample, as compared to the synthetic compounds with approximately 1.80 formula units of copper. This correction gave an estimated cell edge of 5.717Å which in turn indicates 19 atomic % S in the (Se:S) position. It is interesting to note that when a similar correction is applied to sample 157 the relationship between sulphur content and cell edge becomes nearly linear for sulphur-bearing berzelianites with approximately 1.8 formula units of copper.

The presence of very fine intergrowths of berzelianite and athabascaite possibly represents a low temperature re-equilibration of an original umangite phase. Bernardini and Catini (1968) state that at 150°C, umangite breaks down to a mixture of Cu_3Se_2, $Cu_{2-x}Se$ and CuSe. Harris et al. (1970a) state that attempts to synthesize athabascaite at 100°C with 3% S were unsuccessful. These authors also state that umangite is unstable at 135°C and can be synthesized only with difficulty at 120°C.

References

Bernardini, G.P. and Catini, A.
1968: The Cu-Se system; Mineral. Deposita, v. 3, p. 375-380.

Colby, J.W.
MAGIC IV – a computer program for quantitative electron microprobe analysis. Bell Telephone Laboratories, Allentown, Pennsylvania.

Earley, J.W.
1950: Description and synthesis of the selenide minerals; Am. Mineral., v. 35, p. 337-364.

Harris, D.C., Cabri, L.J., and Kaiman, S.
1970a: Athabascaite: A new copper selenide mineral from Martin Lake, Saskatchewan; Can. Mineral., v. 10, pt. 2, p. 207-215.

Harris, D.C., Cabri, L.J., and Murray, E.J.
1970b: An occurrence of a sulphur-bearing berzelianite; Can. Mineral., v. 10, pt. 4, p. 737-740.

Rucklidge, J.C. and Gasparrini, E.L.
1969: Electron microprobe analytical data reduction, EMPADR VII; Univ. Toronto, Dept. Geol.

Project 750037

A.P. Annan and J.L. Davis
Resource Geophysics and Geochemistry Division

Introduction

The maximum range of a radar system is a function of the system parameters, the target parameters and the electrical properties of the medium being probed. The radar range equation can be found in any standard text on radar and electromagnetic radiation (Ridenour, 1947). In the following analysis, the radar range equation is used to determine the maximum range at which smooth and rough, plane, specular targets can be detected given the geologic material properties, attenuation characteristics and system parameters. The range characteristics of various ground probing radars can then be compared.

Radar Range Equation

The radar range equation is

$$Q = 10 \log\left(\frac{\varepsilon_{TX} \cdot \varepsilon_{RX} \cdot G_{TX} \cdot G_{RX} \cdot c^2 \cdot g\sigma \cdot e^{-4\alpha L}}{64\pi^3 f^2 L^4}\right) \qquad (1)$$

The individual terms in this equation are defined with the aid of the block diagram shown in Figure 24.1. Q is the system performance factor expressed in decibels. Q is the ratio of the minimum detectable signal power to the power input to the transmitting antenna.

$$Q = 10 \log\left[\frac{P_{MIN}}{P_s}\right] \qquad (2)$$

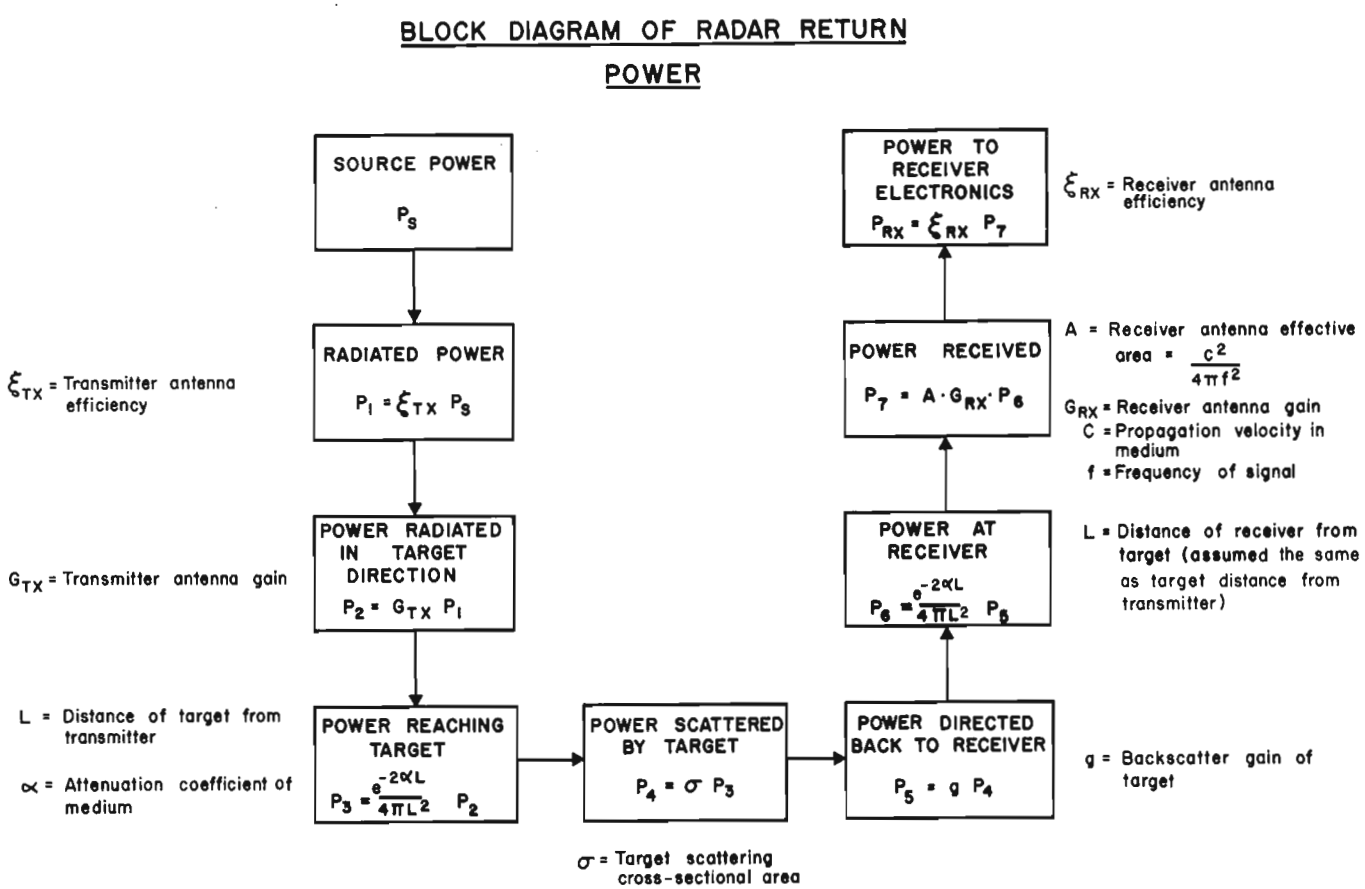

Figure 24.1. Block diagram of radiated and return power for a radar system.

From: Report of Activities, Part B;
Geol. Surv. Can., Paper 77-1B (1977)

Table 24.1

Backscatter-gain and cross-sectional area simple model coefficients

	B_1	B_2	B_3
Smooth, Plane Reflector	$\log(\pi R)$	2	0
Rough Plane Reflector	$\log \frac{\pi c R}{2}$	1	-1
Rayleigh Point Target	$\log \frac{64\pi^5 a^6}{c^4}$	0	4

Table 24.2.

List of ground probing radars to be compared

SYSTEM NAME	SYSTEM KEYWORD	SYSTEM TYPE	REFERENCE
GSSI	2 ns	impulse	
GSSI	10 ns	impulse	
Unterberger	440 MHz	pulse	Stewart & Unterberger, 1976
Unterberger	230 MHz	pulse	
SCR 718	440 MHz	pulse	Weber & Andrieux, 1970
SCR 718 (a)	440 MHz	pulse	Davis, et. al., 1973
Goodman	620 MHz	pulse	Evans, 1970
Goodman (a)	620 MHz	pulse	Evans, 1970
SPRI MK III	480 MHz	pulse	Davis, 1973
HALS	205 MHz	pulse	Evans, 1970
HALS (a)	205 MHz	pulse	Evans, 1970
SPRI MK III	150 MHz	pulse	Davis, 1973
HALS	80 MHz	pulse	Evans, 1970
HALS (a)	80 MHz	pulse	Evans, 1970
SPRI MK III	60 MHz	pulse	Davis, 1973
SPRI MK II	35 MHz	pulse	Davis, 1973
SPRI MK III	23.4 MHz	pulse	Davis, 1973
SPRI MK III	16.9 MHz	pulse	Davis, 1973
SPRI MK III	12.8 MHz	pulse	Davis, 1973
Cambridge	3.5 MHz	monopulse	Ferrari, et. al., 1976
Watts	5 MHz	monopulse	Watts & England, 1976
Watts	1.4 MHz	monopulse	Watts & England, 1976

For analysis purposes, it is convenient to regroup equation 1 as follows

$$40 \log L + 2AL - 10 \log \left(\frac{c^2 g\sigma}{f^2} \right) = 10 \log \left[\frac{\varepsilon_{TX}\, \varepsilon_{RX}\, G_{TX}\, G_{RX}}{64\, \pi^3} \right] - Q \qquad (3)$$

where A is the attenuation factor for the medium in dB/unit length

$$A = 20 \log e^{-\alpha} = 8.69\alpha \qquad (4)$$

For computational purposes, the units of length are determined by the units chosen for propagation velocity, c (see Appendix 1).

The expression in equation (3) has been grouped to indicate range dependence as a function of system, target and material properties. The major factors still to be specified are the target parameters σ and g. In the following section, the scattering cross-section and backscatter gain are discussed.

Target Properties

The targets of interest when probing geological materials are often planar boundaries. To this end, estimates of the "gσ" factor for specular reflecting, smooth and rough boundaries are outlined.

Smooth, Plane, Specular Reflector

The power returned by a smooth, plane, specular reflector is most easily computed using image theory as illustrated in Figure 24.2. The plane reflects the incident signal in such a manner that it appears as if an image of the transmitter, reduced in power by the power reflection coefficient, R, of the boundary, is radiating upwards from a distance twice as far away as the plane. The power received in this case is

$$P_{RX} = P_{source} \cdot R \cdot \frac{\varepsilon_{TX}\, \varepsilon_{RX}\, G_{TX}\, G_{RX} c^2 e^{-4\alpha L}}{16\, \pi^2\, f^2\, (2L)^2} \qquad (5)$$

Thus, the backscatter-gain, scattering-cross-section product is

$$g\sigma = \pi L^2 R \qquad (6)$$

Rough, Plane, Specular Reflector

The exact power returned from a rough, planar, reflector is not readily calculated. One estimate of the cross-sectional area of such a target suggested by Cook (1975) is the area of the first Fresnel zone. The first Fresnel zone is that area of the surface for which reflected signals travel a path length less than $(L + \frac{\lambda}{4})$ where L is the normal distance to the plane and λ is the wavelength of signal in the medium. This yields an effective radius for a circular area on the target of

$$r = \left[\left(L + \frac{\lambda}{4} \right)^2 - L^2 \right]^{1/2} \qquad (7)$$

The area of the first Fresnel zone is

$$\sigma = \pi r^2 = \pi \left(\frac{\lambda^2}{16} + \frac{\lambda L}{2} \right) \qquad (8)$$

When L is large compared with λ, σ becomes

$$\sigma \simeq \frac{\pi \lambda L}{2} \qquad (9)$$

The returned energy depends on the reflectivity of the surface. The "gσ" product is therefore

$$g\sigma = \frac{\pi \lambda L R}{2} = \frac{\pi\, L R\, c}{2 f} \qquad (10)$$

where R is the power reflection coefficient of the boundary.

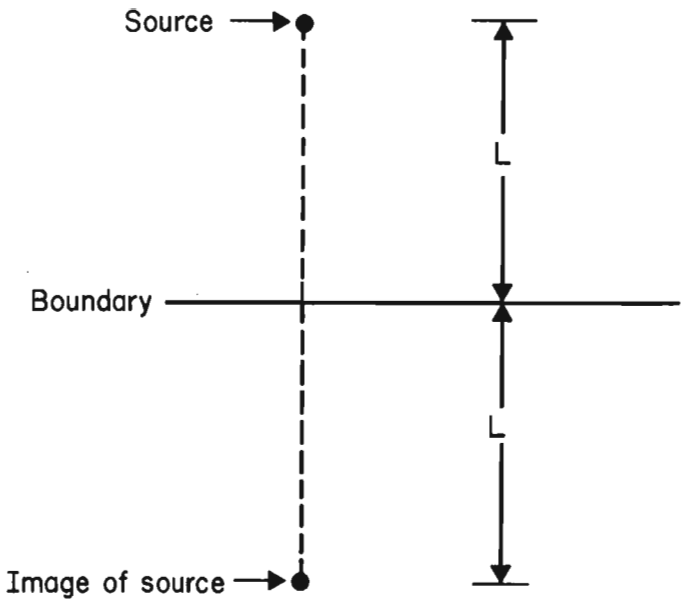

Figure 24.2. Reflection from a smooth, planar boundary.

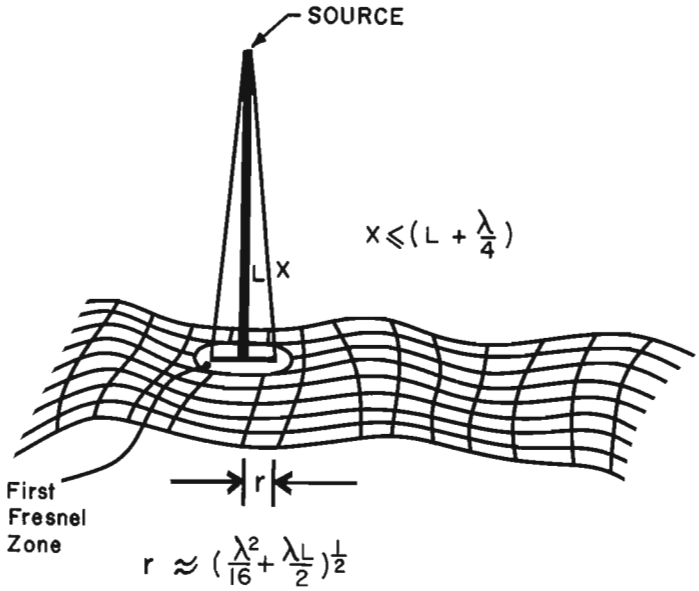

Figure 24.3. Reflection from a rough, planar boundary.

Table 24.3

System parameters for the radar systems given in Table 24.2

System	Q	ϵ_{TX}	ϵ_{RX}	G_{TX}	G_{RX}	T	f
	dB	dB	dB	dB	dB	ns	MHz
GSSI 2ns	-110	-13	-13	2	2	2	500
GSSI 10ns	-110	-13	-13	2	2	10	100
Unterberger 440 MHz	-110	- 3	- 3	30	30	1000	440
Unterberger 230 MHz	-110	- 3	- 3	15	15	1000	230
SCR 718 440 MHz	-120	- 3	- 3	4	4	300	440
SCR 718 440 MHz (a)	-120	- 3	- 3	8	8	300	440
Goodman 620 MHz	-154	- 3	- 3	15	15	100	620
Goodman 620 MHz (a)	-159	- 3	- 3	15	15	500	620
SPRI MK III 480 MHz	-145	- 3	- 3	11	11	100	480
Hals 205 MHz	-120	- 3	- 3	12	12	200	205
Hals 205 MHz (a)	-120	- 3	- 3	12	12	500	205
SPRI MK III 150 MHz	-145	- 3	- 3	11	11	180	150
Hals 80 MHz	-120	- 3	- 3	9	9	200	80
Hals 80 MHz (a)	-120	- 3	- 3	9	9	500	80
SPRI MK III 60 MHz	-150	- 3	- 3	2.5	2.5	120	60
SPRI MK II 35 MHz	-145	- 3	- 3	1.6	1.6	240	35
SPRI MK III 23.4 MHz	-105	- 3	- 3	1.6	1.6	360	23.4
SPRI MK III 16.9 MHz	- 90	- 3	- 3	1.6	1.6	480	16.9
SPRI MK III 12.8 MHz	-100	- 3	- 3	1.6	1.6	600	12.8
Cambridge Monopulse 3.5 MHz	- 62	-10	-10	1.6	1.6	300	3.5
Watts Monopulse 5 MHz	- 67	-10	-10	1.6	1.6	600	5
Watts Monopulse 1.4 MHz	- 67	-10	-10	1.6	1.6	1400	1.4

Table 24.4

Maximum detectable range in metres of a smooth, perfectly reflecting plane target as a function of material loss for the systems listed in Table 24.2

System	ATTENUATION dB/m						RESOLUTION
	0	0.001	0.01	0.1	1	10	r
GSSI 2ns	3×10^2	281	192	66	14	2.2	0.15
GSSI 10ns	1.5×10^3	1150	488	112	19	2.7	0.75
Unterberger 440 MHz	2.2×10^6	20300	2870	376	47	5.6	75
Unterberger 230 MHz	1.4×10^5	10900	1860	270	36	4.5	75
SCR 718 440 MHz	1.7×10^4	5180	1170	194	28	3.7	22.5
SCR 718 440 MHz (a)	4.3×10^4	7550	1470	228	31	4.0	22.5
Goodman 620 MHz	7.6×10^6	25000	3360	425	52	6.1	7.5
Goodman 620 MHz (a)	1.36×10^7	27000	3580	448	54	6.3	37.5
SPRI MK III 480 MHz	1.4×10^6	18700	2710	359	45	5.4	7.5
Hals 205 MHz	2.3×10^5	12600	2050	290	38	4.7	7.5
Hals 205 MHz (a)	2.3×10^5	12600	2050	290	38	4.7	37.5
SPRI MK III 150 MHz	4.5×10^6	22900	3150	404	50	5.9	13.5
Hals 80 MHz	3.0×10^5	13400	2140	300	39	4.8	15
Hals 80 MHz (a)	3.0×10^5	13400	2140	300	39	4.8	37.5
SPRI MK III 60 MHz	2.8×10^6	21200	2970	386	48	5.7	9
SPRI MK II 35 MHz	2.2×10^6	20300	2880	377	47	5.6	18
SPRI MK III 23.4 MHz	3.3×10^4	6820	1380	218	30	3.9	27
SPRI MK III 16.9 MHz	8.1×10^3	3560	936	168	25	3.4	36
SPRI MK III 12.8 MHz	3.4×10^4	6900	1390	219	30	3.9	45
Cambridge Monopulse 3.5 MHz	3.1×10^2	290	197	67	14	2.2	22.5
Watts Monopulse 5 MHz	3.9×10^2	356	228	73	14	2.2	45
Watts Monopulse 1.4 MHz	1.4×10^2	1080	469	110	19	2.7	105

Point Target

No simple solution exists for the "$g\sigma$" product of any real, small target. In general "$g\sigma$" is a complicated function of frequency and angle of illumination. For most computational purposes, it is necessary to specify "$g\sigma$" from detailed knowledge of the specific, point target under consideration.

For some special applications, the Rayleigh law of scattering is useful. A conducting sphere with radius, a, which is much less than the wavelength of the exciting signal has an effective cross-sectional area and backscatter-gain. (Stratton, 1941).

$$g\sigma = \frac{64\,\pi^5\,a^6\,f^4}{c^4} \tag{11}$$

The important feature of the Rayleigh scattering law is that it demonstrates the strong frequency dependence of the "$g\sigma$" product.

Simple Target Model

For range computations, a simple, mathematical model is devised here. The backscatter-gain, cross-sectional-area product is assumed to be of the form

$$g\sigma = 10^{B_1}\ L^{B_2}\ f^{B_3} \tag{12}$$

Table 24.5

Maximum detectable range in metres of a rough perfectly reflecting plane target as a function of material loss for the systems listed in Table 24.2

System	ATTENUATION - dB/m						Resolution r
	0	0.001	0.01	0.1	1	10	
GSSI 2ns	28	28	27	20	8.2	1.8	0.15
GSSI 10ns	142	139	118	58	15	2.6	0.75
Unterberger 440 MHz	11000	5060	1360	247	37	5	75
Unterberger 230 MHz	2200	1700	724	168	28	4.1	75
SCR 718 440 MHz	438	411	283	98	20	3.2	22.5
SCR 718 440 MHz (a)	8090	7240	423	123	23	3.5	22.5
Goodman 620 MHz	22900	7370	1690	286	41	5.4	7.5
Goodman 620 MHz (a)	33500	8750	1880	306	43	5.6	37.5
SPRI MK III 480 MHz	8010	4200	1220	231	35	4.8	7.5
Hals 205 MHz	3210	2270	859	186	30	4.3	15
Hals 205 MHz (a)	3210	2270	859	186	30	4.3	37.5
SPRI MK III 150 MHz	25600	7770	1750	292	42	5.5	13.5
Hals 80 MHz	5190	3180	1040	209	33	4.6	15
Hals 80 MHz (a)	5190	3180	1040	209	33	4.6	37.5
SPRI MK III 60 MHz	25500	7750	1750	291	42	5.5	9
SPRI MK II 35 MHz	25900	7820	1750	292	42	5.5	18
SPRI MK III 23.4 MHz	1800	1440	657	158	27	4.0	27
SPRI MK III 16.9 MHz	789	707	416	122	23	3.5	36
SPRI MK III 12.8 MHz	2240	1720	731	169	29	4.1	45
Cambridge Monopulse 3.5 MHz	152	148	125	60	15	2.6	22.5
Watts Monopulse 5 MHz	156	152	128	61	15	2.6	45
Watts Monopulse 1.4 MHz	556	514	333	107	21	3.3	105

The factor "$g\sigma$" in equation 3 yields the 3 terms

$$10 \log g\sigma = 10 \left[B_1 + B_2 \log L + B_3 \log f\right] \tag{13}$$

The coefficients for the smooth-plane-specular reflector, the rough-plane-reflector and the Rayleigh point target are tabulated in Table 24.1. The simple form of equation (12) permits rapid numerical simulation of quite a wide variety of targets. Obviously, a particular point target can be specified for a fixed frequency and look angle by specifying B_1 and setting $B_2 = B_3 = 0$.

Range Calculation

The calculation of the maximum range at which a target can be detected reduces to solving equation (3) for L once all other variables have been specified. Using the simple scattering model, equation (12), the range equation (3) becomes

$$\text{Log } L + D_1 \cdot L = D_2 \tag{14}$$

$$D_1 = \frac{2\,A}{40 - 10\,B_2} \tag{15}$$

$$D_2 = \left[\frac{-Q + 10 \log \left(\frac{\epsilon_{TX}\, \epsilon_{RX}\, G_{TX}\, G_{RX}}{64\pi^3} \right) + 10 \log c^2 + 10 (B_1 + (B_3 - 2) \log f)}{40 - 10 B_2} \right] \quad (16)$$

Equation 13 is a transcendental equation for which there is no simple, analytical solution. For computational purposes, a quick and simple numerical procedure is used to solve for L given D_1 and D_2. Details of FORTRAN and HP-65 computer programs can be found in Annan and Davis (Computer Programs for Radar Range Analysis in Geologic Materials, internal report, 1977). The solution algorithm is a Newton iterative scheme.

Computed Results

A number of different radar systems were chosen for a comparative study (Table 24.2). The various system parameters are given in Table 24.3 along with the units for each variable. One additional system parameter has been introduced which has a significant bearing on the utility of radar for probing geologic materials; this is the system resolution. For a pulse or impulse system with a pulse-time duration, τ, the minimum spatial separation between targets for which the system can still resolve two distinct events is

$$r = \frac{c\,\tau}{2} \quad (17)$$

For FM-CW systems, the resolution can be found by equating τ to $1/f_b$ where f_b is the system frequency bandwidth. The maximum range of each system listed in Table 24.2 for a perfectly reflecting, smooth, planar target is summarized in Table 24.4. Maximum range is listed as a function of attenuation factor. The medium in which the target is embedded is taken to have a velocity one half of that in a vacuum. This value is quite typical of many geological materials. Table 24.5 is a tabulation of the same results for a rough, perfectly reflecting, plane boundary. The wide frequency range of the systems being considered precluded examination of Rayleigh scattering.

Summary and Conclusions

The results listed in Tables 24.4 and 24.5 yield estimates of maximum target ranges for various systems and geological materials. One result becomes quite apparent when comparing the systems. The system efficiencies ϵ_{TX} and ϵ_{RX} as well as antenna gains G_{TX} and G_{RX} are very important in determining maximum range in low-loss material. In high-loss media, these parameters have much less influence on the maximum range. For example, the Unterberger pulse systems have several orders of magnitude greater range than the GSSI impulse systems do when considering low-loss media. When losses are high, the maximum range is about a factor of 2 to 4 greater with the higher power pulse systems. Basically, D_2 can be viewed as a system variable given a specific target. In low-loss materials, range is approximately given by

$$L \simeq 10^{D_2} \quad (18)$$

In a high-loss material

$$L \simeq \frac{D_2}{D_1} \quad (19)$$

L is exponentially proportional to the system parameter, D_2, in low-loss media while it is only linearly proportional to D_2 in high-loss media. Thus, factors such as high antenna gain and efficiency may not necessarily be the most important parameter to optimize in high-loss media. For the two Unterberger systems, the pulse lengths are on the order of 1 μs, which gives a spatial resolution of about 75 m. The GSSI impulse systems have pulse lengths of 10 and 2 ns which gives resolutions of 75 cm and 15 cm. While the GSSI systems have much lower efficiencies and gains, these parameters have been reduced to obtain high resolution. Since the resolution of the Unterberger systems are less than the maximum range of losses of 1 to 2 db/m, typically found in geological materials (Cook, 1975), resolution is an important parameter to be considered in system design. Before using a radar system, a reasonable knowledge of the electrical properties of the environment must be available in order that a rational decision can be made as to the optimum system to employ.

References

Cook, J.C.
1975: Radar transparencies of mine and tunnel rocks; Geophysics, v. 40, p. 865-885.

Davis, J.L.
1973: The problem of depth sounding temperate glaciers; Unpubl. M.Sc. thesis, Univ. Cambridge.

Davis, J.L., Halliday, J.S., and Miller K.J.
1973: Radio-echo sounding on a valley glacier in east Greenland; J. Glaciol., v. 12, no. 64, p. 87-91.

Evans, S.
1970: Review of radio-echo system performance. (Gudmandsen, P. ed) Proceedings of the International Meeting on Radioglaciology, Lyngby, May 1970; Lyngby, Technical University of Denmark, Laboratory of Electromagnetic Theory, p. 100-102.

Ferrari, R.L., Miller, K.J., and Owen, G.
1976: The 1976 Cambridge – Reykjavik Universities expedition to Vatnajökull, Iceland; Cambridge University Engineering Department. Special Report 5, Department of Engineering, Univ. Cambridge, 34 p.

Ridenour, L.N. (ed)
1947: Radar systems engineering; McGraw-Hill Book Co. Inc., New York, NY, 748 p.

Stewart, R.D. and Unterberger, R.R.
1976: Seeing through rock salt with radar; Geophysics, v. 41, p. 123-132.

Stratton, J.A.
1941: Electromagnetic theory; McGraw-Hill Book Co. Inc., New York and London, 615 p.

Watts, R.D. and England, A.W.
1976: Radio-echo sounding of temperate glaciers: Ice properties and sounder design criteria; J. Glaciol. v. 17, no. 76, p. 39-48.

Weber, J.R. and Andrieux, P.
1970: Radar soundings on the Penny Ice Cap, Baffin Island; J. Glaciol. v. 9, no. 55, p. 49-54.

APPENDIX I

Phase Velocity and Attenuation Factor in Terms of Dielectric Constant and Loss Tangent

For radar sounding analysis it is important to be able to convert quickly from electric property parameters to wave velocity and attenuation parameters. The complex dielectric constant of a material is expressed by

$$K^{*} = K'(1 + i \tan\delta) \qquad (1-1)$$

where K' is the real dielectric constant and tan δ is the loss tangent which is the ratio of the imaginary component of K* to the real component of K*.

For bulk geologic materials the magnetic permeability does not vary significantly from that of free space. As a result, a plane wave travelling in a geologic material can be expressed as

$$e^{i(kx - \omega t)} \qquad (1-2)$$

where x is position, t is time, ω is angular frequency and k is the propagation constant in the medium. k depends on the electrical properties as follows

$$k = \frac{\omega}{c_o}\sqrt{K^{*}} \qquad (1-3)$$

where c_o is the velocity of light in vacuum, 3×10^8 m/s. k is re-expressed as

$$k = \frac{\omega}{c} + i\alpha \qquad (1-4)$$

where c is the phase velocity in the medium

$$c = \frac{c_o}{\left[\frac{K'\left((1 + \tan^2\delta) + 1\right)}{2}\right]^{1/2}} \simeq \frac{c_o}{K'} \qquad (1-5)$$

and α is the attenuation coefficient for the medium

$$\alpha = \frac{\omega}{c_o}\left[\frac{K'\left((1 + \tan^2\delta)^{1/2} - 1\right)}{2}\right]^{1/2} \simeq \frac{\omega\sqrt{K'}\tan\delta}{2c_o} \qquad (1-6)$$

The approximate forms of c and α for small values of tan δ are given to the right of equations 1 – 5 and 1 – 6.

BAFFIN ISLAND SHELF – SHALLOW COREHOLE DRILLING, 1976

Projects 760015 and 760039

Brian MacLean and R.K.H. Falconer
Atlantic Geoscience Centre, Dartmouth

Shallow corehole drilling was undertaken at nine principal localities on the southeastern Baffin Island shelf (Fig. 25.1, Table 25.1) from **CSS Hudson** during cruise 76-029, September 22 to October 23, 1976 (Falconer, 1977) as part of the program to map the offshore geology of that region. The coring was carried out by means of the Bedford Institute of Oceanography's underwater electric rock core drill which cuts a 25 mm diameter core and penetrates to a maximum of 6 m below the seafloor. Site selection was on the basis of data obtained with continuous seismic reflection and Huntec deep tow high resolution seismic systems. The drilling procedure was similar to that used in 1975 (MacLean and Srivastava, 1976).

Cores of consolidated and semi-consolidated rock were recovered at six localities. These samples are considered to represent material in situ at these localities as opposed to the other stations (Table 25.1 and Fig. 25.1) where no samples other than from erratics in the overburden were recovered. The cores averaged 61 cm in length, but most were relatively short. This resulted from several factors, principally: 1. difficulties in coring some of the material encountered (loss of sample in the case of semi-consolidated strata, and limited bedrock penetration at some stations due to core fragments jamming in the core barrel); 2. mechanical problems; and 3. the difficulty of landing the drill on the prime target area. The strong southbound current (up to about 3 knots) along the Baffin Island Shelf caused some station keeping problems that led to the early termination of drilling at four stations. On the whole, however, the **Hudson** kept station well during drilling by means of the main propulsion system and bow thruster.

The continental shelf off southeastern Baffin Island was investigated previously by Grant (1975) who outlined six main bedrock units on the basis of data from seismic reflection and magnetic profiling. McMillan (1973), Wallace (1973) and Beh (1975) discussed the geology of parts of the Baffin Island shelf. Jansa (1976) and MacLean et al. (in press) reported on middle-late Ordovician strata and Precambrian rocks sampled by drilling in this area in 1975. The geology of adjacent southern Baffin Island was mapped on a reconnaissance basis by Blackadar (1967). Clarke and Upton (1971) reported on Tertiary sedimentary and volcanic rocks which occur in a narrow belt along the coast northwestward from Cape Dyer.

Cores composed of semi-consolidated sandstone with scattered gravel fragments were recovered at drill stations 6A, 16, and 16A (Fig. 25.1, Table 25.1). The cores from these stations consist of poorly sorted, mainly angular, silt to pebble sized particles with a matrix of

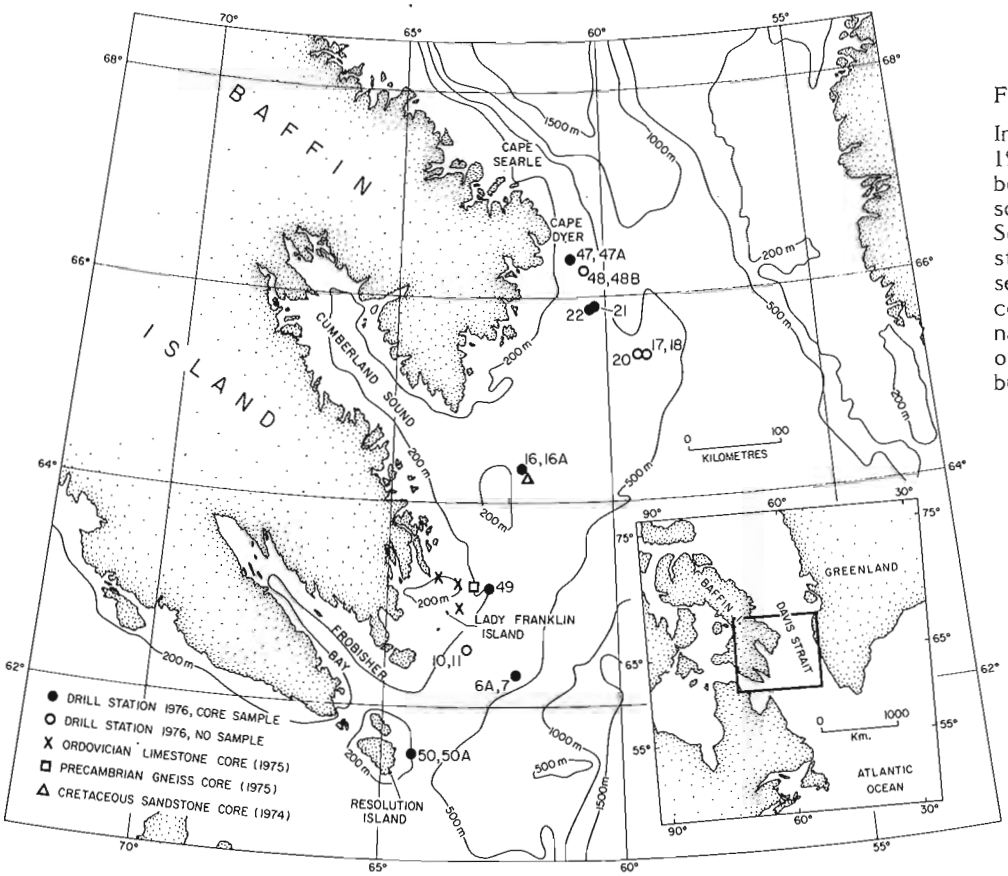

Figure 25.1

Index map showing locations of 1976 drill stations and previous bedrock sample localities on the southeastern Baffin Island Shelf. Solid circles designate 1976 stations where consolidated or semi-consolidated rocks were cored in situ. Open circles designate stations where no samples other than erratics from the overburden were recovered.

From: Report of Activities, Part B; Geol. Surv. Can., Paper 77-1B (1977)

Table 25.1

Drill Station Data

Station	Location		Water Depth (m)	Sea Floor Penetration (cm)	Results
6A	62°18.5'N	62°11.7'W	385	364	5 cm gravel, 53 cm sandstone core (semi-consolidated)
7	62°17.5'N	62°14.9'W	398	124	no core recovery.
10	62°33.1'N	63°14.0'W	223	545	18 cm gravel
11	62°32.7'N	63°16.3'W	224	545	no core recovery.
16	64°19.8'N	62°02.3'W	283	519	44 cm sandstone core (semi-consolidated)
16A	64°19.9'N	62°00.6'W	285	523	16 cm gravel, 33 cm sandstone core (semi-consolidated)
17	65°25.1'N	59°05.4'W	448	545(approx)	30 cm gravel
18	65°24.9'N	59°05.6'W	453	530	73 cm gravel
20	65°25.7'N	59°16.4'W	439	345	14 cm gravel
21	65°55.3'N	60°18.7'W	408	120	13 cm basalt core
22	65°54.2'N	60°20.2'W	404	118	37 cm basalt core
47	66°22.5'N	60°50.3'W	391	295	29 cm gravel, 37 cm basalt core
47A	66°21.6'N	60°48.6'W	391	545	30 cm gravel
48	66°16.6'N	60°30.9'W	422	545	19 cm gravel
48B	66°16.6'N	60°30.5'W	427	101	16 cm gravel
49	63°10.5'N	62°46.2'W	199	318	8 cm gravel, 104 cm gneiss core
50	61°33.3'N	64°23.1'W	199	250	no core recovery
50A	61°33.7'N	64°23.0'W	194	253	172 cm gneiss core

calcareous mud. Foraminifera are present in the cores, and the core from station 6A also contains fragments of plant material (R.H. Fillon, pers. comm.). Station 6A is 100 km east of the coast of Baffin Island and is underlain by strata that regionally have, for the most part, a regular gentle seaward dip, but in the vicinity of the drill station the strata in the upper part of the sequence prograde. Huntec data across the site reveal a continuous near surface reflector that is overlain by a hummocky layer of unconsolidated sediment ranging from near zero to 8 m or more in thickness. A grab sample of this material consisted of silty and clayey sand with some gravel. The near surface reflector appears to mark the top of the sequence cored, but whether this forms part of the progradational sequence or a thin overlying younger sequence unresolved on the seismic profiles is not clear from the present data.

Stations 16 and 16A are on the shelf seaward from the entrance to Cumberland Sound approximately 8 km north-northwest of the site where Srivastava, (1974) recovered 18 cm of sandstone core of late Albian-Cenomanian age (G.L. Williams, pers. comm.). The 1976 drilling locality is underlain by strata which flank a possible diapiric? or fault structure and have an apparent southeasterly dip of some 15°. Huntec and grab sample data from this locality reveal a near surface reflector and overlying unconsolidated sediments that closely resemble those at station 6A in texture and hummocky surface. Seismic reflection (air gun) data in the general area indicate that a thin sequence of younger strata in places unconformably overlies the more steeply dipping beds associated with the underlying structure. Core samples obtained at stations 16 and 16A may be from this younger sequence.

Foraminifera and other shelly microfossils in the cores from stations 6A, 16, and 16A were examined by F.M. Gradstein and spores and dinoflagellates by G.L. Williams and they consider the sediment to be of probable Pliocene-Recent age (F.M. Gradstein, G.L. Williams, pers. comm.). Palynomorphs in the core from station 6A were of Paleozoic, Cretaceous and Plio-Pleistocene ages whereas those in the cores from stations 16 and 16A were predominantly of Aptian-Cenomanian age together with some Senonian-Early Paleocene, Eocene and Plio-Pleistocene forms (G.L. Williams, pers. comm.). In view of the broad spread of ages represented by the palynomorphs and the post Miocene age assigned to the shelly microfossils by Gradstein, the older palynomorphs are considered to have been derived through reworking of material from older strata. The microfossil assemblage at station 6A is indicative of deposition in a brackish-shallow marine environment whereas the assemblage at stations 16 and 16A is characteristic of a shallow open shelf environment (Gradstein, pers. comm.). The presence of plant remains is compatible with a nearshore environment for the material cored at station 6A. The texture of the sediments suggests that floating ice was an important transporting agent at both localities. The interpretation that the sediments in the cores are products of earlier and different environments than those presently prevailing there is supported by contrasts between the microfossil assemblages in the cores and those of grab samples of material from the present sea floor at these localities. R.H. Fillon (pers. comm.) found the latter to be generally consistent with the deeper open shelf marine environment that currently exists in those areas.

Short cores of basalt were recovered at two main localities on the shelf southeast of Cape Dyer (Table 25.1). These are 33 km (station 47) and 89 km (stations 21 and 22) south-southeast of Cape Dyer, respectively (Fig. 25.1), in an area where Grant (1975) inferred the presence of volcanic rocks on the basis of seismic and magnetic data. The core samples from stations 21 and 22 are reddish brown and dark grey in colour respectively, and both consist of fine grained basalt and contain numerous zeolite filled vesicles. The core from station 47 consists of dark grey fine grained basalt in which some vesicles, mainly unfilled, are present.

Basaltic rocks occur on eastern Baffin Island as discontinuous outcrops within a narrow zone some 10 km wide that extends along the coast from just north of Cape Dyer to near Cape Searle 45 km to the northwest. Clarke and Upton (1971) reported a K-Ar age of 58 ± 2 m.y. for the basalt which in places lies on sediments containing fossil flora dated by W.A. Bell as Paleocene. Offshore the seismic reflection data reveal an acoustically relatively uniform sequence of rocks that except for a few local structures seems to dip southeasterly at an apparent angle of approximately 10° from the vicinity of Cape Dyer to station 22 and beyond. The attitude of these rocks on the seismic reflection profiles resembles that of the sub-aqueous breccias of eastern Baffin Island illustrated by Clarke and Upton (1971). Radiometric ages of the core samples are not yet available, but on the basis of relationships inferred from the seismic profiles, the sequence cored offshore appears to postdate the breccias examined on land by Clarke and Upton.

Cores of rocks of presumed Precambrian age were recovered at two localities, stations 49 and 50A, that were sampled to investigate variations observed on magnetic profiles in those areas. The core from station 49 consists of quartz-biotite-feldspar gneiss. This station lies 17 km east of a 1975 drilling locality where cores composed of biotite gneiss were obtained. These stations are located on a basement high that extends east-northeasterly through Lady Franklin Island (MacLean et al., in press). Station 50A lies 13 km east of Resolution Island. The core recovered at this locality comprises 172 cm of light grey garnetiferous gneiss.

Preliminary compressional wave velocity measurements were performed onboard the **Hudson** on sections cut from the cores of basalt and gneiss. Eight basalt bedrock samples from stations 22 and 47 were found to have velocities ranging between 5.2 and 6.0 km/sec, the average velocity for those rocks being 5.6 km/sec. A small cobble-sized fragment composed of dense, fine grained basalt encountered in the unconsolidated sediment at station 48A had a velocity of 6.8 km/sec. Four gneiss bedrock samples from stations 49 and 50A yielded velocities ranging from 5.0 to 6.1 km/sec, the average velocity being 5.5 km/sec. Measurements on gneiss fragments from the overburden at stations 18, 47 and 48 yielded velocities ranging from 4.8 to 5.8 km/sec, the average velocity being 5.4 km/sec. Velocity data on the semi-consolidated sandstone cores from stations 6A, 16, and 16A are not yet available. These cores could not be cut with the equipment onboard ship without risk of disintegration of the samples due to their poorly lithified nature.

References

Beh, R.L.
1975: Evolution and geology of western Baffin Bay and Davis Strait; in Canada's Continental Margins and Offshore Petroleum Exploration, C.J. Yorath, E.R. Parker and D.J. Glass, Eds.; Can. Soc. Petrol. Geol., Mem. 4, p. 453-476.

Blackadar, R.G.
1967: Geological reconnaissance, southern Baffin Island, District of Franklin; Geol. Surv. Can., Paper 66-47, 32 p.

Clarke, D.B. and Upton, B.G.J.
1971: Tertiary basalts of Baffin Island: field relations and tectonic setting; Can. J. Earth Sci., v. 8, no. 2, p. 248-258.

Falconer, R.K.H.
1977: Marine geophysical and geological research in Baffin Bay and the Labrador Sea, **CSS Hudson**, 1976; in Report of Activities, Part B, Geol. Surv. Can., Paper 77-1B, rep. 46.

Grant, A.C.
1975: Geophysical results from the continental margin off southern Baffin Island; in Canada's Continental Margins and Offshore Petroleum Exploration, C.J. Yorath, E.R. Parker and D.J. Glass, Eds.; Can. Soc. Petrol. Geol., Mem. 4, p. 411-431.

Jansa, L.F.
1976: Lower Paleozoic Radiolaria-bearing limestones from the Baffin Island Shelf; in Report of Activities, Part B, Geol. Surv. Can., Paper 76-1B, p. 99-105.

MacLean, B. and Srivastava, S.P.
1976: Shallow corehole drilling on the Baffin Island Shelf; in Report of Activities, Part A, Geol. Surv. Can., Paper 76-1A, p. 141-143.

MacLean, B., Jansa, L.F., Falconer, R.K.H., and Srivastava, S.P.
Ordovician strata on the southeastern Baffin Island Shelf revealed by shallow drilling; Can. J. Earth Sci. (in press)

McMillan, N.J.
1973: Shelves of Labrador Sea and Baffin Bay, Canada; in The Future Petroleum Provinces of Canada (R.G. McCrossan, Ed.), Can. Soc. Petrol. Geol., Mem. 1, p. 473-517.

Srivastava, S.P.
1974: Cruise report **Hudson** 74-026, Phase IV, September 26 to November 1, Bedford Institute of Oceanography.

Wallace, F.K.
1973: Geology of the Davis Strait bathymetric sill and associated sediments, offshore Baffin Island, Canada; in Proceedings of the Symposium on the Geology of the Canadian Arctic, Saskatoon, May 1973 (J.D. Aitken and D.J. Glass, Eds.); Geol. Assoc. Can./Can. Soc. Petrol. Geol., p. 81-97.

OCEAN BOTTOM SEISMOMETER DEVELOPMENTS

Projects 750107 and 770010

D.L. Barrett, D.E. Heffler, and C.E. Keen
Atlantic Geoscience Centre, Dartmouth

Introduction

A continuing research project on the technological development and use of ocean bottom seismometers (OBS) has been active at the Atlantic Geoscience Centre for almost three years. The interest in these instruments arose from our successes with marine seismic refraction techniques in solving the deep crustal and sedimentary processes near the continental margins of Eastern Canada (Keen et al., 1975; van der Linden and Srivastava, 1975; Keen and Barrett, 1972; Jackson et al., in press). These results, although valuable, have been limited by the use of surface sonobuoys which are intrinsically restricted in the kind and quality of data which can be collected. Specifically, sonobuoy systems, unlike OBS, depend on good weather conditions, are subject to drift with wind and current over unknown subsurface structures and have only one sensor, a hydrophone, near the sea surface. OBS's, on the other hand, do not have these disadvantages and in addition have between one and three geophones which are located on the sea floor, allowing both compressional (P) and shear (S) wave velocities to be measured.

The use of OBS near continental margins should significantly advance our knowledge of details of the sedimentary and crustal structure at continental margins. A knowledge of both P and S wave velocities within the layering should allow a more positive relationship between rock type and seismic velocities to be established; the ratio V_S/V_P is presently being investigated by the petroleum industry for the identification of gas layers (Tatham and Stoffa, 1976). Also, signals from OBS geophones, rather than near surface hydrophones, have proved to be extremely valuable in the identification of later arrivals.

In order to obtain some experience with the OBS systems used by other institutions, the authors as well as R. Falconer, R. Jackson and B.D. Loncarevic have participated in cruises where seismic refraction or microseismicity studies were conducted. The results from OBS's designed by Lamont Doherty Geological Observatory used on three separate occasions in the North Atlantic were disappointing for various electronic and mechanical reasons. The main problem was the lack of high frequency response and hence the direct water wave used for shot-receiver distance was not recorded. In addition, the horizontal geophone in these instruments did not output discrete bursts of energy but appeared to oscillate continuously after the first onset of compression waves. This is probably due to the compound pendulum effect of the self-levelling suspension of the geophone. We have observed at first hand such limitations of the systems operated by others and the bad and good features of these other systems have influenced the specifications set in acquiring our own systems. These considerations included:

1. The OBS packages should be pop-up devices; that is they should be unattached in any way to the sea surface but should fall freely to the sea floor and rise again to the surface at a particular pre-set time or on a command from the ship.

2. They should be as inexpensive as possible without sacrificing reliability and data of good quality. Many OBS units which have been deployed by other institutions have failed to pop-up, or have done so when least expected. In either case many have been lost and the recovery rate is about 80-90%. This means replacement of the lost units and consequently the need for relatively inexpensive instruments without sacrificing reliability. One disadvantage of OBS's is the complete loss of all data if the instrument is not recovered.

3. They should contain at least two seismometers, one horizontal and one vertical, to detect and separate P and S wave arrivals, both first and later events.

4. They should be as compact as possible to avoid difficulties in handling over the side of a ship.

5. They should be capable of recording seismic signals in the frequency range 3 – 30 Hz and water wave arrivals (about 100 Hz) for about 10 days while located on the sea floor, in water depths up to 5000 m.

6. In addition to low noise amplifiers and tape recorder electronics, a clock for recording time accuracy to about 10 ms over 10 days is required. This clock should also trigger the release mechanism. A complete back-up timer is also needed to ensure release and recovery of the OBS.

Two OBS units which met most of the above specifications were purchased from the Hawaiian Institute of Geophysics (Sutton et al., in press) and modified to include a release mechanism so that they could be used as pop-up instruments (Heffler and Locke, in press). After initial tests, several modifications had to be made to these instruments to increase their frequency response and dynamic range on the taped recordings and to lower the electronic noise pick-up on all channels. This involved the damping of pulses to the tape drive mechanism and increasing the bias and signal level to the tape recording heads. Levels of gain were adjusted so that minimum background noise in the oceans could be recorded on tape. After these modifications and refinements were carried out the instruments were moored on the continental shelf and several airgun shots were fired to verify that their sensitivity, dynamic range and frequency response were appropriate for ocean monitoring of artificial seismic sources. They were first used as operational instruments in August 1976, during an experiment near the Juan de Fuca Ridge. This OBS experiment, during which both microseismic events and explosive shots for crustal studies were recorded, was initiated by R.D. Hyndman, Seismology Division, Earth Physics Branch. D.L. Barrett participated in this experiment in which both the Atlantic Geoscience Centre OBS units were deployed as well as the OBS units of the Seismology Division which were designed by Lister and Lewis (1976).

From: Report of Activities, Part B; Geol. Surv. Can., Paper 77-1B (1977)

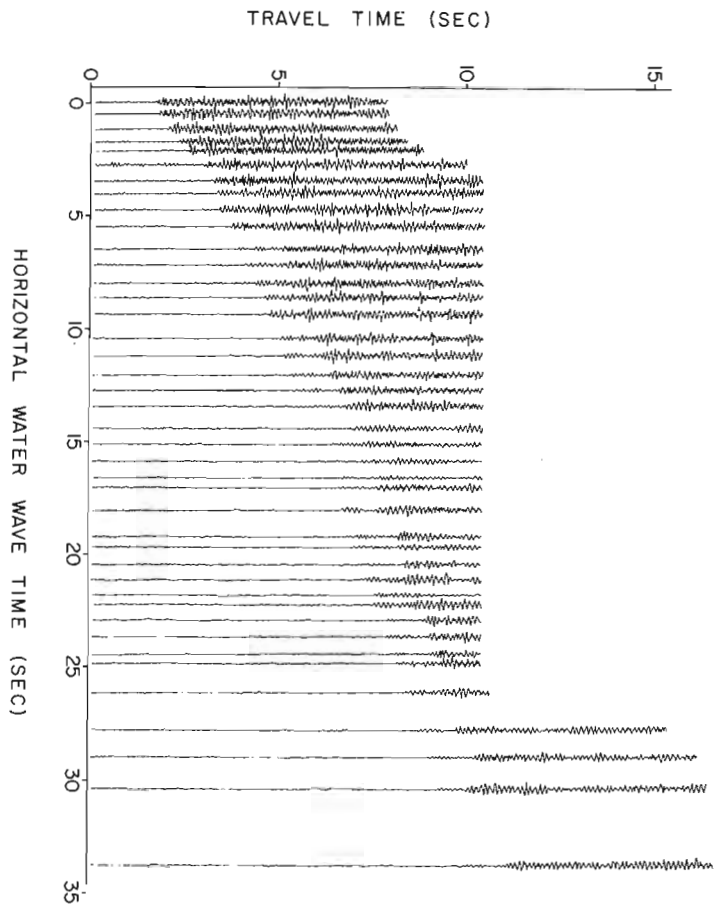

Figure 26.1. A record section from the vertical geophone. Note the high background noise levels on some of the traces. This is due to the high microseismic activity in the area. A water wave velocity of 1.5 km/s was used to derive the velocities noted in the text.

Results

The four OBS units were deployed along a 75 km line near the Explorer spreading centre (50°N, 130°W) off southwestern British Columbia. Eighty-two shots along the refraction line gave clear arrivals for a well-defined crustal structure. Figure 26.1 is a record section of seismograms from the vertical geophone in one of our OBS units. During the experiment, approximately 300 earthquakes were detected by the OBS and as a result, the background noise level was about 20 db higher than that observed by surface sonobuoys and OBS in non-active areas of the deep ocean. In spite of this high background noise, the compressional wave velocities observed from first and second arrivals are well defined. At distances over 7 seconds of horizontal water wave travel time an event is quite apparent arriving about 1 second after first arrival and must represent a P-S converted wave. From first arrivals, three velocities can be identified: 2.2, 5.7 and 7.0 km/sec respectively. The low mantle velocity of 7 km/sec is common in areas of young, rapidly spreading oceanic crust. The main crustal velocity of 5.7 km/sec is relatively high and must be indicative of a somewhat metamorphosed massive basalt. The lowest velocity arises from a thin layer of sediment overlying the basalts.

In addition to the explosive shots, a profile was shot to the OBS using a 1000 cu. in. airgun with a firing rate of 2 minutes and ship's speed of 6 knots. Figure 26.2 shows the resulting profiles recorded by the vertical geophone (left), the horizontal geophone (centre) and hydrophone (right). Several interesting features are noteworthy. (1) A good vertical reflection is clear about 1 second below the bottom on both the vertical and horizontal phones but is not observed on the hydrophone; the hydrophone only detects the direct and water column multiple compressional wave, (2) sedimentary refractors are recorded by all three detectors, (3) clear first arrivals of compressional waves are detected by the vertical geophone which exhibit the same velocities as the explosive results in Figure 26.1, (4) the compressional wave first arrivals are barely visible on the horizontal geophone recordings, and are not detected by the hydrophone, and (5) good mantle shear waves are detected by the horizontal geophone exhibiting a velocity of 4.0 km/sec; a small component of these shear waves is detected by the vertical geophone but not by the hydrophone.

The compressional-shear wave velocity ratio for the highest velocity refractor is comparable to that observed in laboratory measurements on metamorphosed basalts. A better playback and display of results should reveal the shear velocities in the upper layers and afford the calculation of elastic parameters of these rocks.

From the vertical component of motion, both Figures 26.1 and 26.2 display a zone of attenuated first and second arrivals within the first half second of travel time at distances of between 13 and 17 seconds of water wave time. Our first contention is that this attenuation is due to phase interference of arrivals from the main crustal layer and the highest velocity layer. In order to solve this problem adequately, pseudo-seismograms from a layered elastic model will have to be generated to completely fit the times and amplitudes of both vertical and horizontal components. A computer program to achieve this end has been written and is presently being tested. We feel that this method of solving compressional and shear wave seismic data resulting from oceanic and continental structure will replace the outmoded and relatively uninformative simple layered models from surface-recorded compressional wave data. With this approach, the problem of identifying submerged or floundering continental material as opposed to crust generated from ocean spreading, transform faulting and fracturing, and later oceanic crustal readjustments should be alleviated.

With the encouragement of the one successful instrument on the West Coast, the Atlantic Geoscience Centre decided to build several copies of the Hawaiian OBS for use in the 1977 field season. Although the new OBS's were mainly copies, there have been several changes due to unavailability of older parts and several constructional improvements. The basic specifications of two 4.5 Hz geophones and a hydrophone continuously recorded on one magnetic tape cassette for up to 10 days, remains the same.

A microprocessor based clock has been designed for timing and control. This low power computer replaces about 6 digital logic cards, but its most important feature is its adaptability. It will be easy to reprogram to control functions such as a pinger or a command release.

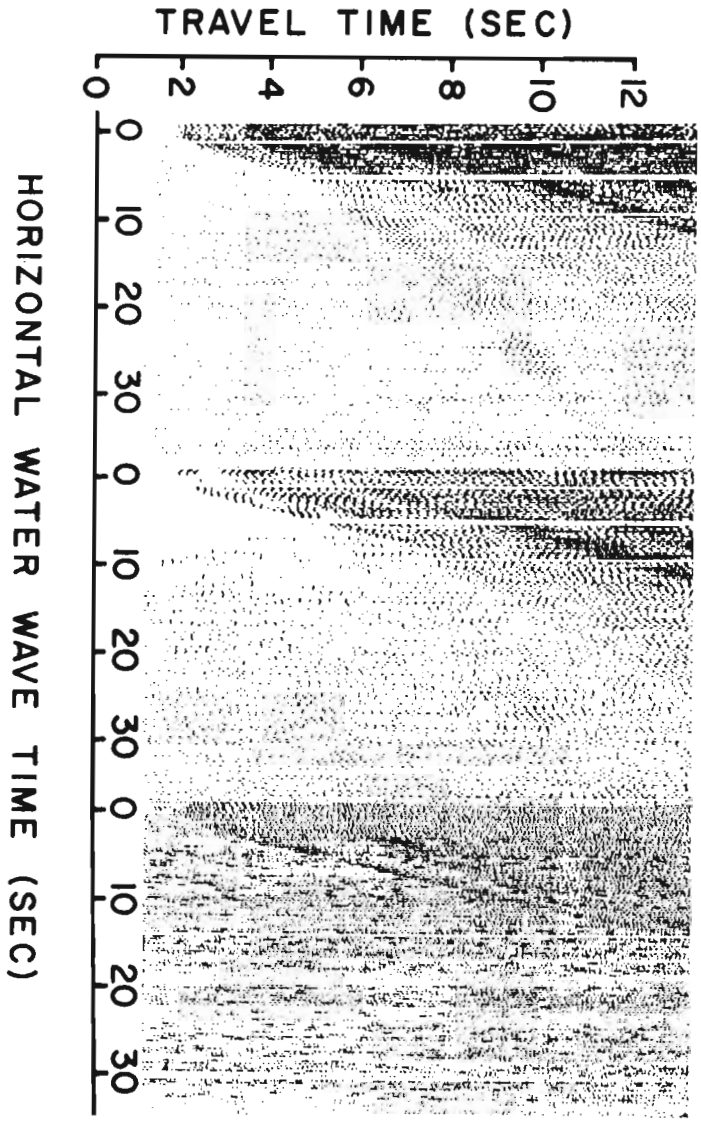

Figure 26.2. Record sections recorded using a 1000 cu. in. air gun. From left to right are shown the vertical and horizontal components and the hydrophone respectively. The variable density display shows clear first arrivals of compressional wave energy at the vertical geophone and clear later shear wave arrivals on the horizontal geophone between about 10 and 30 seconds water wave travel time. The hydrophone shows a much lower signal-noise ratio and only defines sedimentary velocities.

The release mechanism (Heffler and Locke, in press) is being altered for more reliability and fewer consummable parts. Extensive tests will be carried out before field use this year.

Perhaps the weakest part of the previous design was the physical construction of the electronic cards and wiring. Wire wrap boards, high quality connectors and better mechanical design should improve this. The exterior dimensions remain unchanged except that the single glass flotation sphere used previously is being replaced by two cylindrical synthetic foam floats. In addition to increasing reliability, these should lower the profile and reduce current induced noise.

Present Improvements in Instrumentation and Future Work

In the summer of 1977 we hope to use these improved instruments on the continental margin off Newfoundland, in Flemish Pass and off Orphan Knoll. This will be the first time, to the authors' knowledge, that OBS experiments have been conducted at continental margins.

Hopefully by the 1979 field season, several advances should be included in the Atlantic Geoscience Centre design. The two obvious requirements now are:

1. A pinger to provide an acoustic link to the surface so that a ship can make periodic checks on the functioning of the instrument and to aid in its recovery.

2. A command release system rather than a preset timer. This is particularly necessary in the ice-infested arctic waters and the fog-bound eastern Canadian margins if reliable recovery is to be ensured.

In addition to the future use of the improved instruments, work is in progress to construct earth models from which synthetic seismograms can be computed which may be matched with real data obtained by the OBS. Also, inversion of time-distance data to produce velocity models, including bounds on depths and velocities, will be performed. With the present capability of obtaining data of superior quality, it is hoped that these more advanced analytical techniques will help to resolve still further the velocity structure in the crustal layers of our offshore margins.

Acknowledgments

We are grateful to R.D. Hyndman and his co-workers of the Earth Physics Branch for the opportunity to participate in the refraction experiments. D.I. Ross and H.R. Jackson critically read the manuscript.

References

Heffler, D.E. and Locke, D.L.
An OBS release mechanism; Mar. Geophys. Res. (in press)

Jackson, H.R., Keen, C.E., and Barrett, D.L.
Geophysical studies on the eastern continental margin of Baffin Bay and in Lancaster Sound; Can. J. Earth Sci. (in press)

Keen, C.E. and Barrett, D.L.
1972: Seismic refraction studies in Baffin Bay: an example of a developing ocean basin; Geophys. J., v. 30, p. 253-271.

Keen, C.E., Keen, M.J., Barrett, D.L., and Heffler, D.E.
1975: Some aspects of the ocean-continent transition at the continental margin of eastern North America; in Offshore Geology of Eastern Canada, Geol. Surv. Can., Paper 74-30, v. 2, p. 189-197.

Lister, C.R.B. and Lewis, B.T.R.
1976: An ocean bottom seismometer suitable for arrays; Deep Sea Res., v. 23, p. 113-124.

Sutton, G.H., Kasahara, Y., Ichinose, N.N., and Byrne, D.A.
Ocean bottom seismograph development at Hawaii Institute of Geophysics; Mar. Geophys. Res. 3. (in press)

Tatham, R.H. and Stoffa, P.L.
1976: V_p/V_s – a potential hydrocarbon indicator; Geophysics, v. 41, p. 837-849.

van der Linden, W.J.M. and Srivastava, S.P.
1975: The crustal structure of the continental margin off central Labrador; in Offshore Geology of Eastern Canada, Geol. Surv. Can., Paper 74-30, v. 2, p. 233-246.

THE DELPHI FORECASTING TECHNIQUE

Project 720094

K.R. Dawson
Regional and Economic Geology Division

In 1972, as a result of high interest in techniques for predicting future supplies of heavy metals in Canada, a project was initiated to examine the Delphi technique developed in 1953 by the Rand Corporation, Santa Monica, California (Helmer and Rescher, 1959; Dalkey and Helmer, 1963). For a variety of practical reasons it was decided to maintain a bibliography of publications relating to the Delphi technique and other methods for predicting future developments.

The bibliography, operated as a computer based file, is maintained on magnetic tape, is arranged in alphabetical order by author, and is manipulated by remote Teleterm 1030 terminal. The bibliography is moved from backup tape to permanent file for processing using the INTERCOM EDITOR feature. This also is used to produce listings (Table 27.3), do updates and make 'character string' retrievals. EDITOR has provision for the insertion of 10 lines between existing lines of text which is used for all update runs. Specific 'keywords' or 'character strings' can be retrieved and the complete reference can be examined by a retrieval of the lines enclosing the 'keyword' (Table 27.1). Similarly, the EDITOR can be used to generate an index for any specified 'word' or 'character string', for example for two words, 'education' and 'business' that are scattered through more than 1300 lines of text (Table 27.2).

The bibliography, which now consists of 230 entries, typically includes author, corporate author, title, reference and a short list of keywords. The papers describe efforts to predict future developments in a wide variety of scientific and social fields including communications, urban planning, environmental problems, education, business and finance, transportation and medicine. Regrettably, only two references (Cetron and Ralph, 1971; and Torries, 1975) have any connection with either geology or minerals except in a general way. One hundred and seventy-four (174) entries refer directly to the Delphi technique and many refer to other techniques or modifications of the former.

Table 27.1

A computer listing for keywords galena, copper, metal, mineral, smelting, mill.
Each is followed by the appropriate reference where such exists.

```
!LIST,ALL,/GALENA/
NO SUCH LINES
..LIST,ALL,/COPPER/
  2660=  COPPER INDUSTRY
..LIST,2610,2670
  2610=
  2620=  CETRON, M., AND C. RALPH
  2630=  INDUSTRIAL APPLICATIONS OF TECHNOLOGICAL FORECASTING
  2640=  WILEY-INTERSCIENCE, TORONTO, 1971.
  2650=  BOOK   TECHNICAL FORECASTING   T/F   DELPHI   PETROCHEMISTRY
  2660=  COPPER INDUSTRY
  2670=
..LIST,ALL,/METAL/
  6140=  METALLURGIA AND METAL FORMING 1973 V 40 ISS N9 P 273
..LIST,6140,6170
  6140=
  6150=  FUTURE OF FORGING - A DELPHI PROBE
  6160=  METALLURGIA AND METAL FORMING 1973 V 40 ISS N9 P 273
  6170=
..LIST,ALL,/MINERAL/
 13990=          PRODUCED U308 IN THE UNITED STATES, MINERALS ECONOMIST,
..LIST,13990,14040
 13990=
 14000=  TORRIES, T.F.
 14010=    1975  A PROBABILISTIC MODEL OF THE AVAILABILITY OF DOMESTICALLY
 14020=          PRODUCED U308 IN THE UNITED STATES, MINERALS ECONOMIST,
 14030=          STANFORD RESEARCH INSTITUTE.
 14040=
..LIST,ALL,/SMELTING/
NO SUCH LINES
..LIST,ALL,/MILL/
   210=  THIRD EDITION, MACMILLAN, NEW YORK, 1968.
..LIST,14040
 14040=
.. RID,14041,1
```

From: Report of Activities, Part B;
Geol. Surv. Can., Paper 77-1B (1977)

Table 27.2

A terminal listing of indices for the keywords education and business.

```
..LIST,ALL,/EDUCATION/
   390=  STANDARDS   EDUCATIONAL TESTS   PSYCHOLOGICAL TESTS
   900=  ELECTRONIC SHOPPING   PROGRAMMED EDUCATION   INFORMATION RETRIEVAL
  1090=  HEALTH CARE   MEDICAL EDUCATION
  1560=  EDUCATION
  1570=  LIBRARY INFORMATION SCIENCE   EDUCATION
  2030=  MILITARY EDUCATIONAL   BUSINESS PLANNING   STRATEGIC
  2420=  EDUCATION   DELPHI
  2680=   1970   COMPUTERS SUPER MEDIA FOR EDUCATION? COMPUTER DECISIONS,
  3760=  TRANSPORTATION   REGIONAL ENVIRONMENT   HOUSING   EDUCATION
  3830=  DELPHI   VALUE JUDGMENTS   GENERAL INFORMATION   HIGHER EDUCATION
  4070=  GROUP - COMPUTER ASSISTED EDUCATION AS A CASE EXAMPLE
  4100=  COMPUTER ASSISTED EDUCATION   CAE   INTERDISCIPLINARY RESEARCH
  4160=  FUTURE APPLICATIONS   COMPUTER   COMMUNICATIONS   EDUCATION
  4810=  AN EXPLORATION OF THE FUTURE IN EDUCATIONAL TECHNOLOGY IN H. A.
  4830=  THE WORST OF TIMES--CONTEMPORARY ISSUES IN CANADIAN EDUCATION HOLT,
  4850=  BELL CANADA RESEARCH   EDUCATION   DELPHI   VALUES OF SOCIETY
  4890=  AN EXPLORATION OF THE FUTURE IN EDUCATIONAL TECHNOLOGY
  5050=  DELPHI   POLITICS   FORECASTING   EDUCATION OF EXPERTS
  5920=  SOCIETAL IMPACTS   EDUCATION   BUSINESS
  6200=  DELPHI TECHNIQUE IN AN EDUCATIONAL ENVIRONMENT.
  7570=  AUTOMATION   EDUCATION   SOCIAL ENVIRONMENT
  8320=  THE USE OF THE DELPHI TECHNIQUE IN PROBLEMS OF EDUCATIONAL INNOVATIONS
  8340=  DELPHI   TECHNIQUE   EXPER OPINIONS   EDUCATIONAL PLANNING
  8420=  OPERATIONS RESEARCH   EXPERT OPINION   URBAN RENEWAL   EDUCATION
  9520=  EDUCATIONAL NEED ASSESSMENT
 10120=  EDUCATIONAL POLICY CENTER, SYRACUSE UNIVERSITY RESEARCH COR-
 11280=  NATIONAL EDUCATION ASSOCIATION, 1961.
 13200=  THE USE OF CONTEXTUAL MAPPING TO SUPPORT LONG-RANGE EDUCATIONAL POLICY
 13550=  EXPERT JUDGMENT   EDUCATIONAL RESEARCH  SYRACUSE UNIVERSITY
..

LIST,ALL,/BUSINESS/
   680=  OF THE WIRED CITY  BUSINESS PLANNING PAPER #39
   690=  BUSINESS PLANNING GROUP BELL CANADA MONTREAL
   720=  BELL CANADA, BUSINESS PLANNING PAPER NO. 12, MAY, 1973.
   900=  BELL CANADA BUSINESS PLANNING, SEPTEMBER 1972.  (PORPRIETARY)
   950=  BELL CANADA, BUSINESS PLANNING GROUP
   970=  DELPHI   WIDUCATION   MEDICINE   BUSINESS   HOME COMMUNICATIONS
  2030=  MILITARY EDUCATIONAL   BUSINESS PLANNING   STRATEGIC
  2320=  A METHODOLOGICAL STUDY OF THE UTILIZATION OF EXPERTS IN BUSINESS FORE-
  2350=  BUSINESS FORECASTING   GROUP FORECASTING   DELPHI   FORECAST DATA
  2600=  TECHNICAL EVENTS   BUSINESS   POLITICS   SOCIAL CHANGES
  4060=    1975  INTERDISCIPLINARY RESEARCH AT THE BUSINESS PLANNING
  4080=  BUSINESS PLANNING PAPER #44  BUSINESS PLANNING GROUP BELL CANADA
  4170=  BUSINESS TRAVEL   HOME   DELPHI
  4230=  BUSINESS PLANNING   TECHNOLOGICAL FORECASTING   DELPHI
  4290=  DELPHI   CORPORATE ENVIRONMENT   BELL CANADA[S BUSINESS PLANNING
  4960=  BELL CANADA BUSINESS PLANNING, MONTREAL, MARCH 1971.  (PROPRIETARY)
  5900=  BELL CANADA, BUSINESS PLANNING, AUGUST 1972 (INTERNAL DOCUMENT).
  5920=  SOCIETAL IMPACTS   EDUCATION   BUSINESS
  5970=  BUSINESS WEEK, NO. 2115, MARCH 1970, PP. 130-34.
  6660=  AN EXPLORATION OF THE FUTURE BUSINESS INFORMATION PROCESSING TECHNOLOG
  6670=  BELL CANADA BUSINESS PLANNING, OCTOBER 1971.  (PROPRIETARY)
  6680=  DELPHI   FUTURE  SOCIAL IMPACT   BUSINESS PROCEDURES   TECNOLOGY
  8840=  DELPHI TECHNIQUE  A TOOL FOR BUSINESS FORECASTING
  9980=  BUREAU OF BUSINESS RESEARCH, UNIVERSITY OF MICHIGAN, WORKING PAPER 22,
 10260=  BUSINESS STUDIES   ANALYSIS OF TECHNIQUE   TRW DATA
 10320=  CONVAIR DIVISION   BUSINESS PLANNING   DECISION MAKING   CHART
 10690=  MODIFIED DELPHI METHOD OF SOLVING BUSINESS PROBLEMS
 11360=  HARVARD BUSINESS REVIEW, VOL. 47, MAY 1969, PP. 68-82.
 12130=          ENQUIRY,GRAD.SCHOOL OF BUSINESS, UNIV.TEXAS APR 1968.
 12580=  HARVARD BUSINESS REVIEW FORECAST SERIES, NO. 21215 (1971), PP. 51-53.
 14180=   1970   BLUEPRINT FOR MIS, HARVARD BUSINESS REVIEW, NOVEMBER-
..
```

The Delphi technique (Dalkey and Helmer, 1963) was developed to supplement objective scientific facts with subjective opinions using a panel of experts who remain anonymous during the sessions. The technique (Pill, 1971, p. 57-71) has three main characteristics:

(1) Anonymity, accomplished by use of questionnaires and/or on-line computer communication, is a method to reduce the effect of dominant individuals.

(2) Controlled feedback, that is conducting the exercise in a sequence of rounds between which a summary of results of the previous round is communicated back to the participants, is done to reduce large fluctuations in the elicited opinions.

(3) Statistical Group Response. Use of the statistical group response is a device to reduce group pressure for conformity. More important it also assures all opinions

Table 27.3

A computer listing sequenced by author and printed from the Delphi bibliography. Individual entries consist of author, corporate author, title, reference and keywords.

DROR, Y.
LA PREDICCION DE LO POLITICAMENTE POSSIBLE
REVISTA ESPANOLA DE LA OPINION PUBLICA, JULY -DECEMBER 1970, PP. 21-22 89-98. (SEE ALSO THE RAND CORPORATION, P-4044, APRIL 1969.)
DELPHI POLITICS FORECASTING EDUCATION OF EXPERTS
POLITICAL ANALYSIS UNPREDICTABLE HUMAN FORCES

DUDA J. L., HEPPE R. J., SELMAN, V., SELMAN, J.
(YALE UNIV.SCH ORG & MANAGEMENTY, DEPT ADM SCI NEWHAVEN CT 06520)
MARKOVIAN CROSS-IMPACT MODEL FOR EVALUATING MANAGEMENT INFORM ATION-SYSTEMS
OPERATIONS RESEARCH 1975 V 23 ISS S2 P B278

ENGLISH, J. M., KERNAN, G. L.
(UNIV CALIF LOS ANGELES CA 90024)
PREDICTION OF AIR-TRAVEL AND AIRCRAFT TECHNOLOGY TO YEAR 2000 USING DELPHI METHOD
TRANSPORTATION RESEARCH 1976 V 10 ISS N1 P 1-8

ENZER, SELWYN
SOME DEVELOPMENT IN PLASTICS AND CAMPETING MATERIAL BY 1985
INSTITUTE FOR THE FUTURE, R-17, JANUARY 1971.
OWENS-CORNING DELPHI MATERIALS USE INDUSTRIAL ENVIRONMENT
ENGINEERING PLASTICS GLASS FIBER REINFORCED PLASTICS
FOAMED PLASTICS FORECASTS

ENZER, SELWYN
SOME PROSPECTS FOR RESIDENTIAL HOUSING BY 1985
INSTITUTE FOR THE FUTURE, R-13, JANUARY 1971.
OWENS-CORNING FIBERGLAS RESIDENTIAL HOUSING FORECASTING
HOUSING SUPPLY TECHNOLOGICAL DEVELOPMENTS SOCIETY
ILLUSTRATIONS

ENZER, SELWYN
DELPHI AND CROSS-IMPACT TECHNIQUES AN EFFECTIVE COMBINATION FOR SYS-TEMATIC FUTURES ANALYSIS
INSTITUTE FOR THE FUTURE, WP-8, JUNE 1970.
DELPHI CROSS-IMPACT TECHNIQUE EFFECTIVENESS FUTURES

ENZER, SELWYN
A CASE STUDY USING FORECASTING AS A DECISIONMAKING AID
INSTITUTE FOR THE FUTURE, WP-2, DECEMBER 1969.
CASE STUDY FORECASTING DECISION MAKING

ENZER, SELWYN, AND R. DE BRIGARD
ISSUES AND OPPORTUNITIES IN THE STATE OF CONNECTICUT 1970-2000
INSTITUTE FOR THE FUTURE, R-8, MARCH 1970.
SOCIAL ENVIRONMENT POLITICS

THE EXPLORATION OF THE FUTURE
REALITES, NO. 245, JUNE 1966, PP. 50-58. TRANSLATED FROM THE FRENCH B R. NEISWENDER, THE RAND CORPORATION, P-3540, FEBRUARY 1967.
TRANSLATION FROM FRENCH FUTURE FORECASTING METHODS
DELPHI SOCIETY 21ST CENTURY INTERNATIONAL INSTITUTE

influence the final response. The procedure is a rapid, efficient way to sound the individual opinions of a group of knowledgeable persons. It takes less time to complete a questionnaire than it does to write a technical paper. Moreover, the Delphi exercise, properly managed, can be highly motivating for respondents because the feedback can be stimulating, anonymity and group response is refreshing, and the technique releases participants from the inhibitions that result from face-to-face encounters.

To apply the Delphi technique would involve a number of people, including an advisory or steering committee, a co-ordinator, clerical staff, a panel of experts and computer programmers. The committee assigned to carry out the exercise would identify the subject matter of the questions and the persons to be invited as panel members. The co-ordinator would manage the session. The questions are carefully worded, background material is assembled and these are circulated to the panel members. The responses are processed and the results calculated after each round. Two or three rounds with feedback between, are commonly necessary and the results tend to converge into a useful concensus related to the questions asked.

Delphi has been widely used in North America, Europe and India. Reports indicate use of the classical procedure as well as a variety of modifications to the original. One modification relates to the selection of the expert panel members. Individual members are required to qualify themselves for panel duty by self-rating their personal expertise in the subject and in the results their opinions are weighted by a corresponding factor (Brown and Helmer, 1964). Dean and Mathis (1969) described a modified Delphi procedure that required linear regression treatment of the results. This was believed to facilitate interpretation of the final results. Anderson and Sproull (1972) describe the PATTERN technique (Planning Assistance Through Technical Evaluation of Relevance Numbers) which has a slight resemblance to Delphi.

Bell Canada, Business Planning Group is in the forefront of Canadian users of Delphi and other forecasting techniques. "Delphi: The Bell Canada Experience", a collection of five papers by the Business Planning Group of Bell Canada is a useful compilation of experiences with the procedure in corporate activities. Information Canada used the technique to study policy options for the Canadian Government. The Canadian Pulp and Paper Institute used it to study future developments likely to occur in that industry.

Opinion regarding the usefulness of the procedure ranges from complete rejection to enthusiastic acceptance. Pill (1971) suggests the results should be used at a high level of uncertainty; that one should accept the difficulty of gauging its usefulness and measure its eventual usefulness by its performance. Rockwell (1973) is less kind claiming the Delphi is not a substitute for more rigorous scientific methods. On the other hand, the large number of universities and businesses using the procedure indicates strong acceptance in spite of these limitations.

References

Anderson, R.C. and Sproull, N.C.
1972: Requirement analysis, need forecasting, and technology planning using the Honeywell PATTERN technique; Technological Forecasting and Social Change, v. 3, p. 255-265.

Brown, B. and Helmer, O.
1964: Improving the reliability of estimates obtained from a concensus of experts; The Rand Corporation P-2986, September 1964.

Cetron, M. and Ralph, C.
1971: Industrial applications of technological forecasting; Wiley Interscience, Toronto, 1971.

Dalkey, N.C. and Helmer, O.
1963: An experimental application of the Delphi method to use of experts; Mangement Science, v. 9, no. 3, p. 458-467.

Dean, B.V. and Mathis, S.
1969: Department of Operations Research, Case Western Reserve University, Technical Memorandum no. 165.

Helmer, O. and Rescher, N.H.
1959: On the epistemology of the inexact sciences; The Rand Corporation, R-353, February 1960.

Pill, J.
1971: The Delphi Method: Substance, contexts, a critique and an annotated bibliography; Socio. Econ. Plannings Science, v. 5, p. 57-71.

Rockwell, M.A.
1973: The Delphi procedure: knowledge from goat viscera?; The New England Journal of Medicine, v. 288, no. 24, p. 1298-1299.

Torries, T.F.
1975: A probabilistic model of the availability of domestically produced U_3O_8 in the United States; Minerals Economist, Stanford Research Institute.

28. DISTRIBUTION OF URANIUM IN AN ACTIVE GEOTHERMAL AREA IN THE AZORES

E.M.R. Research Agreement 1135-D13-4-13/76

W.S. Mitchell[1], M. Zentilli[1], and K.A. Taylor[1]
Regional and Economic Geology Division

Introduction

In the summer of 1973 a 981-m borehole was drilled in the island of Sao Miguel, Azores as part of a continuing investigation of the oceanic crust by deep drilling. The drillhole is located 72 m above sea level on the northwest flank of volcano, Agua de Pau (Fig. 28.1). Core recovery to a depth of 148 m was sporadic because of the unconsolidated nature of the pyroclastic and lahar deposits but recovery for the remainder of the hole was almost complete. The core is subdivided (Fig. 28.2) into three subaerial sequences, a transition sequence and a subaqueous sequence (Muecke et al., 1974; McGraw, 1976). Temperature measurements (Fig. 4, Muecke et al., 1974) increased rapidly to 100°C between 100 and 175 m, below which there was a gradual increase to around 200°C at 500 m. Boiling occurred when drilling ceased and steam was produced at the drill head. Muecke et al. (1974) suggested that at 550 m water at 205°C is flowing parallel to the almost horizontal strata and that 100°C water is flowing just below an impermeable layer at 110-120 m depth.

Clearly, hydrothermal conditions exist within the drilled volcanic sequence and abundant material was available to us for a preliminary investigation into the behaviour of uranium within an active hydrothermal volcanic environment.

Methods

A total of 72 samples from different units in the drill core were analyzed by the fission track method (Fisher, 1970) for homogenized whole rock uranium concentration. Detailed uranium variation through a single flow unit was also investigated with a further 14 whole rock uranium analyses and distributions of the element within several porphyritic basaltic units were mapped using techniques similar to those described by Kleeman and Lovering (1967).

Data

Whole rock uranium concentrations in samples selected from the drill core are plotted versus depth in Figure 28.3. Average concentrations of the element in the different volcanic units are tabulated in Table 28.1. The trachytic units contain more uranium than any of the basaltic units with the exception of highly oxidized flow tops which have been exposed to subaerial weathering. Most of the flows encountered in the drill core are basaltic in chemistry and mineralogy (McGraw, 1976). Average uranium concentration in the basalts is 1.33 ppm with slight increase in coarse flows and brecciated portions of the flows. Uranium, like other elements analyzed by McGraw (1976), shows no obvious variation with depth through the basalts.

The sequence of pillowed flows below 900 m depth contains an average 2.12 ppm U, a considerably greater concentration than is normal for true ocean floor basalts. Average uranium concentration in MORBS recovered from leg 37 DSDP range from 0.10 to 0.29 ppm U for over 300 samples from five different drillholes. Basalts of the Bermuda seamount sampled by the 800 m Deep Drill borehole of 1972 contain an average 0.18 ppm U (66 analyses).

It therefore appears that the relatively higher average concentration of uranium in Azores basalts relative to oceanic basalts may either be an original feature of their more alkalic chemistry or a secondary enrichment through hydrothermal alteration. A combination of both factors is likely and possible evidence of

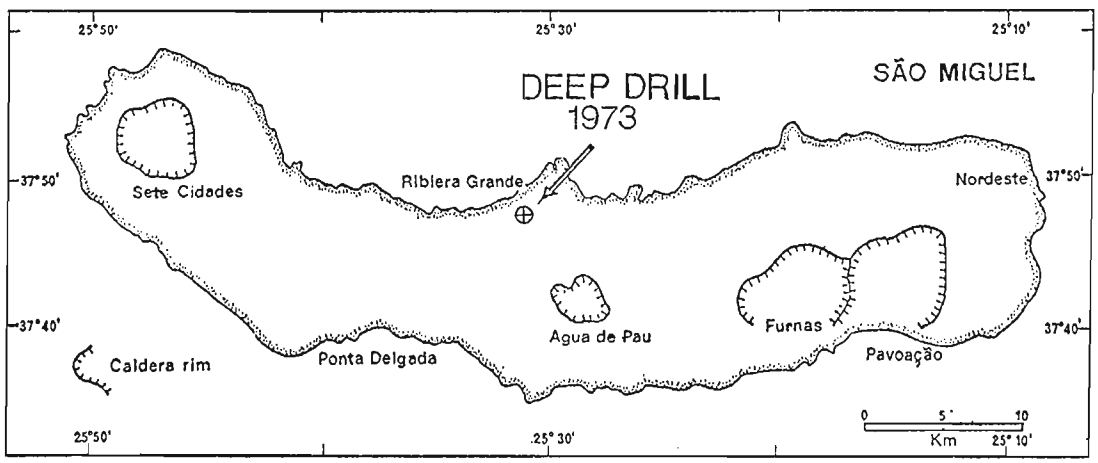

Figure 28.1. Location of 981-m deep borehole (Deep Drill 1973) on Sao Miguel, Azores.

[1] Department of Geology, Dalhousie University, Halifax, Nova Scotia

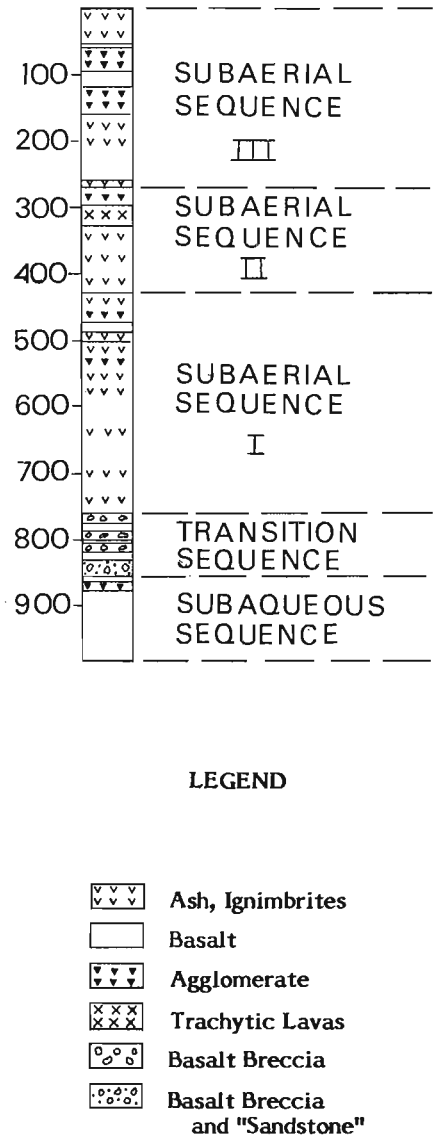

Figure 28.2. Log showing major lithologic variations in the Sao Miguel drill core.

at least some uranium enrichment by hydrothermal activity is seen if the distribution of the element through a flow from 879.41 – 884.29 m depth is examined (Fig. 28.4). A distinct increase of uranium can be seen at 884.29 m, the lower contact of the flow and also in the pillowed flow top region between 880.26 m and 879.4 m. Although the central part of the flow contains significantly less uranium than the marginal areas, the concentration of the element is variable and is much greater than in normal pillowed basalts. It is not possible to tell what the original uranium content of these alkaline basalts was and therefore no estimate of any overall increase in uranium can be made. A similar study of uranium distribution through several flows of the Bermuda

Table 28.1

Table of average uranium concentrations in different volcanic units encountered down the 981-m drillhole

Volcanic Unit	Average ppm U	Number of Whole Rock Analyses
Basalt Flows	1.33	41
Coarse Basalt Flows	1.57	11
Basalt Flow Margins (oxidized)	5.51	4
Flow Breccia	1.53	5
Pillowed Flows	2.12	4
Trachytic Flows	4.78	7

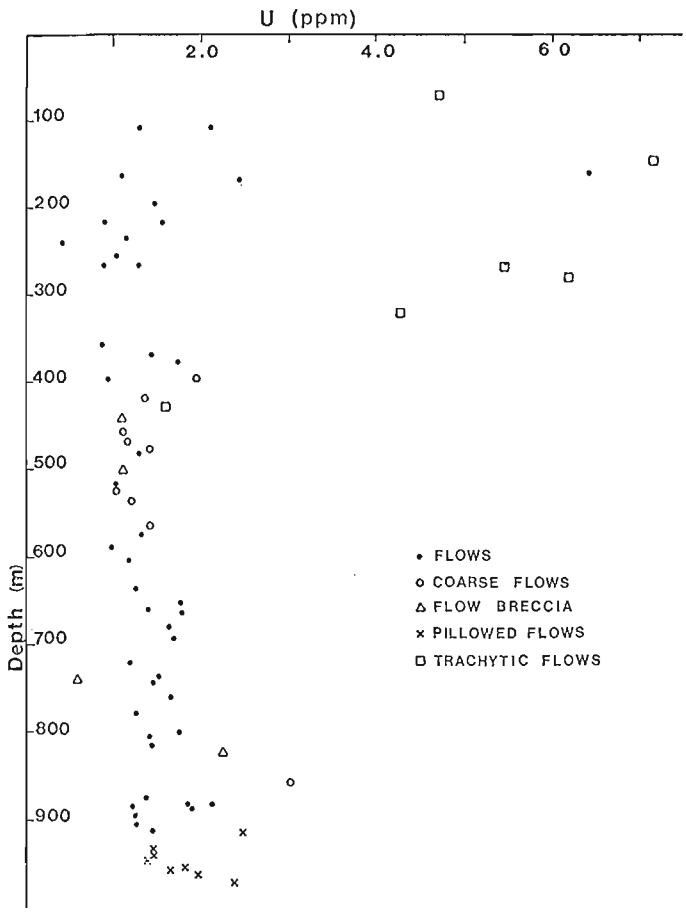

Figure 28.3. Plot of uranium versus depth in different volcanic units.

seamount indicated slight increases in the element at only one flow margin and of the many volcanic units penetrated by DSDP leg 37 drilling, few show any signs of marginal uranium enrichment. Those that do are invariably altered by fluids migrating along flow boundaries. It therefore seems reasonable to suggest that the relatively high uranium concentrations found at the boundaries of the Azores flow is a secondary enrichment caused by alteration in the presently active hydrothermal

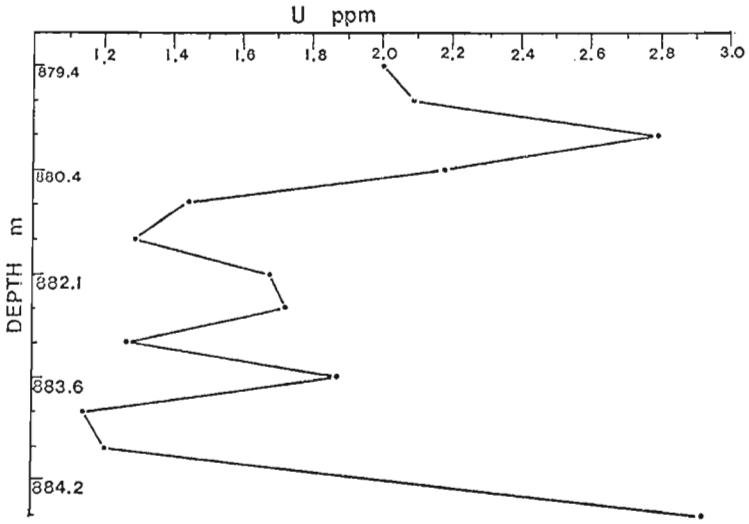

Figure 28.4. Plot of uranium versus depth through a single volcanic flow from 879.4 to 884.2 m. The base of the flow is strongly chloritized at 884.2 m and the flow top is pillowed above 880.4 m.

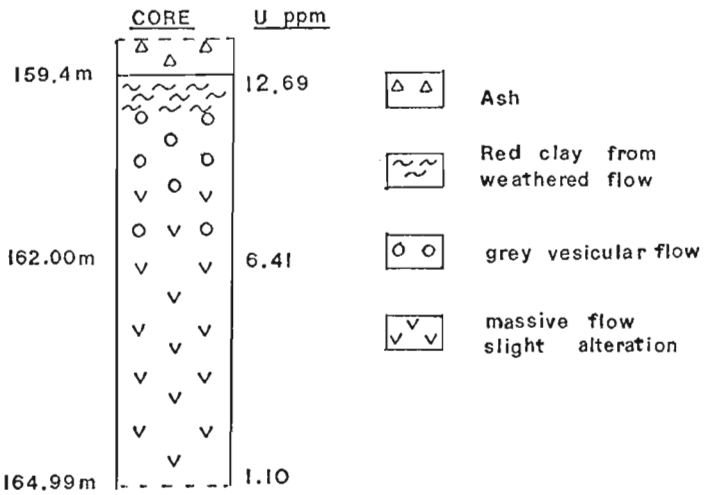

Figure 28.5. Schematic representation of uranium distribution through one subaerially oxidized volcanic unit.

environment. However, it has not yet been possible to tell whether uranium has been introduced to the system or whether the element is simply being redistributed through the volcanic pile with the trachytic units acting as possible uranium rich source rocks.

In oceanic basalts it is possible to use partition coefficients of uranium as a reasonable indication of alteration intensity (Mitchell and Aumento, 1977). Uranium mapping enables us to determine concentrations of the element in both matrix and minerals and partition coefficients calculated for uranium in different minerals enclosed in fresh sideromelane are considered true values. However, any alteration of the glass normally results in erroneously low calculated partition coefficients and the same is true for coefficients calculated for minerals set in progressively more altered microcrystalline basalt matrix. Mapping of uranium in six thin slices of subaerial porphyritic basalt from the Azores indicates that the average concentration of uranium in olivine, plagioclase and clinopyroxene is 10 ppb, 18 ppb and 30 ppb respectively, virtually identical to values previously reported (Mitchell and Aumento, 1977) for uranium in the same minerals from oceanic basalts and ultramafic rocks. However, because of pervasive strong hydrothermal alteration no glass could be located to enable us to calculate true partition coefficients of uranium and thus we are unable to use this technique as a measure of uranium enrichment through alteration.

A noteworthy feature of uranium distribution in several of the subaerially weathered lava flows is the strong concentration of the element in red weathered areas at flow tops. Uranium concentration decreases with decrease in intensity of red oxide weathering down through the basalt flow to normal values for the basalt. An example of this is seen between 159.4 and 164.9 m depths and is illustrated graphically in Figure 28.5. Thus there is evidence that uranium is strongly concentrated by weathering in oxidized tops of subaerial flows. Uranium in these weathered friable zones may in part be derived from trachytic ash units which subsequently covered the basalt flows.

Conclusions

1. The average uranium concentration in basalts from the Azores is an order of magnitude greater than in oceanic tholeiites or Bermuda basalts.

2. Pillowed basalts appear to contain more uranium on average than coarse-grained flows which in turn contain more uranium than fine-grained flows.

3. Trachytic flows contain much more uranium than basalts.

4. Uranium is commonly concentrated at flow margins probably by hydrothermal alteration.

5. Very high concentrations of uranium occur in red oxidized, weathered tops of subaerial flows.

6. It is not yet possible to quantify completely the amount of uranium redistribution throughout the volcanic pile by migrating hydrothermal fluids.

References

Fisher, D.E.
1970: Homogenized fission track determination of uranium in whole rock geologic samples; Anal. Chem., v. 42, p. 414-416.

Kleeman, J.D. and Lovering, J.F.
1967: Uranium distribution in rocks by fission track registration in lexan plastic; Science, v. 156, p. 512-513.

McGraw, P.A.
1976: A petrological/geochemical study of rocks from Sao Miguel, Azores, Portugal. Unpubl. M.Sc. thesis, Dalhousie Univ., Halifax, Nova Scotia.

Mitchell, W.S. and Aumento, F.
1977: Uranium in oceanic rocks: DSDP Leg 37; Can. J. Earth Sci. (in press)

Muecke, G.K., Ade-Hall, J.M., Aumento, F., Macdonald, A., Reynolds, P.H., Hyndman, R.D., Quintino, N., Opdyke, N., and Lowrie, W.
1974: Deep drilling in an active geothermal area in the Azores; Nature, v. 252, p. 281-285.

29. STUDIES OF DISTRIBUTION OF URANIUM IN SELECTED ORE ENVIRONMENTS USING NUCLEAR TRACK TECHNIQUES

E.M.R. Research Agreement 1135-D13-4-13/76

M. Zentilli,[1] W.S. Mitchell,[1] K.A. Taylor,[1] and P.F. Taylor,[1]
Regional and Economic Geology Division

Introduction

The distribution of uranium in host rocks, ore and alteration minerals of non-uraniferous deposits is poorly known. Uranium occurs as trace amounts in a variety of ore environments, but significant concentrations have been reported from porphyry copper, "kuroko" type massive sulphides, red bed copper, fluorite and other deposits. This study is designed to document the variation and distribution of uranium in mineral assemblages from some of these environments.

Besides its usefulness for dating glass or minerals (i.e. Fleischer and Price, 1964; Aumento, 1969), the fission track techniques, as refined at Dalhousie by F. Aumento and co-workers, are an effective method for detecting small amounts of uranium (to a few ppb) in minerals and rocks (i.e. Mitchell and Aumento, 1977; Dostal et al., 1975). The uranium concentration is inferred from the track density on a film of sensitive material in contact with the powder (bulk analysis) or the polished thin section (track mapping) of the material produced by irradiation with a known dose of neutrons in a nuclear reactor. The equivalence of track density with uranium concentration is calibrated by means of standards exposed to the same irradiation as the samples in every run. Precision of the determinations of bulk samples is better than ± 12 per cent and somewhat lower (± 25 per cent) in mineral phases of low uranium concentration (1-2 ppb). The precision is sufficient, however, to detect zonal distribution, concentration contrasts and to calculate fractionation coefficients between coexisting phases. It permits one to discern whether the uranium is evenly distributed throughout the crystals or if it occurs along grain boundaries, in cracks, or in inclusions. Uranium distributions have been successfully measured in a number of natural systems, including skarns (Dikov et al., 1971) and other mineral assemblages (Berzina and Demidova, 1966; Berzina, 1972; Alekseyev et al., 1969).

Results

As part of a preliminary survey, over 350 bulk analyses for uranium have been completed on mineral separates, whole-rock and ore samples. In addition, polished thin sections of a number of rocks and ores have been prepared for uranium track mapping. Preliminary results are reported here.

Fluorites

Fluorite occurs as an associated mineral in a variety of ore deposits. In pipelike bodies associated with felsic volcanics from the Thomas Range, Utah, fluorite is reported to contain as much as 0.3 per cent U (Staatz and Osterwald, 1959; Staatz and Griffitts, 1961). The violet coloration in some fluorites of the USSR has been correlated with high uranium content (Baranov, 1966). Radon gas has been detected in some mine workings of the St. Lawrence fluorite deposits, Newfoundland. In view of these observations, a survey of the uranium content of fluorite appeared justified.

Uranium analyses of a number of fluorites from Eastern Canada are summarized in Table 29.1. The highest values were found in St. Lawrence, Newfoundland (5.76 ppm) and at Gays River, Nova Scotia (2.59 ppm). At St. Lawrence, fluorite occurs in veins and miarolitic cavities and is disseminated in a shallow-level, peralkaline, granitic pluton (Teng, 1974). Within an individual vein in this deposit, the uranium content of purple fluorite (interpreted as an early-formed fluorite by Teng, 1974) is generally higher than in green, yellow or colourless fluorites of the same deposit. The highest value (5.76 ppm), however, was found in white, milky fluorite at a vein wall in contact with granite with 7.8 ppm U. A possible positive correlation of uranium content with temperature of crystallization will be investigated using fluid inclusions. The detailed distribution of uranium in banded fluorite is being studied by fission track mapping. At Gays River, Nova Scotia (a Zn-Pb deposit in Carboniferous carbonate rocks), the purple colour or the association with hydrocarbon material does not appear to correlate with higher uranium content.

Massive Sulphides and Barite

The distribution of uranium in volcanogenic massive sulphide environments has not been studied in detail. Previous investigations (Mitchell and Aumento, 1977) indicate that the separate processes of hydrothermal and halmyrolitic alteration play an important role in the redistribution of uranium in submarine volcanic rocks. Our study of distribution of uranium in an active geothermal system in submarine to subaerial rocks of the Azores (Mitchell et al., 1977), indicates that hydrothermal alteration has led to a considerable U-enrichment in parts of that system. Superimposed on primary differentiation trends, uranium distribution is clearly affected by factors such as permeability of the formations and physico-chemical parameters. The presence of felsic rocks relatively rich in uranium, higher sulphur activities, and prevalent reducing conditions in some massive sulphide environments, probably strongly influenced the mobility of uranium. In fact values as high as 900 ppm U have been determined in some horizons of the Kuroko deposits of Japan (T. Sato, pers. comm., 1977). Samples from the Buchans and Rambler massive sulphides of Newfoundland have been analyzed. From Buchans, values from 3 to 10 ppm were detected in specimens of ore from the MacLean orebody, although the galena- or barite-rich ores are generally much lower (0.02 – 0.08 ppm). Associated volcanic rocks have from 0.9 ppm U (amygdular andesitic

[1]Department of Geology, Dalhousie University, Halifax, N.S.

From: Report of Activities, Part B;
Geol. Surv. Can., Paper 77-1B (1977)

Table 29.1

Contents in ppm of U in Fluorite

Mean	Range	No. of Specimens	Locality	
2.60	(0.23 – 1.80 – 5.76)	3	Church vein, in granite with 7.8 ppm U	St. Lawrence, Newfoundland
0.30	(0.18 – 0.26 – 0.46)	3	Canal vein	"
0.13		1	Tarefare	"
0.07	0.07	2	Lord and Lady Gulch	"
0.09		1	Quarry. In felsite with 1.11 ppm U	"
1.21		1	In sample with galena, sphalerite	"
0.82	(0.11 – 1.53)	2	In greisen	New Ross, N.S.
0.38	(0.13 – 0.92)	5	In rhyolite (10.3 ppm U) with barite (0.16 ppmU)	Lake Ainslie, N.S.
1.47	0.34 – 2.59	2	In mineralized carbonates	Gays River, N.S.
1.02		1	Locality unknown	Quebec

basalt) to 2.6 ppm U (dacite-rhyolite). The specimens from ore at the Ming deposit at Rambler Mines, Newfoundland also contain variable but relatively higher concentrations of U (up to 4.5 ppm); samples of the schistose metavolcanic host rocks are low (0.5 ppm U).

Massive white barite from the Magnet Cove barium-lead-zinc-silver deposit near Walton, Nova Scotia contains 0.03 ppm U, even when associated with black bituminous inclusions, but a sample of yellow-stained barite with hydrocarbon-rich nodules has 0.36 ppm U. One specimen with erythrite contains 2.17 ppm U. Specimens of banded sulphides contain 1 to 2.6 ppm U and the higher values are found in specimens containing tennantite or described as rich in silver. One anomalous value of 13.57 ppm U was determined for massive orange barite, but the uranium appears to be concentrated in very small, yet unidentified, inclusions.

Some of the above values for barite are lower by 2 to 3 orders of magnitude than those reported from barite in the U.S.S.R. by Plyuschchev and Ryabova (1974) which range from 1.8 to 10.6 ppm (mean 5.0 ppm). It is unclear whether the barite from the above Appalachian deposits is anomalously low in U, or if the methods used by the above authors (fluorescence and colorimetric) do not differentiate between uranium in barite proper or in inclusions within this mineral.

Pb-Zn Deposits in Carbonate Rocks

Samples from four Canadian Pb-Zn deposits in carbonate rocks were studied: 1) Pine Point, District of Mackenzie; 2) Polaris Mine, Little Cornwallis Island, District of Franklin; 3) Newfoundland Zinc, Daniel's Harbour, Newfoundland, and 4) Gays River, Nova Scotia. The sulphides from the four deposits contain extremely low concentrations of U: galena (0.002 – 0.012 ppm), sphalerite (0.006 – 0.068 ppm), marcasite (0.775 – 1.068 ppm). Associated sparry carbonate minerals (calcite, dolomite) are poor in uranium (0.011 – 0.472) except those of the Polaris Mine, which are anomalously rich (2.438 – 3.435 ppm). The concentration of uranium in the host carbonate rocks falls within the expected range (0.9 – 2.3 ppm) for these kinds of rocks (Bell, 1963). Hydrocarbons associated with the Daniel's Harbour and Gays River deposits (1.2 and 3.6 ppm average, respectively) are unexpectedly uranium-poor. The results are being evaluated in relation to geochemical considerations and genetic models for Mississippi Valley type deposits.

Felsic, Porphyritic Igneous Rocks

During magmatic crystallization, uranium is strongly partitioned into the residual melts and thus the groundmass of porphyritic volcanic and subvolcanic rocks contains the bulk of the uranium (Dostal et al., 1975). It can be expected that during devitrification-alteration by hydrothermal processes uranium will be redistributed in the different alteration assemblages formed. In some porphyry coppers, radioelements appear to be zonally distributed (Davis and Guilbert, 1973). There is a good possibility that if uranium demand follows current projections, future uranium requirements will necessitate the exploration of large low-grade uranium "porphyry" type deposits (Armstrong, 1974). At the low grades envisaged (0.05% U_3O_8) it is important for extractive milling and metallurgical ore beneficiation processes to know how the uranium is bound up and distributed in the rock. Preliminary results from a small number of samples from the El Salvador porphyry copper (Chile) indicates that: 1) the highest uranium concentration (average 2 ppm) occurs in an altered rhyolite porphyry; 2) relatively high uranium concentrations are found in rocks which have undergone strong potassic alteration, and 3) uranium concentrations are low (average 0.2 ppm) in biotitized

andesite country rock and in an early porphyry intrusive. Unmineralized felsic volcanics from the same region contain an average 2 ppm but some dacites and rhyolites contain twice as much and up to 15 ppm U. Fission track mapping of specimens of these porphyritic volcanics indicates that the bulk of the uranium is in the groundmass and that most of the uranium found within plagioclase crystals occurs in zones rich in fluid inclusions. Early, magmatic magnetite has very low uranium content, while deuteric or secondary magnetite, formed at the expense of ferromagnesian minerals, is relatively enriched in uranium.

Uranium content in a suite of 16 samples from a small felsic porphyritic pluton associated with Mo mineralization at Deep Cove, Cape Breton Island, Nova Scotia, varies from 0.65 to 6.07 ppm U (average 2.76). The highest values are in the groundmass of coarse porphyritic phases and in mineralized zones with phyllic alteration (5.56 ppm U) but values are relatively lower (1-2 ppm U) in phases rich in hydrothermal biotite, K-feldspar, quartz and molybdenite.

The preliminary results indicate that the fission track techniques as used are an effective tool in the study of the distribution of uranium in hydrothermal environments. An attempt to analyze for thorium is being made using a similar technique, as it has been shown (Plyushchev and Ryabova, 1974) that U and Th follow separate paths in certain hydrothermal processes, such as the formation of greisen.

References

Alekseyev, F.A., Gottikh, R.P., Vorob'yeva, V. Ya., and Murav'yeva, L.V.
1969: Uranium distribution in sedimentary rocks in the western part of the Amu Darya Petroleum Basin; Geochem. Int., v. 6, p. 963-970 (Translation from Geokhimiya 10, p. 1238-1247).

Armstrong, F.C.
1974: "Porphyry" uranium deposits. Formation of uranium ore deposits; Int. Atomic Energy Proc., p. 625-638.

Aumento, F.
1969: The Mid-Atlantic Ridge near 45°N: fission track and manganese chronology; Can. J. Earth Sci., v. 6, p. 1431-1440.

Baranov, E.N.
1966: Uranium content in fluorite; Geokhimiya, no. 8, p. 1006-1009.

Bell, K.G.
1963: Uranium in carbonate rocks; U.S. Geol. Surv. Prof. Paper 474A.

Berzina, I.G. and Demidova, P.G.
1966: Determination of the growth of minerals by the tracks from fission fragments from uranium; Atomnaya Energiya, 21, p. 304-306. In: Fleischer et al. (1975).

Berzina, I.G., Mel'nikov, I.V., and Popenko, D.P.
1972: Determination of the quantity and spatial distribution of uranium in fluorites from the tracks of uranium fission fragments; Atomnaya Energiya, 32, p. 211-215. In: Fleischer et al. (1975).

Davis, J.D. and Guilbert, J.M.
1973: Distribution of the radioelements potassium, uranium and thorium in selected porphyry copper deposits; Econ. Geol, v. 68 p. 145-160.

Dikov, Yu, P., Kaikova, T.M., and Perelygin, V.P.
1971: Geochemistry of uranium in skarn deposits; International Geochemical Congress (Book II), A.I. Tubarinov (ed.), 532, Moscow Acad. Sci. U.S.S.R. In Fleischer et al. (1975).

Dostal, J., Capedri, S., and Zentilli, M.
1975: Distribution of uranium in calc-alkaline volcanic rocks from Sardinia (abstract); EOS, v. 56, no. 6, p. 474.

Fleischer, R.L. and Price, P.B.
1964: Uranium content of ancient man-made glass; Science, v. 144, p. 841-842.

Fleischer, R.L., Price, P.B., and Walker, R.M.
1975: Nuclear tracks in solids: principles and applications; Univ. California Press, 605 p.

Lambert, I.B. and Sato, T.
1974: The Kuroko and associated ore deposits of Japan: a review of their features and metallogenesis. Ec., Geol. Vol. 69, p. 1215-1236.

Mitchell, W.S., Zentilli, M., and Taylor, K.A.
1977: Distribution of uranium in an active geothermal area in the Azores; in Report of Activities, Part B, Geol. Surv. Can., Paper 77-1B, rep. 28.

Plyushchev, Ye. V. and Ryabova, L.A.
1974: Accumulation levels of U and Th in hydrothermal minerals; Geokhimiya no. 8, p. 1192-1203.

Staatz, M.H. and Ostenwald, F.W.
1959: Geology of the Thomas Range fluorspar district, Juab County, Utah; U.S. Geol. Surv., Bull. 1069, 97 p.

Staatz, M.H. and Griffitts, W.R.
1961: Beryllium-bearing tuff in the Thomas Range, Juab County, Utah; Econ. Geol., v. 56, p. 941-950.

Teng, H.C.
1974: A lithogeochemical study of the St. Lawrence granite, Nfld; Unpubl. M.Sc. thesis, Memorial University of Newfoundland, 200 p.

GEOLOGY OF THE SOUTHERN PARK RANGES, BRITISH COLUMBIA

E.M.R. Research Agreement 1135-D13-7-165/76

D. Craw[1]
Institute of Sedimentary and Petroleum Geology, Calgary

The Southern Park Ranges lie immediately east of the Rocky Mountain Trench at the Big Bend of the Columbia River (McNaughton Lake, Parts of 83D/1, 8). Reconnaissance mapping and sampling in late August 1975, and detailed mapping and sampling during the summer of 1976, were carried out by the author, aided by P.S. Simony, University of Calgary, Department of Geology.

The rocks are quartzites, carbonates and pelites in an apparently uninterrupted sequence from the Proterozoic Windermere Supergroup, through the Lower Cambrian Gog Group, to the Middle Cambrian Tsar Creek and Kinbasket units (Fyles, 1960).

Four major subdivisions of the Windermere Supergroup rocks, closely corresponding to the divisions of Young et al. (1973), were mapped:

(1) A grit unit at the bottom of the sequence, consisting of interbedded quartzose grit and pelite units, about 10 m thick, with minor thin beds of calcareous grit. Total thickness is in excess of 1000 m (base was not seen).

(2) A slate unit, which consists of 800 to 1000 m of fine grained pelite with rare thin (<30 m) sandstone, grit, and calcareous sandstone interbeds.

(3) A carbonate unit, which contains pure grey marble, sandy dolomitic carbonates, and calcareous quartzites and pelites. Thickness is variable, but does not exceed 200 m. At least some of the thickness variation is a tectonic effect, since the carbonates are structurally incompetent.

(4) An upper clastic unit, containing interbedded fine grained pelite and quartzite in units from 1 to 10 m thick. The proportion of quartzite increases upward in the section to an apparently gradational contact with the overlying Gog quartzite. Thickness is less than 200 m.

The Gog Group consists of three recognizable formations:

(1) The McNaughton Formation at the base, is made up mainly of medium to coarse grained quartzite, with very minor pelitic partings. The proportion of pelite increases up-section, and the top of the formation is characterized by interbedded quartzite and pelite in units about 1 m thick. Total thickness of the McNaughton Formation is about 600 m.

(2) The Mural Formation, a carbonate unit, includes pure marble (with micaceous partings), dolomitic sandy carbonate, and calcareous sandstone. Thickness variation from 20 to 150 m probably is due to deformation as for the carbonate unit in the Windermere Supergroup (above).

(3) The Mahto Formation with lenses of basal conglomerate (up to 20 m thick) in some parts of the area overlies the Mural Formation. The unit comprises fine grained pink quartzite with minor amounts of interbedded pelite and carbonate. Total thickness of the unit generally is about 250 m, although it thins to a minimum of approximately 30 m in the southeastern part of the area.

Immediately overlying the Gog Group is the Tsar Creek unit. This unit contains mainly pelite, with irregular lenses and beds, up to 200 m thick, of sandy carbonate and quartzite (and rare, thin marble layers). Total thickness of the unit ranges from 200 to 600 m. Above the Tsar Creek unit is the Kinbasket unit, a thick (>1000 m, top not seen) monotonous succession of sandy carbonate with layers or lenses of grey marble (up to 200 m thick), with some intercalated pelite.

The area has suffered two phases of deformation associated with the rise of the Porcupine Creek Anticlinorium, a major structural complex trending northwest-southeast through the eastern part of the area (Fig. 30.1). Folding was mainly of concentric style, with minor thickening of incompetent units in the fold hinges. Major structures are broad, open concentric folds and associated thrust faults. Late-stage west-dipping normal faults are parallel to the trend (NW-SE) of the compressive structures.

The Park Ranges have undergone a major phase of Barrovian-type metamorphism which occurred during and after the first phase of deformation. The pervasive mineral cleavage which passes through first-phase fold hinges and is folded around second phase folds, is a result of this phase of metamorphism. A second (minor) phase of metamorphism associated with the second phase of deformation is characterized by the recrystallization of muscovite and chlorite in an incipient cleavage parallel to the axial planes of second phase folds.

The major (Barrovian) metamorphic phase resulted in a metamorphic progression, ranging from chlorite zone rocks in the eastern part of the area, to sillimanite zone rocks in the west, near the Purcell Fault (a major structural break near the Rocky Mountain Trench). The staurolite disappearance isograd and the sillimanite isograd are approximately coincident. The isogradic configuration (thermal antiform, Fig. 30.1) and trend in the Park Ranges is different from that observed on the west side (hanging wall) of the Purcell Fault (Campbell, 1968; Robbins, 1976; P.S. Simony, pers. comm.) and there is significant repetition of metamorphic zones across the fault, suggesting that the Purcell Fault has had post-metamorphic thrust displacement. Quartz c-axis orientation studies at a thrust fault in the Park Ranges also suggest that motion occurred after the main metamorphic phase.

[1] Geology Department, University of Calgary

From: Report of Activities, Part B; Geol. Surv. Can., Paper 77-1B (1977)

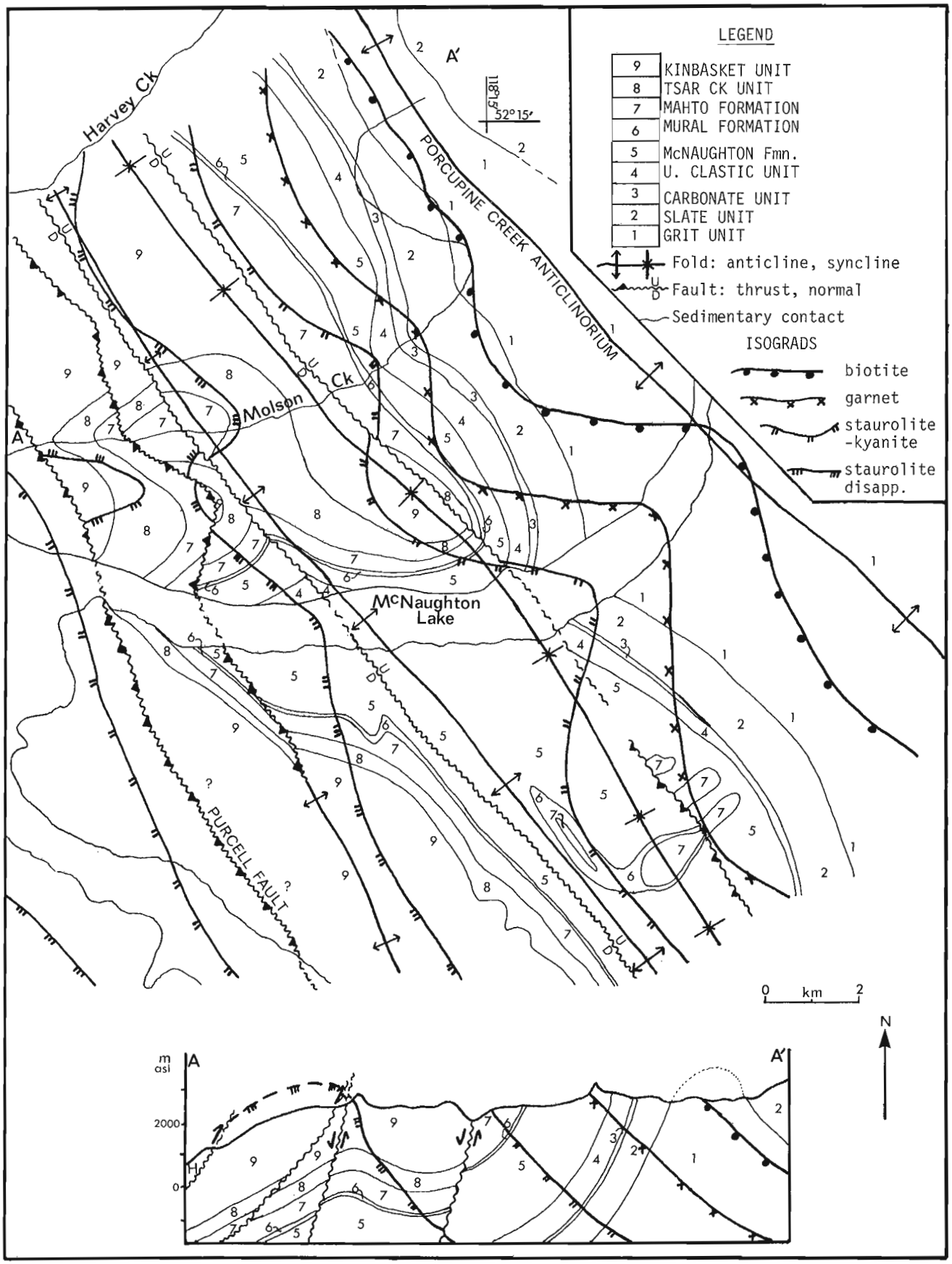

Figure 30.1. Sketch geologic map and cross-section, Southern Park Ranges.

References

Campbell, R.B.
1968: Canoe River, British Columbia; Geol. Surv. Can., Map 15-1967.

Fyles, J.T.
1960: Geological reconnaissance of the Columbia River between Bluewater Creek and Mica Creek; British Columbia Minister of Mines Ann. Rept., 1959, p. 90-105.

Robbins, D.G.
1976: Metamorphism and structure of the Encampment Creek area, British Columbia; Unpubl. M.Sc. thesis, University of Calgary, Alberta.

Young, F.G., Campbell, R.B., and Poulton, T.P.
1973: The Windermere Supergroup of the southeastern Canadian Cordillera; Belt Symp., Univ. of Idaho Dept. of Geol. and Idaho Bur. Mines and Geol., Moscow, Idaho, v. 1, p. 181-203.

31. BEDDED VOLCANIC CHERT NEAR COALSPUR, CENTRAL FOOTHILLS, ALBERTA

Project 760018

T. Jerzykiewicz and J.R. McLean
Institute of Sedimentary and Petroleum Geology, Calgary

Introduction

A section containing several chert and bentonite beds was encountered near the old coal mining town of Sterco, southeast of the town of Coalspur, Alberta (Fig. 31.1).

The location is on the northeastern wall of the No. 5 Pit, originally mined by Sterling Collieries Ltd., but closed since the early 1950's. The area is currently being actively explored and developed for its coal potential but, because of a paucity of good stratigraphic markers associated with the coal, the stratigraphy and structure of the area are problematic. This chert-bentonite zone has potential as a stratigraphic horizon and, also, as a time-stratigraphic marker.

The term "chert" is employed herein for compositional and textural reasons discussed later. Probably similar beds elsewhere have been called silicified tuffs. This chert as well as tuff and bentonite beds are from the same source – airborne volcanic ejecta – but have undergone different diagenetic processes.

Stratigraphy

The stratigraphy of the Upper Cretaceous-lower Tertiary succession in the Foothills of central Alberta has never been clear because of a lack of persistent stratigraphic markers in a wholly continental sequence 1000+ m thick. The current nomenclature in this and adjacent areas is shown in Table 31.1.

The occurrence documented here has not been described previously in the literature, although tuff beds in the same vicinity were observed by Sanderson (1931). Bentonite beds are common in the Cretaceous and Tertiary succession of western Canada but few occurrences of tuff have been reported (Sanderson, 1931). The best documented and most widespread tuff recognized to date is the Kneehills Tuff of Late Cretaceous age which forms the uppermost unit of the Edmonton Group in the central Alberta Plains (Table 31.1). This tuff bed has not been identified in the Foothills of west-central Alberta, but the chert-bentonite sequence described here may be equivalent.

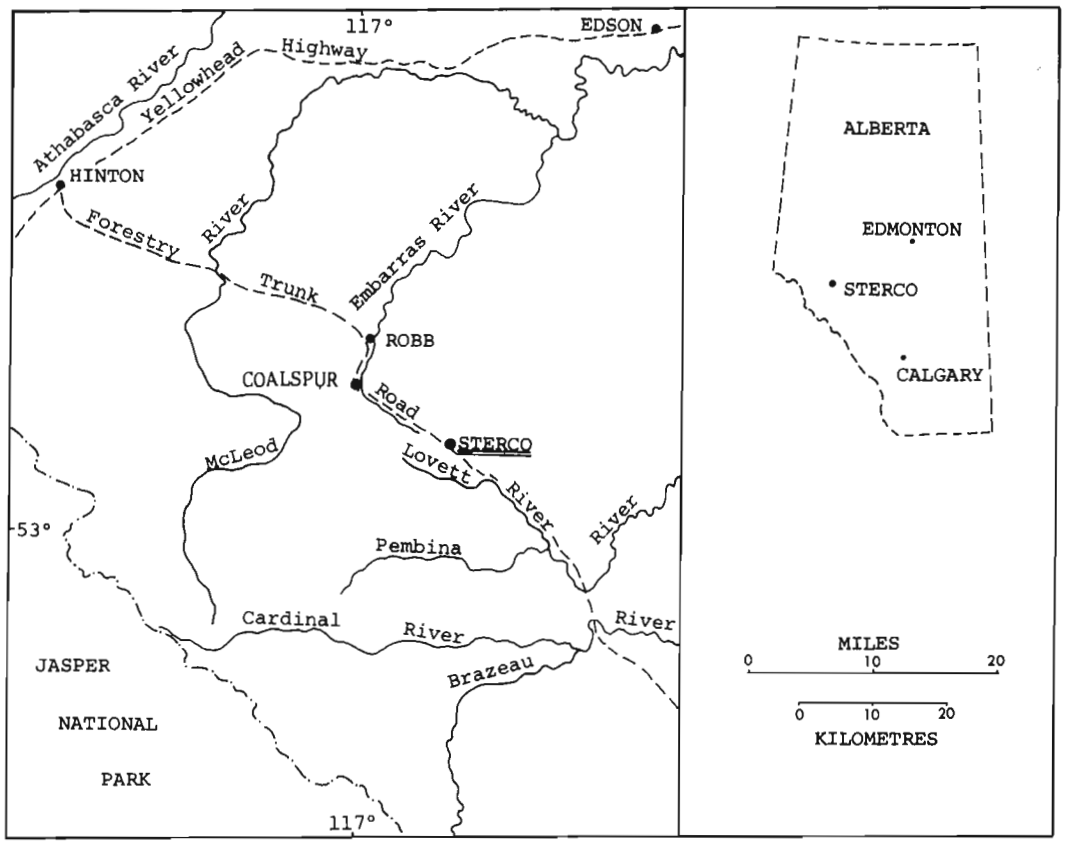

Figure 31.1. Location map.

From: Report of Activities, Part B;
Geol. Surv. Can., Paper 77-1B (1977)

Table 31.1.

Lithostratigraphic Nomenclature

	SOUTHWEST FOOTHILLS	CENTRAL FOOTHILLS	CENTRAL PLAINS	NORTHWEST PLAINS
PALEOCENE	PORCUPINE HILLS FM.	PASKAPOO FM.	PASKAPOO FM.	PASKAPOO FM.
UPPER CRETACEOUS	WILLOW CREEK FM.	*Coal "Zone" ?*	*Ardley Coal "Zone"*	*Ardley "Zone"*
	KNEEHILLS	ENTRANCE CGL.	KNEEHILLS	WAPITI GP.
	ST. MARY RIVER FM.	BRAZEAU FM.	EDMONTON GP.	
	BEARPAW FM.		BEARPAW FM.	
	BELLY RIVER FM.		JUDITH RIVER FM.	SMOKY GP.
	ALBERTA GP.	ALBERTA GP.	LEA PARK FM.	

Sanderson (1931) described the Saunders Tuff bed near Coalspur which he estimated to be 274 m (900 ft) stratigraphically below the lowest coal seam, the Mynheer, in the coal zone of that area. The stratigraphic position of the chert-bentonite zone described here is uncertain due to unresolved structural complications. It is situated in the hanging wall of a northeast-dipping fault whereas the Mynheer coal seam is in the footwall, where it is greatly thickened structurally (Alexander, 1977). The vertical displacement on the fault is not known at this time, but the fact that the block containing the chert-bentonite zone is displaced upward relative to the coal seam suggests that the chert-bentonite zone may be lower stratigraphically and may correlate with the Saunders Tuff, although this is purely speculative at present.

The occurrence of the Saunders Tuff below the main coal zone at Coalspur is comparable to the position of the Kneehills Tuff below the Ardley coal zone (Irish, 1970; Carrigy, 1970; Holter et al., 1975) in the Plains, although the intervening succession is thinner than the 274 m (900 ft) reported by Sanderson (1931) from the Foothills. However, this is not a serious obstacle to correlation as the whole succession thickens markedly from east to west.

The chert beds are confined to the interval from 13 to 22 m (43-73 ft) in Figure 31.2. Beds below are silty claystones to clayey siltstones, with one very fine grained sandstone. Carbonaceous debris is present in minor amounts but evidence of indigenous plant growth was not observed. The presence of two bentonite beds indicates that volcanic ash was being supplied to the area. The chert beds (Plate 31.1A, B) are extremely finely crystalline to aphanitic, very hard, and laminated (Plate 31.2A). They are interbedded with hard, light grey, very fine grained, ripple-laminated sandstones (Plate 31.2B). The contacts between the beds are abrupt. At the top of the succession is a thin bed of silty claystone, overlain by another bed of chert, in turn overlain by a thick bentonite bed.

Description of the Cherts

The cherts exhibit distinct lamination with alternating dark- and light-coloured lamina sets (Plate 31.2A). Set thickness ranges from one to several centimetres. The sets are continuous over several metres of exposure and consist of very fine laminae which are commonly inclined slightly to the set boundary. Penecontemporaneous deformational structures are common and consist of: (1) convolute lamination (Plate 31.2C), probably caused by instability in density stratification together with a horizontal shear force (Anketell and Dzulynski, 1968); and (2) small, irregular vertical structures which disrupt the lamination (Plate 31.2A) and are believed to be water escape structures (Lowe, 1975). Evidence of biotic activity is not apparent. Small scours in the lamina sets (Plate 31.2A) indicate weak wave or current activity.

Microscopically, the cherts are predominantly cryptocrystalline with a small percentage of microcrystals. Much of the cryptocrystalline groundmass and most of the crystals show a preferred extinction position parallel to the lamination.

The darker laminae sets differ from the lighter ones in containing small amounts (less than 5%) of opaque to translucent, reddish brown grains that probably represent organic carbonaceous matter.

Composition of Cherts

Semi-quantitative X-ray diffractography (without internal standards) indicated that the dark bands are composed of 86 per cent quartz, 10 per cent feldspar, and 4 per cent illite. The light bands are composed of 91 per cent quartz and 9 per cent feldspar. For comparison, X-ray diffraction analysis of the bentonite bed at the top of the succession showed a whole rock composition of 57 per cent montmorillonite, 42 per cent quartz and 1 per cent feldspar.

Chemical analyses by X-ray fluorescence (SiO_2 and Al_2O_3 checked by wet chemistry) on two samples from Sterco are compared in Table 31.2 with a sample of Kneehills Tuff from the central Plains area.

It is apparent that there is not a close correlation between the two Sterco samples (one from a light-coloured lamina set, the other from a dark set) and the Kneehills Tuff. A further comparison with nine samples of the Kneehills Tuff from widely spaced localities recorded by Irish (1968, p. 25), also suggests significant differences from the Sterco samples. In particular, the high K_2O and Al_2O_3 content of the Sterco samples indicates a much higher proportion of potassium feldspar than is present in the Kneehills Tuff. It is not certain if these chemical differences definitely indicated different sources, as there may have been post-depositional differences which produced the chemical differences.

An interesting observation by A.E. Foscolos (pers. comm.), who carried out the X-ray fluorescence analyses, was that the temperature necessary to fuse the samples (1000° C +) was markedly higher than that for most quartz-rich samples (less than 800°C). He suggested that this was due to the silica being present as a high temperature form. X-ray diffraction indicated the high temperature form of quartz rather than tridymite, which has a distinctly different lattice spacing.

Table 31.2

Chemical Analyses by X-ray Fluorescence

Oxide	Sterco A	Sterco B	Kneehills
Fe_2O_3	1.56	2.12	0.78
MnO	0.01	0.02	0.01
TiO_2	0.27	0.43	0.79
CaO	0.46	0.49	0.24
K_2O	4.58	6.09	0.89
SiO_2	76.90	71.70	89.66
Al_2O_3	12.34	13.95	5.02
MgO	0.09	0.16	0.06
Na_2O	0.49	0.49	0.53
Ignition Loss	3.30	4.55	2.02

There is a discrepancy between the amount of quartz indicated by X-ray diffraction and the amount of silica determined by X-ray fluorescence. The error is believed to be in the diffraction analyses where a high proportion of crystalline quartz will mask the contribution of other minerals (A.E. Foscolos, pers. comm.).

Depositional Environment

A low energy environment is indicated by the fineness of all sediments and by the formation and preservation of very fine lamination. The lamination in the siliceous sandstones (Plate 31.2B) is lenticular to flaser indicating periods of turbulence alternating with periods of quiescence in an aqueous body. This is common in intertidal sediments, but may also form in a shallow body of standing water with periods of strong wind and wave action alternating with periods of calm.

There has been no evidence of any marine influence in the Upper Cretaceous-lower Tertiary section anywhere in the central Foothills, but terrestrial fauna and flora are common (Allan and Rutherford, 1924; Irish, 1965). A lacustrine environment seems most probable.

Origin of Bedded Chert

The origin of siliceous sediments is often enigmatic. However, there is a common association between silica-rich sediments and contemporaneous volcanism (Rubey, 1928; Taliaferro, 1933). The close relationship, in the section under consideration, of the chert beds with bentonites, acknowledged to be of volcanic origin, strongly suggests that the cherts are also of volcanic origin. The high temperature form of quartz is also suggestive of a volcanic origin.

Airborne volcanic detritus is usually in the form of a very porous tuff when it first settles in the depositional area but, because of the instability of the high

Figure 31.2. Stratigraphic section.

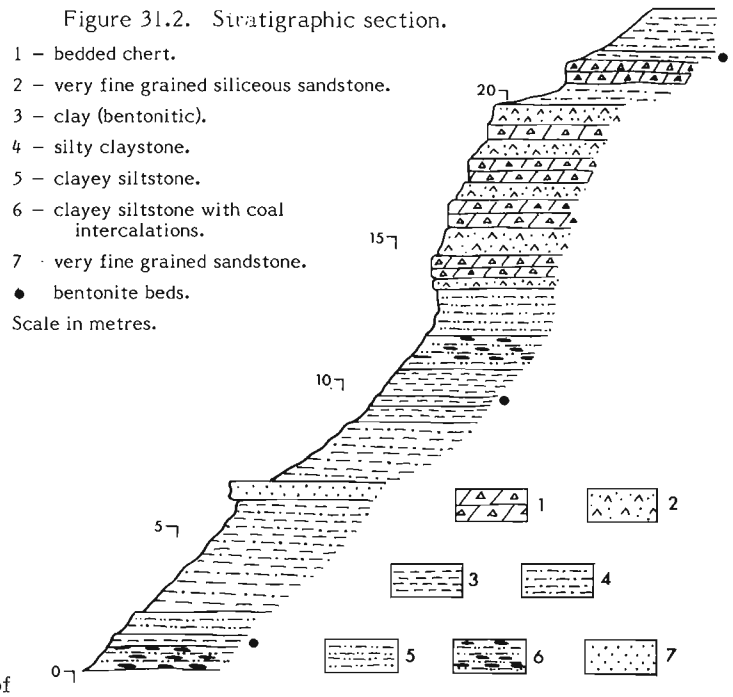

temperature volcanic constituents and the accessibility to migrating fluids due to their porosity, it is the exception rather than the rule to find tuffs in their freshly deposited condition (Pettijohn, 1975, p. 308).

"One of the earliest changes in vitric tuff is the release of silica and deposition of hydrated silica--opal and chalcedony--which may convert these felsic tuffs to a dense flinty rock very much resembling a chert" (Pettijohn, 1975, p. 308).

In outcrop and in macroscopic examination, the Sterco samples, indeed, resemble cherts. The definition of chert (Gary et al., 1972) is: "A hard, extremely dense or compact, dull to semivitreous, cryptocrystalline rock, consisting chiefly of cryptocrystalline silica (chiefly fibrous chalcedony) with lesser amounts of micro- or cryptocrystalline quartz and amorphous silica (opal); . . . ". These characteristics apply to the samples shown in Plate 31.2 and thus they are called cherts. However, it should be noted that the appearance of these cherts under the microscope is distinctly different from the microcrystalline aggregate type of chert that is familiar to most geologists in western Canada, such as in the upper Paleozoic carbonate units of the Rocky Mountain Front Ranges or the Cache Creek Group of south-central British Columbia.

The most enticing question seems to be the genetic relationship of the siliceous sandstones to the chert beds and to the bentonite beds. Why are some beds hard and cherty, while others are soft and clayey, and why are ripple-laminated sandstones interbedded with the cherts?

The sequence in Figure 31.2 illustrates 4 cycles or alternations of siliceous sandstone (Plate 31.2B) and chert (Plate 31.2A, C) starting with a sandstone. The contact between the two lithologies is abrupt. The sand fraction of the sandstones is composed mainly of angular quartz and twinned feldspar grains, but with some rock fragments of a finely textured siliceous felsic volcanic aspect, and a

Plate 31.1A. General view of outcrop looking northeast. White unit is the interbedded siliceous sandstone and chert. Geologist is 1.82 m (6 ft) tall.

Plate 31.1B. Close-up view of a chert bed. Divisions on hammer handle are one inch apart.

Plate 31.2A. Polished slab of laminated chert showing water escape structures and small-scale truncation of lamination.

Plate 31.2B. Slab of siliceous sandstone showing ripple lamination.

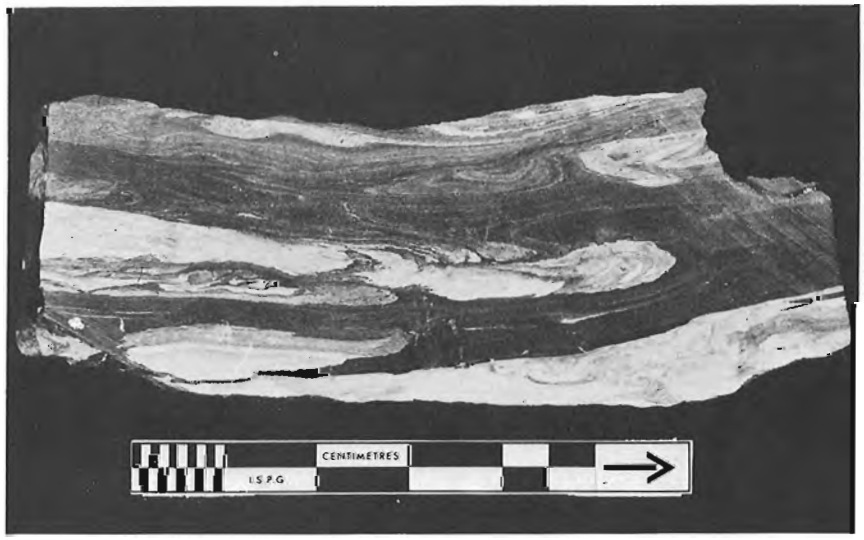

Plate 31.2C. Polished slab of laminated chert with convolutions.

small percentage of detrital carbonate grains (probably dolomite). The matrix-cement appears to be composed of micro- to cryptocrystalline silica and clay minerals. The plagioclase and the finely textured felsic rock fragments almost certainly are ultimately of volcanic, possibly pyroclastic, origin, whereas the carbonate grains appear to have been derived from sedimentary formations. The quartz is not diagnostic but is believed to be mostly volcanic in origin because it is similar in grain size and angularity. It seems likely that the siliceous sandstone beds are not primary pyroclastic deposits but that they were derived from penecontemporaneous volcanic, as well as some nonvolcanic, sediments and redeposited in the inferred lake. The angularity of quartz and feldspar grains, however, indicates that little abrasion has occurred and that the distance of transport was apparently short.

The cherts contain very little recognizable detrital material, the exceptions being a small amount of carbonaceous debris and illite. They are prominently laminated (Plate 31.2A, C), with some truncation of lamination indicating weak erosional forces, but certainly they were deposited under more tranquil conditions than the associated sandstones. This may have been a seasonal effect. The lake was continually supplied with airborne volcanic ash but, during certain times of the year, there was an influx of clastic detritus which formed the sandstone beds. At other times, detrital input was negligible and the airborne ash settled out, forming the chert beds.

This does not account for the lamination within the tuff, which itself could very probably be due to seasonal variation in the influx of small quantities of organic matter and clay. The sandstones, then, would be due to unusual events, perhaps exceptional floods, which spread the coarser debris over a larger area than normal of the postulated lake.

The reason for the very prominent differences in hardness and composition of the chert and bentonite beds is not clear. Some of the observations and conclusions of Rubey (1928) on the siliceous Mowry Shale of Wyoming may be pertinent. The Mowry consists of interbedded siliceous shales and bentonite beds, the origin of which he was attempting to resolve. He concluded that the bentonites were the product of large ash falls which accumulated very rapidly with little opportunity for solution of silica. The shales were formed by slow accumulation of very fine grained volcanic dust, possibly from smaller eruptions. The slow accumulation also permitted accumulation of organic matter which Rubey believed was the chief agent in precipitation of silica. He suggested that the original volcanic dust was very acidic, containing an unusually large proportion of the most soluble constituents--the alkalies--of the original igneous rock.

The small size and angularity of the original particles facilitated solution of the soluble constituents, so that the water in contact with the dust would become alkaline. Silica, the chief component of the volcanic dust, is much more soluble in alkaline solution than in pure water. If not soon buried, the particles of the original dust would be partially to completely dissolved and the surrounding water would be rich in silica. Rubey (1928) suggests that ammonium carbonate from decaying organic matter would then cause precipitation of a portion of this silica as a gel.

The evidence of silica being present as the high temperature form of quartz indicates that it did not crystallize at atmospheric temperature and pressure where only the low temperature form of quartz is formed (Berry and Mason, 1959, p. 474). Therefore, the quartz must have crystallized at the source and been transported as very finely crystalline material. This, however, does not indicate why chert was formed rather than bentonite. Probably, only part of the quartz was transported as high temperature crystalline dust, the rest being precipitated in the lake as amorphous silica which then crystallized as low temperature quartz.

The bentonite beds differ, as suggested by Rubey (1928), in being deposited rapidly from a heavy ash fall. The ash was then diagenetically altered to montmorillonite, with a removal of some silica from the original ash. Why the silica is removed rather than precipitated as cement is unclear, but presumably the chemistry of the groundwater precludes its precipitation.

Examination of the cherts under high magnification indicates faint, subspherical masses with a slightly brownish coloration relative to "matrix" between. These may represent original floccules of precipitated silica. The preferred orientation of crystals in the tuff indicate that they were able to reorient themselves subsequent to deposition or were formed after deposition in a stress field dominated by gravity. Preservation of floccules suggest that crystallization and lithification were accomplished soon after deposition, in order to preserve these fragile structures.

As suggested earlier, the alternating siliceous sandstone and chert may represent alternate rapid and slow sedimentation. Possibly the body of water in which they were deposited maintained a high level of silica saturation. Introduction of detrital carbonaceous material to the lake facilitated precipitation. During periods of high sediment influx by streams, the precipitated silica formed only a subordinate part of the deposit but, when there was little or no sediment influx, slowly settling volcanic dust, precipitated silica and associated minor constituents formed the bulk of the deposit.

The thick bentonite bed at the top of the section signalled the end of the dominance of airborne sediment in this area. The bed of silty claystone near the top suggests the beginning of a new influx of terrigenous clastics into the area which overshadowed the volcanic contribution.

Acknowledgments

We are grateful to H.P. Trettin and E.J.W. Irish for critically reading the original manuscript and suggesting improvements. Suggestions by D.F. Long and F.G. Young were also valuable. A.E. Foscolos and A.E. Heinrich carried out the chemical and X-ray diffraction analyses and aided in their interpretation.

References

Allan, J.A. and Rutherford, R.L.
1924: Geology along the Blackstone, Brazeau and Pembina Rivers in the Foothills Belt, Alberta; Res. Council Alberta, Rept. 9.

Alexander, F.J.
1977: The structural geology of the Mynheer "A" zone, Coal Valley, Alberta; unpubl. M.Sc. Thesis, Univ. Alberta.

Anketell, J.M. and Dzulynski, S.
1968: Patterns of density controlled convolutions involving statistically homogeneous and heterogeneous layers; Annals Geol. Soc. Poland, v. 38, p. 401-409.

Berry, L.G. and Mason, B.
1959: Mineralogy: concepts, descriptions, determinations; Freeman and Co., San Francisco.

Carrigy, M.A.
1970: Proposed revision of the boundaries of the Paskapoo Formation in the Alberta Plains; Bull. Can. Petrol. Geol., v. 18, p. 156-165.

Gary, M., McAfee, R., Jr., and Wolf, C.L. (eds.)
1972: Glossary of geology; Am. Geol. Inst., Washington, D.C.

Holter, M.E., Yurko, J.R., and Chu, M.
1975: Geology and coal reserves of the Ardley coal zone of central Alberta; Res. Council Alberta, Rept. 75-7.

Irish, E.J.W.
1965: Geology of the Rocky Mountain Foothills, Alberta (between Latitudes 53°15' and 54°15'); Geol. Surv. Can., Mem. 334.

1968: Surface distribution and mineralogy of the Whitemud and Battle Formations ("Kneehills Tuff Zone"), Part 1; in Irish, E.J.W. and Havard, C.J., The Whitemud and Battle Formations ("Kneehills Tuff Zone"): A stratigraphic marker, Geol. Surv. Can., Paper 67-63.

1970: The Edmonton Group of south-central Alberta; Bull. Can. Petrol. Geol., v. 18, p. 125-155.

Lowe, D.R.
1975: Water escape structures in coarse-grained sediments; Sedimentology, v. 22, p. 157-204.

Pettijohn, F.J.
1975: Sedimentary Rocks (3rd ed.); Harper and Row, New York

Rubey, W.W.
1928: Origin of the siliceous Mowry Shale of the Black Hills region; U.S. Geol. Surv., Prof. Paper 154, p. 153-170.

Sanderson, J.O.G.
1931: Upper Cretaceous volcanic ash beds in Alberta; Trans. Roy. Soc. Can., ser. 3, v. 25, sec. IV, p. 61-70.

Taliaferro, N.L.
1933: The relation of volcanism to diatomaceous and associated siliceous sediments; Univ. Calif. Publ. in Geol. Sci., v. 23, p. 1-56.

Project 750083

R.A. Rahmani
Institute of Sedimentary and Petroleum Geology, Calgary

Introduction

The purpose of this paper is to demonstrate the influence of basin faulting on sediment dispersal within, and on thicknesses of the Isachsen Formation of the Sverdrup Basin and adjoining areas of the Arctic Archipelago. The writer has drawn his conclusions in large part from published and unpublished works by H.R. Balkwill, K.J. Roy and A.D. Miall and the published works of others referred to below. Data on Mackenzie King Island are those of the present writer, collected in the summer of 1976. The geological setting of the Sverdrup Basin is discussed briefly with an account of the stratigraphy and fault control on sedimentation of the Isachsen Formation.

Geological Setting

In the Sverdrup Basin, a largely terrigenous clastic sequence, 12 000 m thick, was deposited between Pennsylvanian and Late Cretaceous time. The basin has a nearly triangular shape, elongated approximately east-northeast to west-southwest, and is asymmetrical, with the thickest rock sequence occurring near its east-northeast end (Tozer and Thorsteinsson, 1964; Thorsteinsson and Tozer, 1970; Plauchut, 1971; Meneley et al., 1975). Deposition of the Isachsen Formation marks a northwestern Arctic-wide period of alluviation during which sedimentation transgressed beyond the margins of the Sverdrup Basin. Geophysical evidence suggests that the basin is underlain by continental crust, thinned at the basin's axis (Balkwill, in prep.). Abrupt facies transitions between upper Paleozoic evaporites and coeval rocks suggest the possibility that rifting and crustal stretching were responsible for initial basin subsidence (Balkwill, in prep.).

Stratigraphic Setting

The Isachsen Formation of the Sverdrup Basin is a Lower Cretaceous, fluvio-deltaic, terrigenous clastic sequence. Near the depocentre of the basin, at Strand Fiord, Axel Heiberg Island, it consists of about 1400 m of quartzose sandstone, sand and shale with subordinate conglomerate and coal. Near the basin margins and beyond, it thins to less than 150 m of usually coarser clastics, including quartzose granule sandstone and sand (in places conglomeratic), with minor amounts of shale.

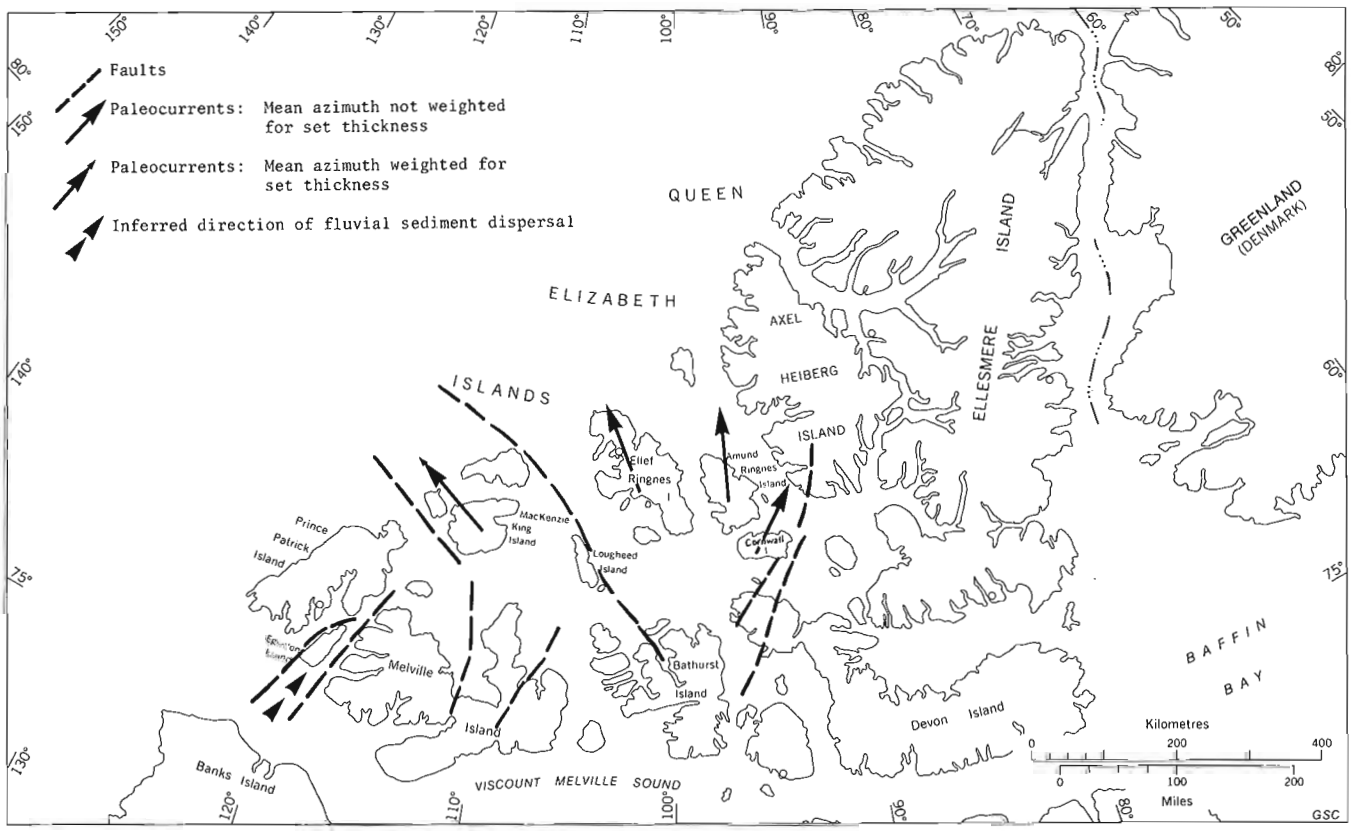

Figure 32.1. Map showing relationship of Isachsen Formation paleocurrents and faulting, Arctic Islands (faults adapted from Plauchut, 1971, Fig. 1).

From: Report of Activities, Part B;
Geol. Surv. Can., Paper 77-1B (1977)

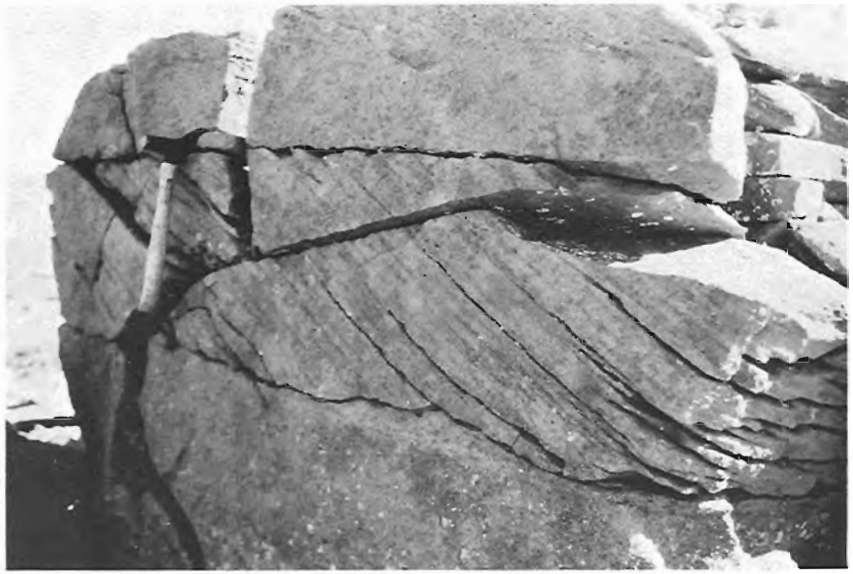

Figure 32.2. Large-scale planar cross-stratification (type alpha of Allen, 1963).

Figure 32.3. Large-scale tangential cross-stratification.

Figure 32.4. Small-scale cross-stratification.

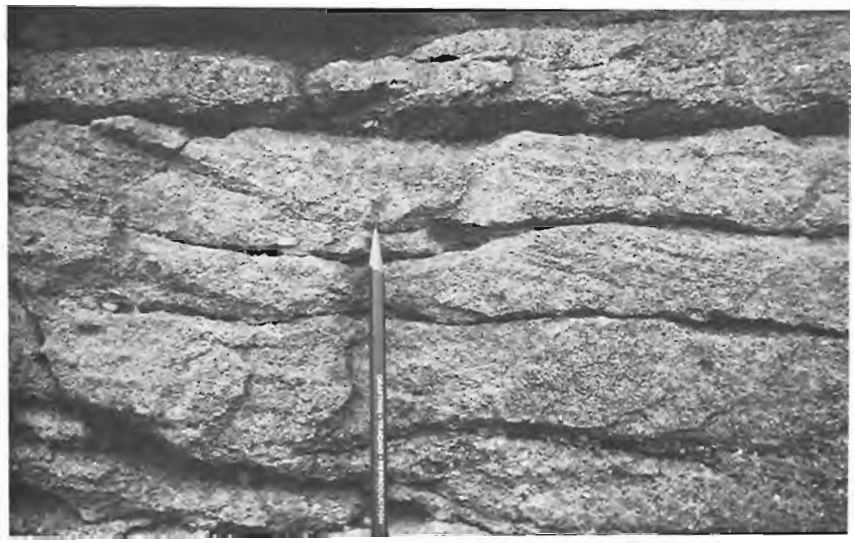

Figure 32.5. Antidune bedform in granule sandstone. Note cross-lamination dipping parallel to gentle side of bedform.

Data of Plauchut (1971) and Balkwill (in prep.) show that the basal contact of the Isachsen Formation is conformable and gradational with the underlying Deer Bay marine shale on Ellef Ringnes, Amund Ringnes, western Cornwall, parts of Axel Heiberg and, perhaps, central Mackenzie King islands (all near the depocentre) where the basal beds are of late Valanginian age. Near and beyond the basin margins, however, the basal contact is unconformable on older rocks and the basal beds are of Aptian age (Miall, 1975; Balkwill, in prep.).

On Amund Ringnes, Ellef Ringnes, King Christian and Cornwall islands, in the central parts of the Sverdrup Basin, the Isachsen Formation consists of medium grained sandstone and shale with subordinate conglomerate and coal (Roy, 1974). These rocks commonly occur as poorly developed fining-upward sequences of channel and overbank deposits. These fining-upward sequences usually have coarse members (conglomerate and sand) as thick as 30 m which suggested to Roy (1974) that the depositing streams in this area were in the order of 30 m deep at bankfull stage. This depth would be correct assuming that the coarse members represent single point bar sequences. Paleocurrent analysis of Isachsen cross-strata in this region shows a major northward transport direction suggesting the "Possibility of a major river system entering the depositional basin from the south in the vicinity of Bathurst Island and Grinnell Peninsula and forming a fan-shaped distribution system in the vicinity of the Sverdrup Islands" (Roy, 1974) (Fig. 32.1). Unpublished paleocurrent data from Axel Heiberg and Ellesmere islands suggest fluvial sedimentary transport to the west and southwest (K.J. Roy, pers. comm., 1976). However, post-Isachsen deformation (Eurekan Orogeny) in Axel Heiberg and Ellesmere islands made difficult the task of relating paleocurrents to faulting. On northern Bathurst Island, beds correlative with the Isachsen Formation consist of coarse grained sandstone with pebble beds; no paleocurrent data are available (Kerr, 1974). On Mackenzie King Island, where the Isachsen Formation thins to 150 m, it is composed almost entirely of quartzose, coarse grained sandstone and sand with abundant granule-size scattered grains and less common small pebbles. The sand fraction is very well sorted and rounded, silica cemented and, in places, slightly calcareous. Sedimentary structures in approximate order of abundance are: (1) large-scale planar cross-stratification (thicker than 50 cm, alpha and epsilon types of Allen, 1963) (Figs. 32.2, 32.3); (2) non-stratified pebbly sandstone; (3) small-scale cross-stratification (thinner than 15 cm) (Fig. 32.4); (4) inverse graded pebbly sandstone; (5) inverse graded small-scale cross-stratification; and (6) rare occurrences of antidunes (Fig. 32.5). On Mackenzie King Island, 28 paleocurrent measurements were made from small- and large-scale cross-stratification, and the weighted vector mean azimuth of 306° indicates transport direction toward the northwest (Fig. 32.1). The unimodal, unidirectional, low-variance transport along with the almost unfossiliferous nature of the sandstone on Mackenzie King Island suggest a fluvial origin for the Isachsen Formation. Textures and sedimentary structures indicate that the Isachsen streams on Mackenzie King Island were of the high gradient, low sinuosity, braided type by analogy with sediments in modern braided streams (Collinson, 1970; Smith, 1971). In fact, the sedimentary characteristics of the Isachsen Formation on Mackenzie King Island compare so closely with those of Isachsen strata on Banks Island that the inferred paleohydrological parameters for the Banks Island Isachsen paleostreams arrived at by Miall (1976) could be used to describe the Isachsen paleostreams of Mackenzie King Island. With some margin of error, Miall (1976) estimated that the mean channel depth of Isachsen streams ranged between 2.5 and 4.0 m and the bankfull water depth ranged between 4 and 5 m. Estimates of mean annual discharge ranged between 250 and 640 m^3/s. and mean annual flow velocity at 50 cm/s. Among others, Miall (1975, Fig. 7; 1976, Fig. 10) suggested that there was a fluvial communication, during Isachsen time, between Banks and Sverdrup Basins. Miall (1975, p. 572) stated that the "...Banks Island area is believed to have provided the headwaters of the streams which flowed into the west end of Sverdrup Basin" via the Eglinton Island graben valley, hence transporting sediments in an essentially northward direction.

Sedimentary Transport and Faulting

The available paleocurrent data for the Isachsen Formation are plotted on a map showing major faults (adapted from Plauchut, 1971). It portrays an interesting relationship between transport directions and orientation of fault blocks (Fig. 32.1). Transport directions on Ellef Ringnes, Amund Ringnes, King Christian and Cornwall islands appear to suggest a fluvio-deltaic system that fans-out northward within a fault block having similar directional orientation (Fig. 32.1). On Mackenzie King Island, a fluvial system flowing northwestward has been established for the Isachsen Formation and it appears to occur also in a fault block of similar orientation (Fig. 32.1). Also, as mentioned earlier, a north-flowing fluvial system is inferred to have entered the western end of the Sverdrup Basin through the fault-bound valley of Eglinton Island (Fig. 32.1).

Review of some recent literature on the Sverdrup Basin suggests that differential basin subsidence due to vertical faulting had a significant influence on patterns of sedimentation and stratigraphic thicknesses (e.g. Meneley et al., 1975, p. 536-539, Figs. 6-8; Balkwill, in prep. on the Cornwall Island Hinge; Plauchut, 1971, p. 676, Fig. 1). It is suggested here that faulting or sharp flexing of the basin floor exerted sufficient influence on the basin's paleotopography to control fluvial transport and dispersal systems in the manner discussed above and seen in Figure 32.1. Additional paleocurrent data are needed in areas such as Prince Patrick and Melville islands in order to test the validity of this suggestion.

Available evidence suggests to the writer that, during Isachsen time, the "northwest rim" of Meneley et al. (1975), a tectonically active ridge situated near the northwestern margin of the Sverdrup Basin, had no detrimental influence on style of sedimentation and paleodrainage.

Depositional History

Any detailed and comprehensive account of the sedimentary history of the Isachsen Formation awaits the collection of additional data in the areas of Melville, Prince Patrick, Lougheed and Graham islands. The following, however, is a brief treatment of the depositional history based on what is available to the writer at the time of writing.

Figure 32.6. Schematic representation of sedimentary history of the Isachsen Formation, Arctic Islands.

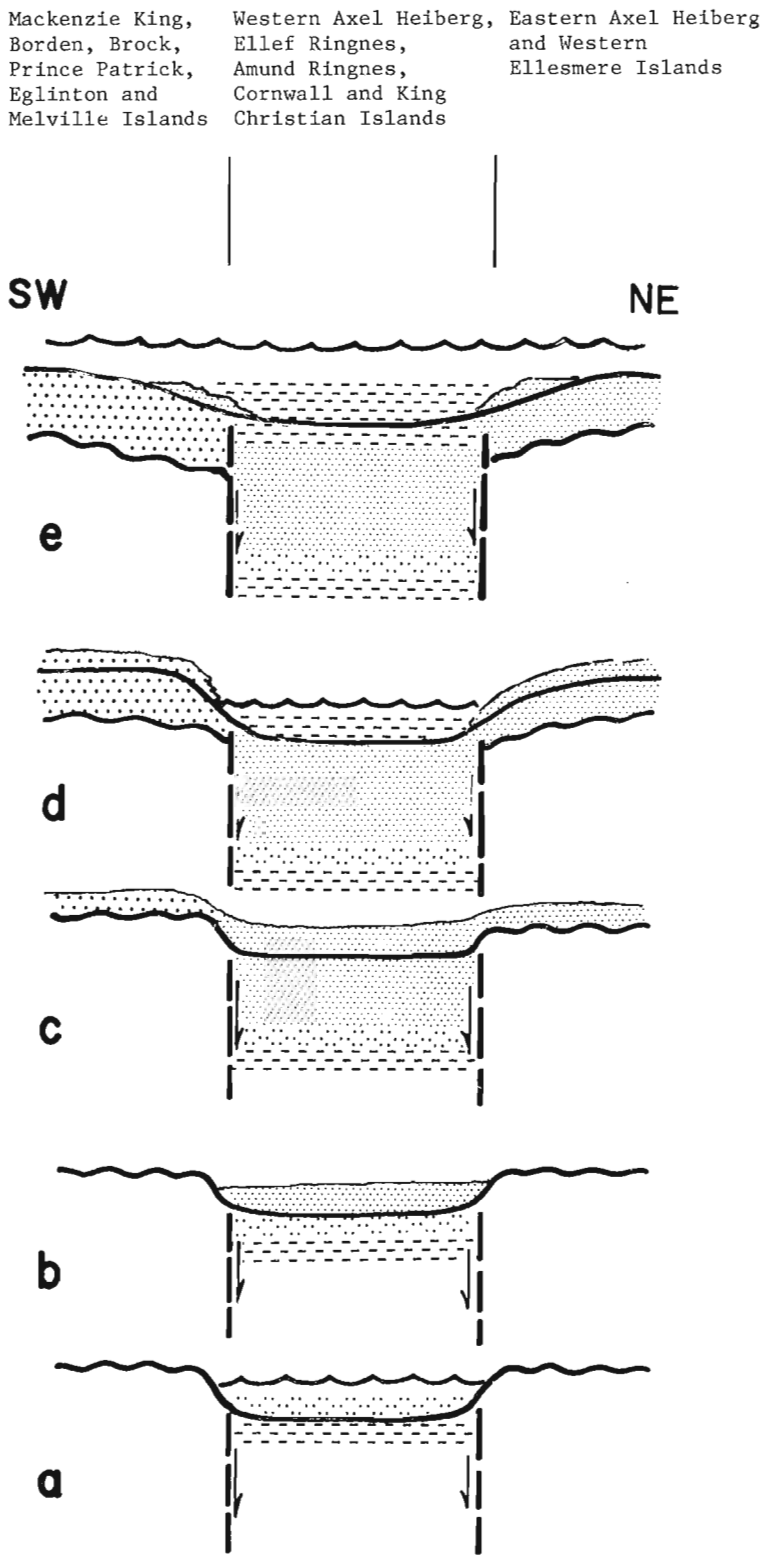

e. ALBIAN: Marine transgression and deposition of the Christopher Formation.

d. LATE APTIAN-EARLY ALBIAN: Marine invasion of central block deposited lower beds of Christopher Formation. Coeval upper beds of Isachsen Formation were deposited on bordering blocks by meandering and braided streams.

c. EARLY APTIAN: Fluvial deposition by meandering streams continued in central block and also in the northeastern block. Southwestern block received sediments deposited by braided streams.

b. BARREMIAN: Fluvial (meandering streams) and deltaic deposition in the central block caused north and northwest sedimentary progradation and sea withdrawal. Bordering blocks were still areas of net non-deposition.

a. VALANGINIAN-HAUTERIVIAN: Marine prodelta deposition of the lower beds of the Isachsen in the central block. Bordering blocks, relatively uplifted, were areas of erosion or non-deposition.

Figure 32.6 is a schematic representation of the depositional history of the Isachsen Formation. The representation is simply to suggest that those parts of the basin within each block have undergone similar depositional history. Within the central, strongly subsiding block, the Isachsen is normally thicker than 1000 m, finer grained, and has a conformable lower contact and basal beds of late Valanginian age. By contrast, in marginal zones with less subsidence (i.e. relatively uplifted blocks), the Isachsen is normally thinner than 150 m, and is coarser grained (northeast block contains finer grained Isachsen). In the latter situation, the basal beds, Aptian in age, rest unconformably on the underlying rocks (with the exception, perhaps, of central Mackenzie King Island; Balkwill, pers. comm., 1976).

In late Valanginian-early Hauterivian time, the Deer Bay sea was retreating northward as a result of progradation from the south of the fluvio-deltaic environments in that direction. Therefore, in the central block, shallow marine and transitional sediments were deposited during this period to form the basal beds of the Isachsen Formation (Fig. 32.6a). The bordering blocks were places of non-deposition or erosion. Further uplift of source areas during Hauterivian-Barremian time resulted in the complete northward withdrawal of the sea, leaving the entire Sverdrup Basin subaerially exposed (Fig. 32.6b). During this time, streams entered the central block via Bathurst Island from the south and Ellesmere Island from the northeast, draining source areas in the southern Arctic Islands and mainland and northwestern Greenland, respectively. These streams were of high-gradient, low-sinuosity, braided type at their proximal end, and deposited coarse sand and gravel (e.g. on northern Bathurst Island). They changed progressively to low-gradient, high-sinuosity meander type at their intermediate and distal parts where finer sand with subordinate pebble beds was deposited. During that time, the bordering blocks were areas of some positive relief and received no appreciable volume of sediments; nor were they contributing much detritus, if any, to the central block (based on available paleocurrent data). At the onset of Aptian time, continued uplift in the source area and slowdown in the rate of differential subsidence in the central block caused a northwest Arctic-wide period of alluviation (Fig. 32.6c). The central block continued to receive alluvial sediments from low-gradient meandering streams flowing northward and west to south-westward. The northeast block also appears to have received sediments from streams of similar nature to those of the central block. However, the southwest block was the site of alluvial deposition by high-gradient, low-sinuosity, braided streams, transporting sediments to the northwest from sources in the southern Arctic Islands and mainland, and to the north-northeast through the Eglinton Island graben valley from source areas near Banks Island (Fig. 32.1). During late Aptian-early Albian time, the sea entered the Sverdrup Basin from the north and northwest to occupy the central block, as a result of increasing rate of subsidence. This subsidence resulted in the deposition of marine beds of the lower Christopher Formation while, simultaneously, arenaceous continental beds of the coeval upper Isachsen Formation were being deposited on the bordering blocks that remained subaerially exposed (Fig. 32.6d). Finally, in Albian time, the entire Sverdrup Basin and vicinity (e.g. Banks Island) were invaded by marine environments in which were deposited sediments of the Christopher Formation (Fig. 32.6e).

References

Allen, J.R.L.
1963: The classification of cross-stratified units, with notes on their origin; Sedimentology, v. 2, p. 93-114.

Collinson, J.D.
1970: Bedforms of the Tana River, Norway; Geogr. Ann., v. 52A, p. 31-55.

Kerr, J. Wm.
1974: Geology of Bathurst Island Group and Byam Martin Island, Arctic Canada; Geol. Surv. Can., Mem. 378.

Meneley, R.A., Henao, D., and Merritt, R.K.
1975: The northwest margin of the Sverdrup Basin in Canada's Continental Margin, C.J. Yorath, E.R. Parker and D.J. Glass, eds.; Can. Soc. Pet. Geol., Mem. 4, p. 531-544.

Miall, A.D.
1975: Post-Paleozoic geology of Banks, Prince Patrick and Eglinton Islands in Arctic Canada in Canada's Continental Margins, C.J. Yorath, E.R. Parker and D.J. Glass, eds.; Can. Soc. Pet. Geol., Mem. 4, p. 557-587.

1976: Paleocurrent and paleohydrologic analysis of some vertical profiles through a Cretaceous braided stream deposit, Banks Island, Arctic Canada; Sedimentology, v. 23, p. 459-483.

Plauchut, B.P.
1971: Geology of the Sverdrup Basin; Bull. Can. Pet. Geol., v. 19, p. 659-679.

Roy, K.J.
1974: Transport directions in the Isachsen Formation (Lower Cretaceous) Sverdrup Islands, District of Franklin; in Report of Activities, Part A, Geol. Surv. Can., Paper 74-1A, p. 351-353.

Smith, N.D.
1971: Transverse bars and braiding in the lower Platte River, Nebraska; Bull. Geol. Soc. Am., v. 82, p. 3407-3420.

Thorsteinsson, R. and Tozer, E.T.
1970: Chapter X, the Arctic Archipelago in Geology and Economic Minerals of Canada, R.J.W. Douglas, ed.; Geol. Surv. Can., Econ. Geol. Rep. No. 1, 5th ed., p. 547-590.

Tozer, E.T. and Thorsteinsson, R.
1964: Western Queen Elizabeth Islands, Arctic Archipelago; Geol. Surv. Can., Mem. 332.

33. CORRELATION OF MICROPLANKTON ASSEMBLAGES WITH AMMONITE FAUNAS FROM THE JURASSIC WILKIE POINT FORMATION, PRINCE PATRICK ISLAND, DISTRICT OF FRANKLIN

Project 500029

B.G.T. van Helden[1]
Institute of Sedimentary and Petroleum Geology, Calgary

Introduction

Ammonite faunas from the Wilkie Point Formation of Toarcian to Early Bathonian age on Prince Patrick Island, Canadian Arctic Archipelago (Fig. 33.1), were collected in 1954 and 1958 (Tozer and Thorsteinsson, 1964; Frebold, 1975). Samples from the matrices of macrofossils were obtained from GSC localities 24643, 24648, 24651, 24661, 24664 and 35324. Figure 33.2 indicates the geographic and stratigraphic positions of these localities.

Age assignments of the samples from the Wilkie Point Formation are based on the recovered ammonite faunas (Fig. 33.3).

The samples were processed for palynology with standard processing techniques and palynomorphs were recovered from six samples (Fig. 33.3); GSC locality 24664 contained no microplankton. The productive samples yielded a diversity of fossil spores and pollen (not discussed in this paper) and well-preserved microplankton.

The latter listed in order of abundance include:

Nannoceratopsis gracilis Alberti
N. senex sp. nov.
Meiourogonyaulax sp. cf. **M. deflandrei** Sarjeant
Micrhystridium sp.
Veryhachium sp.
?**Dictyopyxidia** sp.

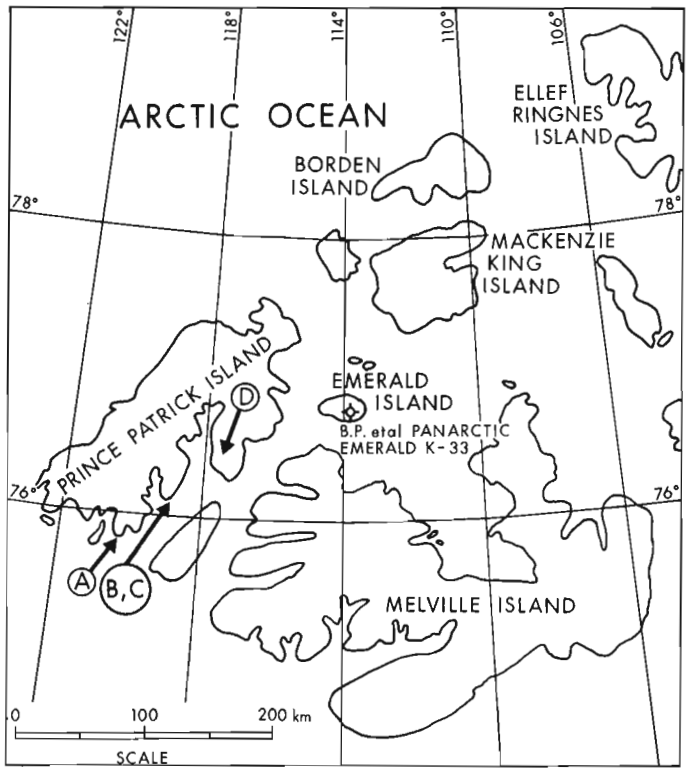

Figure 33.1. Location map of Wilkie Point Formation outcrops A, B, C and D, with studied fossil localities, western Queen Elizabeth Islands, Arctic Archipelago.

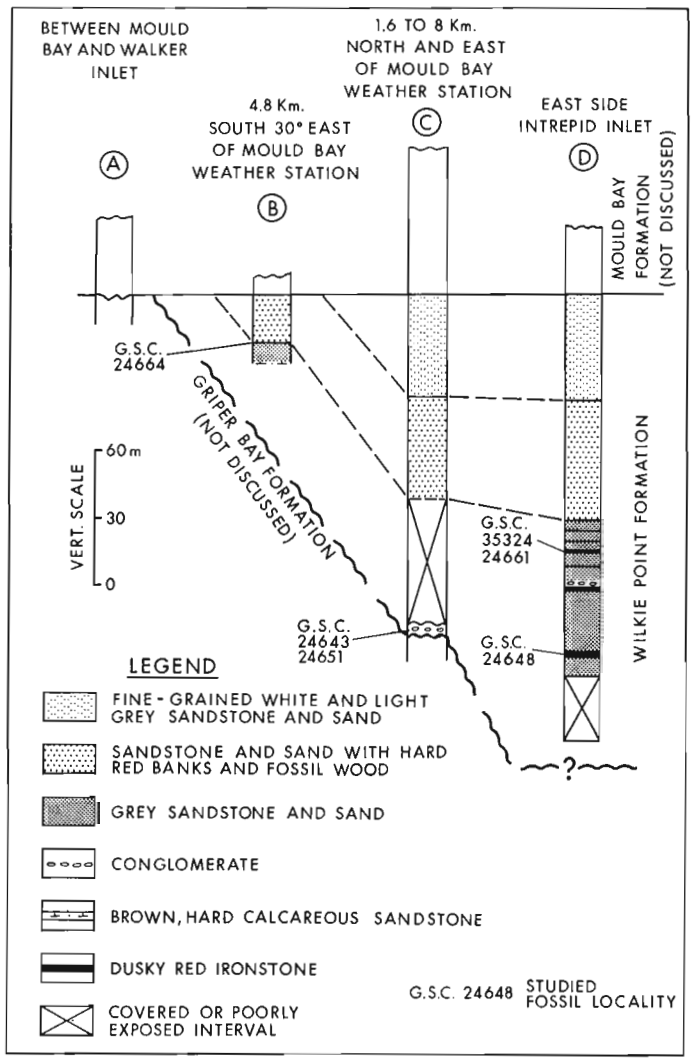

Figure 33.2. Columnar sections of Wilkie Point Formation, Prince Patrick Island, with studied fossil localities (after Tozer and Thorsteinsson, 1964, p. 128, Fig. 8).

[1]Chevron Standard Limited

From: Report of Activities, Part B; Geol. Surv. Can., Paper 77-1B (1977)

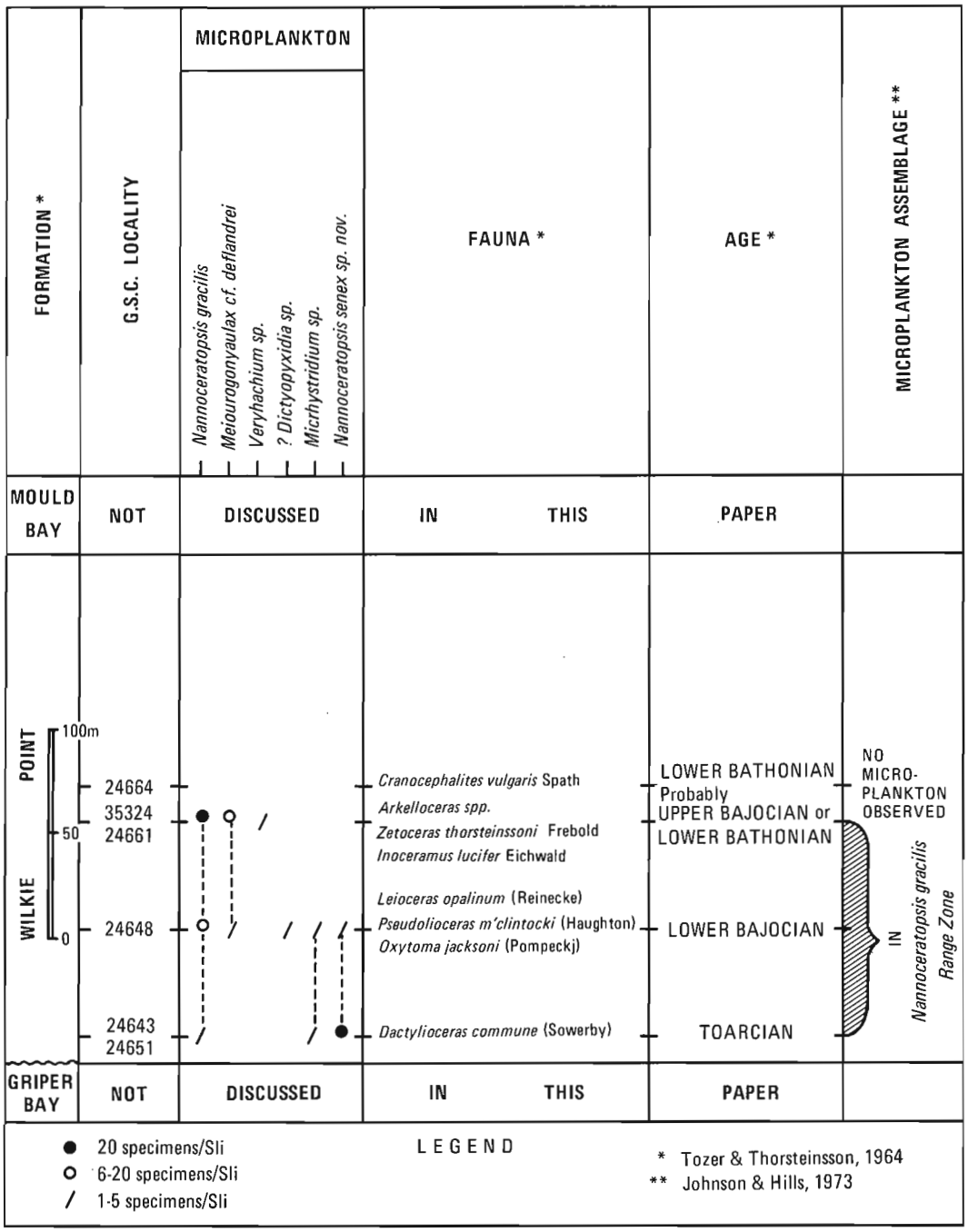

Figure 33.3. Correlation of microplankton assemblages with ammonite faunas, Wilkie Point Formation, Prince Patrick Island.

Of particular interest was the occurrence of a new species of **Nannoceratopsis** Deflandre. This species, recorded by several authors (Evitt, 1961; Morgenroth, 1970; Johnson and Hills, 1973) as a variant of **Nannoceratopsis gracilis** Alberti, did not occur as high in the section of **N. gracilis** and, in most cases, could be distinguished readily from that species by its morphology. The new species is considered stratigraphically significant and has a range from (?Late) Pleinsbachian to Early Bajocian.

The occurrence and frequency distribution of the recorded microplankton is summarized in Figure 33.3. The samples and slides bearing type specimens and figured specimens used in this study are stored in the collections of the Geological Survey of Canada, 601 Booth Street, Ottawa.

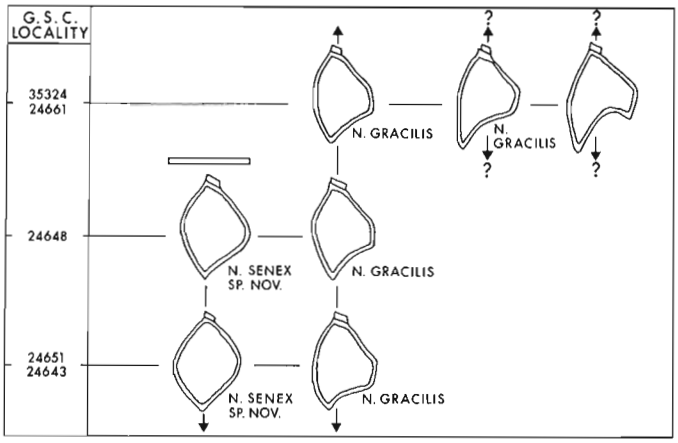

Figure 33.4. Diagrammatic sketch showing the vertical distribution and the variability of **Nannoceratopsis gracilis** Alberti emend. and **Nannoceratopsis senex** sp. nov.

Acknowledgments

The author thanks the Geological Survey of Canada for permitting examination of the material and for the opportunity to publish, and Chevron Standard Limited for permission to publish these data. W.W. Brideaux and H.R. Balkwill (Institute of Sedimentary and Petroleum Geology, Calgary critically read the manuscript and their suggestions for improvement are greatfully acknowledged.

Systematics

Order DINOPHYSIALES Lindemann, 1928

Family NANNOCERATOPSITACEAE Sarjeant and Downie, 1974

Genus **Nannoceratopsis** Deflandre, 1938

Nannoceratopsis gracilis Alberti, 1961 emend.

Plate 33.1, figures 10-14, Plate 33.2, figures 1-13

Nannoceratopsis? **gracilis** Alberti, 1961, p. 30, Pl. 7, figs. 16, 17.
Nannoceratopsis deflandrei Evitt, 1961, p. 308, Pl. 1, figs. 2-14.

Emended diagnosis. Lateral outline variable: subtriangular with two antapical horns (ventral horn always much shorter and less well developed than the dorsal horn) to nearly ovoid with a poorly developed ventral horn and a pronounced dorsal horn. Postcingular ventral area above ventral horn and below parasulcal area more or less straight and parallel to apical-antapical axis, sometimes pronouncedly bulging. Periphragm sculpture reticulate. All other features as in Evitt (1961).

Remarks. The emended diagnosis of **Nannoceratopsis gracilis** Alberti restricts the morphology of the species to forms having a distinctly reticulate ornamentation, one dorsal antapical horn and one short ventral antapical horn, which may be poorly developed.

This emended diagnosis excludes forms having a microreticulate to scabrate or nearly smooth ornamentation and a distinctly ovoid, rounded outline with only the dorsal antapical horn developed.

Occurrence (see Fig. 33.3). **Nannoceratopsis gracilis** occurs in abundance at GSC localities 24661 and 35324, represented by two morphotypes which differ in outline: one form with a well-developed dorsal antapical horn and a short ventral antapical horn, separated by a concave area (Pl. 33.2, figs. 5-13), and one form with a very prominent dorsal antapical horn and one poorly to slightly developed ventral antapical horn (Pl. 33.2, figs. 1-4, Fig. 33.4). The stratigraphic significance of this difference in outline has not yet been evaluated.

The form **Nannoceratopsis gracilis** var. A of Johnson and Hills (1973, p. 208, Pl. 3, fig. 16) was not encountered in the samples.

Nannoceratopsis senex sp. nov.

Plate 33.1, figures 1-9, Figure 33.4

Nannoceratopsis gracilis Alberti, Morgenroth, 1970, Pl. 11, fig. 6 only.
Nannoceratopsis deflandrei Evitt, 1961, Pl. 1, fig. 1 only.
Nannoceratopsis gracilis Alberta, Johnson and Hills, 1973, Pl. 3, figs. 18, 19 only.

Diagnosis. A species of **Nannoceratopsis** having a distinctly rounded, ovoid outline, being dorso-ventrally more or less symmetrical, with a nearly smooth to microreticulate or scabrate surface.

Description. Lateral outline distinctly rounded to ovoid. Ventral side smoothly curved. A dorsal antapical horn with a finely pointed end is usually well developed. Ventral antapical horn absent. Surface sculpture microreticulate or scabrate to nearly smooth. Paracingulum and a small precingular area visible in some specimens. Other features as for genus.

Comparison. This species differs from **Nannoceratopsis gracilis** Alberti 1961, emend. and from all other known species of the genus in possessing an extremely rounded outline, both dorsally and ventrally, with only the dorsal antapical horn (well) developed, and in the reduction or absence of the ornamentation (reticulation) on its surface that is characteristic for **N. gracilis** Alberti, emend. **Nannoceratopsis senex** sp. nov. lacks a ventral antapical horn, which distinguishes it from **N. pellucida** Deflandre, 1938 and from **N. spiculata** Stover, 1966.

The (?Late) Pleinsbachian to Early Bajocian stratigraphic range of **N. senex** sp. nov. differs from the ranges of all other species of the genus **Nannoceratopsis**.

Holotype (Pl. 33.1, figs. 6, 7). GSC 53017, single mount. Wilkie Point Formation, B.P. et al. Panarctic Emerald K-33 well, interval 4280 to 4300 feet (1425-1430 m), where it is associated with **Nannoceratopsis gracilis** Alberti, emend, **Micrhystridium** spp., **Mancodinium semitabulatum** Morgenroth and small "?algal spheres" (abundant). This interval is considered (?Late) Pleinsbachian to Toarcian in age.

Plate 33.1

Nannoceratopsis senex sp. nov.

Figure 1. Paratype GSC 53018 from GSC locality 24651, slide 18527-1, co-ordinates 364X1032 (interference contrast).

Figure 2. Paratype GSC 53019 from GSC locality 24651, slide 18527-1, co-ordinates 369X1044 (interference contrast).

Figures 3, 4. Paratype GSC 53029 from GSC locality 24651, slide 18527-3, co-ordinates 318X1149, showing pronounced, pointed, dorsal antapical horn (Fig. 3, interference contrast).

Figure 5. Paratype GSC 53021 from GSC locality 24651, slide 18527-1, co-ordinates 131X1178 (interference contrast).

Figures 6, 7. Holotype GSC 53017 from B.P. et al. Panarctic Emerald K-33 well (4280-4300 ft.), slide 18087, single mount No. 201 (Fig. 7, interference contrast).

Figures 8, 9. Paratype GSC 53022 from GSC locality 24651, slide 18527-1, co-ordinates 247X1008 (interference contrast), showing paracingulum, apical region, microreticulation.

Nannoceratopsis gracilis Alberti emend.
(pronounced reticulation, ventral antapical horn poorly developed)

Figures 10, 14. GSC 53023 from GSC locality 24651, slide 18527-3, co-ordinates 310X1074 (Fig. 10, interference contrast).

Figure 11. GSC 53024 from GSC locality 24648, slide 18526-4, co-ordinates 212X1062.

Figure 12. GSC 52035 from GSC locality 24648, slide 18526-2, co-ordinates 284X1068.

Figure 13. GSC 53026 from GSC locality 24648, slide 18526-2, co-ordinates 392X1025.

?**Dictyopyxidia** sp.

Figures 15, 16. GSC 53027 from GSC locality 24648, slide 18526-4, co-ordinates 141X1174; 1250 (Fig. 16, interference contrast).

Micrhystridium sp.

Figure 17. GSC 53028 from GSC locality 24643, slide 18525-3, co-ordinates 364X1035.

Meiourogonyaulax cf. **M. deflandrei** Sarjeant

Figure 18. GSC 53029 from GSC locality 24648, slide 18526-3, co-ordinates 402X1161.

PLATE LEGENDS

All photographs x500 (except Pl. 33.1, figs. 15, 16; x1250) and, unless otherwise indicated, taken in brightfield on Ilford Pan F film, 50 A.S.A., with a Leitz Orthomat camera mounted on Leitz Ortholux microscope, frame no. 646 441, property of Chevron Standard Limited, Calgary, Alberta. The distance between the small vertical lines in all figures is 50 μ.

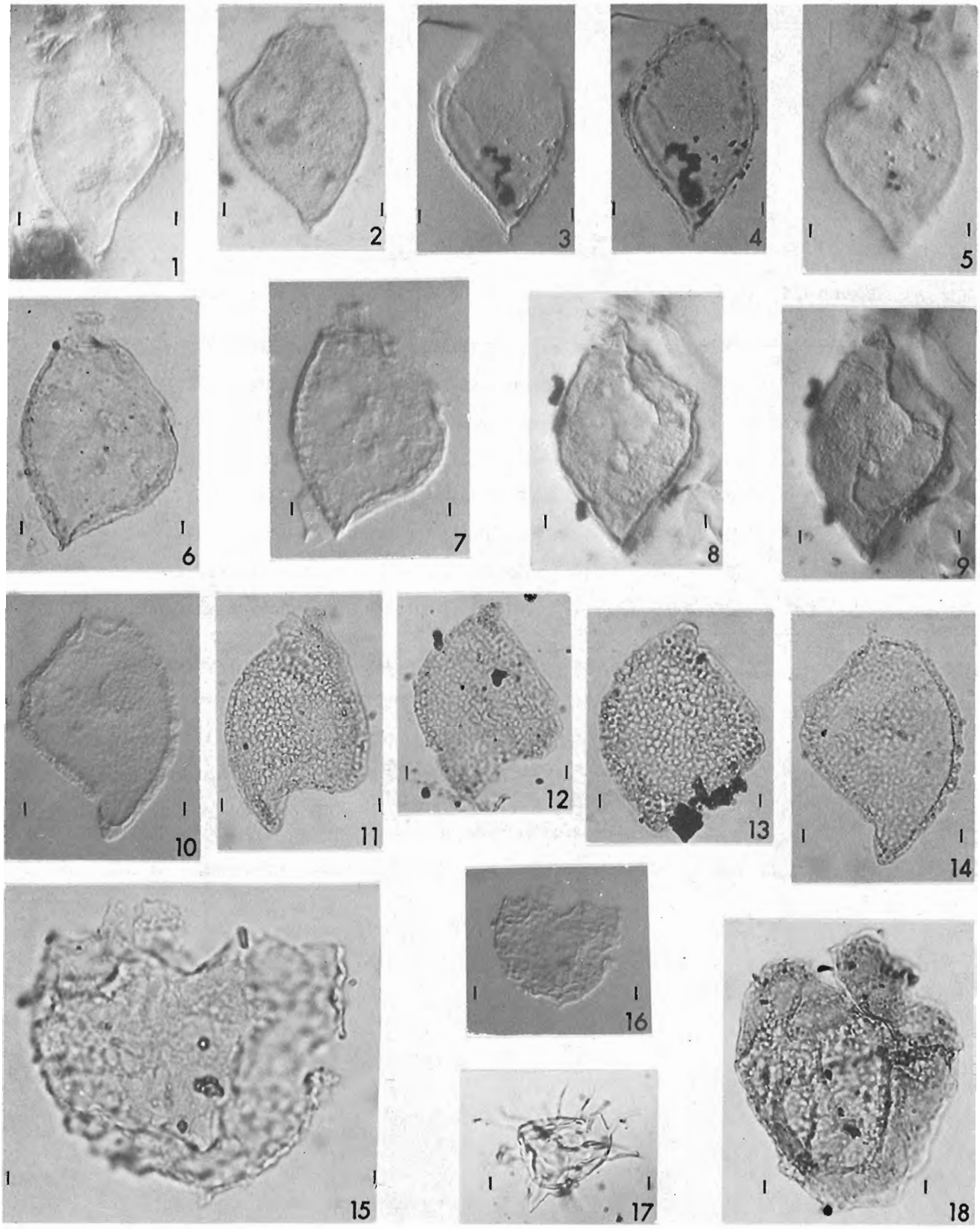
1
2
3
4
5
6
7
8
9
10
11
12
13
14
15
16
17
18

Plate 33.2

Nannoceratopsis gracilis Alberti emend.
(forms with prominent dorsal antapical horn)

Figures 1, 2. GSC 53030 from GSC locality 35324, slide 18530-4, co-ordinates 204X1108 (Fig. 1, interference contrast).

Figure 3. GSC 53031 from GSC locality 35324, slide 18530-4, co-ordinates 136X1072.

Figure 4. GSC 53032 from GSC locality 24661, slide 18528-4, co-ordinates 362X1201.

Nannoceratopsis gracilis Alberti emend.

Figure 5. GSC 53033 from GSC locality 35324, slide 18530-4, co-ordinates 173X1005.

Figure 6. GSC 53034 from GSC locality 35324, slide 18530-4, co-ordinates 203X1011.

Figure 7. GSC 53035 from GSC locality 24661, slide 18528-4, co-ordinates 438X1104.

Figure 8. GSC 53036 from GSC locality 24661, slide 18528-4, co-ordinates 229X1095.

Figure 9. GSC 53047 from GSC locality 35324, slide 18530-4, co-ordinates 359X1123 (interference contrast).

Figure 10. GSC 53058 from GSC locality 35324, slide 18530-4, co-ordinates 244X1046.

Figure 11. GSC 53049 from GSC locality 35324, slide 18530-4, co-ordinates 440X1131.

Figure 12. GSC 53040 from GSC locality 35324, slide 18530-4, co-ordinates 324X1142.

Figure 13. GSC 53041 from GSC locality 35324, slide 18530-4, co-ordinates 153X1103 (interference contrast).

Meiourogonyaulax cf. **M. deflandrei** Sarjeant

Figures 14, 15. GSC 53042 from GSC locality 35324, slide 18530-4, co-ordinates 373X1004 (Fig. 15, interference contrast).

Veryhachium sp.

Figure 16. GSC 53043 from GSC locality 35324, slide 18530-4, co-ordinates 509X1125.

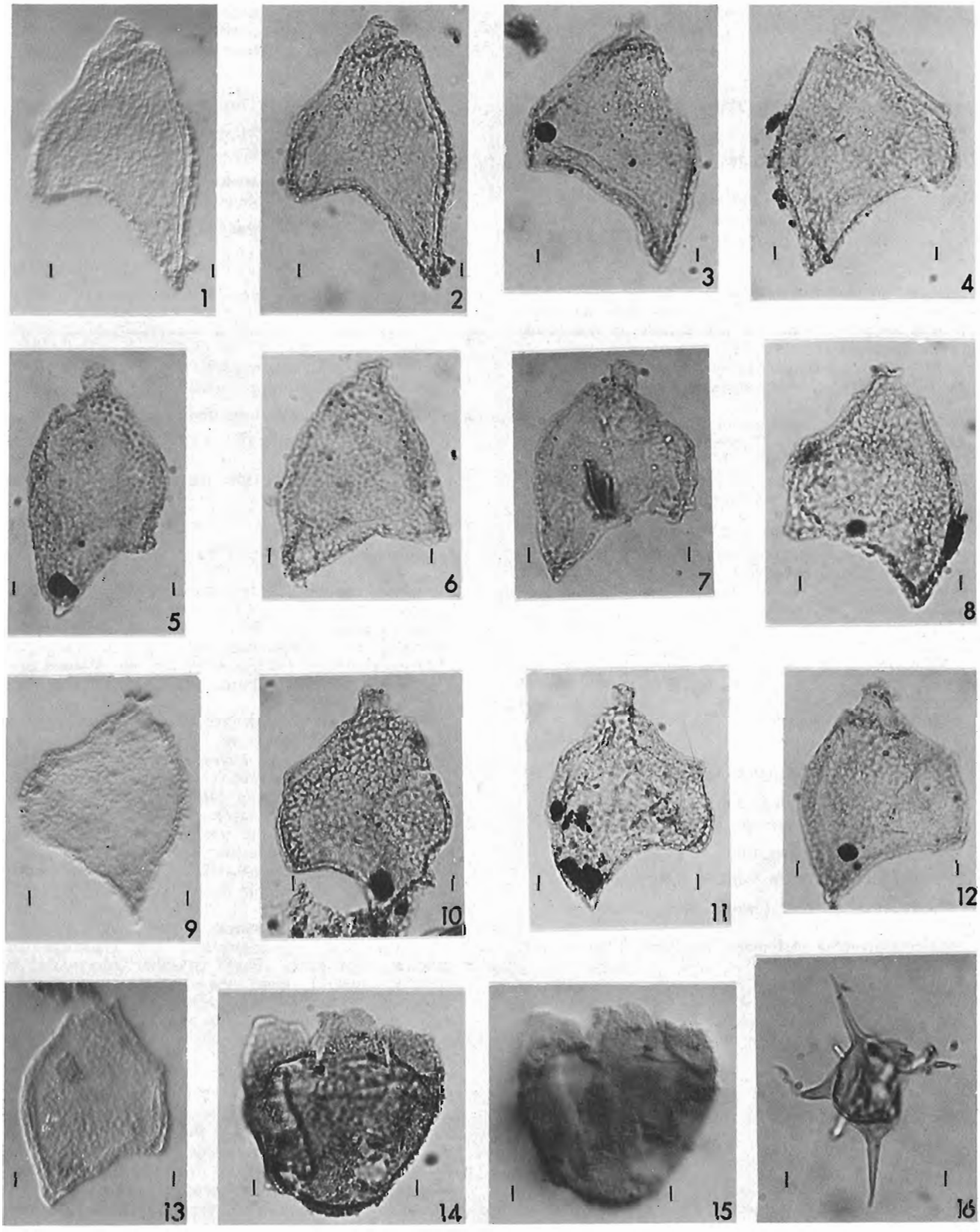
1
2
3
4
5
6
7
8
9
10
11
12
13
14
15
16

Paratypes (Pl. 33.1, figs. 1-5). GSC 53018 to 53021 from GSC locality 24651.

Dimensions	Length	Width
Holotype	72 µ	49 µ
Paratypes	72-79 µ	42-48 µ
Average size	72-76 µ	42-47 µ

Derivatio nominis. **Senex** (Latin) meaning: old man, referring to the top of its stratigraphic range in the Wilkie Point Formation below the top of the local range of **N. gracilis.**

Occurrence. Wilkie Point formation (lower part), GSC localities 24643, 24651 (abundant), 24648 (one specimen only); also reported from the lower part of the Savik Formation (Johnson and Hills, 1973); also in the lower part of the Bug Creek Formation in subsurface sections in the Mackenzie Delta (van Helden, unpubl.).

Age. The earliest occurrence of **Nannoceratopsis senex** sp. nov. is in the Lias Delta (?Upper Pliensbachian) from Lühnde, Germany (Morgenroth, 1970) where it is recorded as **Nannoceratopsis gracilis** Alberti (Morgenroth, 1970, Pl. 11, fig. 6 only), occurring together with **Mancodinium semitabulatum** Morgenroth.

The youngest occurrence of **Nannoceratopsis senex** sp. nov. is in GSC locality 24648, dated as Early Bajocian. Therefore, the total known stratigraphic range of **Nannoceratopsis senex** sp. nov. is from (?Late) Pliensbachian to Early Bajocian.

Johnson and Hills (1973) also noted the restricted stratigraphic range of this form, being restricted to the lower part (±0-70 m) of the Savik Formation at Vantage Point (Johnson and Hills, 1973, p. 199, 200, Textfig. 10).

Order PERIDINIALES Schutt, 1896

Family MICRODINIACEAE Eisenack, emend. Sarjeant and Downie, 1966

Genus **Meiourogonyaulax** Sarjeant, 1966

Meiourogonyaulax cf. **M. deflandrei** Sarjeant, 1968

Plate 33.1, figure 18, Plate 33.2, figures 14, 15

cf. **Meiourogonyaulax deflandrei** Sarjeant, 1968, p. 288, Pl. 1, fig. 20, Pl. 3, fig. 13.

Remarks. This species resembles **M. deflandrei** Sarjeant in possessing an "infrareticulate" sculpture on the pericyst. The paratabulation could not be determined exactly.

Occurrence. Five specimens were encountered in slides from GSC locality 35324; only one specimen was found in GSC locality 24648.

Family CANNINGIACEAE Sarjeant and Downie, 1966, emend. Sarjeant and Downie, 1974

Genus **Dictyopyxidia** Eisenack, 1961

?**Dictyopyxidia** sp.

Plate 33.1, figures 15, 16

Remarks. Only one specimen was encountered (GSC loc. 24648). The preservation did not allow further refinement of the identification.

Group ACRITARCHA Evitt, 1963

Subgroup ACANTHOMORPHITAE Downie, Evitt and Sarjeant, 1963

Genus **Veryhachium** Deunff, 1958, emend. Downie and Sarjeant, 1963

Veryhachium sp.

Plate 33.2, figure 16

Remarks. Only a few specimens were encountered (GSC loc. 35324).

Genus **Micrhystridium** Deflandre, 1937, emend. Lister, 1970

Micrhystridium sp.

Plate 33.1, figure 17

Remarks. Only a few specimens were recorded (GSC locs. 24643, 24648).

Conclusions

The presence of **Nannoceratopsis gracilis** Alberti emend. in GSC localities 24643, 24648, 24651 and 35324 indicates that these samples contain an assemblage belonging in the **Nannoceratopsis gracilis** range zone (Johnson and Hills, 1973, p. 199), with an assigned age of Toarcian to Bajocian (Johnson and Hills, 1973, Fig. 7).

The age of GSC localities 24643, 24648, 24651 and 35324 is from Toarcian to Early Bathonian, based on ammonites (Fig. 33.3). **Nannoceratopsis senex** sp. nov. occurs singly at GSC locality 24648 and in abundance at GSC localities 24643 and 24651. The top of its local stratigraphic range occurs within the lower part of the **Nannoceratopsis gracilis** range zone in the Lower Bajocian. This observation is in agreement with the writer's unpublished observation on other sections (mostly subsurface) within the Arctic Archipelago.

Nannoceratopsis senex sp. nov. can be used for biostratigraphic subdivision of the **Nannoceratopsis gracilis** range zone. Based on other information (van Helden, unpubl.) about the Jurassic section in the Canadian Arctic, the writer believes that **N. senex** sp. nov. ranges farther down into the Toarcian and probably into the Pleinsbachian (?Upper).

Summary

Outcrops of the Wilkie Point Formation on Prince Patrick Island, Canadian Arctic Archipelago, have been dated as Early Bathonian to Toarcian using ammonites. Microplankton has been recovered from the matrices of the macrofossils and, thus, the microfloral ages can be correlated with those derived from studies of the ammonites. The microplankton is dominated by dinoflagellate cysts of **Nannoceratopsis gracilis** Alberti, emend. and **N. senex** sp. nov.

References

Alberti, G.
1961: Zur Kenntnix mesozoischer und alttertiären Dinoflagellaten und Hystrichosphaeriden von Nord – und Mitteldeutschland sowie einige anderen europaischer Gebieten; Palaeontographica, Abt. A, v. 116, p. 30, Pl. 7.

Evitt, W.R.
1961: The dinoflagellate **Nannoceratopsis** Deflandre: morphology, affinities and intraspecific variability; Micropaleontology, v. 7, no. 3, p. 305-316, Pls. 1, 2.

1962: Dinoflagellate synonyms: **Nannoceratopsis deflandrei** Evitt junior to **N.? gracilis** Alberti; Paleontology, v. 36, p. 129, 130.

Frebold, H.
1975: The Jurassic faunas of the Canadian Arctic. Lower Jurassic ammonites, biostratigraphy and correlations; Geol. Surv. Can., Bull. 243.

Johnson, C.D. and Hills, L.V.
1973: Microplankton zones of the Savik Formation (Jurassic), Axel Heiberg and Ellesmere Islands, District of Franklin; Bull. Can. Pet. Geol., v. 21, p. 178-218, Pl. 1-3.

Morgenroth, P.
1970: Dinoflagellate cysts from the Lias Delta of Lühnde, Germany; N. Jb. Geol. Paleont., Abt. 136, p. 345-359, Pl. 11.

Sarjeant, W.A.S.
1968: Microplankton from the Upper Calovian and Lower Oxfordian of Normandy; Rev. Micropaléontologie, v. 10, p. 221-242, Pls. 1, 3.

1974: Fossil and living dinoflagellates; Academic Press, London and New York.

Tozer, E.T. and Thorsteinsson, R.
1964: Western Queen Elizabeth Islands, Arctic Archipelago; Geol. Surv. Can., Mem. 332.

SYSTEMATICS AND BIOSTRATIGRAPHIC IMPORTANCE OF THE LOWER DEVONIAN RUGOSE CORAL GENUS **EXILIFRONS**

Project 680093

A.E.H. Pedder
Institute of Sedimentary and Petroleum Geology, Calgary

Introduction

Crickmay (1968) proposed the genus **Exilifrons** with no discussion of its relationships, other than to comment that three of its species that had previously been placed in **Hexagonaria** are not "true **Hexagonariae** or even related to the family", and the indication that he considered it to be an arachnophyllid. Several years later, Merriam (1974b) established a new subgenus **Hexagonaria (Pinyonastraea)** for a species that he considered differed from **Hexagonaria**, strict sense, by "lacking crossbar or yardarm carinae and other septal thickenings". Merriam made no mention of Crickmay's work.

In its original concept, **Exilifrons** embraced three genera or species groups. The purpose of the present contribution is to refine the genus, so that it becomes restricted to one of these, and to demonstrate that it is apparently a good index of upper, but probably not uppermost, Lower Devonian strata in northern Yukon Territory and central Nevada. In addition, the author argues the almost certain synonymy of **Pinyonastraea** and **Exilifrons** and shows that a newly discovered occurrence of **Exilifrons** in east-central British Columbia is likely to be of about the same age as the Yukon and Nevada occurrences. The paper also includes the first photographs of thin sections of the holotype and a paratype of the type species of **Exilifrons.**

Acknowledgments

The writer is indebted to R.I. Thompson for comments concerning the stratigraphic position of **Exilifrons** in British Columbia, to W.A. Oliver for advance access to Johnson and his publication on Merriam's Nevada coral zones, and to B.S. Norford and E.W. Bamber for suggesting improvements to the original typescript of this paper.

Systematics

Family CYATHOPHYLLIDAE Dana, 1846

Subfamily ARACHNOPHYLLINAE Dybowski, 1873

Genus **Exilifrons** Crickmay, 1968, p. 3, 4

Type species. **Exilifrons exilis** Crickmay, 1968, p. 4, Pl. 1, fig. 1, Pl. 2, figs. 1, 2, 9, Pl. 3, fig. 5, Pl. 4, fig. 1. "Ogilvie River area, Yukon Territory; 65°23'N. lat., 138°24'W. long.; near the base of the Bear Rock equivalent, with **Spongonaria parca** sp. n.; 700 feet below zone of **Spirinella collina.** 900 feet below **Exilifrons** ogilviensis, and 1800 feet below **Taimyrophyllum vescibalteatum** Pedder". Crickmay's Bear Rock equivalent is evidently the unit known as the Ogilvie Formation. The basal part of this formation is estimated tentatively to be late Zlichovian in terms of the Czechoslovakian standard and Emsian in terms of the Rhenish standard (see under heading Distribution). The type locality is one of several sections exposed on an unnamed range of the Ogilvie Mountains, 1 to 9 km west-northwest of the bridge carrying the Dempster Highway over the Ogilvie River. Perry et al. (1974, Sec. 8) published one of these sections, giving the co-ordinates as latitude 65°21'N, longitude 138°26'W. The present author and G. Klapper briefly examined another in 1976 at latitude 65°22'30"N, longitude 138°27'W.

Description. Corallum compound, phaceloid to cerioid, most commonly subcerioid with some rounded and a few free corallites. Intercorallite walls thin. Septal trabeculae monacanthine, fine, typically 0.1 to 0.2 mm in diameter, apparently developed only in parts of some septa. Septa alternate, smooth or more commonly bearing zigzag carinae; typically markedly folded in both horizontal and vertical senses. Septa of both orders may be discontinuous peripherally and withdrawn from the wall. Major septa extend to or near the axis in most corallites, but in some extend adaxially as little as half the radius of the tabularium. Adult dissepimentaria comprise a few or,

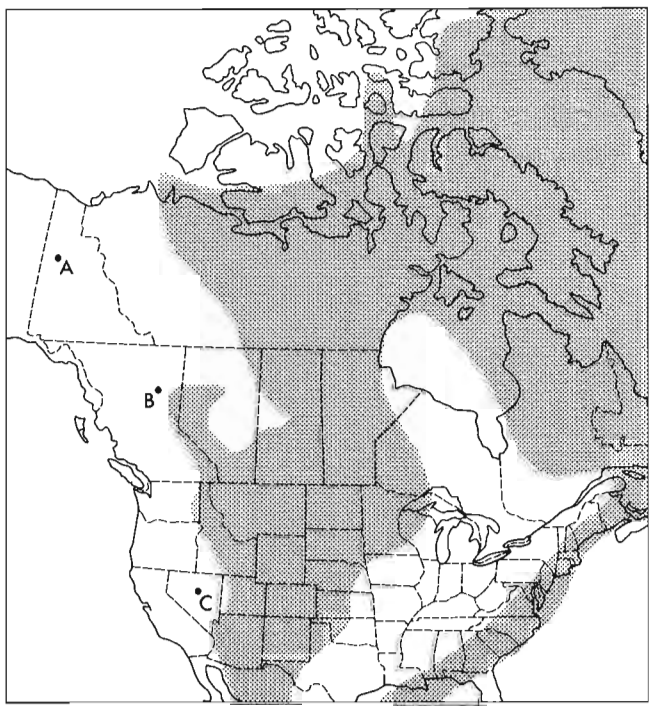

A – Ogilvie Mountains, Yukon Territory.
B – Mount Lady Laurier, British Columbia.
C – southern Sulphur Springs Range and Lone Mountain, Nevada.

Figure 34.1. Map showing occurrences of species of **Exilifrons** and approximate position of the major land masses (stippled) in late Early Devonian time.

the tabularium. Adult dissepimentaria comprise a few or, more typically, many rows of dissepiments. Inner dissepiments smaller and more steeply inclined than the outer ones. Parts of the dissepimentaria formed during periods of rapid growth have larger, noticeably much less globose dissepiments and may include prominently elongate presepiments. The outer dissepimentarial surface is more or less flat or, less commonly, slightly everted. Tabulae and tabularial surfaces vary considerably within one colony depending on the length of the septa; where the septa are long, tabulae are generally very incomplete and axially domed; where they are short, tabulae are normally flat, or slightly sagging axially, and elevated periaxially or marginally.

Synonymy The type and only species referred to **Hexagonaria** (Pinyonastraea) by Merriam was **Prismatophyllum kirki** Stumm (1937, p. 437, Pl. 55, figs. 7a, b), which also has been figured or discussed by Merriam (1940, Pl. 16, fig. 5; 1974b, p. 62, Pl. 23, figs. 5-10) and Stumm (1949, Pl. 15, figs. 16, 17). Although the single longitudinal section of the holotype shows some unusually flat and complete tabulae, there can be little doubt that Stumm's species is congeneric with **Exilifrons exilis**. Merriam's (1974b, p. 62) diagnosis of **Hexagonaria (Pinyonastraea) kirki** reads "this **Pinyonastraea** has large corallites, minutely undulant, very weakly zigzag, thin carinate septa and thin, even, commonly straight walls. Some of the outer dissepiments are sublonsdaleioid in the peripheral

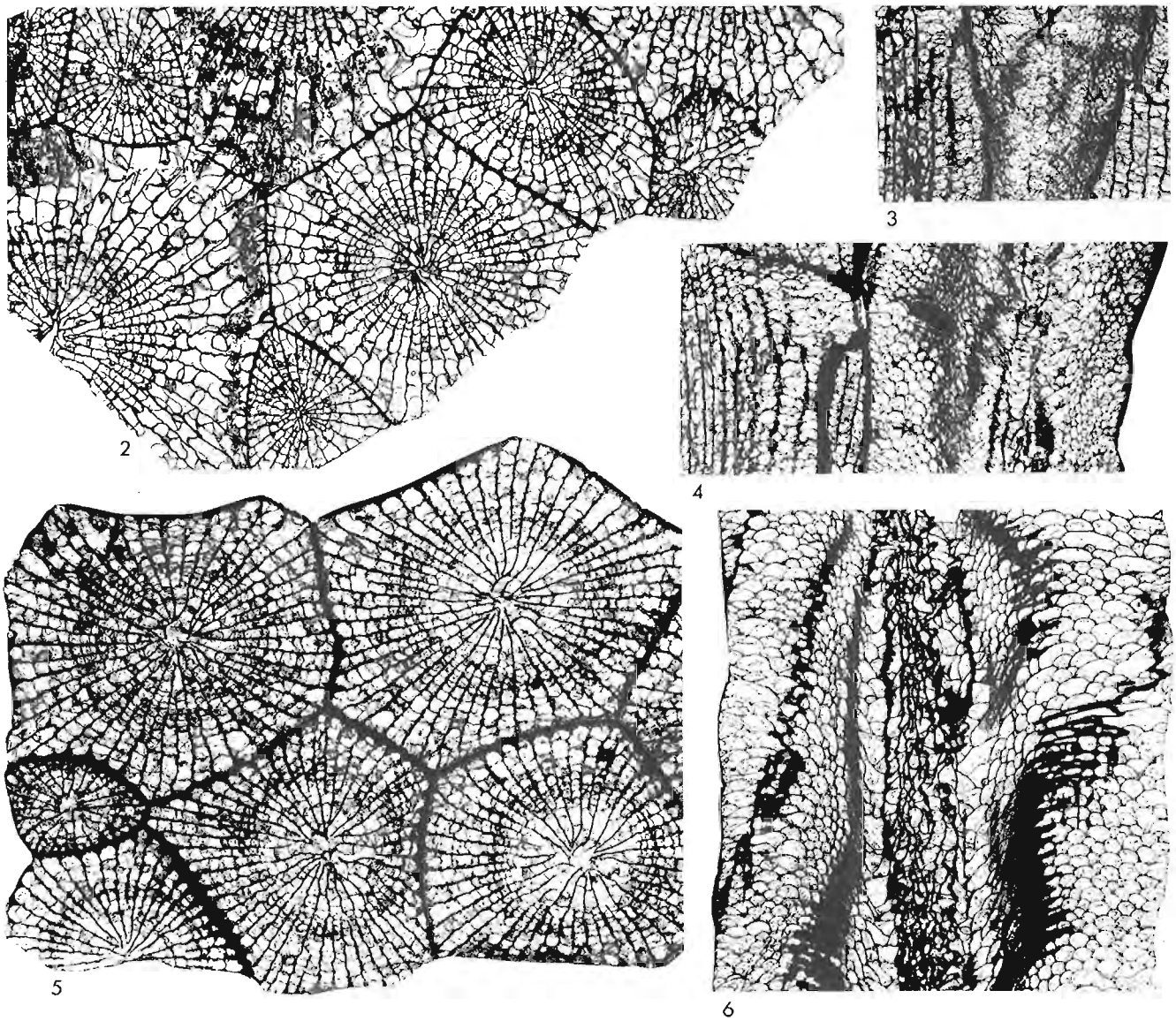

Figures 34.2 to 34.6. **Exilifrons exilis** Crickmay, x3. Figures 34.2, 34.6, paratype, GSC 25534. Figures 34.3 to 34.5, holotype (designated as such in Crickmay's hand-writing on the specimen and also in anonymous publication, 1971, p. 97), GSC 25533. Both specimens are from near the base of the Ogilvie Formation on an unnamed range of the Ogilvie Mountains, Yukon Territory. Latitude 65°23'N, longitude 138°24'W. Collector and date of collection not recorded.

irregular zone of the dissepimentarium". This might have been written as well for **Exilifrons** exilis as for **Prismatophyllum kirki**.

Familial assignment. Merriam placed **Hexagonaria** (H.) and H. (**Pinyonastraea**) with **Disphyllum, Acinophyllum, Cylindrophyllum, Billingsastraea, Aphroidophyllum** and **Taimyrophyllum** in the family Disphyllidae. True **Hexagonaria** and **Disphyllum** have fusiforme or cuneate septa and well-delineated monacanthine trabeculae, and certainly belong to the Disphyllinae as diagnosed by Jell (1969, p. 68). However, **Acinophyllum** and **Cylindrophyllum** have very fine trabeculae and septa and well-developed zigzag carinae, and therefore belong to the Craspedophyllidae as that family is interpreted by Oliver (1974, 1976), whereas **Aphroidophyllum** and **Taimyrophyllum**, which have axially modified septa and closely spaced and adaxially depressed peripheral tabulae, are clearly to be assigned to the Ptenophyllidae as interpreted by Birenheide (1972) and other workers.

Crickmay's assignment of **Exilifrons** to the Arachnophyllidae is justified by the alternate carinae and tabularial morphology of **Exilifrons.** But so little separates the Cyathophyllidae from the Arachnophyllidae that the latter is better regarded as a subfamily of the Cyathophyllidae.

Generic distinctions. **Exilifrons** has been confused at different times with **Spongophyllum** Milne Edwards and Haime, 1851, **Prismatophyllum** Simpson, 1900, **Disphyllum** de Fromentel, 1861, **Hexagonaria** Gürich, 1896 and **Spongonaria** Crickmay, 1962. Another taxon with which it is in danger of being confused is **Orthocyathus** Merriam, 1974.

Satisfactory interpretation of **Spongophyllum** is impossible on existing data. The type species, by monotypy, is **S. sedgwicki** Milne Edwards and Haime, 1851. Unfortunately, the entire type series of this species is lost and apparently has never been either thin sectioned or photographed. A neotype chosen by Jones (1929, p. 89) may not have been prepared adequately, and to date has only been crudely figured (Birenheide, 1962, Pl. 9, fig. 8, Pl. 10, fig. 10). The stratigraphic and geographic origin of the type series is not known more precisely than Torquay, Devonshire. Information on the neotype is even more vague because the specimen is a pebble labeled South Devonshire. As far as it is possible to determine, **Exilifrons** is distinguished from **Spongophyllum** by its undulant and typically carinate septa, better developed minor septa, relatively smaller and less elongate dissepiments, and by its tabulae which should be more incomplete in corallites having septa as long as those of the neotype of **Spongophyllum sedgwicki**.

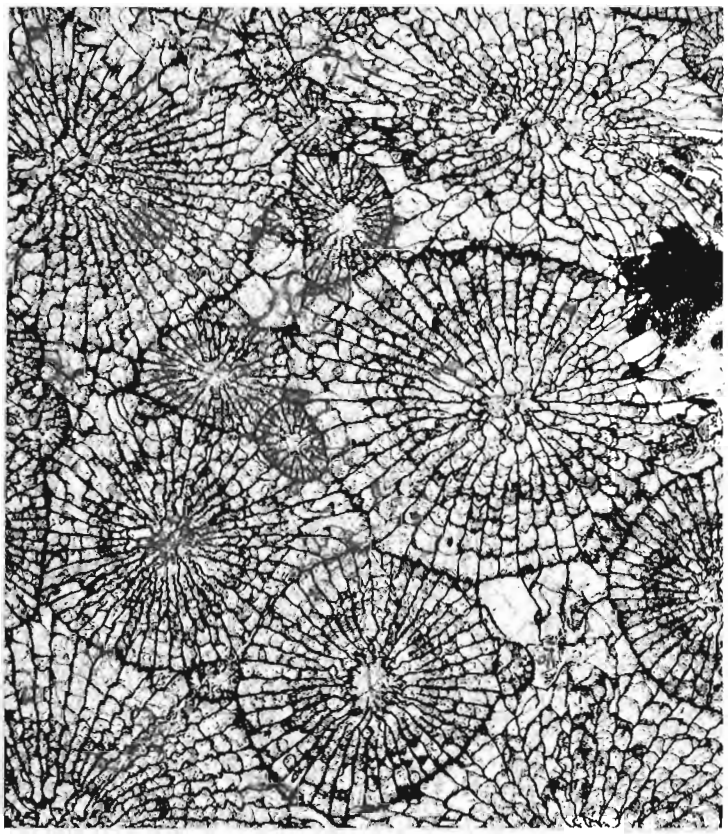

7

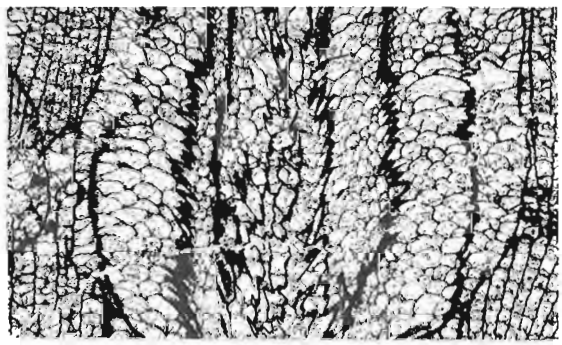

8

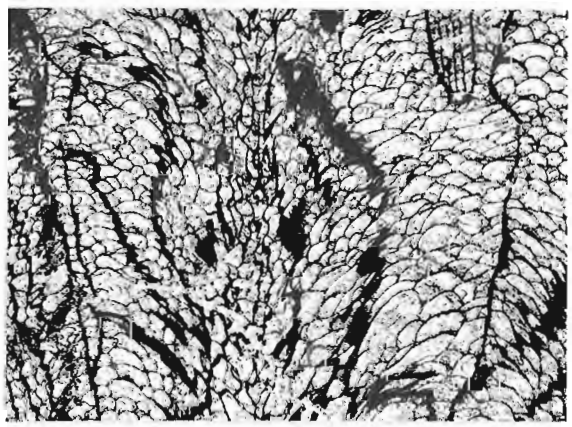

9

Figures 34.7 to 34.9. **Exilifrons** sp. cf. **E. exilis** Crickmay, x3. Figure 34.7, GSC 46111. Figures 34.8, 34.9, GSC 46110. Both specimens are from approximately 78 m above the base of the Ogilvie Formation on an unnamed range of the Ogilvie Mountains, Yukon Territory. Latitude 65°22'30"N, longitude 138°27'W. GSC locality C-63133. Collected by A.E.H. Pedder, 1976.

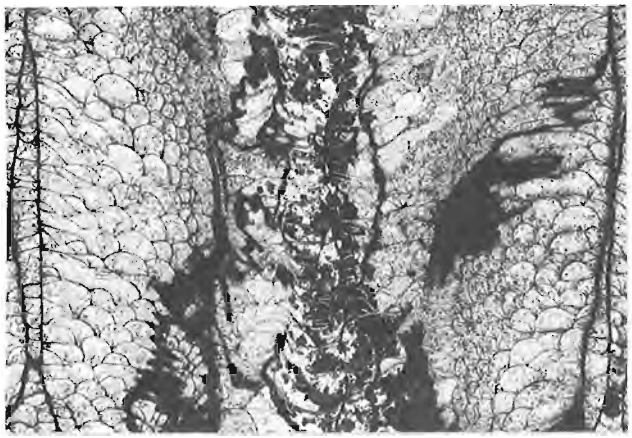

10

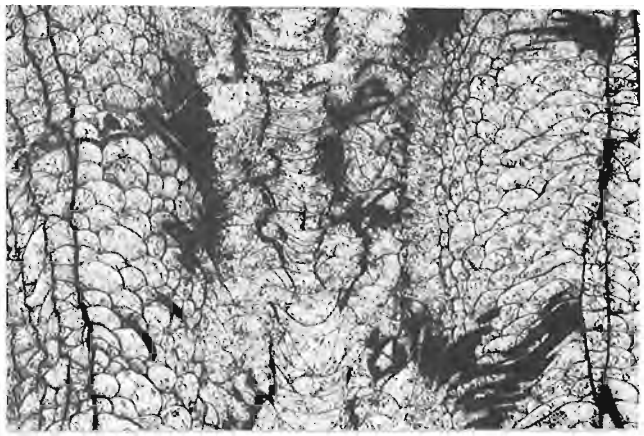

11

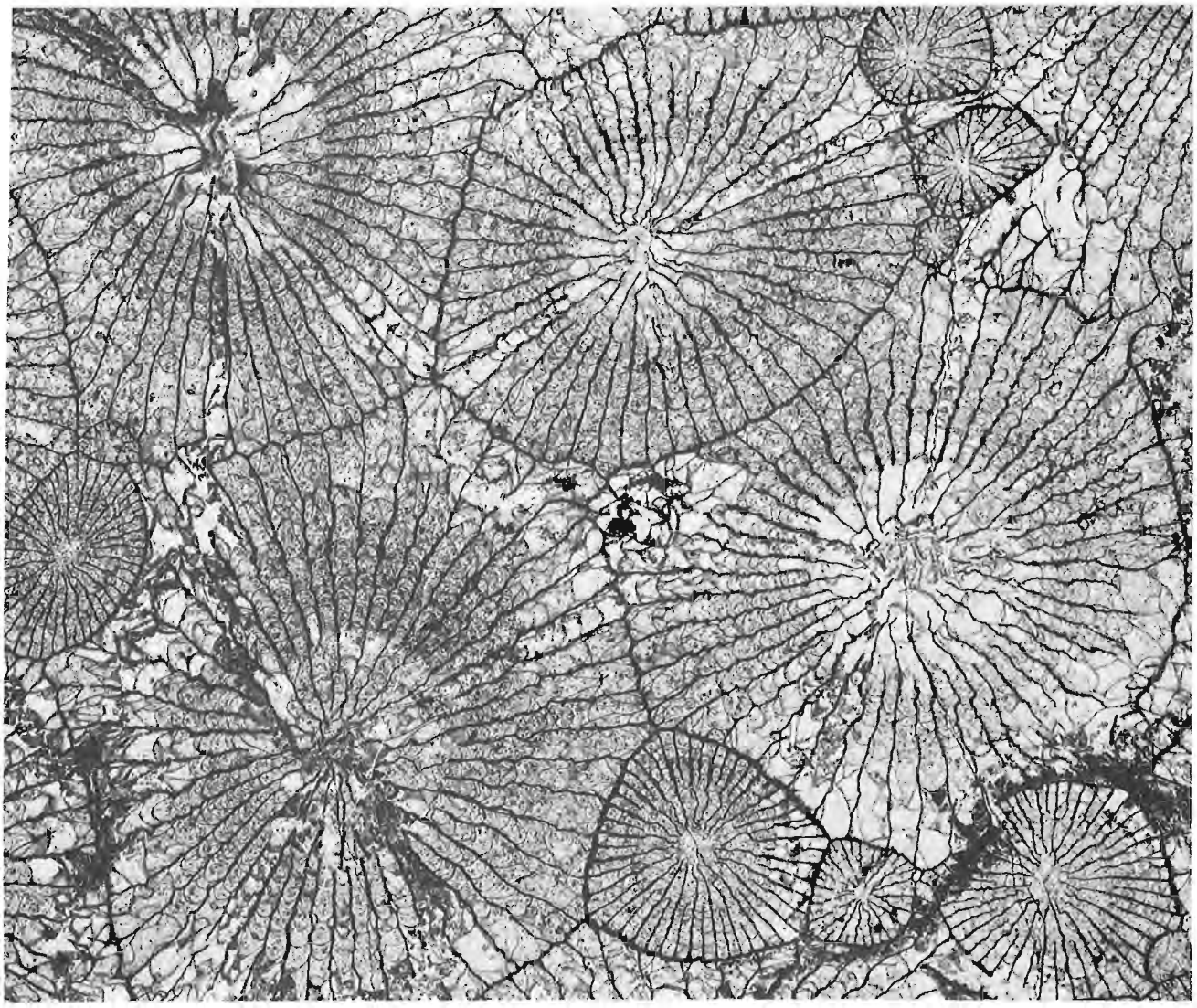

12

Figures 34.10 to 34.12. **Exilifrons** sp. cf. **E. occidens** (Stumm), x3. GSC 46109. Approximately 75 m above the base of the Ogilvie Formation on an unnamed range of the Ogilvie Mountains, Yukon Territory. Latitude 65°22'30"N, longitude 138°27'W. GSC locality C-63132. Collected by A.E.H. Pedder, 1976.

Prismatophyllum is typified by **P. prisma** Lang and Smith, 1935. The holotype of this species is from the presumed early Eifelian part of the Jeffersonville Limestone of Indiana, but Oliver's (1976, p. 79-83, Pl. 46-48) recent and thorough monography of the species demonstrates that it is distributed widely in the Appalachian Basin. Neither Crickmay nor Merriam discussed differences between Exilifrons or **Pinyonastraea** and **Prismatophyllum**. This is unfortunate since the morphology of **Exilifrons,** on the whole, more closely resembles that of **Prismatophyllum** than any other genus. It differs from **Prismatophyllum** in having less highly developed carinae that normally are never of the yardarm type, prominently undulant septa and abundant peripheral tabellae.

Cyathophyllum caespitosum Goldfuss, 1826, was designated the type species of **Disphyllum** by Lang and Smith (1934, p. 80). These authors also chose a lectotype for the species, which has since been figured by both Lang and Smith (1935, Pl. 35, figs. 4-6) and Birenheide (1969, Pl. 2, figs. 7a, b, Pl. 5, fig. 14). It is believed to have come from the Middle Devonian (Givetian) Bücheler Schichten of the Paffrather Mulde, Bergisch Gladbach, Germany. Interpreted on this and other obviously congeneric species, **Disphyllum** is distinguished from **Exilifrons** in having cuneate septa, coarser trabeculae and uniformly small dissepiments. It also lacks the characteristic septal undulations of **Exilifrons.**

The type species of **Hexagonaria** has been established by Lang et al. (1940, p. 69) as **Cyathophyllum hexagonum** Goldfuss, 1826. A lectotype for this species, chosen earlier by Lang and Smith (1935, p. 550, 551) is lost, but has been replaced by a neotype designated and illustrated by Birenheide (1969, p. 40, 41, Pl. 1, figs. 1a-d, Pl. 4, fig. 11). This specimen probably derives from the Upper Devonian (Frasnian) Refrath Schichten of the Paffrather Mulde, Bergisch Gladbach, Germany, and differs from **Exilifrons** in having strongly fusiforme septa, coarse monacanths, and broad tabulae despite the considerable length of the major septa.

The holotype of **Spongonaria filicata** Crickmay, 1962, which is the type species of **Spongonaria,** was said to be from "supposed equivalent of the Bear Rock formation . . . . on Houston River, Yukon Territory;

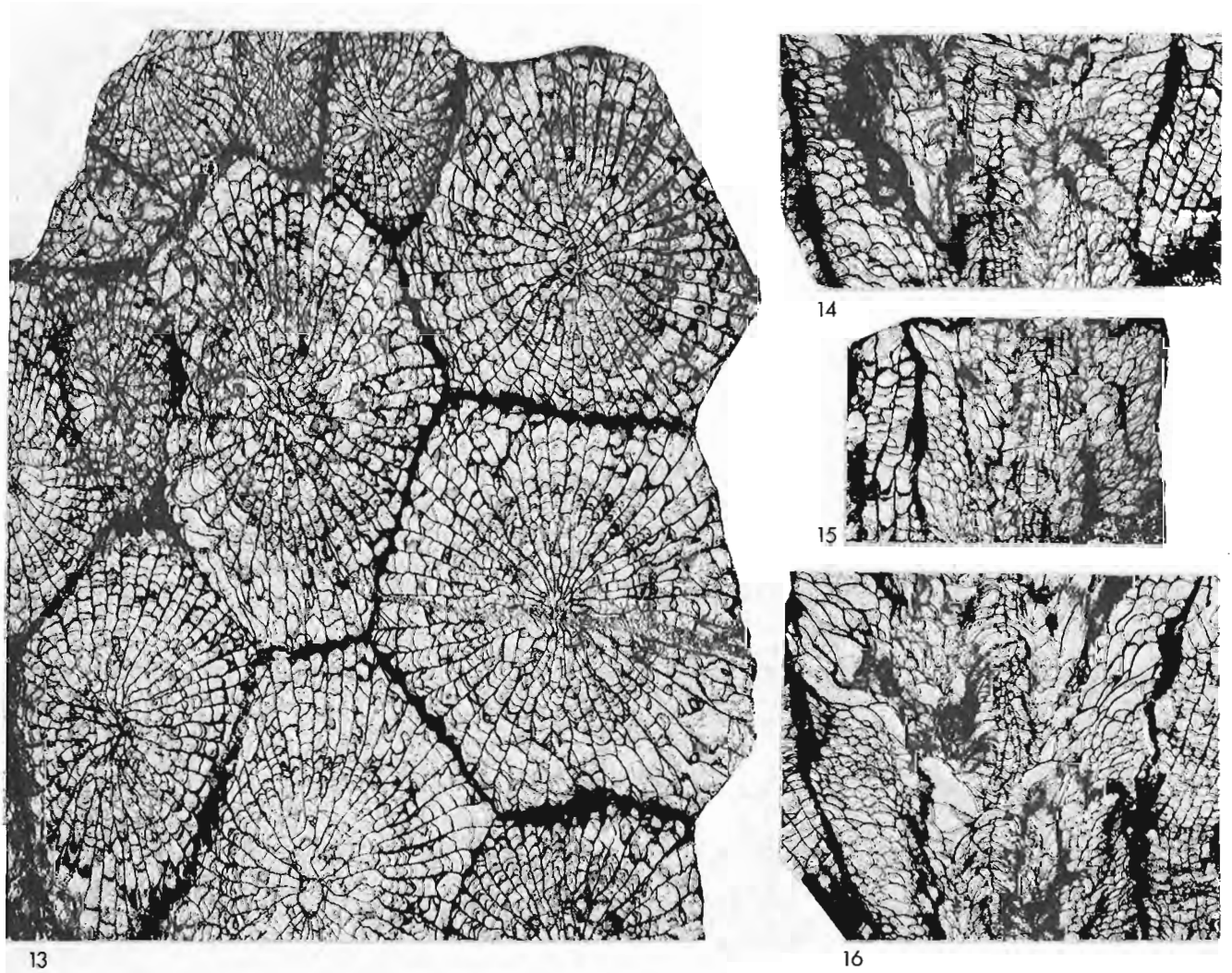

Figures 34.13 to 34.16. **Exilifrons** sp. nov., x3. GSC 53073. Upper Lower Devonian limestone in an unnamed shale-siltstone succession exposed on a ridge 6.5 km northeast of Mount Lady Laurier, British Columbia. Latitude 56°43'N, longitude 123°42'W. GSC locality C-51791. Collected by D.K. Noakes, 1975.

65°30'N. lat., 131°15'W. long.". This statement is in error because no Lower Devonian rock outcrops at the locality defined by these co-ordinates; furthermore, this locality is in the District of Mackenzie, not Yukon Territory. Finally, the name Houston River does not appear in the current gazetteers of either Yukon Territory or Northwest Territories. Despite this minor problem, **Spongonaria** is assessed easily since its species are common in upper Lower and lowest Middle Devonian strata of western and arctic Canada. Compared with **Exilifrons,** they normally have shorter, smoother septa that lack undulations, and have lath-like septal spines in the axial region, and relatively broader and less complicated tabularia.

To the present time, the only species referred to **Cyathophyllum (Orthocyathus)** is the type species **Prismatophyllum flexum** Stumm, 1938, from Lone Mountain, Nevada. Stumm believed that it came from the upper

17

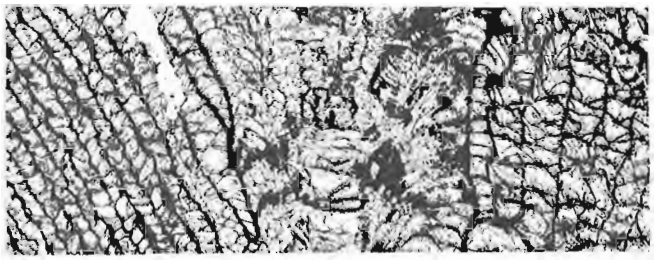

18

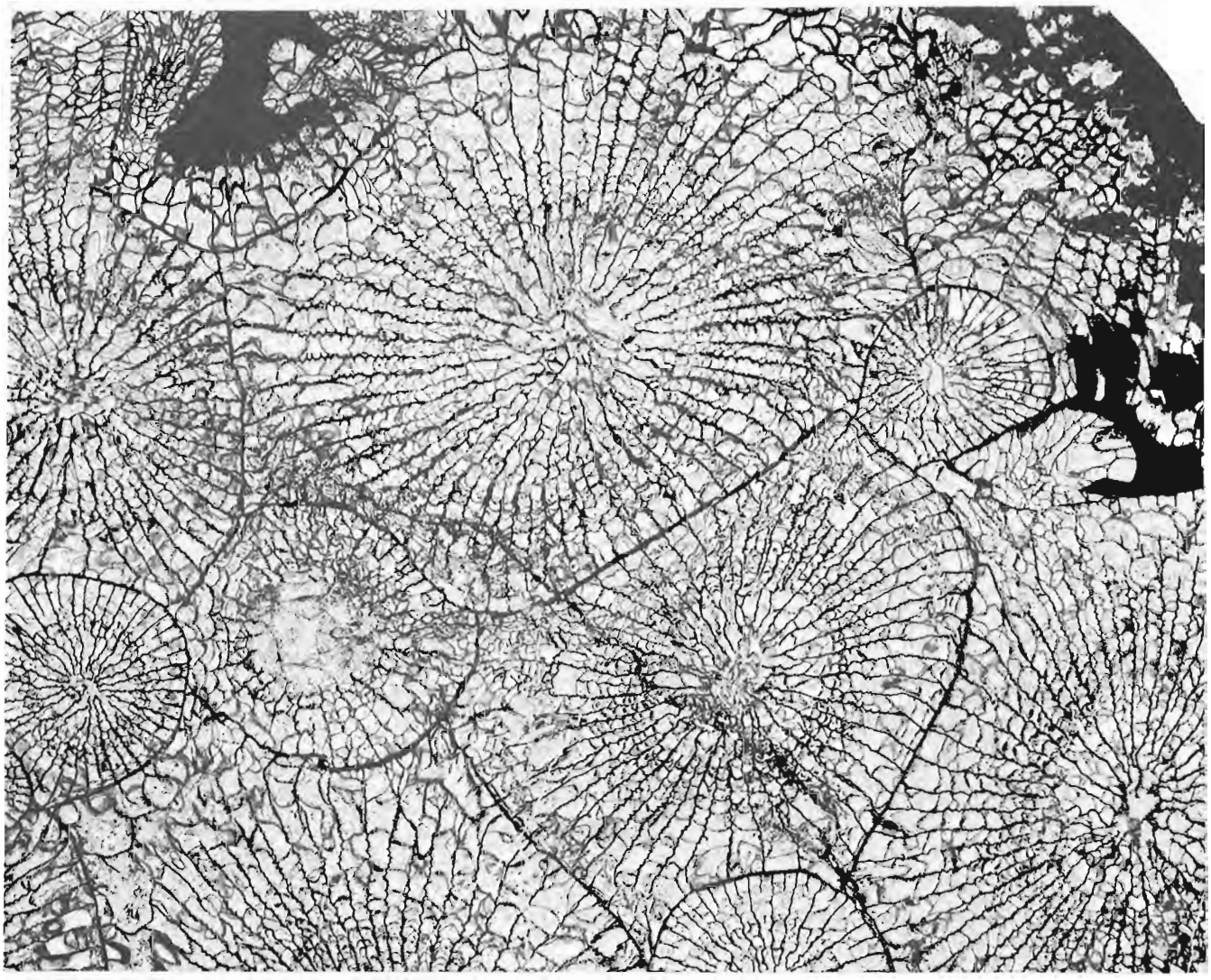

19

Figures 34.17 to 34.19. **Exilifrons** sp. cf. **E. occidens** (Stumm), x3. USNM 245251. 43.9 m above the base and 116.4 m below the top of the Bartine Member of the McColley Canyon Formation, Lone Mountain, Nevada. Twp. 20 N, Rge. 51 E. Bartine Ranch Quadrangle, Eureka County. Collected by A.E.H. Pedder, 1970.

Middle Devonian part of the Nevada Limestone, but Merriam (1974a, p. 35) regarded it as a constituent of his Devonian Fauna F, which both he (1974b, p. 18) and Johnson and Oliver (in press) consider to be late Eifelian or late Couvinian. A specimen from Lone Mountain collected by the writer came from talus above occurrences of **Warrenella kirki** and could be early Givetian rather than late Eifelian. **Orthocyathus flexum** is close to some species of **Exilifrons,** but its septa are not folded to any extent and its dissepiments are uniformly smaller. Hill and Jell (1969, p. 5), and others before, have speculated that it may be related closely to **Cyathophyllum,** strict sense.

Species composition. The following described species are assigned to **Exilifrons** with varying degrees of confidence: **Spongophyllum nevadense** Stumm, 1937, **S. expansum** Stumm, 1937, **Prismatophyllum kirki** Stumm, 1937, **Disphyllum occidens** Stumm, 1938, **Exilifrons exilis** Crickmay, 1968 and **Disphyllum** eurekaense Merriam, 1974.

Hexagonaria impedita, H. atypica and **H. furtiva,** all described by Crickmay in 1960 and transferred by him to **Exilifrons** in 1968, are part of a species group that is well represented in certain Eifelian strata of western Canada. Its members differ from typical species of **Exilifrons** in lacking carinae and septal undulations, and in having more uniform and inwardly sloping dissepimentaria. They are likely to be related to **Exilifrons** but are sufficiently distinct, morphologically and stratigraphically, to be excluded from the genus, strict sense. Possibly they could be accommodated satisfactorily in a subgenus of **Exilifrons.**

Exilifrons ogilviensis Crickmay, 1968, **E. excavata** Crickmay, 1968 and **E. horiae** Crickmay, 1968 do not conform to the present concept of **Exilifrons** and are transferred unequivocally to **Spongonaria.**

Distribution. Known occurrences of **Exilifrons** in Yukon Territory are confined to the lower beds of the Ogilvie Formation on an unnamed range of the Ogilvie Mountains (point A in Fig. 34.1). Species present are **Exilifrons exilis** from "near the base" (Crickmay, 1968) of the formation, and forms identified as **Exilifrons** sp. cf. **E. occidens** from about 75 m up in the formation (Figs. 34.10 to 34.12) and **E.** sp. cf. **E. exilis** (Figs. 34.7 to 34.9), 3 m higher. **Polygnathus dehiscens** and **Teicherticeras lenzi** are present in the underlying Michelle Formation in this area (Fåhraeus, 1971; House and Pedder, 1963) and the early Eifelian conodont **Polygnathus costatus costatus** has been isolated 462 m above the base of the Ogilvie Formation (Perry et al., 1974), that is about 384 m above the highest known occurrence of **Exilifrons.** In the headwaters area of Royal Creek, **Polygnathus** dehiscens occurs just above the highest occurrence of **Monograptus yukonensis,** which is a late Pragian species in Czechoslovakia (Chlupáč, 1976). From these data, a late Zlichovian age is deduced for the Yukon occurrence of **Exilifrons.**

A new species of Exilifrons has been identified recently from a ridge 6.5 km northeast of Mount Lady Laurier, between the headwater areas of Halfway and Graham rivers in east-central British Columbia (Figs. 34.13 to 34.16 and point B in Fig. 34.1). It derives from a limestone interbed in an unnamed shale-siltstone succession, currently mapped as Middle Devonian (unit 6 of Irish, 1970, Map 1232A). Eifelian corals have been identified from high in this unit, but the beds providing **Exilifrons,** which, despite structural complications, are almost certainly lower in the sequence, contain abundant crinoid ossicles with double axial canals, and are therefore likely to be of late Zlichovian or Dalejan age.

Several species of **Exilifrons** are known from Nevada (localities around point C in Fig. 34.1). Merriam (1974b) documented occurrences of **Exilifrons** kirki, **E. eurekaensis** and **E.** (?) **nevadensis** in his Devonian coral zone D_2 on Lone Mountain. Johnson and Oliver (in press) estimate that this fauna is from the upper subzone of the **Eurekaspirifer pinyonensis** Zone. They also suggest that it is within the range of **Polygnathus gronbergi** (Klapper and Johnson, 1975) and is late Zlichovian in age. The present author has collected **E.** sp. cf. **E. occidens** (Figs. 34.17 to 34.19), 41.8 m above the base of the Bartine Limestone on Lone Mountain, that is 24.7 m above Klapper and Johnson's (1975, p. 75) LM 12 sample with **Polygnathus dehiscens** and 9.8 m below their LM 16 sample at the base of the **P. gronbergi** Teilzone as it is currently established. This occurrence may be below those documented by Merriam, but since it is still above the level of **Polygnathus dehiscens,** it is presumably also late Zlichovian. Stumm (1938, p. 481) reported **Exilifrons occidens** from "approximately 1000 feet above the base of the Nevada limestone just west of Romano Ranch Mountain, east side of the Sulphur Spring Mountains quadrangle, Nevada". Thicknesses given by Carlisle et al. (1957, Fig. 2) would seem to place this occurrence in their Union Mountain Member of the Nevada Formation. This member consists mainly of unfossiliferous dolomite and sandstone (Johnson and Niebuhr (1976, p. 1695) consider it a westward-prograding tongue of the Sevy Dolomite), but is reported to yield the **Eurekaspirifer pinyonensis** fauna in places (Carlisle et al., 1957, Fig. 2). A more plausible interpretation is that the **Exilifrons occidens** came from near the top of Merriam's (1974b, Fig. 14) Nevada unit 2, which is the Bartine Limestone of present terminology (Murphy and Gronberg, 1970). Probably this would place it just above the **Polygnathus dehiscens/P. gronbergi** transition, and would again suggest a late Zlichovian age.

References

Anonymous

1971: Type specimens of species of fossils described by C.H. Crickmay; in Report of Activities, Part A, Geol. Surv. Can., Paper 71-1A, p. 97-101.

Birenheide, Rudolf

1962: Revision der koloniebildenden Spongophyllidae und Stringophyllidae aus des Devon; Senckenbergiana Lethaea, Bd. 43, p. 41-99.

1969: Typen mittel- und oberdevonischer Rugosa aus der Sammlung Goldfuss; Senckenbergiana Lethaea, Bd. 50, p. 37-55.

1972: Ptenophyllidae (Rugosa) aus dem W-deutschen Mitteldevon; Senckenbergiana Lethaea, Bd. 53, p. 405-437.

Carlisle, Donald, Murphy, M.A., Nelson, A.A., and Winterer, E.L.
1957: Devonian stratigraphy of Sulphur Springs and Pinyon Ranges, Nevada; Bull. Am. Assoc. Pet. Geol., v. 41, p. 2175-2191.

Chlupáč, Ivo
1976: The oldest goniatite faunas and their stratigraphical significance; Lethaia, v. 9, p. 303-315.

Crickmay, C.H.
1960: The older Devonian faunas of the Northwest Territories; Evelyn de Mille Books, Calgary.

1962: New Devonian fossils from western Canada; Evelyn de Mille Books, Calgary.

1968: Lower Devonian and other coral species in northwestern Canada; Evelyn de Mille Books, Calgary.

Fåhraeus, L.E.
1971: Lower Devonian conodonts from the Michelle and Prongs Creek Formations, Yukon Territory; J. Paleontol., v. 45, p. 665-683.

Hill, Dorothy and Jell, J.S.
1969: Devonian corals from Ukalunda; Geol. Surv. Queensland, Publ. 340, Palaeontol. Papers 16.

House, M.R. and Pedder, A.E.H.
1963: Devonian goniatites and stratigraphical correlations in western Canada; Palaeontology, v. 6, p. 491-539.

Irish, E.J.W.
1970: Halfway River map-area, British Columbia; Geol. Surv. Can., Paper 69-11.

Jell, J.S.
1969: Septal microstructure and classification of the Phillipsastraeidae in Stratigraphy and palaeontology essays in honour of Dorothy Hill, K.S.W. Campbell, ed.; Austral. Natl. Univ. Press, Canberra, p. 50-73.

Johnson, J.G. and Niebuhr, W.W.
1976: Anatomy of an assemblage zone; Bull. Geol. Soc. Am., v. 87, p. 1693-1703.

Johnson, J.G. and Oliver, W.A.
Silurian and Devonian coral zones in the Great Basin; Bull. Geol. Soc. Am. (In press)

Jones, O.A.
1929: On the coral genera **Endophyllum** Edwards and Haime and **Spongophyllum** Edwards and Haime; Geol. Mag., v. 66, p. 84-91.

Klapper, Gilbert and Johnson, D.B.
1975: Sequence in conodont genus **Polygnathus** in Lower Devonian at Lone Mountain, Nevada; Geologica et Palaeontologica, v. 9, p. 65-83.

Lang, W.D. and Smith, Stanley
1934: Ludwig's 'Corallen aus Paläolithischen Formationen' and the genotype of **Disphyllum** de Fromentel; Ann. Mag. Nat. Hist., ser. 10, v. 13, p. 78-81.

1935: **Cyathophyllum caespitosum** Goldfuss, and other Devonian corals considered in a revision of that species; Quart. J. Geol. Soc. London, v. 91, p. 538-590.

Lang, W.D., Smith, Stanley, and Thomas, H.D.
1940: Index of Palaeozoic coral genera; Brit. Mus. (Nat. Hist.), London.

Merriam, C.W.
1940: Devonian stratigraphy and paleontology of the Roberts Mountains region, Nevada; Geol. Soc. Am., Spec. Paper 25.

1974a: Middle Devonian rugose corals of the central Great Basin; U.S. Geol. Surv., Prof. Paper 799.

1974b: Lower and Lower Middle Devonian rugose corals of the central Great Basin; U.S. Geol. Surv., Prof. Paper 805.

Murphy, M.R. and Gronberg, E.C.
1970: Stratigraphy and correlation of the Lower Nevada Group (Devonian) north and west of Eureka, Nevada; Bull. Geol. Soc. Am., v. 81, p. 127-136.

Oliver, W.A.
1974: Classification and new genera of noncystimorph colonial rugose corals from the Onesquethaw Stage in New York and adjacent areas; U.S. Geol. Surv., J. Research, v. 2, p. 165-174.

1976: Noncystimorph colonial rugose corals of the Onesquethaw and Lower Cazenovia Stages (Lower and Middle Devonian) in New York and adjacent areas; U.S. Geol. Surv., Prof. Paper 869.

Perry, D.G., Klapper, Gilbert, and Lenz, A.C.
1974: Age of the Ogilvie Formation (Devonian), northern Yukon: based primarily on the occurrence of brachiopods and conodonts; Can. J. Earth Sci., v. 11, p. 1055-1097.

Stumm, E.C.
1937: The Lower Middle Devonian tetracorals of the Nevada Limestone; J. Paleontol., v. 11, p. 423-443.

1938: Upper Middle Devonian rugose corals of the Nevada Limestone; J. Paleontol., v. 12, p. 478-485.

1949: Revision of the families and genera of the Devonian tetracorals; Geol. Soc. Am., Mem. 40.

35. LOUGHEED ISLAND AND NEIGHBOURING SMALL ISLANDS, DISTRICT OF FRANKLIN (NTS 69C, 79D)

Project 760019

H.R. Balkwill, W.S. Hopkins, Jr., and J.H. Wall
Institute of Sedimentary and Petroleum Geology

Introduction

Five weeks (mid-July to mid-August) were spent in mapping and stratigraphic study of Mesozoic strata in the west-central part of the Sverdrup Basin (69C, 79D). Mapping was completed on Lougheed and Mackenzie King islands, and at Sabine Peninsula (Melville Island); also, small areas of the Ringnes Islands and northwestern Melville Island were examined (Fig. 35.1a). Widespread snow cover hampered operations until the third week of July. Prolonged fog and high winds brought the field season to a premature end in early August, preventing completion of mapping on Borden and Brock islands. The following paragraphs summarize the surface bedrock geology of Lougheed Island (Fig. 35.1b).

Stratigraphy and Structure

A conformable succession of Lower and Upper Cretaceous strata, assigned to the Isachsen, Christopher, Hassel, Kanguk, and Eureka Sound formations, comprises exposed bedrock on Lougheed Island and neighbouring small islands (Edmund Walker, Grosvenor, and Patterson islands; Fig. 35.1b). The formations are arranged about a shallow syncline – here named Lougheed Syncline – which has a gentle, southeastward-plunging, broad trough, and a subdued, reversed sigmoid trace. The oldest bedrock at the surface of Lougheed Island consists of partly calcite-cemented, carbonaceous and coaly, buff and light grey weathering sandstones of the upper part of the Isachsen Formation (Lower Cretaceous), exposed locally near the northern coast of the island. This incomplete Isachsen succession is estimated to be about 270 m (900 ft.) thick. [A complete Isachsen succession, about 340 m (1130 ft.) thick, was penetrated in the Sun KR Panarctic Skybattle Bay C-15 drill hole, near the southwestern coast of the island (Fig. 35.1b)].

The lower part of the Christopher Formation (Lower Cretaceous) consists of dark olive-grey to dark grey silty shale, with characteristically large and colourful, buff-orange-weathering, calcareous mudstone concretions. Some tan-weathering, calcite-cemented, fine to medium grained, partly fossiliferous sandstones, about 1 m to 3 m thick, are intercalated with shales in the lower part of the Christopher succession. Upper Christopher strata are dark grey to black, partly silty shale, with small, dark red-brown ironstone concretions and, near the top, upwardly increasing numbers of very thin beds of fine grained, buff, noncemented to weakly cemented, partly glauconitic sandstone, as a transitional succession to overlying Hassel Formation sandstones. About 700 m (2325 ft.) of Christopher strata were penetrated in the Skybattle Bay C-15 drill hole.

The Hassel Formation (Lower and Upper Cretaceous) is the most widely distributed and best exposed unit on Lougheed Island. The formation, which is estimated to be about 300 m (1000 ft.) thick, consists mainly of buff to tan, mainly medium grained sandstone, weakly cemented by ferruginous clay. There are abundant, very thin, dark grey shale intercalations in the basal part of the formation and, in the upper part, some black, pyritic shales, resembling the black shales of the overlying Kanguk Formation. [In that regard, the Christopher and Hassel formations are transitional over wide areas of central Sverdrup Basin, but the Hassel and Kanguk formations in most places have an abrupt contact (Stott, 1969; Balkwill and Hopkins, 1976)]. The middle part of the Hassel Formation consists of quartzose sandstones, with high-angle, tabular cross-strata, carbonaceous detritus, scour channels, and some pebble lenses; the strata lack marine faunas.

The Kanguk Formation (Upper Cretaceous) underlies a large part of southeastern Lougheed Island. The succession consists mainly of black, cohesive, papery, clay-rich shales, with very thin, yellow-grey, tuffaceous clay beds. The shales are sulphurous, with yellow and white secondary sulphate mineral crusts on many outcrops, and are so acidic that the formation supports almost no vegetation. The lower part of the Kanguk succession contains intervals of buff to yellow-brown, weakly cemented to noncemented, fine grained sandstone. The most prominent of the Kanguk sandstones is a few tens of metres thick, and lies about 100 m (330 ft.) above the base of the shale-dominated succession. Such well-developed sandstones are not common in the Kanguk Formation of central and eastern Sverdrup Basin; but Plauchut (1971, p. 675) indicated that the Kanguk Formation at Eglinton Island (Fig. 35.1a) has abundant sandstones. The Kanguk Formation is estimated to be about 200 m (660 ft.) thick.

The youngest strata on Lougheed Island are light grey, medium to coarse grained, weakly cemented sandstones of the Eureka Sound Formation. The unit, which is present only in the eastern part of Lougheed Island, is not more than about 60 m (200 ft.) thick, and contains large fragments of carbonized wood. Palynomorphs from the Eureka Sound beds indicate that the rocks are Maastrichtian, and thus approximately coeval with the formation on the Ringnes Islands, in those places where the Eureka Sound Formation lies conformably on the Kanguk Formation (Balkwill, 1974; Balkwill and Hopkins, 1976).

Lougheed Syncline has a nearly flat trough region that plunges southeastward about 1 degree (20 m/km or 100 ft./mile). The northeastern flank dips about 4 degrees toward the trough. The southwestern flank is locally interrupted by a system of low-amplitude regularly spaced folds. Some disharmonic, flexural-flow folds are particularly well developed in the upper part of the Christopher Formation on Edmund Walker Island. Folds there are asymmetric northward (some have overturned forelimbs), and have wavelengths as great as several tens of metres. Near Skybattle Bay, the Christopher/Hassel contact is locally overturned toward

From: Report of Activities, Part B; Geol. Surv. Can., Paper 77-1B (1977)

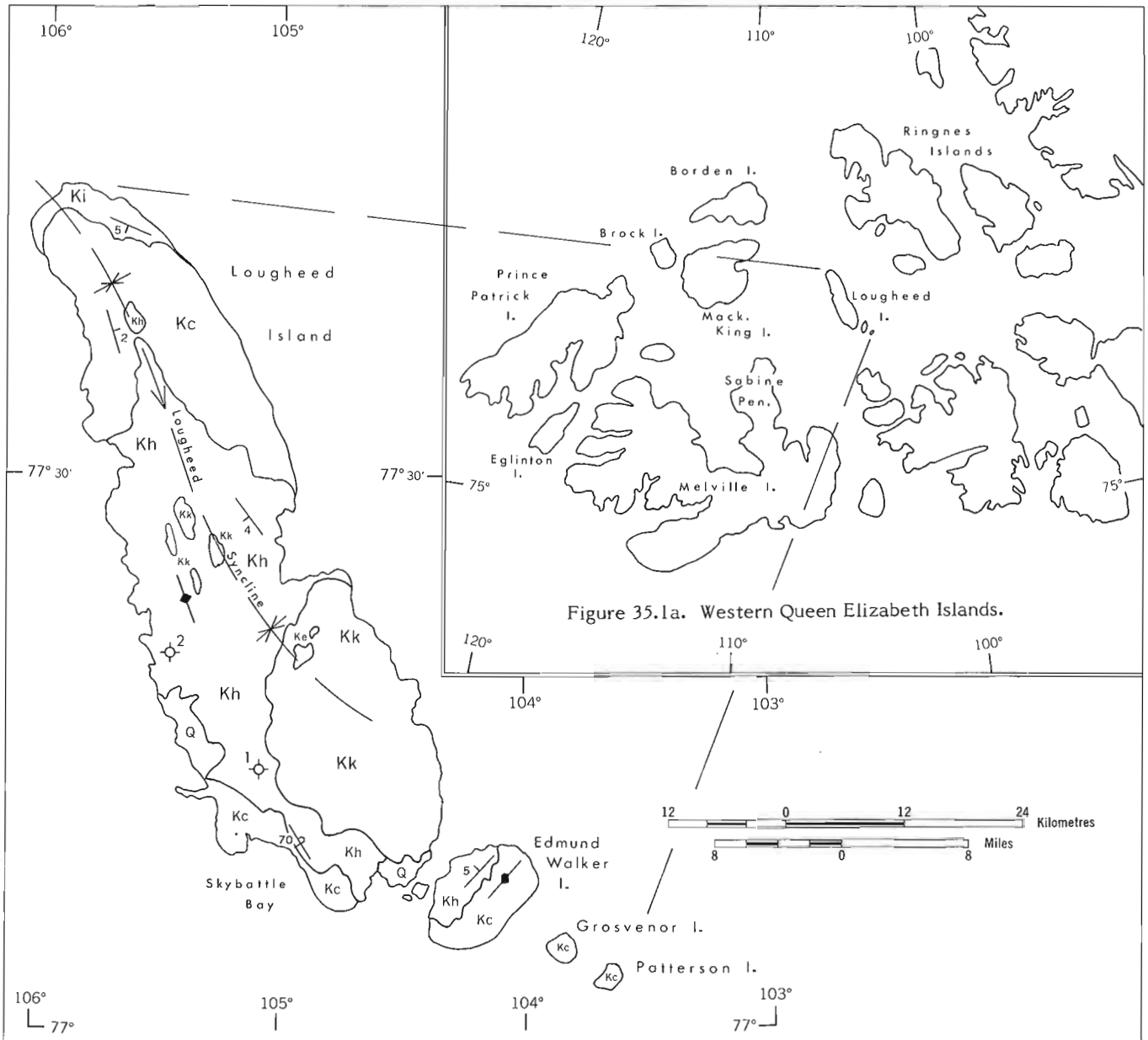

Figure 35.1a. Western Queen Elizabeth Islands.

Q	Quaternary: sand and mud
Ke	Eureka Sound Formation: sandstone
Kk	Kanguk Formation: shale
Kh	Hassel Formation: sandstone
Kc	Christopher Formation: shale
Ki	Isachsen Formation: sandstone

Strike and dip of bedding

Overturned bedding

Syncline: approximate axial trace and plunge

Trend of small folds

1 Sun KR Panarctic et al. Skybattle Bay C-15

2 Panarctic Tenneco et al. Pat Bay A-72

Figure 35.1b. Geology, Lougheed Island.

the northeast. The general structural style is suggestive of large-scale, slope-induced, northeastward- and northward-directed flow of ductile upper Christopher pelites toward the trough region of Lougheed Syncline. This would require the existence of a structurally high domain peripheral to the southwestern and southern coasts of Lougheed Island and adjacent small islands.

References

Balkwill, H.R.
1974: Structure and tectonics of Cornwall Arch, Amund Ringnes and Cornwall Islands, Arctic Archipelago; in Proc. Vol., 1973 Symposium on the Geology of the Canadian Arctic, J.D. Aitken and D.J. Glass, eds., Geol. Assoc. Can./Can. Soc. Petrol. Geol., p. 39-62.

Balkwill, H.R. and Hopkins, W.S., Jr.
1976: Cretaceous stratigraphy, Hoodoo Dome, Ellef Ringnes Island, District of Franklin; in Report of Activities, Part B, Geol. Surv. Can., Paper 76-1B, p. 329-334.

Plauchut, B.P.
1971: Geology of the Sverdrup Basin; Bull. Can. Petrol. Geol., v. 19, p. 659-679.

Stott, D.F.
1969: Ellef Ringnes Island, Canadian Arctic Archipelago; Geol. Surv. Can., Paper 68-16.

36. GEOLOGICAL AND PALYNOLOGICAL INTERPRETATION OF EUREKA SOUND FORMATION ON SABINE PENINSULA, NORTHERN MELVILLE ISLAND, DISTRICT OF FRANKLIN

Projects 750083 and 680068

R.A. Rahmani and W.S. Hopkins, Jr.
Institute of Sedimentary and Petroleum Geology, Calgary

Introduction

A 33 m composite section of the Eureka Sound Formation, exposed on the northern tip of Sabine Peninsula, Melville Island (Fig. 36.1), is described. The significance of this section lies in the fact that this is one of the few locations where the Eureka Sound Formation is exposed in the western half of Sverdrup Basin (Tozer and Thorsteinsson, 1964). Therefore, age determination and structural and stratigraphic relationships of these rocks with the underlying formations are critical for the elucidation of Late Cretaceous-early Tertiary geological history of the western part of Sverdrup Basin and its relationships with the geological events of the same time span of the eastern part of Sverdrup Basin.

Preliminary studies of the structural and stratigraphic relationships of Mesozoic and Tertiary rocks in the eastern Sverdrup Basin (Balkwill, 1974; Balkwill and Bustin, 1975; Balkwill et al., 1975; Balkwill and Hopkins, 1976) resulted in recognition of three phases of the Eurekan Orogeny: (1) a phase of uplift (Maastrichtian/late Paleocene) exemplified by such features as the Princess Margaret Arch on Axel Heiberg Island and the Cornwall Arch of Amund Ringnes Island; (2) a phase of regional compression [(?)Middle Eocene/Oligocene] which produced large folds and faults in Eocene and older rocks in eastern Axel Heiberg and western Ellesmere Islands; and (3) a renewed phase of uplift with local normal faulting (Miocene/Pliocene) as exemplified along the eastern flank of Princess Margaret Arch in eastern Axel Heiberg Island, accompanied by the syntectonic deposition of the coarse clastic sediments which characterize the Beaufort Formation.

Description

About 33 m of moderately well exposed Eureka Sound Formation were measured in two closely spaced sections directly west of Colquhoun piercement dome on the northern tip of Sabine Peninsula (Fig. 36.1). Section 1 (Fig. 36.2) is 16 m thick and contains the gradational Kanguk-Eureka Sound contact near the base; the beds dip about 12 degrees westward away from the piercement dome. Section 2 (Fig. 36.2) is 23 m thick, composed entirely of Eureka Sound beds. It overlaps with and is better exposed than Section 1. The Eureka Sound beds of Section 2 are nearly horizontal and the top of the section is the present erosional surface. Stratigraphic evidence suggests that these two sections are separated by a reverse fault, probably as a result of the evaporite intrusion nearby. The base of the Eureka Sound Formation in this location was placed at the first appearance of light grey sand beds above the dark brown silty and argillaceous rock types of the underlying Kanguk Formation. The Kanguk-Eureka Sound contact is gradational and conformable, as indicated by lithological and paleontological

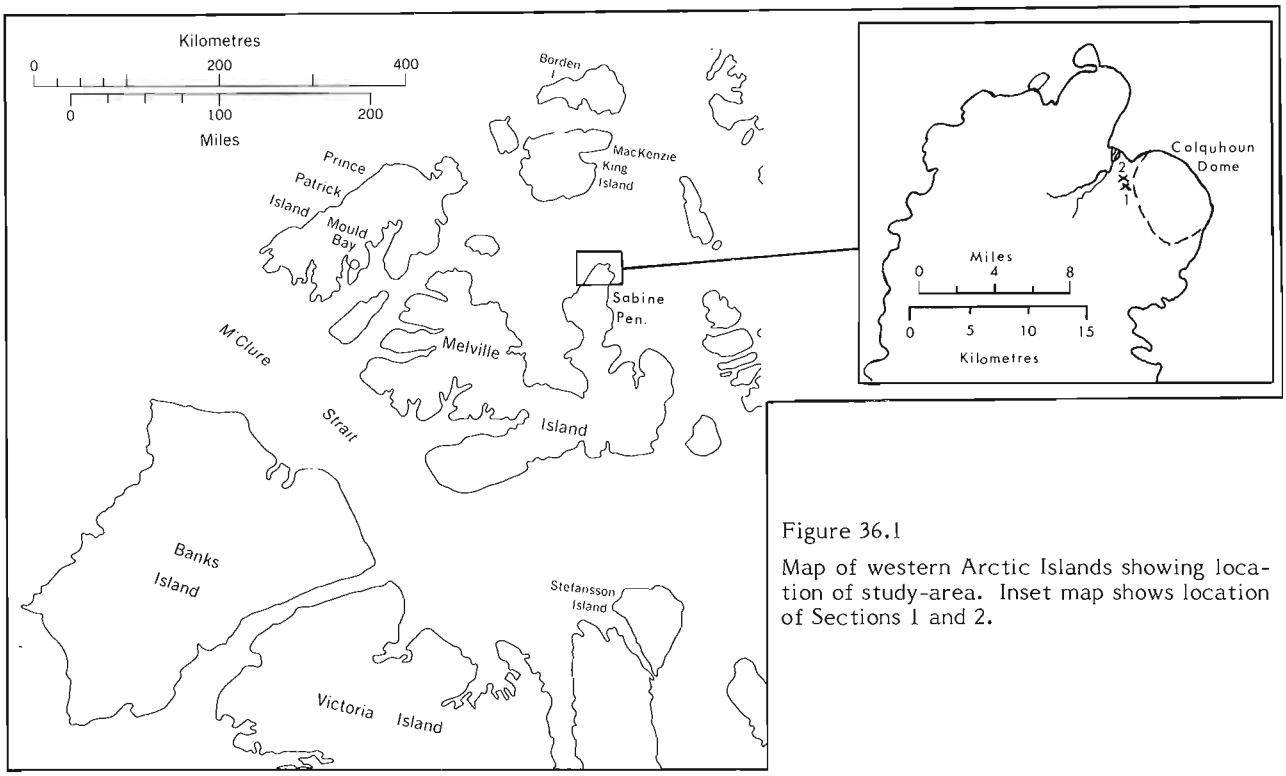

Figure 36.1

Map of western Arctic Islands showing location of study-area. Inset map shows location of Sections 1 and 2.

From: Report of Activities, Part B; Geol. Surv. Can., Paper 77-1B (1977)

evidence discussed below. For reasons of time shortage in the field, Section 1 only was sampled and detailed lithological notes were not taken (Fig. 36.2).

This exposure of Eureka Sound Formation generally represents a coarsening-upward sequence of sand, silt, and mud. The rocks of the upper part of the Kanguk Formation are generally argillaceous and of shallow-marine nature based on micropaleontological interpretations by J.H. Wall. Lithological and palynological data suggest that this sequence becomes progressively nonmarine upward. In Section 2, the Eureka Sound Formation is composed mainly of very fine to medium grained sand, except for the uppermost 3.5 m which are shale.

Friability of the silt and sand beds tends to obscure the sedimentary structures. However, the volumetrically dominant sedimentary structure observed is large-scale cross-stratification which comprises the entire thickness of two thick (6 m each) sand beds in the middle part of Section 2 (Fig. 36.2). The lower of these two beds contains ripple laminations in the top 1 m, and both beds are fining upward. The foresets of the cross-stratified beds dip southeasterly (120°). These cross-stratified beds extend the entire width of the outcrop, a distance of about 200 to 250 m. Lack of time prevented tracing the extent of the sedimentary structures along the third dimension. The remaining beds, in the lower part of Section 2, are laminated only vaguely. A carbonaceous shale-filled channel, oriented approximately NE-SW (30°), occurs near the 4 m level above the base of Section 2. This channel, scoured into the underlying very fine grained sand, contains incompletely carbonized wood and logs. Other sedimentary structures observed are organic burrows in two beds near the base of Section 2 and plant root remnants (Fig. 36.2, Sec. 2).

Sieve grain size data are shown in Figure 36.3 plotted on probability paper using quarter phi intervals. Three of the seven sand samples shown have bimodal size distribution. The sands of the Eureka Sound Formation are moderately well to moderately sorted [using Folk's (1966) terminology] and are generally angular to very angular (Power's scale) in the modal and fine grades, but generally show better rounding in the coarser grades. In some of the samples, however, it was observed that the finer sand grade, which is usually angular, also commonly contains rounded grains. Quartz makes up 90 per cent or more of the sand, whereas feldspar, dark rock fragments, accessory minerals, and muscovite constitute the remaining fraction. Carbonaceous debris is present throughout, either disseminated or concentrated in discrete laminae.

Palynology

Eleven samples were collected for palynological analysis from these two sections (see Fig. 36.2). Ten of the eleven were productive in both microspores and megaspores. The stratigraphic position and GSC locality numbers are indicated on the accompanying range chart (Fig. 36.4). Samples C-60024 and C-60030 are isolated samples taken from what was considered in the field to be the oldest exposed strata of the Eureka Sound Formation, a conclusion borne out by palynological analysis. Section 1 is represented by samples C-60020 (20) to C-60023 (23) and Section 2 by samples C-60025 (25) to C-60029 (29), inclusive.

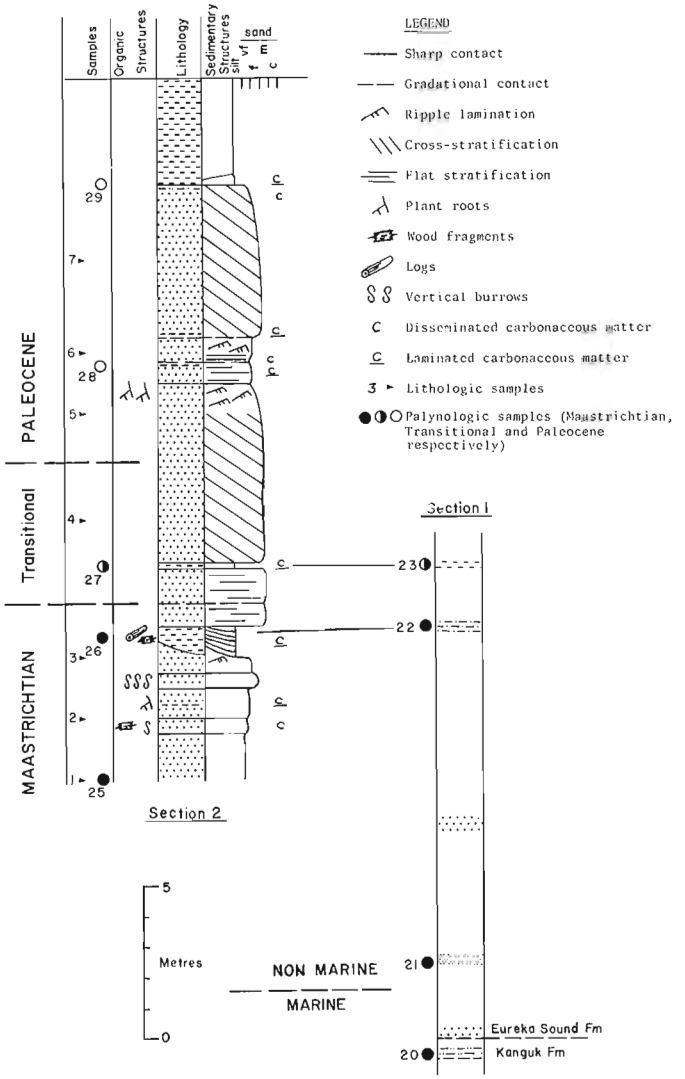

Figure 36.2. Sections 1 and 2 of the Eureka Sound Formation on Sabine Peninsula. See Figure 36.4 for GSC locality numbers of palynologic samples.

The total microflora is itemized on the microfloral list (Table 36.1), and age-significant palynomorphs are indicated on the accompanying range chart (Fig. 36.4). Two comparatively distinct groups of key palynomorphs are present, indicating a transition from Maastrichtian to Paleocene. Pollen characteristic of, and almost completely restricted to, the Maastrichtian include **Aquilapollenites, Fibulapollis mirificus, Orbiculapollis globosus, Expressipollis barbatus, E. accuratus, Azonia, Clanculatus, Wodehouseia spinata,** and **Integricorpus.** The Maastrichtian microflora appears to be common to the entire circumpolar area (see for example, Felix and Burbridge, 1973; Brattseva, 1965; Chlonova, 1961; Hopkins, unpubl. data). The second assemblage is marked by more typical Tertiary forms, especially **Alnus,** which becomes abundant near the top of Section 2. Although **Alnus** (alder) may occur sporadically in upper Maastrichtian rocks, it does not become abundant until the Paleocene. Early forms of **Pterocarya, Carya** and

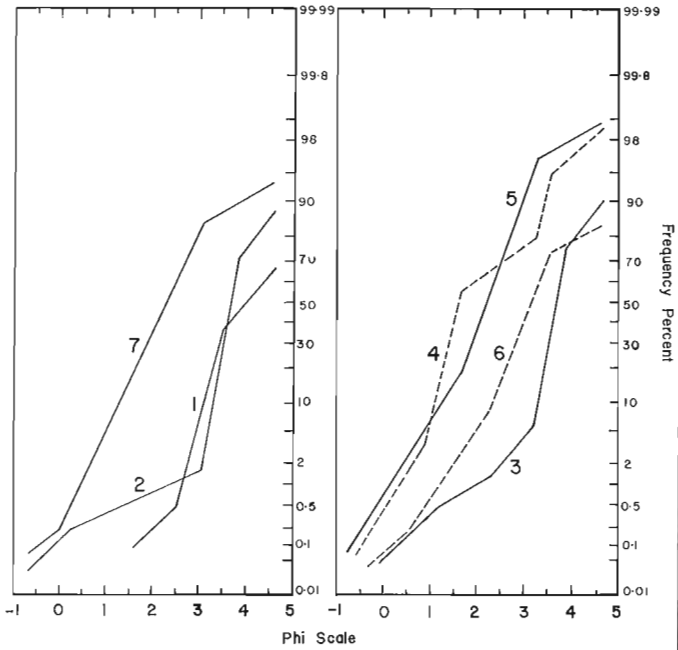

Figure 36.3. Grain-size probability plots of Eureka Sound sands of Section 2. See Figure 36.2 for stratigraphic positions of samples numbered 1 to 7.

Carpinus are present and appear to be Paleocene forms. Sample C-60023 (23) is somewhat ambiguous in that it contains some Tertiary palynomorphs and the Late Cretaceous **Orbiculapollis.** This appears to be a transition sample, occurring at the boundary between the Cretaceous and Tertiary strata. Although it is not discussed in this report, the megaspore data basically support the interpretations derived from microspore analysis (A.R. Sweet, pers. comm.).

Consequently, we can conclude only that this is a transition unit, essentially representing deposition during the latest Cretaceous and early Tertiary. The top two samples of Section 2, on the basis of both micro- and megaspores, clearly are Paleocene. Therefore, sample C-60023 (23) at the top of Section 1 would seem to be equivalent essentially to C-60027 (27).

The indicated environment of deposition is deltaic with a lowland of lakes, swamp and meandering streams. The abundance of **Sphagnum** spores, plus the excellent preservation of all pollen and spores indicates, at least locally, the presence of **Sphagnum** bogs. **Lycopodium** and **Selaginella** are both moderately common which suggest moist conditions; some of the **Lycopodium** may have been epiphytic. Representatives of the ferns such as **Osmunda** and **Laevigatosporites** occur in some places and rare spores of **Gleichenia** and **Cicatricosisporites** are present. All of these suggest a warm, damp climate.

With the exception of the Taxodiaceae, the gymnosperms are not common. **Taxodium** and/or **Glyptostrobus** are common palynomorphs, again suggesting damp and warm conditions. However, the microflora of all samples is dominated by the angiosperms. Unfortunately, more than one half of these cannot be related to modern forms and, although some are age diagnostic, they are not particularly useful environmentally.

To summarize the microspore data, the rocks from this locality are uppermost Cretaceous to lowermost Tertiary, and exemplify a rare exposure of the Cretaceous-Tertiary transition in the Sverdrup Basin. This transition, based on both lithologic and palynologic evidence, lies about 15 m above the Kanguk-Eureka Sound boundary. The depositional environment appears to be deltaic in a warm temperate to even subtropical climate. The overall climatic and environmental conditions probably were not dissimilar to those now prevailing in the Mississippi delta area.

30	24	25	26	27	28	29	20	21	22	23	
X	X	X	X	X	X	X	X	X	X	X	Inaperturopollenites sp.
							X				Cycadopites follicularis
X	X	X	X	X	X	X	X			X	Extratriporopollenites sp.
X	X	X	X			X	X	X	X	X	Osmunda sp.
X	X	X					X				Aquilapollenites spp.
X	X	X	X	X	X	X	X	X	X	X	Sphagnum spp.
X	X	X	X	X	X	X	X	X	X	X	Glyptostrobus-Taxodium
X	X	X	X	X	X	X	X	X	X	X	Lycopodium sp.
X		X	X		X		X	X			Gleicheniidites sp.
X	X	X	X		X	X	X	X		X	Lycopodiacidites sp.
							N				Fibulapollis mirificus
N	N	N	N					N	N	N	Orbiculapollis globosus
X	X	X	X		X			X	X	X	Sequoiapollenites sp.
								N			Expressipollis barbatus
N	N		N					N	N		E. accuratus
X	X	X	X		X	X		X	X	X	cf. Betula sp.
								N			Azonia sp.
								N			Clanculatus sp.
		X						X			cf. Ulmus sp.
								N	N		Aquilapollenites cf. A. attenuatus
X	X	X	X		X	X		X	X	X	Engelhardtia (= Momipites sp.)
X	X	X	X		X	X			X		Podocarpus sp.
	N	N							N		Wodehouseia spinata
			N								W. fimbriata
		N							N		Integricorpus sp.
		O			O	O				O	Pterocarya sp.
					O	O				O	Alnus sp.
		X				X				X	Cicatricosisporites sp.
					O					O	Carya cf. C. paleocenica
					O	O				O	Carpinus cf. C. subtriangula
										X	Selaginella sp.
					X	X				X	Ericaceae
										X	Corylus sp.
										X	Typha sp.
				X	X	X				X	Paraalnipollenites sp.
	X	X	X		X	X					Schizosporis cf. S. scabratus
			X								Castanea-type
					X	X					Tsuga sp.

X Palynomorph present

N Characteristic Maastrichtian palynomorph

O Characteristic Paleocene palynomorph

Geological Survey Locality Numbers

20 = C-60020
21 = C-60021
22 = C-60022
23 = C-60023
24 = C-60024
25 = C-60025
26 = C-60026
27 = C-60027
28 = C-60028
29 = C-60029
30 = C-60030

Figure 36.4. Stratigraphic distribution of selected palynomorphs.

Table 36.1

Microflora of Eureka Sound Formation, northern Sabine Peninsula

Bryophyta	Sphagnaceae	**Sphagnum** spp.
Lycopodophyta	Lycopodiaceae	**Lycopodium** sp. **Lycopodiacidites** sp.
	Selaginellaceae	**Selaginella** sp.
Pterophyta	Osmundaceae	**Osmunda** sp.
	Schizaeaceae	**Cicatricosisporites** sp.
	Gleicheniaceae	**Gleicheniidites** sp.
	Polypodiaceae-Dennstaedtiaceae	**Laevigatosporites** sp. **Deltoidospora** sp. verrucate monolete spores
	Incertae sedis	**Undulatisporites** sp.
Cycadophyta	Cycadaceae	**Cycadopites follicularis** Wilson and Webster
Coniferophyta	Pinaceae	**Pinus** sp. **Tsuga** sp.
	Taxodiaceae	**Inaperturopollenites** sp. **Glyptostrobus** sp. **Taxodium** sp. **Sequoia pollenites** cf. **paleocenicus** Stanley
	Podocarpaceae	**Podocarpus** sp.
Anthophyta	Cyperaceae	Cyperaceae
	Liliaceae	**Liliacidites** sp.
	Typhaceae	**Typha** sp.
	Betulaceae	**Alnus** sp. **Paraalnipollenites** sp. cf. **Betula** sp. **Carpinus** cf. **C. triangula** Stanley cf. **Corylus** sp.
	Fagaceae	**Castanea** sp.
Anthophyta	Juglandaceae	**Carya** cf. **C. paleocenica** Stanley **Engelhardtia (Momipites-type)** sp. **Pterocarya** sp.
	Ulmaceae	?**Ulmus** sp.
	Ericaceae	Ericaceae
	Dicotyledonae – **Incertae sedis**	**Extratriporopollenites** sp. **Aquilapollenites** cf. **A. attenuatus** Funkhouser **Aquilapollenites** spp. **Fibulapollis mirificus** (Chlonova) Chlonova **Expressipollis accuratus** Chlonova E. **barbatus** Chlonova **Orbiculapollis globosus** Chlonova **Azonia** sp. **Clanculatus** sp. **Wodehouseia spinata** Stanley **Integricorpus** sp. (McIntyre, 1974, Pl. 21, figs. 1-3) **Schizosporis** cf. **S. scabratus** Stanley **Tricolpites** sp. **Triporopollenites** spp. **Tricolporopollenites** spp.

Interpretation

The overall coarsening upward and the disappearance upward of marine influence (the latter assumption based on paleontological evidence) suggest that the sedimentary regime of the Eureka Sound Formation in this locality was that of prograding, shallowing-upward environments.

Comparison of the grain size probability curves (Fig. 36.3) with those published by Visher (1969) and Glaister and Nelson (1974) suggests that the thick, cross-stratified sand beds of the present study-area were formed in deltaic distributary channel environments, probably as laterally migrating sand waves.

The above lithological and paleontological evidence suggests that these sediments were deposited as a fluvial-dominated delta (see deltaic classification of Galloway, 1975) prograding, probably in a northeasterly direction, into a marine basin where waves and tidal current influence were too weak to keep up with the rapid rate of fluvial sediment influx and to sort and round the sand grains. Diagnosis of the specific deltaic subenvironments of the study sequence is difficult due to lack of more detailed field observations. Texture (bimodal grain size and shape) of the sand suggests a multi-source rock provenance.

Palynological evidence suggests that deposition of rocks of the Eureka Sound Formation, especially the upper part, took place largely in lowlands of lakes, swamps and streams in warm, humid temperate to subtropical climate.

Conclusions

The Cretaceous-Tertiary transition in northern Sabine Peninsula is gradational within the detrital, arenaceous sequence of the Eureka Sound Formation, about 15 m above its base. Deposition was rapid and continuous as a fluvially dominated deltaic sequence prograding into a marine basin of low wave and tidal current energy under humid and warm temperate to subtropical climate. The gradual change of sedimentary regime from marine Kanguk to the nonmarine Eureka Sound marks a period of gradual uplift of the source area. This period of uplift (Maastrichtian in age) may be synchronous with the late Maastrichtian/late Paleocene "phase of local uplift" (Balkwill et al., 1975) in the eastern part of the Sverdrup Basin.

References

Balkwill, H.R.
1974: Structure and tectonics of Cornwall Arch, Amund Ringnes and Cornwall Islands, Arctic Archipelago; in Canadian Arctic Geology, J.D. Aitken and D.J. Glass, eds., Proceedings Volume, 1973 Symposium of the Geol. Assoc. Can./Can. Soc. Petrol. Geologists, p. 39-62.

Balkwill, H.R. and Bustin, R.M.
1975: Stratigraphic and structural studies, central Ellesmere Island and eastern Axel Heiberg Island, District of Franklin; in Report of Activities, Part A, Geol. Surv. Can., Paper 75-1A, p. 513-517.

Balkwill, H.R., Bustin, R.M., and Hopkins, W.S., Jr.
1975: Eureka Sound Formation at Flat Sound, Axel Heiberg Island, and chronology of the Eurekan Orogeny; in Report of Activities, Part B, Geol. Surv. Can., Paper 75-1B, p. 205-207.

Balkwill, H.R. and Hopkins, W.S., Jr.
1976: Cretaceous stratigraphy, Hoodoo Dome, Ellef Ringnes Island, District of Franklin; in Report of Activities, Part B, Geol. Surv. Can., Paper 76-1B, p. 329-334.

Brattseva, G.M.
1965: Pollen and spores of the Maastrichtian deposits of the Far East; Akad. Nauk SSSR, Geol. Inst., Tr., no. 129.

Chlonova, A.F.
1961: Spores and pollen of the upper half of the Upper Cretaceous in the eastern part of the western Siberian Lowland; Akad. Nauk SSSR, Geol. Geofiz. Inst. Sib. Otd., Tr., v. 7.

Felix, C.J. and Burbridge, P.P.
1973: A Maastrichtian age microflora from Arctic Canada; Geoscience and Man., v. 7, p. 1-29.

Folk, R.L.
1966: A review of grain-size parameters; Sedimentology, v. 6, p. 73-93.

Galloway, W.E.
1975: Process framework for describing the morphological and stratigraphic evolution of deltaic depositional systems; in Deltas, Models for Exploration, 2nd ed., M.L. Broussard, ed.; Houston Geol. Soc., p. 87-98.

Glaister, R.P. and Nelson, H.W.
1974: Grain-size distributions, an aid in facies identification; Bull. Can. Petrol. Geol., v. 22, p. 203-240.

Leffingwell, H.A.
1970: Palynology of the Lance (Late Cretaceous) and Fort Union (Paleocene) Formations of the type Lance area, Wyoming; Geol. Soc. Am., Spec. Paper 127, p. 1-64.

Stanley, E.A.
1965: Upper Cretaceous and Paleocene plant microfossils and Paleocene dinoflagellates and hystrichosphaerids from northwestern South Dakota; Bull. Am. Paleont., v. 49, p. 179-384.

Tozer, E.T. and Thorsteinsson, R.
1964: Western Queen Elizabeth Islands, Arctic Archipelago; Geol. Surv. Can., Mem. 332.

Visher, G.S.
1969: Grain size distributions and depositional processes; J. Sediment. Petrol., v. 39, p. 1074-1106.

37. SOME OBSERVATIONS ON THE HORN PLATEAU, DISTRICT OF MACKENZIE

Projects 710011 and 710033

G.K. Williams
Institute of Sedimentary and Petroleum Geology, Calgary

During the past few years, several wells have been drilled on and near the Horn Plateau. In this report, by means of several maps and cross-sections, the writer summarizes the subsurface information and integrates it with surface data.

Physiography

The plateau rises about 1500 feet (450 m) above the surrounding plain. It has a streamlined form (Fig. 37.2) with an irregularly bowl-shaped surface. The plateau is bounded by a steep scarp on the south, more moderate scarps on the east and north, and by a gentle slope on the west (paraphrased from Craig, 1965).

Regional Geological Setting

The plateau lies near the eastern margin of the Interior Plains (Fig. 37.1). Regional dip is to the southwest. The plains from which the plateau rises are underlain by Upper Devonian shales with a veneer, a few tens of feet thick, of glacial drift. The core of the plateau is an outlier of Lower Cretaceous shale capped, along part of the south rim, by a few tens of feet of sandstone. The sandstone is probably of Late Cretaceous age.

Outcrop Summary

There are only three small areas of outcrop; the locations of these are shown on Figure 37.3.

At area 1, first visited by Whittaker (1922, p. 54B), about 80 feet (24 m) of dark fissile shale outcrop at an elevation between 1500 and 1600 feet (450 and 480 m) (Douglas and Norris, 1960, p. 20). The stratigraphic position of this outcrop is shown on Figure 37.6.

Outcrop 2, on the north side of the plateau (Douglas and Norris, 1960), consists of black pyritic shale with a 10-inch (25.4 cm) bed of argillaceous limestone. This outcrop, at an elevation of about 1300 feet (390 m), is probably the lower of the two radioactive shale zones (Figs. 37.4, 37.8).

Area 3, on the south rim of the plateau, was examined by Whittaker (1923, p. 99B). Whittaker described scattered exposures of rather coarse, white to rusty-yellow, friable sandstone, and common large ironstone concretions and partings of soft black shale. He named this the Rabbitskin Sandstone. The stratigraphic position of this outcrop is shown on Figure 37.7.

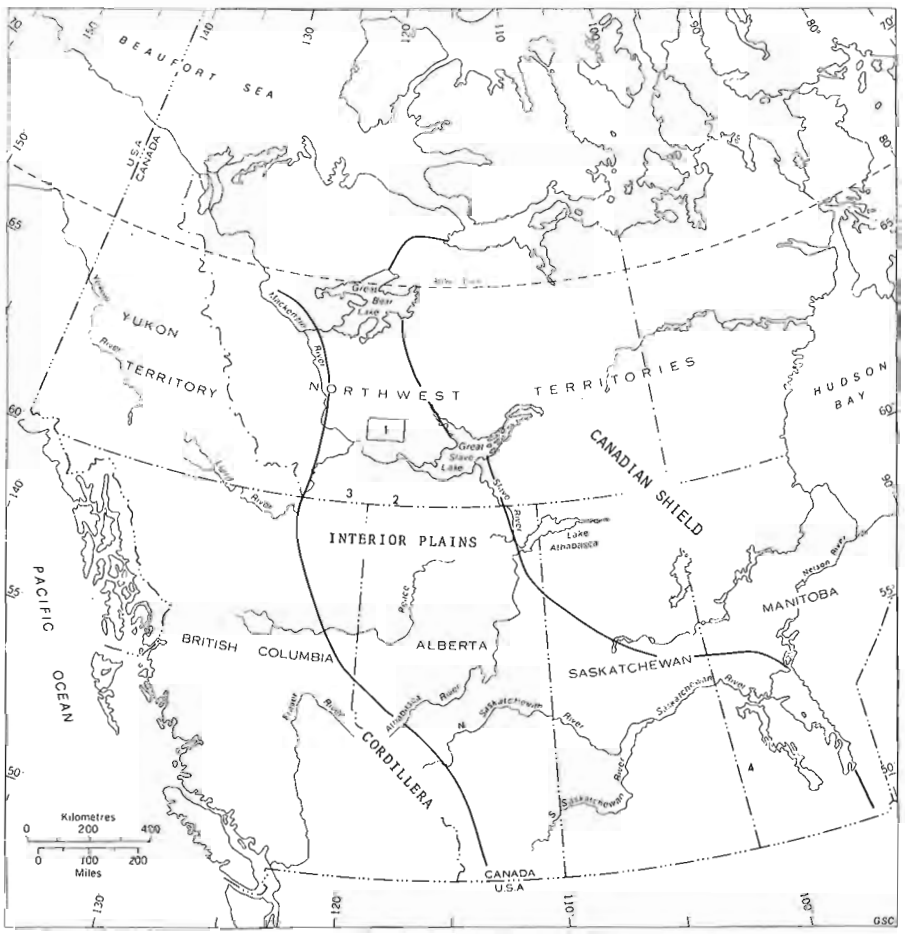

Figure 37.1. Index map.

1. Horn Plateau
2. Cameron Hills
3. Trout Lake Highlands
4. Duck Mountain

No useful fossils have been found in any of the outcrops. It is assumed that the shales are of Early Cretaceous age, equivalent to the Fort St. John Group, and that the sandstone probably is of Late Cretaceous age, equivalent to the Dunvegan Formation (Douglas, 1959; Douglas and Norris, 1960; Stott, 1960).

Cretaceous Lithology (subsurface)

The Rabbitskin Sandstone was not encountered in any of the wells.

Well samples, although of poor quality, indicate that the Lower Cretaceous shales are medium grey, rarely dark grey, variably bentonitic, with traces of glauconite, silt, sand, ironstone, fish remains and a coal-like material which is probably bitumen. Fish scales and bitumen seem to be more common in the radioactive zones. Two radioactive zones are present in well P-02 (Fig. 37.8). The log character of the Cretaceous section of the Horn Plateau wells is similar to that of wells farther south. Although detailed correlation is not possible, this similarity tends to confirm an Early Cretaceous age.

From: Report of Activities, Part B; Geol. Surv. Can., Paper 77-1B (1977)

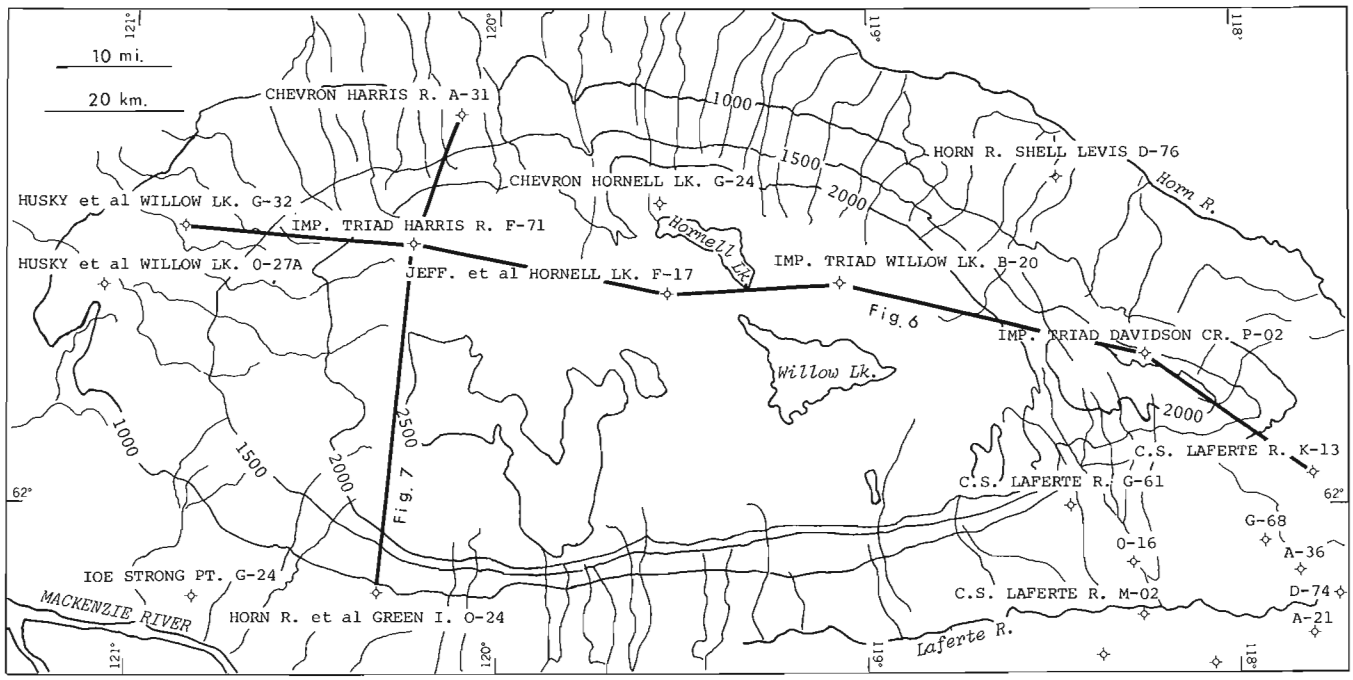

Figure 37.2. Main topographic features (contour interval 500 ft.), and well names, Horn Plateau.

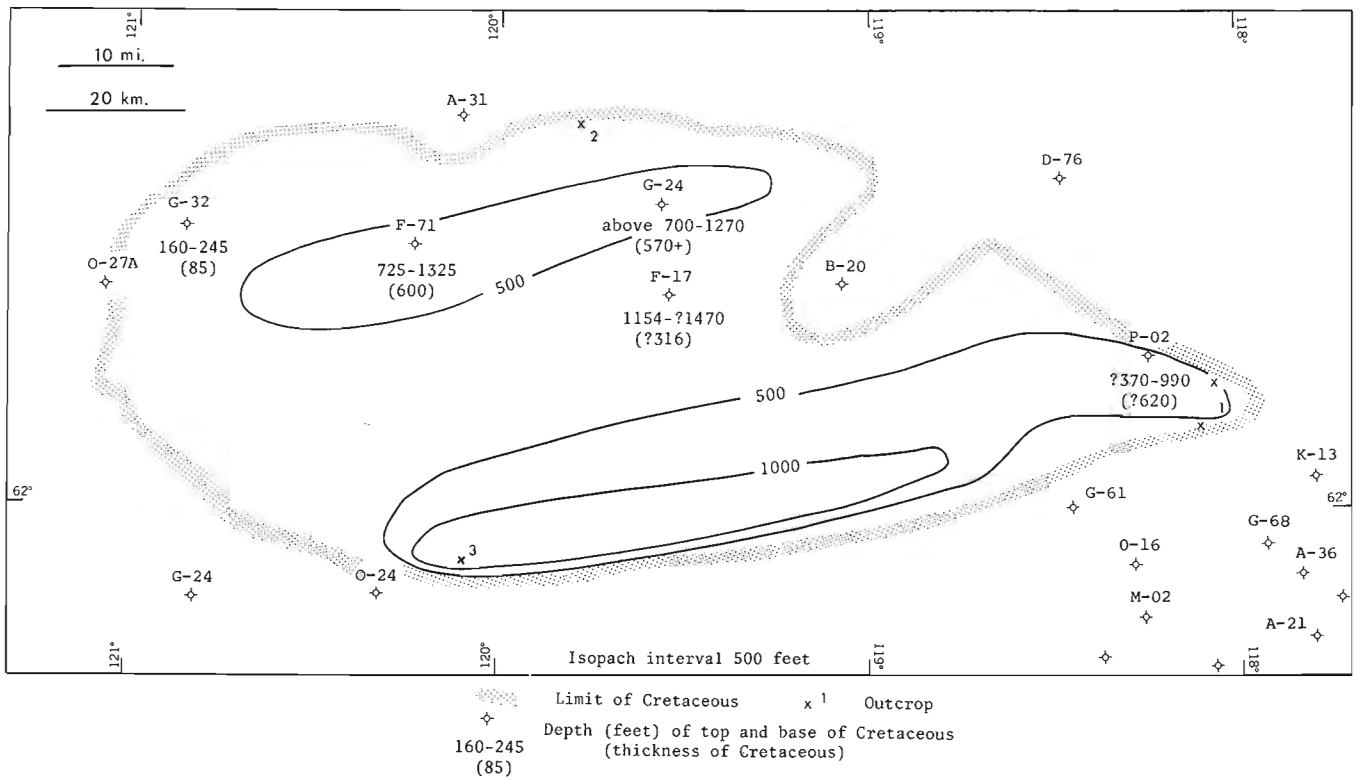

Figure 37.3. Cretaceous distribution and thickness, Horn Plateau. The isopach interval is 500 feet.

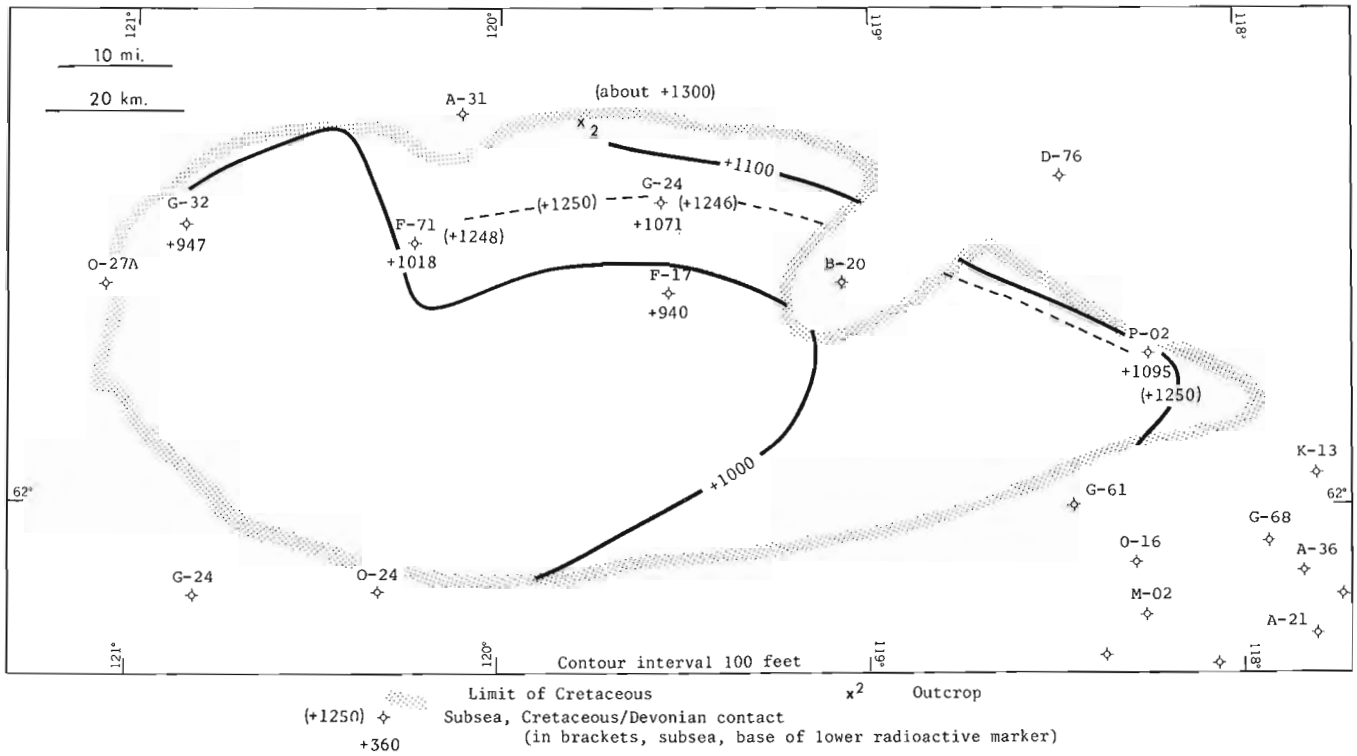

Figure 37.4. Structure, base of Cretaceous, Horn Plateau. The contour interval is 100 feet.

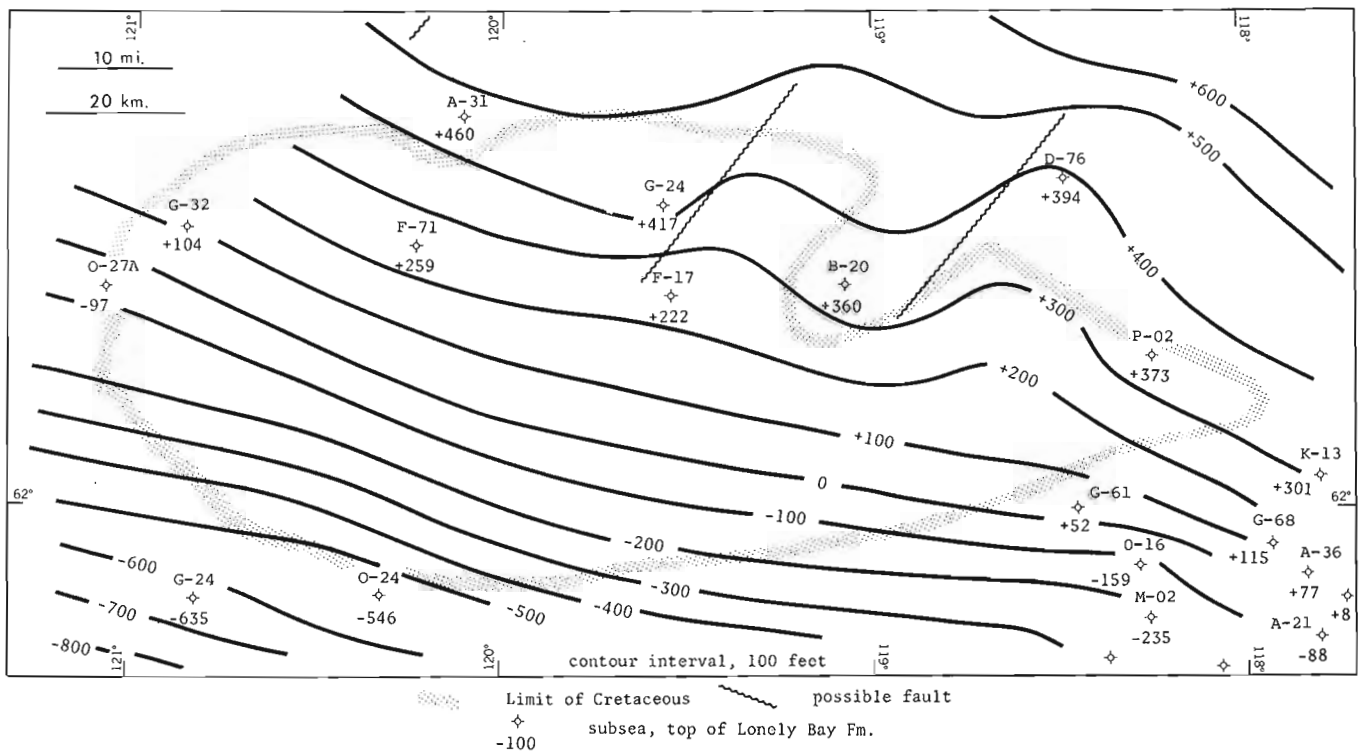

Figure 37.5. Structure, top of Lonely Bay Formation, Horn Plateau. The contour interval is 100 feet.

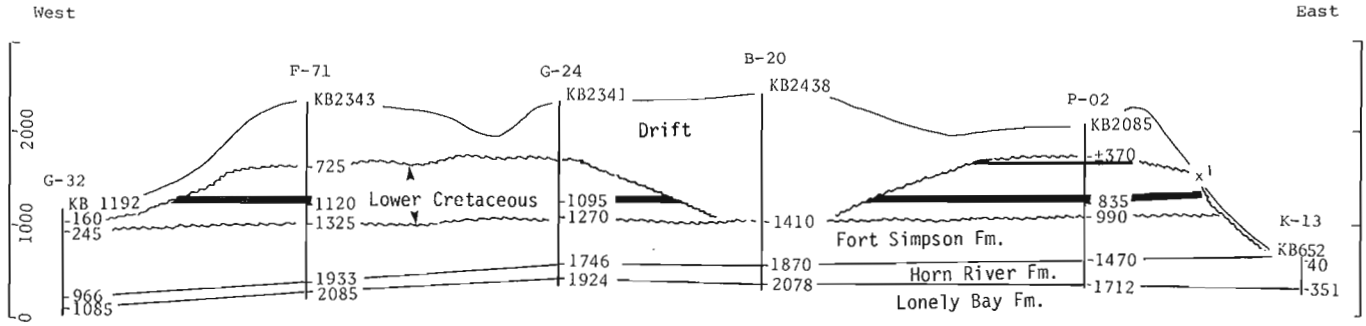

Figure 37.6 East-west cross-section, Horn Plateau. Datum: sea level.

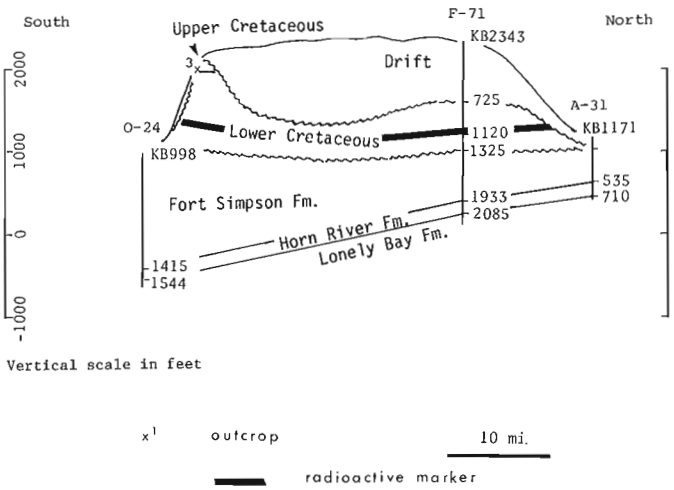

Figure 37.7 North-south cross-section, Horn Plateau. Datum: sea leve.

Development of the Plateau

There is not any structural reason, apparently, for the existence of the plateau (Fig. 37.5). There is a suggestion of a slight anomaly at the pre-Cretaceous erosion surface (Fig. 37.4) but this is an erosional, not a tectonic, feature. If the regional tilt in Figure 37.5 was removed, Figure 37.4 would display a very slight topographic terrace south of the plateau.

Marine Lower Cretaceous shale once covered the entire area. If the Rabbitskin Sandstone is indeed Upper Cretaceous, the total thickness of the Lower Cretaceous is in the order of 1000 feet (300 m) (Figs. 37.3, 37.7). This is thinner than would be expected from regional isopachs (Shell Oil Company Exploration Department, Houston, Texas, 1975; see map: Cretaceous unit II Isopachs). The presence of radioactive shale zones suggest that, through part of Early Cretaceous time, this area was sediment-starved. The topographic terrace, mentioned above, may have some bearing on the deposition or preservation of the Rabbitskin Sandstone.

One can speculate that the ancestral Horn Plateau, i.e. in preglacial time, was similar in shape and relief to the present plateau. It was probably a sandstone-capped mesa, a product of post-Cretaceous erosion. Pleistocene ice erosion almost obliterated this mesa, leaving only a part of the southern rim intact (Fig. 37.3). The sandstone cap was removed almost entirely and a deep valley was gouged through the ancestral plateau (Fig. 37.3). The resulting topography was later buried in thick drift; for some reason the ice-created depressions became Pleistocene depocentres.

Although much of the foregoing is speculative, the presence of thick drift (up to 1400 ft. (420 m)) and high pre-drift relief is well documented (Fig. 37.8). A somewhat comparable situation occurs in other uplands: the Cameron Hills and Trout Lake Highlands near the Alberta-Northwest Territories boundary (Fig. 37.1) and areas such as Duck Mountain in Manitoba (Klassen et al., 1970).

Some Questions

What are the conditions of ice-age sedimentation that lead to the deposition of such thick drift? Did preglacial hills divert the erosive power but encourage the depositional power of glaciers, or did the hills survive because some other factor so influenced the glaciers? How much of this unusual drift thickness is a result of bulldozing by successive ice sheets?

Why is the Lower Cretaceous section so thin – onlap over a broad topographic high, starved sedimentation in a basin deep, or erosion at the top? Is the Rabbitskin Sandstone Upper Cretaceous? It lies over 100 miles (161 km) northeast of the Dunvegan delta's depocentre – is it reasonable to consider it as part of that delta?

Perhaps students of the Pleistocene know the answers to the first questions. Possibly a micropaleontological study of available well and surface samples will answer some of the questions on Cretaceous history. The affinities of the Rabbitskin Sandstone are likely to remain conjectural.

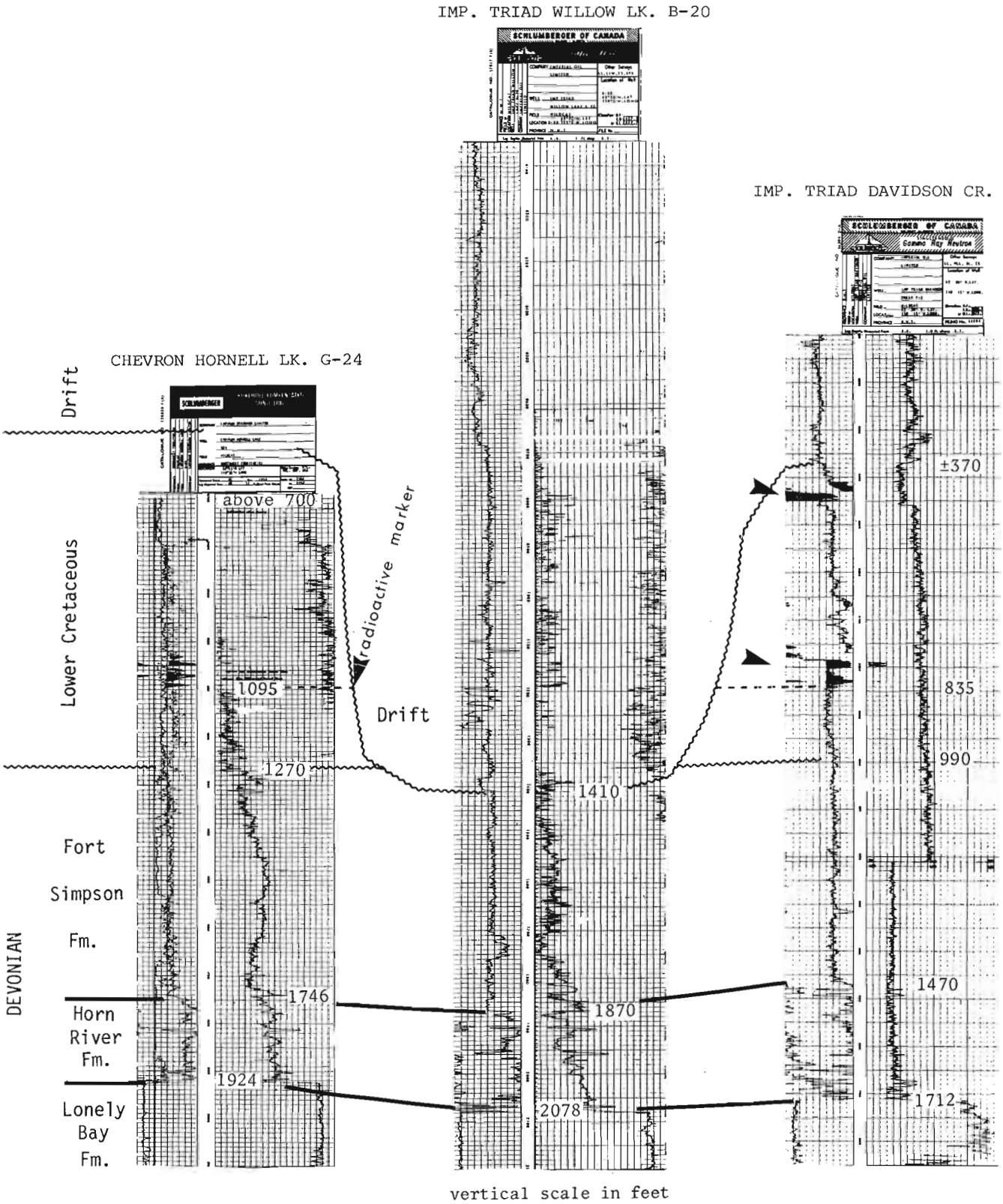

Figure 37.8. Gamma log evidence for a deep drift-filled channel, northern Horn Plateau. Datum: sea level. Vertical scale in feet.

References

Craig, B.G.
1965: Glacial Lake McConnell, and the surficial geology of parts of Slave River and Redstone River map-area, District of Mackenzie; Geol. Surv. Can., Bull. 122.

Douglas, R.J.W.
1959: Great Slave and Trout River map-areas, Northwest Territories; Geol. Surv. Can., Paper 58-11.

Douglas, R.J.W. and Norris, A.W.
1960: Horn River map-area, Northwest Territories; Geol. Surv. Can., Paper 59-11.

Klassen, R.W., Wyder, J.E., and Bannatyne, B.B.
1970: Bedrock topography and geology of southern Manitoba; Geol. Surv. Can., Paper 70-51.

Shell Oil Company Exploration Department, Houston, Texas
1975: Stratigraphic atlas, north and central America.

Stott, D.F.
1960: Cretaceous rocks in the region of Liard and Mackenzie Rivers, Northwest Territories; Geol. Surv. Can., Bull. 63.

Whittaker, E.J.
1922: Mackenzie River district between Great Slave Lake and Simpson; Geol. Surv. Can., Sum. Rept. 1921, pt. B, p. 45-55.

1923: Mackenzie River district between Providence and Simpson; Geol. Surv. Can., Sum. Rept. 1922, pt. B, p. 88-100.

REMANENT MAGNETISM OF AN ULTRAMAFIC FLOW FROM MUNRO TOWNSHIP, ONTARIO

Project 730160

E.J. Schwarz
Regional and Economic Geology Division

In the course of other field work ten oriented drill cores were obtained from an ultramafic (komatiite) flow west-northwest of Munro Lake to investigate its potential for paleomagnetic study. The outcrop (80°10'W; 48°35'N) is well known (Pyke et al., 1973) and consists of a large number of subvertical flows. Two 2.5 by 2.5 cm cylindrical specimens were cut from each core and the stability of the remanent magnetization of each specimen was tested, using alternating field (AF) demagnetization. Additional specimens were cut for thermal demagnetization experiments.

The intensity of the natural remanent magnetization (NRM) is in the 10^{-3} emu/cc range. The north-seeking NRM directions point upwards and form a distribution streaked towards east-southeast. Intensity is decreased strongly during stepwise AF demagnetization (Fig. 38.1A). Directions were well grouped after the 200 and 300 oe treatment, but tended to scatter after treatment in higher fields up to 500 oe (Fig. 38.1B).

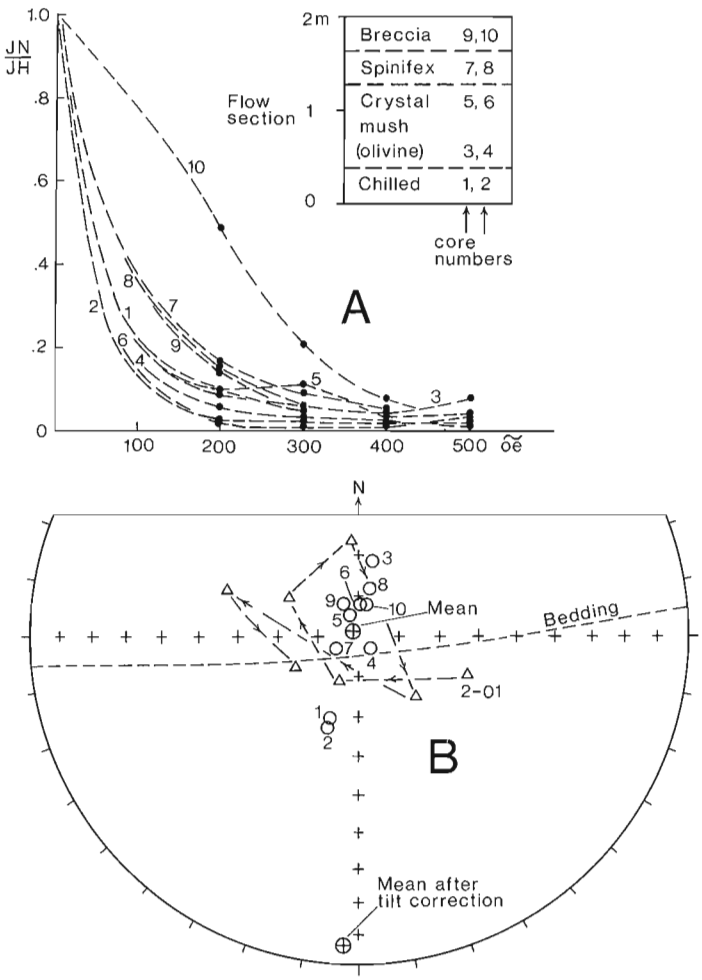

Figure 38.1A. Effect of stepwise AF demagnetization in fields up to 500 oersteds. $\frac{JN}{JH}$ indicates relative intensity.

B. Circles are equal area stereographic projections of north-seeking directions after cleaning at 200 oe. Triangles show directional changes of sample 1 from core 2 during step cleaning. Mean directions after cleaning at 200 oe are shown before and after bedding tilt correction. Note that all north-seeking directions are up.

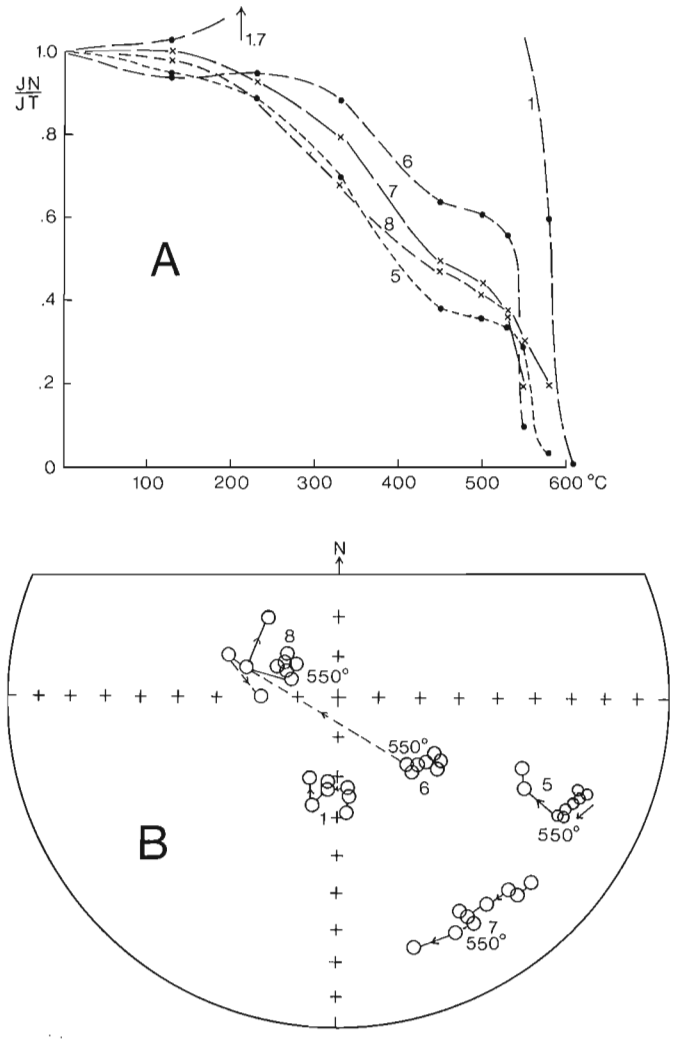

Figure 38.2. Results obtained by thermal step-cleaning one specimen from each of five cores. Symbols as in Fig. 38.1.

From: Report of Activities, Part B; Geol. Surv. Can., Paper 77-1B (1977)

During thermal demagnetization intensities decreased in two steps. The first drop took place between 250° and 450°C and accounted for about half of the NRM intensity. The second drop took place in a narrow range from 500° to 570°C (Fig. 38.2A). The thermal change of the saturation magnetization shows the presence of only one magnetic compound, almost pure magnetite. The two blocking temperature ranges may be explained by the presence of two distinct ranges of grain sizes of magnetite in most of the cores, which may correspond to two different generations of magnetite. The remanent magnetization does not show a well-defined end point direction similar to that obtained by AF demagnetization (Fig. 38.2B); however, some movement towards the AF direction was observed during the thermal cleaning. The specimen directions after heating are also more scattered than directions obtained after AF treatment in 200 oe.

The core directions are best grouped after treatment in 200 and 300 oe AF. The 200 oe treatment yields an average direction of Declination (D) = 3.4°, Inclination (I) = -88°, α_{95} = 8°. This direction is D = 183°, I = 6° after correction for tilt of the flows, which would apply if the magnetization is prefolding. The results suggest that the flows possess a stable magnetization carried by multidomain magnetite which is worth being investigated further for paleomagnetic purposes.

Guidance in the field by Mr. Howard Lovell, Ontario Department of Mines geologist, is greatly appreciated.

Reference

Pyke, D.R., Naldrett, A.J., and Eckstrand, O.R.
1973: Archean ultramafic flows in Munro Township, Ontario; Geol. Soc. Am. Bull., v. 84, p. 955-974.

39. URE-3 (URANIUM RESOURCE EVALUATION FILE) – A DATA BASE FOR URANIUM RESOURCE EVALUATION

Project 750010

N. Prasad
Regional and Economic Geology Division

URE-3 is a computer-processable data file for the evaluation of uranium resources. As work on this file is still in progress, this report contains the concepts and description of the proposed data base. The data on one area (Makkovik[1] in Labrador) have been entered in the file and coding of data for other areas is in preparation. The file when complete will represent, it is hoped, all the uraniferous areas in Canada and will have about 500 records. An overview of URE-3 is given by Ruzicka (1976).

The selection of data items (Appendix) was made in consultation with the scientists of the Uranium Resource Evaluation Section. Significant contributions and discussions were made by L.P. Tremblay, V. Ruzicka, R.T. Bell, and J.Y.H. Rimsaite.

In resource assessment a common approach is to compare known areas with unknown areas (United States Atomic Energy Commission, 1973). Many computer based files on mineral deposit data cannot easily be used for resource assessment of areas. This is because they are made to meet other objectives or are not flexible enough to deal with the concept of areas. URE-3 file is designed to deal with uraniferous areas in a systematic way (see Fig. 39.1). A unit subdivision is a 'unit record' of the file and by definition may represent an area as well as a uranium occurrence. On the basis of this principle the URE-3 file may be considered as unique with respect to other mineral deposit files, e.g. CANMINDEX (Picklyk, 1976), MINDEP (Wynne-Edwards et al., 1976), MOLYFILE (Prasad et al., 1974). The latter strictly consider a mineral occurrence as a unit record, which may be represented as a point on a map.

Since the objective of building the URE-3 file is to assist in the estimation of resources of specific areas, the areas are defined and outlined in a systematic way. The

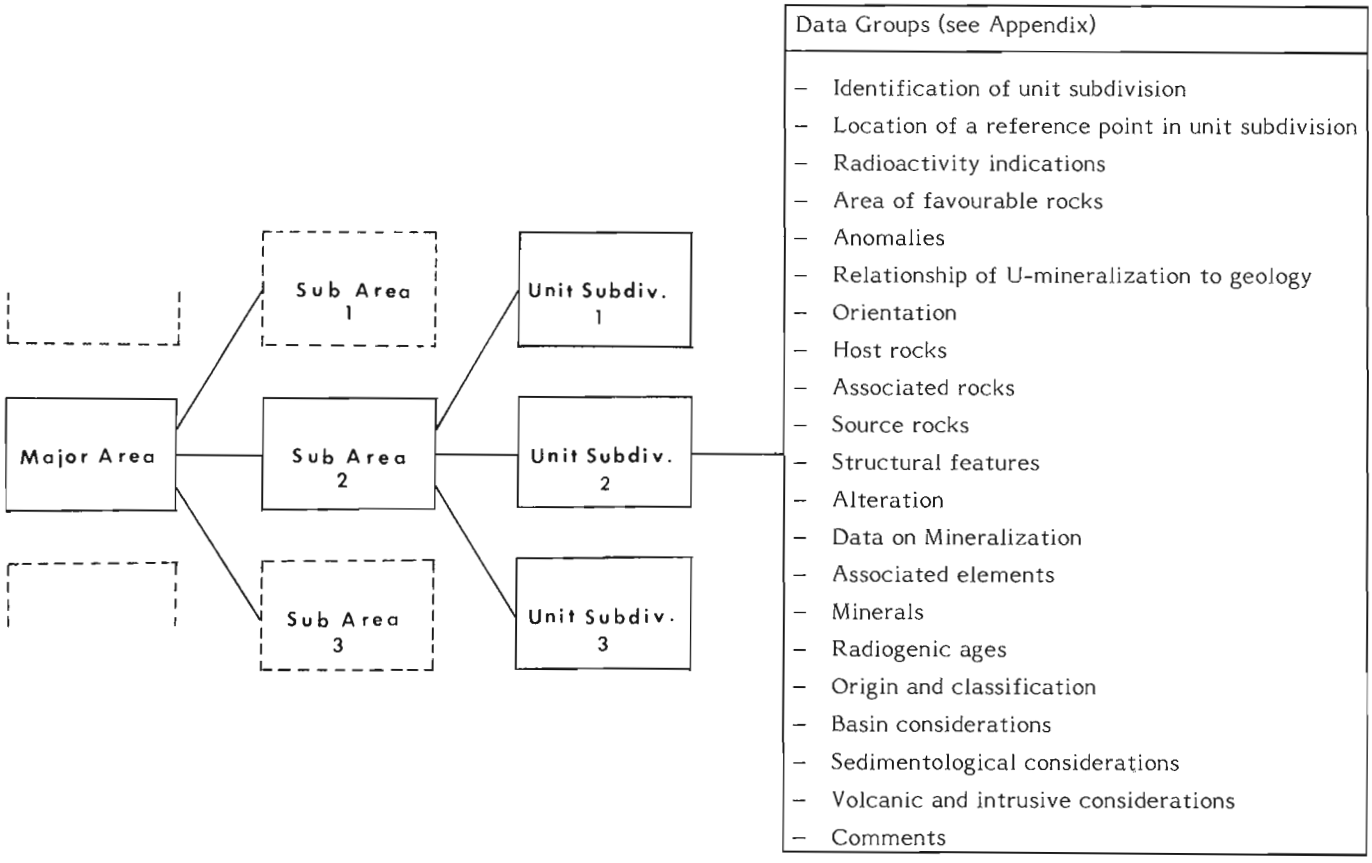

Figure 39.1. Division of an area into smaller logical units preceding the coding in URE-3 file. Each unit subdivision may contain data which can be grouped in 'data groups' listed on the right side.

[1] Compilation and coding of data in this area were done by J.A. Kerswill.

From: Report of Activities, Part B;
Geol. Surv. Can., Paper 77-1B (1977)

delineation of areas is a critical step and has to precede the data entry in the coding sheets. Definitions of the heirarchical terms for areas are:

Major areas – These broad areas are based on known uranium mineralization and/or favourable geological environment. Examples: Makkovik area, Wollaston Lake fold belt, and the southern part of Canadian Cordillera. Major areas are outlined on 1:5 000 000 scale map of Canada.

Subareas – Subdivision of a major area is based on metallogenic criteria. Each type of uranium occurrence in a major area would have at least one corresponding subarea. Subareas need not be geographically continuous. They are the working blocks for which resources will be calculated. For example, the Makkovik area has two important subareas: the Kitts belt and the Michelin belt.

Unit subdivision – The basic principle behind a unit subdivision is that it is geologically a homogeneous unit. Presence of favourable host rocks and quality and quantity of exploration data available are some of the criteria for defining a unit subdivision. Subareas and unit subdivisions may be outlined on 1:250 000 or larger scale maps. The dimensions of unit subdivision may be highly variable, depending on the available data. Thus, (i) a single developed prospect or a mine where grades or tonnages are known, (ii) an area containing several radioactive occurrences or (iii) an area with favourable geology but no known uranium occurrences, could each be an individual unit subdivision. Examples: Kitts deposit, Nash Prospect, Inda prospect in Kitts belt-subarea.

The data are entered on specially designed coding sheets which consist of ten eighty-column computer cards for each unit subdivision. The smallest unit of record is called a 'data item'. There are 237 data items which constitute a 'unit record'. However all the data would not always be known to code 237 data items and hence there will be many blank fields. In areas of continuing exploration and development work some of these blanks could be filled later. The related data items of a geological feature, e.g. alteration, occur together in the file and may be considered as links of a chain (see Appendix). These data items are collectively called 'data group'. The Appendix lists all the data items and corresponding data groups contained in URE-3 file data base. The data base management system used is MARS VI (Multi Access Retrieval System) version 2.1, available on CONTROL DATA's CYBER-74 hardware. A preprocessor program is used before loading data in MARS. The reasons for using MARS – besides its being available at our departmental Computer Science Centre – are its simple structure, efficient retrieval-update features and ease of subsetting data out of MARS for other statistical and application programs.

Data Acquisition – Data are acquired from federal and provincial government reports, geological and mining publications, Atomic Energy Control Board reports, mining company reports and from field observations by the staff of Uranium Resource Evaluation Section. Location of uranium occurrences and deposits will eventually be derived from Geological Survey of Canada's computer-based CANMINDEX file (Picklyk, 1976). Uranium data for CANMINDEX file are currently being coded in the Uranium Resource Evaluation Section.

References

Picklyk, D.D.
1976: An index to Canadian Mineral Occurrences – Preliminary consideration; Computers and Geosciences, v. 2, p. 317-319.

Prasad, N., Kirkham, R.V., and Vokes, F.
1974: MOLYFILE; Geol. Surv. Can., Paper 74-60, p. 45-48.

Ruzicka, V.
1976: Uranium resources evaluation model as an exploration tool; IAEA/NEA Symp. on Explor. of uranium ore deposits, March/April, 1976, Vienna, Austria.

United States Atomic Energy Commission (USAEC)
1973: Nuclear fuel resource evaluation, concepts, uses and limitations, p. 17.

Wynne-Edwards, H.R. and Sinclair, A.J.
1976: MINDEP, Computer-processable files of mineral deposits information; Western Miner, February 1976, p. 10-18.

APPENDIX

A list of the 'data items' and corresponding 'data groups' contained in a 'unit record' (unit subdivision) of URE-3 file. The data groups listed here are the same as shown in Figure 39.1.

Data group	Data item
Identification of unit subdivision	Major area: number, area, volume; sub area: number, area, volume; unit subdivision: number, area, units of area, units of volume, unit subdivision as per cent of sub area; political province, geological province.
Location of a reference point	NTS number, latitude, longitude, description of a reference point.
Radioactivity indicators	U-orebodies, radioactive outcrops, radioactive boulders, drilling, predominant type of U-mineralization, other types of U-mineralization, spatial relationship of U-occurrences, distribution of U-occurrences.
Favourable area	Area of favourable rocks, units.
Anomalies	Geophysical anomalies: airborne-total counts, airborne-U, ground-total counts, ground-U; Geochemical anomalies: U-in water, Radon in water, U-in soil, Radon in soil, U-in lake sediments, U-in rock; Non-radiometric anomalies; Geobotanical anomalies.
Relationship of U-mineralization with geology	Relationship of mineralization with: -structure, -alteration, -metamorphism, -carbon and -hydrocarbon.
Orientation	Foliation: -dip, -strike geologic formation: -dip, -strike.
Host rocks or host rocks in 'basement'	Basement/cover distinction, major class, genetic class, rock names (up to 4), stratigraphic age -lower, -upper.
Host rocks in 'cover'	Major class, genetic class, rock names (up to 3), stratigraphic age -lower, -upper.
Source rocks	Major class, genetic class, rock names (up to 2), stratigraphic age -lower, -upper.
Structural features	Number of major fault-sets, faults -strike, -dip (up to 3 sets) subsidiary faults, folding, periods of folding, unconformity, mylonitization, brecciation, zoning, metamorphism, periods of metamorphism.
Alteration	Level of information, granitization, metasomatism, retrograde metamorphism, hydrothermal, regolith, bleaching, felspathization, chloritization, limonitization, hematitization, carbonatization, silicification.
Alteration (cont.)	Mineralized direction (up to 3): number of mineralized occurrences, strike, dip, average length, maximum length, average width, maximum width, average depth, maximum depth, U_3O_8 grade, ThO_2 grade, U_3O_8/ThO_2, sample-type, -condition, type of assay.
Data on Mineralization	Mineralization data for whole unit subdivision: average length, maximum length, average width, maximum width, average depth, maximum depth, estimated grades - U_3O_8, - ThO_2, - U_3O_8/ThO_2, estimated tonnage U_3O_8.
	Data on orebodies: trend, plunge, U_3O_8 grade, ThO_2 grade, tonnage U_3O_8 (reserve + production).
Associated elements	Element – amount (up to 5).
Minerals	Radioactive minerals (up to 4), accompanying minerals (up to 6).
Radiogenic ages	Host rocks – method of determination, cover host rocks – method of age determination, metamorphism – method of age determination, mineralization – method of age determination.
Origin and classification	Origin of mineralization, tentative genetic classification.
Basin considerations	Basin type, environment of sedimentation, reducing conditions.
Sedimentologic considerations	Lithologic components: -feldspathic, -lithic, -volcanic, -carbonate, cement/matrix, friability, framework, grain size, porosity, permeability, sorting, roundness, bedding, evaporites, sandstone/shale ratio, sandstone/conglomerate ratio, sandstone/limestone ratio, lateral facies changes, local dip, vergence, direction of paleoslope, direction of main distributing channels.
Volcanic and intrusive considerations	Distribution of volcanics in relation to host rocks, nature of volcanism, distribution of intrusive rocks in relation to host rocks, nature of intrusive rocks.
Comments	Comment identifier, comment.
	Intials of coder, month and year of coding and initials of person making updates, month and year of updating are also entered in each record.

40. GEOLOGICAL INVESTIGATIONS OF THE COAL-BEARING KOOTENAY FORMATION IN THE SUBSURFACE OF THE UPPER ELK RIVER VALLEY, BRITISH COLUMBIA

Project 760056

P.S. Graham, P.R. Gunther, and D.W. Gibson
Institute of Sedimentary and Petroleum Geology, Calgary

In 1975, a preliminary study was undertaken by the British Columbia Department of Mines and Petroleum Resources to determine the mining potential of the upper Elk River valley. A preliminary geological map was prepared (Pearson and Duff, 1976) but, because of poor bedrock exposure, problems were encountered in trying to evaluate the coal potential at the north end of the valley (Fig. 40.1). In co-operation with the British Columbia Department of Mines and Petroleum Resources, the Geological Survey of Canada began a program to expand the earlier work of Pearson and Duff (1976).

In the summer and fall of 1976, a geological mapping and coring program was undertaken in the upper Elk River valley (Fig. 40.2), the objectives of which were: (1) to obtain additional geological information in the area and prepare a detailed geological map in support of a test drilling program; (2) to study the Kootenay Formation in the subsurface as a means of linking the economically important Fernie and Cascade Coal basins to the south and north, respectively; (3) to obtain information on the quality, quantity and distribution of the coal seams in the area, as part of the Federal Coal Resource Evaluation Program; and (4) to test new coal rank correlation techniques.

The area was mapped in July by Graham at a scale of approximately 1:16 000 to determine the feasibility of and the best location for drilling. Between September and December, Graham, assisted by B.R. Cormier of the Geological Survey, supervised the drilling of four H.Q. size coreholes. The core was re-examined and logged in detail by Gibson, with petrographic rank studies initiated by Gunther. Additional work is currently in progress by other officers of the Geological Survey, including A.R. Cameron (maceral analyses), A.R. Sweet (palynology), J.H. Wall (microfossils), and Prof. E. Ghent, University of Calgary (low-grade metamorphism). The results of these investigations will be reported at a later date pending completion of all laboratory phases of the investigation.

Figure 40.1. Upper Elk River valley, looking northwest. GSC 199244.

Approximately 30 km^2 (11 sq miles) of the coal-bearing Kootenay Formation were studied between Cadorna Creek on the south and the British Columbia-Alberta border on the north, and the northern extension of the Lizard Range and the Elk Range on the west and east, respectively. The area studied lies 55 km (30 miles) north of Elkford, British Columbia in the southeastern corner of the province (Fig. 40.2), accessible by a gravel road connecting Elkford to the Kananaskis Forestry Trunk Road in Alberta, via the West Elk Pass. The upper Elk River valley area of this report is presently being withheld from coal licensing by the British Columbia Government.

Mapping Program

Additional geological mapping was required to confirm the previous structural interpretations of Pearson and Duff (1976), and also to obtain surface information on coal seams as an aid in planning the drilling program. Results of the mapping are illustrated by Figure 40.2. Structurally, the study-area is dominated by the Bourgeau(?) Thrust and the Alexander Creek Syncline. The thrust runs northwest along the western edge of the valley bottom, bringing Paleozoic carbonate rocks in contact with the Kootenay Formation. Additional smaller reverse faults occur on the east side of the valley north of Elk River, and may join the main Bourgeau Thrust at depth. Running parallel to the main thrust and through the centre of the valley is the asymmetrical Alexander Creek Syncline (Fig. 40.2). This syncline, more correctly termed a synclinorium, comprises two right-hand, en echelon synclines separated by a short connecting anticline. The syncline plunges both to the north and south. Other small, simple-linkage anticline-syncline pairs are present and associated with the major syncline. Ollerenshaw (1968) observed similar fold structures 150 km (93 miles) to the north in the Limestone Mountain area of Alberta.

Coring Program

Results of the mapping were sufficiently encouraging to initiate the drilling phase of the program. Because of depth limitation on the drilling apparatus, four coreholes were necessary to penetrate the entire Kootenay Formation. The first hole (EV-1; see Fig. 40.2) was located so that it

From: Report of Activities, Part B;
Geol. Surv. Can., Paper 77-1B (1977)

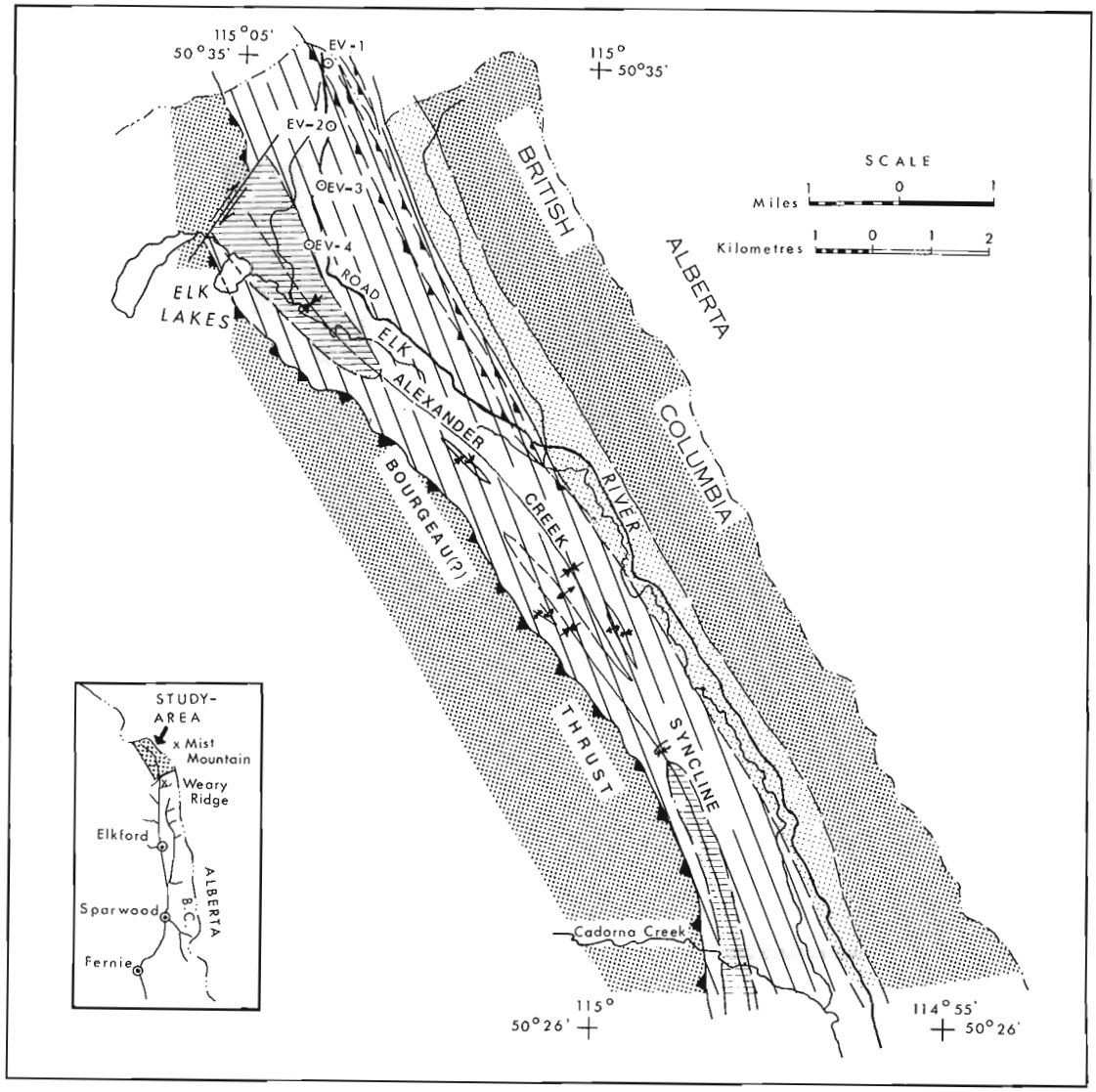

LEGEND

LOWER CRETACEOUS

BLAIRMORE GROUP

JURASSIC-LOWER CRETACEOUS

KOOTENAY FORMATION

JURASSIC

FERNIE FORMATION

PRE-JURASSIC

SPRAY RIVER GROUP AND OLDER

Geological Contact (defined, approximate, assumed).....

Thrust Fault (defined, approximate, assumed; teeth on upthrust side).....

Anticline (defined, approximate, assumed)...

Syncline (defined, approximate, assumed)....

Core Hole Location and Number..... ⊙ EV-4

Figure 40.2. Geological map, upper Elk River valley, British Columbia.

would penetrate the lower contact of the Kootenay. The location of each succeeding hole was designed to penetrate younger strata and overlap with the upper strata of the previous hole, thus giving a complete core of the Kootenay Formation. Each hole was planned to penetrate the strata as close as possible to right angles in order to reduce total footage to be drilled, hole deviation problems, and to improve core recovery.

During the operation, 1641 m (5385 ft) were drilled at a cost of $156 600.00 or $95.35 per metre ($29.00 per ft). Operational costs included equipment and moves, bulldozer operation and geophysical logging.

Lithostratigraphy

Recent work by Gibson (1977a, b) in Alberta and British Columbia has demonstrated that the Kootenay Formation can be subdivided readily into three main stratigraphic units. The nomenclature tentatively applied to these units is, in ascending order: the Basal Sandstone member, the Coal-Bearing member, and the Elk member. Results of the Kootenay coring project described in this report have demonstrated that surface Kootenay subdivisions are both practical and applicable to subsurface investigations.

The Kootenay Formation in the subsurface of the upper Elk River valley consists of an interstratified sequence of probable nonmarine siltstone, sandstone, mudstone-shale, and coal. Unfortunately, the coring project failed to intersect the upper and lower contacts of the formation. However, graphic calculations from mapped contacts and geographic proximity to surface sections measured by Gibson in 1976 (1977a), suggest approximately 90 m (300 ft) of missing strata. The total Kootenay Formation thickness in the report-area is estimated to be approximately 1000 m (3300 ft). The Kootenay conformably but abruptly overlies sandstone, siltstone, and shale of the marine Jurassic "Passage Beds" of the Fernie Formation (Gibson, 1977a). The formation is overlain unconformably by sandstone and conglomerate of the Cadomin Formation. The Pocaterra Creek Member of the Blairmore Group, exposed in the Mist Mountain area to the east (Gibson, 1977a), was not observed in exposures in the vicinity of the four cored holes.

Basal Sandstone member

The thick, medium to light grey, very fine to medium grained quartzose sandstone recorded at the base of hole EV-1 (Fig. 40.3) is interpreted tentatively as the upper part of the Basal Sandstone member (Gibson, 1977a). The uppermost 13 m (43 ft) are medium to very fine grained and display normal graded bedding (i.e. fining upward). This facies may be equivalent to Unit A observed elsewhere in exposures in geographically adjacent areas of British Columbia and Alberta (Gibson, 1977a). The lower 8 m (26 ft) are finer grained, and may be equivalent to only the upper part of Unit B (Gibson, 1977a). For example, at Mist Mountain, 9.6 km (6 miles) east of hole EV-1 (Fig. 40.2), the Basal Sandstone is 79 m (260 ft) thick, with Unit B attaining a thickness of 43.6 m (143 ft). At Weary Ridge, 22.4 km (14 miles) to the south of hole EV-1 (Fig. 40.2), the Basal Sandstone is 75.3 m (247 ft) thick with Unit B recorded with a thickness of 36 m (118 ft).

Sedimentary structures are uncommon in the member. Thin to thick, light and dark grey, planar laminations were observed in the lower 7.6 m (25 ft). Poorly preserved fine-scale planar crossbedding was noted only in the upper few metres of the member.

The contact with the overlying Coal-Bearing member is abrupt but conformable. It is placed at the base of the first occurrence of dark grey, carbonaceous siltstone overlying the thick sandstone of the Basal Sandstone member (EV-1; Fig. 40.3). It must be noted, however, that, in exposures and core from Fording Coal property 43.2 km (27 miles) to the southeast, Gibson has recorded thick, fine to coarse grained sandstone lithofacies in the overlying Coal-Bearing member. Some of these units are in excess of 24.4 m (80 ft) thick, and are lithologically similar to the sandstone at the base of hole EV-1 (Fig. 40.3). Until all phases of the investigation are complete, one cannot eliminate the possibility that the thick sandstone at the base of hole EV-1 is one of the thick sandstones of the Coal-Bearing member. Further petrographic and coal rank work is required to resolve the problem.

Coal-Bearing member

The Coal-Bearing member, a name temporarily used by Gibson (1977a, b), comprises a thick succession of interbedded siltstone, sandstone, mudstone, shale, and economically important thin to thick seams of medium to high volatile bituminous coal. The member has an approximate thickness of 483.7 m (1587 ft) (EV-1, EV-2, EV-3; Fig. 40.3). However, because of the faulting in the area, and evidence of faulting in cores of the Elk Valley drilling project, the recorded thickness of the Coal-Bearing member may be in error. Gibson has recorded thicknesses in adjacent surface areas of 381 and 487.7 m (1250 and 1600 ft) for the Coal-Bearing member at Mist Mountain and the property of Fording Coal Company near the headwaters of Fording River, respectively. These surface values suggest that the thickness obtained in the subsurface of the upper Elk Valley may be approximately correct.

Medium dark to dark grey carbonaceous-argillaceous siltstone forms the predominant lithology of the member, and is most commonly interbedded and interlaminated with very fine grained sandstone (Fig. 40.3). Siltstone also occurs in many of the coal, mudstone and shale intervals, where it is characteristically darker grey, more carbonaceous-argillaceous, and contains a noticeable concentration of vegetal matter. The sandstone is medium to light grey, quartzose, rarely calcareous, and very fine to fine grained. Medium to coarse grained sandstone is rare, but does occur, as can be seen, for example, in the intervals from 32 to 41.1 m (105-135 ft) and 304.2 to 311.2 m (998-1021 ft) below the surface in hole EV-2 (Fig. 40.3). These coarse grained sandstones become finer upward, are calcareous in places, and commonly contain vitreous coal fragments or thin coaly laminations near their base. In addition, the base of the thick sandstone units is commonly characterized by elongate, well rounded to angular clasts of siltstone or mudstone.

Mudstone or shale is associated with the siltstone and coal lithofacies. It is dark grey to black, very carbonaceous-argillaceous, with the mudstone in part displaying a distinctive subconchoidal fracture. The

mudstone may contain brown ferruginous nodules or lenticular brown ferruginous or pyritiferous laminations and banding. Poorly- to well-preserved pelecypods and ostracodes have been collected from the member. Similar fossils have been recorded by Pearson and Duff (1976) in the Coal-Bearing member at Weary Ridge to the south (Fig. 40.2). In core from holes EV-2 and EV-3 at levels of 260.0 and 396.2 m (855 and 1300 ft), respectively (Fig. 40.3), two unusual pale yellowish brown bands of claystone-mudstone were encountered, up to 0.06 m (0.2 ft) thick, associated with dark grey mudstone and coal. These samples were submitted for X-ray diffraction and chemical analysis. Preliminary results indicate a mineral composition of 75 per cent kaolinite and 25 per cent quartz for the sample from EV-2, and a composition of 100 per cent kaolinite for the sample from EV-3. These two samples are thought to be "Tonsteins" (Meriaux, 1972), and may eventually serve as a useful tool for correlation in the area.

Coal forms a lithologically characteristic and conspicuous component of the member in the report-area. More than 50 seams ranging in thickness from 0.12 to 5.5 m (0.5 – 18 ft) of medium to high volatile bituminous coal have been recorded (Fig. 40.2). Further discussion of the coal is present elsewhere in this report.

Sedimentary and biogenic structures are common. Micro- to fine-scale planar and festoon crossbedding occur in some of the siltstone and finer grained sandstone strata and less commonly in the coarser grained sandstone beds of the member. Contorted or convolute, ripple and ripple drift laminations are common in the thin to medium bedded sandstones interbedded with the siltstones. Trace fossils or burrow structures occur in many of the sandy siltstones. These biogenic structures are generally uncommon in adjacent exposures of the Kootenay Formation (Gibson, 1977b). This absence, however, may be attributable to the weathered nature of the strata and, as a result, may have gone unrecognized. The sedimentary structures and structure combinations suggest that the strata of the member are characteristic of fluvial flood plain, flood basin, swamp, channel, and point bar depositional environments.

Facies changes between the subsurface, and geographically adjacent exposures in the Mist Mountain and Weary Ridge area of Alberta and

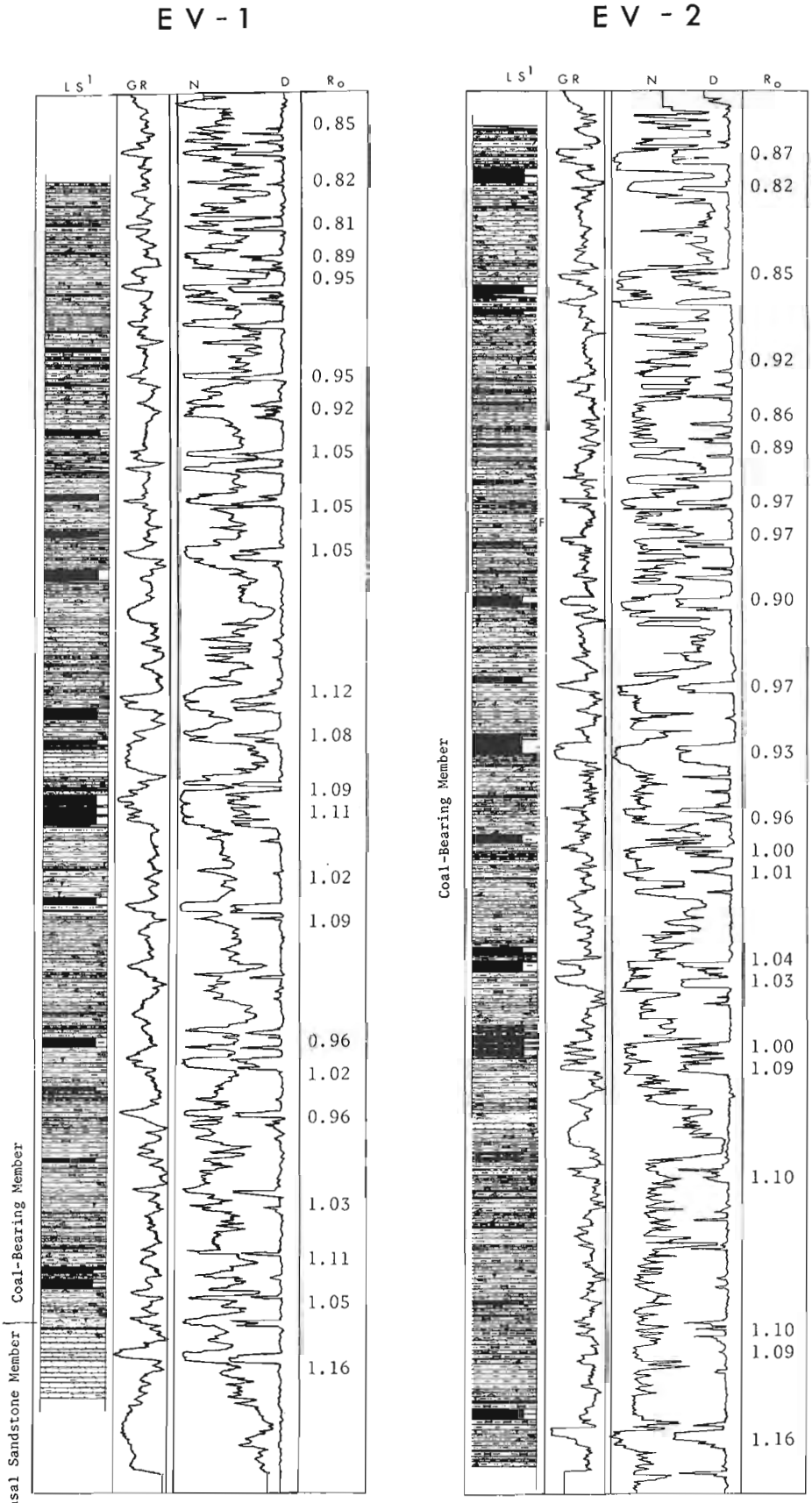

Figure 40.3. Lithostratigraphy logs, geophysical logs and mean maximum reflectance of coals, upper Elk River valley coring program.

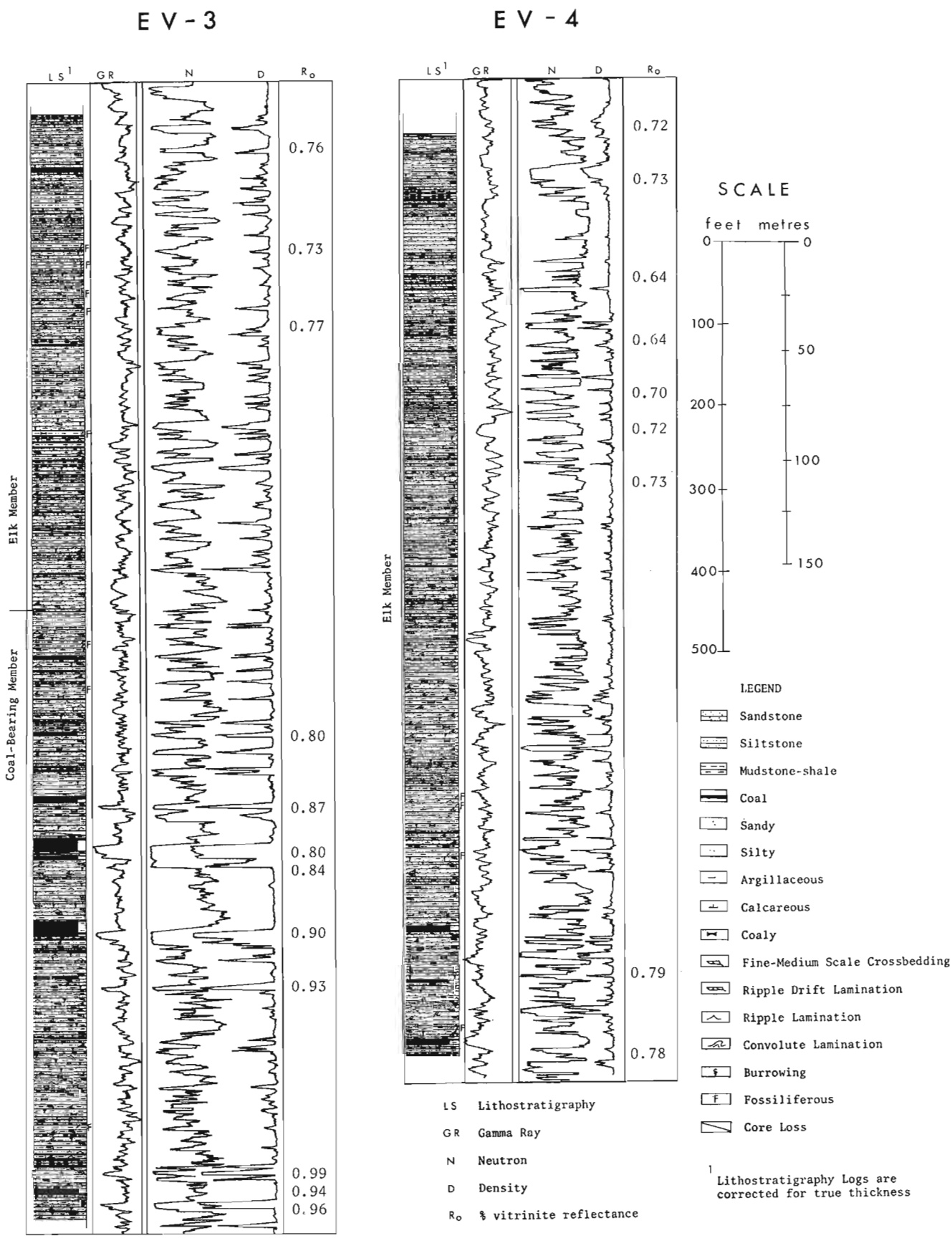

Figure 40.3. continued

British Columbia are uncommon in the Coal-Bearing member. Gibson, however, has noted that, to the east, coal seams in the Mist Mountain area of Alberta (Fig. 40.2) display a decrease in number and thickness.

The contact with the overlying Elk member is placed at the base of the first major sandstone above the last or uppermost major coal seam in the Coal-Bearing member (EV-3; Fig. 40.3). Coal seams, although present in the Elk member, are thin and relatively uncommon in comparison with those of the Coal-Bearing member. Accordingly, the presence or absence of thick seams serves as a major criterion for differentiating strata of the Coal-Bearing and Elk members. However, four seams were recorded in the Elk member near the base of hole EV-4 (Fig. 40.3). These seams are very shaly and may, upon analysis, be classed mainly as shaly coal. Because of the impurities, these seams, although thick in part, are interpreted as atypical of the Coal-Bearing member and, accordingly, are assigned to the Elk member.

Elk member

In the subsurface of the upper Elk River valley, the Elk member is lithologically similar to strata of the underlying Coal-Bearing member. It consists of interbedded siltstone, sandstone, mudstone, shale, and thin seams of coal. As noted above, the top of the member was not penetrated during drilling and, consequently, the exact or true thickness of the member is speculative; 396.2 m (1300 ft) of probable Elk strata were drilled in holes EV-3 and EV-4 (Fig. 40.3). Between 30 and 60 m (100 – 200 ft) of additional strata have been estimated to occur between the top of EV-4 and the contact with the Blairmore Group. However, it must be noted that, as in the underlying Coal-Bearing member, some of the Elk member core is characterized by slickensiding, numerous calcite-filled fractures, micro-faults, and thin fault breccia zones, all criteria suggesting possible faulting or bedding plane movement. Further work is needed to resolve the thickness problem.

Siltstone appears to form the predominant lithology of the member, and is most commonly interbedded and interlaminated with sandstone. It is dark to medium dark grey, carbonaceous-argillaceous, and in some cases calcareous. Siltstone is also interbedded with mudstone, shale and coal. The sandstone is light to medium grey, commonly calcareous, and very fine to medium grained. Mudstone and shale are common in the member, and commonly contain brown ferruginous nodules and lenses, and thin bands of vitreous coal. Some of the mudstones

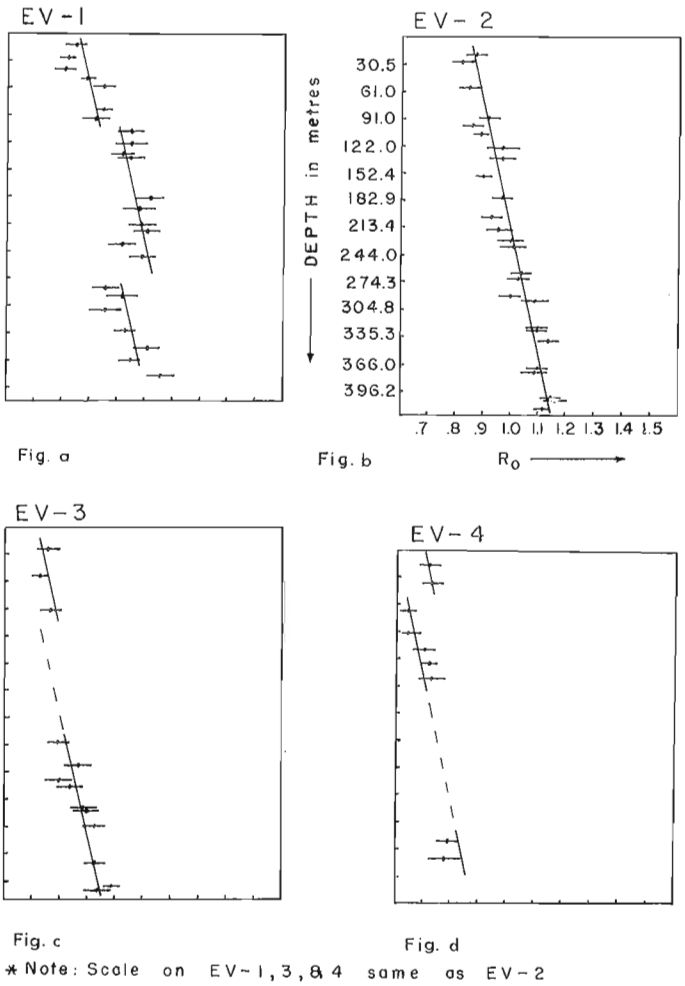

Figure 40.4. Depth versus reflectance (Ro) graphs.

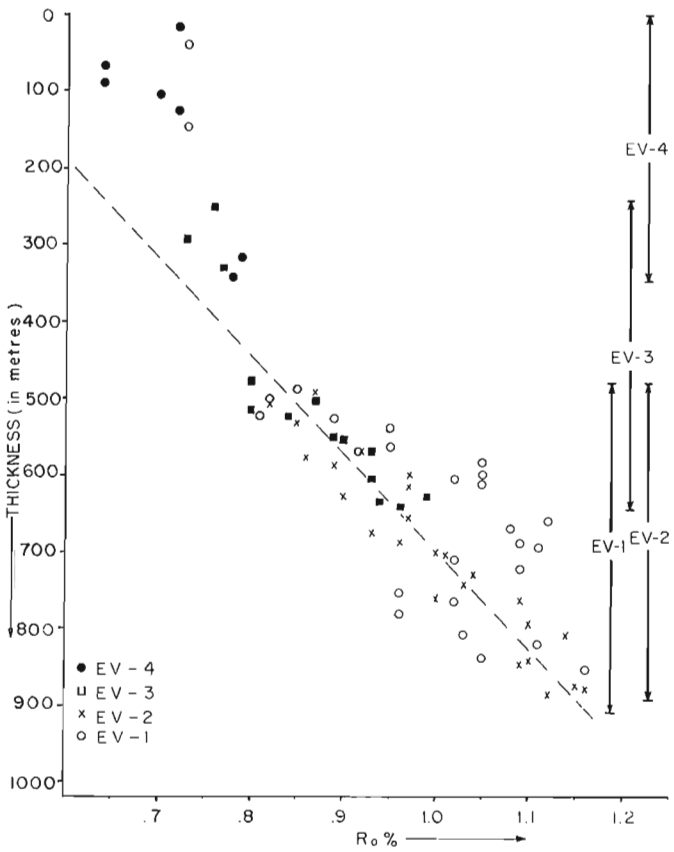

Figure 40.5. Composite thickness versus reflectance (Ro) graph of coal seams in EV-1 to EV-4.

near the base and top of holes EV-4 and EV-3, respectively (Fig. 40.3), contain poorly- to well-preserved pelecypods, gastropods, and ostracodes. Coal seams, although present, are thin. "Needle coal", a diagnostic component of the upper Elk member in many surface exposures (Gibson, 1977a), was not encountered in core of EV-4. However, in an exposure near hole EV-4, a thin unit of "needle coal" was observed immediately underlying the Cadomin Formation. In the Fernie area 112 km (70 miles) to the south, chert-pebble conglomerate and conglomeratic sandstone form a diagnostic facies of the Elk member (Gibson, 1977a, b). This distinctive facies was not observed in core from the upper Elk River valley.

Sedimentary and biogenic structures are common and similar to those observed in the underlying Coal-Bearing member. They consist of fine-scale crossbedding, ripple, ripple drift, and convolute or contorted laminations, all characteristic of flood plain and fluvial depositional environments. The mudstones, shales, and coals probably represent former lacustrine and swamp depositonal environments. Biogenic structures are similar, but less common than those in the Coal-Bearing member.

Facies changes between the subsurface and exposures of the Elk member in adjacent areas are shown by the sandstones and by the occurrence and concentration of mudstone, shale and coal/coaly shale. For example, in the Mist Mountain area to the east (Fig. 40.2), Gibson has noted that medium to coarse grained sandstone is more common, and in general is coarser grained than that encountered in the subsurface Elk of the upper Elk River valley. In addition, mudstone, shale, coal and coaly strata were observed to decrease in concentration toward the Mist Mountain area.

The contact of the Elk member and Cadomin Formation was not penetrated in hole EV-4 (Fig. 40.3); however, it was observed in exposures near hole EV-4. The darker grey, carbonaceous siltstone, mudstone, sandstone, and coal of the upper Elk member are overlain unconformably by thick-bedded chert-pebble conglomerate and sandstone of the Cadomin Formation.

Coal Rank Studies

Coal rank studies were initiated as a correlation technique. It has been demonstrated by Hacquebard and Donaldson (1974) that coal rank (Ro) values in the Kootenay increase with depth. Coal seams of similar depth will locally show similar ranks and, therefore, can be used as a tool for correlation.

Coal samples for petrographic studies were collected from all seams 0.3 m (1 ft) thick or greater. From the four cored holes, a total of 130 samples were taken, of which 73 now have been examined to determine petrographic rank. In addition, 64 of these samples were submitted for proximate analyses; these were collected from all seams 1.2 m (4 ft) thick or greater.

Samples were prepared using the standard procedures outlined in the handbook of the American Society for Testing and Materials (1973, p. 411-414). The samples were crushed to minus 20 mesh size and then riffled, so that an unbiased split could be obtained. Next, pellets were made in a pressure bomb at 5000 p.s.i., using a thermal setting mounting medium. Finally, they were polished with 0.3 μm and 0.05 μm alumina grits. The mean vitrinite reflectance, value for each sample was calculated from 50 values of maximum reflectance measured on vitrinite in the sample. Hacquebard and Donaldson (1970, p. 1141) describe the method and equipment in detail.

The mean maximum reflectance (Ro) values and standard deviations were plotted on graphs of depth versus Ro (Fig. 40.4a-d). A best-fit straight line (Ro gradient) was plotted initially on the graph containing the Ro information pertaining to the EV-2 hole. Because this hole appeared to be the least disturbed as far as increasing rank was concerned (Fig. 40.4a-d), the EV-2 Ro gradient was then used as the norm or standard. This standard gradient was then plotted through the data points on the other three graphs using a best-fit. At this stage, correlation and structural interpretations were possible.

For example, from geological mapping and core examination, it has been demonstrated that major and minor faults occur in the report-area. Figure 40.4a, when compared with Figure 40.4b (the norm), demonstrates evidence of probable faults. Between the coal sample at 250 m (820 ft) and the sample at 285 m (935 ft), as suggested by the offsetting of the best-fit Ro gradient line, a thrust fault is proposed. A thin zone of fault gouge was observed at 260 m (854 ft), further supporting the interpretation. Between the coal samples at 91 and 122 m (298 and 400 ft), because of missing Ro values, a normal fault is proposed. The total span of reflectance values for EV-1 (0.81 – 1.16 Ro; Fig. 40.4a) and EV-2 (0.82 – 1.16 Ro; Fig. 40.4b) are, statistically speaking, the same. Evidence from Ro and geophysical logs strongly suggest EV-1 and EV-2 are in part repeat sections, probably caused by thrust faulting.

Figure 40.5 is a plot of mean Ro values for all four holes. If the best-fit Ro gradient (Fig. 40.4b) is plotted on this graph, complications are apparent. When the gradient is plotted through the points below 487.7 m (1600 ft), it does not intersect the points above the position. In contrast, one may suggest that the gradient over the total Kootenay Formation may be a curved rather than a straight line. Accordingly, the discrepancy in Figure 40.5 may be attributed to a curving gradient, and not necessarily a fault. Additional samples and further analyses are needed to clarify the problem so that a reasonable explanation can be derived.

Another unusual aspect of the rank study is the low range of absolute rank values when compared to other adjacent areas. For example, Hacquebard and Donaldson (1974) document Ro values from two sections in the Elk River valley: Fording River at Eagle Mountain, and Line Creek Ridge. They recorded Ro values from the Coal-Bearing member ranging from 1.13 to 1.43 at Fording River (337 m (1124 ft) thick) and from 0.97 to 1.49 at Line Creek (308 m (1026 ft) thick). The highest Ro value in the study area approaches 1.16 Ro. In terms of ASTM rank, coals obtained from the coring project in the upper Elk River valley are medium to high volatile bituminous whereas, generally, Kootenay coals from other areas are low to medium volatile bituminous. The lower ranks found in the study-area may be explained, in part, by a lower geothermal gradient, which in turn is reflected by the lower Ro gradient. The gradients are as follows: study-area, 0.079 Ro/100 m (0.024 Ro/100 ft); Fording River,

0.092 Ro/100 m (0.028 Ro/100 ft); and Line Creek, 0.164 Ro/100 m (0.050 Ro/100 ft). These gradients would tend to indicate a regional trend in the geothermal gradient, which increases in a southerly direction in the Elk River valley.

Conclusions

1. The restored thickness of the Kootenay Formation is consistent with other sections in the same geologic setting to the north and south.

2. Seams of mineable thickness were encountered but their lateral extent was not determined.

3. The average rank of the coal seams in the study-area is unusually low in comparison to the ranks of adjacent studied areas.

4. Petrographic rank studies can be used as an aid to coal seam correlation and to delineate major tectonic movement in the Kootenay Formation of the upper Elk River valley.

References

American Society for Testing and Materials
1973: Book of ASTM standards, Part 19, Gaseous fuels, coal and coke; Philadelphia, Pennsylvania, p. 416-419.

Gibson, D.W.
1977a: The Kootenay Formation of Alberta and British Columbia – a stratigraphic summary; in Report of Activities, Part A, Geol. Surv. Can., Paper 77-1A, p. 95-106.

Gibson, D.W. (cont.)
1977b: Sedimentary facies in the Jura-Cretaceous Kootenay Formation, Crowsnest Pass area, southwestern Alberta and southeastern British Columbia; Bull. Can. Petrol. Geol, special guidebook issue, Waterton Lakes.

Hacquebard, P.A. and Donaldson, J.R.
1970: Coal metamorphism and hydrocarbon potential in the upper Paleozoic of the Atlantic Provinces, Canada; Can. J. Earth Sci., v. 7, p. 1139-1163.

1974: Rank studies of coals in the Rocky Mountains and inner Foothills Belt, Canada; Geol. Soc. Am., Spec. Paper 153, p. 75-94.

Meriaux, E.
1972: Les tonsteins de la veine de charbon no. 10 (Balmer) à Sparwood Ridge dans le bassin de Fernie (Columbie Britannique); in Report of Activities, Part B, Geol. Surv. Can., Paper 72-1B, p. 11-22.

Ollerenshaw, N.C.
1968: Preliminary account of the geology of Limestone Mountain map-area, southern Foothills, Alberta; Geol. Surv. Can., Paper 68-24.

Pearson, D.E. and Duff, P.McL.D.
1976: Coal investigations. Studies in the East Kootenay coalfields in Geological field work, 1975. A summary of field activities of the Geological Division, Mineral Resources Branch; British Columbia Dep. Mines Petrol. Res., p. 93-98.

41. SUMMARY OF CONODONT BIOSTRATIGRAPHY OF THE READ BAY FORMATION AT ITS TYPE SECTIONS AND ADJACENT AREAS, EASTERN CORNWALLIS ISLAND, DISTRICT OF FRANKLIN

Project 680101

T.T. Uyeno
Institute of Sedimentary and Petroleum Geology, Calgary

Introduction

Thorsteinsson and Fortier (1954) introduced the term Read Bay Formation, and subdivided the formation into four informal members: A, B, C and D, in ascending order. The type sections of members A and B were located at Goodsir Creek, eastern Cornwallis Island, whereas those of members C and D were located some 23 km to the north, in an unnamed creek entering the southwestern side of Read Bay (Thorsteinsson, 1958, p. 49, 64, 65, 69). The type sections and other collecting sites are shown on Figure 41.1. Thorsteinsson (in Thorsteinsson and Tozer, 1970, p. 558, 559) gave the following summary account of the Read Bay Formation at its type sections: "Member A, 1875 feet [571.5 m] of mainly thin bedded argillaceous limestone alternating with generally thick bedded biostromal and fossil fragmental limestone; Member B, 60 to 100 feet [18.3-30.5 m] of shale and minor sandstone; Member C, 3775 feet [1150.6 m] of beds similar to Member A, but with biostromal and biohermal developments that are thicker and commonly dolomitized; Member D, about 1800 feet [548.6 m] of alternating red calcareous sandstone and argillaceous limestone." Subsequently, the lower beds of member A at its type section have been assigned to the Cape Storm Formation of Kerr (1975), and the base of member A now is drawn at the base of lithologic unit no. 46 of Thorsteinsson (1958, p. 51) (Thorsteinsson, pers. comm., Dec. 1976). At Goodsir Creek, the revised thicknesses of members A and B are 335.4 and 64.9 m, respectively (Thorsteinsson, pers. comm., March 1977). For the most recent account on the geology of Cornwallis Island, the reader is referred to Thorsteinsson and Kerr (1968).

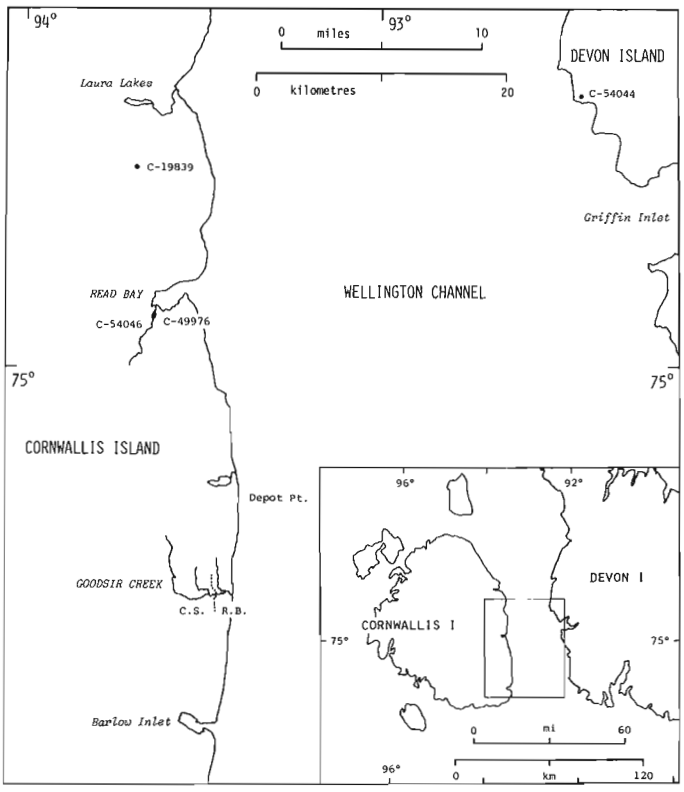

Figure 41.1. Index map showing the collecting sites of the Read Bay Formation on eastern Cornwallis and western Devon Islands. At Goodsir Creek, dotted line marks the boundary between the Cape Storm (C.S.) and Read Bay (R.B.) formations. Inset map shows the geographic position of the enlarged map.

In 1968, the writer collected from some of the localities at Goodsir Creek reported herein (GSC locs. 83335-83349) (see McGregor and Uyeno, 1969). Material from all other localities was provided by and collected over a period of several field seasons by R. Thorsteinsson.

The conodont faunas summarized herein are discussed in full taxonomy by Uyeno and Thorsteinsson (in prep.). The writer is indebted to Dr. Thorsteinsson for access to the stratigraphic information contained in that manuscript.

Previous Conodont Studies

Previous investigations of conodonts in strata equivalent in time to the type Read Bay Formation include the following: Weyant's (1971) study of member C, Read Bay Formation, south of Laura Lakes (Fig. 41.1), and the Douro Formation east of Camp Creek and in an area north of Prince Alfred Bay, both on Devon Island. Conodont species from these localities were listed (Weyant, 1971, Table 8, p. 40). Of the three critical platform elements (all spathognathodontan) on the list, only one was illustrated and described. Correlation of Weyant's faunas with those of the present report, consequently, is extremely difficult. Mirza (1976) studied the conodonts of the Cape Storm and Cape Phillips formations at Vendom Fiord, southwestern Ellesmere Island. In that study, parts of the Cape Phillips Formation are shown as correlatives of the Douro Formation (in revised sense, allowing for the Cape Storm Formation; Fig. 4, p. 12, Sec. B, p. 191-193) but, unfortunately, no conodonts were recovered from this interval.

Conodont Biostratigraphy

The conodont biostratigraphy of parts of the Read Bay Formation and its subjacent unit, the Cape Storm Formation, at Goodsir Creek and the Read Bay area, is summarized in Figure 41.2. In the following discussion, all morphotypes of **Ozarkodina confluens** (Branson and Mehl) are those of Klapper and Murphy (1974). The figured specimens are in the collections of the Geological Survey of Canada, Ottawa.

From: Report of Activities, Part B; Geol. Surv. Can., Paper 77-1B (1977)

PLATE 41.1

All figures x40. Figures 1, 2, 7 and 8 from Cape Storm Formation; all others from Read Bay Formation on eastern Cornwallis Island

Figures 1, 2. Asymmetrical palmate element

Posterior and anterior views, GSC 49769, Cape Storm Formation, Goodsir Creek, GSC loc. 83335.

Figures 3-6. **Ozarkodina** cf. **O. eurekaensis** Klapper

3. Outer lateral view of a P element, GSC 49770.

4-6. Upper, outer lateral and lower views of a P element, GSC 49771; both from member C, GSC loc. C-19839.

Figures 7, 8. **Ozarkodina** cf. **O.** n. sp. B of Klapper (in Klapper and Murphy, 1974)

Outer lateral and upper views of a P element, GSC 49772, Cape Storm Formation, Goodsir Creek, GSC loc. 83343.

Figures 9, 10. **Pedavis latialata** (Walliser)

Upper and lower views of an I element, GSC 49773, member C, Goodsir Creek, GSC loc. C-63576.

Figures 11, 12. **Ozarkodina remscheidensis remscheidensis** (Ziegler)

Lateral and lower views of a P element, GSC 49774, member C, Read Bay area, GSC loc. C-54046.

Figures 13, 14. **Pelekysgnathus** n. sp. A

Lateral and upper views of an I element, GSC 49775, member C, Goodsir Creek, GSC loc. C-19837.

Figures 15, 16. **Pelekysgnathus** n. sp. B

Inner lateral and lower views of an I element, GSC 49776, member D, Read Bay area, GSC loc. C-49976.

Figure 17. **Kockelella variabilis** Walliser

Inner lateral view of a Pb element, GSC 49777, member B, Goodsir Creek, GSC loc. 83349.

Figure 18. **Ozarkodina confluens** (Branson and Mehl) morphotype γ of Klapper (in Klapper and Murphy, 1974)

Lateral view of a P element, GSC 49778, member C, Goodsir Creek, GSC loc. C-19837.

Figures 19, 20. **Polygnathoides siluricus** Branson and Mehl

Upper and lower views of a P element, GSC 49779, member A, Goodsir Creek, GSC loc. C-63573.

Figures 21, 26. **Ozarkodina** n. sp. A of Klapper (in Klapper and Murphy, 1974)

Lateral views of two P elements, GSC 49780 and 49781, respectively, both from member C, Goodsir Creek, GSC loc. C-63576.

Figures 22-24. **Ozarkodina** n. sp. G.

22, 23. Inner lateral and lower views of a P element, GSC 49782.

24. Outer lateral view of a P element, GSC 49783; both from member D, Read Bay area, GSC loc. C-49976.

Figure 25. **Ancoradella ploeckensis** Walliser

Upper view of a P element, GSC 49784, member A, Goodsir Creek, GSC loc. 83347.

Figures 27-30. **Pedavis** n. sp. T

27-29. Upper, outer lateral and lower views of an I element, GSC 49785.

30. Upper view of an I element, GSC 49786; both from member C, Goodsir Creek, GSC loc. C-19837.

Figure 31. **Ozarkodina confluens** (Branson and Mehl) morphotype α of Klapper (in Klapper and Murphy, 1974)

Lateral view of a P element, GSC 49787, member A, Goodsir Creek, GSC loc. 83348.

Figure 32. **Ozarkodina** n. sp. B of Klapper (in Klapper and Murphy, 1974)

Upper view of a P element, GSC 49788, member A, Goodsir Creek, GSC loc. C-63573.

1
2
3
4
5
6
7
8
9
10
11
12
13
14
15
16
17
18
19
20
21
22
23
24
25
26
27
28
29
30
31
32

Cape Storm Formation

The lowest sampled interval of the Cape Storm Formation is 398.1 m below the top (GSC loc. 83335). This yielded a meagre conodont fauna which includes asymmetrical palmate elements (Pl. 41.1, figs. 1, 2). If this form were laterally skewed, it would resemble remotely the blade element of **Rhipidognathus symmetricus** Branson, Mehl and Branson, a Late Ordovician form (Kohut and Sweet, 1968). A similar form also is present in a sample from the Leopold Formation at the Port Leopold area in northeastern Somerset Island (GSC loc. C-30089), collected by B. Jones (see Jones and Dixon, 1975). At this stage, it is difficult to assess the biostratigraphic significance of the palmate form.

At the level of 9.1 m below the top of the Cape Storm Formation (GSC loc. 83345) is **Ozarkodina** n. sp. B of Klapper (in Klapper and Murphy, 1974) and 55.2 m below that (GSC loc. 83343), **O.** cf. **O.** n. sp. B (Pl. 41.1, figs. 7, 8) occurs. The later differs from **O.** n. sp. B only in the degree of development of accessory denticles on the inner side, and may be its progenitor. **Ozarkodina** n. sp. B was reported, in the Roberts Mountains Formation of Nevada, to be associated with **Polygnathoides siluricus** Branson and Mehl (Klapper and Murphy, 1974, p. 12, 15). Weyant (1971, Table 8, p. 40, sample 15836) also recorded its presence in the Douro Formation, 325 m above the base, east of Camp Creek on Devon Island. **Ozarkodina confluens** (Branson and Mehl) morphotype γ and **O. excavata excavata** (Branson and Mehl) occur at GSC locality C-63575, located 3.0 m below the top of the formation. In Nevada, the range of the former is from **Polygnathoides siluricus** Zone to **Pelekysgnathus index** fauna (i.e., about middle-late Ludlovian boundary to early Pridolian) (Klapper and Murphy, 1974, p. 16). On this basis, at least the upper 9.1 m of the Cape Storm Formation are considered to belong to the **siluricus** Zone.

Read Bay Formation

Member A. The lowest sample from member A that yielded conodonts is from 125.0 m above the base (GSC loc. 83347). This locality, and another which is 213.4 m above the base (GSC loc. 83348), yielded collections with **Ozarkodina confluens** morphotype α, **Ancoradella ploeckensis** Walliser and **Polygnathoides siluricus** (Pl. 41.1, figs. 25, 31). The overlap of the latter two zonal markers occurs in the lower part of the **siluricus** Zone at Cellon (Walliser, 1964, p. 97) and at Pete Hanson Creek IIE in Nevada (Klapper and Murphy, 1974, p. 12). At GSC locality C-63573, located 2.9 m below the top of member A, **Ozarkodina** n. sp. B of Klapper and **Polygnathoides siluricus** were recovered (Pl. 41.1, figs. 19, 20, 32), indicating that the **siluricus** Zone extends at least as high as this locality. Chitinozoans also were recovered from GSC locality 83348 (F.H. Cramer, pers. comm., Jan. 1970). By tracing the carbonate units northward into the graptolite-bearing shale facies of the Cape Phillips Formation on eastern Cornwallis Island, R. Thorsteinsson (pers. comm., March 1977) found that member A is entirely above the **fritschi-linearis** Zone.

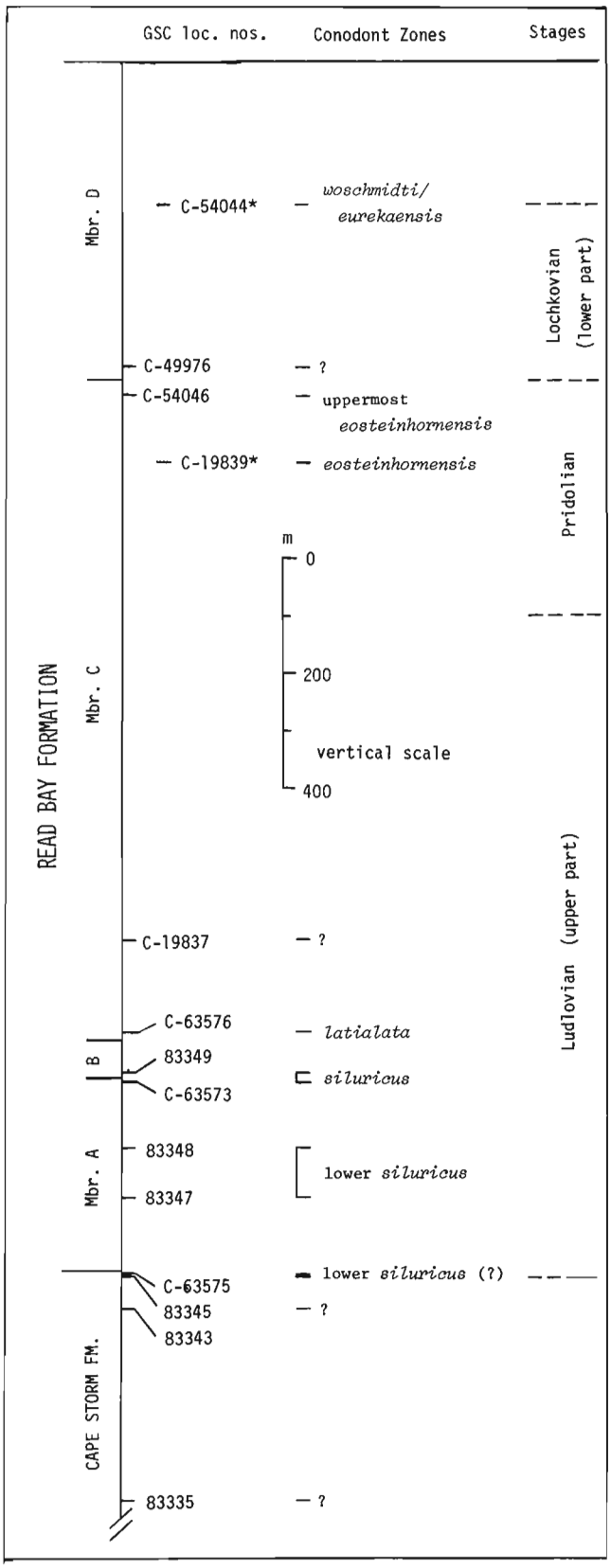

Figure 41.2 (opposite)

Summary of conodont biostratigraphy of the Read Bay Formation at its type sections and the upper part of the Cape Storm Formation at Goodsir Creek. Localities with asterisk (*) are not from the type sections and their stratigraphic positions are only approximate.

Member B. The only sample of member B that yielded any conodonts is from 6.1 m above the base of the unit (GSC loc. 83349). The recovered fauna is poorly preserved, with only a few specimens that are sufficiently complete to allow identification. These specimens include the Pb (Pl. 41.1, fig. 17), M and Sa elements that can be assigned to **Kockelella variabilis** Walliser (apparatus G of Walliser, 1964; locational notation after Sweet and Schönlaub (1975), and adopted by Barrick and Klapper (1976)). The upper limit of the range of **K. variabilis** is the **siluricus** Zone (Walliser, 1964, p. 40, 56, 63), which suggests that the lower part of member B is still within that zone. Chitinozoans were recovered also from this locality (F.H. Cramer, pers. comm., Jan. 1970).

Member C. The lowest conodont-bearing sample of member C at Goodsir Creek is from 15.2 m above the base (GSC loc. C-63576). This sample yielded **Pedavis latialata** (Walliser), **P.** cf. **P.** n. sp. T, and **Ozarkodina** n. sp. A of Klapper (in Klapper and Murphy, 1974) (Pl. 41.1, figs. 9, 10, 21, 26), and indicate the **latialata** Zone. **Ozarkodina** n. sp. A also occurs in the **latialata** Zone in the Roberts Mountains Formation at Birch Creek II in Nevada, and in the Cellon section in the Carnic Alps, according to Klapper and Murphy (1974, p. 15). In the same section at Goodsir Creek, 174 m above the base of member C (GSC loc. C-19837), are **Pedavis** n. sp. T, **Ozarkodina confluens** morphotypes α and γ, and **Pelekysgnathus** n. sp. A (Pl. 41.1, figs. 13, 14, 18, 27-30). Associated with these conodonts are **Atrypella** cf. **A. foxi** Jones and **Hemiarges aquilonius** Whittington (R. Thorsteinsson, pers. comm., March 1977). On the basis of conodonts, the age of this sample cannot be determined precisely, but **O. confluens** morphotype γ and the stratigraphic position of the sample suggest an assignment between the **latialata** and **eosteinhornensis** Zones.

At the type section of member C, 24.4 m below the top of the unit (GSC loc. C-54046) are **Ozarkodina confluens** morphotype α and **O. remscheidensis remscheidensis** (Ziegler) (Pl. 41.1, figs. 11, 12). These conodonts can be assigned to the uppermost **Ozarkodina remscheidensis eosteinhornensis** Zone of late Pridolian age (see Klapper and Murphy, 1974, p. 19).

At GSC locality C-19839, located some 12 km north of the member C type section, and stratigraphically near the top of member C, the fauna contains **Ozarkodina confluens** morphotypes α and γ, and **O.** cf. **O. eurekaensis** Klapper (Pl. 41.1, figs. 3-6). The latter has been reported previously from the Roberts Mountains Formation at Birch Creek II in Nevada in the **eosteinhornensis** Zone (in restricted sense; Klapper and Murphy, 1974, Table 2), and is of late Pridolian age.

Member D. Faunal control of member D at its type section is restricted to the basal part of the unit. At GSC locality C-49976, 21.3 m above the base of member D, are **Ozarkodina** n. sp. G with large basal cavity, and **Pelekysgnathus** n. sp. B (Pl. 41.1, figs. 15, 16, 22-24). In lateral view, the former has the general outline of some morphotypes of **O. confluens** or **O. remscheidensis remscheidensis**, but the basal cavity is similar to that of **O.** n. sp. F of Klapper (in Klapper and Murphy, 1974). The age of this fauna can be stated only in broad terms of late Pridolian through early Lochkovian.

The only other available collection of conodonts from member D is from western Devon Island (GSC loc. C-54044). The exact stratigraphic position of this locality within the member is difficult to determine accurately, but R. Thorsteinsson estimates it to be about 1000 feet (300 m) above its base. The collection includes **Ozarkodina remscheidensis remscheidensis** and **O.** n. sp. F of Klapper. The first occurrence of **O.** n. sp. F at Birch Creek II in Nevada is well above (48.5 m) the base of the **Icriodus woschmidti** Zone, and is within the early Lochkovian age strata (Klapper and Murphy, 1974, Table 2). **O.** n. sp. F continues higher into the **Ozarkodina eurekaensis** Zone in Nevada.

References

Barrick, J.E. and Klapper, G.
1976: Multielement Silurian (late Llandoverian-Wenlockian) conodonts of the Clarita Formation, Arbuckle Mountains, Oklahoma, and phylogeny of **Kockelella**; Geol. Palaeontol., v. 10, p. 59-100.

Jones, B. and Dixon, O.A.
1975: The Leopold Formation: an Upper Silurian intertidal/supratidal carbonate succession on northeastern Somerset Island, Arctic Canada; Can. J. Earth Sci., v. 12, p. 395-411.

Kerr, J. Wm.
1975: Cape Storm Formation – a new Silurian unit in the Canadian Arctic; Bull. Can. Petrol. Geol., v. 23, p. 67-83.

Klapper, G. and Murphy, M.A.
1974: Silurian-Lower Devonian conodont sequence in the Roberts Mountains Formation of central Nevada; Univ. Calif. Publn. Geol. Sci., v. 111.

Kohut, J.J. and Sweet, W.C.
1968: The American Upper Ordovician standard. X. Upper Maysville and Richmond conodonts from the Cincinnati region of Ohio, Indiana and Kentucky; J. Paleontol., v. 42, p. 1456-1477.

McGregor, D.C. and Uyeno, T.T.
1969: Mid-Paleozoic biostratigraphy of the Arctic Islands (58F, 69A, 78H); Geol. Surv. Can., Paper 69-1A, p. 134, 135.

Mirza, K.
1976: Late Ordovician to Late Silurian stratigraphy and conodont biostratigraphy of the eastern Canadian Arctic Islands; unpubl. Master's thesis, Univ. Waterloo.

Sweet, W.C. and Schönlaub, H.P.
1975: Conodonts of the genus **Oulodus** Branson and Mehl, 1933; Geol. Palaeontol., v. 9, p. 41-54.

Thorsteinsson, R.
1958: Cornwallis and Little Cornwallis Islands, District of Franklin, Northwest Territories; Geol. Surv. Can., Mem. 294.

Thorsteinsson, R. and Fortier, Y.O.
1954: Report on progress on the geology of Cornwallis Island, Arctic Archipelago, Northwest Territories; Geol. Surv. Can., Paper 53-24.

Thorsteinsson, R. and Kerr, J. Wm.
1968: Cornwallis Island and adjacent smaller islands, Canadian Arctic Archipelago; Geol. Surv. Can., Paper 67-64.

Thorsteinsson, R. and Tozer, E.T.
1970: Geology of the Arctic Archipelago; in Geology and Economic Minerals of Canada, R.J.W. Douglas, ed., Geol. Surv. Can., Econ. Geol. Rept. 1, p. 548-590.

Walliser, O.H.
1964: Conodonten des Silurs; Abh. Hess. Landesamtes Bodenforsch., v. 41.

Weyant, M.
1971: Recherches micropaléontologiques sur le Paléozoïque inférieur et moyen de l'Archipel Arctique Canadien; Doctoral dissertation, Univ. Caen, France, v. 1, 2.

42. STRATIGRAPHIC RECONNAISSANCE OF LOWER PALEOZOIC ROCKS, EASTERN DEVON ISLAND, ARCTIC ARCHIPELAGO

Project 680015

R.L. Christie
Institute of Sedimentary and Petroleum Geology, Calgary

Introduction

This report provides preliminary results of a reconnaissance stratigraphic study of the eastern part of Devon Island east of 87°W, an area of about 26 000 km^2 (10 000 sq. miles) (see Fig. 42.1). Field work along the coasts was carried out during April and May of 1968 and 1969 using dog sleds, motor toboggans, and aircraft for support. The stratigraphic sections were measured during the summer months (June to August) from camps established by aircraft.

Eastern Devon Island forms part of the elevated eastern edge of the Canadian Arctic Archipelago. The eastern extremity of the island is a mountainous area underlain by Precambrian crystalline rocks whereas, to the west, a dissected plateau is underlain mainly by flat-lying Paleozoic beds. Ice-cover is widespread.

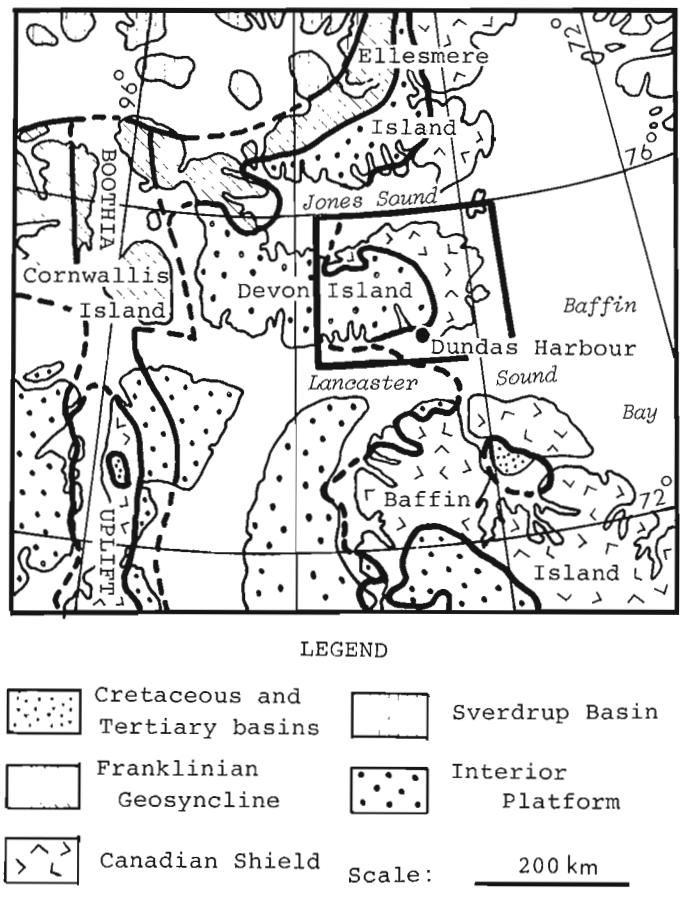

Figure 42.1. Stratigraphic-structural provinces of the eastern part of the Canadian Arctic Archipelago.

Previous Geological Work

The earliest geological observations on (the then-called) North Devon Island were made in 1824 by Dr. Neill, the ship's doctor on W.E. Parry's third voyage to the Arctic Archipelago. Further data were obtained during Leopold M'Clintock's voyage in the **Fox** in 1858. The information from these voyages, mainly of the coast between Philpotts Island and Cape Warrender, were incorporated in Haughton's geological appendix to M'Clintock's published account (see Haughton, 1859). A.P. Low, of the Geological Survey of Canada, described the geological and physiographic features of the south-eastern part of the island after cruising the south coast in the **Neptune** in 1904, and landing at Cuming Inlet (Low, 1906). Other descriptions were provided by L.J. Weeks (1927, p. 137) of the Survey, who accompanied the **CGS Arctic** in 1925 on her annual cruise to the eastern parts of the Archipelago.

D.B. Wales, R.P. Nickelsen, and V.E. Kurtz collected Middle Cambrian fossils near Dundas Harbour in 1948 and 1949 and measured the local Paleozoic section (Wales, 1949; Kurtz et al., 1952). Dundas Harbour was visited briefly in 1950 by V.K. Prest, of the Geological Survey of Canada, who collected Precambrian rocks and measured the heights of beach terraces (Prest, 1952). D.A. Nichols (1936) earlier had published notes on shell remains from these raised beaches.

Localities at Burnett Inlet, on the south coast, and others between Sverdrup Inlet and Cape Sparbo, on the north coast, were visited by B.F. Glenister and E.F. Roots during the Geological Survey of Canada's "Operation Franklin" in 1955 (Fortier et al., 1963, p. 179-194). Stratigraphic sections were measured and the basement rocks were examined. In 1960, the Arctic Institute of North America established, under the leadership of S. Apollonio, a scientific research station near Cape Skogn. Geological studies were done by J.W. Cowie and A. Ormiston (Cowie, 1961). Glacial, periglacial, and beach studies have been carried out by other researchers in following years.

Dr. J.W. Cowie, of the University of Bristol, accompanied the author in 1968 in the measuring of stratigraphic sections at Cuming Inlet.

Stratigraphy of Lower Paleozoic Rocks

The Paleozoic rocks described in this report form a little-disturbed veneer that is dissected to expose the older, Precambrian rocks in certain valleys and fiords. Paleozoic rocks form a structurally conformable succession that strikes generally north-south and dips at a very gentle angle to the west. The border of the Paleozoic region is much indented and marked by scattered outliers of bedded rocks.

From: Report of Activities, Part B; Geol. Surv. Can., Paper 77-1B (1977)

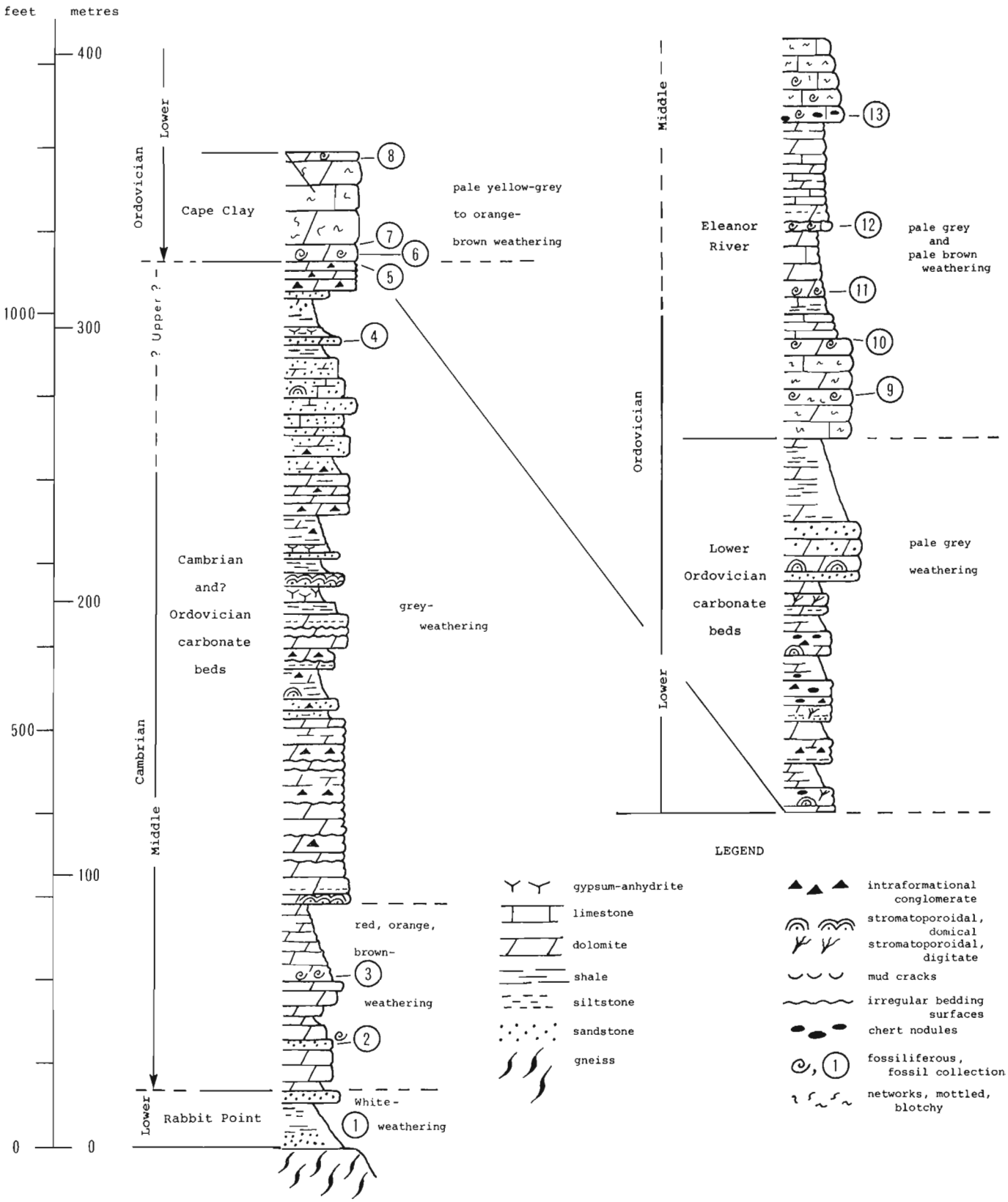

Figure 42.2. Graphic representation of composite stratigraphic section, lower Paleozoic rocks of eastern Devon Island.

The Paleozoic, bedded rocks include sandstone, dolomite, limestone, intraformational conglomerate, and gypsum. The units range in age from Early Cambrian to Middle Ordovician.

The stratigraphy of the Lower Paleozoic rocks, as presented here, is based on several measured sections at localities on both the south and north coasts of the island. The sections studied by Kurtz et al. (1952) at Dundas Harbour, although referred to in the text, were not visited by the author. This report is preliminary in nature and the correlation of units is tentative.

Cambrian

Lower and Middle Cambrian

The Precambrian crystalline rocks of eastern Devon Island are overlain unconformably by a thin- to medium-bedded sequence of carbonate and clastic rocks in which are found, near Dundas Harbour, fossils of Early and Middle Cambrian age. The Lower Cambrian beds described here are assigned to the Rabbit Point Formation of Kurtz et al. (1952). Overlying beds appear to be correlative with the Bear Point and Ooyahgah formations of the same authors. The uppermost thin beds, here considered to be probably Middle Cambrian, form a basal member of the Ordovician Mingo River Formation of Kurtz et al. (1952).

Rabbit Point Formation. A basal sandstone unit, the Rabbit Point Formation (Kurtz et al., 1952), is widespread but in places rather thin or perhaps absent. At the type section, west of Dundas Harbour (Fig. 42.3, loc. 4), the unit is 26.5 m (85 ft.) thick and consists of calcareous, medium to fine grained sandstone, in part glauconitic. **Olenellus** and linguloid brachiopods (1)[1] were collected by Kurtz and Wales 7.6 m (25 ft.) above the base. At Cuming Inlet, about 80 km (50 miles) to the west (Fig. 42.3, loc. 6), about 21 m (70 ft.) of white-weathering, medium and fine grained sandstone with green shale beds were measured. At Burnett Inlet, 32 km (20 miles) west of Cuming Inlet (Fig. 42.3, loc. 7), Glenister (1963, p. 181) noted about 14 m (45 ft.) of quartzose sandstone, coarse at the base and medium grained upward.

The Rabbit Point Formation appears much reduced in thickness at locality 3 (Fig. 42.3), 24 km (15 miles) northwest of the type locality, where a basal sandstone bed about 1.5 m (5 ft.) thick is present and overlain by a dolomitic limestone bed. The overlying 15 m (50 ft.) of strata are covered but there is no evidence in the talus that sandstone is present.

Basal sandstones of the Rabbit Point Formation are more prominent on the north coast of Devon Island, where Glenister (1963, p. 186, 187) measured an incompletely exposed section of sandstone about 60 m (200 ft.) thick (Fig. 42.3, loc. 1).

Undivided Bear Point-Ooyahgah Formations. Conformably overlying the Rabbit Point Formation is a sequence consisting mainly of thin-bedded dolomite and dolomitic limestone with minor amounts of sandstone and shaly to silty carbonate. The thin bedded carbonate sequence forms rubbly slopes, in many places interrupted in the lower part by lines of small cliffs due to more resistant dolomite beds. The beds are characterized by variable lithology but have a uniform thickness of about 300 m (1000 ft.).

The Middle Cambrian sequence described here is presumed to comprise mainly the Bear Point and the Ooyahgah formations of Kurtz et al. (1952), but it includes also about 12 m (40 ft.) of beds assigned by them to the Mingo River Formation. The Middle Cambrian sequence is treated as a unit because a mappable contact separating the formations was not evident in the field. The difficulty in separating the Bear Point and Ooyahgah formations may have been due to the reconnaissance nature of the recent field work, but it is suspected that division is not practical outside the type area.

The Middle Cambrian carbonate beds include mainly grey to yellow-grey, thin-to medium-bedded, fine grained dolomite, limy dolomite, and dolomitic limestone, and shaly to silty dolomite. Sandstone, commonly limy or dolomitic, forms 10 to 20 per cent of the section, and intraformational conglomerate forms an abundant and conspicuous component of the unit. Locally conspicuous, mainly in the middle part of the unit, are stromatolitic beds variously with digitate and domal or layered forms. Thin gypsum-anhydrite or gypsiferous shale strata occur locally in the middle and upper parts of the section. Sandstone and sandy beds occur generally as medium or thick beds in the upper half of the unit. In addition, one or two thin sandstone beds occur locally within about 30 m (100 ft.) of the base. A prominent sandstone member is widely distributed in the upper part of the Middle Cambrian carbonate beds (Fig. 42.3).

Several fossil collections were obtained by Kurtz and Wales from thin carbonate beds equivalent to beds described here. The early collections (Kurtz et al., 1952) were made west of Dundas Harbour but, in spite of careful search by J.W. Cowie in 1960 and by Cowie and Christie in 1968, similar collections were not found outside the type locality, although linguloid brachiopods were found at two horizons (2, 3) at Cuming Inlet. Evidently conditions for preservation – perhaps less dolomitization – were more favourable in the Dundas Harbour region than elsewhere.

Middle Cambrian **Paterina** was collected (4) in the type section of the Ooyahgah Formation, from shale beds a few tens of feet below fossiliferous Lower Ordovician beds and it appears, therefore, that Upper Cambrian beds are missing from the section.

Ordovician

Lower Ordovician

Cape Clay Formation. The thin-bedded dolomite, limestone, intraformational conglomerate, and sandstone of Middle Cambrian age are overlain conformably by distinctive thick-bedded dolomite, here assigned to the Cape Clay Formation. The Cape Clay Formation was defined by Koch (1929a, p. 14; 1929b, p. 230) in Washington Land, Greenland, where it conformably overlies the Cass Fiord Formation.

[1] Fossiliferous horizons are identified on Figure 42.2 by appropriate circled numbers.

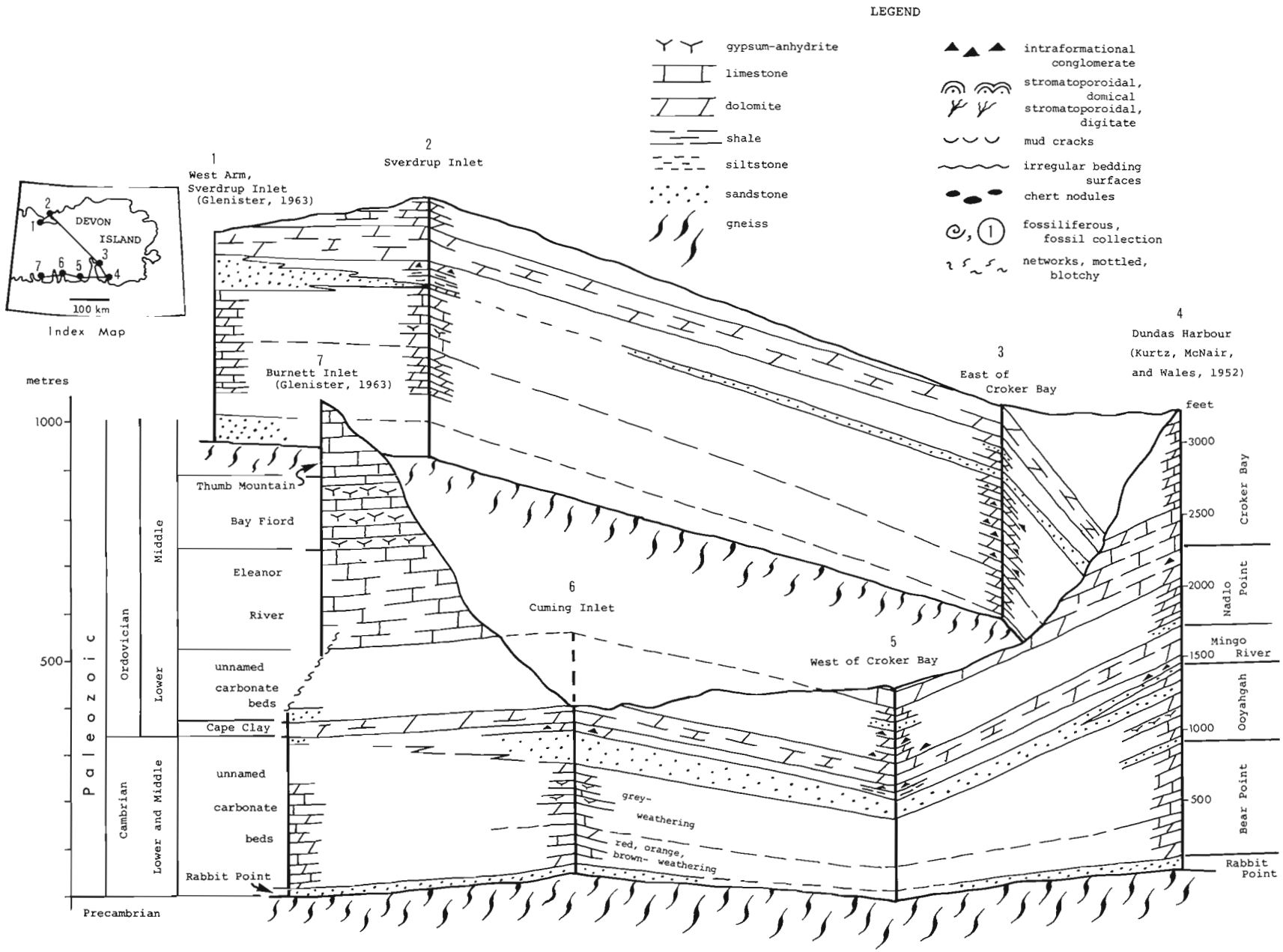

Figure 42.3. Fence diagram showing lower Paleozoic formations of eastern Devon Island.

Table 42.1

Table of Formations

Era	Period or Epoch		Formations: This paper	Formations: Kurtz, McNair, and Wales, 1952	Lithology Thickness: feet (metres)
Cenozoic	Quaternary to Recent				Till, gravel, sand, alluvium
Paleozoic	Ordovician	M	Cornwallis Gp.	Croker Bay	Limestone, gypsum-anhydrite 750 (230)
		M	Eleanor River	Croker Bay	Limestone, dolomite, intraformational conglomerate 700 (210)
		L	carbonate beds	Nadlo Point	Dolomite, dolomitic limestone, intraformational conglomerate, sandstone 400 (120)
		L	Cape Clay	Mingo River	Dolomite, dolomitic limestone 120-230 (37-70)
	Cambrian	U	disconformity	disconformity	Dolomite, dolomitic limestone, intraformational conglomerate, sandstone, shale, gypsum-anhydrite 1000 (300)
		M	carbonate beds	Ooyahgah	
		M		Bear Point	
		L	Rabbit Point	Rabbit Point	Sandstone, shale 10-87 (3-26)
nonconformity					
Precambrian					Diabase (dykes)
					Gneiss, granitoid gneiss; quartz-feldspar-biotite gneiss, garnetiferous gneiss, quartz-feldspar-garnet rock; pegmatite

The thick-bedded dolomite, here called the Cape Clay Formation, and the uppermost few tens of feet of the thin-bedded sequence were named the Mingo River Formation by Kurtz et al. (1952). The unity of the formation presumably was based on the cliff-forming character of both the uppermost thin beds and the thick-bedded dolomite, and on the presence, in certain thin beds, of **Symphysurina** and **Dendrograptus** (5). **Hystricurus**? **nudis** was found (7) in the lowermost part of the thick-bedded member, and an early Ordovician age was assigned to the formation. The boundary between units is placed, in this report (as noted),at the base of the thick-bedded part of the Mingo River Formation. The reasons are:

1. The upper part of the Mingo River Formation is a distinctive, thick-bedded dolomite and limy dolomite unit that may be correlative with the Cape Clay Formation of Northwest Greenland and central Ellesmere Island (as noted by Kurtz et al., 1952, p. 653; see also Christie, 1967, p. 38-40);

2. The interbedded carbonate and intraformational conglomerate evidently are not present everywhere beneath the thick-bedded part of the Mingo River Formation; at some localities, sandstone directly underlies the thick-bedded unit. In any case, the lower beds are lithologically similar to the underlying beds and are in marked contrast to the overlying thick-bedded unit; it seems preferable, therefore, to place the formational boundary at a distinctive and widely distributed lithological break.

Only a few tens of feet separate fossiliferous beds assigned a Middle Cambrian age from those of Early Ordovician age in the type section of Kurtz et al. and it appears probable, as noted by those authors, that Upper Cambrian beds are absent. The disconformity representing this hiatus is presumed, in the present report, to lie at the base of the thick beds of the Cape Clay Formation. Kurtz et al. (1952, p. 652), on the other hand, place the disconformity beneath the lower, thin-bedded part of their Mingo River Formation (see Table 42.1).

The Cape Clay Formation of Devon Island is very thick bedded, finely to coarsely crystalline, grey to brown dolomite and dolomitic limestone characteristically weathering to yellow-brown, red-brown, or orange, with distinctive lighter patches of irregular or amoeboid form. The weathered surface may be scoriaceous. Parts or all of the unit, especially where coarsely crystalline, are vuggy to cavernous. The Cape Clay is identified easily, even from a distance, because of its cliff-forming nature and distinctive colours; the lower beds are commonly darker and brownish, and the upper, yellow-white weathering. Kurtz et al. (1952, p. 645) described the unit (the upper part of the Mingo River Formation, 53.6 m (176 ft.) thick) as follows: "brownish grey, . . . fine-grained, massive, weathers yellowish brown. Broad light coloured bands, discernible from a distance, occur in the middle part of the unit".

The Cape Clay Formation is 37 to 70 m (120-230 ft.) thick in measured sections on Devon Island.

Poorly preserved orthocerid cephalopod fossils may be found at most localities in the Cape Clay Formation. In addition, **Hystricurus** was collected (7) by Kurtz and Wales near Dundas Harbour, and Glenister obtained **Goniotrema**? sp., **Eotomaria** sp., **Ophileta** sp., **Cyrtocerina** sp., and "cf. **Piloceras** sp." south of the west arm of Sverdrup Inlet (Fig. 42.1, loc. 1). **Ophileta** and **Hystricurus** were among fossils identified by Foerste (1921) and Poulsen (1946) in collections from the Cape Clay Formation at Bache Peninsula (Ellesmere Island) and Northwest Greenland; an "Upper Ozarkian" (Early Canadian) age was assigned.

Orthocerid cephalopod fossils were collected (6, 8) at most Cape Clay localities visited during recent field work. Fossils were obtained (8) from the uppermost part of the unit west of Croker Bay (Fig. 42.3, loc. 5); these are reported by E.L. Yochelson as follows (GSC loc. C-3305):

echinoderm plates
fragment of brachiopod or pelecypod indet.
?mollusk fragment with prominent spiral ornament
?**Priscochiton** sp. indet.
gastropod indet. aff. **Loxoplocus (Lophospira)**
?**Bridgeina** or **Helicotoma**
lenticular gastropod genus indet. (step-like umbilicus)
macluritid gastropod indet.
?macluritid gastropod indet. (very low whorls)
gastropod indet. aff. **Trochonema** sp.
high-spired gastropod indet. (possibly two genera)
cephalopod indet.

Regarding the age, Yochelson remarks as follows: "The ?**Bridgeina** is known from early Early Ordovician. The macluritid could be into Early Ordovician or Middle Ordovician. The possible **Trochonema** could be Middle Ordovician".

The evidence described above supports the assignment of the fossiliferous unit of Devon Island to the Cape Clay Formation, and of an Early Ordovician age to the beds.

Kurtz and Wales describe (as noted earlier), in their type section of the Mingo River Formation, about 4.5 m (15 ft.) of greenish grey calcareous shale and interbedded brownish limestone immediately beneath the upper, massive dolomite unit. **Symphysurina** and **Dendrograptus gracilis**? were collected (5) from the middle of these beds. A green shale bed, 20 cm (8 in.) thick, but not fossiliferous, was noted by Christie in a section at locality 5, about 50 km (30 miles) west of Kurtz and Wales' locality. At no other section studied on Devon Island were these shale beds seen. Possibly the shale and associated limestone should be considered as discontinuous basal beds of the Cape Clay Formation.

Unnamed Lower Ordovician carbonate beds. Conformably overlying the Cape Clay Formation is a sequence of thin-bedded dolomite, dolomitic intraformational conglomerate, and lesser amounts of dolomitic sandstone about 120 m (400 ft.) thick. This unit evidently is present everywhere in eastern Devon Island but usually forms greyish talus slopes between prominent cliffs formed by the underlying and overlying, relatively resistant, brown-weathering units. This unnamed map-unit is presumed to be equivalent to the lower part (about two-thirds) of the Nadlo Point Formation of Kurtz et al. (1952).

A complete section of the unnamed carbonate beds was examined by the writer at only one locality: that west of Croker Bay (loc. 5). There, the unit consists of about 90 m (300 ft.) of thin-bedded, fine grained, pale brown weathering dolomite and dolomite intraformational conglomerate overlain by about 21 m (70 ft.) of medium-bedded, white-grey weathering, dolomitic sandstone and about 30 m (100 ft.) of talus-covered, greenish grey, slaty carbonate, probably argillaceous dolomite. The lower dolomites are silty to sandy, and contain abundant dark grey chert nodules. Both digitate and domal stromatolites are abundant in the lower two-thirds of the unit.

Beds similar to those described above were examined by Kurtz and Wales at the type section of the Nadlo Point Formation. There, the basal 14 m (47 ft.) of the unit are greenish grey, glauconitic, calcareous sandstone. The sandstone is overlain by about 46 m (150 ft.) of mainly brownish grey, silty dolomitic limestone, above which is a covered interval of 46 m (150 ft.).

A sequence of about 60 m (200 ft.) of the lower beds was examined east of Sverdrup Inlet, on the north coast of the island (Fig. 42.3, loc. 2). These beds are thin- to medium-bedded, fine grained dolomite and, when

weathered, have a hard, silvery grey surface. Some greenish shaly beds are present, but few intraformational conglomerates were observed.

No fossils have been collected from the unnamed carbonate unit overlying the Cape Clay Formation, but its stratigraphic position clearly indicates an Early Ordovician age. The unit probably contains equivalents of the gypsiferous Baumann Fiord Formation and of the underlying beds ("map-unit 6" of Bache Peninsula region; Christie, 1967) of central Ellesmere Island (see Kerr, 1967, 1968a). Although gypsum-anhydrite may be present in some of the covered intervals on Devon Island, it was nowhere observed.

Lower and Middle Ordovician

Eleanor River Formation. A series of cliff-forming, fossiliferous, brown-weathering limestone beds, tentatively assigned to the Eleanor River Formation, conformably overlies the unnamed carbonate rocks described above. The Eleanor River Formation was defined by Thorsteinsson (1958, p. 31) on Cornwallis Island. The unit was redescribed and assigned a new reference section on Ellesmere Island by Kerr (1967, p. 103; see also Kerr, 1968a, p. 26, 80, 81).

The Eleanor River Formation is widely exposed on eastern Devon Island, where it comprises generally resistant, thick beds of pale brown weathering limestone and less resistant interbeds. The writer nowhere traversed the whole unit, but probably all or nearly all of it is represented in the section studied by Glenister (1963) at Burnett Inlet (loc. 7), where a succession of about 210 m (700 ft.) of Eleanor River beds was measured.

Included in the Eleanor River Formation in this report are the upper beds, about 76 m (250 ft.) thick, of the Nadlo Point Formation of Kurtz et al. (1952). The upper part of the Eleanor River Formation presumably is represented by lower beds of the type Croker Bay Formation.

The position of the upper boundary of the Eleanor River Formation in the section near Dundas Harbour is uncertain; if the unit described by Kurtz and Wales as forming a "structural terrace" is taken to underlie less resistant, perhaps gypsiferous beds (of the Cornwallis Group), then this would be the top of the Eleanor River Formation. A thickness approaching 180 m (600 ft.) would then be present.

The Eleanor River Formation of southeastern Devon Island (the unit was not visited elsewhere) includes thick-bedded, fine grained, grey and pale brown weathering limestone; thin-bedded, yellow-grey-weathering dolomitic limestone and intraformational conglomerate; and minor amounts of light grey weathering shaly carbonate beds. The thick-bedded limestones are characteristically marked on the weathered surface by irregular patches or an anastomosing network of a lighter brown colour, and emit a strongly petroliferous odour on breaking. Silicified fossils are abundant at numerous horizons and, in addition, siliceous networks and chert nodules occur in upper, competent beds. Bedding planes in the thin- to medium-bedded dolomitic rocks are commonly wavy and argillaceous. Numerous fossiliferous beds also are present in the less competent part of the unit.

Fossils were obtained from various levels in the interval assigned to the Eleanor River Formation on southeastern Devon Island (9-13). Some of these are reported below.

Fossil collections examined by B.S. Norford of the Geological Survey of Canada are reported as follows:

Bed about 37 m (120 ft.) above the base west of Croker Bay (GSC loc. C-3307) (10):

Ceratopea sp.
Maclurites sp.
?**Palliseria** sp.
Polytoechia sp.
Diparelasma sp.
bryozoan
echinoderm
trilobite fragment
gastropods
straight cephalopods
age: early Middle Ordovician (Whiterock) or possibly latest Early Ordovician (Canadian)

Bed about 76 m (250 ft.) above the base west of Croker Bay (GSC loc. C-3308) (12):

?**Maclurites** sp.
echinoderm debris
gastropods indet.
ostracode
trilobites undetermined
age: probably Middle Ordovician

Bed about 55 m (180 ft.) above uncertain base, west of Croker Bay (GSC loc. C-3310) (not shown in Fig. 42.2):

Ozarkispira sp.
?**Nanorthis** sp.
gastropod indet.
age: Early Ordovician, probably Middle Canadian (about late Tremadoc)

About 135 m (450 ft.) above base, west of Croker Bay (GSC loc. C-3313) (13):

Maclurites sp.
echinoderm debris
brachiopod indet.
ostracode
trilobite undet.
age: Middle Ordovician

About 200 m (650 ft.) of limestone at Burnett Inlet (loc. 7) were assigned to the Eleanor River Formation by Glenister (1963, p. 181, 182) on the basis of lithology and position below the Cornwallis Formation (Group). Fossil collections from these beds were dated provisionally by G.W. Sinclair as Middle Ordovician.

Kurtz and Wales obtained several fossil collections from the upper, resistant beds of the Nadlo Point Formation, which beds, as noted, are here included with the Eleanor River Formation (see Kurtz et al., 1952, p. 642-644). A probable late Canadian age was suggested for the beds.

Table 42.2

Correlation of lower Paleozoic formations of Devon, Ellesmere, and Cornwallis Islands.
Age assignments for tops and bottoms of formations follow Table 1 of Barnes, 1974.

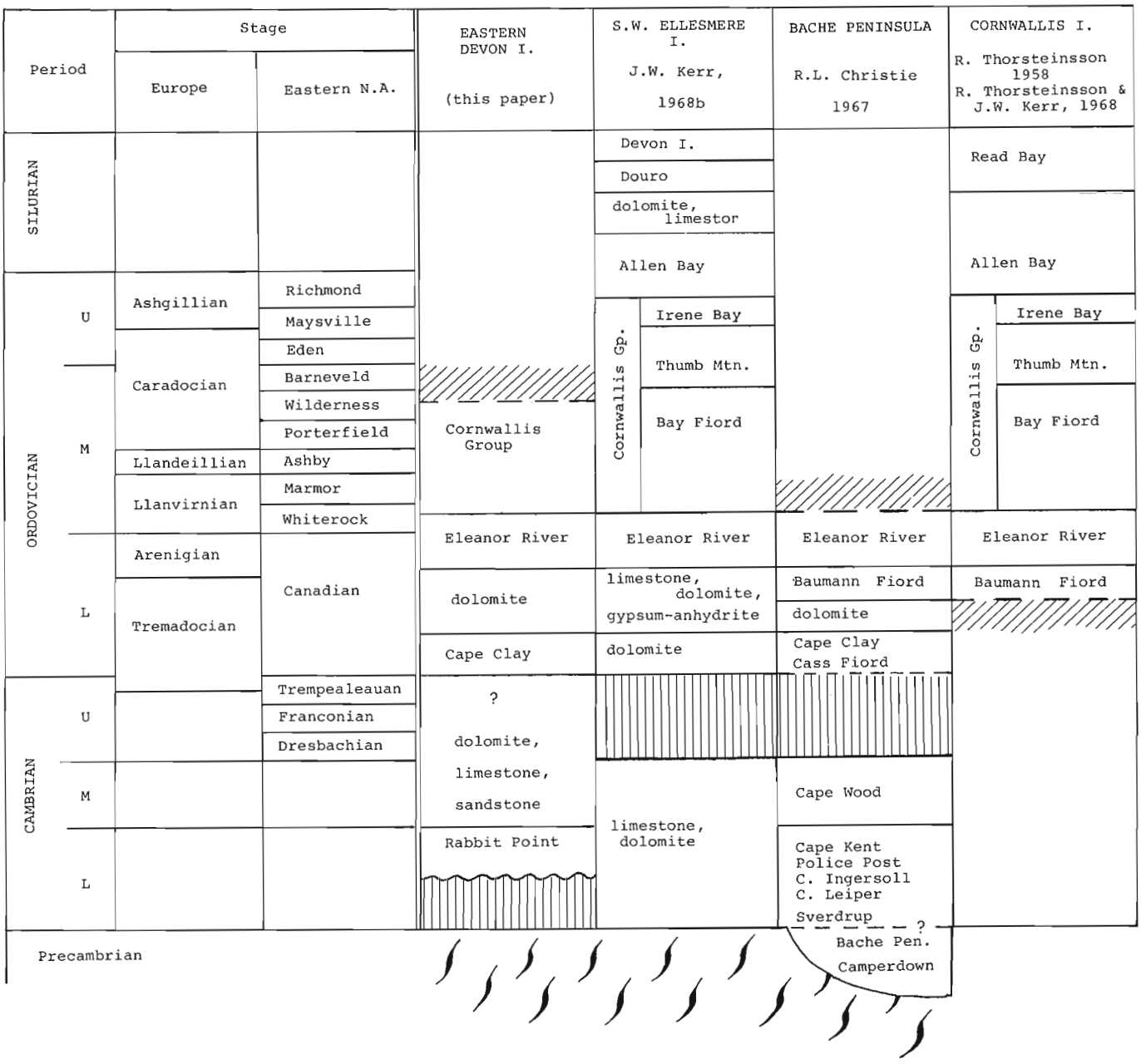

The lowermost 90 m (300 ft.) of the Croker Bay Formation of Kurtz et al. comprise mainly brown, petroliferous limestone and these beds, as noted, are included here tentatively in the Eleanor River Formation[1]. **Maclurites** and **Isotelus** were obtained, for which a "Middle Ordovician or possibly early Upper Ordovician" age was assigned.

Middle and Upper Ordovician

Cornwallis Group. The Cornwallis Group was defined originally by Thorsteinsson (1958, p. 33) on Cornwallis Island as the Cornwallis Formation. The unit was redefined and raised to group status by Kerr (1967), who named three reference sections near Irene Bay on Ellesmere Island.

[1] This correlation was suggested earlier by Thorsteinsson (in Fortier et al., 1963, p. 34).

The Cornwallis Group typically comprises a basal gypsum-anhydrite and thin-bedded limestone formation, a middle, bluff-forming limestone formation, and a thin, recessive shaly limestone formation. These are named, respectively, the Bay Fiord, Thumb Mountain, and Irene Bay formations. Beds described by Glenister (1963, p. 182, 183) at Burnett Inlet clearly are assignable to the Bay Fiord and Thumb Mountain formations. The Cornwallis Group forms some of the uplands of southern Devon Island and is exposed widely west of Burnett Inlet. The group was not examined, however, by the author during the recent field work.

A section composed of light brownish grey, medium- to thin-bedded limestone about 340 m (1100 ft.) thick and containing Maclurites and Receptaculites arcticus was examined by Kurtz and Wales west of Dundas Harbour. These beds were included in the Croker Bay Formation, of Middle Ordovician age (Kurtz et al., 1952). It is suggested here tentatively that most or all of this 340 m (1115 ft.) section is correlative with the Cornwallis Group, as proposed by Thorsteinsson (in Fortier et al., 1963, p. 34).

Whether the basal, gypsiferous unit of the Cornwallis Group, the Bay Fiord Formation, is present immediately west of Dundas Harbour is uncertain. At Burnett Inlet, 100 km (60 miles) to the west (loc. 7), this formation is 160 m (530 ft.) thick and consists of thin gypsum beds alternating with limestone and shale (Glenister, 1963, p. 182). A whitish, recessive unit below resistant beds east of Croker Bay was discerned in 1969 by fieldglass and appeared to be in the correct stratigraphic position for the Cornwallis Formation.

A Middle Ordovician age is assigned to the Cornwallis beds of Burnett Inlet based on fossil collections from upper beds (Glenister, 1963, p. 182, 183). The group is known, elsewhere, to range in age from early Middle to Late Ordovician (Whiterock to early Richmondian), based on conodont biostratigraphy (see Barnes, 1974; this paper, Table 42.2).

References

Barnes, C.R.
1974: Ordovician conodont biostratigraphy of the Canadian Arctic; in Symp. on the Geology of the Canadian Arctic; Geol. Assoc. Can./Can. Soc. Petrol. Geologists, Proc., p. 221-240.

Christie, R.L.
1967: Bache Peninsula, Ellesmere Island, Arctic Archipelago; Geol. Surv. Can., Mem. 347.

Cowie, J.W.
1961: Geology; in The Devon Island expedition; Arctic, v. 14, no. 4, p. 255.

Foerste, A.F.
1921: Notes on Arctic Ordovician and Silurian cephalopods, chiefly from Boothia Felix-King William Land, Bache Peninsula, and Bear Island; Denison Univ. Bull., J. Sci., Labs, v. 19, p. 247-306, Pls. 27-35.

Fortier, Y.O., Blackadar, R.G., Glenister, B.F., Greiner, H.R., McLaren, D.J., McMillan, N.J., Norris, A.W., Roots, E.F., Souther, J.G., Thorsteinsson, R., and Tozer, E.T.
1963: Geology of the north-central part of the Arctic Archipelago, Northwest Territories (Operation Franklin); Geol. Surv. Can., Mem. 320.

Glenister, B.F.
1963: Burnett Inlet; in Geology of the north-central Part of the Arctic Archipelago, Northwest Territories (Operation Franklin); Geol. Surv. Can., Mem. 320, p. 179-184.

Haughton, S.
1859: Geological account of the Arctic Archipelago; in M'Clintock, F.L. 1859: The Voyage of the **Fox** in the Arctic Seas; a narrative of the discovery of the fate of Sir John Franklin and his companions; John Murray, London, Appendix IV, p. 372-399.

Kerr, J.Wm.
1967: New nomenclature for Ordovician rock units of the eastern and southern Queen Elizabeth Islands, Arctic Canada; Bull. Can. Petrol. Geol., v. 15, no. 1, p. 91-113.

1968a: Stratigraphy of central and eastern Ellesmere Island, Arctic Canada, Pt. II, Ordovician; Geol. Surv. Can., Paper 67-27, Pt. II.

1968b: Geology, southwestern Ellesmere Island; Geol. Surv. Can., Map 10-1968, 1:125 000.

Koch, Lauge
1929a: The geology of the south coast of Washington Land; Medd. om Grønland, Bd. 73, Afd. 1, Nr. 1.

1929b: Stratigraphy of Greenland; Medd. om Grønland, Bd. 73, Afd. 1, Nr. 2.

Kurtz, V.E., McNair, A.H., and Wales, D.B.
1952: Stratigraphy of the Dundas Harbour area, Devon Island; Am. J. Sci., v. 250, p. 636-655.

Low, A.P.
1906: Cruise of the **Neptune**; report on the Dominion Government Expedition to the Hudson Bay and the Arctic Islands on board the **DGS Neptune** 1903-04; Government Printing Bureau, Ottawa.

M'Clintock, F.L.
1859: The voyage of the **Fox** in the Arctic Seas; a narrative of the discovery of the fate of Sir John Franklin and his companions; John Murray, London.

1875: The voyage of the **Fox** in the Arctic Seas in search of Franklin and his companions; John Murray, London, 4th ed.

Nichols, D.A.
1936: Post-Pleistocene fossils of the uplifted beaches of the eastern Arctic regions of Canada; Can. Field Naturalist, v. L, p. 127-129.

Poulsen, Chr.
1946: Notes on Cambro-Ordovician fossils collected by the Oxford University Ellesmere Land Expedition, 1934-35; Quart. J. Geol. Soc. London, v. 102, p. 299.

Prest, V.K.
1952: Notes on the geology of parts of Ellesmere and Devon Islands, Northwest Territories; Geol. Surv. Can., Paper 52-32.

Thorsteinsson, R.
1958: Cornwallis and Little Cornwallis Islands, District of Franklin, N.W.T.; Geol. Surv. Can., Mem. 294.

Thorsteinsson, R. and Kerr, J.Wm.
1968: Cornwallis Island and adjacent smaller islands, Canadian Arctic Archipelago; Geol. Surv. Can., Paper 67-64.

Wales, D.B.
1949: Cambrian strata on the southern shore of Devon Island in the Arctic Archipelago; J. Geol., v. 57, p. 330.

Weeks, L.J.
1927: The geology of parts of eastern Arctic Canada; Geol. Surv. Can., Sum. Rept. 1925, Pt. C, p. 136-142.

43. FAUNA AND CORRELATION OF THE TYPE SECTION OF THE CRANSWICK FORMATION (DEVONIAN), MACKENZIE MOUNTAINS, YUKON TERRITORY

Project 680093

A.E.H. Pedder and Gilbert Klapper[1]
Institute of Sedimentary and Petroleum Geology, Calgary

Introduction

As proposed by A.W. Norris (1968a, p. 27, 28; 1968b, p. 771), the Cranswick Formation comprises an unnamed lower member of "medium brownish grey to black, aphanitic to fine-grained, thin-bedded to massive limestone" and an upper, also unnamed member of "black, fine-grained limestone and argillaceous limestone, interbedded with black calcareous shale". At the composite type section on the Mackenzie Mountain Front, 6 to 12 km west of Snake River (65°26-27.5'N; 133°34-35'W), thicknesses of these members were given as 208.2 ft. (63.5 m) and 234.5 ft. (71.5 m) respectively.

A short distance westward (probably in the order of 15 km) from the type locality, the Cranswick passes into a predominantly shale facies now mapped as the Road River Formation (D.K. Norris, 1975). Relationships to rock units situated to the north, east and south of the type outcrop section are more problematical, although the problem may be more nomenclatorial than stratigraphic. For example, D.K. Norris (1975) has mapped the Cranswick and overlying Ogilvie formations to the eastern margin of the Snake River sheet (NTS 106F) whereas, in the adjacent Rampart River sheet (NTS 106G), these are combined and mapped under the formational name of Landry (Aitken and Cook, 1975). It should be noted also that the unit mapped as Cranswick by D.K. Norris corresponds only to the lower of the two original members of the formation. The anonymous authors of the 15th Schedule of Wells (1976, p. 72) do not use the terms Cranswick, Ogilvie or Landry in listing the subsurface sequence penetrated by the Amoco PCP B-1 Cranswick Y.T. A-42 well (65°41'13"N; 133°07'52"W), which is only 18.5 km north of the Cranswick outcrop near the centre of the Snake River sheet; the Gossage Limestone Member of their terminology (8364-9863 ft.) probably corresponds, in part, to D.K. Norris' Cranswick Formation and A.W. Norris' lower member of the formation. South of the east-west trending mountain front, in the area of the headwaters of Cranswick River in the southeast part of the Snake River sheet, the name Cranswick was applied to a member of the Ogilvie Formation by A.W. Norris (1967, p. 16, 30-36), but appears to have been dropped in a later paper (A.W. Norris, 1968b, Sec. 4, p. 761). D.K. Norris (1975) and Perry et al. (1974, Sec. 16, p. 1094) also have recognized the Cranswick, as a formation, in this area. And again D.K. Norris' units pass eastward into the lower Landry Formation of the Ramparts River sheet.

These nomenclatorial problems could only be resolved by a regional surface and subsurface stratigraphic analysis. In the present contribution, the writers confine themselves essentially to identification and correlation of faunas collected by them in the immediate vicinity of the type section of the Cranswick Formation in July 1976.

[1]Department of Geology, University of Iowa; Iowa City, Iowa 52242

Previous Paleontological Data

A.W. Norris reported the presence of stromatoporoids, later identified by Stearn and Mehrotra (1970, p. 4) as specimens of **Trupetostroma** sp. and **Ferestromatopora** sp., cup corals, **Alveolites** sp., **Coenites** sp., **Gypidula** sp., **Atrypa** sp., **Warrenella** sp., ostracodes and echinoderm ossicles with single, double and cross-like canals from the lower member in the type area, and **Lingula** sp., **Orbiculoidea**? sp., **Warrenella** sp., **Styliolina** sp., **Tentaculites** sp. and echinoderm ossicles with double axial canals in the upper member of the type area. At that time such echinoderm ossicles had been reported from the early Middle Devonian of Europe and were considered indicative of this age in western Canada.

Perry et al. (1974, p. 1069, 1070, 1094, Pl. 1, figs. 14-18) figured a species of **Carinagypa** and listed **Parachonetes macrostriatus** (Walcott)?, **Phragmostrophia** sp. and **Strophochonetes** sp. from 73 m below the top of the Cranswick Formation in the southeast part of Snake River sheet (65°07'40"N; 132°19'W). Their Figure 3 shows the formation at this locality to be equivalent to all but the lowest part of the Lower Devonian Emsian Stage. No mention was made of fossils from the type Cranswick outcrop.

New Paleontological Data

In the type area, the lower member of the Cranswick Formation is a resistant cliff-forming limestone with a thickness of 60.8 m (base not exposed) at 65°24'40"N, 133°35'40"W. The cliff at this locality is illustrated in A.W. Norris' (1968a, p. 283) Plate 13. In the lists of our collections, given below, bracketed numbers after conodont names indicate the number of specimens obtained from a 2 kg sample. Conodonts are identified by Klapper, the megafaunas by Pedder, except the goniatites which were examined by W.W. Nassichuk.

42.7-42.9 m below top of lower cliff-forming member; GSC locality C-63102.

Amphipora sp.
bulbous stromatoporoids, not studied
Alveolites sp.
Spongonaria sp. cf. **S. richardsonensis** Crickmay
S. sp. nov.?
Planetophyllum sp. nov.

39.2-39.3 m below top of lower cliff-forming member; GSC locality C-63103.

Polygnathus inversus Klapper and Johnson (1)

27.1-27.3 m below top of lower cliff-forming member; GSC locality C-63106.

Polygnathus inversus Klapper and Johnson (4)
Panderodus sp. (5)

From: Report of Activities, Part B; Geol. Surv. Can., Paper 77-1B (1977)

23.3-24.3 m below top of lower cliff-forming member; GSC locality C-63107.

Favosites sp. cf. **F. goldfussi** sensu Hill and Jell, 1969
Crassialveolites sp.
Cavanophyllum sp. nov.
Dohmophyllum (sensu lato) sp.
Taimyrophyllum sp. nov.
Carinatina sp. cf. **C. lowtherensis** Johnson and Boucot
trilobite fragments, not studied
echinoderm ossicles with double and cross-like axial canals

21.3-21.7 m below top of lower cliff-forming member; GSC locality C-63108.

Echyropora sp. nov.
Crassialveolites sp.
Bogimbailites sp. nov.
echinoderm ossicles with double and cross-like axial canals

21.4-21.5 m below top of lower cliff-forming member; GSC locality C-63109.

Polygnathus inversus Klapper and Johnson (8)
Pandorinellina exigua exigua (Philip) (23)
Panderodus sp. (5)
Belodella sp. (2)

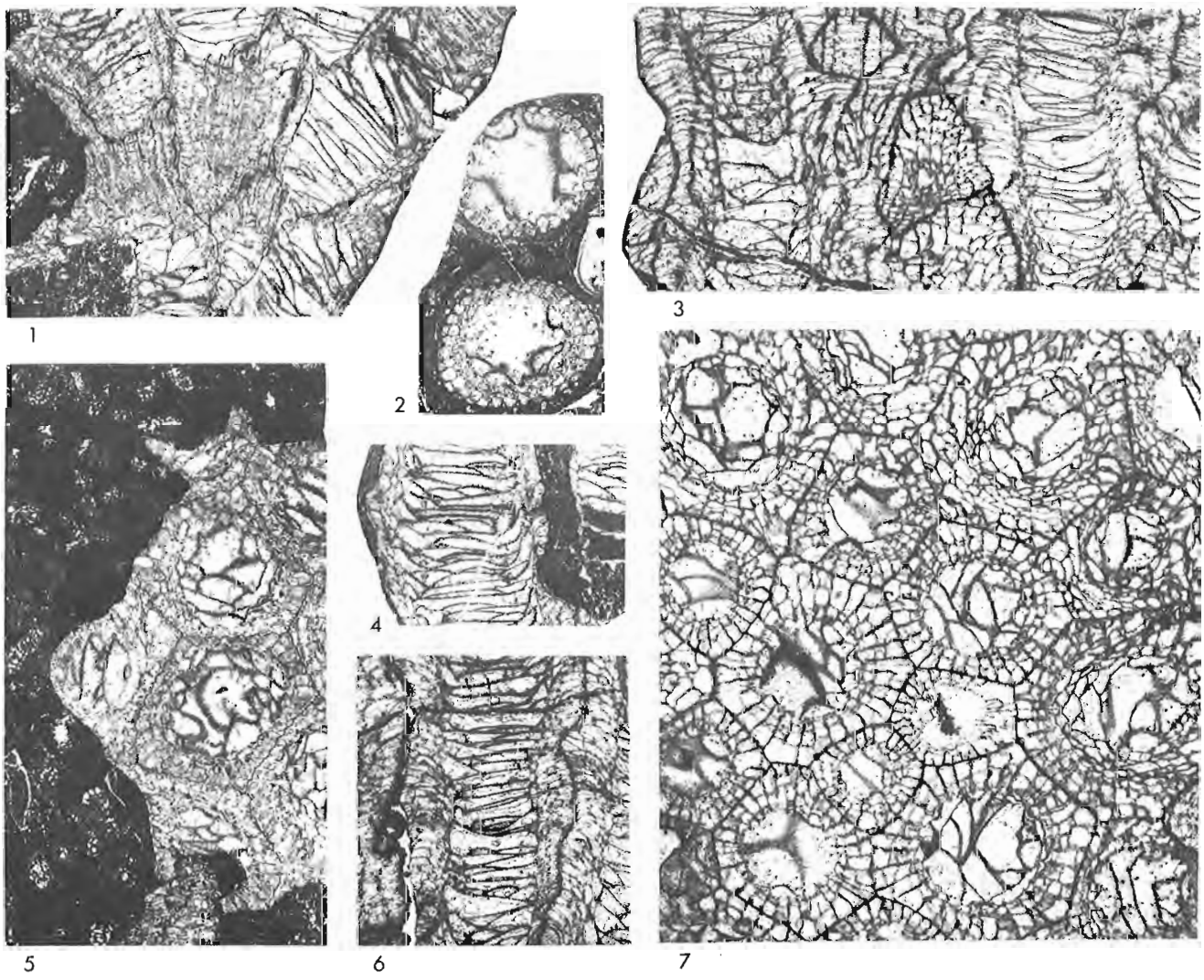

Figures 43.1-43.7. Megafauna from 17.9-18.1 m above base of exposure and 42.7-42.9 m below top of lower resistant member of the Cranswick Formation. Cliff overlooking a tributary of Snake River, Mackenzie Mountain Front, Yukon Territory (65°24'40"N; 133°35'40"W). GSC locality C-63102. Figures 43.1, 5, **Amphipora** sp. undet. and **Spongonaria** sp. nov.?, x3, GSC 53074. Figures 43.2, 4, **Planetophyllum** sp. nov., x3, GSC 53075. Figures 43.3, 6, 7, **Spongonaria** sp. cf. **S. richardsonensis** Crickmay, x3,GSC 53076.

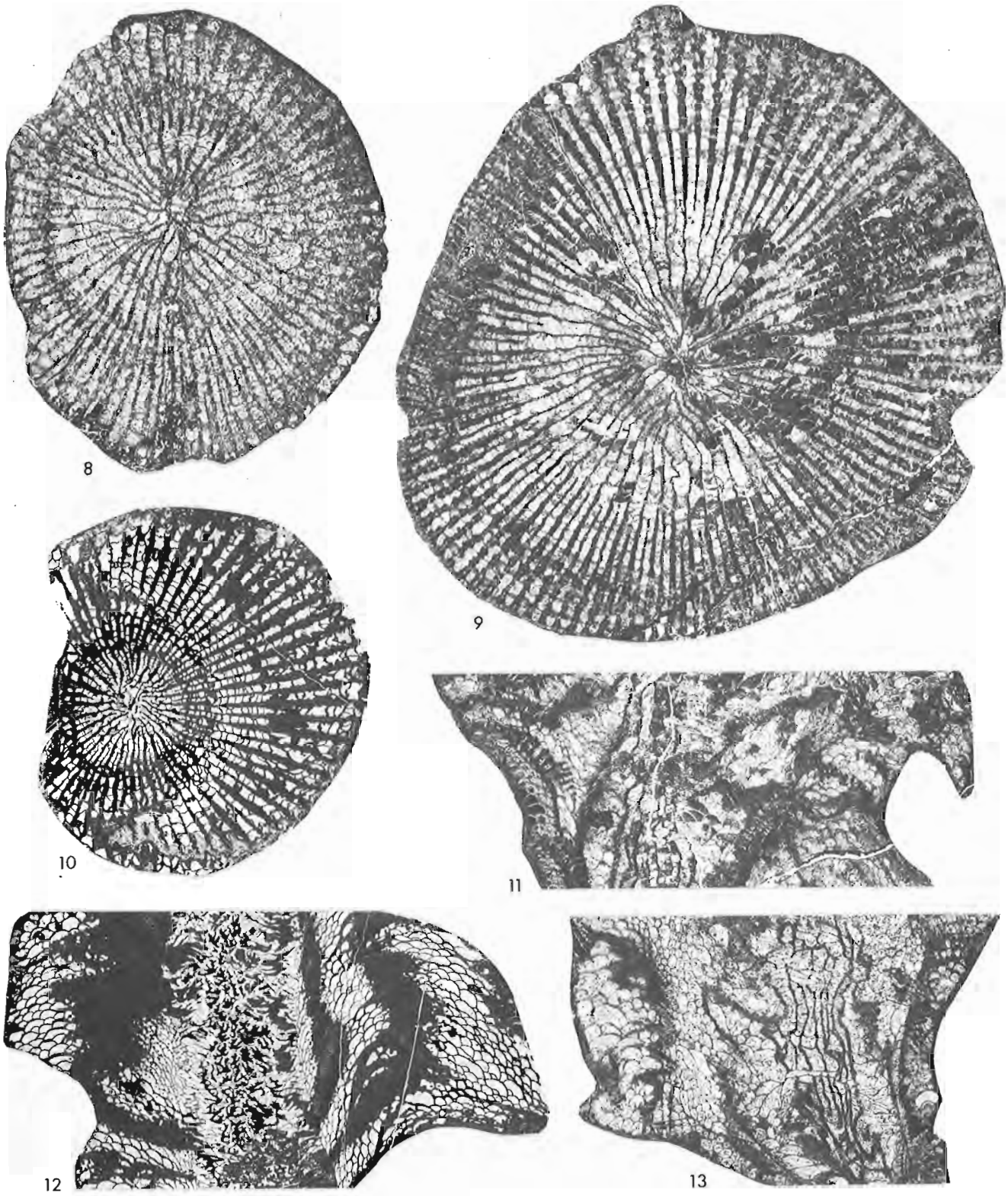

Figures 43.8-43.13. Megafauna from 36.5-37.5 m above base of exposure and 23.3-24.3 m below top of lower resistant member of the Cranswick Formation. Cliff overlooking a tributary of Snake River, Mackenzie Mountain Front, Yukon Territory (65°24'40"N; 133°35'40"W). GSC locality C-63107. Figures 43.8, 9, 11, 13, **Cavanophyllum** sp. nov., x2.5. Figures 43.8, 13, GSC 46112. Figures 43.9, 11, GSC 53077. Figures 43.10, 12. **Dohmophyllum** (broad sense) sp. undet., x2.5, GSC 46114.

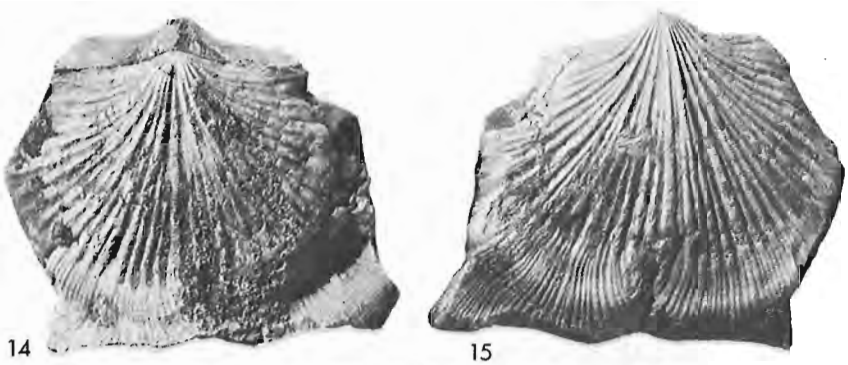

14

15

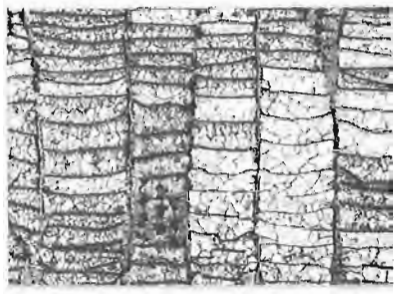

16

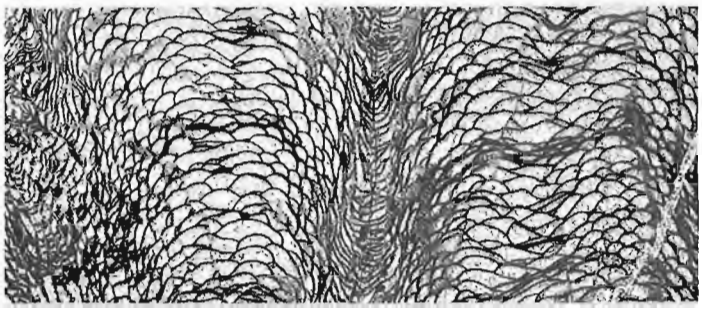

17

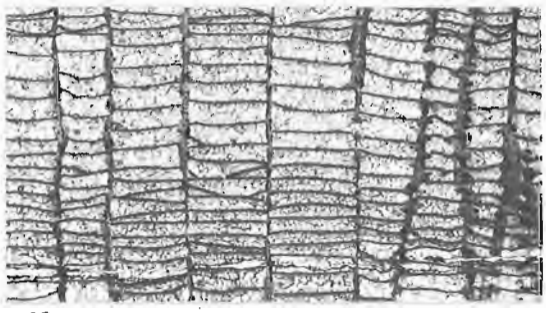

18

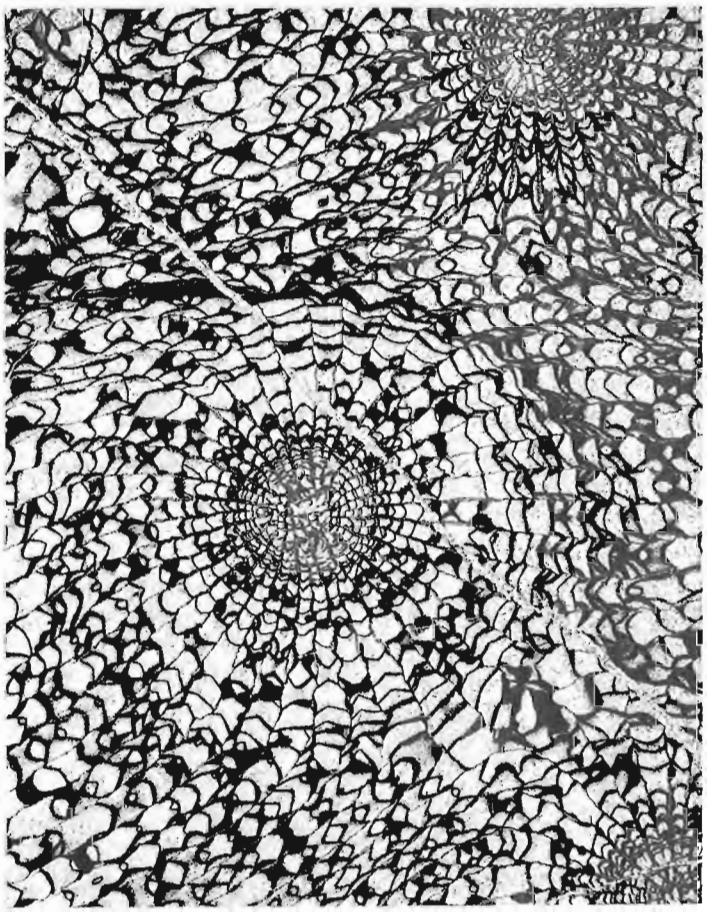

20

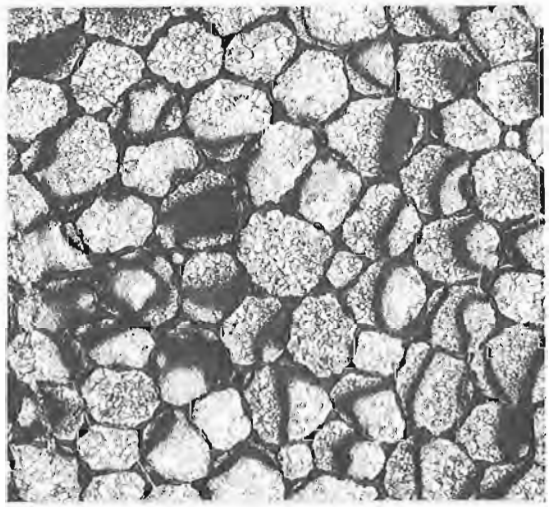

19

21

22

Figures 43.14-43.22. Megafauna from 36.5-37.5 m above base of exposure and 23.3-24.3 m below top of lower resistant member of the Cranswick Formation. Cliff overlooking a tributary of Snake River, Mackenzie Mountain Front, Yukon Territory (65°24'40"N; 133°35'40"W). GSC locality C-63107. Figures 43.14, 15, **Carinatina** sp. cf. **C. lowtherensis** Johnson and Boucot, x2, GSC 53084. Figures 43.16, 18, 19, **Favosites** sp. cf. **F. goldfussi** sensu Hill and Jell, 1969, x4, GSC 53078. Figures 43.17, 20, **Taimyrophyllum** sp. nov., x2.5, GSC 46117. Figures 43.21, 22, **Crassialveolites** sp. indet., x8, GSC 53079.

18.8-19.0 m below top of lower cliff-forming member; GSC locality C-63110.

Polygnathus inversus Klapper and Johnson (16, 5 of which appear transitional to **P. aff. P. perbonus** (Philip))
Pandorinellina exigua exigua (Philip) (27)
Belodella sp. (1)
Panderodus sp. (1)

17.1-17.2 m below top of lower cliff-forming member; GSC locality C-63111.

Polygnathus inversus Klapper and Johnson (3)
P. aff. P. perbonus (Philip) (2)
Pelekysgnathus glenisteri Klapper (1)
Pandorinellina exigua exigua (Philip) (1)

14.2-14.4 m below top of lower cliff-forming member; GSC locality C-63112.

Polygnathus inversus Klapper and Johnson (1)
P. aff. P. perbonus (Philip) (1)
Pandorinellina exigua exigua (Philip) (1)
Belodella sp. (4)
Panderodus sp. (1)

8.2-8.4 m below top of lower cliff-forming member; GSC locality C-63114.

Polygnathus inversus Klapper and Johnson (1)

0
0-0.2 m below top of lower cliff-forming member; GSC locality C-63117.

Polygnathus inversus Klapper and Johnson (4)
Pelekysgnathus glenisteri Klapper (5)
Pandorinellina exigua exigua (Philip) (1)

The upper argillaceous recessive member was examined on a tributary of Snake River (65°27'45"N; 133°30'35"W). The lower part of the unit and lower contact are well exposed here, but minor faulting and absence of the upper contact preclude accurate measurement. A.W. Norris measured the thickness of this member as 234.5 ft. (71.5 m) at a nearby locality (65°27-27.5'N; 133°34-35'W). This included a covered interval of about 50 ft. (15.2 m) at the base of the member. We collected the following fossils:

Talus from lower 15 m of upper recessive member; GSC locality C-63119.

"crushed indeterminate goniatites and one uncrushed specimen that may be a species of **Foordites**" (W.W. Nassichuk).

Approximately 10 m above base of upper recessive member; GSC locality C-63120.

Polygnathus inversus Klapper and Johnson (1)
Pandorinellina sp. (1)
Panderodus sp. (11)
Belodella sp. (10)

8 m below top exposure of upper recessive member; GSC locality C-63122.

Polygnathus serotinus Telford (30)
P. linguiformis linguiformis Hinde α morphotype (4)
Pandorinellina expansa Uyeno and Mason (9)
Panderodus sp. (2)

With the exception of **Polygnathus linguiformis linguiformis** α morphotype, which has been described by Bultynck (1970, p. 126, Pl. 9, figs. 1-7), the **Polygnathus** species identified in the Cranswick Formation have been monographed by Klapper and Johnson (1975), although in that publication **Polygnathus serotinus**, named by Telford (1975, p. 43, 44, Pl. 7, figs. 5-8), was referred to as **Polygnathus** sp. nov. D. **Pandorinellina exigua exigua** and **Pandorinellina expansa** have been monographed by Klapper (in Klapper et al., 1973, p. 319, **Ozarkodina** Pl. 2, fig. 10) and Uyeno and Mason (1975, p. 718-720, Pl. 1, figs. 6, 9, 11-19) respectively. For description and figures of **Pelekysgnathus glenisteri** readers are referred to Klapper's 1969 work (p. 12, Pl. 2, figs. 22-27, 30-34).

The megafossil species of the Cranswick Formation are either new or show some differences from described species. For this reason most are illustrated in accompanying Figures 43.1 to 43.32.

Discussion of Conodonts

Conodont collections from 21.5-21.6 m (C-63103) above the base of the exposed Cranswick Formation, up through the sample at approximately 10 m above the base of the upper recessive member (C-63120), contain **Polygnathus inversus** Klapper and Johnson. Consequently, these collections are referable to the **inversus** Zone, proposed by Klapper and Johnson (in Klapper, in press), on the basis of the sequence at Lone Mountain in central Nevada. The **inversus** Zone is late Early Devonian in age in terms of the European succession (Klapper and Johnson, 1975, p. 71). The zone replaces the **P. perbonus perbonus** Faunal Unit of Perry et al. (1974, locs. S-3, 11, 13-15), which was used informally for strata within the Ogilvie Formation 140-340 km west and northwest of the type Cranswick outcrop. The **inversus** Zone also is present within the Blue Fiord Formation at Sör Fiord, southwest Ellesmere Island (Pedder and Klapper, in prep.), and within the Stuart Bay Formation, Bathurst Island (McGregor and Uyeno, 1972).

The occurrence of **Polygnathus** aff. **P. perbonus** (Philip) in collections C-63111 and C-63112 represents an upward range extension for this distinctive form, which was previously known only in the older **gronbergi** Zone in Nevada and in strata below the **inversus** Zone at Sör Fiord (Klapper and Johnson, 1975, Fig. 4).

The **serotinus** Zone (Klapper and Johnson, in Klapper, in press) is represented by collection C-63122, near the top of the upper recessive member of the Cranswick Formation. In terms of the European succession, the **serotinus** Zone is believed to be older than the base of the Couvinian (Cola), which is taken as the base of the Middle Devonian in Belgium.

Discussion of Megafossils

Much of the Cranswick material is too poorly preserved to be identified with certainty. **Spongonaria** sp. cf. **S. richardsonensis** (C-63102), which differs from **S. richardsonensis**, sensu stricto, in having distinctly flatter dissepiments, is present also in the lower part of the Blue Fiord Formation at Sör Fiord, Ellesmere Island. There its stratigraphic position is above **Polygnathus dehiscens**, below **P. inversus** and within the range of **Pandorinellina exigua exigua** (Pedder and Klapper, in prep.), and is probably equivalent to the Lower Devonian **Polygnathus**

23

24

25

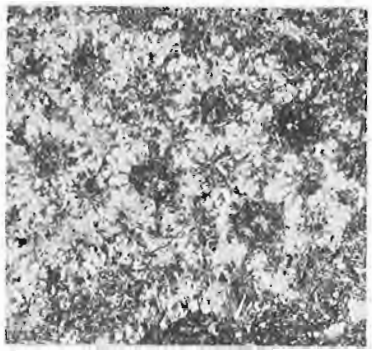

26

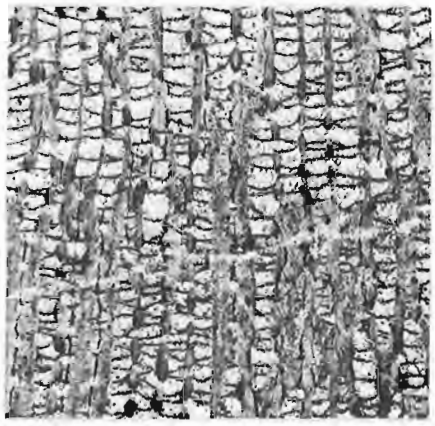

27

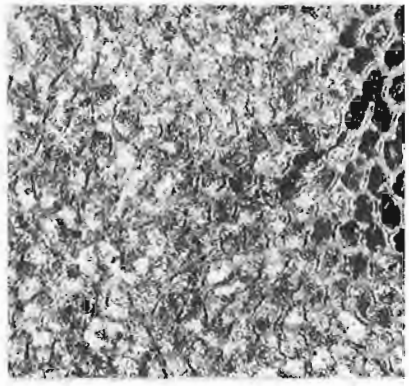

28

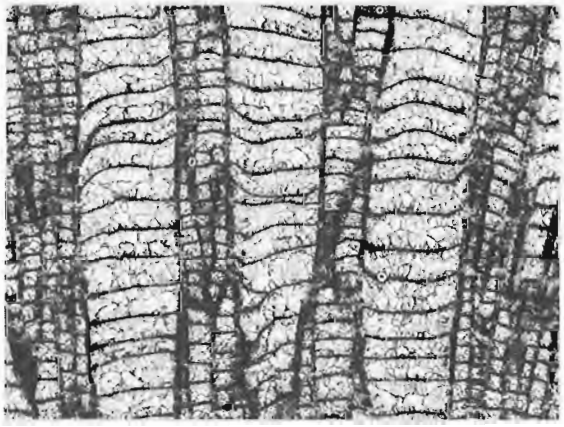

29

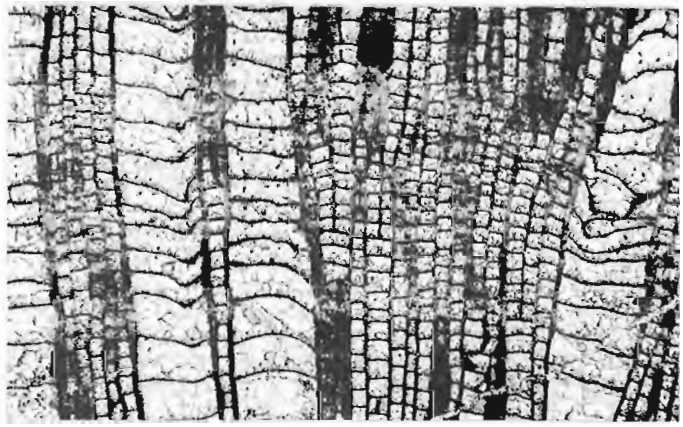

30

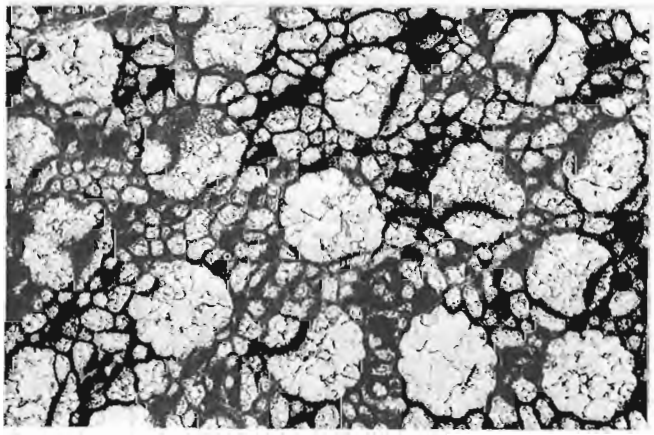

31

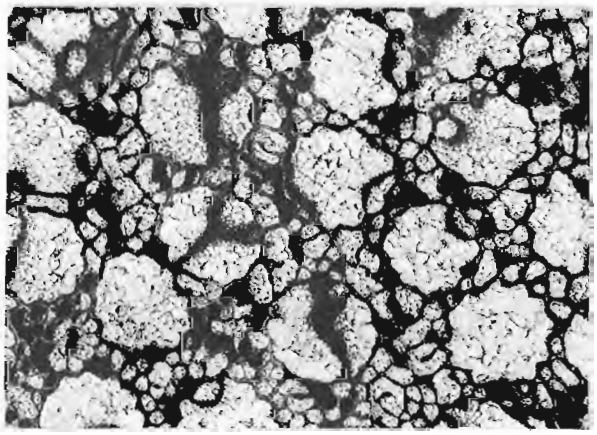

32

Figures 43.23-43.32. Megafauna from 39.1-39.5 m above base of exposure and 21.3-21.7 m below top of lower resistant member of the Cranswick Formation. Cliff overlooking a tributary of Snake River, Mackenzie Mountain Front, Yukon Territory (65°24'40"N; 133°35'40"W). GSC locality C-63108. Figures 43.23-43.26, **Echyropora** sp. nov., x7. Figure 43.23, GSC 53080. Figures 43.24-43.26, GSC 53081. Figures 43.27, 28, **Crassialveolites** sp. undet., x8, GSC 53082. Figures 43.29-43.32, **Bogimbailites** sp. nov., x6, GSC 53083.

gronbergi Zone of Klapper and Johnson (in Klapper, in press). The species of **Planetophyllum** in C-63102 has not been named, but may be identical with forms identified as **P. planetum** by Rice (1967, Pl. 2, figs. 7, 8) from the subsurface Fitzgerald Formation of northeastern Alberta.

The double and cross-like axial canals of some of the echinoderm ossicles, which may have derived from **Gasterocoma**(?) **bicaula** Johnson and Lane, in C-63107, indicate a late Early or early Middle Devonian age. Cyathophyllids such as **Cavanophyllum** have a known range equivalent to the **sulcatus-inversus** conodont zones (Klapper, in press) in Australia and Canada. **Carinatina lowtherensis** was described first (Johnson and Boucot, 1972, p. 37, Pl. 1, figs. 1-14, Textfig. 3) from the Disappointment Bay Formation on Lowther Island, where it occurs with **Polygnathus inversus** (T.T. Uyeno, pers. comm., March 1977). The Cranswick specimen in C-63107 is slightly larger and has a better developed anterior geniculation and frill than figured topotypes of **C. lowtherensis**. However, these differences probably are not very significant either taxonomically or stratigraphically. The **Favosites** in C-63107 is identical with the form identified as **F.** sp. cf. **F. goldfussi** d'Orbigny by Hill and Jell (1969, p. 19, 20, Pl. 6, figs. 1, 2) from the upper Lower Devonian Ukalunda Beds of Queensland, Australia. The age indicated by these identifications is clearly late Early Devonian, provided the Lower/Middle Devonian boundary is maintained as post-**inversus** Zone.

No forms comparable to the new species of **Bogimbailites** and **Echyropora** in C-63108 were known previously in North America. **Echyropora** was proposed by Tong-Dzuy Thanh (in Dubatolov and Tong-Dzuy Thanh, 1965, p. 49-52, Pl. 7, figs. 1a-d; Tong-Dzuy Thanh, 1966, p. 23-27, Textfigs. 1a, b, Pl. 1, figs. 1-5) for **E. grandiporosa** from the Sông Nho Quẽ Limestone in Ha Giang Province, north Vietnam. Tong-Dzuy Thanh (1966, p. 25) dated the type stratum as "coblencien supérieur-eifélien inférieur". In addition to the Vietnamese occurrence, three species are known now from the northern Urals and northeast Soviet Union. These were considered Middle Devonian when the pre-Eifelian **Favosites regularissimus** Zone was considered Middle Devonian. Tables in more recent works by Dubatolov (1972, p. 72) and Dubatolov and Spasskiy (1973, p. 14) give the range of Russian occurrences of **Echyropora** as Gedinnian to Zlichovian, that is, lower to upper, but possibly not uppermost Lower Devonian. **Bogimbailites** is best known from central Kazakhstan (Bondarenko, 1966), where its range is believed to be restricted to the "Gedinnian" Kokbaytal' Horizon (Bondarenko et al., 1975; Bondarenko, 1975). It is present also in the Agrelopos Limestone on the Island of Chios in the Aegean Sea (Weissermel, 1938, p. 71-73, Textfigs. 1, 2). The age of this occurrence is not known precisely, but Herget and Roth (1968, Textfig. 2) regarded the Agrelopos Limestone to be of Ludlow to Early Devonian age.

Conclusions

Fossils collected from the upper 42.9 m of the lower cliff-forming limestone member, and lower 10 m of the upper recessive limestone and shale member of the Cranswick Formation, at the type outcrop, suggest correlation with parts of the following formations: Lower Blue Fiord Formation as developed at Sör Fiord, southwest Ellesmere Island; Stuart Bay Formation on Bathurst Island; Disappointment Bay Formation on Lowther Island; Lower Ogilvie Formation of northern Yukon Territory; Fitzgerald Formation of northeastern Alberta; and McColley Canyon Formation of Nevada.

In terms of the conodont zonation proposed by Klapper (in press), the lower 20.3 m of the Cranswick Formation are possibly equivalent to either the **gronbergi** or **inversus** Zone; the upper 39.3 m of the lower member and lower 10 m of the upper member of the formation are referred to the **inversus** Zone; higher beds in the upper member pertain to the **serotinus** Zone.

Provided the Lower/Middle Devonian boundary is maintained at its current North American level, the Cranswick Formation is upper Lower Devonian in the type area.

Acknowledgments

We extend our thanks to D.G. Cook, D.K. Norris and G.K. Williams for discussing regional correlations with Pedder. W.W. Nassichuk examined goniatites from the lower part of the upper member of the Cranswick Formation. At our request, T.T. Uyeno kindly revised earlier identifications (in Johnson, 1975, p. 951) of conodonts from the Disappointment Bay Formation on Lowther Island (GSC loc. C-2682).

Klapper's laboratory work was supported partly by National Science Foundation, Earth Sciences Section, NSF Grant GA-43791.

References

Aitken, J.D. and Cook, D.G.
1975: Geology of Upper Ramparts River (106G) and Sans Sault Rapids (106H) map-areas, District of Mackenzie, N.W.T.; Geol. Surv. Can., Open File Rept. 272.

Anonymous ("officers of the Oil and Minerals Division")
1976: Schedule of wells 1973-1975. Northwest Territories and Yukon Territory, 15; Department of Indian and Northern Affairs, Ottawa.

Bondarenko, O.B.
1966: Geliolitoidei isen'skoy svity; in Stratigrafiya i fauna siluriyskikh i nizhnedevonskikh otlozheniy Nurinskogo sinklinoriya, A.A. Bogdanov, ed.; Izdatel'stvo Moskovskogo Univ., p. 145-197.

1975: Geliolitoidei; in Kharakteristika fauny pogranichnykh sloev silura i devona Tsentral'nogo Kazakhstana, B.B. Menner, ed.; Moskva "Nedra", p. 50-61.

Bondarenko, O.B., Stukalina, G.A., and Ushatinskaya, G.T.
1975: Kharakteristika stratigraficheskoy skhemy verkhnego silura i nizhnego devona Tsentral'nogo Khazakhstana; in Kharakteristika fauny pogranichnykh sloev silura i devona Tsentral'nogo Kazakhstana, B.B. Menner, ed.; Moskva "Nedra", p. 5-39.

Bultynck, P.
1970: Révision stratigraphique et paléontologique (brachiopodes et conodontes) de la coupe type du Couvinien; Inst. Géol. Univ. Louvain, Mém., tome 26.

Dubatolov, V.N.
1972: Zoogeografiya devonskikh morey evrazii (po materialam izucheniya tabulyat); Akad. Nauk SSSR, Sib. Otdel., Inst. Geol. i Geofiz., Trudy, vyp. 157, p. 1-128.

Dubatolov, V.N. and Spasskiy, N.Ya.
1973: O printsipakh paleobiogeograficheskogo rayonirovaniya morey; Akad. Nauk SSSR, Sib. Otdel., Inst. Geol. i Geofiz., Trudy, vyp. 169, p. 11-18.

Dubatolov, V.N. and Tong-Dzuy Thanh
1965: Nekotorye novye tabulyaty i tabulyatomorfnye tselenteraty severnogo V'etnama; in Tabulyatomorfnye korally devona i karbona SSSR, B.S. Sokolov and V.N. Dubatolov, eds.; Izdatel'stvo "Nauka", Moskva, p. 41-64.

Herget, Günter and Roth, Werner
1968: Stratigraphie des Paläozoikums im Nordwest-Teil der Insel Chios (Ägäis); Neues Jahrb. Geol. Paläont., Abh., Bd. 131, p. 46-71.

Hill, D. and Jell, J.S.
1969: Devonian corals from Ukalunda; Geol. Surv. Queensland, Publ. 340, Palaeontology Papers, no. 16.

Johnson, J.G.
1975: Late Early Devonian brachiopods from the Disappointment Bay Formation, Lowther Island, Arctic Canada; J. Paleontol., v. 49, p. 947-978.

Johnson, J.G. and Boucot, A.J.
1972: Origin and composition of the Carinatininae (Devonian Brachiopoda); J. Paleontol., v. 46, p. 31-38.

Klapper, Gilbert
1969: Lower Devonian conodont sequence, Royal Creek, Yukon Territory, and Devon Island, Canada, with a section on Devon Island stratigraphy by A.R. Ormiston; J. Paleontol., v. 43, p. 1-27.

Lower and Middle Devonian conodont sequence in western North America; in Devonian System of western North America, Murphy, M.A., Berry, W.B.N., and Sandberg, C., eds.; Univ. California, Riverside, Campus Museum, Contrib. 4. (in press)

Klapper, Gilbert and Johnson, D.B.
1975: Sequence in conodont genus **Polygnathus** in Lower Devonian at Lone Mountain, Nevada; Geologica et Palaeontologica 9, p. 65-83.

Klapper, G., Lindström, M., Sweet, W.C., and Ziegler, W.
1973: Catalogue of conodonts, v. 1; E. Schweizerbart'sche Verlagsbuchhandlung, Stuttgart.

McGregor, D.C. and Uyeno, T.T.
1972: Devonian spores and conodonts of Melville and Bathurst Islands, District of Franklin; Geol. Surv. Can., Paper 71-13.

Norris, A.W.
1967: Descriptions of Devonian sections in northern Yukon Territory and northwestern District of Mackenzie (106F, G; 107C; 116F, G, H, J and P); Geol. Surv. Can., Paper 66-39.

1968a: Reconnaissance Devonian stratigraphy of northern Yukon Territory and northwestern District of Mackenzie; Geol. Surv. Can., Paper 67-53.

1968b: Devonian of northern Yukon Territory and adjacent District of Mackenzie; in International Symposium on the Devonian System, Calgary, 1967, D.H. Oswald, ed.; Alberta Soc. Petrol. Geologists, Calgary, v. 1, p. 753-780.

Norris, D.K.
1975: Geological maps comprising Hart River, Y.T., Wind River, Y.T. and Snake River, Y.T. and N.W.T.; Geol. Surv. Can., Open File Rept. 279.

Perry, D.G., Klapper, Gilbert, and Lenz, A.C.
1974: Age of the Ogilvie Formation (Devonian), northern Yukon: based primarily on the occurrence of brachiopods and conodonts; Can. J. Earth Sci., v. 11, p. 1055-1097.

Rice, D.D.
1967: Stratigraphy of the Chinchaga and older Paleozoic formations of the Great Slave Lake area, southern Northwest Territories and northern Alberta; M.Sc. Thesis, Univ. Alberta, Department of Geology, Edmonton.

Stearn, C.W. and Mehrotra, P.N.
1970: Lower and Middle Devonian stromatoporoids from northwestern Canada; Geol. Surv. Can., Paper 70-13.

Telford, P.G.
1975: Lower and Middle Devonian conodonts from the Broken River Embayment, north Queensland, Australia; Palaeont. Assoc., Spec. Papers Palaeont., no. 15.

Tong-Dzuy Thanh
1966: Nouveux genre et sous genre chez les coelentérés tabulatomorphes dévoniens du Nord Viêtnam; Act. Sci. Vietnam.,Sect. Biol. Geogr. et Geol., tom 1, p. 23-32.

Uyeno, T.T. and Mason, David
1975: New Lower and Middle Devonian conodonts from northern Canada; J. Paleontol., v. 49, p. 710-723.

Weissermel, W.
1938: Eine altpaläozoische Korallenfauna von Chios; Zeit. Deutsch. Geol. Ges., Bd. 90, p. 65-74.

44. MINERAL ASSEMBLAGES AT THE RABBIT LAKE URANIUM DEPOSIT, SASKATCHEWAN: A PRELIMINARY REPORT

Project 750059

J. Rimsaite
Regional and Economic Geology Division

This report is based on the study of specimens collected in 1975 of principal rock types and mineralized zones at the Rabbit Lake uranium deposit. The specimens of ore are mainly core from diamond-drill holes in the northeastern part of the deposit, near and under the lake. This paper documents and extends an oral presentation to the Mineralogical Association of Canada (Rimsaite, 1976a).

Geological Background

The Rabbit Lake uranium deposit is west of Wollaston Lake at 58°11'00"N, 103°42'36"W, in northeastern Saskatchewan. General geology of the area has been described by Wallis (1971) and Knipping (1974). In 1976, the Saskatchewan Geological Survey in co-operation with the Saskatchewan Research Council commenced a long term research project of metallogenic, petrographic and isotopic studies, and detailed mapping of the Rabbit Lake open pit. The program and first results of these studies are discussed by Sibbald (1976).

Uranium mineralization in the Rabbit Lake deposit occurs in Aphebian brecciated metasediments within the Wollaston Lake Fold Belt, in the hanging wall of a northeast-trending thrust fault, near the unconformity with the overlying Athabasca Formation. The metasediments listed by Knipping (1974) include quartzite, meta-arkose, biotite paragneiss, calc-silicate rocks and marble. They are brecciated and transected by pegmatites. Metasediments that occur above the thrust fault are here referred to as "upper", and those below the fault as "lower" quartzites and gneisses. There is no marked difference between low grade ore and wall rock, because both are composed dominantly (> 99%) of the same common rock-forming minerals. Characteristic textures and features of minerals and rocks, such as cross-cutting fractures, alterations and recurring mineral growths are illustrated in photomicrographs (Fig. 44.1). Also chemical analyses of selected minerals and principal rock types are given in Tables 44.1 and 44.2.

Mineralogy

Minerals identified in the present study, listed according to Dana's classification, are the following:

Native elements:

Carbon, C.

Sulphides, Selenides and Arsenides:

Galena, PbS; clausthalite, PbSe; sphalerite, ZnS; Fe-Cu sulphides listed in order of apparent sequence of crystallization: pyrite, FeS_2; chalcopyrite, $(Cu, Fe)S_2$ (Fig. 44.4b); bornite Cu_5FeS_4; chalcocite, Cu_2S; covellite, CuS; nickeline, NiAs (Fig. 44.4a); carrollite, Co_3S_4, and minerals of linnaeite-siegenite group (Fig. 44.3f); cobaltiferous pyrite.

Oxides and hydrated oxides:

Quartz, SiO_2, many varieties and generations (Figs. 44.1a, 44.1d); hematite, Fe_2O_3; goethite, $2Fe_2O_3 \cdot 3H_2O$, commonly siliceous; rutile and anatase, TiO_2(Fig. 44.2);

Uranium and U-Pb oxides:

Pitchblende, U_3O_8, five varieties and several generations (Figs. 44.3, 44.4); triuranium heptaoxides, $U_3O_7(nH_2O)$; Pb-bearing, $PbU_2O_7 \cdot xH_2O$; masuyite-becquerelite, $UO_2(OH)_2 \cdot H_2O - UO_2(OH)_2 \cdot 4H_2O$; vandendriesscheite, $4(UO_2)(OH)_2 \cdot Pb(OH)_2 \cdot H_2O$; woelsendorfite, $2[UO_2](OH)_2(Pb, Ca)O$.

From: Report of Activities, Part B; Geol. Surv. Can., Paper 77-1B (1977)

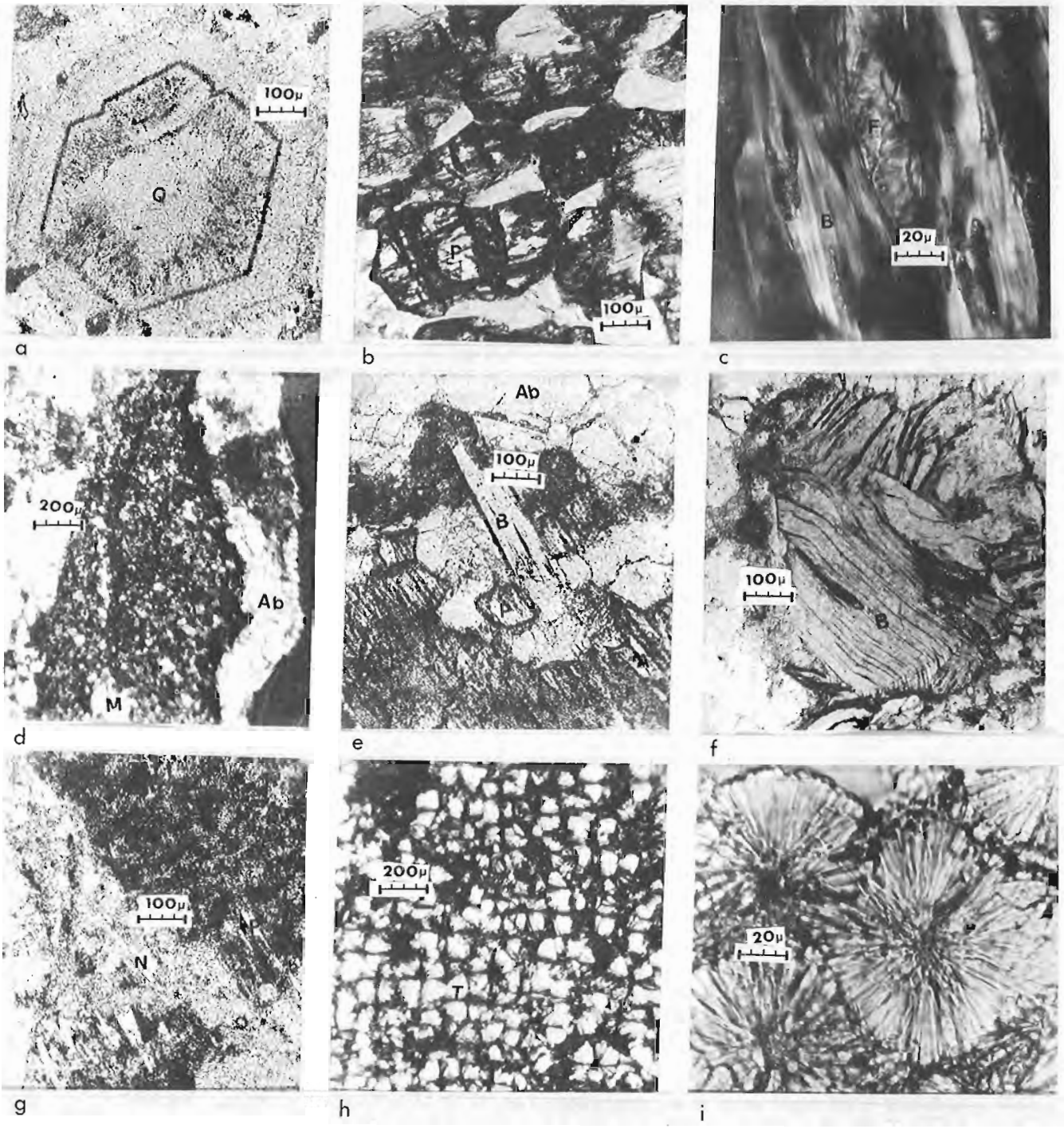

Figure 44.1.

Mineral and rock textures in the Rabbit Lake U-deposit. (All photomicrographs taken in transmitted light)

1a. Zoned quartz in "upper quartzite", from 38-foot depth.

1b. Banded "upper gneiss" composed of scapolite, pyroxene (P), amphibole, garnet, biotite and feldspar in sericite, chlorite, eastonite, talc groundmass, all transected by carbonate veins, from outcrop.

1c. Biotite partly replaced by K-feldspar in "upper gneiss" (Fig. 44.1b).

1d. Mylonitized zones in "lower gneiss" below the "main fault", composed of fine-grained mylonitic quartz (M), plagioclase (Ab), K-feldspar, amphibole, chlorite, cordierite, phlogopite, allanite, anatase, zircon and "yttrialite" (Fig. 44.2), from 397-foot depth.

1e. Remnant pyroxene (P) partly replaced by amphibole (A), biotite laths (B) and plagioclase (Ab) in "lower gneiss" below the "main fault", from 417-foot depth.

1f. Deformed band of chloritized biotite (B) in quartzite breccia, from 85-foot depth.

1g. Deformed mylonite composed of dark chloritic paleosome patches in recrystallized leucocratic neosome consisting dominantly of zoned quartz (as in Fig. 44.1a), from 636-foot depth.

1h. White radiating tourmaline recrystallized in paleosome patches in silicified "upper quartzite" breccia, from 85-foot depth.

1i. White radiating tourmaline aggregates, enlarged from Figure 44.1h.

Carbonates:

Calcite, $CaCO_3$; magnesian calcite; dolomite, (CaMg) CO_3; ankerite; siderite, $FeCO_3$; malachite, $CaCO_3 \cdot Cu(OH)_2$.

Silicates: Feldspars, several generations:

Albite, oligoclase, antiperthite, microcline, orthoclase, (Fig. 44.1c), perthite; garnet; diopside, $Ca,Mg(SiO_3)_2$, Fe-diopside: tremolite, $Ca,Mg_3(SiO_3)_4$; actinolite, $Ca(Mg,Fe)_3(SiO_3)_4$ (Fig. 44.1e); cordierite, $Mg_2Al_4Si_5O_{18}$; scapolite, $CaCO_3 \cdot 3CaAl_2Si_2O_8 - NaCl \cdot 3NaAlSi_3O_8$; zircon, $ZrSiO_4$; zoisite-epidote, $Ca_2(AlOH)Al_2(SiO_4)_3 - Ca_2(FeOH)Fe_2(SiO_4)_3$; allanite $(Ca, Fe)_2(AlOH)(Al, Ce, Fe)_2(SiO_4)_3$, some radioactive; tourmaline, $H_9(Mg, Fe, Ca)Al_3(B \cdot OH)_2Si_4O_{19}$, three varieties; black-green, orange-yellow and white, radiating, (Figs. 44.1h, 44.1i); biotite $H_2K(Mg,Fe)_3AlFe(SiO_4)_3$, (Figs. 44.1c, 44.1f); muscovite, $H_2KAl_3(SiO_4)_3$; eastonite, $H_4K_2Mg_5Al_4Si_5O_{24}$; phlogopite, $H_2KMg_3Al(SiO_4)_3$; glauconite, $K(Al, Mg, Fe)(Al, Fe)(OH)_2Si_3AlO_{10}$; celadonite (ferric glauconite); chlorite, $H_4(Mg,Fe,Al)_{2-3}AlSiO_9$, many varieties and several generations, (Figs. 44.1a, 44.1f, 44.4f); serpentine, $H_4Mg_3Si_2O_9$; talc, $H_2Mg_3(SiO_3)_4$; kaolinite, $H_4Al_2Si_2O_9$; halloysite, $Al_2O_3 \cdot 2SiO_2 \cdot nH_2O$ (hydrous kaolinite); montmorillonite $(Mg,Ca)O \cdot Al_2O_3 \cdot 5SiO_2 \cdot nH_2O$ (Fig. 44.4f); sphene, $CaTiSiO_5$; U-bearing silicates; coffinite, $USiO_4$; kasolite, $Pb(UO_2)SiO_4 \cdot H_2O$; α – & β-uranophane, $CaO \cdot 2UO_3 \cdot 2SiO_2 \cdot 7H_2O$; sklodowskite, MgO, $2UO_3 \cdot 2SiO_2 \cdot 7H_2O$; boltwoodite, $K_2H_2(UO_2)(SiO_4)_2 \cdot 4H_2O$; yttrialite, $Y_2(Th,U,Pb)Si_2O_7$ (Fig. 44.2); allophane (amorphous clay).

Phosphates:

apatite, (Ca,F) $Ca_4(PO_4)_3$ and Cl-apatite; monazite $(Ce,La,Di)PO_4$, some radioactive.

Sulphates:

anhydrite, $CaSO_4$; gypsum, $CaSO_4 \cdot 2H_2O$; zippeite, $2UO_3 \cdot SO_4 + 3\text{-}6H_2O$; barite, $BaSO_4$.

Oxygenated hydrocarbons:

"thucholite", $C \cdot nH_2O \pm U_3O_8$, uranium is usually present as thin rims of pitchblende, type P-5, on "thucholite", and as fracture fillings, (Figs. 44.4b, 44.4d).

Mineral Assemblages

Nine modes of occurrence of radioactive elements have been distinguished and are described in order of the apparent sequence of crystallization. However, it is important to point out that some of the primary and secondary radioactive minerals, such as pitchblende, uranophane, coffinite and others, can be present in more than one generation.

1. Thorium- and rare earths-bearing grains, "yttrialite" (Fig. 44.2) have been observed in "lower gneisses" and quartzites as small radioactive grains associated with anatase aggregates. These "yttrialite" grains produce prominent pleochroic halos in micaceous minerals. They are commonly heterogeneous, suggesting breakdown of chemically complex radioactive minerals into simple oxides. Partial analysis of an altered uraniferous titanium-rare earths-bearing grain is given in Table 44.3-13. Relics of these rare earths-bearing grains account for the relatively large amount of rare earths in brightly coloured Pb-rich uranium oxides and silicates (Table 44.4).

2. Pitchblende-bearing assemblages. On the basis of chemical compositions and modes of occurrence, five principal types of pitchblende have been distinguished and are illustrated in Figures 44.3, 44.4. The "oldest primary" pitchblende, type P-1, occurs as colloform bands and/or breccia fragments in green phyllosilicate matrix, commonly composed of poorly crystalline (metamict) chlorite-mica-montmorillonite intergrowths, containing quartz gragments, yellow tourmaline, abundant apatite, anatase, and occasionally potassium feldspar (Figs. 44.3a, 44.3b, 44.4f). The pitchblende bands of type P-1 and the host rock are transected by numerous fractures filled with secondary U-minerals, calcite and serpentine. As a result of alteration and partial resorption, this pitchblende exhibits various reflectivities. It grades from the well reflecting type P-1 to the poorly reflecting P-2 type of pitchblende (Figs. 44.3c, 44.3d and Table 44.3). The poorly reflecting pitchblende, type P-2, is usually depleted of radiogenic lead, partly hydrated, and contains Si, Al and Ca impurities. In some specimens, a portion of partly resorbed pitchblende is surrounded by fine grained euhedral pitchblende, type P-3, that is, pitchblende crystallized in phyllosilicate matrix from remobilized uranium, Figure 44.3e, Table 44.3-7. The major remobilization of pitchblende accompanied by the removal of radiogenic lead and the crystallization of galena, is related to the time of emplacement of sulphides, arsenides and selenides (Fig. 44.4a), and was followed by the formation of very fine grained ($<1\mu$) aggregates consisting of pitchblende, sulphide, calcite and coffinite (pitchblende type P-4,

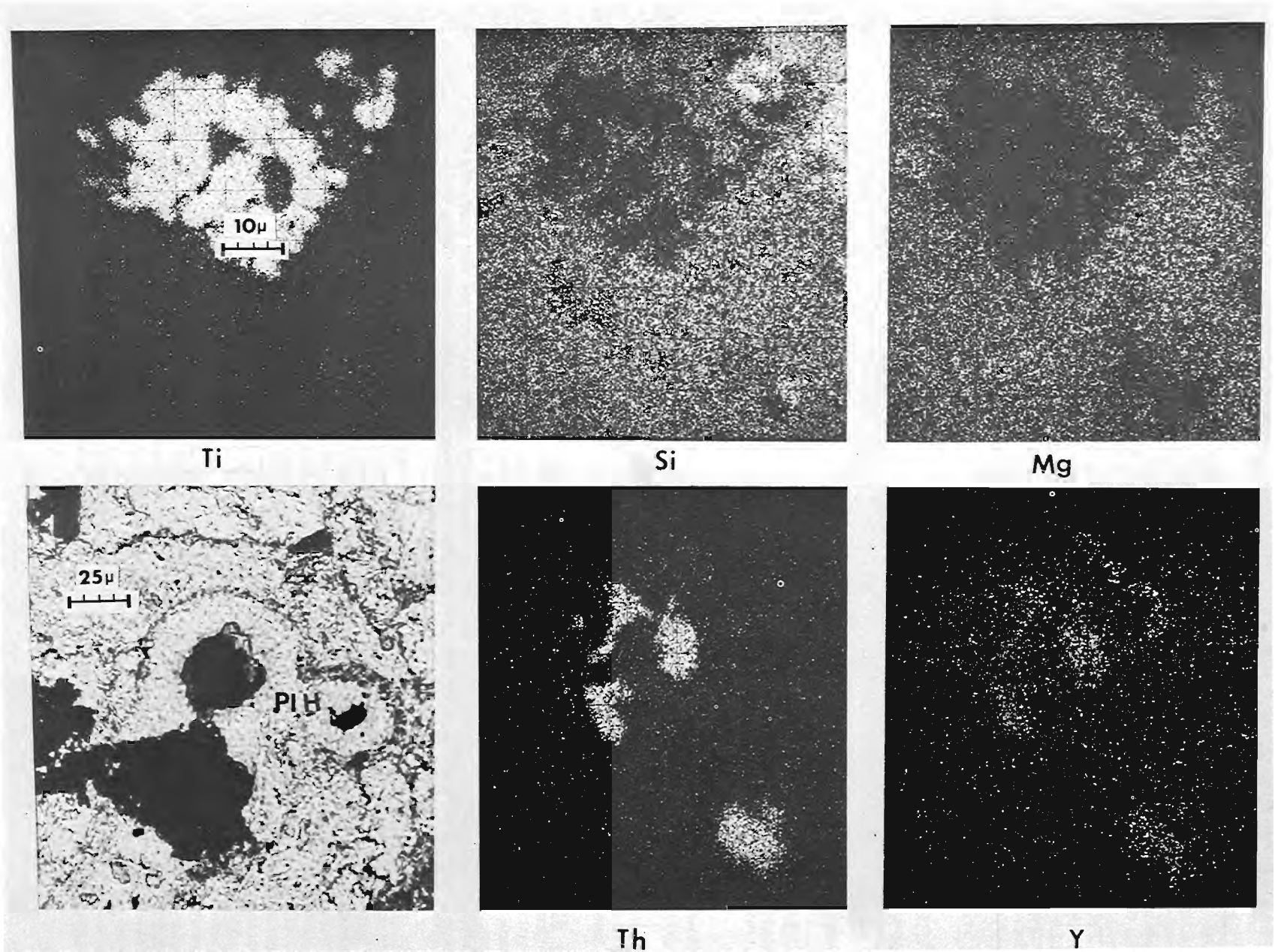

Figure 44.2.

Anatase-"yttrialite" intergrowths in mylonitic rock (Fig. 44.1d). The photomicrograph at lower left shows double pleochroic halos (PlH) surrounding "yttrialite" in chloritized phlogopite. The remaining illustrations are X-ray scanning images for Ti, Si, Mg, Th and Y that show the distribution of these elements in the radioactive grains at a higher magnification (x2.5) than does the photomicrograph. The white spots in the X-ray scanning image for Ti are anatase needles whose interstices (black holes) are filled with Si, Th and Y contained in the radioactive "yttrialite", (compare X-ray scanning images for Ti, Si, Th and Y). The X-ray scanning images for Si and Mg show distribution of these elements in silicates. The black spots coincide with anatase aggregates and, in the Mg image, with the "yttrialite". (Electron microprobe analysis by A.G. Plant)

Fig. 44.3f, Table 44.3-8). A further portion of remobilized pitchblende postdates crystallization of sulphides as it forms narrow rims (type P-5, Fig. 44.4) around chalcopyrite, pyrite, quartz, calcite, Ti-minerals, and "thucholite". Some pitchblende rims of type P-5 are speckled (sooty) and overgrown by secondary uranium minerals (Fig. 44.4e). There are two types of fine grained speckled or "sooty" pitchblende: one being the result of newly recrystallized pitchblende grains, the other representing fine grained remnants of old resorbed pitchblende (Types 1, 2) in phyllosilicate or carbonate groundmass. Small radioactive grains (< 1 μ) detected by electron microprobe in apatite are probably related to "sooty pitchblende" rims. Radioactive minerals observed in the gneisses below the main fault are "yttrialite" grains and rims of pitchblende of the type P-5 coating anatase crystals.

3. Coffinite-bearing assemblages. Coffinite occurs in five spatially and temporally different modes: (a) as narrow rims coating massive and colloform pitchblende; (b) in quartz- and calcite-filled fractures (Fig. 44.4f); (c) interbanded with zoned quartz, thus indicating recurring recrystallizations; (d) as fracture fillings in quartz and other minerals and associated with fine grained speckled ("sooty") pitchblende (Fig. 44.4e), and (e) filling vugs within phyllosilicate patches in altered, impure quartzite. The coffinite associated with the massive pitchblende or other strongly radioactive minerals is poorly crystalline ("metamict"), and as such it may easily be overlooked or mistaken for the associated "sooty" pitchblende. In thin section, and thin chips, it is slightly transparent and green or brown. It is an abundant mineral in the "regolith" and recent weathered rocks. Coffinite associated with hydrated, montmorillonite-rich, phyllosilicates contains about 8 per cent H_2O, determined by thermogravimetric method of analysis.

4. Uraniferous phyllosilicates. The uranium-bearing phyllosilicates were discovered in this study as a result of their abnormal optical and X-ray properties. They are greenish in reflected light, brown to opaque in transmitted light and somewhat resemble fine grained coffinite; they exhibit marked variations in refractive indices which increase with increasing uranium content from 1.56 (U_3O_8 <1 wt. per cent) to 1.67 (U_3O_8ca 20 wt. per cent), and appear isotropic. The uraniferous phyllosilicates produce very faint, poor and broad X-ray diffractometer patterns, suggesting the presence of poorly crystalline intergrowths of glauconite-, chlorite- and montmorillonite-like minerals. The U-bearing phyllosilicates contain more potassium and less iron than the associated related varieties of the groundmass (Table 44.2-11, -12, -15, -16). The unusual optical properties are apparently due to uranium present in the crystal structure. The uraniferous phyllosilicates were observed in the groundmass of high grade ore (Figs. 44.3a, 44.3b, 44.4f), in argillitized quartzites containing abundant radiating (secondary) tourmaline (as in Fig. 44.1i), and in late fractures and vugs. The U-coated and impregnated altered biotite flakes (Rimsaite, 1975, Fig. 1b) are present in all mineralized rocks containing bands or single flakes of altered biotite (as in Fig. 44.1f). The uranium concentration in uraniferous phyllosilicates varies from trace amounts to ca 60 wt. per cent (Table 44.2-12,-16).

5. Brightly coloured uranium-lead hydrated oxides. The brightly coloured uranium oxides are common in the "regolith", in recent weathering zones and along open fractures to various depths. In general the bright orange and yellow oxides are closely associated with black pitchblende. The hydrated U-oxides either pseudomorphously replace parent pitchblende or occur as bright coatings on minerals and fractures. The alteration reactions are usually complex; they involve silica and other ions liberated from decomposing silicates to form U-Pb oxides and U-Pb-bearing secondary silicates. The fine grained uraniferous silicates and bright oxides commonly occur together as fine grained compact crusts disintegrating into powdery layers when exposed to weathering.

6. Brightly coloured uranium-lead silicates. Kasolite pseudomorphs after pitchblende were observed in drill core samples. The bright orange kasolite aggregates adjoin relatively fresh black pitchblende in the same thin section. These kasolite-pitchblende assemblages are fractured and replaced by fine grained carbonates and clays. The kasolite grains adjacent to carbonate and clay alter to yellow uranophane by losing lead and gaining Ca, U and H_2O. The brightly coloured ore samples with abundant lead, contain appreciable quantities of rare earths (Table 44.4). The rare earths content decreases with decreasing orange coloration which is apparently related to lead content of the U-Pb silicates and oxides. Uranophane is a common mineral in veins transecting the U-ore and in vugs. As a result of recurring brecciations, there are numerous cross-cutting fractures filled with several generations of uranophane; well-crystallized radiating crystals of β-uranophane occur in earlier fractures, whereas very fine grained to submicroscopic α-uranophane is common in late fractures and vugs filled with clay. Some radiating uranophane needles grade to sklodowskite due to increasing Mg and decreasing Ca contents during crystal growth. Boltwoodite within a groundmass of phyllosilicate occurs filling fractures and vugs in quartzite containing patches of dolomite and radiating white tourmaline (Fig. 44.1i). Secondary hydrated U-silicates coat and fill fractures in argillitized rocks. Uranophane needles with sklodowskite tips form globular aggregates.

Table 44.1

Chemical analyses* of selected rocks and minerals from the Rabbit Lake Uranium Deposit

	Specimens****												
Weight %	1	2	3	4	5	6	7***	8	9	10	11	12	13
SiO_2	91.	57.	42.	45.	6.	0.6	38.	47.	34.	36.	69.	51.	62.
Al_2O_3	3.	20.	16.	20.	0.0	0.0	10.	18.	7.	7.	11.	18.	16.
TiO_2	0.06	0.68	1.0	0.34	0.00	0.00	0.45	0.21	0.45	0.4	0.47	0.72	0.76
Fe_2O_3**	1.	5.	3.1	2.5	1.	1.1	10.	2.5	12.	20.	4.3	8.	1.1
FeO	0.3	1.1	1.4	1.1	0.7	0.9		1.2			4.	6.4	1.
MgO	3.	5.	24.	19.	20.	20.	15.	8.	12.	7.	9.	14.	9.
MnO	0.02	0.04	0.06	0.05	0.20	0.07	0.04	0.08	0.2	0.6	0.01	0.01	0.02
K_2O	0.08	3.7	0.17	0.36	0.60	0.04	0.1	3.2	1.2	1.	1.1	1.7	0.7
Na_2O	<0.2	0.8	0.5	<0.2	<0.2	<0.2	<0.2	<0.2	<0.2	< 0.2	<0.2	<0.2	7.6
CaO	0.37	0.83	1.0	0.44	29.	31.	0.5	0.85	1.4	8.	0.2	0.2	1.7
PbO	0.02	0.03	0.02	<0.02	<0.02	<0.02	0.1	0.04	1.	0.5	0.00	0.00	0.00
U_3O_8	0.79	0.06	0.33	0.31	0.04	0.02	4.5	3.8	13.4	2.4	0.4	0.8	0.4
H_2O	1.8	7.2	12.4	11.1	0.0	0.0	8.2	14.9	11.5	8.6	5.2	7.4	3.5
F	0.04	0.08	0.22	0.10	0.02	0.02	0.07	0.2	0.07	0.06	0.11	0.15	0.04
Cl	0.02	0.01	0.06	0.04	0.02	0.02	0.04	0.02	0.03	0.03	0.02	0.05	0.04
C	0.00						2.7	0.07		0.00	0.5	0.1	0.3
CO_2	0.00	0.00	0.00	0.00	44.	48.	0.00	0.00	0.3	6.1	0.00	0.00	0.7
P_2O_5	0.12	0.25	0.47	0.08	0.08	0.05	0.40	0.15	0.18	0.34	0.18	0.15	0.18
S	0.02	0.00	0.04	0.22	0.10	0.00	5.	0.23	0.3	0.10	0.10	0.10	0.07
B	0.05	0.05	0.05	1.	<0.05	<0.05	0.1	0.1	0.1	0.03	<0.05	0.10	<0.05
Ba	0.000	0.044	0.04	0.006	0.00	0.00	0.02	0.01					
Rb	0.004	0.014	0.01	0.01	0.00	0.00		0.00					
Sr	0.000	0.062	0.00	0.00	0.00	0.00	0.00	0.00					
Cu	0.002	0.02	0.03	0.03	0.3	0.02	3.	0.05	0.1	0.05	0.01	0.002	<0.001
Ni	0.006	0.01	0.03	0.02	0.03	0.00	0.3	0.01	0.05	0.015	0.01	0.01	0.00
Co							5.		0.1	0.05	0.00	0.00	0.00

* Analysts: J.-L. Bouvier, P.G. Bélanger and G.R. Lachance.

** Total iron as Fe_2O_3; total uranium as U_3O_8; total water as H_2O. In U-bearing samples FeO values are not reliable.

*** Ag = 0.005%.

**** Specimens 1 to 8 are from the pit; specimens 9 to 13 are drill core samples.

1. "Upper quartzite" composed of quartz and coatings of secondary U-minerals and sulphides, minor phyllosilicates (Table 44.2-2).
2. "Pink surface clay" with detrital quartz, sericitized feldspar and calcite.
3. "Grey paleoclay – a regolith" with small quartz chips.
4. Quartzite with interstitial chloritized biotite and secondary tourmaline, similar to that in Figures 44.1h, 1i.
5. Red euhedral (impure) dolomite crystals coated with covellite and hematite from vugs in quartzite.
6. Clean white tops of the euhedral dolomite crystal at No. 5 tourmaline-bearing quartzite.
7. Fine grained black pyrite-carrollite-carbon-bearing interstices in quartzite.
8. Grey glauconite-thucholite-bearing "regolith" containing quartz chips and coffinite.
9. Uranium ore from 155-foot depth composed of pitchblende (Figs. 44.3a, 44.3b, Table 44.3-1, 2, 3), coffinite, uraniferous and non-radioactive phyllosilicates (Table 44.2-11, 12) and yellow tourmaline (Fig. 44.4f, Table 44.2-14) transected by calcite and serpentine veinlets.
10. Red banded quartzite from 187-foot depth. Quartz-tourmaline bands alternate with phyllosilicate bands <1 mm in width. Phyllosilicates (Table 44.2-15, 16) are U-bearing or coated with iron oxides. Numerous fractures are filled with calcite.
11. "Lower quartzite" from main fault zone, from 320-foot depth.
12. "Gouge" and mylonitized "lower quartzite" just below the main fault zone, from 332-foot depth (rock similar to that in Fig. 44.1d).
13. "Footwall gneiss" from 430-foot depth, composed of alkalic plagioclase, diopside, amphibole, phlogopite, chlorite. Rock similar to that in Figures 44.1e, 44.1g, mineral analysis in Table 44.2-25, 26.

Table 44.2

Electron microprobe analyses* of selected silicates from the Rabbit Lake Uranium Deposit

Specimens	Weight % SiO_2	Al_2O_3	TiO_2	FeO**	MgO	MnO	K_2O	Na_2O	CaO
"Upper quartzite"									
1. Fibrous chlorite	34.	18.	0.0	4.5	28.	0.1	0.1	0.0	0.5
2. Bleached chlorite	30.	22.	0.4	2.0	32.	0.1	0.1	0.0	0.1
"Upper gneiss"									
3. Scapolite***	51.8	20.9	0.0	0.0	0.1	0.0	0.3	9.2	6.5
4. "Eastonite-like"	51.7	20.9	0.0	2.3	6.2	0.0	9.5	0.4	0.2
5. "Sericite"	54.7	20.0	0.0	1.9	8.1	0.0	10.0	0.6	0.3
6. Diopside	52.8	1.3	0.0	5.8	14.5	0.1	0.1	1.4	24.0
7. Amphibole	54.3	2.0	0.1	8.0	19.1	0.1	0.2	1.2	12.9
8. Groundmass "clay"	59.	1.1	0.0	5.6	22.6	0.1	1.0	1.1	2.4
9. Biotite	36.6	14.4	2.0	14.4	19.5	0.1	7.5	0.7	0.9
10. Chloritized biotite	30.8	15.7	1.2	14.2	20.8	0.1	2.7	0.6	0.1
"U-ore" Figs. 44.3a, 44.3b, 44.4f, Table 44.1-9)									
11. Groundmass "clay"	39.2	16.6	0.0	9.7	14.1	0.1	3.9	0.8	0.4
12. U-phyllosilicate****	21.5	6.5	0.0	0.0	0.9	0.0	2.9	0.0	1.7
13. "Eastonite" in ore	41.9	19.9	0.1	7.7	9.5	0.1	6.5	0.6	0.6
14. Tourmaline, orange	35.8	29.1	1.3	4.1	11.4	0.0	0.0	2.0	2.2
Banded chloritic U-quartzite (Table 44.1-10)									
15. Phyllosilicate	39.1	16.1	0.1	18.5	12.4	0.2	1.4	0.0	0.7
16. U-phyllosilicate****	44.6	21.3	0.0	5.6	10.8	0.0	3.8	0.2	0.1
Mylonitized "lower quartzite" (Table 44.1-11)									
17. Colourless flakes	26.8	25.5	0.0	1.5	31.2	0.0	0.0	0.0	0.0
18. Green flakes	28.3	18.8	0.1	20.3	20.0	0.0	0.1	0.2	0.1
19. Groundmass "clay"	28.9	18.3	0.1	19.6	19.4	0.0	0.1	0.3	0.0
20. Groundmass "clay"	33.0	21.4	0.1	14.6	17.0	0.1	1.9	0.2	0.1
"Lower quartzite" breccia (Figs. 44.1d, 44.2)									
21. Phlogopite	39.3	14.0	1.2	8.7	21.5	0.0	9.9	0.5	0.3
22. Chlorite pleochr. halo	33.7	14.8	0.0	9.4	30.3	0.1	0.0	0.0	0.1
23. Chlorite green	32.8	14.5	0.0	7.5	31.7	0.1	0.1	0.8	0.1
24. Chlorite bleached	34.1	15.0	0.0	5.2	32.5	0.0	0.0	0.0	0.3
"Lower gneiss"									
25. Amphibole	56.2	0.6	0.0	5.9	20.7	0.1	0.1	0.4	12.9
26. "Talc-like"	59.8	0.9	0.0	3.3	28.4	0.0	0.1	0.3	0.1

* Electron microprobe analyses by M. Bonardi, G.R. Lachance and A.G. Plant using an energy dispersive spectrometer (Lachance and Plant, 1973) combined with manually adjusted spectrometers for the uranium, lead (and potassium).

** Total iron reported as FeO.

*** Scapolite No. 3 contains 1.7% chlorine.

**** U-phyllosilicate No. 12 contains, in addition, UO_2 = 54.4% and PbO = 0.4%; and No. 16, UO_2 = 5.8%.

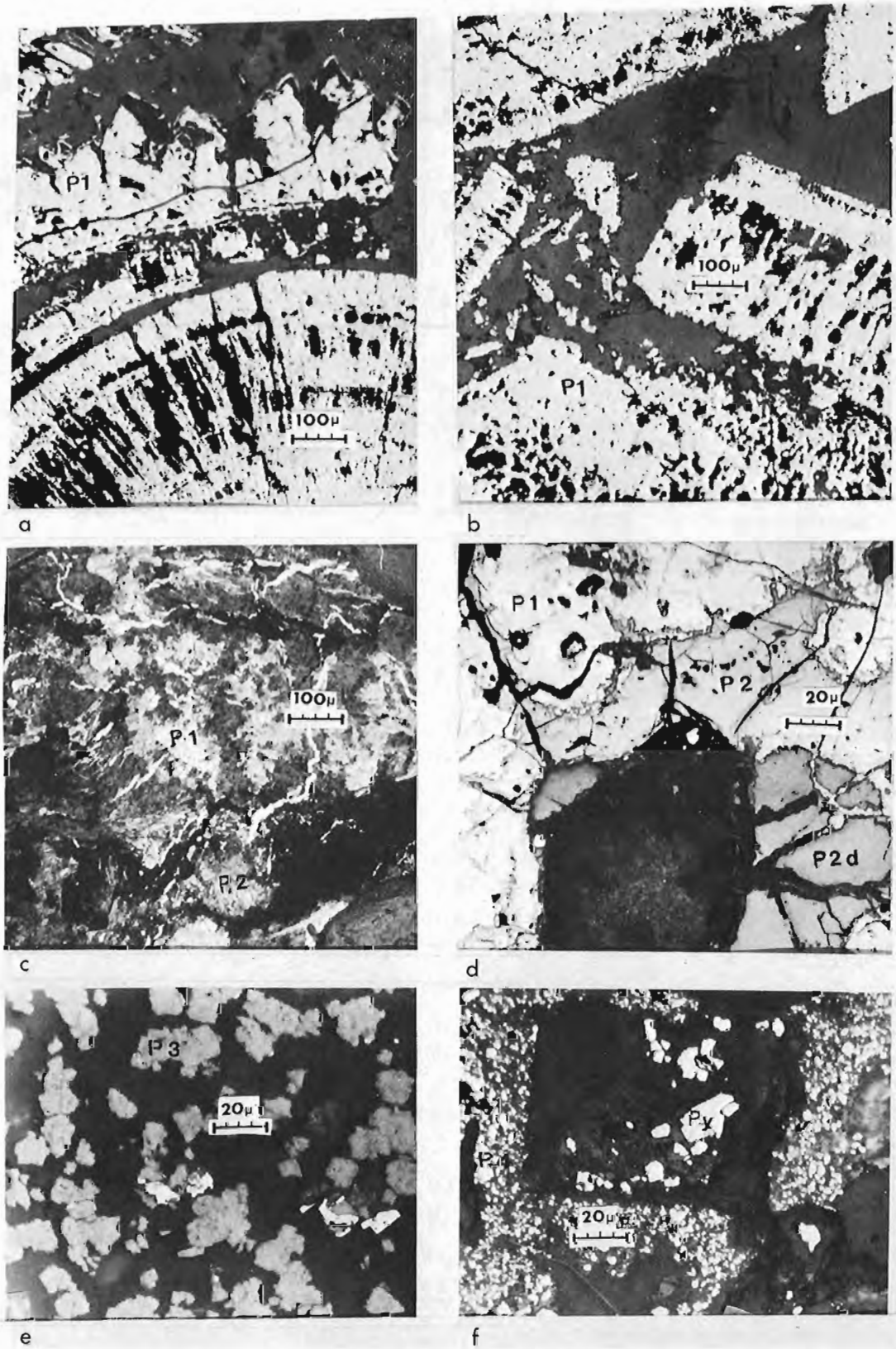
P1
100μ
a
P1
100μ
b
100μ
P1
P2
c
P1
P2
20μ
P2d
d
P3
20μ
e
Py
Py
20μ
f

Table 44.3

Selected electron microprobe analyses* of five types of pitchblende and of associated secondary U-minerals from the Rabbit Lake Uranium Deposit

Specimen	Weight % SiO_2	Al_2O_3	TiO_2	FeO	CaO	MgO	PbO	UO_2	Total	100-total	PbO/UO_2
Pitchblende type											
1. Massive P-1	0.1	0.0	0.3	0.1	1.3	0.0	11.7	85.1	98.6	1.4	1/7.3
2. Massive P-1	0.3	0.0	0.5	0.2	1.4	0.0	8.7	85.4	96.5	3.5	1/9.8
3. Massive P-1	0.7	0.2	0.5	0.1	1.7	0.0	10.1	83.5	96.9	3.1	1/8.2
4. Resorbed P-1	3.6	0.0	0.0	0.0	1.1	0.0	18.6	51.5	74.8	25.2	1/2.8
5. Resorbed P-2	3.2	0.0	0.0	0.0	2.8	0.0	13.6	61.6	81.2	18.8	1/4.5
6. Pb-depleted P-2	3.2	0.0	0.0	0.0	6.0	0.0	1.0	78.8	89.0	11.	1/78.8
7. Recrystallized P-3	0.0	0.0	0.0	0.0	0.6	0.0	4.8	81.9	87.3	12.7	1/17
8. Recrystallized with sulphide P-4	9.9	0.0	0.0	0.0	5.9	0.0	0.1	77.3	93.3	6.7	1/700
9. Rims P-5	13.9	0.0	0.0	0.0	2.8	0.0	0.1	63.1	79.8	20.2	1/800
Secondary U-minerals											
10. Coffinite	16.7	1.7	0.0	0.0	1.2	0.2	0.3	75.8	95.9	4.1	1/253
11. Uranophane	12.4	0.0	0.0	0.0	6.2	0.0	0.2	68.2	86.9	13.1	1/341
12. U in Fe oxides	22.2	22.0	0.2	44.6	0.6	1.9	0.3	2.0	93.8	6.2	1/6.7
13. U with Ti and RE	5.1	1.2	7.2	0.0	1.8	0.0	1.1	62.3	78.7	21.3	1/53

* Analysts: M. Bonardi, G.R. Lachance and A.G. Plant.

1-3. Massive, fractured pitchblende P-1 (Figs. 44.3a, 44.3b).

4-6. Resorbed pitchblende having different reflectivities P-1 and P-2 (Figs. 44.3c, 44.3d) from brecciated ore.

7. Rectangular recrystallized pitchblende P-3 in phyllosilicate groundmass, as in Figure 44.3a.

8. Impure pitchblende P-4 recrystallized with fine grained Fe, Cu, Co, Ni-sulphides coffinite and carbonate (Fig. 44.3f).

9. Narrow pitchblende rims P-5 surrounding chalcopyrite (Fig. 44.4b) commonly speckled or sooty, overgrown by "metamict" clay or coffinite, as in Figure 44.4e.

10. Coffinite associated with calcite in a vein, Figure 44.4f.

11. Uranophane filling fractures in brecciated ore.

12. U-bearing iron oxides adsorbed on groundmass silicates in red "oxidized" sample.

13. Uranium-titanium-rare earths-bearing grains, similar to those in Figure 44.2 in red "oxidized" ore containing abundant radiating tourmaline, as in Figure 44.1h, 44.1i.

Figure 44.3. (opposite)

Various types of pitchblende in the Rabbit Lake U-deposit. (All photomicrographs taken in reflected light)

3a. Massive and colloform pitchblende P-1, from ore zone at 155 feet.

3b. Brecciated bands of massive and colloform pitchblende P-1 in phyllosilicate groundmass, from the same sample as in Figure 44.3a.

3c. "Primary" massive pitchblende P-1 surrounded by partly resorbed and Pb-depleted pitchblende P-2 (note decreasing reflectivity), transected by galena and clausthalite veinlets in breccia ore, from 177-foot depth.

3d. Decreasing reflectivities from relatively fresh pitchblende P-1, resorbed edges P-2, to Pb-depleted impure pitchblende P-2d, enlarged from Figure 44.3c.

3e. Fine-grained euhedral pitchblende aggregates P-3, recrystallized in phyllosilicate groundmass adjacent to resorbed edges of massive pitchblende P-1. Euhedral pitchblende P-3 has lower Pb/U ratio than the adjacent massive pitchblende P-1; brecciated U-ore from 107-foot depth.

3f. Pseudomorphs of chlorite after euhedral pyrite (dark rectangle) with pyrite remnants (Py), surrounded by speckled coffinite-calcite-carrollite-chalcopyrite-covellite-pitchblende aggregates P-4 in U-ore partly replaced by sulphides, from 183.5-foot depth.

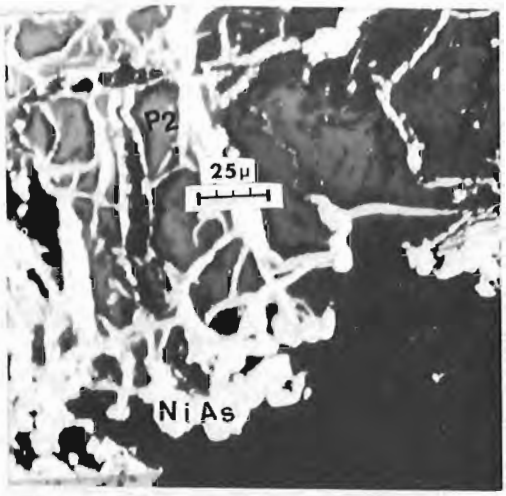
P2
25µ
NiAs

a

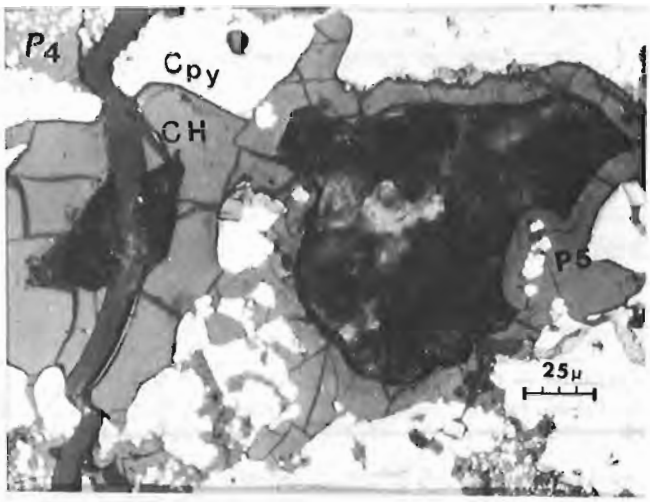
P4
Cpy
CH
P5
25µ

b

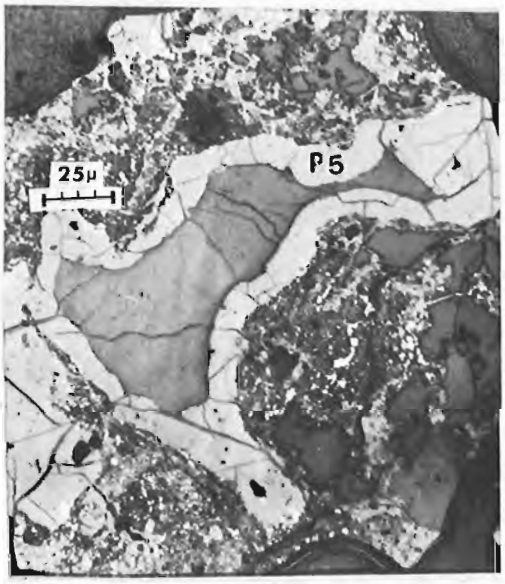
25µ
P5

c

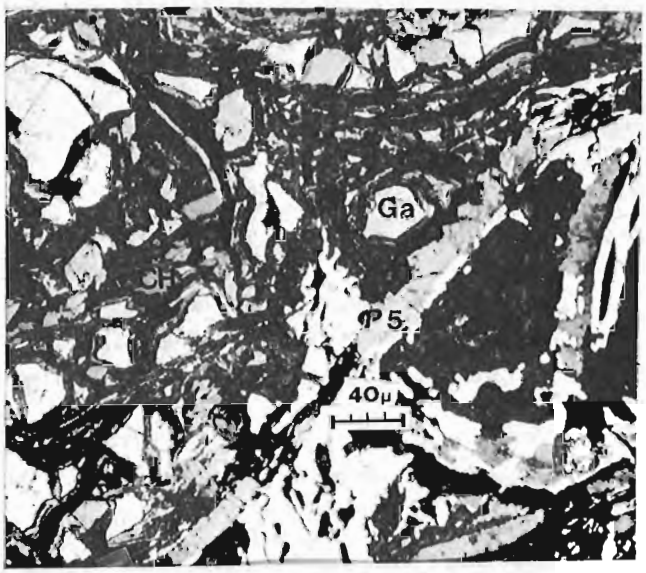
Ga
CH
P5
40µ

d

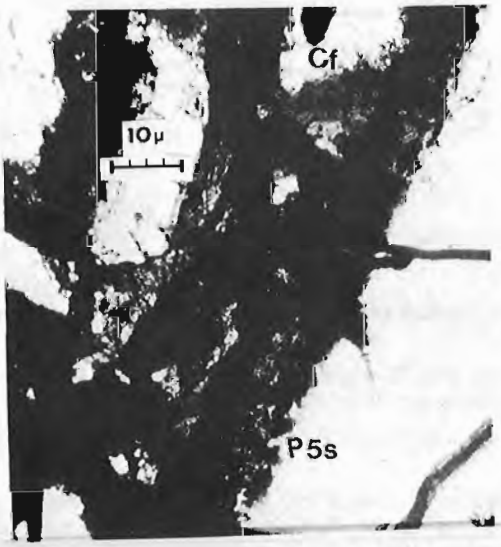
Cf
10µ
P5s

e

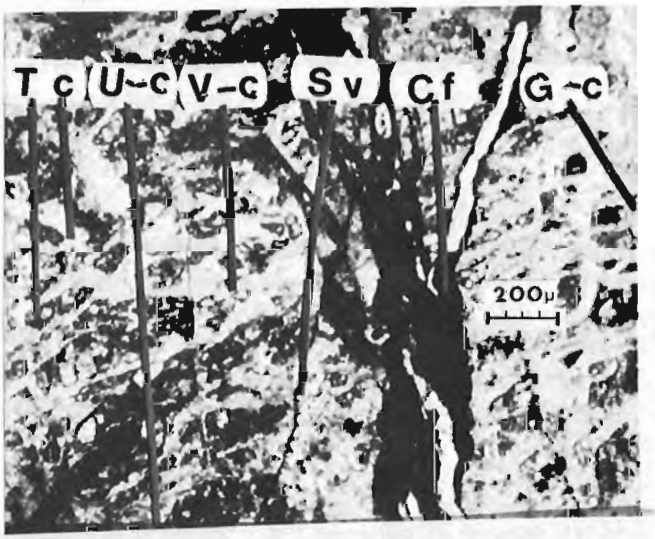
T c
U-c
V-c
Sv
Cf
G-c
200µ

f

7. Oxygenated hydrocarbons and U-C impregnated clays. Black, coarse (ca 1 mm) round grains, transected by curved fractures were observed in drill core samples in close association with massive pitchblende (Figs. 44.4b, 44.4d). In the pit they occur associated with black euhedral quartz and grey clay. These black grains, commonly referred to as "thucholite", are composed of carbon, water and traces of calcium and sulphur. Some of them are coated with thin pitchblende rims, type P-5, which extend into the fractures of the black grain, thereby accounting for the uranium content of the "thucholite". Altered "thucholite" grains are replaced by fine grained calcite.

Some argillitized patches in the "upper" quartzite are grey to almost black as a result of finely dispersed black carbon (Table 44.1-7). The black C-bearing patches contain uranium and occasionally fine grained Co-Ni sulphides. Fine grained U-C coatings were also observed on euhedral dolomite and on black quartz containing interstitial "thucholite". The black colour disappears on ignition and the trace residue after ignition gives the uraninite and anhydrite X-ray patterns.

8. Uranium-bearing and common sulphates. Fine grained, apple-green, glassy zippeite globules (< 1 mm), associated with gypsum, sklodowskite and uranophane were observed in fractures in montmorillonitic clay which caps fragments of brecciated ore in the pit. Anhydrite and gypsum were identified in "thucholite" ashes; barite was found in carbonate veinlets transecting "upper" gneiss; and malachite associated with covellite and secondary U-minerals form thin coatings on coarse grained euhedral dolomite.

9. Uranium associated with red iron-rich patches. Red, oxidized rocks which occur just above the groundwater level in the open pit and along fracture zones in several drill core samples, contain patches of red phyllosilicates coated with fine grained hematite and/or goethite. Some of these Fe-rich coatings are radioactive in spots, probably because of uranium adsorbed on iron oxides (Table 44.3-12).

Table 44.4

Selected analyses* of brightly coloured hydrated Pb-U oxides and silicates from the Rabbit Lake Uranium Deposit

	Weight %											
Specimen**	U_3O_8	ThO_2	PbO	Y	Nd	Sm	Eu	Dy	Ho	Er	Tm	Yb
1. Orange ore	59.	0.08	20.	0.23	0.0676	0.0444	0.0105	0.19	0.0245	0.0550	0.0057	0.0352
2. Green ore	70.	<0.02	1.5	0.0242	0.0024	0.0044	0.0007	0.0088	0.0014	0.0020	0.0003	0.0020
3. Yellow ore	74.	<0.02	2.5	0.006	0.0008	0.0023	0.0002	0.0033	0.0006	0.0007	0.0001	0.0008

* X-ray spectrographic analysis for U, Th and Pb by G.R. Lachance; atomic absorption spectrometric analysis for the rare earths by J.G. Sen Gupta (for method used, see Sen Gupta, 1976).

** All specimens are from the pit.

1. Orange U-ore consists of fine grained intergrowths of uranophane, masuyite-becquerelite, and woelsendorfite.
2. Green U-ore consists dominantly of fine grained uranophane-montmorillonite intergrowths.
3. Yellow U-ore consists dominantly of fine-grained uranophane. Isotopic analysis of lead by TELEDYNE ISOTYPES, Westwood, New Jersey, U.S.A. indicated following Atom %: Pb 204 = 0.005; Pb 206 = 92.975; Pb 207 = 6.470; Pb 208 = 0.550.

Figure 44.4. (opposite)

Illustrations of replaced pitchblende and of pitchblende rims P-5 (Photomicrographs 44.4a to 44.4d taken in reflected light; 44.4e and 44.4f in transmitted light)

4a. Remnant of pitchblende P-2 partly replaced by nickeline (NiAs) in U-ore replaced by sulphides and arsenides, from 143-foot depth.

4b. Pitchblende rims P-5 surrounding calcite-clay pseudomorphs after "thucholite" in U-ore partly replaced by chalcopyrite (Cpy), "thucholite" (CH), and by speckled coffinite-calcite-sulphide-pitchblende P-4 aggregates, from 153-foot depth.

4c. Pitchblende rims P-5 surrounding recrystallized carbonate in a breccia, from 177-foot depth.

4d. Remnants of pitchblende rims P-5 on resorbed "thucholite" (CH) with abundant galena (Ga, white) in partly resorbed ore from 107-foot depth.

4e. Speckled rims of "sooty" pitchblende P-5s (opaque specks), enclosed in semi-transparent coffinite (Cf) in quartz, from 147-foot depth.

4f. Host rock to massive pitchblende P-1 (Figs. 44.3a, 44.3b), consisting of phyllosilicates or "clays" (G-c), uraniferous "clay" (U-c) including disintegrating orange-yellow tourmaline (T) and quartz, and transected by veinlets of calcite and coffinite (Cf) and serpentine (S), from 155-foot depth.

Summary and Conclusions

The present mineralogical-chemical study of selected samples from the Rabbit Lake deposit provides additional information on the mineralogy of the uranium ore and of the surrounding rocks. The results obtained on the specimens examined are as follows:

1: The pyroxene-amphibole-biotite layers in the "upper" gneisses and their alteration products are similar to those in the "lower" gneisses.

2: The occurrences of radioactive elements in nine mineral groups and different modes, along with Co, Ni, Cu, Se, Th and rare earths minerals indicate the mineralogical complexity of the deposit. Because of the deformed, fractured and displaced nature of the "primary" pitchblende, the contacts between the pitchblende and the host rock are unclear and commonly masked by subsequent recrystallizations and alterations.

3: In the high grade ore, pitchblende is the dominant U-mineral, and there are lesser amounts of secondary U-minerals. Because the primary pitchblende is much fractured and is partly altered and resorbed along the fractures, it is believed that all secondary U-minerals were derived from the "primary" pitchblende.

The areas of high grade ore are surrounded by zones containing fragments of "primary" pitchblende or high grade ore enclosed within low grade ore material, made up mainly of secondary U-minerals and minor amounts of partly resorbed particles of "primary" pitchblende. This suggests that the high grade ore was originally more extensive.

4: Below the main thrust fault, the radioactive minerals include "yttrialite" grains, which contain U, Th and rare earths, and pitchblende (type P-5) that rims Ti-minerals.

5: Marked differences in Pb/U ratio in U-minerals, as shown in Table 44.3, are attributed to three factors, singly or in combination;

(a) temporal difference in crystallization of primary and secondary U-minerals and different periods of time for natural accumulation of radiogenic lead;

(b) migration and depletion of lead during remobilization of pitchblende; and

(c) recrystallization of liberated U and Pb in different proportions forming secondary U-Pb minerals.

Descriptions of progressive alteration of uranium minerals during emplacement of sulphides and in the oxidation zone, and of phyllosilicates in the Rabbit Lake deposit will be presented in more detail in two separate papers.

Acknowledgments

Optical and X-ray diffractometer studies by the author were supported by: DTA-TG analyses by W.S. Bowman of CANMET; X-ray identifications of minerals by A.C. Roberts; emission spectrographic analyses by P.G. Bélanger, G. Bender and K. Church; rapid chemical analyses by G.R. Lachance and J.-L. Bouvier; atomic absorption spectrometric analyses for selected rare earths by J.G. Sen Gupta; and electron microprobe analyses by M. Bonardi, G.R. Lachance and A.G. Plant, all of the Geological Survey of Canada. The assistance of the members of the Analytical, Cartographic and Photographic Sections, and of all who contributed to this study is greatly appreciated. Special thanks are due to Mr. C.R. Burkhart of Gulf Minerals Limited for his helpful guidance in the pit, to Gulf Minerals Canada Limited and Uranerz Canada Limited for their consent to present these data at two scientific meetings (Rimsaite, 1976a, 1976b), and to Dr. L.P. Tremblay who read the manuscript and made valuable suggestions.

References

Knipping, H.D.
1974: The concepts of supergene versus hypogene emplacement of uranium at Rabbit Lake, Saskatchewan, Canada; Symposium: Formation of Uranium Deposits; IAEA-SM-183/38.

Lachance, G.R. and Plant, A.G.
1973: Quantitative electron microprobe analysis using an energy dispersive spectrometer; in Report of Activities,Part B, Geol. Surv. Can., Paper 73-1B, p. 8-9.

Rimsaite, J.
1975: Natural alteration of mica and reactions between released ions in mineral deposits; Clays and Clay Miner., v. 23, p. 247-255.

1976a: Mineral assemblages at the Rabbit Lake uranium deposit, Saskatchewan; GAC/MAC Meeting, Edmonton; MAC Symposium: Mineralogy and Geochemistry of Uranium Deposits; Program with Abstracts, v. 1, p. 44.

1976b: Progressive alteration of pitchblende in an oxidation zone of uranium deposits; 25th IGC, Sydney, Australia; Abstracts, v. 2, p. 594-595.

Sen Gupta, J.G.
1976: Determination of lanthanides and yttrium in rocks and minerals by atomic absorption and flame-emission spectrometry; Talanta, v. 23, p. 343-348.

Sibbald, T.I.I.
1976: Uranium metallogenetic studies – Rabbit Lake; Sask. Geol. Surv., Summ. Invest., 1976, p. 115-123.

Wallis, R.H.
1971: The geology of the Hidden Bay area, Saskatchewan; Sask. Dep. Min. Res., Rep. 137.

45. A NEW GENETIC MODEL FOR URANIUM-COPPER MINERALIZATION, PERMO-CARBONIFEROUS BASIN, NORTHERN NOVA SCOTIA

Project 760014

H.E. Dunsmore
Regional and Economic Geology Division

A number of uranium-copper occurrences in Upper Carboniferous sandstones of northern Nova Scotia are designated in an accompanying paper (Dunsmore, 1977) as the Pugwash-Tatamagouche style of mineralization. The scattered occurrences bear a striking resemblance, both in style of mineralization and geological setting, to deposits of the Colorado Plateau area of the southwestern United States. In both areas, the mineralization occurs as concordant, tabular deposits closely associated with coalified organic debris within nonmarine, fluviatile sandstones which are interbedded with mudstones. One major difference is that volcanic ash, suspected by many to be the source of the uranium in the Colorado Plateau area (Fischer, 1974) is not present in Nova Scotia, either in the host rocks or in overlying strata.

A new metallogenetic model suggests that the mineralizing solutions, together with most of the uranium for this type of deposit, were derived from thick sequences of underlying marine evaporites. Although still speculative, the model is proposed here in the hope that it will stimulate discussion and perhaps assist exploration in this and other areas. Should the model be valid, significant uranium resources not suspected hitherto may be found in the Pugwash-Tatamagouche district of northern Nova Scotia.

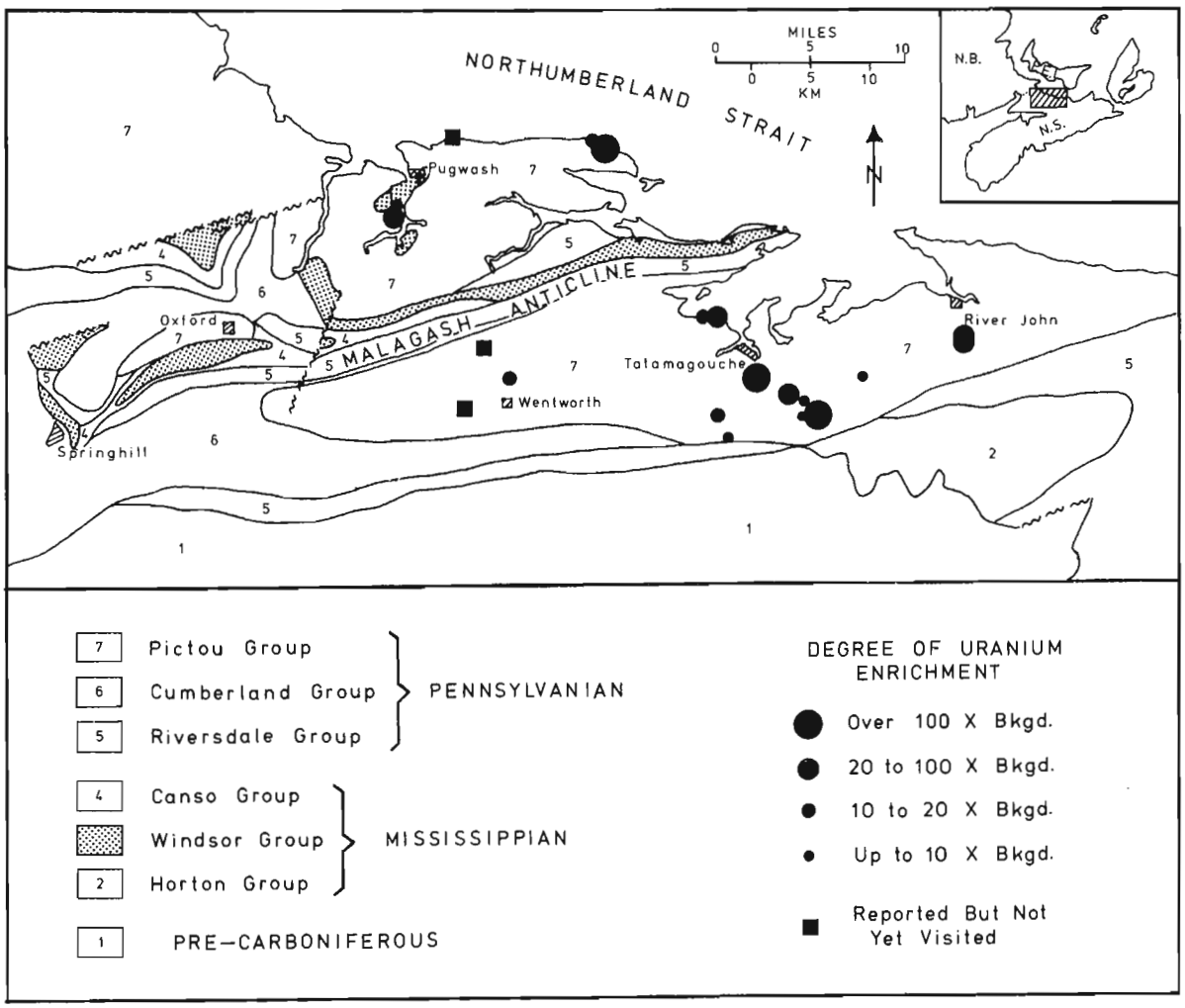

Figure 45.1. Geology and uranium occurrences, northern Nova Scotia. Degree of uranium enrichment in selected hand specimens relative to mean uranium content of unmineralized equivalents (geology after Geological Map of Nova Scotia, N.S. Dept. of Mines, 1965).

From: Report of Activities, Part B;
Geol. Surv. Can., Paper 77-1B (1977)

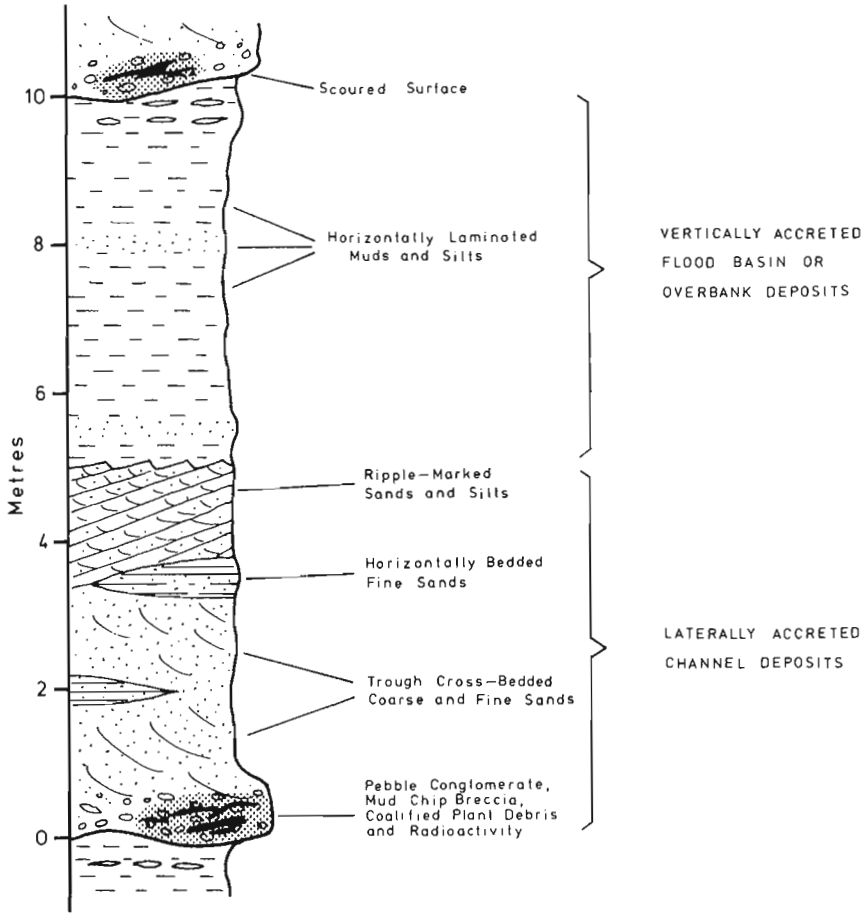

Figure 45.2. Generalized stratigraphic section illustrating fining-upward cycles, lower Pictou Group, northern Nova Scotia. Shaded portions represent radioactivity associated with coalified plant debris.

Distribution of Uranium Occurrences

The geographic distribution of presently known surface occurrences is shown in Figure 45.1. The degree of uranium enrichment relative to background concentrations, as determined by neutron activation analysis of selected rock specimens, is also depicted. A number of these occurrences were previously reported and described in the literature (Brummer, 1958; Gross, 1957). Because copper is frequently associated with uranium, the copper showings recorded by Fletcher (1905), some of which were mined, proved to be useful guides. However, diligent geological prospecting would probably result in the discovery of additional radioactive occurrences.

Geological Setting

The known uranium-copper occurrences in this part of Nova Scotia are in lower Pictou Group red beds which comprise a low-lying erosional remnant of a once much thicker clastic section (van de Poll, 1973). These rocks consist of stacked cycles of conglomerate, sandstone, siltstone and mudstone which were deposited in a non-marine environment by fluvial, palustrine and lacustrine processes. Sediment transport was in an easterly to northeasterly direction (ibid). Unlike uranium mining districts in the southwestern United States, there is no evidence here of volcanic material within the host rocks which might have served as a source of uranium. The dominant structural features are a series of salt-cored diapirs originating from exceptionally thick sequences of underlying, Lower Carboniferous, Windsor Group evaporites.

In detail, uranium-copper mineralization is found at or near the base of fining-upward cycles, in direct association with coalified organic matter (Fig. 45.2). These very localized sites of chemical reduction are visible in outcrop as a pronounced colour change, from the usual reddish brown to greenish grey. The organic matter was observed in two forms: discrete pieces of coalified wood which were originally tree trunks or branches, and flakes of organic matter on the bottomset bedding planes of cross-stratified, coarse sands.

The fining-upward cycles, stacked one on top of the other, are typically about 10 m thick. The channel floor deposits at the base of most cycles consist of a lithic and quartz pebble conglomerate. At many localities, the basal lag deposit is also made up of mud chips eroded locally from the channel walls as the meandering river migrated across the flood plain. Above the coarse lag, laterally accreted deposits of the active channel are generally preserved as trough cross-bedded coarse sands, passing upward to ripple-marked fine sands, both of which are interbedded with varying amounts of horizontally laminated sands (Fig. 45.2). The upper half of each cycle, the vertically accreted flood plain or overbank deposits, consists of laminated, red-coloured silts and muds, commonly containing calcitic concretions or nodules near the top. These more resistant, caliche-like nodules are sometimes ripped up and incorporated in the lag deposit of the succeeding cycle. A summary of our knowledge of fining-upward cycles and an introduction to the literature is provided by Walker (1976).

There are at least two reasons why mineralization is found at or near the base of fining-upward cycles. Firstly, this was presumably the most porous and permeable part of the sequence, and thus the preferred route for laterally migrating formational fluids. Secondly, the coalified plant debris, which began its existence as scattered clumps of vegetation growing on the flood plain, is preferentially found there. As meandering rivers swept back and forth across the valley floor, organic trash was picked up, became waterlogged, and was incorporated as a lag deposit mainly in the basal part of each cycle. Thus, postdepositional, ore-forming solutions would be channelled within those portions of the section where copper and uranium could be chemically fixed. Copper and iron would be precipitated as a result of sulphate reduction in the presence of the organic matter, uranium by the change in redox potential.

Proposed Model of Ore Formation

Of all the various types and styles of uranium enrichment in Atlantic Canada, the Pugwash-Tatamagouche style is perhaps the best understood at present. Not only does the means of fixing the uranium seem clear, but we may also have some insight into the source of the metal and of the ore-forming solutions.

The model of ore formation which presently appears to fit the data best, involves the underlying Windsor Group evaporites. It is proposed that these saline deposits were the source of both the mineralizing solutions and of most of the uranium. During the evaporation of sea water and the systematic precipitation of the various evaporitic minerals, uranium preferentially remains in solution (a low temperature, chemical fractionation), becoming highly concentrated in the saline, residual brines (Dunsmore, 1975). This 'mother liquor' of the sedimentary realm is analogous to the final fluid phases within a cooling magma chamber. On burial and compaction (de-watering), these uranium-enriched connate brines would, in most cases, be expelled to overlying, permeable strata (ibid). Under suitable hydrodynamic and chemical conditions, concentrations of uranium might result at sites of chemical reduction within the overlying strata.

It has been calculated that by the time sea water has evaporated to the point where potash minerals are about to precipitate, the concentration of uranium in solution has increased some 18 times, from a normal marine value of 3.2 ppb to approximately 60 ppb (Dunsmore, 1975). The validity of these calculations is confirmed by Dall'Aglio and Casentini (1970) who determined the uranium content of brines within a solar salt plant in Italy. The curve drawn from their analytical data shows a lower concentration of uranium during the initial stages of evaporation than the calculated curve, but subsequently the two run parallel (Dunsmore, 1975). The difference at the initial stage is almost certainly due to fish-farming operations carried on within the first few evaporating pans (Dall'Aglio and Casentini, 1970). The organic wastes associated with these operations would probably remove unusually large quantities of uranium from solution. However, the bulk of the concentration occurs during the precipitation of halite; this is not surprising when one considers that rock salt is perhaps the least uraniferous of all rocks.

The advantages of working with a simple mathematical model are that one can extrapolate the available data, and also that one can alter the initial conditions to see what the outcome might be. It turns out that the most critical variable in the equation is the initial uranium content of sea water. The values given above assume that the aqueous input to the evaporite basin is normal sea water, as found today in the middle of the North Atlantic and North Pacific. However, many evaporite basins would be expected to process waters with higher trace element contents, perhaps due to an enriched hinterland. This would almost certainly have been the case for the Mississippian, Windsor Group evaporite basin in Atlantic Canada, where older Mississippian and Devonian igneous rocks are known to be enriched in uranium. Assuming an initial uranium content double that of normal sea water, the model predicts a final concentration, at the point where potash salts begin to precipitate, of 195 ppb; if triple, the corresponding value is well over 300 ppb, or 0.3 ppm (Dunsmore, 1975). Such values compare more than favourably with the 12 to 46 ppb uranium found in groundwaters issuing from volcanic and tuffaceous sedimentary terrains (Denson et al., 1956), evidence which apparently convinced many people that the volcanic component was the source of uranium for sandstone-type deposits.

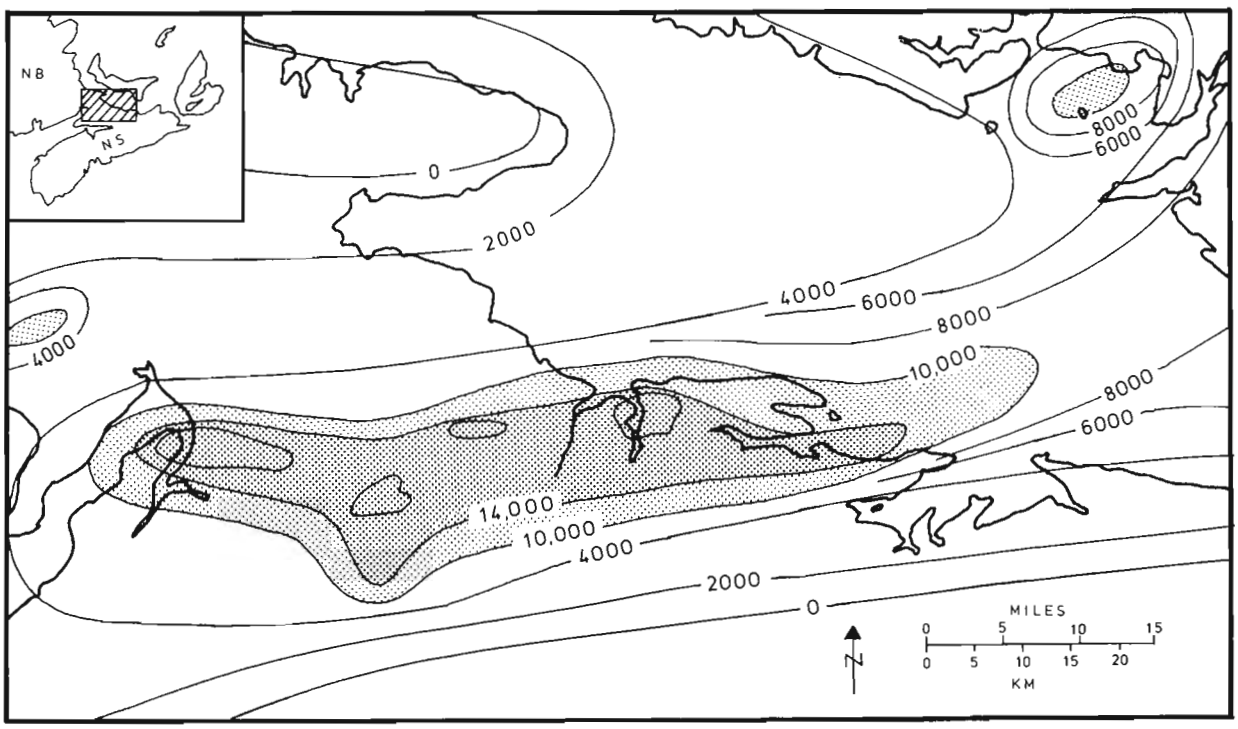

Figure 45.3. Isopach map of Windsor Group, in feet (after Howie and Barss, 1975).

After the concentration of uranium and other elements by evaporitic differentiation, a portion of the highly saline residual brines would be trapped within the saline deposits. During burial and compaction, these connate brines would be ejected, usually to overlying stratigraphic sequences. Proof that this actually occurs was provided by Carpenter et al. (1974). They found highly saline, evaporite-derived brines (original connate brines and not brines of dissolution) throughout many thousands of feet of strata above the Louann Formation evaporites of the Gulf Coast Basin. Faulting associated with compaction or the initial stages of salt diapirism would greatly facilitate the upward migration of these brines. Once higher stratigraphic levels had been reached, the brines could then be channelled laterally within permeable stratigraphic units, such as fining-upward cycles or basal conglomerates along unconformities.

Support for this model of ore formation was recently provided by Rose (1976). Primarily on chemical considerations, Rose argued that the most likely copper-transporting fluid for many red bed, copper-uranium deposits was evaporite-derived, chloride-rich groundwaters.

Mathematical models and theoretical considerations are only useful up to a point. The proof of the puzzle will be in the rocks.

Application of the Model

Although detailed field work has yet to be undertaken, evidence is accumulating to support the proposed model in the Pugwash-Tatamagouche area of northern Nova Scotia. For one thing, there is an obvious areal relationship between known mineralization and thick saline deposits. Figure 45.3 shows part of a Windsor Group isopach map prepared by Howie and Barss (1975). Information from the subsurface is still meagre, but a very thick section of Windsor Group, consisting largely of evaporites (ibid), is known to trend east-west through the area of interest (Fig. 45.3). Salt in the thickest portions of the saline deposit has flowed, forming the salt-cored Malagash anticline and the salt diapirs in the Pugwash area. The known uraniferous anomalies, in outcrop (Fig. 45.1) and in well waters (Fig. 45.4), appear to occur in two broad belts that parallel the axes of the Malagash anticline and the evaporite sub-basin. One belt lies to the north of the anticline, including those occurrences in the vicinity of the Pugwash diapirs. The other lies to the south and is made up of occurrences in the Tatamagouche and Wentworth areas. In all probability, copper-uranium deposits were originally more uniformly distributed throughout the area, but those along the axis of the Malagash anticline have been lost to erosion.

It is most encouraging to compare the Pugwash-Tatamagouche situation to that of uranium-mining districts in the southwestern United States. Figure 45.5 is an isopach map of the salt facies within the Paradox Basin of Utah and Colorado; the locations of known uranium deposits and of salt-cored domes and anticlines are also plotted. Approximately 90 per cent of the uranium reserves of the area coincide areally with the thickest portions of the saline deposit. What is more, a strong positive correlation exists between salt-cored anticlines and some of the more important uranium-mining districts. Uranium-bearing brines may have gained access to the relatively unimportant White Canyon and Monument Valley mining districts following lateral migration through the thick sequences of shelf carbonates deposited seaward of the evaporite basin. The evaporites in this area are Upper Carboniferous in age while the uranium-copper deposits, located some two to six thousand feet stratigraphically above the salt, are in fluviatile sandstones of Jurassic and Triassic age. Although isopachous lines in Figure 45.5 have not been drawn beyond 3000 feet, the salt facies is estimated to have originally been up to 7000 feet (2100 m) thick, but is now locally in excess of 14 000 feet (4300 m) due to salt flow (Hite, 1961). Thus, not only is the thickness of salt in northern Nova Scotia similar to that of the Paradox Basin, but the length of the Malagash anticline is also similar to those in Colorado and Utah.

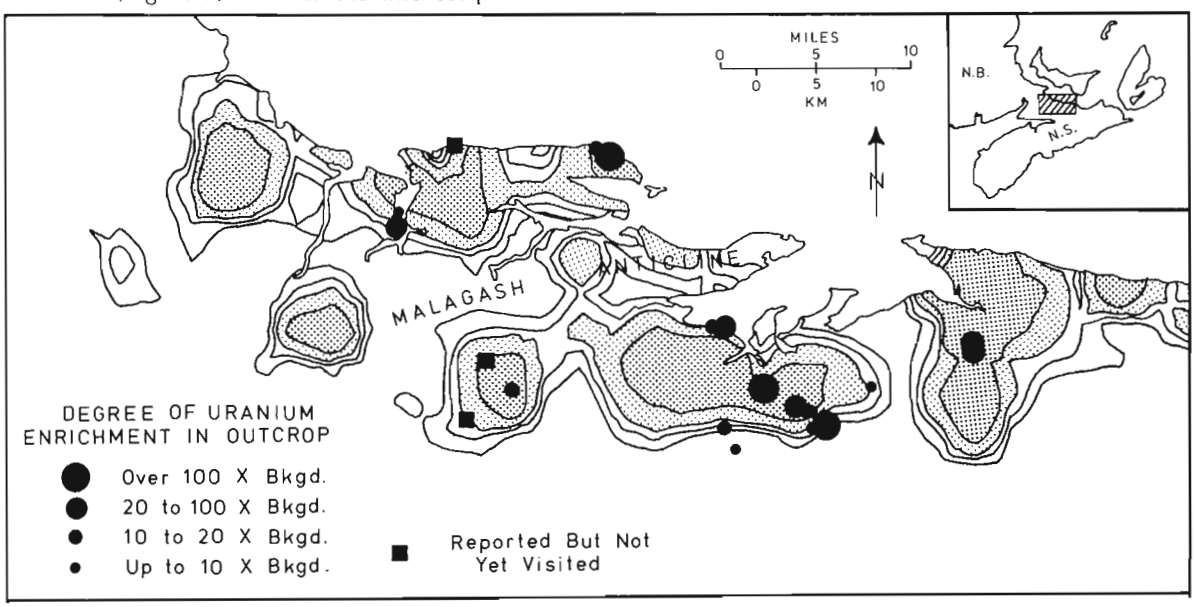

Figure 45.4. Groundwater uranium anomalies (after Dyck et al., 1976) and uranium occurrences, northern Nova Scotia.

In view of the foregoing, it is unfortunate, from a uranium resources point-of-view, that the bulk of the Windsor Group evaporites in eastern Canada lie beneath the Gulf of St. Lawrence. The Magdalen Islands, which probably owe their existence to salt diapirism, are a tiny scrap of land rising above the waters of the Gulf. As reported in an accompanying paper (Dunsmore, 1977), a number of occurrences were discovered there, although the style of mineralization is different from that in the Pugwash-Tatamagouche area. Nevertheless, the association with evaporites is once again clearly evident.

Other evidence to support the suggestion that the ore-forming solutions were residual evaporitic brines is found within the rocks themselves. The host sandstones and conglomerates at a number of the occurrences visited in northern Nova Scotia contain what was identified in hand specimens as dolomitic cements. The limited petrographic studies made to date have revealed the presence of authigenic dolomite rhombs and microcrystalline dolomitic cements. If further studies show that dolomite is a common secondary mineral at the sites of mineralization, the source of the magnesium in

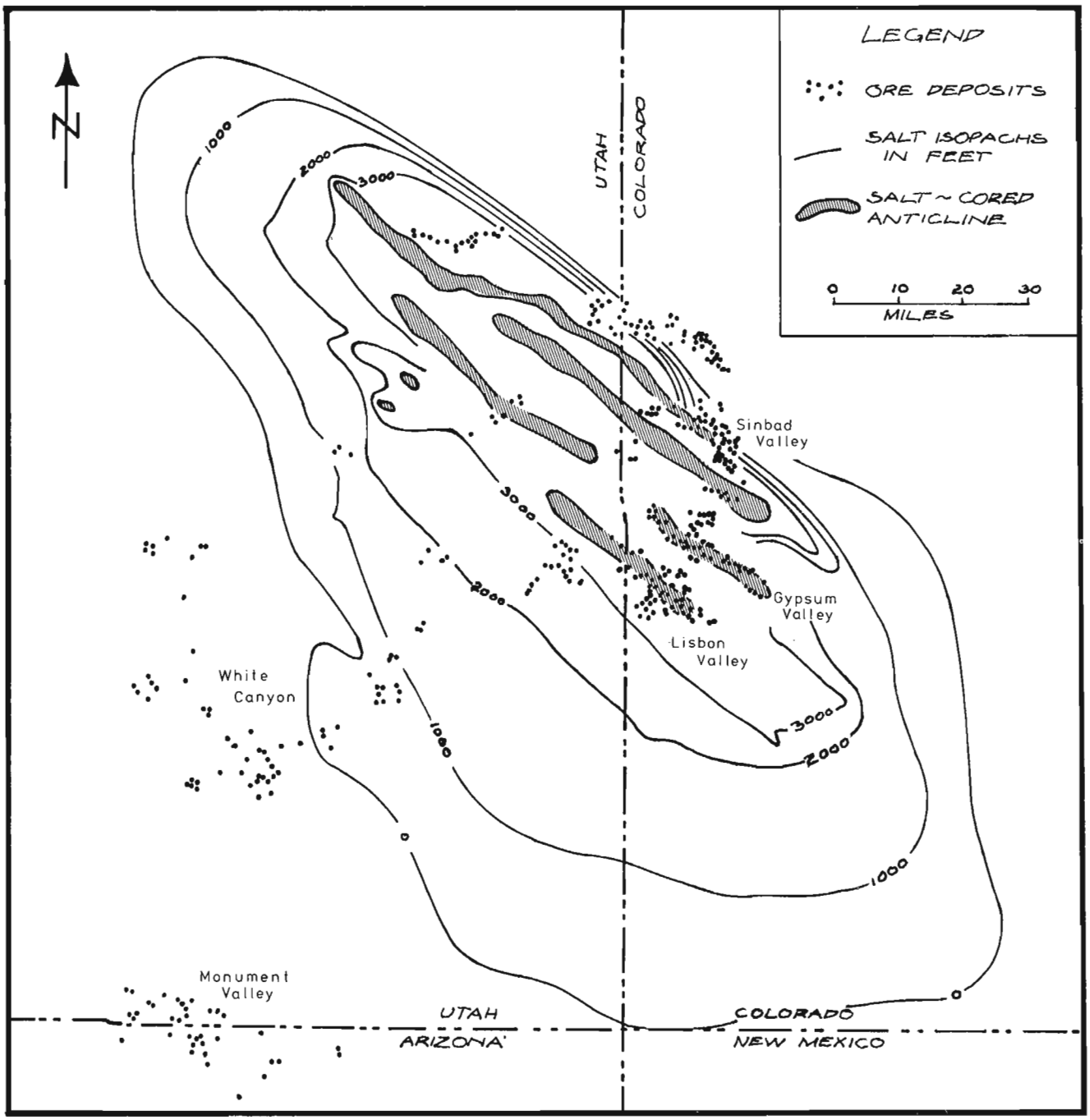

Figure 45.5. Areal distribution of sandstone-type uranium deposits, marine evaporites and evaporite-related structural features in the Colorado Plateau area, southwestern United States (after Lefond, 1969; Malan, 1968; Motica, 1968).

sequences of fluviatile sandstones would pose a problem unless the underlying evaporites were involved. Residual evaporitic brines would be highly charged with magnesium and would be expected to dolomitize any calcitic cements with which they came in contact. In this context it is interesting to note that mineralized portions of the Salt Wash Member, the principal uranium host rock in the Colorado Plateau area, contain three times more magnesium than unmineralized samples of the same unit (Shoemaker et al., 1959). The bulk of the excess magnesium associated with the ore was believed to be present as authigenic dolomite (ibid). Clearly, additional petrographic and geochemical studies of the host rocks in Nova Scotia are warranted.

There are areas in northern Nova Scotia underlain by thick sequences of evaporites where there is no apparent mineralization. For example, presently known uraniferous anomalies do not extend very far west of the Pugwash area (Fig. 45.1, 45.4). One explanation may be found in the nature of the sediments immediately overlying the evaporites. In the Dorchester area of eastern New Brunswick, the Windsor Group is conformably overlain by as much as 700 m of highly impermeable Canso Group mudstones and siltstones. A similar situation is present in the Antigonish area of eastern Nova Scotia. These rocks would present a very effective barrier to upward migrating fluids. In the Pugwash-Tatamagouche area, this fine grained facies is either missing, as indicated by Roliff (1962), or was breached in the early stages of salt diapirism. Thus, we may be looking at a relatively local permeability window which permitted the upward escape of metal-bearing brines to favourable, fluviatile host rocks.

Conclusions

It is generally agreed by those who have worked in the Permo-Carboniferous Basin of Atlantic Canada that economic grades and tonnages of uranium ore will be found only at depth. The rocks here are probably more highly oxidized, and the centres of mineralization more thoroughly leached, than those in the southwestern United States. Only those metals which are inextricably bound up with organic matter remain behind to be viewed on the surface. In other words, we are probably only looking at the pips and not at the fruit. This does not necessarily mean, however, that the fruit has not been preserved in the subsurface.

In order to find hidden ore deposits at reasonable costs, exploration geologists will require a genetic model with predictive capability. Efforts should be directed toward the development of such a model for uranium occurrences in northern Nova Scotia. For example, it was recognized many years ago (Fletcher, 1905) that several of the laterally continuous fining-upward cycles are preferentially mineralized, but the reason why is not yet apparent. The results obtained by Dyck et al. (1976), a small portion of which are shown in Figure 45.4, indicate that groundwater geochemistry may also have an important role in exploration in this area. It will not be an easy task, but if the comparisons made here are valid, the rewards could prove to be substantial.

The model presented here represents but one of a number of ways in which a highly mobile element can be recycled and concentrated in the sedimentary-diagenetic environment.

References

Brummer, J.J.
1958: Supergene copper-uranium deposits in northern Nova Scotia; Econ. Geol., v. 53, p. 309-324.

Carpenter, A.B., Trout, M.L., and Pickett, E.E.
1974: Preliminary report on the origin and chemical evolution of lead- and zinc-rich oil field brines in central Mississippi; Econ. Geol., v. 69, p. 1191-1206.

Dall'Aglio, M. and Casentini, E.
1970: The distribution of uranium between precipitates and brines in the solar salt plant of Margherita Di Savoia. Geochemical and geological considerations; Boll. Soc. Geol. It., v. 89, p. 475-484.

Denson, N.M.,Zeller, H.D., and Stephens, J.G.
1956: Water sampling as a guide in the search for uranium deposits and its use in evaluating widespread volcanic units as potential source beds for uranium; U.S. Geol. Surv., Prof. Paper 300, p. 673-680.

Dunsmore, H.E.
1975: Origin of lead-zinc ores in carbonate rocks: a sedimentary-diagenetic model; Unpubl. thesis, Imperial College, Univ. of London.

1977: Uranium resources of the Permo-Carboniferous basin, Atlantic Canada; in Report of Activities, Part B, Geol. Surv. Can., Paper 77-1B, rep. 63.

Dyck, W., Chatterjee, A.K., Gemmell, D.E., and Murricane, K.
1976: Well water trace element reconnaissance, eastern Maritime Canada; J. Geochem. Explor., v. 6, p. 139-162.

Fischer, R.P.
1974: Exploration guides to new uranium districts and belts; Econ. Geol., v. 69, p. 362-376.

Fletcher, H.
1905: Geol. Surv. Can. Map nos. 793 (Tatamagouche), 794 (Malagash), 795 (Pugwash), and 796 (Wentworth).

Gross, G.A.
1957: Uranium deposits in Gaspe, New Brunswick and Nova Scotia; Geol. Surv. Can., Paper 57-2.

Hite, R.J.
1961: Potash-bearing evaporite cycles in the salt anticlines of the Paradox Basin, Colorado and Utah; U.S. Geol. Surv., Prof. Paper 424-D, p. 135-138.

Howie, R.D. and Barss, M.S.
1975: Upper Paleozoic rocks of the Atlantic provinces, Gulf of St. Lawrence, and adjacent continental shelf; Geol. Surv. Can., Paper 74-30, v. 2, p. 35-50.

Lefond, S.J.
1969: Handbook of World Salt Resources; Plenum Press, New York, p. 22.

Malan, R.C.
1968: The uranium mining industry and geology of the Monument Valley and White Canyon Districts, Arizona and Utah; Ore Deposits in the United States, 1933-1967, Graton-Sales, Vol. 1, J.D. Ridge, ed., p. 790-804.

Motica, J.E.
1968: Geology and uranium-vanadium deposits in the Uravan Mineral Belt, southwestern Colorado; Ore Deposits in the United States, 1933-1967, Graton-Sales Vol. 1, J.D. Ridge, ed., p. 805-813.

Poll, H.W. van de
1973: Stratigraphy, sediment dispersal and facies analysis of the Pennsylvanian-Pictou Group in New Brunswick; Marit. Sediments, v. 9, p. 72-77.

Roliff, W.A.
1962: The maritimes Carboniferous basin of eastern Canada; Geol. Assoc. Can., Proc., v. 14, p. 21-41.

Rose, A.W.
1976: The effects of cuprous chloride complexes in the origin of red-bed copper and related deposits; Econ. Geol., v. 71, p. 1036-1048.

Shoemaker, E.M., Miesch, A.T., Newman, W.L., and Riley, L.B.
1959: Elemental composition of Colorado Plateau sandstone-type uranium deposits; U.S. Geol. Surv. Prof. Paper 320, p. 25-54.

Walker, R.G.
1976: Facies models: 3. Sandy fluvial systems; Geosci. Can., v. 3, p. 101-109.

MARINE GEOPHYSICAL AND GEOLOGICAL RESEARCH IN BAFFIN BAY AND THE LABRADOR SEA, **CSS Hudson** 1976

Projects 760039 and 760015

R.K.H. Falconer
Atlantic Geoscience Centre, Dartmouth

In 1976 the Bedford Institute of Oceanography's ship **CSS Hudson** operated on an eastern Arctic cruise from July 26 to October 23. There were two primary programs for the season: (1) work in Lancaster Sound-Barrow Strait for the period August 19 – September 03 (Cruise 76-025); and (2) work in Baffin Bay and Labrador Sea prior to (Cruise 76-023) and after (Cruise 76-029) the Lancaster Sound work. The Lancaster Sound work was led by C.F.M. Lewis of Terrain Sciences Division, Ottawa and has been reported earlier (Lewis et al., 1977a). The Baffin Bay and Labrador Sea programs are the subject of this report.

The planned 1976 Baffin Bay program was a continuation of work carried out in 1974 (Ross and Falconer, 1975), and in previous years (Keen et al., 1974). Numerous Atlantic Geoscience Centre and Dalhousie University scientists have participated in this work. The 1976 bedrock program off southeastern Baffin Island was a continuation of work begun in 1975 (MacLean and Srivastava, 1976; MacLean et al., in press).

The primary objectives for the season were:

1) to study the margins of Baffin Bay with geophysical techniques; primarily seismic reflection, gravity and magnetic profiles, extending the work of Jackson et al., (in press) and Keen et al., (1974).

2) to extend surveys carried out in central Baffin Bay in 1974 which had revealed magnetic and gravity lineations (Appleton et al., 1975).

3) to extend studies of the crustal structure of central Baffin Bay (Keen and Barrett, 1972), in particular to obtain good quality seismic reflection data penetrating to oceanic basement.

4) to continue studies of the bedrock geology of the southeast Baffin Island shelf (MacLean et al., in press) by obtaining bedrock cores with an electric drill.

Once the initial shiptime allocation had been received, several secondary objectives were identified. Secondary projects are an important part of making full use of the capabilities of **CSS Hudson** and the facilities available at Bedford Institute. These objectives were:

5) to extend previous geophysical studies of the northern Labrador Sea, and Labrador Shelf and slope (Srivastava, Evolution of the Labrador Sea and its bearing on the early evolution of the North Atlantic; Paper submitted to Geophys. J. Roy. Astr. Soc., 1977.

6) to carry out a 3-day geophysical survey on the Labrador Shelf as part of a joint project with the Eastcan Group in order to study the distribution of boulders on the banks.

7) to provide opportunities for ornithology studies in the eastern Arctic (R.G.B. Brown, Canadian Wildlife Service, Department of the Environment)

8) to initiate chemical oceanography studies in Lancaster Sound (Chemistry Division, Atlantic Oceanographic Laboratory, Department of the Environment, Bedford Institute).

9) to obtain sediment cores in Baffin Bay as part of continuing studies of the sedimentology of the Bay, under the leadership of D. Piper, Dalhousie University (A. Aksu, Dalhousie University).

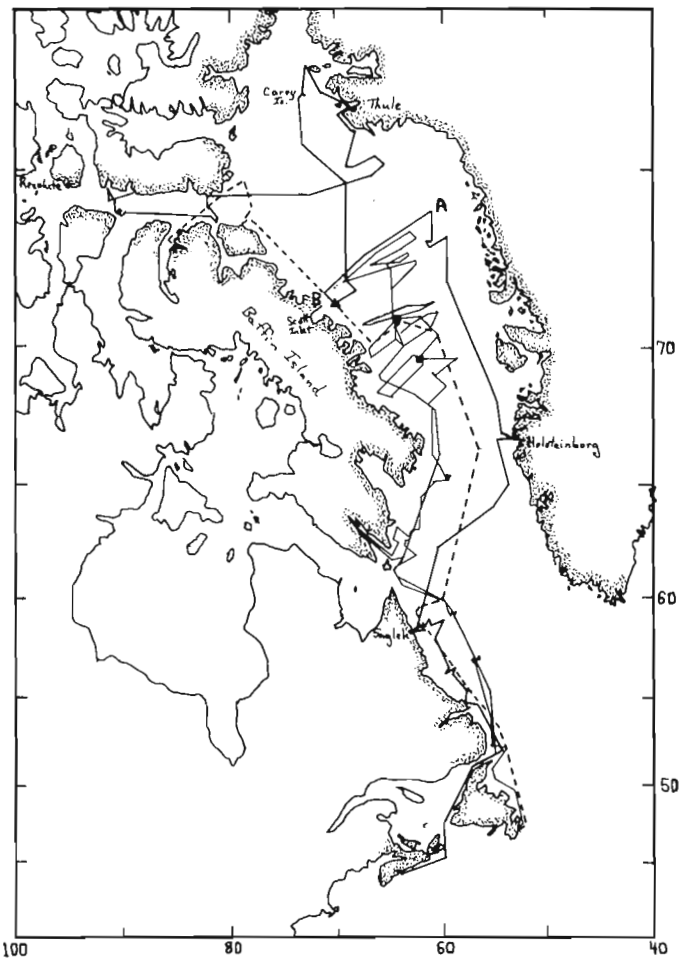

Figure 46.1. **CSS Hudson** 1976 tracks in Baffin Bay and Labrador Sea. Solid lines are cruises 76-023 and 76-029. Dashed line is the return track from Lancaster Sound of cruise 76-025. Filled squares indicate positions of buoy magnetometer moorings. Triangle off Scott Inlet is position of oil slick.

From: Report of Activities, Part B;
Geol. Surv. Can., Paper 77-1B (1977)

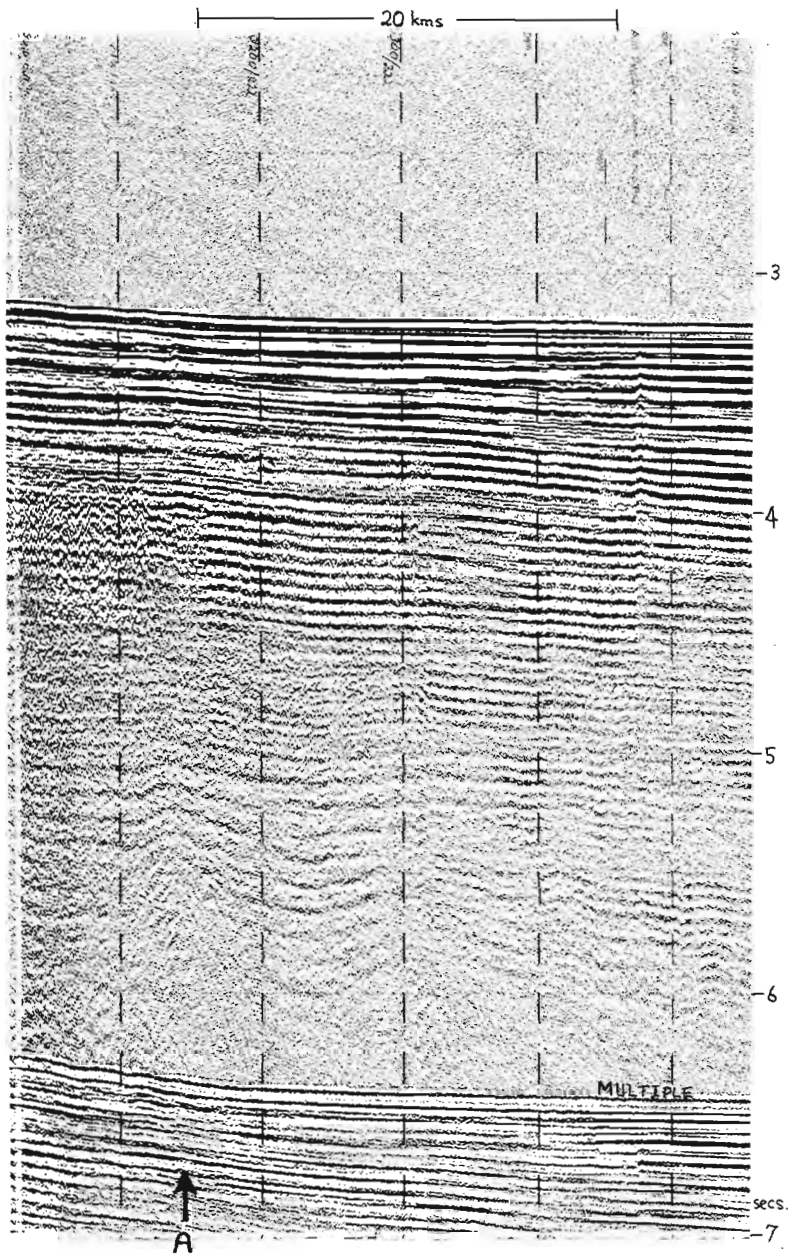

Figure 46.2. Seismic reflection record from Baffin Bay, on line AB. Vertical scale is two-way travel time in seconds. Water depth 2300 m. Letter A marks position of feature seen in Figure 46.3.

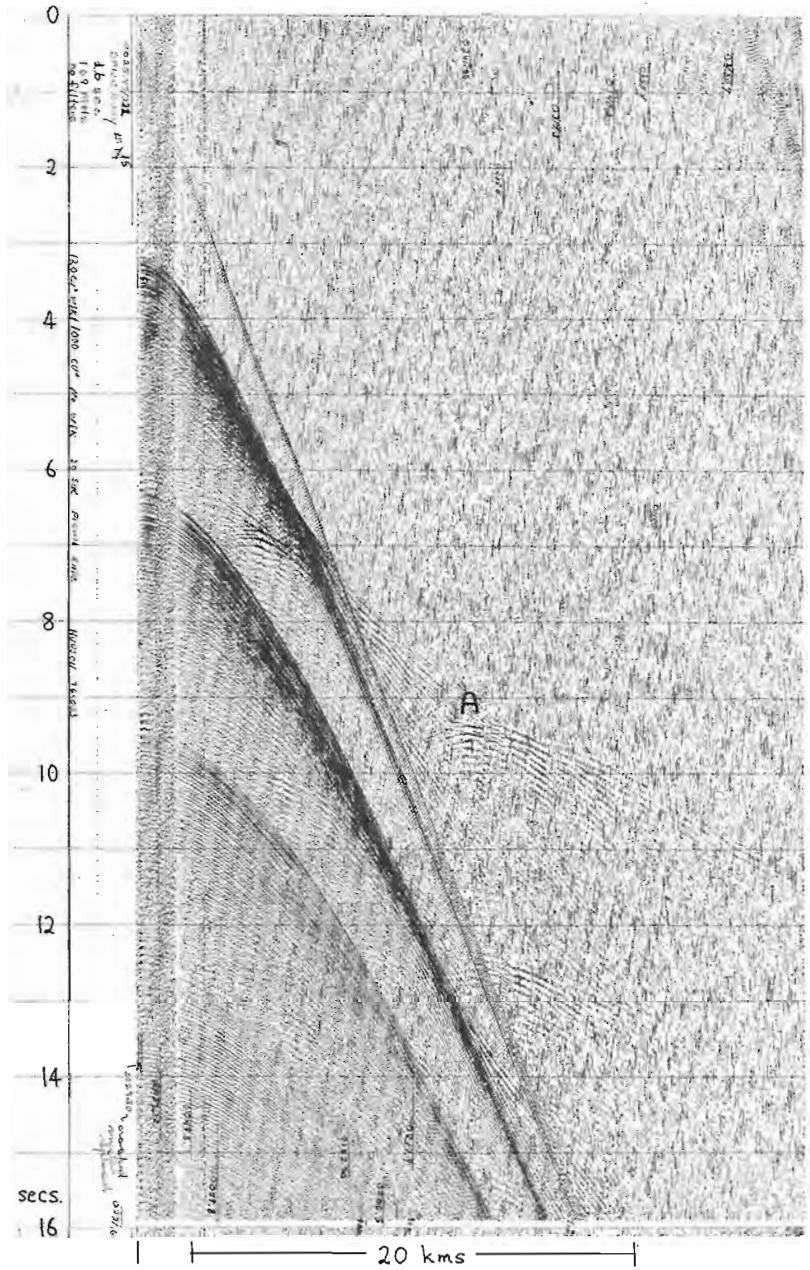

Figure 46.3. Expendable sonobuoy record from Baffin Bay, on line AB. Hyperbolic reflectors at A relate to feature labelled in Figure 46.2.

10) to initiate a geochemical study of eastern Arctic sediments (U. Lobsiger, Dalhousie University).

11) to assist in the calibration and maintenance of the Defence Research Establishment Pacific acoustic range in Lancaster Sound.

12) to compare the performance of Loran C, satellite, and TORAN navigation systems on the Labrador Shelf (D.E. Wells, Navigation Group, Atlantic Oceanographic Laboratory, Bedford Institute).

13) to undertake co-operative research with the Danish Greenland Geological Survey on the northwest Greenland margin.

The planned schedule had to be drastically altered when the ship lost a propellor in Lancaster Sound on August 17, just prior to the end of cruise 76-023. The loss meant that **Hudson** could not operate in ice and had to return for repairs to St. John's, Newfoundland on September 11. The ship sailed again from St. John's on September 22. The main effect of the schedule changes on the Baffin Bay program was that there was not time to do planned work in northern Baffin Bay and most of the planned survey of margins of the bay was abandoned. The ships tracks in Baffin Bay and Labrador Sea for the 1976 season are shown in Figure 46.1.

The first work of the arctic season was a three day geophysical survey of the Labrador Shelf in conjunction with the Eastcan Group, who are carrying out a major petroleum exploration and drilling program on the shelf. A three day extension of the season's shiptime in order to do this work was made possible by direct funding from Eastcan. They defined the survey track and ran a TORAN navigation system which they installed. The Atlantic Geoscience Centre provided and operated: 12 kHz wide-beam and 50 kHz narrow beam echo sounders, air gun seismic reflection, Huntec high resolution deep tow seismic reflection, and sidescan. The data obtained are confidential to Eastcan and the Atlantic Geoscience Centre for 15 months. The survey was very successful and the Eastcan representatives onboard said that the quantity and quality of the data obtained was most satisfactory. This joint program has provided opportunities for closer liaison between Bedford Institute and Institute Francais du Petrole scientists. R.H. Fillon of the Atlantic Geoscience Centre has already visited Paris to consult on the data obtained.

The Eastcan program personnel were dropped off at Saglek on August 2 and the ship then ran a seismic reflection line across the Labrador Sea to Holsteinborg. This line passed close to the Cabot drillsite on the northern Labrador Shelf, and it is interesting to note that there, and at other localities on the Labrador Shelf, gas is visible in the water column and in the nearbottom sediments. At Holsteinborg, M. Roksandic of the Greenland Geological Survey joined, and the ship then headed north to commence surveys of the Greenland margin of Baffin Bay. Unfortunately an extensive tongue of ice extended northward over the margin and it was not possible to carry out the planned surveys south of 72°N.

The unseasonally late ice meant that most of the margins were inaccessible so it was decided to concentrate on obtaining a single good seismic line across the bay. The line (AB in Fig. 46.1) extending from shelf to shelf was done at 4 knots using a 1000 cubic inch airgun. Five expendable sonobuoys provided almost continuous high quality refraction data in the deep part of the bay. Data from two buoys yielded velocities corresponding to 'Moho' at 10 and 14 kms depth. A layer with velocity of 6.4 to 7.0 km/sec was detected at about 8 km depth on records from three of the buoys. Four other sonobuoy refraction lines were shot later farther south in the Bay. Two of these lines were along the axis of the mid-bay gravity negative (Appleton et al., 1975) and there the 6.8 km/sec layer is at least 2 km deeper than elsewhere in the Bay. Velocities typical of oceanic layer 2 were not generally seen on the sonobuoy data. Oceanic basement was not seen on the seismic reflection records as the sediments extend to below the bottom multiple. Sediment thickness is at least 5 km in the centre of the Bay. Diapiric-like structures were observed on line AB near the Greenland margin on both the vertical reflection record (Fig. 46.2) and the sonobuoy record (Fig. 46.3).

On completion of the long seismic line AB some seismic and sidescan work was done on the Baffin Shelf. In the course of that, an oil slick was discovered just off Scott Inlet (Fig. 46.1), as reported earlier by Loncarevic and Falconer (1977). Analysis of the oil samples obtained on cruises 76-023 and 76-025 has not provided a definitive answer on whether the oil is natural or refined. Further investigation of the area is planned for 1977 when the **Hudson** will be engaged on a Bedford Institute chemistry cruise in the area.

Following the work on the Baffin Shelf, the **Hudson** proceeded to Thule for calibration of the gravimeter. En route, a field party from Terrain Sciences Division, Geological Survey (Blake, 1977) was picked up from the Carey Islands. Ornithology studies by R.G.B. Brown were made at the Careys, Haklyut I. north of the Careys, and the coastal areas toward Thule. After the Thule call these studies were continued towards Cape York and at several places in Lancaster Sound. Valuable data were obtained on the breeding and feeding habits of birds in the large breeding colonies of northwestern Greenland and Lancaster Sound.

Sidescan data were obtained at three areas of northwestern Greenland and surprisingly there was virtually no evidence of iceberg scour, despite the areas being infested with large icebergs, some of which are known to ground. The bottom in the surveyed areas was very hard and possibly the lack of scour reflected only lack of sediment soft enough to reveal scour. Figure 46.4 shows data from near the Carey Islands. The "pock-like" marks may be iceberg grounding marks but note the lack of linear scours. Sidescan data obtained earlier off Holsteinborg also showed no scour. However, surveys on the Labrador Shelf and on the Baffin Shelf revealed intensive scouring to water depths of at least 250 m (Fig. 46.5). Sidescan data will be presented at the Geological Association of Canada meeting in Vancouver in April 1977 by C.F.M. Lewis, S.M. Blasco, R.K.H. Falconer, and G. Martin.

In Lancaster Sound the main work was ornithology and chemical oceanography. Two chemistry sections with CTD casts and deep sampling were done, one near the mouth of Lancaster Sound, the other in eastern Barrow Strait. These sections provided preliminary data for the definition of major chemical oceanography programs in the eastern arctic. A 27 day chemistry cruise onboard **CSS Hudson** is scheduled for the eastern arctic in 1977.

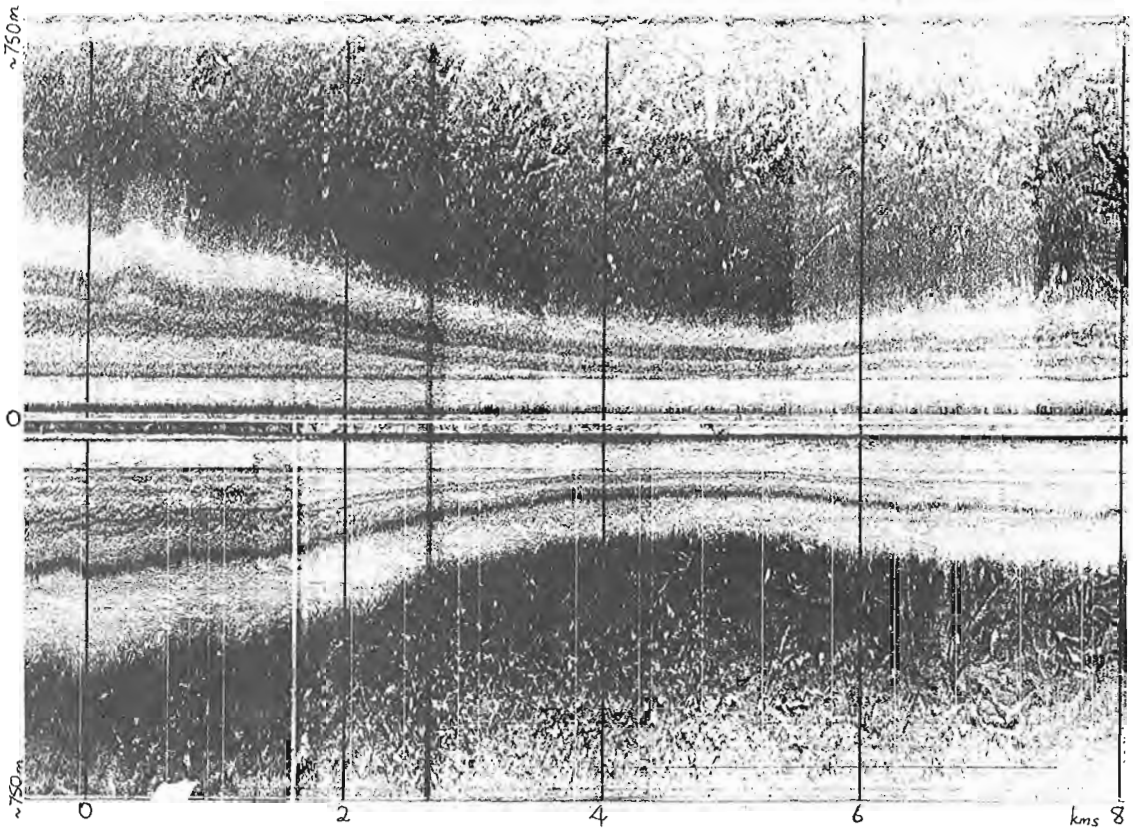

Figure 46.4. Sidescan record from 60 km north of the Carey Islands. Water depth shallows from 300 m to 150 m.

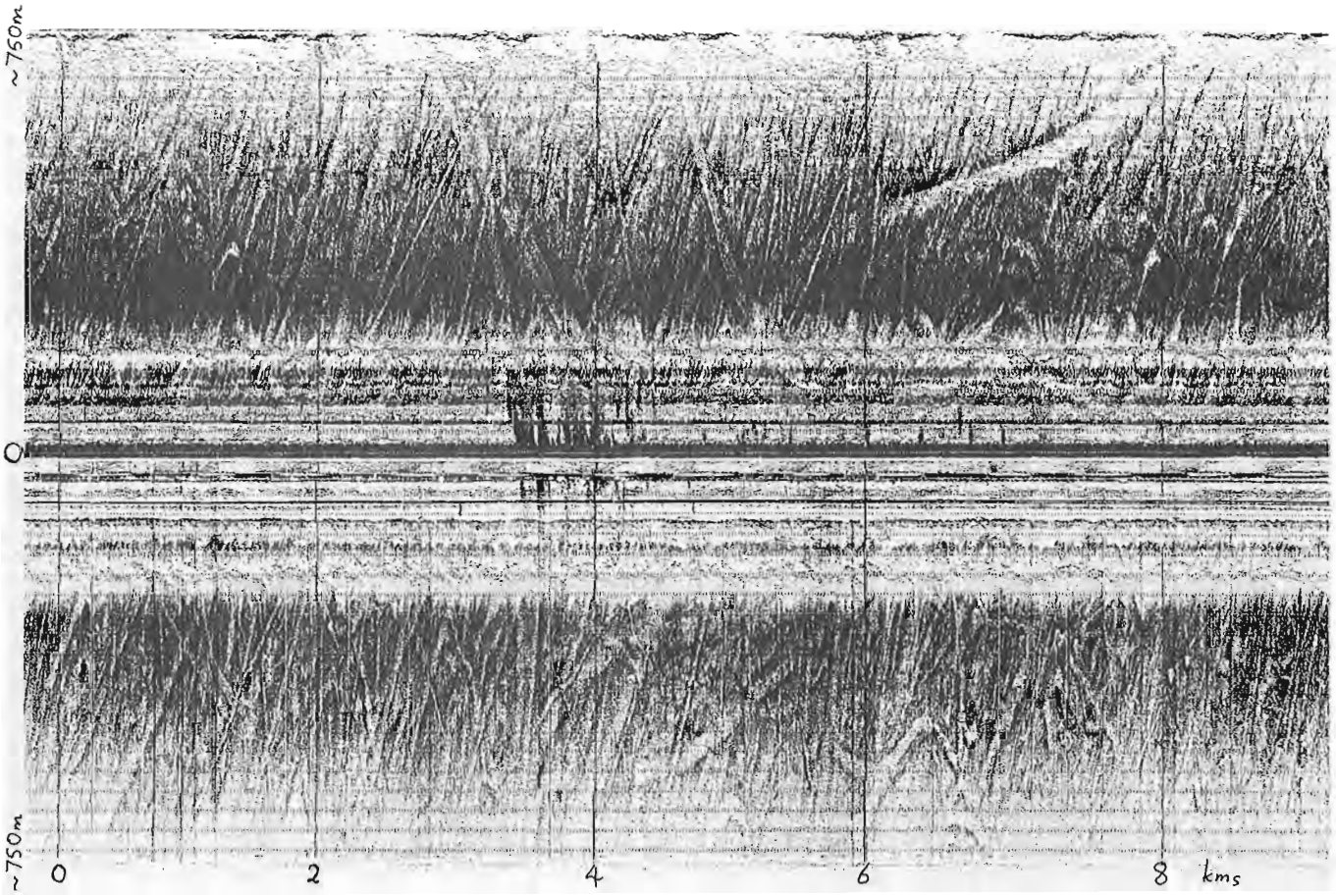

Figure 46.5. Sidescan record from Saglek Bank northern Labrador Shelf, in approximately 150 m water.

Cruise 76-023 had been scheduled to end at Resolute, August 19, but the loss of the ship's propellor on August 17 near Prince Leopold Island altered that. The Defence Research Establishment Pacific work was postponed. The **Hudson** could not go to Resolute because of ice. Scientific and ship's personnel were transferred to Resolute from Maxwell Bay and Gasgoyne Inlet with the help of the Polar Continental Shelf Project.

Cruise 76-025 (Lewis et al., 1977) then worked in Lancaster Sound for 15 days before returning to St. John's, Newfoundland. The return trip provided much good en route data in Baffin Bay and Labrador Sea: the oil slick was investigated, sidescan and seismic reflection data were obtained on the Baffin Shelf, seismic reflection data were obtained in part of Baffin Bay and on the Labrador Shelf, gravity and magnetic profiles were continuous.

The **Hudson** sailed on cruise 76-029 from St. John's after repairs were completed on September 22. En route to the southeastern Baffin Shelf, a small survey was done of steep scarps which had previously been observed at the foot of the Labrador Shelf slope. That survey and more work on the return trip indicate that there has been massive slumping along at least 400 km of the Labrador slope. A seismic reflection profile parallel to the slope crossing toes of some slumps is shown in Figure 46.6.

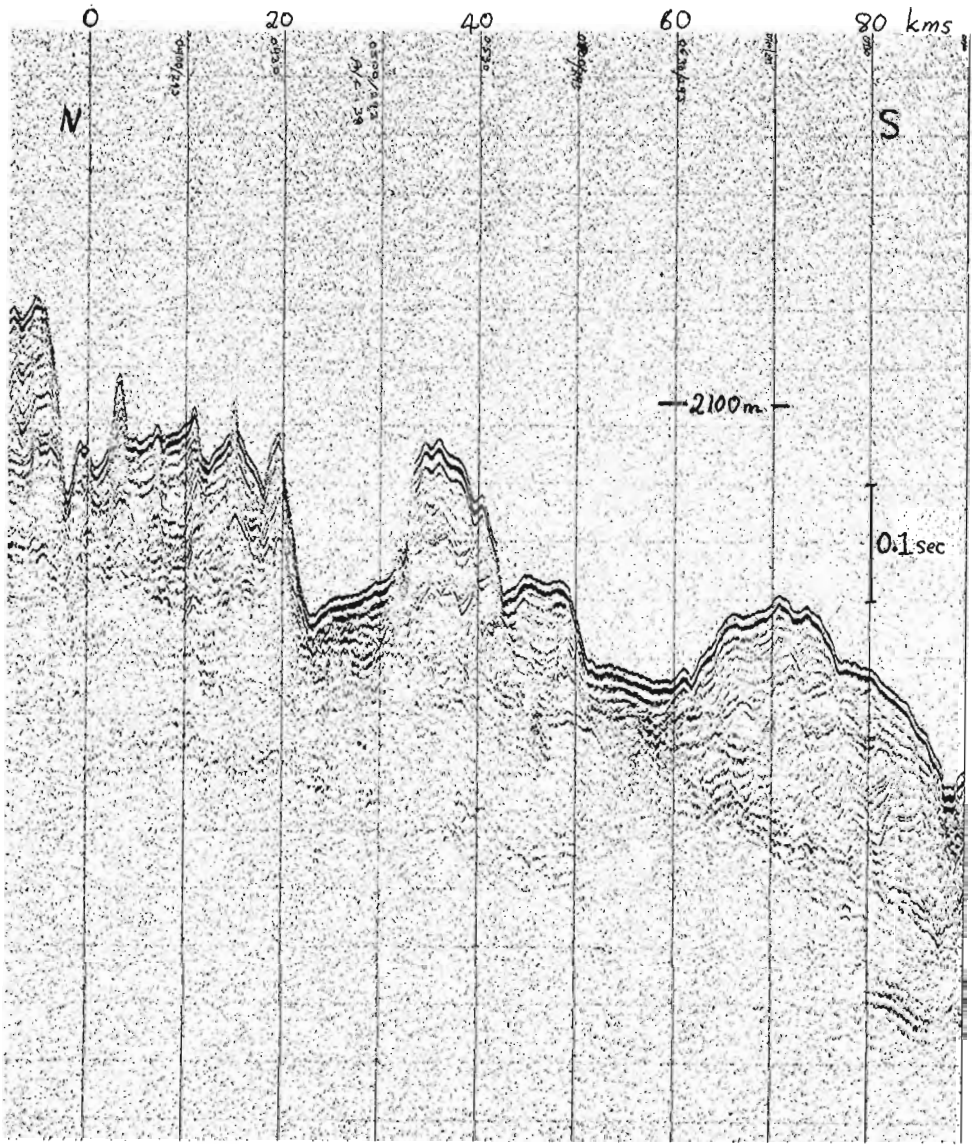

Figure 46.6. Seismic reflection record parallel to the slope off Saglek Bank northern Labrador Shelf. Two-way travel time of 0.1 sec represents about 100 m in the sediments.

Bedrock drilling was carried out off southeastern Baffin Island on both the way northward and the return southward. Cores of consolidated and semi-consolidated rocks were obtained at 6 out of 10 sites. Details of the bedrock program are described by MacLean and Falconer (1977).

In Baffin Bay magnetic surveys were the major work. A buoy magnetometer was used to monitor diurnal variations. It was laid first in the southern area (Fig. 46.1) and picked up 2 days later drifting free 3 miles from its mooring. It appeared that ice had broken the nylon mooring line. The buoy was then moved northward to just south of the 1974 survey. Lines were run south and north of that survey. The magnetic lineations mapped in 1974 (Appleton et al., 1975) do not appear to extend far either side of the 1974 survey but there are other lineations in the southern part of the bay. A limited amount of seismic reflection data was obtained across the Baffin Island margin in the Home Bay area. A thick sedimentary basin is evident in Home Bay.

Piston cores were obtained at 11 sites in Baffin Bay as part of a Dalhousie University project. Analysis of these cores (A. Aksu, pers. comm.) has revealed important marker horizons, mainly ash, which can be mapped in the bay. Material from the cores and grab samples taken at other localities are being used by U. Lobsiger of Dalhousie University in a geochemical study of sediments in the eastern arctic.

Acknowledgments

The success of the 1976 **Hudson** arctic cruises is due in large measure to the support of the Officers and Crew of **CSS Hudson** under the leadership of Captains L. Strum and D. Deer. The contribution of each individual in the scientific party to the results of the whole program is appreciated. The support facilities of Bedford Institute were very valuable. Polar Continental Shelf Project through F. Alt assisted with the transfers through Resolute.

References

Appleton, K.P., Keen, C.E., and Barrett, D.L.
1975: Magnetic lineations in Baffin Bay and their significance to the evolution of the Canadian Arctic; I.U.G.G. 16th Assembly, Grenoble 1975. Abstracts, p. 62.

Blake, W.
1977: Radiocarbon age determinations from the Carey Islands, Northwest Greenland; in Report of Activities, Geol. Surv. Can., Paper 77-1A, p. 445-454.

Jackson, H.R., Keen, C.E., and Barrett, D.L.
Geophysical studies on the eastern continental margin of Baffin Bay and in Lancaster Sound; Can. J. Earth Sci. (in press)

Keen, C.E. and Barrett, D.L.
1972: Seismic refraction studies in Baffin Bay: An example of a developing ocean basin; Geophys. J. Roy. Astr. Soc., v. 30, p. 253-271.

Keen, C.E., Keen, M.J., Ross, D.I., and Lack, M.
1974: Baffin Bay: A small ocean basin formed by seafloor spreading; Am. Assoc. Petrol. Geol., Bull., v. 56, p. 1080-1108.

Lewis, C.F.M., Blasco, S.M., Bornhold, B.D., Hunter, J.A.M., Judge, A.S., Kerr, J.Wm., McLaren, P., and Pelletier, B.R.
1977: Marine geological and geophysical activities in Lancaster Sound and adajacent fiords; in Report of Activities, Part A, Geol. Surv. Can., Paper 77-1A, p. 495-506.

Loncarevic, B.D. and Falconer, R.K.H.
1977: An oil slick occurrence off Baffin Island; in Report of Activities, Part A, Geol. Surv. Can., Paper 77-1A, p. 523-524.

MacLean B. and Srivastava, S.P.
1976: Shallow corehole drilling on the Baffin Island Shelf; in Report of Activities, Geol. Surv. Can., Paper 76-1A, p. 141-142.

MacLean, B., Jansa, L.F., Falconer, R.K.H., and Srivastava, S.P.
Ordovician strata on the southeastern Baffin Island Shelf revealed by shallow drilling; Can. J. Earth Sci. (in press)

MacLean, B. and Falconer, R.K.H.
1977: Baffin Island Shelf – shallow corehole drilling, 1976; in Report of Activities, Part B, Geol. Surv. Can., Paper 77-1B, rep. 25.

Ross, D.I. and Falconer, R.K.H.
1975: Geological studies of Baffin Bay, Davis Strait and adjacent continental margins; in Report of Activities, Part A, Geol. Surv. Can., Paper 75-1A, p. 181-183.

47.

STRUCTURAL GEOLOGY OF THE ALBERT PEAK AREA, SOUTHEASTERN BRITISH COLUMBIA

E.M.R. Research Agreement 1135-D13-4-69/76

J.W. Sears[1] and R.A. Price[1]
Regional and Economic Geology Division

A preliminary geologic map of a 250-km^2 area of the western Selkirk Mountains southeast of Albert Peak, British Columbia, was prepared during the 1976 field season. This area, encompassing the northern end of the Kootenay Arc and the southern margin of the Clachnacudainn salient of the Shuswap metamorphic complex (Fig. 47.1), was chosen for detailed study because it lies within a structural culmination in the transition zone between the infrastructure and suprastructure of the Cordilleran orogen, in a region affected by superposition of Mesozoic and Paleozoic deformations. The purpose of the project is to unravel the structural geometry and stratigraphy and the deformational and metamorphic history of the area; and to clarify the regional tectonic evolution of this part of the Cordillera.

Mapped rock units include Hadrynian (?) and lower Paleozoic sedimentary and igneous rocks, a locally concordant sheet of granodiorite gneiss (Gilman, 1972), and a discordant felsic pluton associated with the Battle Range Batholith. Distinct structural levels can be recognized in the layered rocks. The lower two are separated by the low-angle Standfast Creek extension fault of Thompson (1972). Rocks of the lowest level include the sheet of granodiorite gneiss (unit 1) and overlying rusty weathering pelitic quartzites and grey platy quartzites (unit 2) that are interlayered with light grey micaceous marble, minor pelite and amphibolite (units 3 and 4). This sequence may correlate with the Hadrynian Horsethief Creek Group or may represent isoclinally infolded carbonate rocks and quartzites of the lower Cambrian Badshot Formation and Hamill Group respectively. Rocks in the next level are quartzites and pelites of the Hamill Group, pelitic marble of the Badshot Formation, and dark grey to black carbonaceous phyllite of the lower Paleozoic Index Formation (units 5, 6, 7) folded into the isoclinal Akolkolex anticline of Thompson (1972). The overlying dark grey limestones and phyllites and light green phyllites, greenstone, gritty green phyllite and sandstone, and minor feldspathic conglomerate (units 7 through 11) of the lower Paleozoic Lardeau Group may be separated from the underlying levels by one or more low-angle faults. All units of the upper level appear to have intergradational contacts. In the southeast corner of the area of Figure 47.1, Read (Read and Wheeler, 1975) has mapped black siliceous phyllite of the Sharon Creek Formation (unit 12), green phyllite and metavolcanics of the Jowett Formation (unit 13), and gritty green phyllite of the Broadview Formation (unit 14), all of lower Paleozoic age. A green phyllite unit (unit 9) underlying a thick dark grey pelitic limestone (unit 8) in the eastern part of the map area has been tentatively interpreted as a lateral extension of rocks which Read (Read and Wheeler, 1975) assigned to the Jowett Formation.

The megascopic structural geometry of the area is characterized by an open synform that plunges southeasterly off the flank of the Lauretta Dome of Gilman (1972) and is coaxial with two sets of southeasterly plunging superposed folds. Although many aspects of the gross structure remain enigmatic because of the difficulty in correlating units, several faults that are subparallel to schistosity and compositional layering appear to be important. In addition to the Standfast Creek Fault of Thompson (1972) another fault seems to be required to account for relationships between the Akolkolex Anticline of Thompson (1972), and the thick dark grey pelitic limestone (unit 8) that extends across the central part of the map area. In the southern part of the map area this fault may be responsible for the apparent repetition of the sequence of units 7, 8, 7 and 10. Another fault at the base of unit 9, in the eastern part of the map area, may account for the repetition of units 8 and 10, but the mapped relations also might be explained by facies changes, as favoured by Read (Read and Wheeler, 1975). Further structural complexities are obvious in the northern part of the area where the Standfast Creek Fault or a subsidiary fault is folded about a southeast plunging asymmetric anticline that is probably related to the development of the Lauretta Dome. The relationships between the marble and quartzite units overlying this prominent shear zone and the units below the Standfast Creek Fault, the Akolkolex Anticline, the overlying Lardeau Group and structures northeast of Albert Peak will be studied during the 1977 field season.

Orientation data for six structural elements widely observed in the map area are summarized in Figure 47.2. Composition layering (A), is isoclinally folded about southeast-plunging axes (D). Schistosity (B) parallels the axial surfaces of the isoclinal folds and is itself deformed into upright open folds with southeast plunging axes (E). Crenulation cleavage, (C), parallels the axial surfaces of these upright folds and intersects compositional layering and schistosity in a crenulation lineation (F). In addition to these elements, a relict metamorphic foliation predating the schistosity (B) was observed in some areas, but its significance has not yet been fully evaluated.

Preliminary mapping of mineral isograds defined by the first appearances for each of biotite, garnet, andalusite and sillimanite, shows a deflection in the neighbourhood of the felsic pluton at the northern margin of the map area. Textural relationships suggest that regional metamorphic facies have been overprinted by a contact metamorphic aureole; boudinaged pre-crenulation garnets coexist with undeformed andalusite porphyroblasts. The nearby occurrence of kyanite-bearing mineral assemblages with textures indicative of regional syn-kinematic metamorphism (Thompson, 1972) may indicate that substantial uplift, associated with the development of the Lauretta Dome and the whole of the Clachnacudainn salient, occurred prior to emplacement of the felsic pluton and attendant contact metamorphism. The time of emplacement of the felsic pluton may also place an upper limit on the age of the Standfast Creek fault.

[1]Department of Geological Sciences, Queen's University, Kingston, Ontario

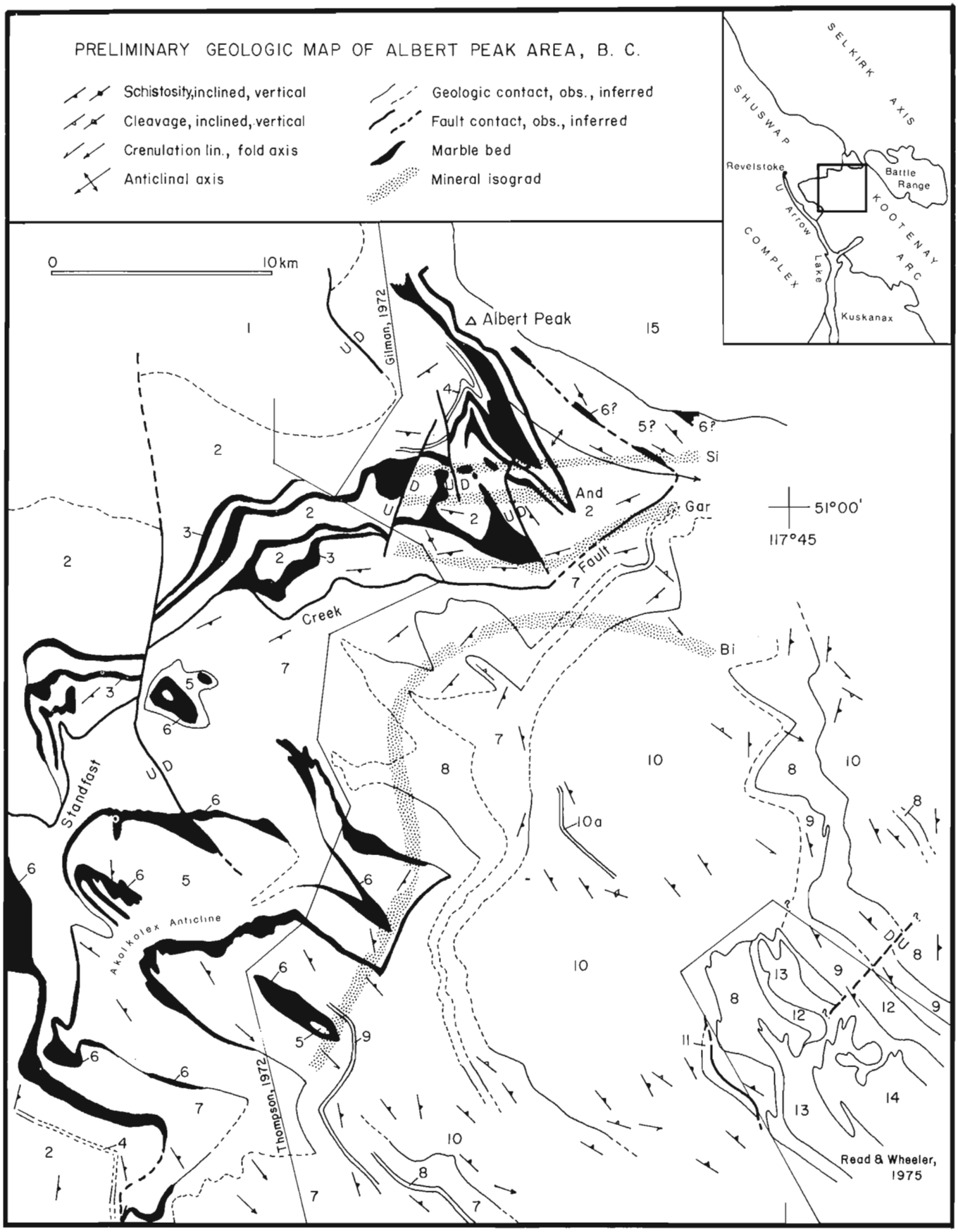
PRELIMINARY GEOLOGIC MAP OF ALBERT PEAK AREA, B. C.
Schistosity, inclined, vertical
Cleavage, inclined, vertical
Crenulation lin., fold axis
Anticlinal axis
Geologic contact, obs., inferred
Fault contact, obs., inferred
Marble bed
Mineral isograd
0
10 km
SELKIRK AXIS
SHUSWAP
Revelstoke
Battle Range
KOOTENAY ARC
COMPLEX
Arrow Lake
Kuskanax
Albert Peak
Gilman, 1972
Si
And
Gar
Bi
51°00'
117°45
Fault
Creek
Standfast
Akolkolex Anticline
Thompson, 1972
Read & Wheeler, 1975

Figure 47.1. (opposite)

Geologic map with superposed mineral isograds: Bi – Biotite; Gar – Garnet; And – Andalusite; Si – Sillimanite

Lithic units numbered on map:

1. Granodiorite gneiss
2. Pelitic quartzite, quartzite, pelite
3. Grey marble
4. Amphibolite
5. Hamill Group: grey micaceous quartzites, green pelites
6. Badshot Formation: grey pelitic marble
7. Black phyllite
8. Grey and black phyllitic limestone
9. Green chloritic phyllite

(7, 8, 9: Index Formation)

10. Green phyllite, sandstone, and gritty green phyllite and sandstone
    10a. Feldspathic conglomerate

(10, 10a: Broadview or Index Formation)

11. Vesicular mafic igneous rock
12. Sharon Creek Formation: black siliceous phyllite
13. Jowett Formation: green phyllite, greenstone
14. Broadview Formation: gritty green phyllite
15. Felsic pluton

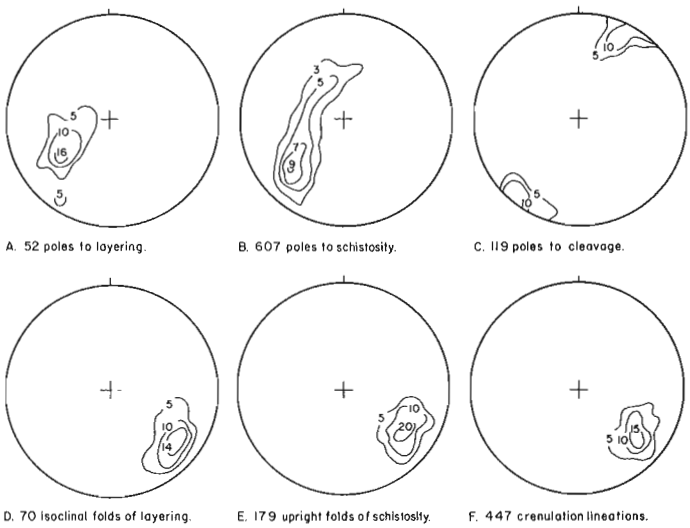

Figure 47.2. Lower hemisphere equal area projections of orientation data for Albert Peak area. Contours in per cent population per 1% area.

References

Gilman, R.A.
1972: Geology of the Clachnacudainn salient near Albert Canyon, British Columbia; Can. J. Earth Sci., v. 9, p. 1447-1454.

Read, P.B. and Wheeler, J.O.
1975: Lardeau west-half geology; Geol. Surv. Can., Open File 288.

Thompson, R.I.
1972: Geology of the Akolkolex River area near Revelstoke, British Columbia; unpubl. Ph.D. thesis, Queen's University, Kingston, Ontario, 125 p.

48. ECHO SOUNDING AND SUBBOTTOM PROFILING IN DOUGLAS CHANNEL AND KITIMAT ARM, BRITISH COLUMBIA

Project 750108

Brian D. Bornhold
Terrain Sciences Division

Introduction

Considerable interest in the marine environments of Douglas Channel and Kitimat Arm (Fig. 48.1) has been generated recently by a proposal to establish a tanker route through these waters and an oil terminal at Kitimat. As part of the assessment of this proposal, a three-day cruise on **CSS Parizeau** was conducted from February 21-23, 1977 along the proposed and alternate routes from Dixon Entrance, north of Queen Charlotte Islands, to Kitimat principally to consider navigational aspects but also to gain an impression of possible environmental concerns. This cruise provided an opportunity to obtain vertical and side-looking echo sounding records along two parallel tracks through the channels and to make some preliminary interpretations of the thickness, nature, and possible origin of the seafloor sediments.

CSS Parizeau is equipped with an 11 kHz Simrad echo sounder, having a beam angle of 20°. In addition to providing a profile of the seafloor topography, the echograms also yielded considerable subbottom information with penetrations of more than 60 m in some areas. A 24 kHz side-looking sonar, with a beam angle of 11° or 30°, capable of looking 360° about the ship from 5° above to 25° below the horizontal, also was used during this cruise. The sonar transducer was aimed at 90° to starboard and 25° below the horizontal with an 11° angle.

Results and Discussion

The distribution of the principal acoustic units in Douglas Channel and Kitimat Arm, their thicknesses, and the locations of bedrock outcrops in the channel floor are summarized in Figure 48.1. Because no information on the seismic velocities of the sediments in this area exists, the thicknesses were taken directly from the echograms assuming the same velocity as sea water. The unusually high subbottom penetration in the channel bottoms suggests rather high sedimentary water contents and, consequently, low seismic velocities. It is unlikely that the velocities of the sediments differ by more than 10 to 15 per cent from that of sea water.

Four distinct sedimentary units could be identified on the basis of their acoustic characteristics. The uppermost unit (A) consists of highly stratified muds in distinct lenses, each up to 60 m thick (Fig. 48.2). The presence of numerous distinct reflectors and the convex upward shape of the sediment bodies suggest episodic sedimentation, perhaps from turbidity currents originating in tributary channels, forming sediment cones which thin and pinch out to the north and south along the axis of the main channel.

Underlying unit A is a massive, unstratified layer (B) of transparent muds which drapes evenly over the bedrock surface (Fig. 48.2). This unit averages 20 m in thickness and is absent only where bedrock rises steeply from the channel floor. It seems probable that this unit is of the same age as the marine clays which directly overlie bedrock in Kitimat Valley and other larger valleys in this area (Duffell and Souther, 1964; Armstrong, 1966). The distribution of postglacial sediments in Kitimat-Terrace Valley indicates an isostatic depression of about 300 m. Thus, deglaciation was accompanied by a marine transgression of at least 80 km up Kitimat Valley and gave rise to extensive deposition of a variety of marine sediments throughout the region (Clague and Hicock, 1976). Unit B is thought to be a deeper water facies, deposited in 500 to 600 m water depth, correlative with the marine clays and deltaic sediments exposed on land.

Delta-front sediments (unit C) (Fig. 48.3) occur near the head of Kitimat Arm and are characterized by undulating, hummocky topography and superimposed lobes of sediment extending down the delta face into deeper water. These lobes and the associated hummocky surface are indicative of mass slumping of unconsolidated sediments from the upper delta front. Large-scale submarine slope failures are not uncommon in this area; on April 27, 1975 approximately 2.5×10^6 m^3 of marine muds slid to the floor of the channel on the eastern side of Kitimat Arm near Kitimat (Bell and Kallman, 1976).

A unit (D) acoustically similar to unit B occurs in southernmost Douglas Channel and grades northward into the highly stratified muds of unit A. These transparent muds appear to be confined to deeper waters in southern Douglas Channel (greater than 400 m) where thicknesses up to 60 m have accumulated.

The side-looking echograms provide an impression of the topography of the channel walls and indicate areas where bedrock outcrops. Continuous profiles of both sides of the channels were obtained except for the west side of Kitimat Arm. A side-looking echogram (Fig. 48.4) from Douglas Channel shows areas of bedrock outcrops along the channel walls and the presence of a major sill. An analysis of both the vertical and side-looking echograms revealed two major bedrock sills and numerous isolated bedrock outcrops on the channel floor (Fig. 48.1).

Further subbottom profiling, using a 3.5 kHz echo sounder, and piston coring are planned in order to delineate better the thickness and extent of the sedimentary units identified in this study and to interpret their origins.

Acknowledgments

The assistance of Mr. H. Blandford, Marine Surveys Directorate, Department of Fisheries and the Environment, who directed the cruise, and Capt. Chamberlain and the officers and crew of the **CSS Parizeau** is greatly appreciated. Drs. C.F.M. Lewis and J.L. Luternauer critically read the manuscript and offered helpful suggestions.

From: Report of Activities, Part B; Geol. Surv. Can., Paper 77-1B (1977)

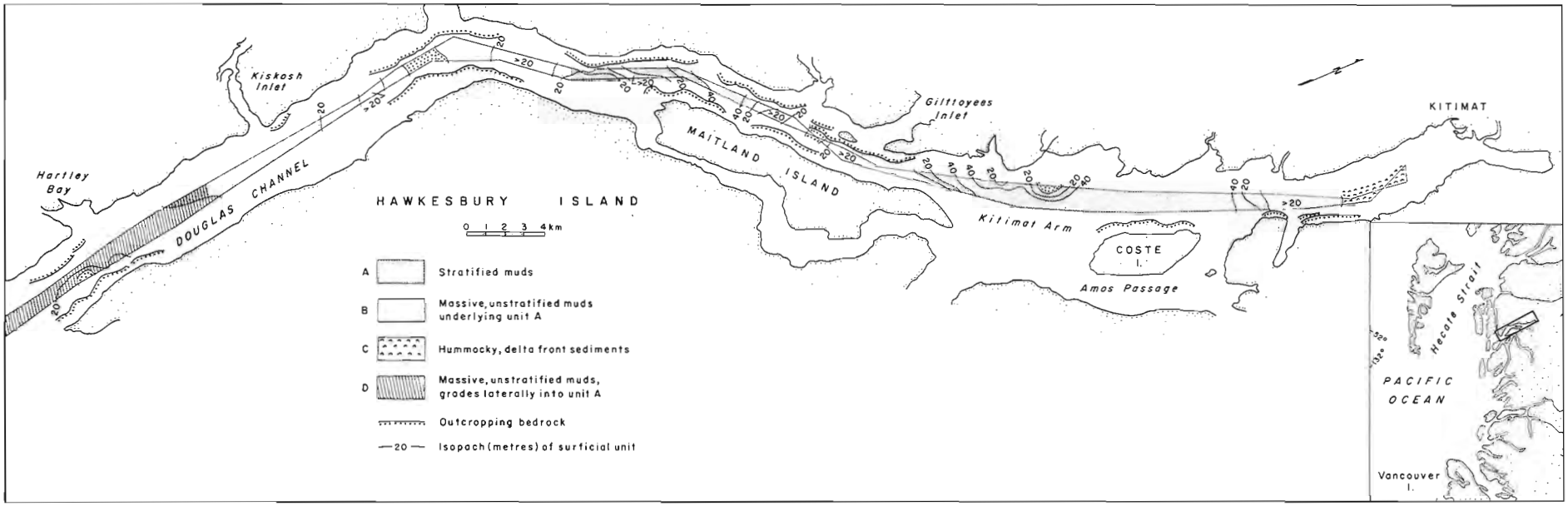

Figure 48.1. Distribution of surficial sediment types in Douglas Channel and Kitimat Arm.

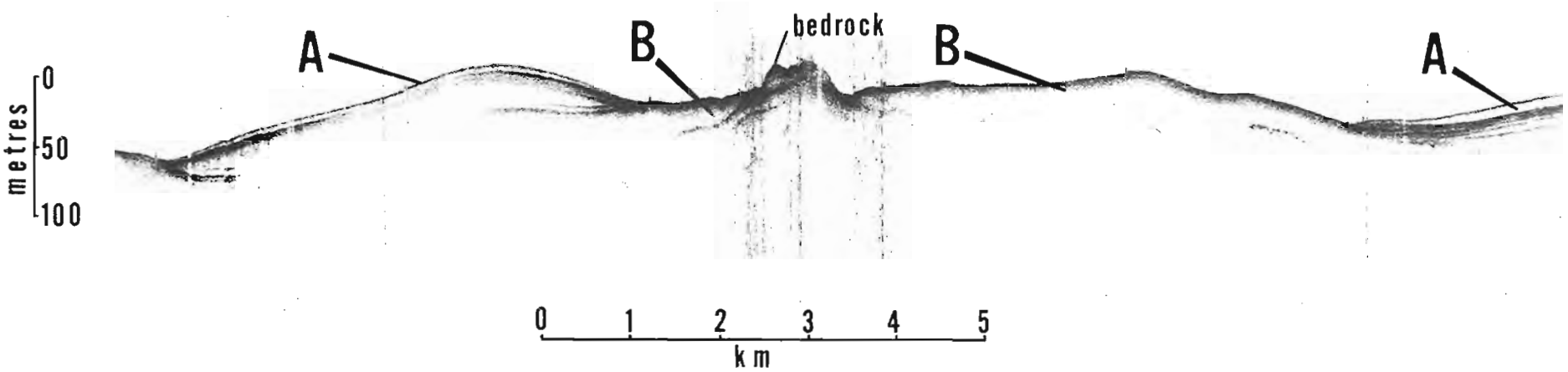

Figure 48.2. Vertical echo sounding record from Douglas Channel showing the relationship between the stratified muds (unit A) and the homogeneous unstratified muds (unit B).

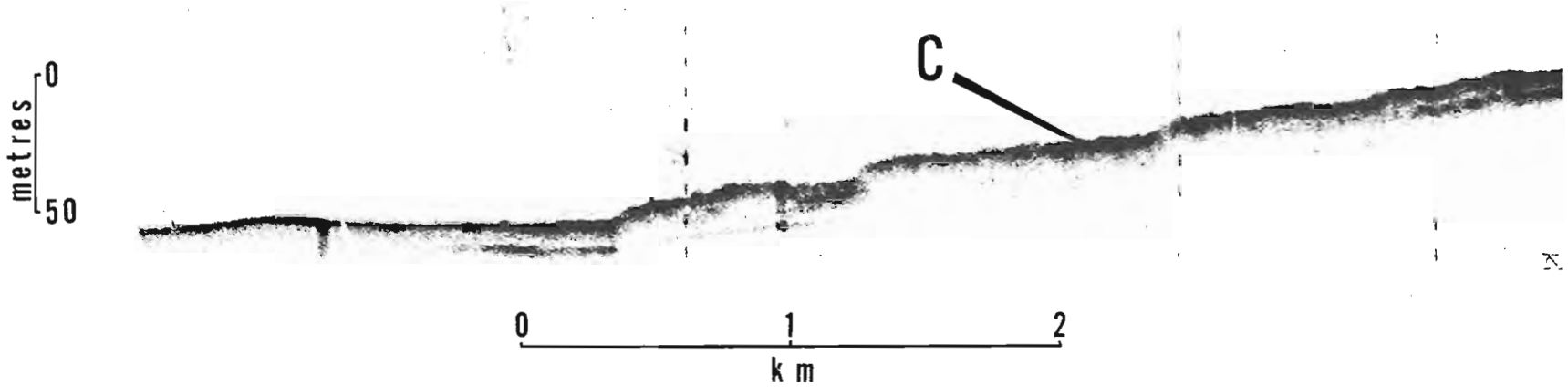

Figure 48.3. Hummocky delta-front sediments on the lower part of the Kitimat Delta.

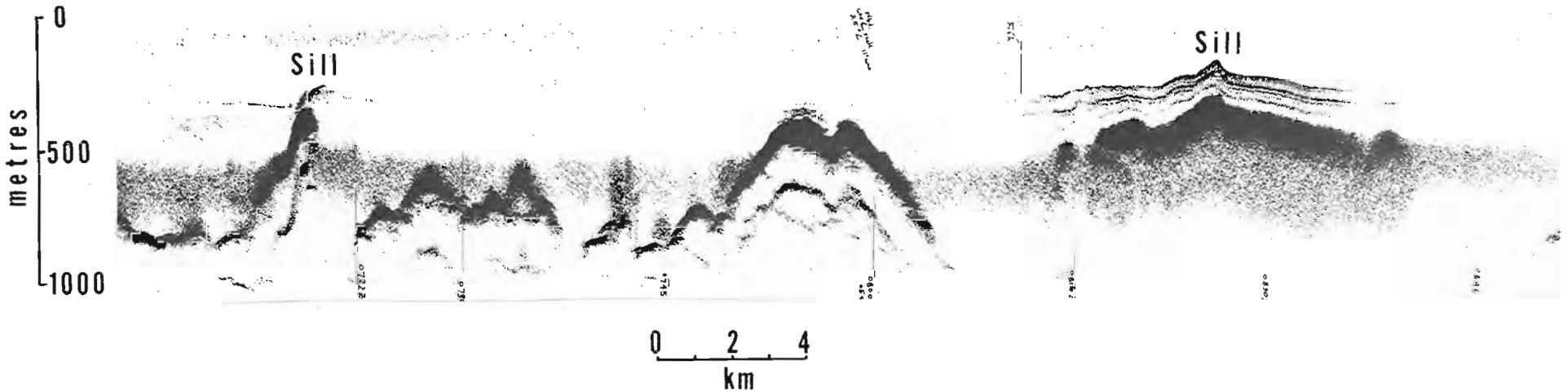

Figure 48.4. Side-looking echogram of the west side of Douglas Channel approximately between Gilttoyees Inlet and Kiskosh Inlet. Vertical scale is the oblique distance (25 degrees below the horizontal) from the ship to the seafloor.

References

Armstrong, J.E.
1966: Glacial studies, Kitimat-Terrace area; in Report of Activities, Part A, Geol. Surv. Can., Paper 66-1A, p. 50.

Bell, L.M. and Kallman, R.J.
1976: The Kitimat River estuary – status of environmental knowledge to 1976; Estuary Working Gr., Can. Dep. Environ., Reg. Board Pacific Reg., Sp. Estuary Ser. No. 6, 296 p.

Clague, J.J. and Hicock, S.R.
1976: Sand and gravel resources of Kitimat, Terrace, and Prince Rupert, British Columbia; in Report of Activities, Part A, Geol. Surv. Can., Paper 76-1A, p. 273-276.

Duffell, S. and Souther, J.G.
1964: Geology of Terrace map-area, British Columbia; Geol. Surv. Can., Mem. 329, 117 p.

Projects 740062, 740063

D. Swan and R. Linden
Terrain Sciences Division, Vancouver

The increasing use of computers has allowed geologists to deal with larger and larger amounts of data. The accurate graphic presentation of large data sets is time consuming and expensive if done by hand and requires a considerable programming effort if done using a computer. Over the last two years a package of thirteen plotting subroutines, written in FORTRAN IV, has been developed to produce a variety of plots of geological data sets. These routines generate plotter output by calling the standard CalComp routines PLOT, SYMBOL, NUMBER, AXIS, and LINE (California Computer Products, 1969). The routines have been made as flexible as possible. For example, most of the routines allow the user to specify plotting of either a symbol or a numerical value at a given location. Parameters such as axis lengths, symbol heights, and labels can be specified in many of the routines. The structure of the subprogram package provides the user with different levels of control. That is, routines which require very little user input are available, as well as routines which require the specification of a large number of parameters.

Figures 49.1 and 49.2 demonstrate the types of plot that can be generated using textural data from a suite of marine sediment samples collected in the Strait of Georgia (Clague, 1975a, b, 1976, 1977). Figure 49.1 displays the geographical location of sediment sampling stations on a standard U.T.M. grid, with latitude and longitude reference crosses along the edges of the figure. Figures 49.2A and 49.2B represent the cumulative and simple frequency grain-size curves for one of the sediment samples. Figures 49.2C and 49.2D demonstrate a popular method of differentiating sedimentary environments using bivariate plots of statistical parameters derived from grain-size frequency distributions. The contours in Figure 49.2D quantify the density of points in the scattergram, allowing easier grouping of the samples into different fields, using a moving average technique. Figure 49.2E demonstrates a more recent trend in sedimentology, that of classifying environments using factor analysis (note that the data presented in Figure 49.2E represent output from a factor analysis model incorporating sediment data from the northern Strait of

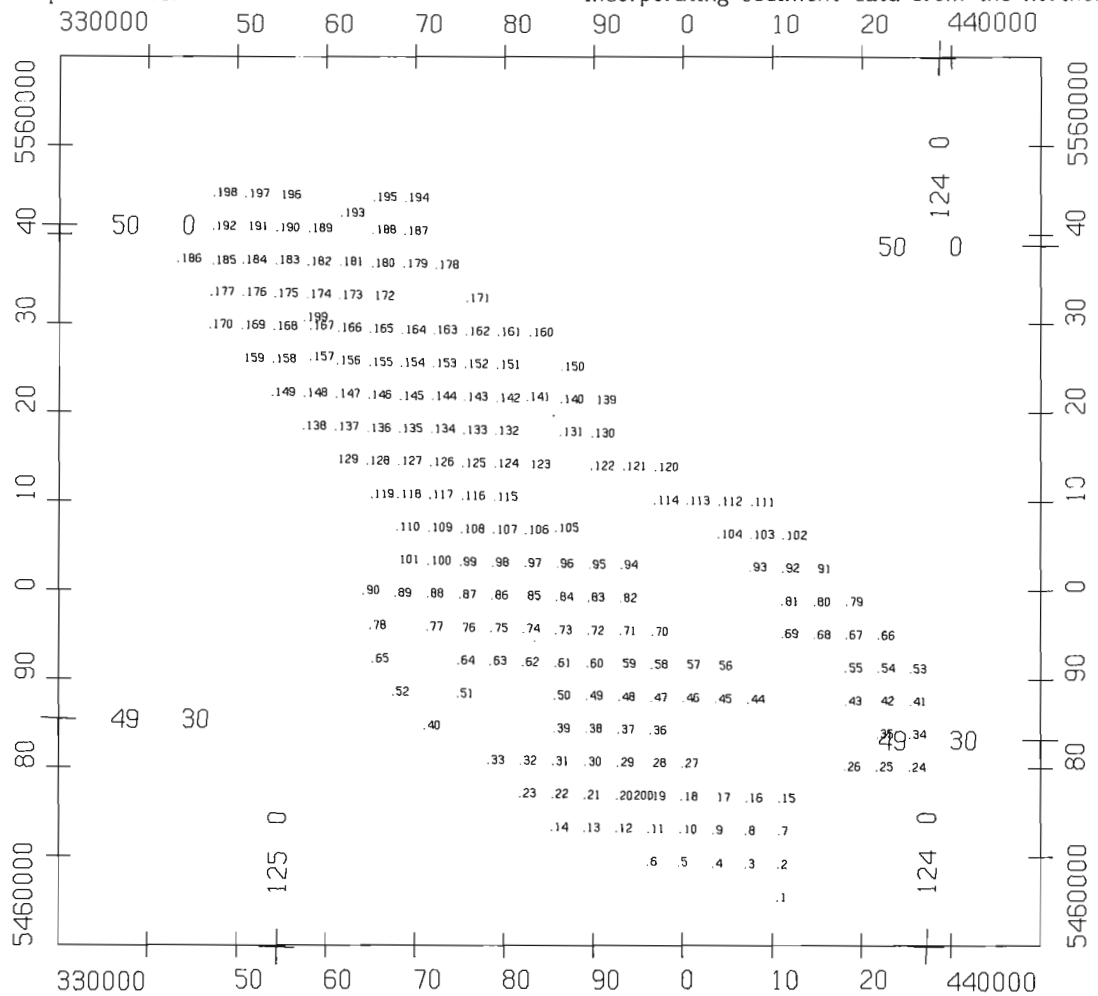

Figure 49.1. Geographic locations for marine sediment samples collected in the Strait of Georgia.

From: Report of Activities, Part B;
Geol. Surv. Can., Paper 77-1B (1977)

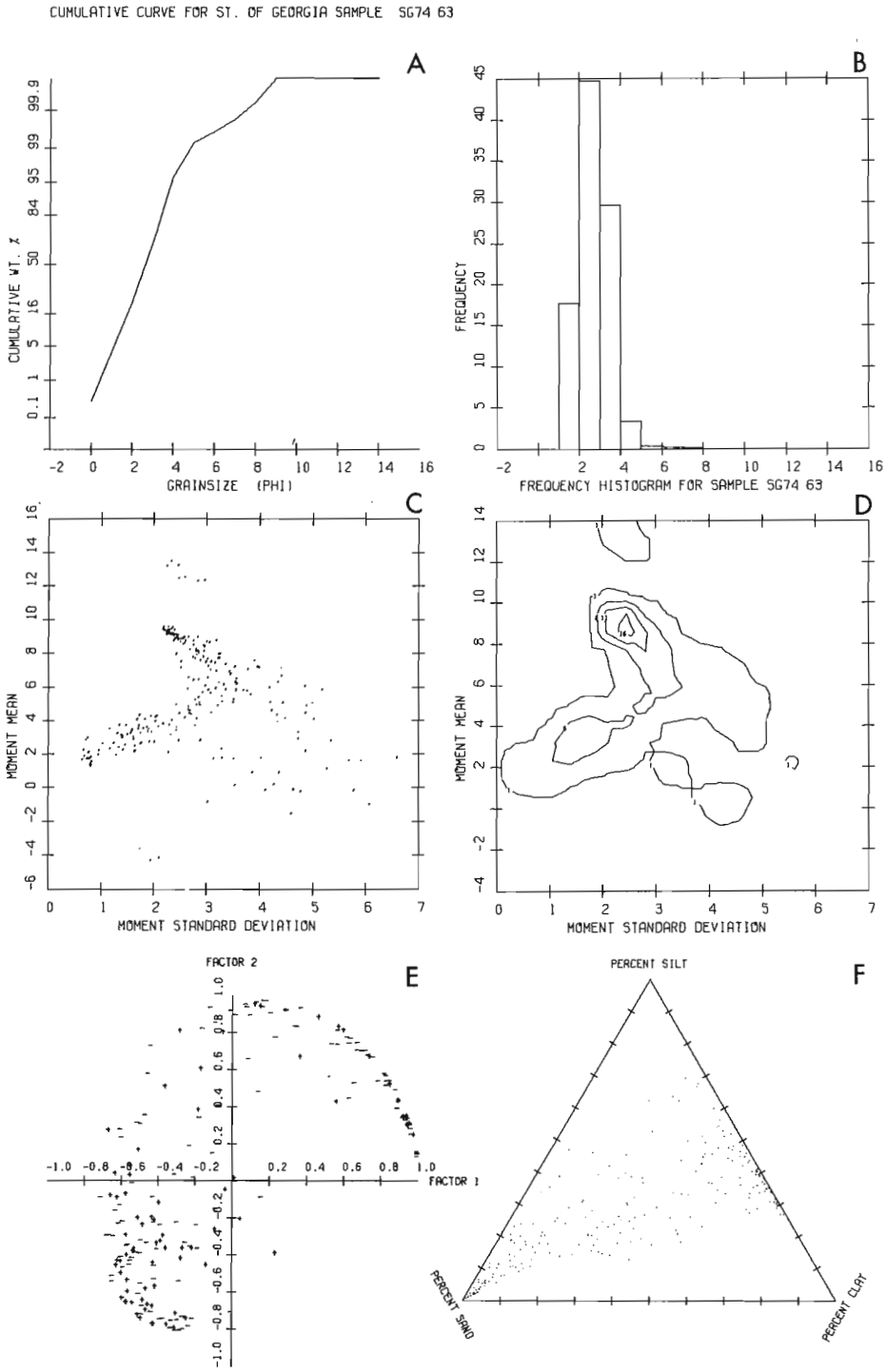

Figure 49.2. Examples of plot output using textural data from Strait of Georgia marine sediment samples.

Georgia with data from the southern Strait of Georgia (Pharo, 1972)). Finally, a sand-silt-clay diagram (Fig. 49.2F) is included as another example of a graphical sedimentological tool.

Program listings and full documentation for these plotting subroutines are available as Data Systems Technical Note 11, Data Systems Group, Geological Survey of Canada.

References

California Computer Products
1969: Programming CalComp Pen Plotters; California Computer Products, Anaheim, California, 25 p.

Clague, J.J.
1975a: Quaternary geology, northern Strait of Georgia, British Columbia; in Report of Activities, Part A, Geol. Surv. Can., Paper 75-1A, p. 397-400.

1975b: Surficial sediments of the northern Strait of Georgia, British Columbia; in Report of Activities, Part B, Geol. Surv. Can., Paper 75-1B, p. 151-156.

1976: Pleistocene sediments in the northern Strait of Georgia, British Columbia; in Report of Activities, Part B, Geol. Surv. Can., Paper 76-1B, p. 157-160.

1977: Holocene sediments in the northern Strait of Georgia, British Columbia; in Report of Activities, Part A, Geol. Surv. Can., Paper 77-1A, p. 51-58.

Pharo, C.H.
1972: Sediments of the central and southern Strait of Georgia, British Columbia; unpubl. Ph.D. thesis, Univ. British Columbia, Vancouver, B.C., 290 p.

50. PALEOMAGNETIC REMANENCE CHARACTERISTICS OF SURFACE TILLS FOUND IN THE PAKOWKI-PINHORN AREA OF SOUTHERN ALBERTA

Project 650027

R.W. Barendregt[1], J.H. Foster[2], and A. MacS. Stalker[3]
Terrain Sciences Division

The number of till sheets present in the Pakowki-Pinhorn area of southern Alberta is still not known. A number of techniques have been used to try to determine the number present and to map the surficial deposits there; one method presently being tried is to map remanent magnetism. Other workers (Stupavsky et al., 1974a, b; Stalker and Foster, 1976; Gravenor and Stupavsky, 1976) previously have used a map of remanent magnetization in differentiating and, in some cases, dating such deposits.

The remanent magnetization of the tills in this area shows strong characteristic magnetizations. This may have been acquired, while the debris was being removed from the base of the ice in the form of a thick slurry, as postdepositional remanent magnetization (PDRM). If the debris forming each till was deposited over a rather long period of time, as is probable, the PDRM variations in each till should reflect the variation in the direction of the earth's magnetic field as the till progressively lost sufficient water to lock in its characteristic magnetization. If the till were time-transgressive, as is probable, this would happen in different areas at different times.

Oriented blocks and drive-core samples of the surface tills were taken at 20 sites, with 6 separately oriented specimens from each site. The natural remanent magnetization (NRM) of each specimen was measured on a Schonstedt D.S.M. spinner magnetometer. Following this, the remanence of each specimen was measured after alternating-field (AF) demagnetization, using a Schonstedt GSD-1 demagnetizer. At least one pilot specimen per site was AF step demagnetized in 100 oersted (oe) steps from 100 to 1000 oe peak intensities. An optimum demagnetizing intensity was selected graphically for the pilot specimen using the method described by Symons and Stupavsky, 1974. If, as happened more than half the time, the pilot specimen demagnetization showed no stable characteristic magnetization, the specimen was discarded and another specimen was step demagnetized as a pilot. This was continued until either (1) all 6 specimens for the site had been discarded or (2) a 'successful' pilot demagnetization was obtained. In the latter case the remaining specimens from the site were AF demagnetized at the selected intensity, and their remanent magnetization was remeasured. The mean direction of remanent

Table 50.1

Remanence Data by Site

Unit	Number of specimens	AF demagnetizing field (oersteds)	Length of resultant vector	Declination (degrees)	Inclination (degrees)	Precision parameter	A95* (degrees)
PC 1101	3	200	2.97	342.5	67.3	57.60	16.39
RS 1202	5	800	4.64	346.9	60.1	11.13	23.98
PS 1303	3	300	2.98	21.5	44.2	117.92	11.40
LS 1404	3	300	2.90	343.6	61.6	19.2	28.94
DC 1505	3	300	2.91	307.0	68.4	22.44	26.66
PR 1606	4	600	3.82	325.2	51.1	16.84	23.06
OR 1707	5	300	4.91	344.2	48.2	44.92	11.92
Mean 7 sites	26	AF demagnetized	6.78	344.4	59.1	27.58	11.70

Virtual Geomagnetic Pole	DP**	DM**
75.6°N, 234.3°W	13.06	17.48

*A95 = radius of 95% confidence
**DP and DM = semi-axes of oval of 95% confidence along and perpendicular to the site-pole great circle.

[1] Department of Geography, Queen's University, Kingston

[2] Regional and Economic Geology Division

[3] Terrain Sciences Division

magnetization was calculated for each site, along with its precision parameter (K) and the radius of the cone of 95 per cent confidence (A95). Sites with A95 greater than 30 degrees were discarded, as each site consisted of samples collected from a single stratigraphic horizon to represent, as closely as possible, a single time.

The remaining 7 till sites of the 20 sites originally sampled had a similar characteristic magnetization. The virtual geomagnetic pole (VGP) was 75.6°N, 234.3°W, i.e. in the Lapteuykh Sea area (northeastern Soviet Union).

The single cluster of characteristic magnetizations obtained from the mapping of remanent magnetization (Table 50.1) did not permit differentiation of tills in the Pakowki-Pinhorn area nor show the presence of more than one till sheet. This result was unexpected, for the samples were collected from what were thought to be two different till sheets (the Labuma and a post-Labuma (Stalker, 1960)) on grounds of morphology, carbonate content, and lithology. In addition, bulk magnetic susceptibility studies carried out earlier on these samples (Barendregt et al., 1976) clearly had identified two till sheets. The single direction shown by the remanent magnetization measurements made by the writers indicates that the PDRM was 'locked-in' with a similar orientation for both the Labuma and post-Labuma tills.

Remanence studies of a glacial till are often difficult in that pebbles may mask the PDRM of the fine grained materials; the 7 sites retained were composed of finer material than the sites discarded. The writers recognize that it is difficult to find and sample suitable material in many till sheets; however, this is necessary for a proper study of PDRM. It is suggested that specimens should be examined by X-ray for the presence of pebbles before measuring remanent magnetization.

References

Barendregt, R.W., Stalker, A. MacS., and Foster, J.H.
1976: Differentiation of tills in the Pakowki-Pinhorn area of southeastern Alberta on the basis of their magnetic susceptibility; in Report of Activities, Part C, Geol. Surv. Can., Paper 76-1C, p. 189-190.

Gravenor, C.P. and Stupavsky, M.
1976: Magnetic, physical and lithological properties and age of till exposed along the east coast of Lake Huron, Ontario; Can. J. Earth Sci., v. 13, no. 12, p. 1656-1666.

Stalker, A. MacS.
1960: Surficial geology of the Red Deer–Stettler map-area, Alberta; Geol. Surv. Can., Mem. 306, 140 p.

Stalker, A. MacS. and Foster, J.H.
1976: Paleomagnetic stratigraphy of the Welsch Valley site, Saskatchewan; in Report of Activities, Part C, Geol. Surv. Can., Paper 76-1C, p. 191-193.

Stupavsky, M., Symons, D.T.A., and Gravenor, C.P.
1974a: Paleomagnetism of the Port Stanley Till, Ontario; Geol. Soc. Am., Bull., v. 85, p. 141-144.

Stupavsky, M., Gravenor, C.P., and Symons, D.T.A.
1974b: Paleomagnetism and magnetic fabric of the Leaside and Sunnybrook Tills near Toronto, Ontario; Geol. Soc. Am., Bull., v. 85, p. 1233-1236.

Symons, D.T.A. and Stupavsky, M.
1974: A rational paleomagnetic stability index; J. Geophys. Res., v. 79, p. 1718-1720.

51. CHANGES IN THE ACTIVE LAYER FROM 1968 to 1976 AS A RESULT OF THE INUVIK FIRE

Project 680047

J. Ross Mackay[1]
Terrain Sciences Division

From 8 to 18 August 1968, a forest-tundra fire burnt in the Inuvik, Northwest Territories area (Hill, 1969). The fire destroyed tens of square kilometres of lichen-rich tundra and forest-tundra. As a direct result of the fire, some bare hillslopes became gullied, sediment was transported into otherwise clear lakes, ice-rich permafrost was exposed to thermal erosion and thermokarst activity, flow slides developed, bulldozed firebreaks subsided, and the active layer thickened over most regions. Natural revegetation has been rapid, in some areas, since 1968. Numerous papers have already been written on various aspects of the Inuvik fire (e.g. Heginbottom, 1973, 1974; Hill, 1969; Mackay, 1970; Wein, 1974; Wein and Bliss, 1973). Some years earlier, Nowosad (1963) discussed the increase in thickness of the active layer, after clearing, at the Inuvik Experimental Farm.

On 15 August 1968, while the forest fire was still burning, five sites were selected to monitor future changes in the terrain. At each site, 1.5 m-long wooden stakes, 2 cm square, were driven to the frost table. Two of the sites, one burnt and the other unburnt, were located by the "Navy Road" 3 km north of Inuvik. Fifteen stakes were placed in a burnt area and another 15 in an adjacent unburnt area. Two more sites were chosen 4 km southeast of Inuvik in adjacent burnt and unburnt areas, and 10 stakes were inserted at each site. A fifth site, on a burnt hillslope but with no nearby unburnt site, was chosen on a hillslope 4 km southeast of Inuvik; 8 stakes were installed at this site (Fig. 51.1). Since 1968 the five sites have been rechecked each August: the heights of the stakes have been measured; the stakes have been tapped down to the frost table when possible; vegetation and terrain changes have been noted; and the sites have been rephotographed frequently. The purpose of this report is to discuss active layer changes between 1968 and 1976 at the hillslope site.

Figure 51.1. Hillslope site showing 8 stakes 1.5 m long driven down to the frost table several days after the fire. The uneven heights of the stakes are the result of alternate stakes being located on ridges and depressions (cf. Fig. 51.2) August 16, 1968.

Hillslope Site

The hillslope site was staked within two days after it had been burnt. The original vegetation was scattered spruce and white birch, with willows, alder, labrador tea, heaths, and a spongy ground cover of mosses, lichens, and organic-rich turf. The fire scarred the trees and reduced the vegetation mat to a layer of ash several centimetres thick, which rose in a cloud with every passing footstep. The 19 degree slope had ridges trending downslope (Fig. 51.1). Eight stakes were driven to the frost table along the contour, 4 on the ridges and 4 in the intervening depressions.

The question can be raised as to whether the heat from the forest fire contributed to active layer thaw, either during the course of the fire or afterwards. The duration of active burning at any given site (trees excluded) was usually far less than half an hour because of the lack of combustible materials. For example, a heat flow calculation (e.g. Ingersoll et al., 1954, eq. 7.14d) shows that if the top of the active layer were at 10°C, and the fire maintained a temperature of 500°C for half an hour, the temperature rise at a depth of 30 cm would hardly be perceptible.

Vegetation Changes (1968-1976)

Natural revegetation of the hillslope site has been rapid. One year after the fire, about 70 per cent of the total area of the inter-ridge depressions was covered with bare ash. Two years after the fire (i.e. 1970), there was a continuous cover of fireweed, marsh-fleabane, and other plants standing

[1]Department of Geography, University of British Columbia, Vancouver, British Columbia V6T 1W5

From: Report of Activities, Part B;
Geol. Surv. Can., Paper 77-1B (1977)

Figure 51.2. The hillslope site of Figure 51.1 as seen on August 28, 1976. The depth of thaw has increased an average of 57 cm in the depressions and 54 cm in the ridges. The vegetation is waist high. Most of the trees have fallen down; the tall tree on the right is identifiable in Figure 51.1.

50 cm high. By 1974, willows and white birch had grown to 1 m high. However, most of the burnt trees, which were upright in 1968, now had toppled over. Eight years after the fire (i.e. 1976), the stakes were largely hidden by a luxuriant growth, and a thickening mat of dead and decaying vegetation had covered the ground, leaving no bare ash (Fig. 51.2).

Active Layer Changes (1968-1976)

The 1968-1976 mean thickness of the active layer for the inter-ridge depressions (mean of 4 stakes) and ridges (mean of 4 stakes) is plotted in Figure 51.3. Several trends are evident. First, although the active layer for both the depressions and ridges thickened rapidly for the first 4 or 5 years after the fire, a slight increase still occurred even eight years after the fire. Second, the absolute increase from 1968-1976 was nearly the same for both the depressions (57 cm) and the ridges (54 cm). Third, the percentage thickening for the depressions (250 per cent) was greater than that for the ridges (190 per cent). Fourth, the 1968-1976 thickening of the active layer for both depressions and ridges can be approximated by an exponential decay curve (Fig. 51.3).

Discussion

The destruction of a vegetation cover by clearing or by fire in a permafrost environment usually results in a thickening of the active layer (e.g. Heginbottom, 1973; Kurfurst, 1976; Mackay, 1970; Nowosad, 1963; Viereck, 1973; Wein and Bliss, 1973), because there is a summer warming of soil temperatures above those previously experienced. On the other hand, the winter temperatures tend to remain the same, unless there has been a change in the snow cover. The net effect is for the amplitude of the ground surface temperature to increase, and the active layer therefore must deepen until a new equilibrium thickness is established.

If permafrost below the active layer has little excess ice, the quasi-equilibrium thickness of the active layer can occur within a year or two following a surface disturbance. However, the top of permafrost at the hillslope site is ice rich, and prior to the fire the ice content may have exceeded 50 per cent by volume (Heginbottom, 1973). The thaw of such ice-rich permafrost is a slow summer process. For example, if the volumetric ice content at the top of permafrost was 50 per cent, then the thickening of the active layer in the depressions required the thaw of about 114 cm of permafrost to yield the 57 cm of new active layer soil; for the ridges, thaw of 108 cm of permafrost was required to supply 54 cm of new active layer soil. On a 50 per cent ice content basis, the hillslope site would have subsided about 50 cm.

The summer thaw in the active layer usually approximates an exponential or modified exponential curve (Kelly and Weaver, 1969). The exponential curve in Figure 51.3 has been applied to many types of naturally occurring data (Ten Brink, 1974). The curve is described by the equation:

$$A_t = A_o \sum_{o}^{t} e^{-kt}$$

where A_t is the thickness of the active layer at the end of August in year t; A_o is the thickness of the active layer at t=o, i.e. 1968; e is the base of natural logarithms; k is an exponential constant which must be fitted for each set of thaw data; and t is time in years. The computed curves in Figure 51.3 have k=0.5 for the depressions and k=0.8 for the ridges. The rate of decay for the depressions apparently is slower than for the ridges.

As a consequence of the fire, there is now less contrast between the thickness of the active layer beneath the depressions as compared to the ridges. In most areas of vegetated patterned ground, such as the hillslope ridges, the active layer is much thinner beneath the depressions than beneath the ridges. At the hillslope site, the greater thickening of the active layer beneath the depressions (250 per cent) as compared to the ridges (190 per cent) shows the former influence of the vegetation cover and microtopography in keeping the depressions colder than the ridges.

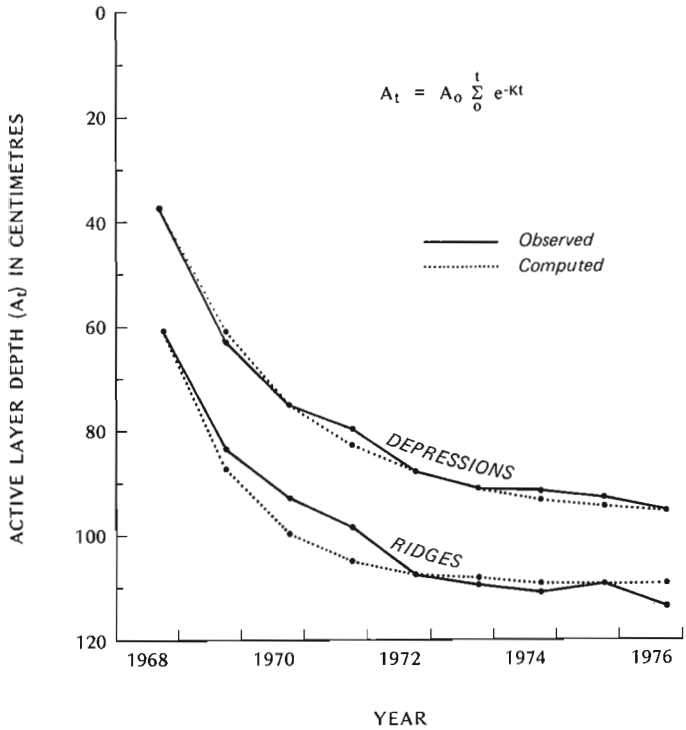

Figure 51.3. The observed thickening of the active layer for the depressions (mean of 4 stakes) and ridges (mean of 4 stakes) from 1968-1976 along with computed curves. See text.

Other Areas

Although not discussed in detail here, the four other staked sites have shown similar changes where a vegetation cover was destroyed. At one site with large vegetated earth hummocks in 1968, some hummocks have now lost their mound relief. In areas of large mud hummocks (cf. Wein and Shilts, 1976) the vegetated depressions now have a thicker active layer, whereas the mud centres have changed little. Along some of the bulldozed firebreaks, subsidence in excess of 100 cm has occurred locally.

Conclusion

The active layer on a burnt hillslope at Inuvik continued to thicken, but at a decreasing rate, from 1968-1976. The deepening occurred despite the rapid growth of a waist-high vegetation cover. The 8-year period required to reach a quasi-equilibrium active layer depth has resulted from the high ice content of the top of permafrost. The burnt hillslope probably has subsided nearly 50 cm. In the future, as the vegetation succession changes, the active layer will probably thin, the upper permafrost surface will aggrade upwards, and some ice lenses at the bottom of the active layer will become incorporated into permafrost. If this happens, the ground surface will rise by an amount equal to the total thickness of the ice lenses incorporated into the upward aggrading permafrost. The hillslope thickening of the active layer over an 8-year period emphasizes the inherent danger of drawing conclusions on the effect of a disturbance only a year or so after disturbance. The long-term active layer effect can only be inferred if the ice content of permafrost is known and the extent of the revegetation is estimated.

References

Heginbottom, J.A.
1973: Some effects of surface disturbance on the permafrost active layer at Inuvik, N.W.T.; Environmental-Social Prog., Northern Pipelines, Task Force Northern Pipelines, Ottawa, Rept. 73-16, 22 p. and appendix.

1974: The effects of surface disturbance on ground ice content and distribution; in Report of Activities, Part A, Geol. Surv. Can., Paper 74-1A, p. 273.

Hill, R.M.
1969: Review of Inuvik Forest Fire August 8-18, 1968. Inuvik, N.W.T.; Inuvik Research Laboratory, 10 p.

Ingersoll, L.R., Zobel, O.J., and Ingersoll, A.C.
1954: Heat Conduction; University of Wisconsin Press, Madison, 325 p.

Kelly, J.J. and Weaver, D.F.
1969: Physical processes at the surface of the arctic tundra; Arctic, v. 22, p. 425-437.

Kurfurst, P.J.
1976: Assessment of terrain performance in the Mackenzie Valley and Arctic Islands; in Report of Activities, Part A, Geol. Surv. Can., Paper 76-1A, p. 277-279.

Mackay, J.R.
1970: Disturbances to the tundra and forest tundra environment of the western Arctic; Can. Geotech. J., v. 7, p. 420-432.

Nowosad, F.S.
1963: Growing vegetables on permafrost; North, v. 10, p. 42-45.

Ten Brink, N.W.
1974: Glacio-Isostasy: new data from West Greenland and geophysical implications; Geol. Soc. Am., Bull., v. 85, p. 219-228.

Viereck, L.A.
1973: Wildfire in the taiga of Alaska; J. Quat. Res., v. 3, p. 465-495.

Wein, R.W.
1974: Recovery of vegetation in arctic regions after burning; Environmental-Social Prog., Northern Pipelines, Task Force Northern Pipelines, Ottawa, Rept. 74-6, 63 p.

Wein, R.W. and Bliss, L.C.
1973: Changes in arctic **eriophorum** tussock communities following fire; Ecology, v. 54, p. 845-852.

Wein, R.W. and Shilts, W.W.
1976: Tundra fires in the District of Keewatin; in Report of Activities, Part A, Geol. Surv. Can., Paper 76-1A, p. 511-515.

Project 740046

P.J. Kurfurst
Terrain Sciences Division

A detailed study of the acoustic properties and behaviour of frozen soils at permafrost temperatures is being carried out both in the laboratory and in the field by Terrain Sciences Division, Geological Survey of Canada. This study, initiated in spring of 1976, is part of a continuing long-term research program of laboratory and field measurements of physical properties of frozen soils and rocks.

Compressional and shear wave velocities are measured in the laboratory on frozen soil samples that differ in type of material and ice content; all samples were collected at drill sites in Mackenzie Valley and Arctic Islands where field measurements of seismic velocities were made at the time of drilling. All samples tested are subjected to a uniaxial state of stress at a range of temperatures varying from +1°C to -7°C.

A special apparatus, consisting of electronic equipment, a fluid-pressure control system, and a loading frame, has been installed in the temperature-controlled cold room. The apparatus, original in design, enables measurement of compressional and shear wave velocities sequentially on the same specimen; a detailed description of the apparatus was reported by Kurfurst (1977).

Frozen soil samples of required dimensions are placed between the transmitter and the receiver and then are placed in the loading frame. The fluid-pressure control system, connected to the loading frame, is used to apply the required pressure on the sample. The entire assemblage is connected to the electronic equipment. A pulsed oscillator is used to apply a short sinusoidal-voltage pulse to one of the two piezoelectric transducers. The pulse of mechanical energy produced by the transmitter travels through the transmitter face, specimen, and the receiver face to the receiver where it is converted into an electrical voltage signal. This signal then is amplified and displayed on a horizontal axis of one beam of a dual-beam oscilloscope. Both the pulsed oscillator and the oscilloscope sweep are triggered by a time-mark generator, which also provides accurate time marks on the second beam of the oscilloscope. The sample preparation and the operational procedure used are similar to those described in detail by Kurfurst and King (1972).

The compressional and shear wave velocities are obtained by measuring the time taken by a pulse to traverse the length of the specimen. Their values are claculated by using the following equation:

$$V_p, V_s = \frac{l/d}{t_1 - t_2}$$

where V_p is compressional wave velocity

V_s shear wave velocity

l length of specimen

d diameter of specimen

t_1 pulse travel time through specimen and transducer holders

t_2 pulse travel time through transducer holders

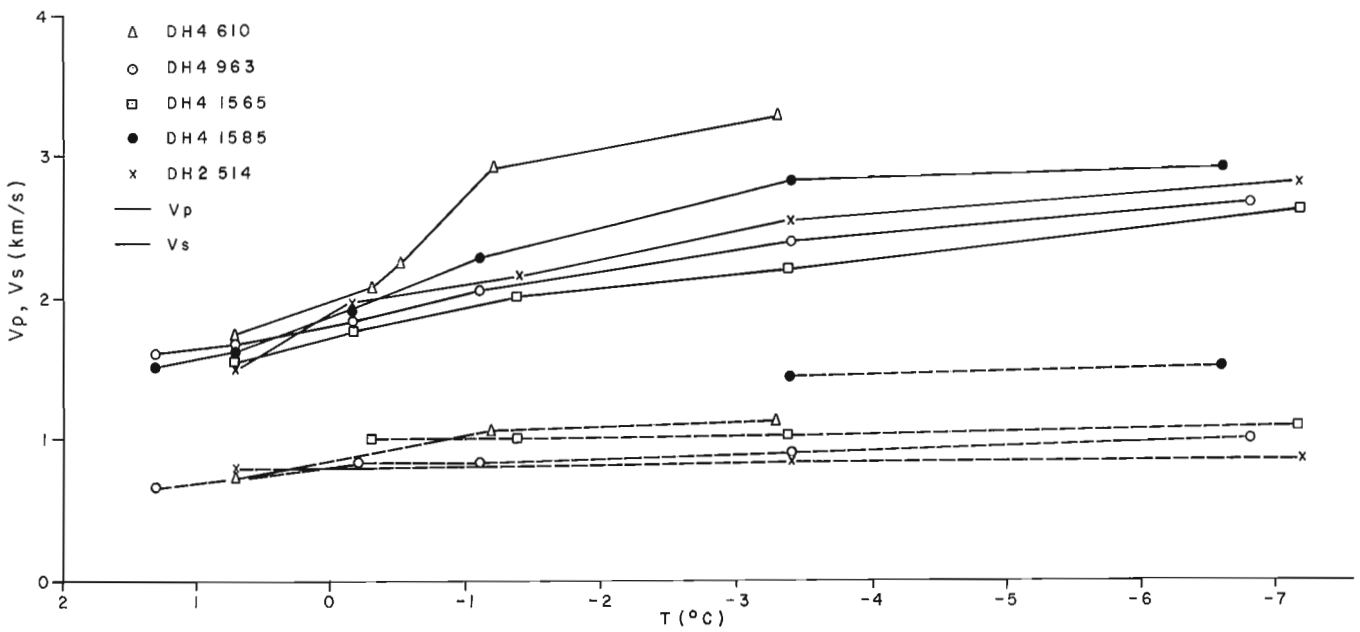

Figure 52.1. Relationship between acoustic wave velocity and temperature: fine grained soils.

From: Report of Activities, Part B;
Geol. Surv. Can., Paper 77-1B (1977)

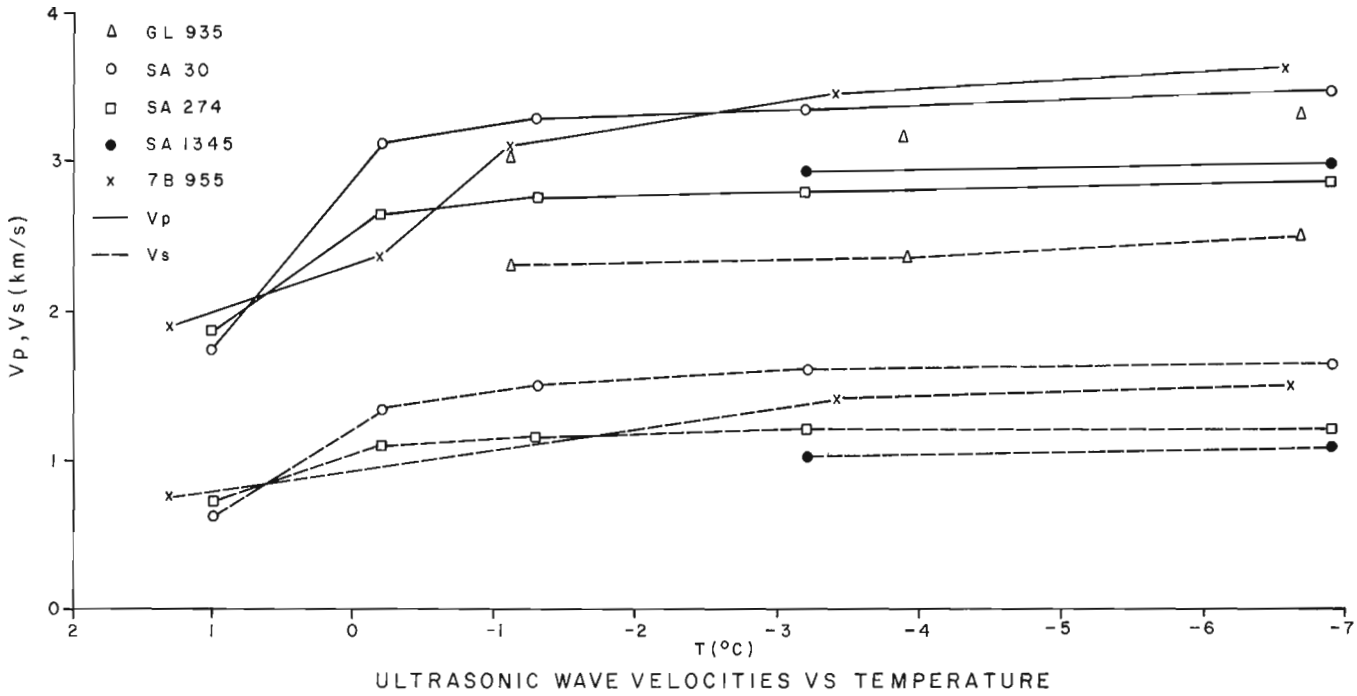

Figure 52.2. Relationship between acoustic wave velocity and temperature: coarse grained soils.

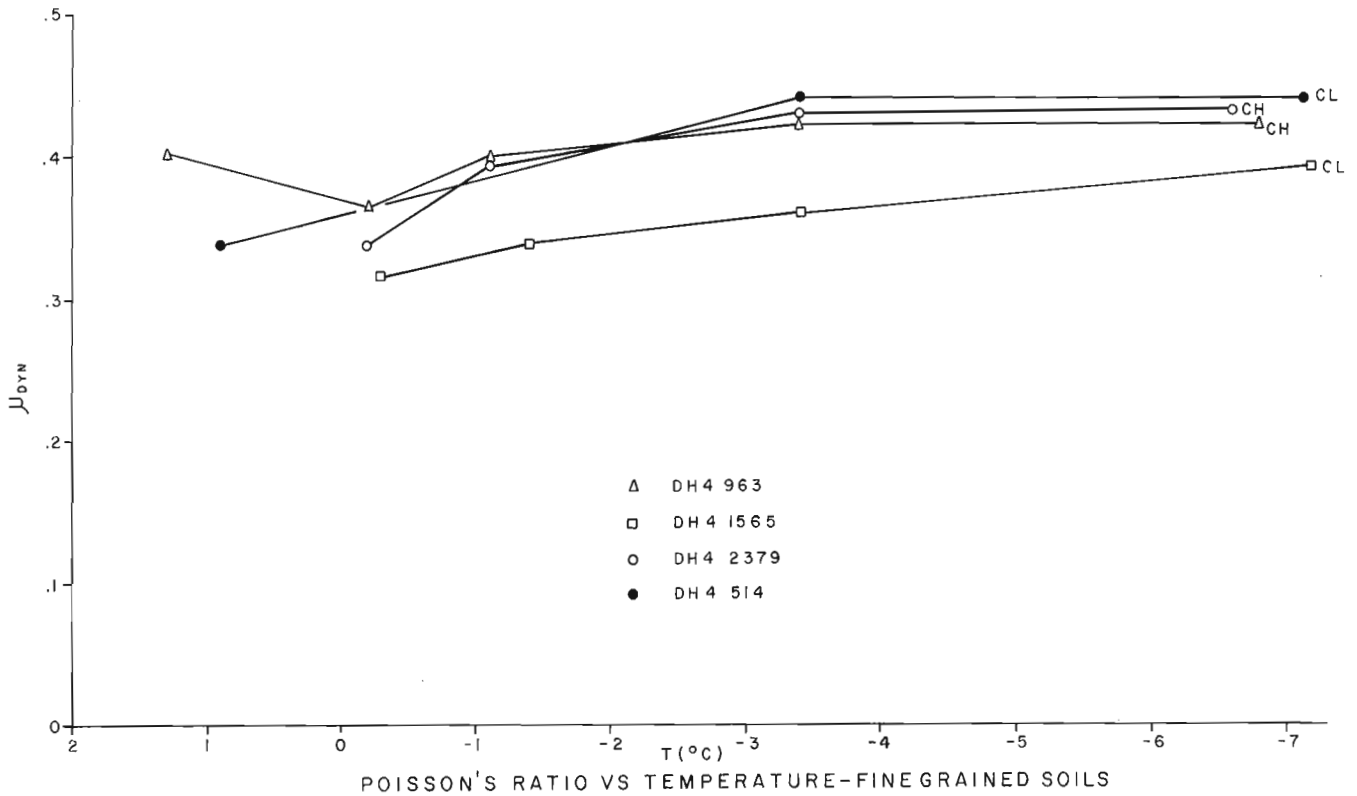

Figure 52.3. Relationship between dynamic Poisson's ratio and temperature: fine grained soils.

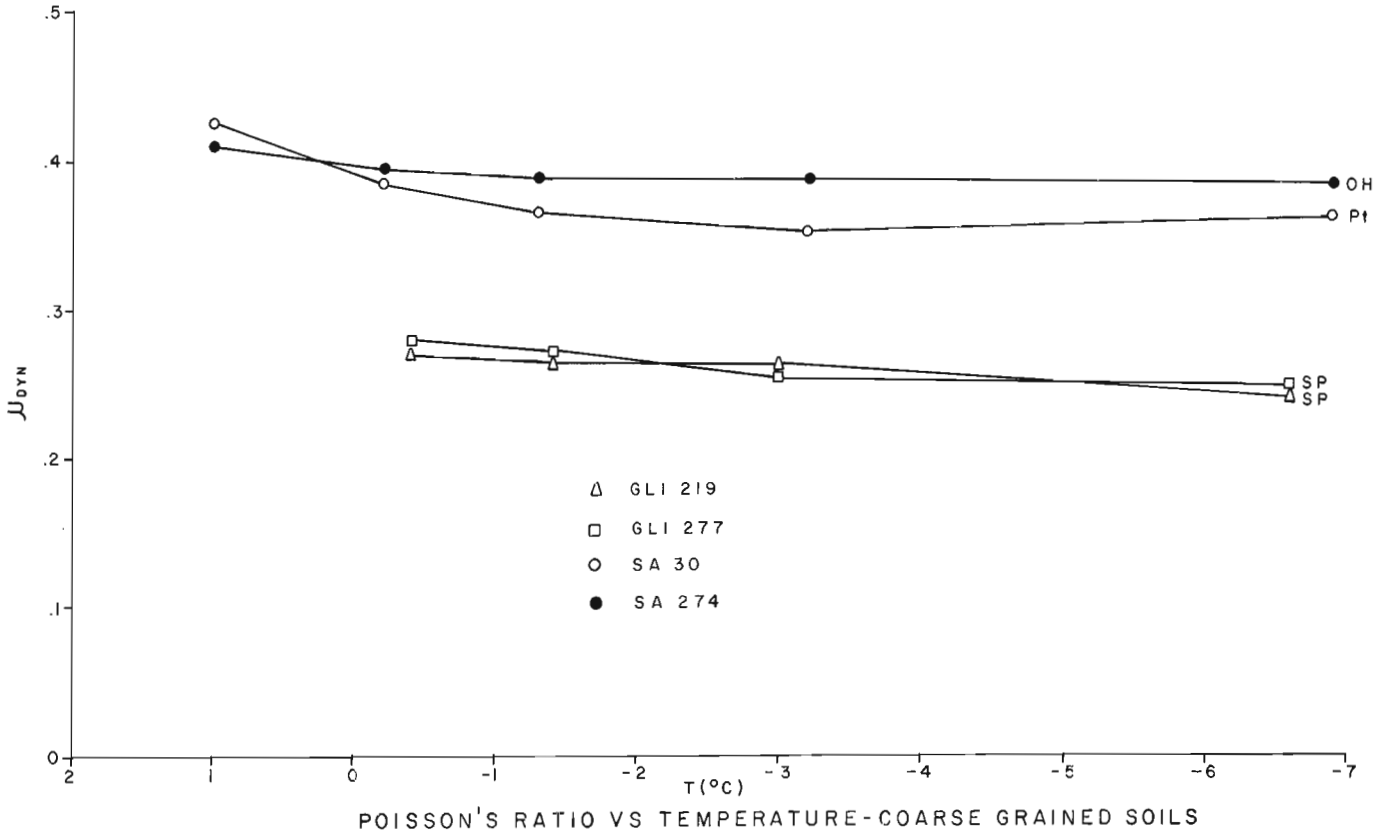

Figure 52.4. Relationship between dynamic Poisson's ratio and temperature: coarse grained soils.

A series of tests was conducted on frozen clay samples of low and high plasticity. Values of compressional and shear wave velocities measured were plotted as a function of temperature and are shown in Figure 52.1. Both compressional and shear wave velocities display similar behaviour. Results indicate that an increase in the measured velocities occurs after the temperature is reduced below 0°C; this increase becomes pronounced around -1°C. After the temperature is reduced further, velocities increase only gradually at a relatively slow rate. This behaviour of frozen clays is attributed to a combination of their high natural moisture content, grain size, and low porosity.

Results of tests on frozen samples of poorly graded sands, organic soils, and peats are presented in Figure 52.2. A sharp increase in compressional wave velocities occurs immediately after reducing the temperature below 0°C; further reduction in the temperature below -1°C results in further gradual velocity increase, which is relatively slow. Although shear wave velocities show the same sharp increase for a temperature range between +1°C and -1°C.

Values of dynamic Poisson's ratio were calculated for all samples tested, using the following formula:

$$\mu_{dyn} = \frac{1}{2} \cdot \frac{(V_p/V_s)^2 - 2}{(V_p/V_s)^2 - 1}$$

where μ_{dyn} is dynamic Poisson's ratio

V_p compressional wave velocity

V_s shear wave velocity

The typical values of dynamic Poisson's ratio were plotted as a function of temperature for both fine and coarse grained soils tested (Figs. 52.3 and 52.4).

Fine grained soils, represented by low and high plasticity clays (Fig. 52.3 – CL and CH groups), display a gradual increase in values of dynamic Poisson's ratio when temperature is reduced from 1°C to -3°C; any further decrease in temperature results in only a slight increase in dynamic Poisson's ratio. However, poorly sorted sands, organic soils, and peats (Fig. 52.4 – SP, OH and Pt groups),representing coarse grained soils, show the opposite trend. When temperature is reduced below +1°C, values of dynamic Poisson's ratio decrease sharply until temperature reaches -3°C; further decrease in temperature to -7°C produces either minor or no decrease in dynamic Poisson's ratio. Differences in grain size, void ratio, and porosity seem to be the major factors affecting the values of dynamic Poisson's ratio and its behaviour.

Field measurements of seismic velocities were made adjacent to boreholes using a 12-channel refraction array laid out on the surface. Only high velocity first arrival events were used in correlation with laboratory results. Because the seismic refraction technique used measured an average velocity over a considerable distance (>100 m) and a considerable depth (20 to 30 m), good correlation between the field and laboratory results is remarkable and attests to the uniformity of materials surrounding the boreholes tested.

Typical results of both field and laboratory values of compressional and shear wave velocities are summarized in Table 52.1.

Table 52.1

Comparison of Field and Laboratory Data

Drillhole	V_p field	V_p lab	V_s field	V_s lab	USCS*
DH 2	3.11	2.79	0.82	0.85	CL
DH 3	3.05	2.88	1.04	0.89	CL
DH 4	2.62	2.90	0.81	1.05	CL, CH
GL 1	3.36	3.48	0.74	0.73	SP, CH
GL 2	2.38	2.45	0.73	0.79	CH
SA	2.74	2.77	0.62	0.63	OH, CL, Pt
7B	3.04	3.09	0.64	0.71	CH, SM-SC
MV	3.58	3.86	0.86	–	MH
TL	2.57	2.47	0.63	–	OH

Note: All values in km/s, temperature -1°C.

* Unified Soils Classification System

The results obtained show that:

(1) an increase in both compressional and shear wave velocities occurs when temperature is reduced below 0°C due to formation of ice in large pore spaces;

(2) the rate of velocity increase is proportional to the increase in the amount of ice within one soil type due to changes in temperature, but varies with different soil types;

(3) there is a depression of temperature, at which most freezing takes place, from 0°C to about -1°C for fine grained soils as a portion of the water remains unfrozen in smaller pores even at and below 0°C;

(4) a correlation exists between the type of material and dynamic Poisson's ratio. In general, values of dynamic Poisson's ratio increase for fine grained soils and decrease for coarse grained soils as the temperature is reduced below 0°C;

(5) good agreement exists between field and laboratory results.

References

Kurfurst, P.J.
1977: Acoustic wave velocity apparatus; in Report of Activities, Part A, Geol. Surv. Can., Paper 77-1A, p. 73.

Kurfurst, P.J. and King, M.S.
1972: Static and dynamic elastic properties of two sandstones at permafrost temperatures; Am. Inst. Mining Eng., Trans., v. 253, p. 495-504.

53 ICEBERG CONCENTRATIONS AS AN INDICATOR OF SUBMARINE MORAINES, EASTERN QUEEN ELIZABETH ISLANDS, DISTRICT OF FRANKLIN

Project 750063

W. Blake, Jr.
Terrain Sciences Division

At a number of localities in southeastern Ellesmere Island and on Coburg Island (Fig. 53.2), submarine moraines are delineated by concentrations of stranded icebergs or, in shallower water, by rafted floes of sea ice. Although the situation varies from year to year, in a general way photographs taken in late spring or early summer, before breakup, are the most useful. This is particularly true if an abundance of icebergs drifted into the area during the preceding summer and autumn.

In areas where detailed soundings have been carried out and hydrographic charts are available (cf. Liestøl, 1972), submarine moraine ridges can be discerned without recourse to indirect methods; but in more remote and less-studied Arctic regions, mapping of moraines by the stranded icebergs aligned along them is a useful tool, as Løken (1973) has demonstrated already off the northeastern coast of Baffin Island. Investigations of the submarine moraines in the northern part of the Canadian Arctic Archipelago are just commencing as part of a long-term project of deciphering the glacial history and geochronology of this vast region. The purpose of this report is to illustrate a few examples of the type of occurrence described above.

The unnamed outlet glacier shown in Figure 53.1 is on the west side of Coburg Island (Fig. 53.2). No chronological data are available as to when the outer submarine moraine formed, but the inner moraine appears to mark the position occupied by the glacier front in 1959, for the aerial photographs taken on July 16th of that year reveal the presence of only a single underwater ridge (Fig. 53.3). In this connection it is interesting to note that photographs (A22540-42 and -43) taken from an altitude of approximately 3090 m on August 19th, 1971, at a time when the waters around Coburg Island were ice free, show no trace of the submarine moraines in front of the glacier illustrated in Figures 53.1 and 53.3. This indicates that

Figure 53.1. View northeastward along the northwest coast of Coburg Island. Note how two submarine moraines are delineated by the patterns in the ice in front of the glacier in the foreground. Part of the outer moraine that is above sea level is indicated by the large arrow, and the two underwater ridges are located by the smaller arrows. July 2, 1970 (GSC-203181).

From: Report of Activities, Part B;
Geol. Surv. Can., Paper 77-1B (1977)

the moraine ridges lie in water deep enough that they are not visible on fairly low level photography. On the opposite side of Coburg Island, 'Laika Glacier' (unofficial name used by the North Water Project, leader F. Müller, ETH, Zürich) advanced across a series of raised beaches some time within the last few thousand years, probably within the last few hundred years, and it reached a terminal position approximately at the shoreline. The glacier has since retreated from the position attained during that advance, leaving a prominent moraine (Fig. 53.4). The outer submarine moraine shown in Figure 53.1 may be related to the same expansion, for it would not be unreasonable if advances of outlet glaciers on both sides of Coburg Island had taken place at approximately the same time.

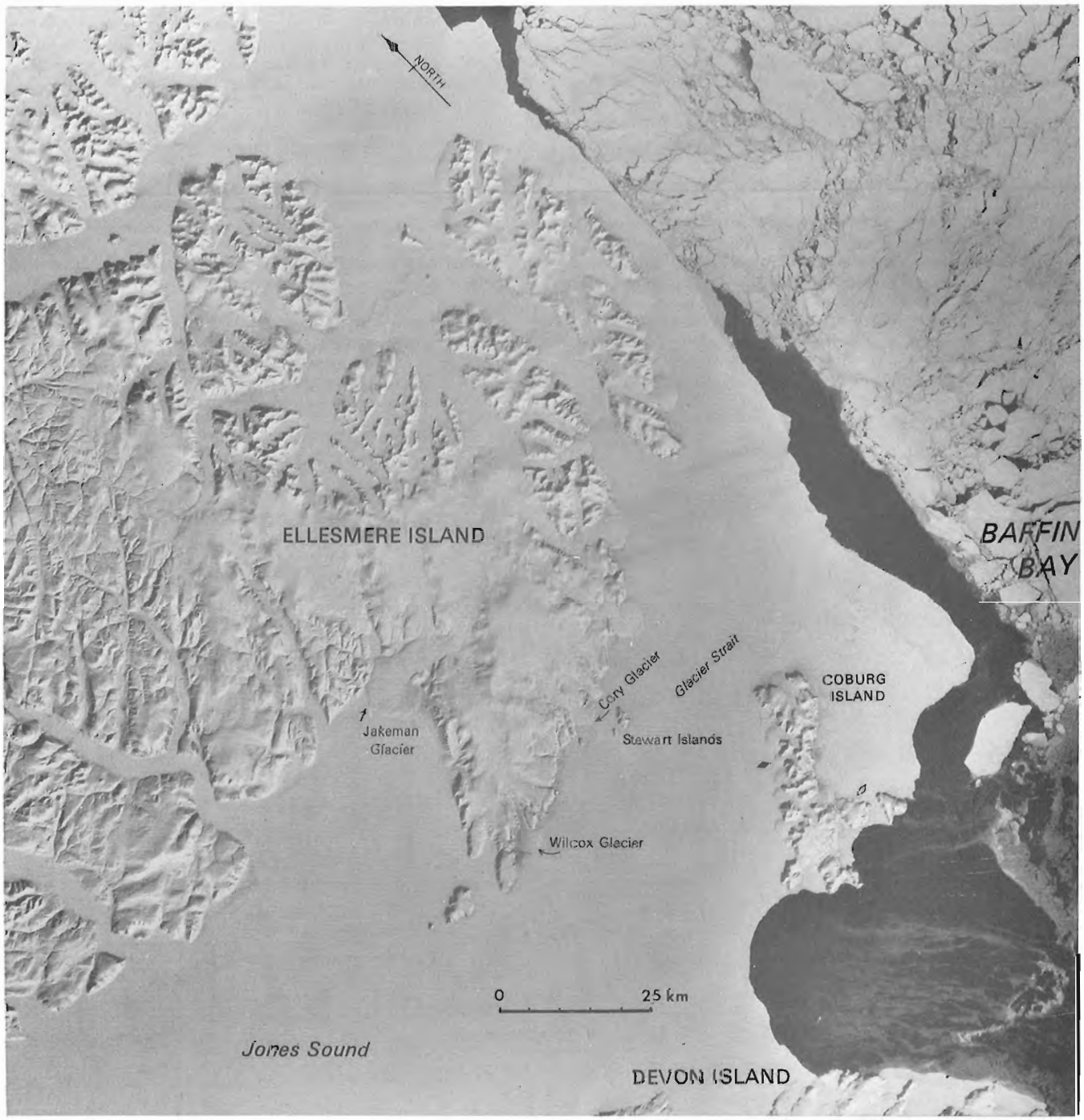

Figure 53.2. LANDSAT image of the eastern part of Jones Sound, showing the location of sites referred to in the text. The position of the unnamed glacier, shown in Figure 53.2, on the northwest side of Coburg Island is indicated by the black diamond; 'Laika Glacier' on the east side of the same island (Fig. 53.3) is indicated by the open diamond. Note the development of the North Water at the time the image was created, April 26, 1975 (image E-11007-17232, spectral band 7).

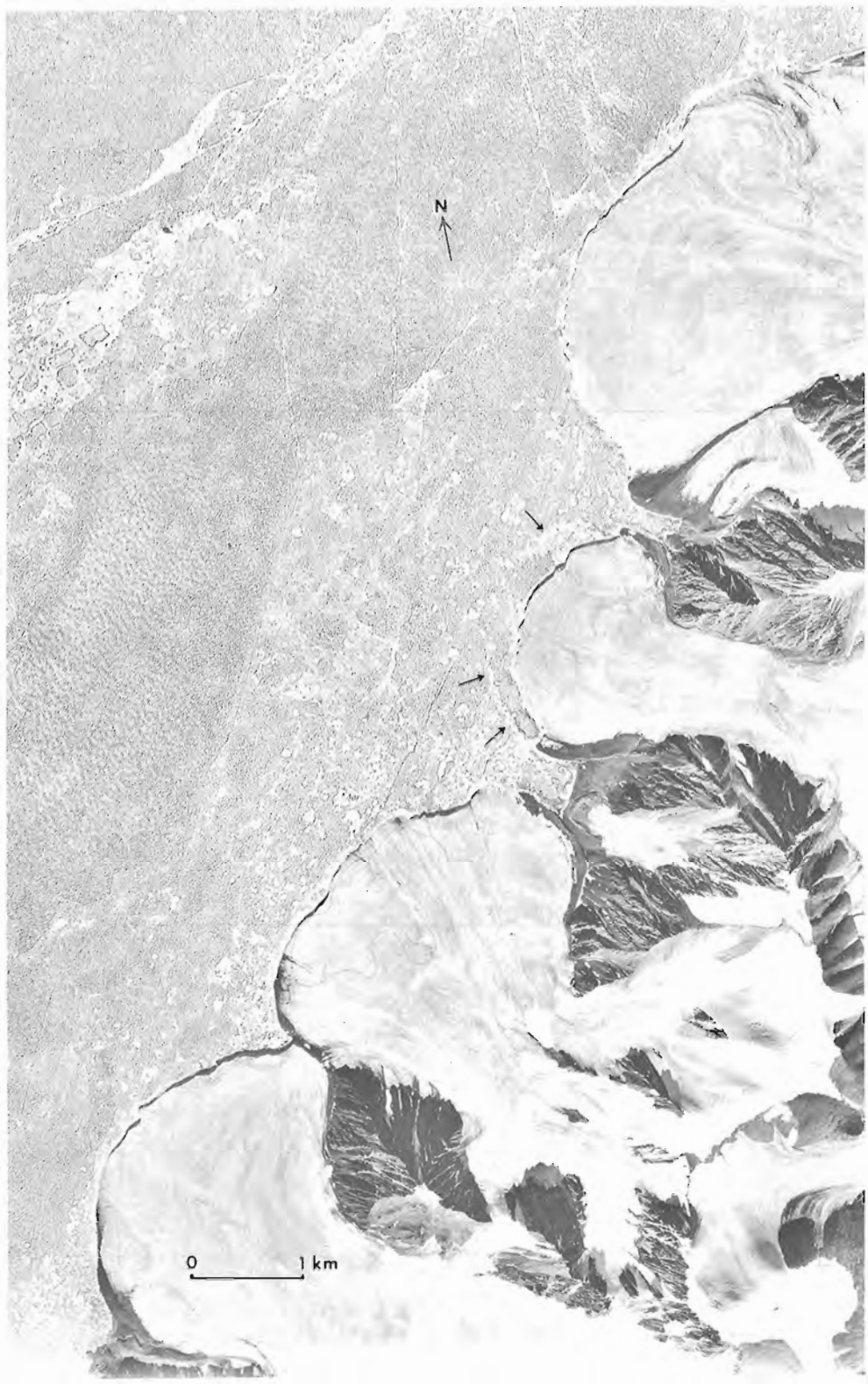

Figure 53.3. Vertical aerial photograph of the same glacier on the northwest side of Coburg Island that is shown in Figure 53.2. Note the single line of bergy bits, rafted ice, etc., extending out from the moraine on the south side of the glacier. Photograph A16682-16 taken from an altitude of ca. 9100 m, July 16, 1959. National Air Photographic Library, Department of Energy, Mines and Resources, Ottawa.

Figure 53.4. Aerial view southeastward along the east coast of Coburg Island. The terminal moraine of 'Laika Glacier' cuts obliquely across the series of raised beaches. July 2, 1970 (GSC-203182).

Figure 53.5. Aerial view northward at Wilcox Glacier, Ellesmere Island, with a group of icebergs aligned in concentric fashion in the foreground. July 2, 1970 (GSC-203183).

The line of icebergs shown in Figure 53.5, south of Wilcox Glacier, southeastern Ellesmere Island (Fig. 53.2), is considerably farther from the glacier than is the case with the moraines on Coburg Island. The only chronological data in the immediate vicinity are from Cory Glacier, some 20 km to the northeast (cf. Fig. 53.6). There, organic material believed to represent a lagoonal deposit (Blake, 1970, 1975) is present within a beach ridge at an elevation of 10 m and over 1 km from the present shore; the organic material was determined to be 6490 ± 140 years old (GSC-1170). Obviously a sequence of younger beaches formed before Cory Glacier readvanced, created a series of moraines, and diverted meltwater to truncate and destroy much of the beach area. In addition, one area on the lowest beaches is occupied by the ruins of typical Thule culture houses (site RbHa-1; Fig. 53.6). It seems

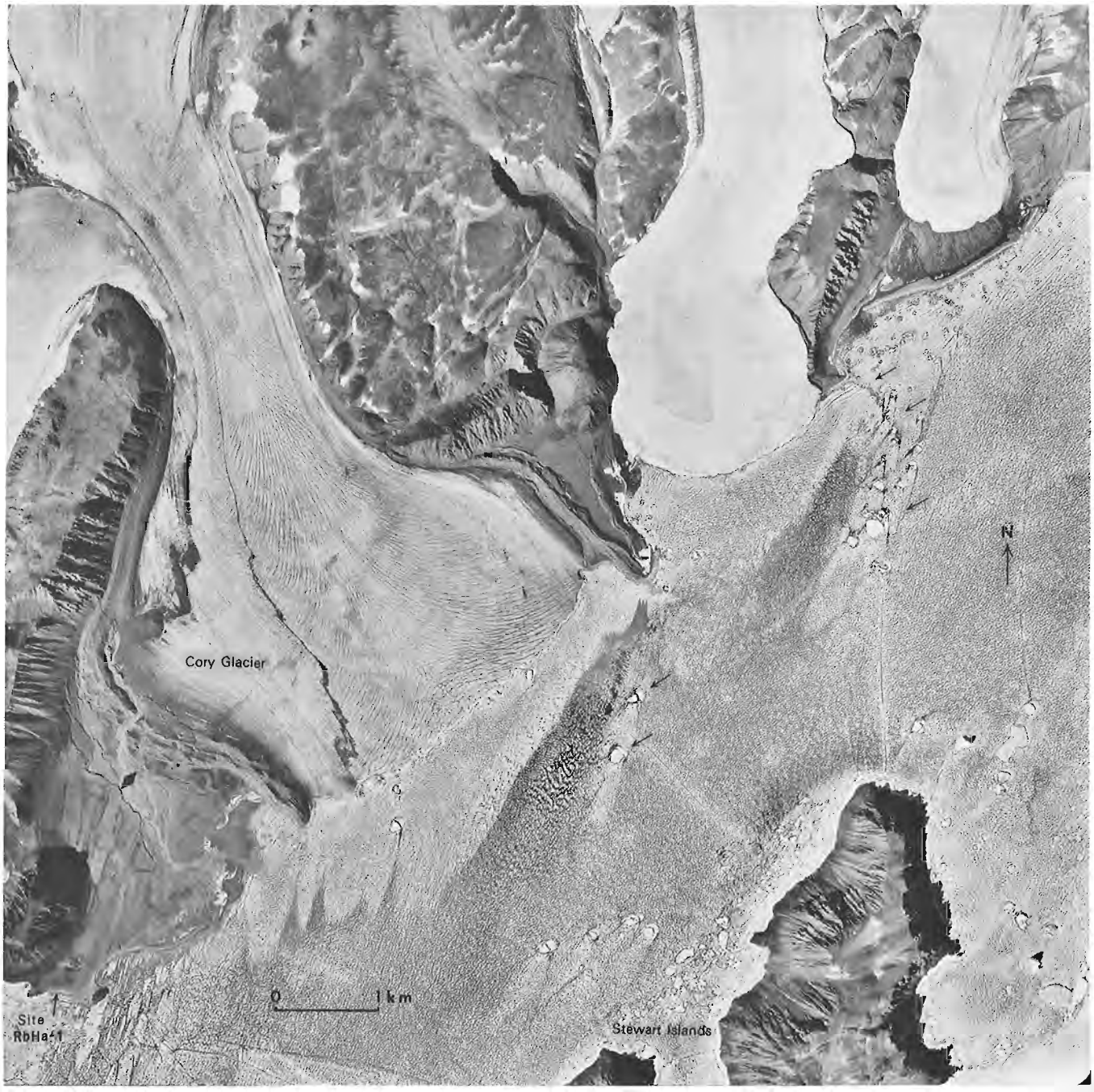

Figure 53.6. Vertical aerial photograph of Cory Glacier and the adjacent unnamed glacier, Ellesmere Island. Note the stranded icebergs (arrows) on the limbs of the submarine moraines and the way in which the beaches have been truncated by the ice-marginal river. The black diamond indicates the location of the dated lagoonal deposit referred to in the text. Photograph A16682-170 taken from an altitude of ca. 9100 m, July 16, 1959. National Air Photographic Library, Department of Energy, Mines and Resources, Ottawa.

reasonable to assume that this site was occupied some time during the last 1000 years, for a Thule settlement farther west along the coast of Jones Sound (site RcHv-1) contains whale bone which is 1110 ± 80 years old (GSC-1899; Blake, 1975)[1]. If this assumption is correct and if it also can be assumed that the readvance of Cory Glacier postdates the occupation of site RbHa-1, then the submarine moraines formed relatively recently, i.e., within the last few hundred years. Another line of evidence is provided by the presence of peat underlying

[1]McGhee (1975) has suggested that "the main thrust of the Thule movement into Arctic Canada occurred between A.D. 1100 and 1400, and that by the latter date the Thule occupation had spread throughout most of the Central and Eastern Arctic".

colluvium or solifluction debris adjacent to Jakeman Glacier (Fig. 53.2); this material is 1470 ± 80 years old (GSC-1562). The advance of the glacier that caused the ice-marginal river to impinge on the succession of marine deposits and to excavate the section where the peat is exposed must postdate the development of the peat.

In Figure 53.6 the stranded icebergs carried onto the submarine moraine in front of both Cory Glacier and the unnamed glacier to the northeast are readily discernible. In this area, because of the southwestward-flowing current in Glacier Strait, the icebergs tend to cluster on the eastern limbs of the submarine moraines. The relationship, if any, of the icebergs nearer the Stewart Islands to moraines beneath the sea is uncertain. As observed earlier with regard to the glacier on the west side of Coburg Island, submarine moraines in front of Wilcox Glacier and Cory Glacier cannot be detected on aerial photographs taken under ice free conditions; e.g., during August 1959 (flight lines A16779 and 16787) and August 1971 (flight line A22540).

Acknowledgments

Comments which helped to clarify a number of points in this manuscript have been made by T.W. Anderson, B.G. Craig, D.A. Hodgson, and R.J. Richardson. The author is solely responsible, however, for its content.

References

Blake, W., Jr.
1970: Studies of glacial history in Arctic Canada. I. Pumice, radiocarbon dates and differential postglacial uplift in the eastern Queen Elizabeth Islands; Can. J. Earth Sci., v. 7, p. 634-664.

1975: Radiocarbon age determinations and postglacial emergence at Cape Storm, southern Ellesmere Island, Arctic Canada; Geogr. Ann., Ser. A, v. 57, p. 1-71.

Liestøl, O.
1972: Submarine moraines off the west coast of Spitsbergen; Nor. Polarinst., Årbok 1970, p. 165-168.

Løken, O.H.
1973: Bathymetric observations along the east coast of Baffin Island: submarine moraines and iceberg distribution; in Earth Science Symposium on Offshore Eastern Canada (Ottawa, February 1971), ed. P.J. Hood; Geol. Surv. Can., Paper 71-23, p. 509-519.

McGhee, R.
1975: An individual view of Canadian Eskimo prehistory; Can. Archaeol. Assoc., Bull. 7, p. 55-75.

54.

FOSSIL RECORD OF **CERATOPHYLLUM DEMERSUM** L., **ELATINE TRIANDRA** VAR. **AMERICANA** (PURSH) FASSETT, AND **LEERSIA ORYZOIDES** (L.) SWARTZ FROM THE MISSINAIBI FORMATION, NORTHERN ONTARIO

Project 690064

Sigrid Lichti-Federovich
Terrain Sciences Division

Interglacial peat beds from Moose River Crossing (50°19'N; 81°18'W) in northern Ontario are producing plant subfossils of considerable paleofloristic interest. An earlier discovery (Lichti-Federovich, 1974) of macrofossils of a species of southern affinity (**Najas guadalupensis**) in these Missinaibi Formation beds was explained in terms of extinction of a northern ecotype. The assemblage recorded to date, both as pollen and macrofossils, is predominantly of boreal affinity, with high pollen frequencies of spruce and pine.

Further analysis has yielded macrofossil finds of three species whose modern ranges do not extend north of the Clay Belt region of Ontario. These are **Ceratophyllum demersum** L., **Elatine triandra** var. **americana** (Pursh) Fassett, and **Leersia oryzoides** (L.) Swartz (Pl. 54.1, figs. 1-3).

Aquatic plants pose several interesting phytogeographical problems illustrated by these discoveries. There is growing evidence (e.g. Harms, 1969) that inadequate information exists about modern ranges of these plants in northern regions, compared with nonaquatic plants. This may be due to the neglect of aquatic habitats by some plant collectors for reasons of access, convenience, and safety. An example is **Ceratophyllum demersum** L. Harms (1969) records sites from Tanana River valley in Alaska which extended its range northward, and he indicates that it might well be expected elsewhere in Alaska and the Yukon. Its range in Canada (W. Cody, pers. comm., 1977) extends from Nova Scotia and the Great Lakes area to stations on the east and west sides of Lake Winnipeg in Manitoba; southern Alberta; southern British Columbia; and sites east, north, and west of Great Slave Lake, Northwest Territories. In light of these range extensions, the paleofloristic inference suggested by Terasmae and Craig (1958) for the record of this species in 5500-year-old lake sediments from a pingo east of Great Slave Lake might no longer be tenable.

The subfossil records for **Leersia oryzoides** and **Elatine triandra** are the first for North America. Watts (1970) found seeds of **Elatine minima** in full-glacial sediments from northwestern Georgia; however, seeds of **E. triandra** are distinguished readily from **E. minima** by their hexagonal surface reticulations. Both these species are at their northern limit in the Great Lakes area (Rousseau, 1974; Fernald, 1950; Mason, 1969; Fassett, 1940). It is significant that the centre of their distribution area is the southern deciduous forest and eastern prairie region – that is, they are not boreal species.

An interpretation of the records in the Missinaibi Formation beds, associated with species whose modern affinities are primarily boreal (Terasmae, 1958; Terasmae and Hughes, 1960), is not obvious. It is likely that these data add further evidence to the growing body of late Quaternary information that "our present plant communities have no long history in the Quaternary but are merely temporary aggregations under given conditions of climate, other environmental factors and historical factors" (West, 1964). In a recent review of North American late Wisconsin vegetation history, Wright (1976) has suggested that traditional pollen zoning has overemphasized relative stability rather than the more interesting times of dynamic alteration due to phytogeographic rather than climatic factors.

Macrofossil records provide information at the species level and precise ecological interpretations are possible, at least theoretically. **Ceratophyllum demersum**, however, has a wide modern geographical range, and the growing evidence indicates that it occurred in widely different environments throughout most of the Holocene. Ritchie and de Vries (1964) record it from late-glacial sediments in the Missouri Coteau, Saskatchewan. Watts and Bright (1968) found **Ceratophyllum demersum** in mid-postglacial sediments from Pickerel Lake, South Dakota; and the records referred to above by Terasmae and Craig (1958) are from a site near Great Slave Lake, Northwest Territories.

Apparently anomalous records such as those presented here force a re-evaluation of the traditional interpretation and in this particular case indicate that the flora and vegetation recorded in the Missinaibi sediments probably have no modern equivalent.

References

Fassett, N.C.
1940: A manual of aquatic plants; University of Wisconsin Press, Madison, 405 p.

Fernald, M.L.
1950: Gray's manual of botany; American Book Co., New York, 1632 p.

Harms, V.L.
1969: Range extensions for some Alaskan aquatic plants; Can. Field Natur., v. 83, p. 253-257.

Lichti-Federovich, S.
1974: **Najas guadalupensis** (Spreng.) Morong. in the Missinaibi Formation, northern Ontario; in Report of Activities, Part A, Geol. Surv. Can., Paper 74-1A, p. 201.

Mason, H.L.
1969: A flora of the marshes of California; University of California Press, Berkley and Los Angeles, 878 p.

Ritchie, J.C. and de Vries, B.
1964: Contributions to the Holocene paleoecology of west-central Canada. A late-glacial deposit from the Missouri Coteau; Can. J. Bot., v. 42, p. 677-692.

From: Report of Activities, Part B; Geol. Surv. Can., Paper 77-1B (1977)

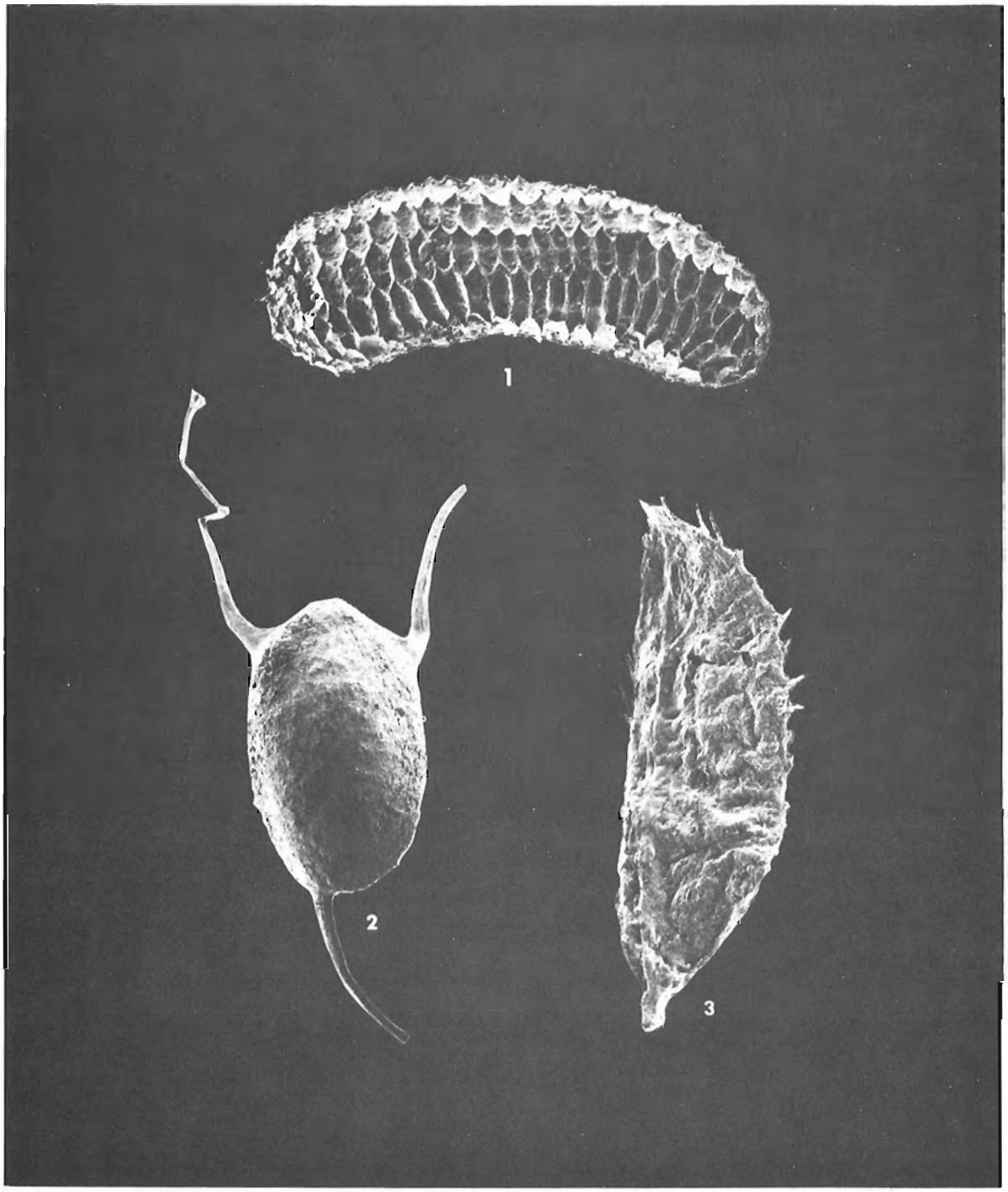

Plate 54.1. Scanning electron micrographs of fossil seeds from the Missinaibi Formation, northern Ontario.

fig. 1. **Elatine triandra** var. **americana** (Pursh) Fassett (x130)
fig. 2. **Ceratophyllum demersum** L. (x10)
fig. 3. **Leersia oryzoides** (L.) Sw. (x26)

Rousseau, C.
1974: Geographie Floristique du Quebec/Labrador; Travaux et Documents du Centre D'Etudes Nordiques, Laval Univ. Press, 799 p.

Terasmae, J.
1958: Non-glacial deposits along Missinaibi River, Ontario; in Contributions to Canadian palynology, Part III; Geol. Surv. Can., Bull. 146, p. 29-35.

Terasmae, J. and Craig, B.G.
1958: Discovery of fossil **Ceratophyllum demersum** L. in Northwest Territories, Canada; Can. J. Bot., v. 36, p. 567-569.

Terasmae, J. and Hughes, O.L.
1960: Pleistocene deposits in the James Bay Lowlands, Ontario; Geol. Surv. Can., Bull. 62, 15 p.

Watts, W.A.
1970: The full-glacial vegetation of northwestern Georgia; Ecology, v. 51, p. 17-33.

Watts, W.A. and Bright, R.C.
1968: Pollen, seed and mollusk analysis of a sediment core from Pickerel Lake, northeastern South Dakota; Geol. Soc. Am., Bull. 79, p. 855-876.

West, R.G.
1964: Inter-relations of ecology and Quaternary palaeobotany; J. Ecol., v. 52 (suppl.) p. 47-57.

Wright, H.E., Jr.
1976: The dynamic nature of Holocene vegetation. A problem in paleoclimatology, biogeography and stratigraphic nomenclature; Quat. Res., v. 6, p. 581-596.

55. ANOMALOUS URANIUM CONCENTRATIONS IN TILL NORTH OF BAKER LAKE, DISTRICT OF KEEWATIN

Project 690095

W.W. Shilts and C.M. Cunningham[1]
Terrain Sciences Division

Samples of till and sediments derived from till were collected during mapping of surficial geology in the vicinity of the Keewatin Ice Divide near Baker Lake (Cunningham and Shilts, 1977). Routine geochemical analyses were performed on the <2μ fractions of these samples, as have been done for samples collected since 1973 during Quaternary mapping projects in Keewatin. Comparison of uranium values in these samples with a few samples collected by A.N. Boydell in 1973 and with several thousand samples collected by R.A. Klassen in 1975-1976 over areas of high uranium potential at the easternmost end of the Dubawnt Group (Helikian age) shows that the area directly north of Baker Lake and east of Thelon River is covered by tills containing anomalously high amounts of uranium in association with high contents of zinc and molybdenum.

Figure 55.1 shows the distribution of uranium and molybdenum values from the <2μ fractions of drift. Most of the samples are till, but some, particularly near Whitehills Lake and the west end of Baker Lake, are of questionable genesis and probably represent marine sediments or till reworked by marine processes. The metal contents of three samples of gossanous mud also are indicated in Figure 55.1. The outcrop areas of Aphebian age quartzites and related rocks and of Dubawnt Group sedimentary and volcanic rocks are generalized from Wright's (1967) map.

The last position of the Keewatin Ice Divide roughly follows an arc drawn from Pitz Lake through Whitehills Lake and along the Aphebian quartzite ridge across Quoich River. Prior to the migration of the divide from

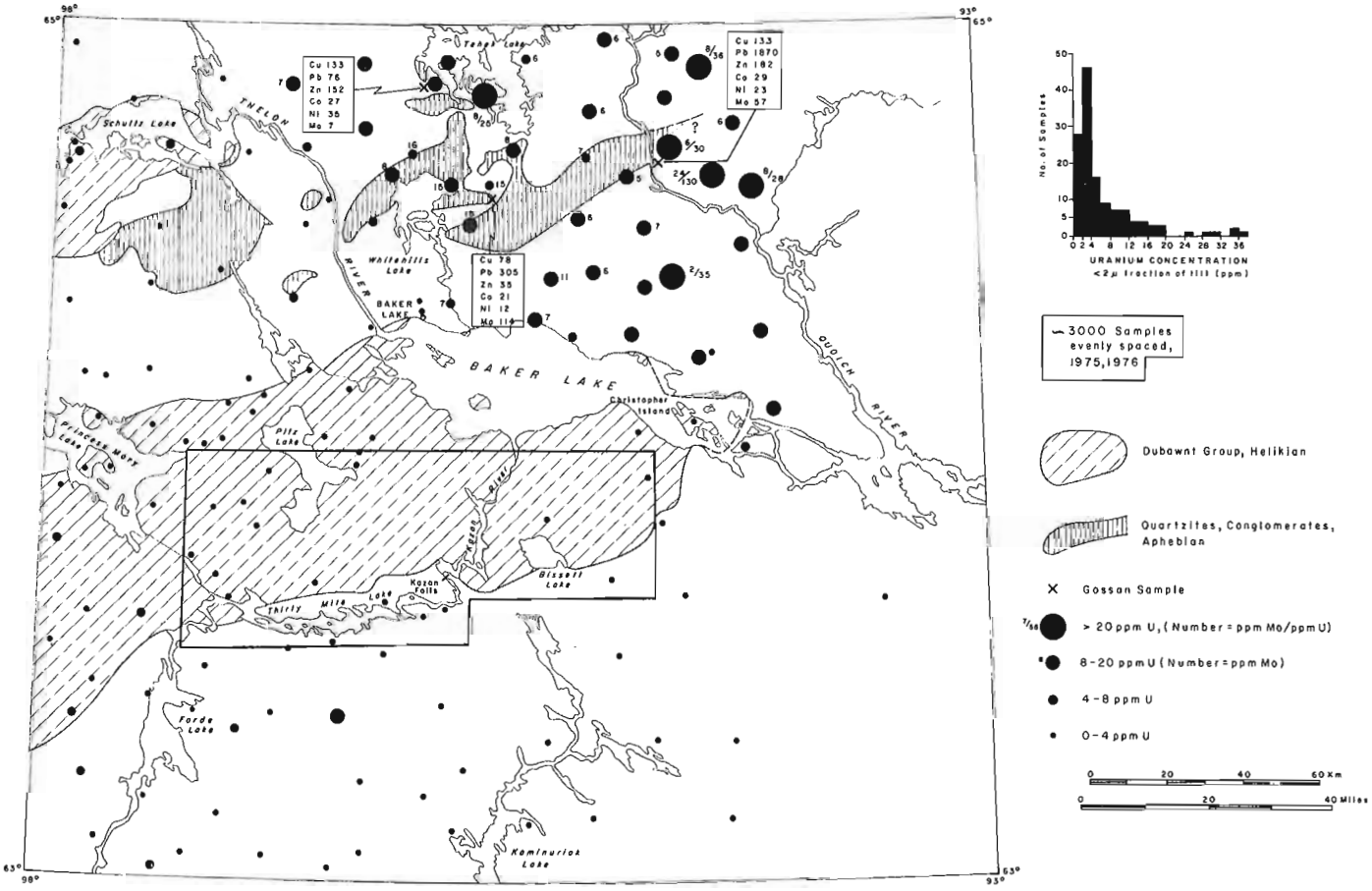

Figure 55.1. Uranium concentrations in <2μ fraction of till samples, Baker Lake area. Note uniformly high uranium concentrations north of Baker Lake and east of Thelon River. Samples from the area between Whitehills Lake and Tehek Lake and southeast of that area also are enriched in Mo and Zn. Fewer than 10 of 3000 samples collected by R.A. Klassen in the outlined area have values above 8 ppm U, although several zones of uranium mineralization occur between Bissett Lake and Kazan Falls and on or near Christopher Island. All samples shown in the figure were collected by C.M. Cunningham and A.N. Boydell.

[1] Department of Geology, University of Massachusetts, Amherst, Massachusetts

north and west into the map area, flow was generally south to southeast. At the time when the ice divide was in the area, however, flow directions changed frequently making studies of the nature of glacial dispersal difficult.

Till samples with anomalous uranium contents are highly enriched compared to the thousands of samples collected elsewhere in Keewatin (cf. Shilts and Klassen, 1976; Klassen and Shilts, 1977). Furthermore, they are confined almost entirely to the area east of Thelon River and north of Baker Lake. Most of the samples with high uranium concentrations also are associated with abnormally high Mo and Zn values, and the tills in the anomalous area generally contain more iron than those outside. In contrast, of the approximately 3000 samples collected on one-mile centres by R.A. Klassen in 1975-1976 in the area indicated in Figure 55.1, fewer than 10 had values higher than 8 ppm U and none were over ∿ 10 ppm U. Although Mo was only measured on a few hundred of those samples chosen at random, in all cases it was below 2 ppm.

Discussion: Origin of Elevated Uranium Contents of Till

The high uranium contents in the <2μ fraction of till may result from one or more of the following: (1) derivation from rocks intruding or forming a part of the Archean basement. Likely sources may be unmapped occurrences of fluorite-bearing granites or syenites that contain elevated uranium values; (2) derivation from presently unknown uranium-bearing beds within the Aphebian quartzites and related rocks – both those shown on Figure 55.1 and similar outcrops directly north of the map area in the Amer Lake area; and (3) the high uranium contents may not be related directly to bedrock sources at all but may be caused by enhanced cation exchange capacity resulting from some uniform mineralogical difference between these tills and surrounding tills with low uranium contents. Although Zn, Mo, and Fe show enrichment roughly corresponding to that of uranium, the elements Cu, Ni, Co, Pb, Mn, and Cd show no corresponding enrichment, making this possibility less likely than the first two.

If the source of the uranium is in some discrete area(s) of bedrock, glacial dispersal probably has spread the detritus southward, which seems to be the predominant direction of effective glacial transport at and south of this latitude, in spite of evidence of northward flow associated with the ice divide.

An alternative explanation of the pattern observed would be that the distance of detectable glacial dispersal was much less than the spacing of samples on this grid (8 to 25 km) so that each value shown represents essentially "local" bedrock sources. Such an interpretation would imply that virtually all rocks of the map area are likely to carry enhanced uranium concentrations. However, this is known to be incorrect at the east end of Baker Lake where uranium-depleted granulites (0.1 to 2 ppm U) underlie glacial deposits which contain 8 to 20 ppm U (M. Schau, pers. comm., 1977).

Of the various possible origins of uranium enrichment in the tills of this area, the authors favour the interpretation that, although some mineralization of the basement may be contributing uranium, the bulk of the uranium has been derived from sources within the Aphebian quartzites. Although not associated with high uranium values, molybdenum is enriched in two gossans in the vicinity of Aphebian quartzite outcrops. Consequently, the observation that Mo occurs in elevated amounts in uranium-rich tills may support the interpretation that both elements come from the same general source area. In addition, similar quartzites are known to be associated with uranium mineralization in the Amer Lake area and elsewhere in Keewatin. Thus, the pattern may represent a complex uranium dispersal train of significant size and probably several sources.

Conclusions

The U content of the clay (<2μ) fraction of tills north of Baker Lake is greater than that of tills in any area measured to date; values >15 ppm are unusual even in proximity to uranium mineralization, and no values that high have been measured in the several thousand samples collected in outcrop areas of the Dubawnt Group south of Baker Lake, an area with several known uranium showings and an area of great economic interest. The size of the anomalous area and magnitude of the anomalies, however, cannot be related easily to economic potential. It is possible that the Aphebian quartzites of the Baker Lake map area (NTS 56 D) contain uranium mineralization in association with Mo and Zn, particularly in the vicinities east of Whitehills Lake and southwest of Tehek Lake. Alternatively, uranium may be enriched in many areas within the Archean basement and Aphebian quartzites.

Properly documented drift samples collected at wide intervals during routine geological mapping can be of great regional geochemical interest, and may outline areas of interest for future mineral exploration.

Acknowledgments

This report has been reviewed by R.N.W. DiLabio, R.A. Klassen, M. Schau, R. Ridler, and R.J. Fulton.

References

Cunningham, C.M. and Shilts, W.W.
1977: Surficial geology of the Baker Lake area, District of Keewatin; in Report of Activities, Part B, Geol. Surv. Can., Paper 77-1B, rep. 59.

Klassen, R.A. and Shilts, W.W.
1977: Uranium exploration using till, District of Keewatin; in Report of Activities, Part A, Geol. Surv. Can., Paper 77-1A, p. 471-477.

Shilts, W.W. and Klassen, R.A.
1976: Drift prospecting in the District of Keewatin - uranium and base metals; in Report of Activities, Part A, Geol. Surv. Can., Paper 76-1A, p. 255-257.

Wright, G.M.
1967: Geology of the southeastern barren grounds, parts of the Districts of Mackenzie and Keewatin; Geol. Surv. Can., Mem. 350, 91 p.

ELECTRICAL PARAMETER CONVERSION TABLE II

Project 630049

T.J. Katsube
Resource Geophysics and Geochemistry Division

Introduction

An electrical parameter conversion table has been described by Katsube (1975). Electrical measurements are made in a large variety of fields and investigators frequently use a different combination of electrical parameters to present their results. The method of data display depends on the application of the method and the objective of the measurement. Results of all investigations are significant to one another even though the field of investigation may be different. The purpose of a conversion table is to make it easy to relate the results from one investigation to another. Significant developments in electrical measurements have taken place in the fields of geophysics, biophysics, electrochemistry and ceramics since the last conversion table was published. It is necessary to produce an updated version of the table.

Direct measurements have usually appeared in terms of complex resistivity amplitude and phase-shift (Vector-impedance meters) or dielectric constant and dissipation factor (capacitance bridges and Q-meters). Results of investigations are often produced in terms of real and imaginary permittivity (e.g. Cole and Cole, 1941; Einolf and Carstensen, 1971; physics and chemistry), real and imaginary conductivity (Bauerle, 1969; electrochemistry) and real and imaginary resistivity (Zonge, In situ mineral discrimination using a complex resistivity method; Presented at the 42nd Annual International Meeting of the Society of Exploration Geophysicists, Anaheim, Calif., Nov. 26-30, 1972; Wynn and Zonge, 1975; geophysics). The parameters used in the Electrical Rock Property Laboratory of the Geological Survey are real relative permittivity and resistivity of a parallel RC circuit (Katsube, 1977).

Acknowledgments

Thanks are expressed to A.P. Annan and W.J. Scott for their criticisms regarding the format of this paper.

Basic Equations

When an alternating voltage (v) at same frequency (f) is applied across a rock sample both ohmic (I_1) and displacement currents (I_C) are observed. The I_1 is in-phase, but I_C is 90° out-of-phase with v so that the total current (I) shows a phase-shift of θ and is expressed as follows:

$$I = I_1 + jI_C = I \angle \theta$$

$$I_1 = I \cos \theta$$

$$I_C = I \sin \theta$$

Since both I_1 and I_C traverse a rock sample it can be simulated for that frequency by a RC parallel circuit with R_x and C_x being the components. Their values are determined by,

$$R_x = \frac{V}{I_1}$$

$$C_x = \frac{I_C}{2\pi f V}$$

All parameters that are used to express the electrical characteristics of rocks are volume independent parameters such as resistivity (ρ_x), permittivity (ε_x) and relative permittivity (K_x), and are related to the actually measured parameters by the following equations

$$\rho_x = kR_x \text{ (ohm metres)}$$

$$\varepsilon_x = C_x/k \text{ (Farads/metre)}$$

$$K_x = \varepsilon_x/\varepsilon_o = C_x/k\varepsilon_o$$

where

$k = \frac{A}{d}$: geometric factor

ε_o = 8.854E-12: permittivity of air or vacuum

A : area of specimen cross-section

d : thickness of specimen

Complex resistivity (ρ^*), complex conductivity (σ^*) and complex relative permittivity (K^*) are the commonly used parametric expressions:

$$\rho^* = \rho' - j\rho'' \quad (1)$$

$$\sigma^* = \sigma' + j\sigma'' \quad (2)$$

$$K^* = K' - jK'' \quad (3)$$

$j^2 = -1$

ρ', ρ'' : real and imaginary resistivity

σ', σ'' : real and imaginary conductivity

K', K'' : real and imaginary relative permittivity

By definition

$$K' = K_x \quad (4)$$

$$\sigma' = 1/\rho_x$$

Also by definition the following two relationships exist:

$$\sigma^* = j\omega K^* \varepsilon_o \quad (5)$$

$$\rho^* = \frac{1}{\sigma^*} \quad (6)$$

ω : angular frequency

From: Report of Activities, Part B; Geol. Surv. Can., Paper 77-1B (1977)

Table 56.1

Electrical Parameter Conversion Table

Parameters \ Combinations	$\rho_x \quad \kappa_x$	$\lvert\rho^*\rvert \quad \theta$	$\kappa' \quad D$	$\rho' \quad \rho''$	$\sigma' \quad \sigma''$	$\kappa' \quad \kappa''$
D, tan δ	$\frac{1}{\omega \rho_x \kappa_x \epsilon_o}$	$\frac{1}{\tan \theta}$	———	$\frac{\rho'}{\rho''}$	$\frac{\sigma'}{\sigma''}$	$\frac{\kappa''}{\kappa'}$
$\lvert\sigma^*\rvert$	$\frac{\sqrt{1+(\omega \rho_x \kappa_x \epsilon_o)^2}}{\rho_x}$	$\frac{1}{\rho^*}$	$\omega \kappa' \epsilon_o \sqrt{1+D^2}$	$\frac{1}{\sqrt{(\rho')^2+(\rho'')^2}}$	$\sqrt{(\sigma')^2+(\sigma'')^2}$	$\omega \epsilon_o \sqrt{(\kappa')^2+(\kappa'')^2}$
σ'	$\frac{1}{\rho_x}$	$\frac{\cos \theta}{\rho^*}$	$\omega \kappa' \epsilon_o D$	$\frac{\rho'}{(\rho')^2+(\rho'')^2}$	———	$\omega \kappa'' \epsilon_o$
σ''	$\omega \kappa_x \epsilon_o$	$\frac{\sin \theta}{\rho^*}$	$\omega \kappa' \epsilon_o$	$\frac{\rho''}{(\rho')^2+(\rho'')^2}$	———	$\omega \kappa' \epsilon_o$
$\lvert\kappa^*\rvert$	$\frac{\sqrt{1+(\omega \rho_x \kappa_x \epsilon_o)^2}}{\omega \rho_x \epsilon_o}$	$\frac{1}{\omega \rho^* \epsilon_o}$	$\kappa' \sqrt{1+D^2}$	$\frac{1}{\omega \epsilon_o \sqrt{(\rho')^2+(\rho'')^2}}$	$\frac{\sqrt{(\sigma')^2+(\sigma'')^2}}{\omega \epsilon_o}$	$\sqrt{(\kappa')^2+(\kappa'')^2}$
κ'	κ_x	$\frac{\sin \theta}{\omega \rho^* \epsilon_o}$	———	$\frac{\rho''}{\omega \epsilon_o [(\rho')^2+(\rho'')^2]}$	$\frac{\sigma''}{\omega \epsilon_o}$	———
κ''	$\frac{1}{\omega \rho_x \epsilon_x}$	$\frac{\cos \theta}{\omega \rho^* \epsilon_o}$	$\kappa' D$	$\frac{\rho'}{\omega \epsilon_o [(\rho')^2+(\rho'')^2]}$	$\frac{\sigma'}{\omega \epsilon_o}$	———
$\lvert\rho^*\rvert$	$\frac{\rho_x}{\sqrt{1+(\omega \rho_x \kappa_x \epsilon_o)^2}}$	———	$\frac{1}{\omega \kappa' \epsilon_o \sqrt{1+D^2}}$	$\sqrt{(\rho')^2+(\rho'')^2}$	$\frac{1}{\sqrt{(\sigma')^2+(\sigma'')^2}}$	$\frac{1}{\omega \epsilon_o \sqrt{(\kappa')^2+(\kappa'')^2}}$
ρ'	$\frac{\rho_x}{1+(\omega \rho_x \kappa_x \epsilon_o)^2}$	$\rho^* \cos \theta$	$\frac{D}{\omega \kappa' \epsilon_o (1+D^2)}$	———	$\frac{\sigma'}{(\sigma')^2+(\sigma'')^2}$	$\frac{\kappa''}{\omega \epsilon_o [(\kappa')^2+(\kappa'')^2]}$
ρ''	$\frac{\omega \rho_x^2 \kappa_x \epsilon_o}{1+(\omega \rho_x \kappa_x \epsilon_o)^2}$	$\rho^* \sin \theta$	$\frac{1}{\omega \kappa' \epsilon_o (1+D^2)}$	———	$\frac{\sigma''}{(\sigma')^2+(\sigma'')^2}$	$\frac{\kappa'}{\omega \epsilon_o [(\kappa')^2+(\kappa'')^2]}$
ρ_x	———	$\frac{\rho^*}{\cos \theta}$	$\frac{1}{\omega \kappa' \epsilon_o D}$	$\frac{(\rho')^2+(\rho'')^2}{\rho'}$	$\frac{1}{\sigma'}$	$\frac{1}{\omega \kappa'' \epsilon_o}$
κ_x	———	$\frac{\sin \theta}{\omega \rho^* \epsilon_o}$	———	$\frac{\rho''}{\omega \epsilon_o [(\rho')^2+(\rho'')^2]}$	$\frac{\sigma''}{\omega \epsilon_o}$	κ'
θ	$\tan^{-1}(\omega \rho_x \kappa_x \epsilon_o)$	———	$\frac{\pi}{2} - \tan^{-1} D$	$\frac{\pi}{2} - \tan^{-1}(\frac{\rho'}{\rho''})$	$\frac{\pi}{2} - \tan^{-1}(\frac{\sigma'}{\sigma''})$	$\frac{\pi}{2} - \tan^{-1}(\frac{\kappa''}{\kappa'})$

The dissipation factor (D) or loss tangent (tan δ) is defined by

$$D = \tan \delta = \frac{\rho'}{\rho''} = \frac{\sigma'}{\sigma''} = \frac{K''}{K'} \qquad (7)$$

The equations in Table 56.1 are derived from equations 1 through 7.

References

Bauerle, J.E.
1969: Study of solid electrolyte polarization by a complex admittance method; J. Phys. Chem. Solids, v. 30, p. 2657-2670.

Cole, K.S. and Cole, R.H.
1941: Dispersion and adsorption in dielectrics: I. Alternating current characteristics; J. Chem. Phys., v. 9, p. 341-351.

Einolf, C.W., Jr. and Carstensen, E.L.
1971: Low-frequency dielectric dispersion in suspensions of ion-exchange resins; J. Phys. Chem., v. 75, p. 1091-1099.

Katsube, T.J.
1975: Electrical parameter conversion table; in Report of Activities, Part A, Geol. Surv. Can., Paper 75-1A, p. 26-27.

1977: Electrical properties of rocks; Proc. Induced Polarization for Exploration Geologists and Geophysicists; Univ. of Arizona, Mar. 14-16.

Wynn, J.C. and Zonge, K.L.
1975: EM coupling, its intrinsic value, its removal and the cultural coupling problem; Geophysics, v. 40, p. 851-864.

Project 740052

Peter Fransham and Denis Battrum [1]
Terrain Sciences Division

Introduction

General

The sensitive clays of eastern Canada are susceptible to slope instability. The determination of the degree of stability of a slope requires an appropriate anayltical model which adequately represents the slope failure mechanism. Input factors into such a model are: slope geometry, stratigraphy, strength parameters for each soil layer, and an estimate of the pore pressures acting along a potential failure plane. Obtaining the actual pore pressure distribution in a slope requires the installation and monitoring of a series of piezometers – a procedure which is both time-consuming and expensive. On a regional scale it is impractical to instrument every potentially critical slope; therefore the slopes investigated in Ottawa Valley were classified into two groups according to their stratigraphy. Typical slopes of each group were monitored, and the data can be extrapolated with a reasonable amount of confidence to other slopes in the region.

Classification of Clay Slopes and Soil Descriptions

The division of sensitive clay slopes into two groups or geological settings was based on data collected during a drilling and mapping project covering Ottawa Valley (Fransham et al., 1976). Typical profiles of the two settings are shown in Figure 57.1. The main difference between the two is the existence of a sand and a clay and silt layer on the surface of setting type A as compared to setting type B which has desiccated clay as an upper layer. The sand acts as a groundwater reservoir thereby maintaining a high water table and saturated conditions in the underlying clay. The desiccated crust is fissured and somewhat more permeable than the intact clay but cannot store a significant volume of water to maintain saturated conditions near the surface. The red-grey colour banded clay and the massive grey clay are not thought to be sufficiently layered to create an anisotropic permeability. On the other hand the banded silt and clay and the varved clay can be expected to have a coefficient of horizontal permeability higher than the vertical permeability.

The till ranges from sandy to silty. Because it is a mixture of sand, silt, and boulders, a relatively low coefficient of permeability can be expected due to its low porosity. During drilling operations open fractures were encountered in the bedrock in some holes, and all the drilling water was lost. The drill rig pump has a capacity of 500 gpm, thus the effective permeability of the fractured bedrock must be relatively high.

All irregularities on the bedrock surface have been ignored for the purpose of this study. This is not the general case in the field where the bedrock surface is undulating and contains many scarps and valleys. A flat bedrock surface does not represent too serious a simplification as some knowledge of the bedrock profile has to be established before a stability analysis can be carried out. The pore pressure profile can be modified assuming that the bedrock is a significant aquifer with permeabilities much higher than the overlying clay. Before an estimate of the pore pressures is made, judgment also is needed concerning the relative influence on the pore pressure distribution of: slope geometry, thickness of overburden, location of any groundwater discharge, and depth of erosion of streams at the toe of the slope.

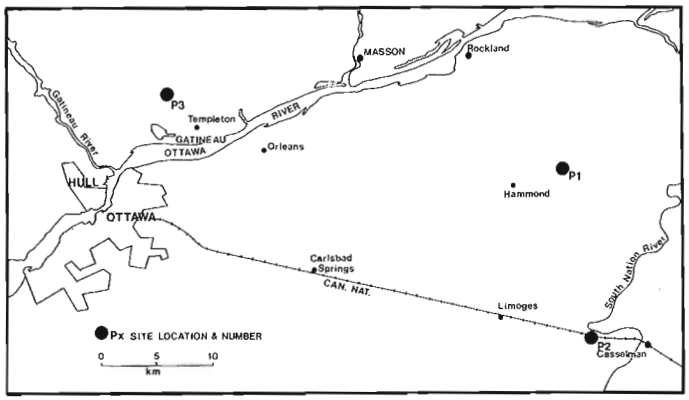

Figure 57.1. Location of instrumented slopes.

Site Locations

Setting Type A

Two sites (P1 and P2) of this geologic setting were instrumented with piezometers; their locations and that of the third site are shown in Figure 57.2. Nine piezometers were installed at location P1: four were at the crest of the slope, three at the midslope, and two at the toe of the slope. At each of the three piezometer locations perforated pipes were driven to a depth of 3 m and served to measure the surface water table elevations. Ten piezometers were installed at site P2: one group of five piezometers was near the crest of the slope, and another group of five piezometers was about 200 m back from the crest. The slope profiles, piezometer elevations, mean pressure heads for each piezometer, and the site stratigraphy for sites P1 and P2 are shown in Figures 57.3 and 57.4 respectively.

Setting Type B

Site P3 is located on the Quebec side of Ottawa River. Nine piezometers were installed on the slope: three at the crest, three at the midslope, and three at the toe. The site profile and mean pressure heads are shown in Figure 57.5. Because a few problems were encountered at this site, the data for site P3 are not as complete as for the other two sites. The piezometers were installed in 1974,

[1] Department of Geology, Queen's University, Kingston, Ontario

From: Report of Activities, Part B
Geol. Surv. Can., Paper 77-1B (1977)

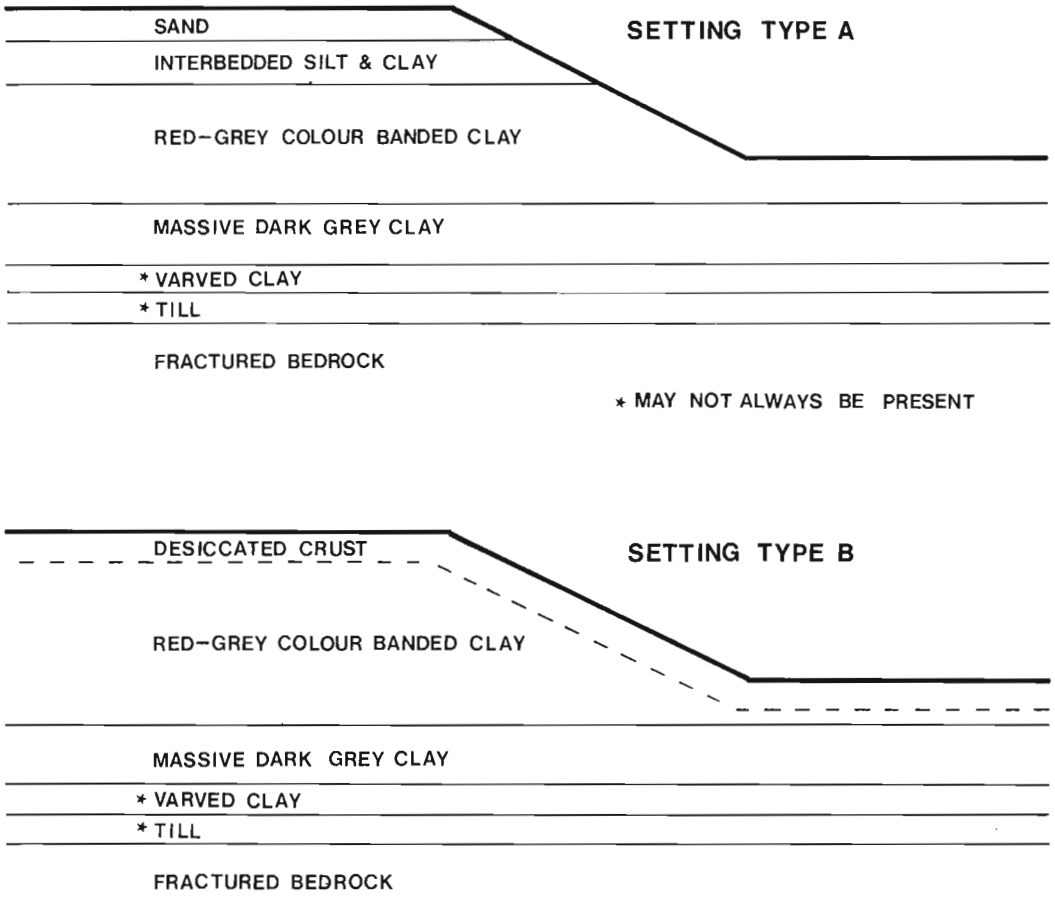

Figure 57.2
Geological settings of sensitive clay slopes.

and the set on the midslope subsequently had become obscured with soil and grass. These piezometers were not located until late in the field season, and only one set of readings was obtained. One of the piezometers at the crest became blocked and was useless for any further readings. Accessibility to the toe of the slope was poor, and readings were difficult to obtain.

Instrumentation

General

Considerable research has been done on the design of piezometers and the relative benefits of each design (Lindberg, 1965; Hvorslev, 1951). Hvorslev (1951) stated that "the total volume or flow of water required for equalization of differences in hydrostatic pressure in the soil and in the measuring device depends primarily on the permeability of the soil, the type and dimensions of the device, and on the hydrostatic pressure difference." The volume of water required to equalize the pressure difference, therefore, should be kept to an absolute minimum and the intake screen should be large so that the water involved in the equalization can be drawn from a greater volume of soil. It is also important that no seepage occurs along the piezometer-soil interface otherwise the pressure head will be influenced by seepage to or from strata other than the one in which the piezometer is set.

Piezometer Design

The piezometer is essentially a well point grouted into the soil or rock at the required depth. A schematic diagram of the piezometer design is shown in Figure 57.6A. The design is much the same as that described by Brooker et al. (1968) with the exception of the procedures described below, which were followed to ensure that no seepage occurred along the soil-piezometer boundary. A 13 cm-diameter borehole was drilled to the required depth; unless the soil was sufficiently stiff, steel casing was used to support the walls of the hole. A known volume of silica sand was poured down the hole to form a sand filter between the clay and the well point. A 5 cm-diameter well point was attached to a steel pipe of similar diameter, and a large rubber stopper was placed at the top of the well point. The stopper acted as a seal between the casing and the piezometer and helped to carry any sand down the hole that might have become lodged in the side of the casing. The rubber also kept the bentonite balls, which were added above the rubber seal, from falling down around the well screen. A steel washer placed between the stopper and the bentonite balls gave the rubber a certain amount of rigidity and prevented it from being displaced. A similar steel washer welded 30 cm above the rubber stopper confined the bentonite balls in the vertical direction and allowed the balls to expand laterally to form a good seal between the piezometer and the soil. Once the piezometer was at the required depth a cement-bentonite grout was pumped down between the

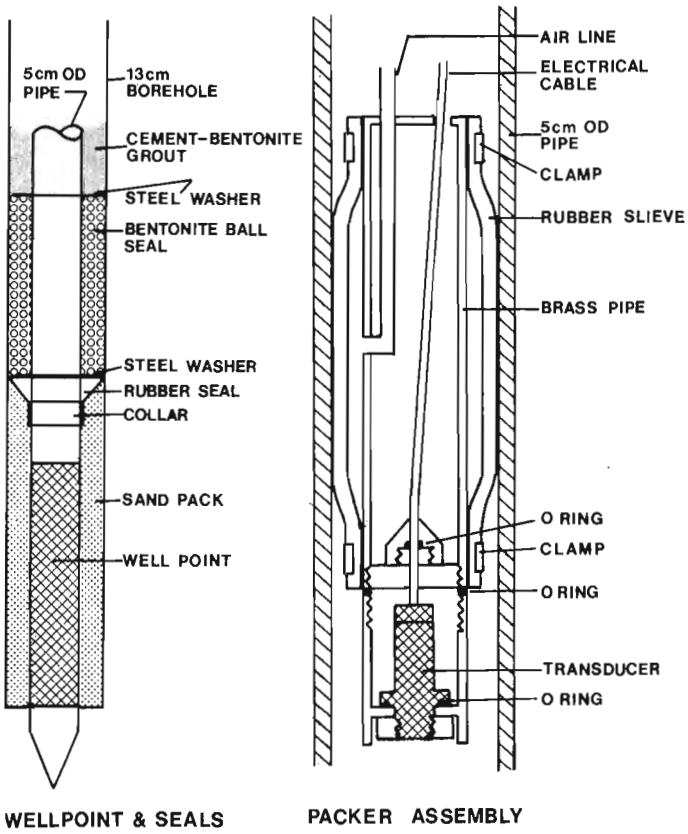

Figure 57.3. Piezometer design.

casing and the piezometer. The casing was then removed, and the hole was filled to the top with grout leaving only the 5 cm pipe showing above ground level. The entire piezometer then was flushed out with clean water, thereby removing any soil which may have entered the piezometer during installation.

Pore Pressure Measurement

An inflatable packer with an electrical transducer (see Fig. 57.6B) was lowered into the piezometer to a depth just above the well screen. The packer then was inflated by air pressure resulting in an instantaneous increase in pore pressure due to the volume of water displaced by the packer. The pressure then decreased to some equilibrium value which equals the pore pressure in the surrounding soil mass. The time required for equalization depends on the permeability of the soil or rock, the geometry of the piezometer, and the response of the packer to the inflation pressure.

Figure 57.7 shows two examples of pressure equalization curves. The bedrock in this case is highly fractured and therefore is permeable. The pressure-time curve decreases rapidly to the equilibrium pressure in six minutes. For the relatively impermeable clay, the decrease is much slower, requiring at least an hour before equilibrium is reached. Experiments are now underway to determine if some relationship can be obtained which will relate the pressure equilibrium curves to the permeability of the soil.

The advantage of this measuring system is that once the packer is inflated it seals off the rest of the pipe from the soil. Because the volume of water required to activate the pressure transducer is small, the response time for changes in the pore pressure in the soil should be rapid.

The main disadvantage of this system is the volume of electronics which are part of the recording unit. A schematic diagram of the apparatus is shown in Figure 57.8. An attempt was made to reduce the size of the generator to 300 watts; however, the voltage was too erratic to allow for accurate readings. The Hewlett Packard Chart recorder, measuring about 15 cm on each side, is about the smallest usable machine available. Some saving in bulkiness may be had by eliminating the DC voltmeter and obtaining a smaller ampliifer. These reductions in size would be marginal and do not represent a major improvement in the equipment design. A more useful change would be to use a pneumatic transducer which would eliminate the need for any electronic equipment. The entire apparatus then could be reduced to a small read-out box and a cylinder of gas to pressurize the packer. Another disadvantage of this system is the length of time required to obtain one reading in clay; generally about one hour is required before equalization is reached therefore restricting the number of piezometers that can be read in a given time period. It would be far more efficient to have several packers, which could be inflated, thereby increasing the number of readings per day. Pneumatic transducers are relativley inexpensive, and the cost for three packer assemblies would be about the same as one electrical transducer packer. Considering the savings in cost and size of the equipment, it would be preferable to change the system over to a series of pneumatic transducer packers.

Results and Discussions

General

The general case of downdrainage in slopes of Ottawa Valley has been reported by various investigators (Jarrett and Eden, 1970; Lefebvre et al., 1976) and was found in the slopes instrumented for this study. For stability calculations the maximum recorded value of pore

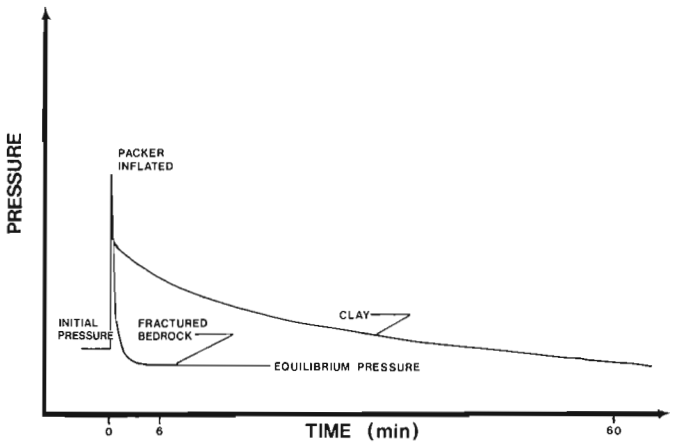

Figure 57.4. Pressure-time curves for clay and fractured bedrock

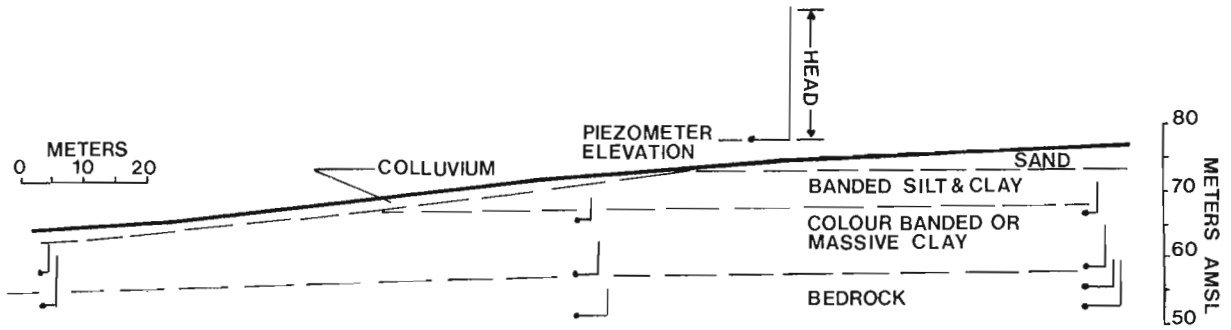

Figure 57.5. Site P1, profile and mean heads.

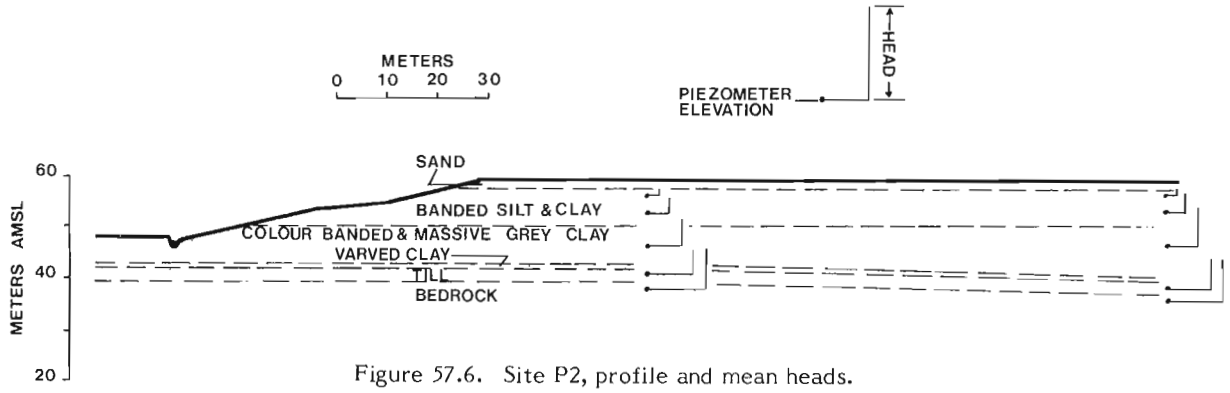

Figure 57.6. Site P2, profile and mean heads.

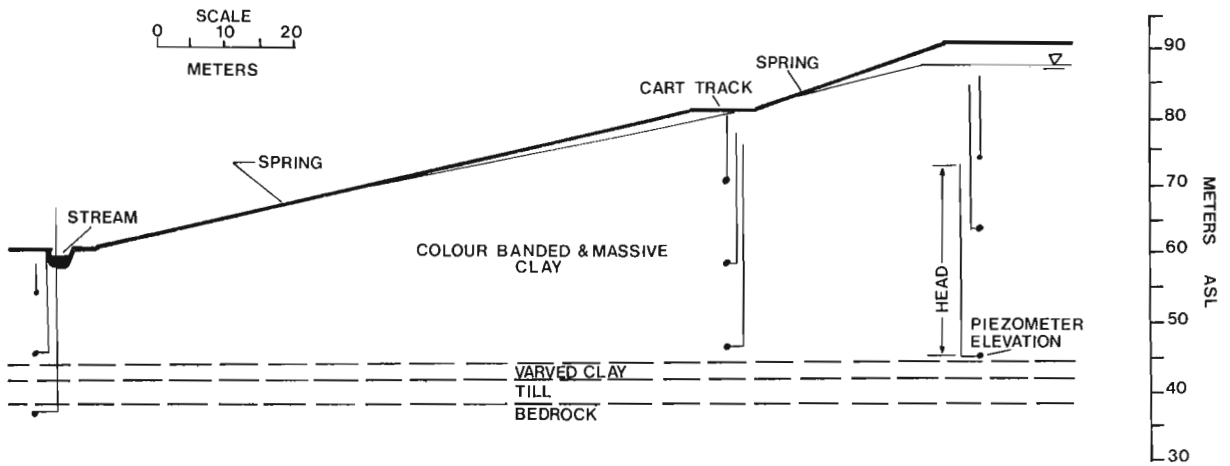

Figure 57.7. Site P3, profile and mean heads.

pressure is critical. A statistical approach is being formulated which will allow for a better estimate of the pore pressure variability and the probability of attaining a maximum value. Only the mean pore pressure will be discussed here so that the general trends of the pore pressure with depth can be seen.

Type A

Figures 57.3 and 57.4 illustrate the main results for the two slopes falling into this group. The difference in vertical gradient is of the order of 1 and in horizontal gradient is about 0.025. This difference in gradients results in flow being almost vertical downward, with only a minor component in the horizontal direction. The results from the piezometer nest at the toe of site P1 shows that the vertical gradients are smaller at the toe of the slope than at the crest of midslope. In wet periods the pore pressures at the toe of the slope approach hydrostatic. No piezometers were installed at the toe of site P2. Because the horizontal gradients are small, however, if an extrapolation were made to the toe area, the pore pressures likely would be hydrostatic and the heads would be close to the level of the small stream at the toe.

Type B

The pore pressure distribution at this site is somewhat different from that at the previous two sites. Downdrainage again was identified at the crest of the slope; however, the toe had artesian pressures. This type of distribution is similar to the neoclassical flow patterns in slopes which have been described by Patten and Hendron (1974). The artesian pressures dissipate near the toe if the depth of river erosion at the base of the slope intersects the fractured bedrock surface (Scott et al., 1976).

Groundwater Development with Time

It is interesting to speculate on the history of groundwater development in Ottawa Valley and how the pore pressure distribution has changed with time. During its early stages Ottawa River meandered and cut several broad channels in Champlain Sea sediments. At this stage the slopes were submerged completely, and no groundwater flow took place. As the land rose, the water level in the channels dropped and mainly hydrostatic conditions prevailed in the portion of the slope above river level. In the final stage, which is in effect today, the rivers and streams have eroded down to bedrock and are able to maintain a lower piezometric surface in the bedrock than in the upland plains. Major rivers are the ultimate local groundwater discharge, and their surface elevations have a strong influence on the piezometric elevation in the surrounding bedrock and clay.

Influence of the Pore Pressure Distribution on the Stability of Natural Slopes

The critical stage for slope instability in the history of Ottawa Valley was when the groundwater profile was essentially hydrostatic. Before this time the slopes were submerged completely and were somewhat stable.

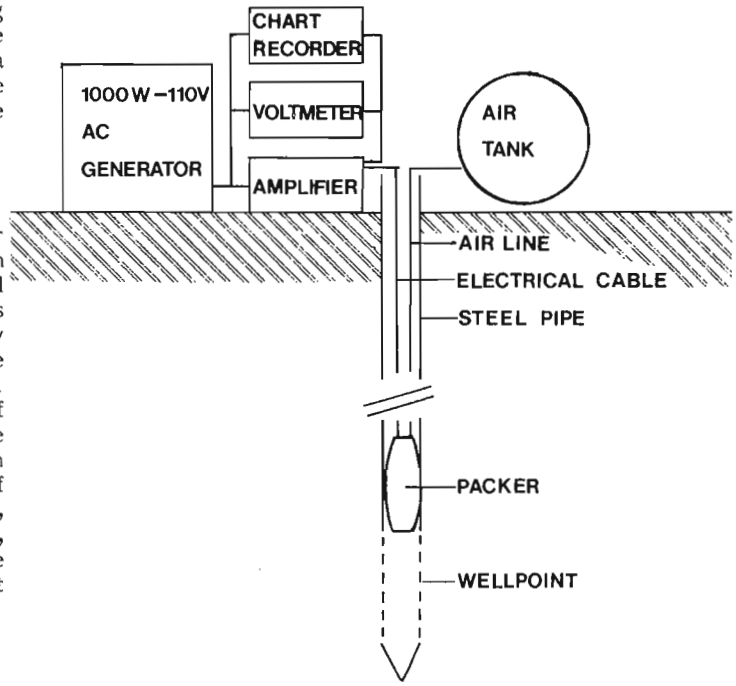

Figure 57.8. Equipment schematic.

The slopes are subjected to downdraining which adds to the overall stability. During periods of prolonged wetness the pressures in the upper part of the soil profile approach hydrostatic, thereby reverting to conditions favourable for instability; however, the clay has been overconsolidated due to the increase in effective stresses resulting from the downward flow. Thus the clays may be somewhat stronger than they were before consolidation. The increase in strength with time may not allow for the development of the extemely large slides like those which have occurred in the past. Groundwater fluctuations, however, may trigger smaller slides like the South Nation River Slide of 1971. The moments resisting failure along the critical failure circle will be dependent partly on the pore pressure distribution in the slope. As the portion of the slope that is subject to near hydrostatic conditions increases, therefore, the probability of failure also increase. This would explain why most slope failures occur during spring when the water table is high and pore pressures are maximum.

References

Brooker, E.W., Scott, J.S. and Ali, P.
1968: Transducer piezometer for clay shales; Can. Geotech. J., p. 256-264.

Fransham, P.B., Gadd, N.R., and Carr, P.A.
1976: Distribution of sensitive clay deposits and asociated landslides in the Ottawa Valley; Geol. Surv. Can., Open File 352.

Hvorslev, M. Juul.
1951: Time lag and soil permeability in groundwater observations; U.S. Army Eng. Waterw. Exp. Stn., Bull. 36.

Jarrett, P.M. and Eden, W.J.
1970: Groundwater flow in eastern Ottawa; Can. Geotech. J., v. 7, p. 326-333.

Lefebvre, G., Lafleur, J., and Chagnon, J.Y.
1976: Vertical drainage as a stabilizing agent in a clay slope at Hull, Quebec; Proc. 29th Can. Geotech. Conf., session 6, p. 16-30.

Lindberg, D.A.
1965: Comparative aspects of five piezometer designs; unpubl. M.Sc. thesis, Dep. of Civil Eng., University of Alberta, Edmonton.

Patten, F.D. and Hendron, A.J., Jr.
1974: General report of "mass movements"; Proc. 2nd Int. Congr., Int. Assoc. Eng. Geol., v. 2, p. 1-57.

Scott, J.D., Shields, D.H., and Bauer, G.E.
1976: Stability of natural slopes of Champlain Sea clay in the Ottawa-Hull region; Proc. 29th Can. Geotech. Conf., session 11, p. 24-36.

58. THE CELIBETA STRUCTURE COMPARED WITH OTHER BASEMENT STRUCTURES ON THE FLANKS OF THE TATHLINA HIGH, DISTRICT OF MACKENZIE

Projects 710011 and 710033

G.K. Williams
Institute of Sedimentary and Petroleum Geology, Calgary

Introduction

This study began as an attempt to understand the Celibeta structure, located on the western end of the Tathlina High in the southern part of the District of Mackenzie, Northwest Territories (NTS 85, 94, 95). The reported presence of Cretaceous rocks on deeply eroded Mississippian strata in some of the Celibeta wells (DIAND, 1973) led some geologists, including the writer, to conclude that the main structural growth was a pre-Cretaceous, post-Mississippian event. If true, the uplift should have had some effect on the facies of Cretaceous rocks. An examination of samples by the writer indicated no unusual facies changes in the vicinity of the structure. Furthermore, the study failed to find Cretaceous rocks in any of the wells drilled on the uplift, hence the evidence for a pre-Cretaceous structure disappeared. The structure (at least most of it) developed, at the earliest, after Early Cretaceous time – probably a Laramide structure.

Subsurface structural data of the Celibeta fold does not conform to the usual Laramide (foothills-type) structures. Of several possible structural interpretations, one bears a close resemblance to the Rabbit Lake fault zone; a closed dome adjacent to a rejuvenated, northeast-trending basement fault. Of the many basement faults known or suspected in the general area of the Tathlina High (Sikabonyi and Rodgers, 1959; Belyea, 1971; de Wit et al., 1973), the Rabbit Lake and Tathlina fault zones are among the best documented; in both cases a segment of the structure has been investigated by deep drilling as well as by shallow structure test holes. A description of these structures is included to serve as a model for interpreting the Celibeta structure. A brief summary of the Pine Point area is included. Although our knowledge of the basement fault zone underlying the Pine Point area is unsatisfactory, the relationship of tectonic adjustments to Middle Devonian facies is well documented (Skall, 1975). Such a relationship can only be suspected in the other areas.

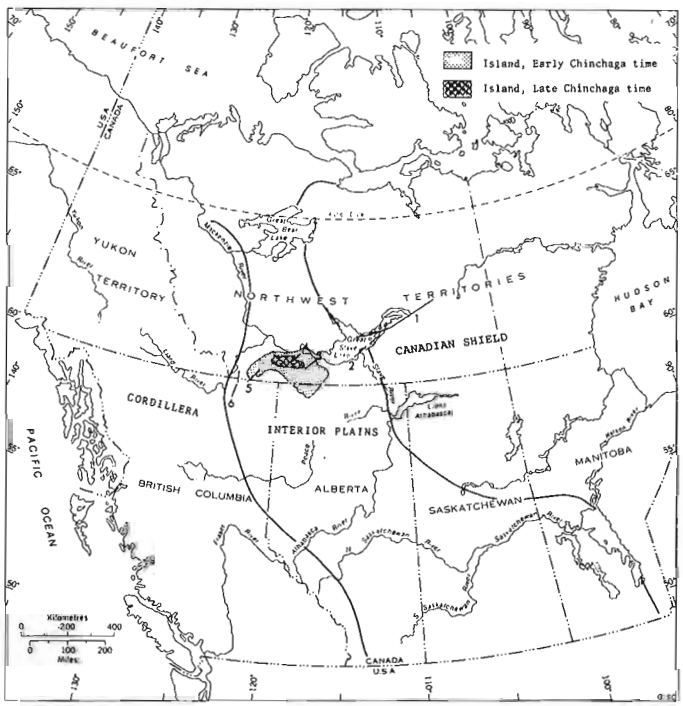

1. McDonald fault system
2. Pine Point mining area
3. Tathlina structure
4. Rabbit Lake structure
5. Celibeta structure
6. Bovie hinge line

Figure 58.1. Index map.

The first hypothesis of this paper is that the Celibeta, Rabbit Lake, Tathlina, and Pine Point fault zones fit a common model which has the following characteristics:

1. A northeast-trending basement fault zone (not a single fault) of ancient, probably Precambrian, origin.

2. Pre-Devonian, erosion-produced topographic relief along the fault zone.

3. Minor tectonic adjustments along the zone, at least during late Middle Devonian time, possibly throughout the Phanerozoic.

All of the fault zones discussed were rejuvenated, producing folds and faults in preserved Phanerozoic cover. The age of this cover ranges from Middle Devonian in the east to Early Cretaceous in the west. To build an

Table 58.1

Table of Formations, Tathlina and Rabbit Lake Areas

PLEISTOCENE	Drift	
DEVONIAN Upper	Wabamun ls.	
	Trout River ss.	
	Kakisa ls.	
	Redknife sltstn., ls.	
	Tathlina ls., sh.	
	Twin Falls ls., sh.	Fort Simpson sh.
	Hay River sh.	Muskwa sh.
	Slave Point ls.	Horn River sh.
	Watt Mountain karsted surface	
Middle & Lower	Pine Point dol., ls.	Lonely Bay ls.
	Chinchaga	dol., anh.
		Ebbutt ss., sh.
		anh.
PRECAMBRIAN	Crystalline rocks	

From: Report of Activities, Part B; Geol. Surv. Can., Paper 77-1B (1977)

Table 58.2

Table of Formations, Celibeta Area

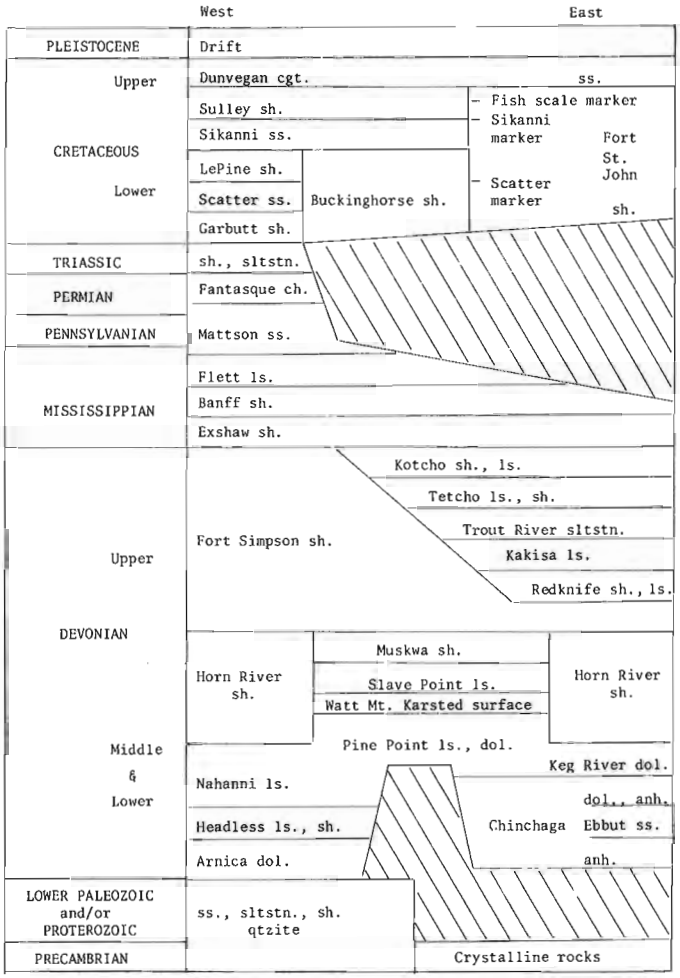

hypothesis on an hypothesis, one can speculate that the time of the last major fault adjustment was the same in all four cases. Or, put another way, the effects of Laramide compression extended entirely across the Interior Plains.

Before discussing the individual structures (treatment of which varies inversely as the amount of published data), it is pertinent to describe, very briefly, the Tathlina High, on the flanks of which three of the four structures are located.

The Tathlina High

The Tathlina High is a large basement feature within the Interior Plains (Fig. 58.1). Its beginnings, whether Precambrian or lower Paleozoic, are unclear. After the period of erosion which preceded Devonian sedimentation, it was a broad topographic upland rising, perhaps, several hundred feet above the surrounding country. The outline depicted on Figure 58.1 is derived from onlap edges of units of the Chincaga Formation (Eifelian). The island was not submerged entirely until late in the Givetian. Although primarily a topographic feature, Belyea (1971) has documented differential subsidence on the flanks of the Tathlina High during Middle Devonian time.

The Pine Point Mining Area

Middle Devonian carbonates, chiefly the well-known Pine Point (or Presqu'ile) reef complex, occur at the surface and host the lead-zinc orebodies. The structure of these rocks (Campbell, 1957; Norris, 1965) consists of numerous small folds, flexures and minor faults. Although these show a great variety of trends, a northeast orientation predominates. Little can be learned regarding basement structure from the outcrop and mining exploration itself. However, the zone of faults which mark the southern shore of the East Arm of Great Slave Lake has been traced, on aeromagnetic maps, beneath the mining area (Burwash, 1957; Campbell, 1957). For a description of part of this fault zone, the following is quoted from Burwash (1957): "In the area northeast of the delta of the Slave River at least three faults, striking northeast, can be traced to the western limit of the exposed Precambrian surface (Brown, 1950). Erosion of the fault blocks, coupled with recurrent movement within this fault zone, has resulted in the development of a graben". The magnetic signature of this graben, Burwash believes, can be recognized in the Pine Point area and beyond. According to Burwash's Figure 4, the northern limb of the graben underlies the mineralized area.

Tathlina Structure

This structure is illustrated in Figures 58.3 to 58.6; topographic names, well names and symbols occur on Figure 58.2. Figure 58.3 incorporates structure test data (J.C. Sproule and Associates, 1956, 1957) as well as some seismic data (Seismograph Service Corp. of Canada, 1956). Figures 58.4 and 58.5 document pre-Devonian topography and Figure 58.6 is a rather schematic interpretation of basement structure.

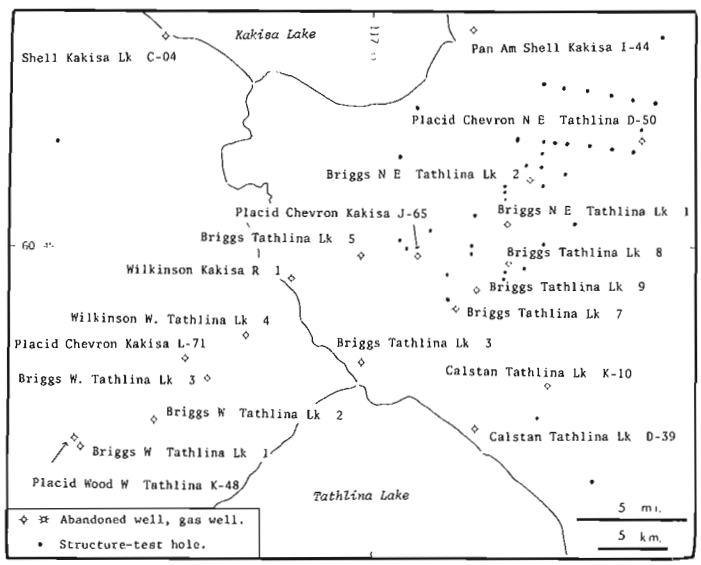

Figure 58.2. Well names, Tathlina area.

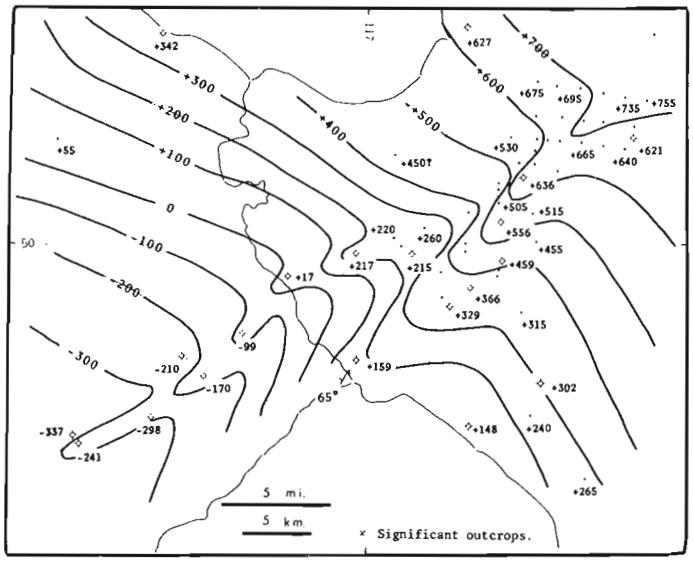

Figure 58.3. Structure contours, top of Twin Falls Formation, Tathlina area. Contour interval 100 feet.

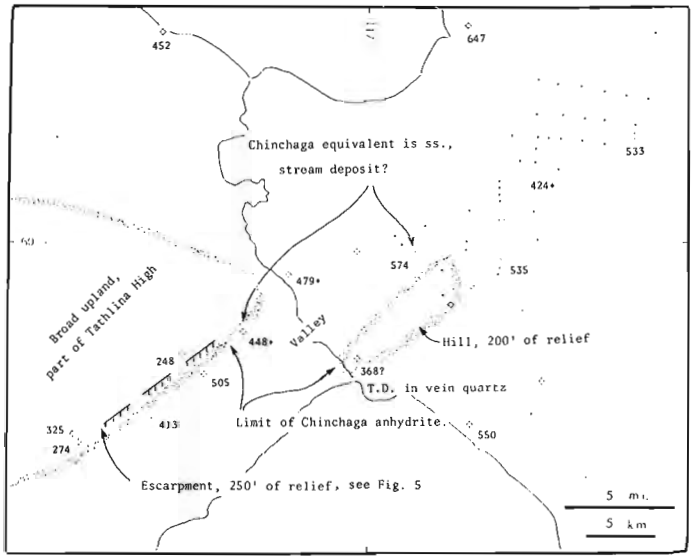

Figure 58.4. Pre-Devonian topography, Tathlina area. Thickness (feet) base of Slave Point Formation to Precambrian.

In shallow horizons (Upper Devonian), the structural belt, about 8 km (5 miles) wide, consists of two tight anticlines separated by a syncline. These folds appear to have been caused by a combination of pre-Devonian topography and post-Devonian basement movement.

The western side of the structural zone coincides with an east-facing pre-Devonian escarpment. The lowest Devonian sediments in this area are evaporites of the Upper Chinchaga Formation (Table 58.1) which lap out against the base of this escarpment (Figs. 58.4, 58.5). The escarpment was not buried until late Pine Point time (Fig. 58.5).

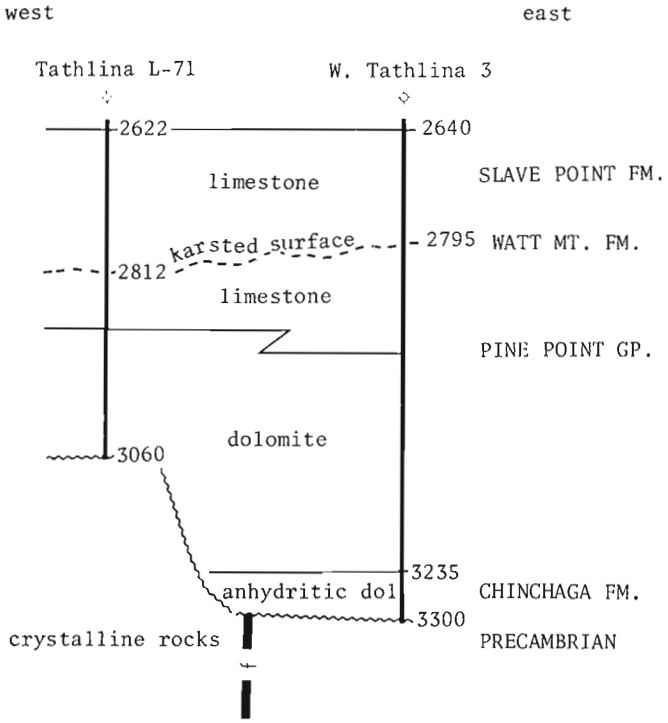

Figure 58.5. Cross-section illustrating pre-Devonian fault and escarpment, Tathlina area. Depths in feet, datum-top of Slave Point Formation.

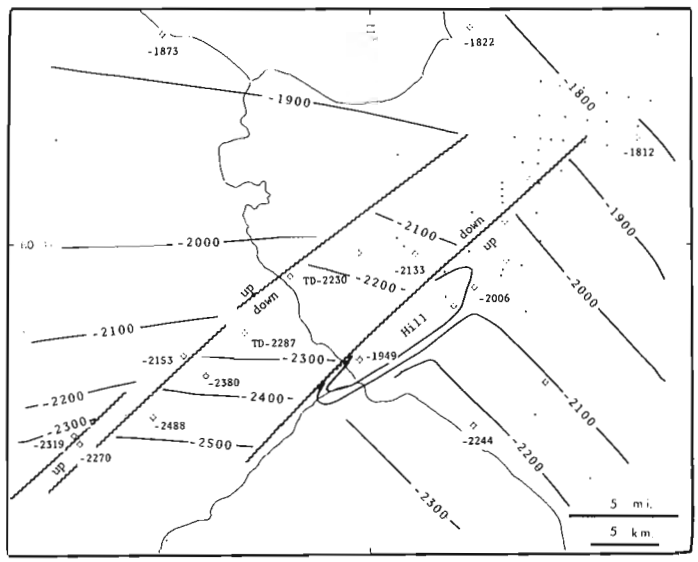

Figure 58.6. Structure contours on Precambrian, Tathlina area. Contour interval 100 feet.

Most wells drilled along the east side of the structural belt did not reach the basement, therefore pre-Devonian relief remains largely unknown. One well, immediately north of Tathlina Lake, bottomed in vein quartz. If this vein quartz is basement, it indicates a hill or ridge (Fig. 58.4); that is, an island never covered by Chinchaga evaporites. However, the quartz vein might be intrusive into Devonian rocks.

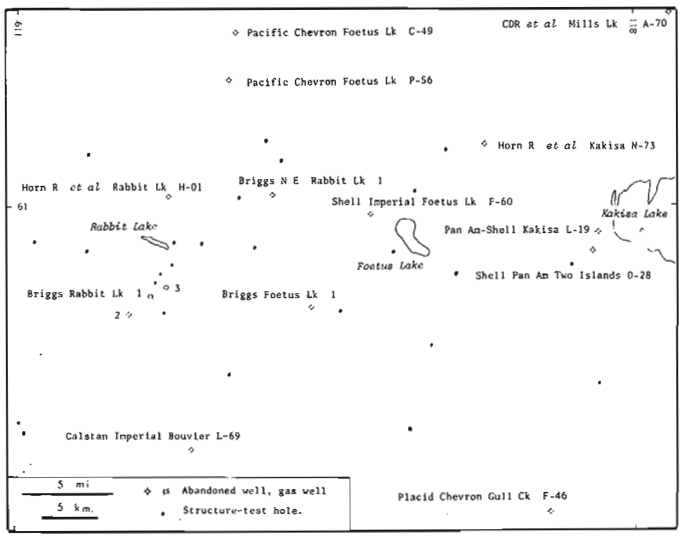

Figure 58.7. Well names, Rabbit Lake area.

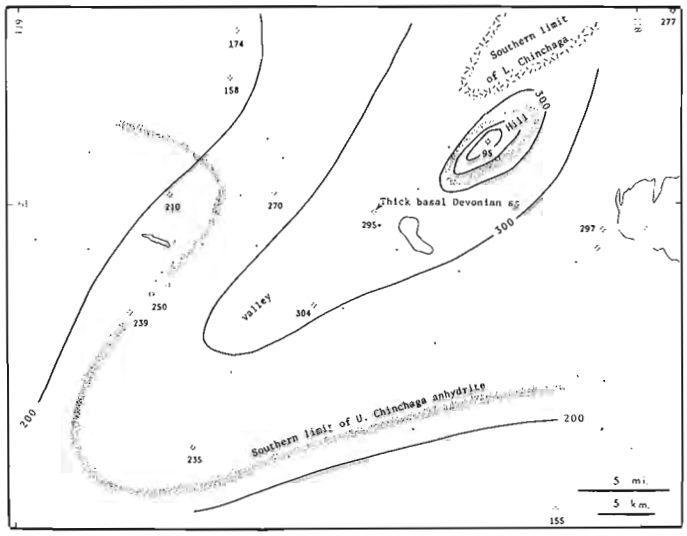

Figure 58.9. Pre-Devonian topography, Rabbit Lake area. Thickness (feet) base of Slave Point Formation to Precambrian. Contour interval 100 feet.

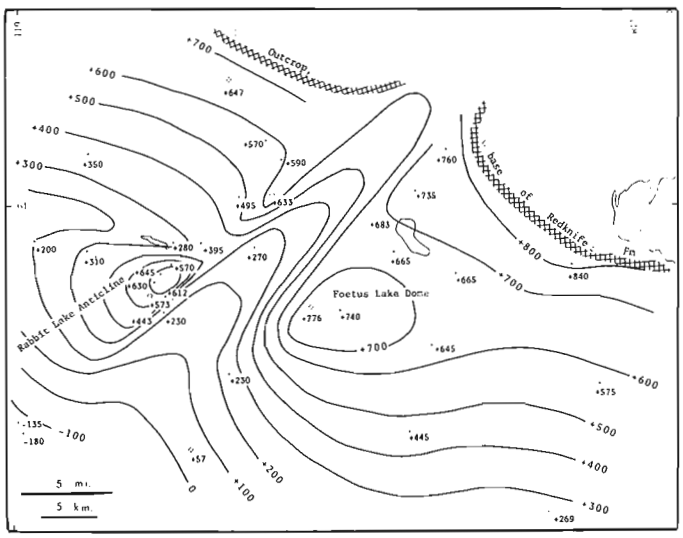

Figure 58.8. Structure contours, base of Redknife Formation, Rabbit Lake area. Contour interval 100 feet.

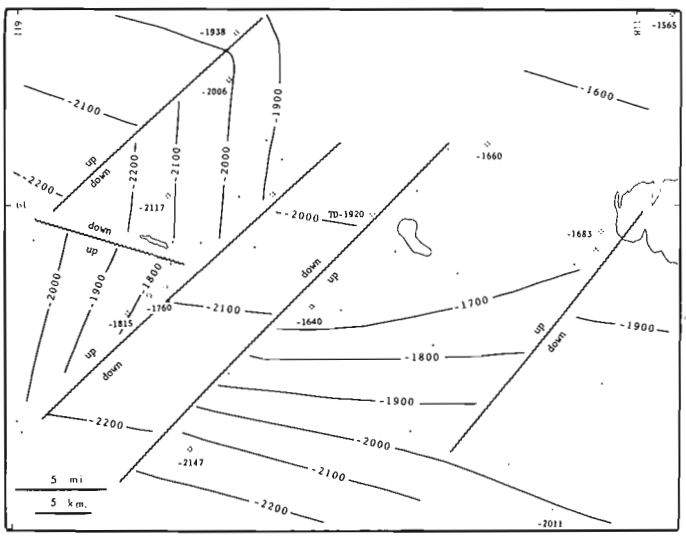

Figure 58.10. Structure contours on Precambrian, Rabbit Lake area. Contour interval 100 feet.

An anomalous thickness of sandstone, in part equivalent to the Chinchage anhydrite, occurs in two wells (Fig. 58.4), one on each side of the valley; this suggests similar topographic relief on both sides. If there is considerable topographic relief on the eastern edge of the fault zone, it must indicate a hill or ridge of local extent, somewhat as depicted in Figure 58.4. The escarpment on the west side, on the other hand, is the edge of a large plateau. Devonian sediments continue to thin westward over this plateau, which is part of the Tathlina High (Fig. 58.1).

The topography indicated on Figure 58.4 is presumably a consequence of pre-Devonian faulting and erosion and, if this topography reflects movement, it was mainly vertical movement and relatively upward on the northwest. Movement during the Devonian cannot be firmly demonstrated. The rapid eastward thickening of the section is a reflection mainly of pre-Devonian topography; however, regional isopachs (not shown) indicate gradual thickening to the southeast. If there was Devonian movement of the Tathlina faults, it must have been down on the southeast.

Facies changes occur within the Pine Point Group in the general area, but no pattern that can be linked directly to the fault zone is apparent. Of course, there is nowhere near the amount of stratigraphic control that is available in the Pine Point area (Skall, 1975).

In summary, the Tathlina structural belt can be interpreted to be the result of: 1) pre-Devonian (probably Precambrian) faulting which resulted in local topographic relief; 2) minor movement on these faults, which probably occurred in late Middle Devonian (Givetian) time, and caused downthrows to the southeast; and 3) post-Devonian tilt and relatively minor adjustments along the earlier faults which folded Devonian strata. In this area, the youngest strata are Upper Devonian; therefore, the age of this last movement cannot be dated more precisely.

Rabbit Lake Structure

A closed anticline south of Rabbit Lake (Fig. 58.8) was mapped first from outcrops (J.C. Sproule and Associates, 1955). Subseuqent drilling discovered a small gas field. The field is about 13 km^2(5 sq. miles) in area; closure is about 85 m (280 ft.). The pay-zone is about 6 m (20 ft.) of porous limestone at the top of the Pine Point Group. Recoverable reserves are estimated at 12 billion cubic feet.

Structure test holes (J.C. Sproule and Associates, 1956, 1957), combined with deep drilling plus outcrop data, result in fairly close control on shallow structure. Pronounced topographic lineations coincide with the northern and southeastern limbs of the Rabbit Lake anticline. The interpretation of shallow structure (Fig. 58.8) has been drawn to conform with the speculative concept of basement faulting (Fig. 58.10).

Like the Tathlina structure, the Rabbit Lake structure consists of a narrow syncline flanked by anticlines; at Rabbit Lake, however, the anticlines are domed rather than linear. The closure of the gas-bearing Rabbit Lake anticline is due to the presence of a narrow east-trending syncline. The Foetus Lake dome, east of the syncline, sits on a structural terrace.

Unlike the Tathlina structure, there is no good evidence for much pre-Devonian topographic relief in the Rabbit Lake area. What evidence there is (Fig. 58.9) suggests a shallow pre-Devonian valley coincident with the syncline or basement graben. The southern limit of the Chinchaga anhydrite may be misleading because this appears to be a facies change (to dolomite) as well as an onlap. Somewhat more convincing evidence is found north of the map-area where, over a distance of 80 km (50 miles), a mild structural flexure (up on the southeast) is mappable, and this coincides with a narrow valley filled with Lower Chinchaga evaporites. Only the southern end

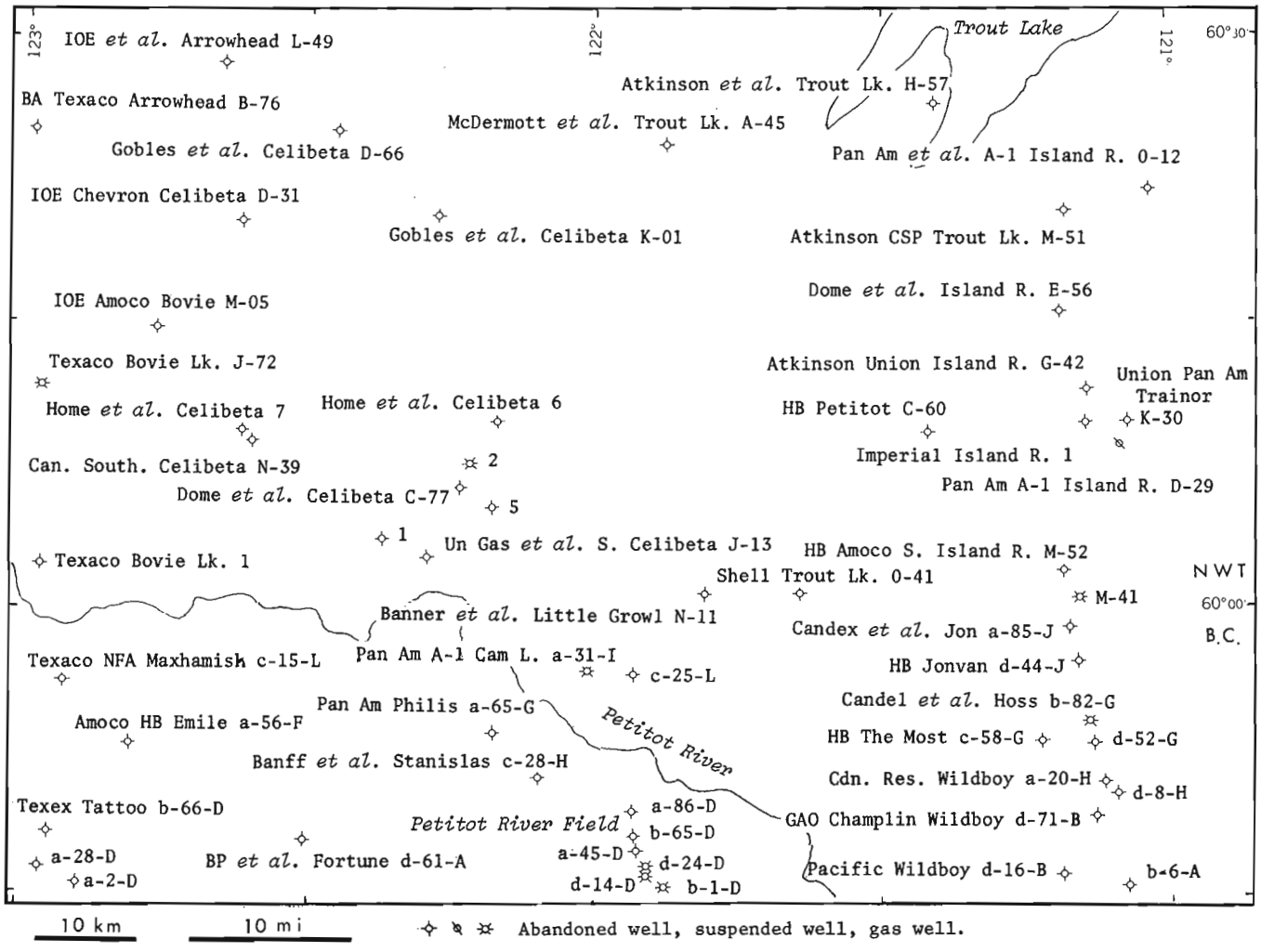

Figure 58.11. Well names, Celibeta area.

of this tongue appears on Figure 58.9. Only one well (just west of Foetus Lake) is located in the graben, and it did not reach basement but bottomed in the basal Devonian sandstone. This sandstone is more than 30 m (100 ft.) thick, in contrast to the 3 to 9 m (10-30 ft.) thickness that is usual in this area. The hill northeast of Foetus Lake remained an island until Pine Point time.

In the stylized structure contours on the basement (Fig. 58.10), the main feature is a graben flanked by differentially tilted blocks. There is rather weak evidence (Fig. 58.9) that the graben coincides with a pre-Devonian valley. There is no evidence to document any movement during Devonian deposition; however, there is insufficient control to deny such movement. The youngest rocks in the area are Upper Devonian, therefore the final movement can only be dated as post-Late Devonian.

Celibeta Structure

The Celibeta anticline is a one-well gas field. About 15 m (50 ft.) of porosity at the top of the Slave Point limestone contain an estimated 10 billion cubic feet of marketable gas (National Energy Board, 1974, Appendix 4).

Many miles of seismic lines have been shot over and in the vicinity of the Celibeta structure. Because the illustrative material (Figs. 58.12 to 58.19) has been compiled without benefit of any geophysical data, the picture therefore is incomplete and the interpretation is subjective.

Unlike the Tathlina and Rabbit Lake structures, the Celibeta structure has no topographic or outcrop expression. Except for one small limestone outcrop on the

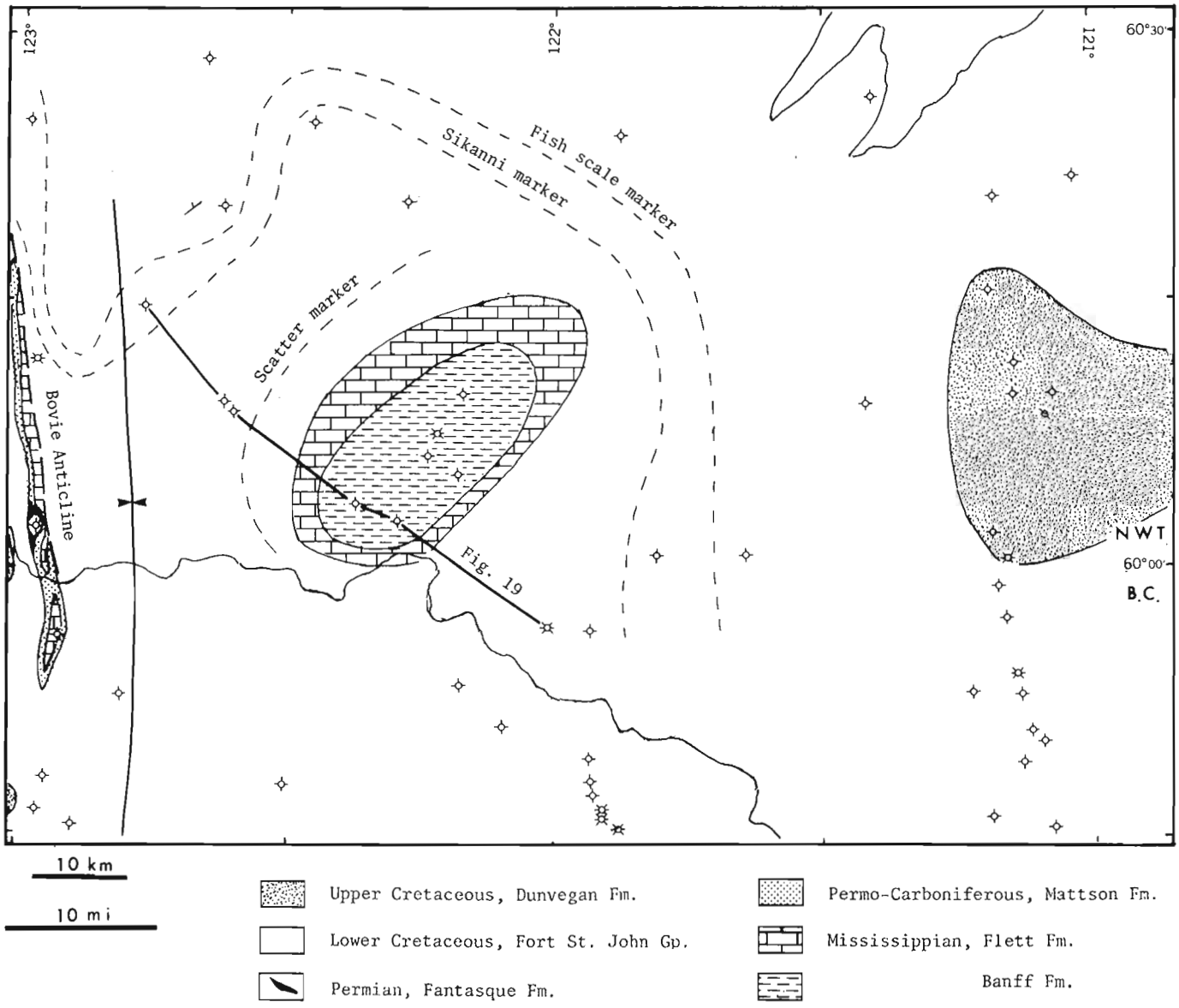

Figure 58.12. Bedrock (pre-drift) geology, Celibeta area.

Petitot River (Douglas and Norris, 1959), the structure is buried below thick glacial drift.

Within the District of Mackenzie portion of the map-area, all near-surface well samples have been re-examined by the writer to determine the nature of the bedrock in this heavily drift-covered area. Markers published in the Schedule of Wells (DIAND, 1973) indicate Cretaceous beds overlying Banff shale in three of the Celibeta wells. No evidence for Cretaceous rocks was found by the writer in any of these wells. In all wells drilled on the Celibeta structure, the Banff shale is overlain by drift, in places up to 180 m (600 ft.) thick.

Bedrock (pre-drift) geology is shown in Figure 58.12. The main change from previous mapping (Douglas and Norris, 1959) is in the extent of Paleozoic rocks in the Celibeta area. The northeast trend of the structure, as will be discussed later, is conjecture.

The tectonic setting of the Celibeta structure is illustrated by isopachs of the upper Paleozoic section (Fig. 58.14). Isopachs of most mappable units display a similar picture. The Celibeta structure is situated on a shelf (broad contour spacing) about 32 km (20 miles) from the Bovie hinge line (close contour spacing). The Bovie hinge line (so named because it coincides with the Bovie anticline, Fig. 58.12) divides the shelf from the western

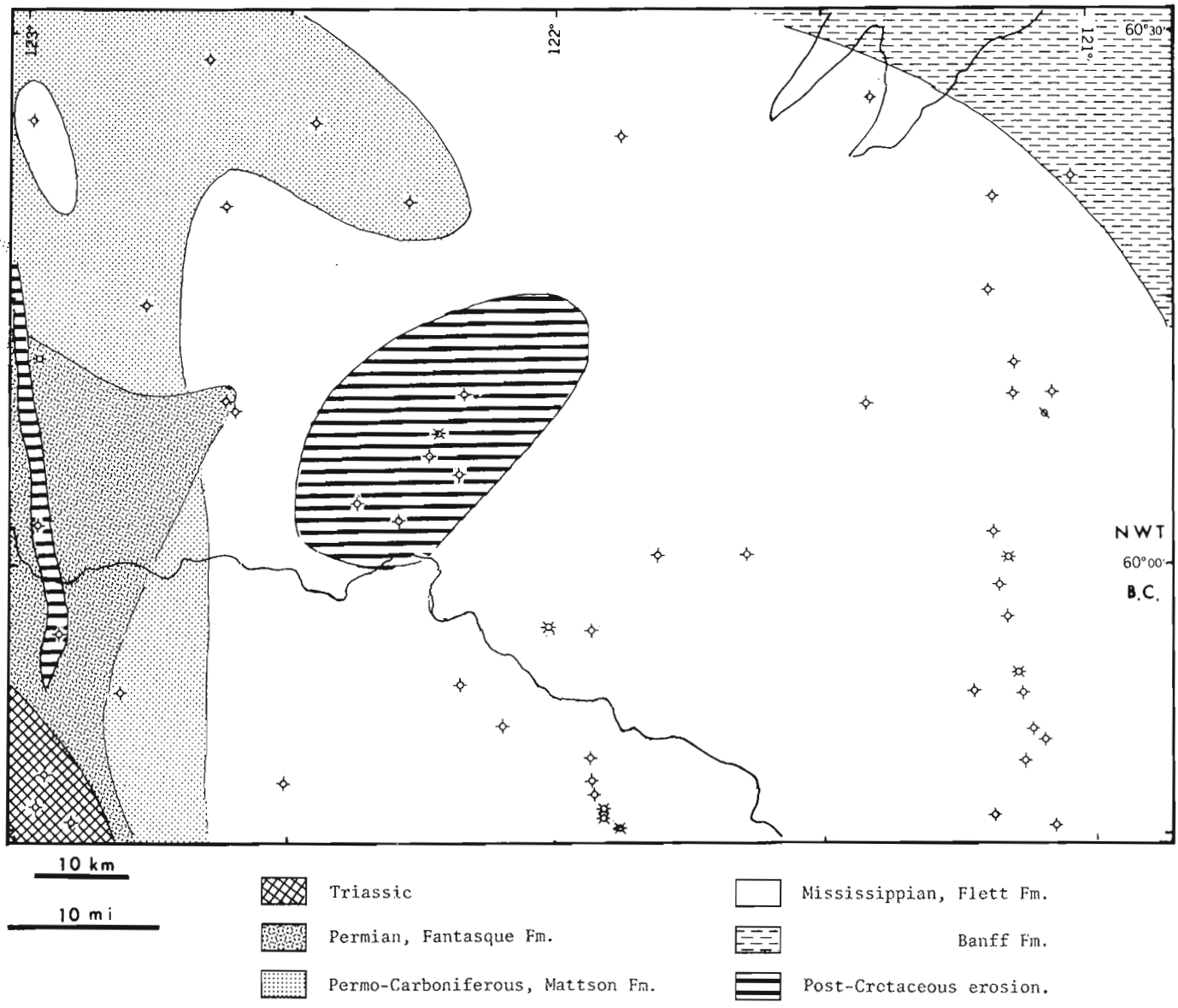

Figure 58.13. Pre-Cretaceous geology, Celibeta area.

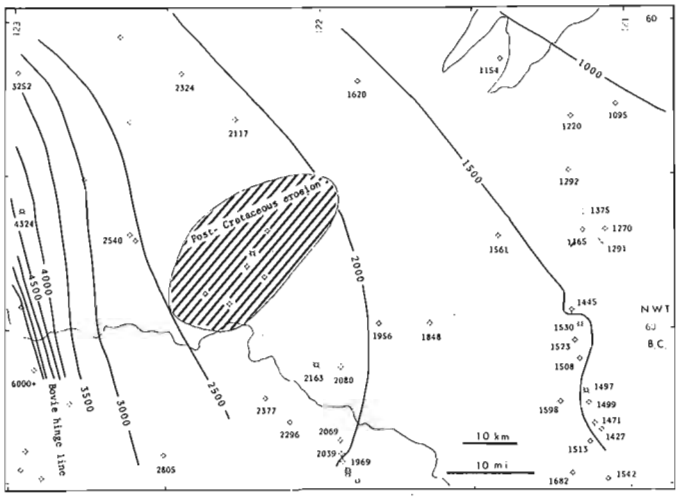

Figure 58.14.

Isopachs, base of Cretaceous to top of Devonian, Celibeta area. Contour interval 500 feet.

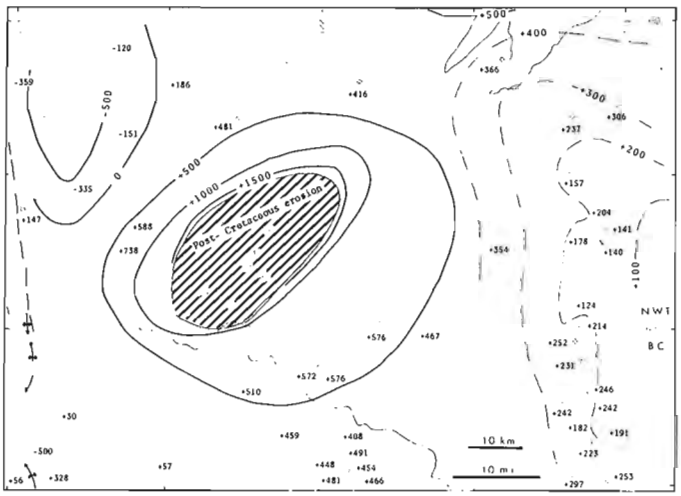

Figure 58.15. Structure contours, base of Cretaceous, Celibeta area. Contour interval 500 feet (solid line) or 100 feet (dashed line).

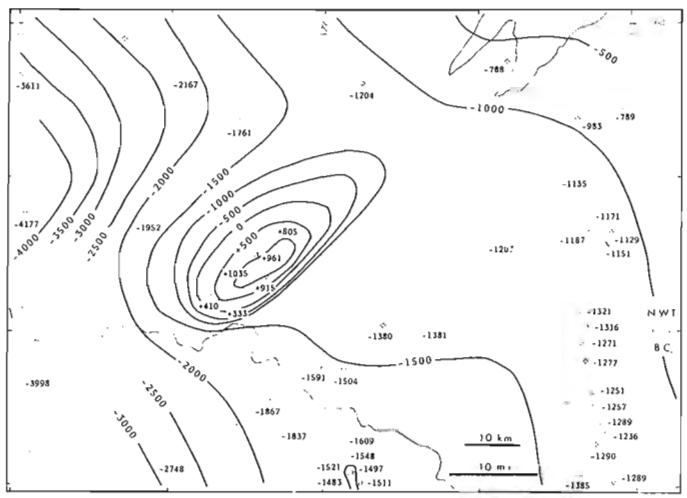

Figure 58.16. Structure contours, top of Devonian, Celibeta area. Contour interval 500 feet.

basin. This hinge is an ancient flexure, down on the west, which was active throughout much of Paleozoic and Mesozoic time. The hinge continues south of the map-area, where its trend changes to south-southwest (Fig. 58.1). The Bovie hinge line marks the eastern limit, except for thin and discontinuous patches, of Pennsylvanian, Permian and Triassic rocks (Fig. 58.13).

The large amount of structural relief on all horizons down to and including basement make it obvious that the Celibeta structure involves basement faulting. The question is, what is the nature of this faulting? The structure of shallow horizons (Figs. 58.15, 58.16) is drawn on the assumption that a northeast-trending basement fault coincides with the southeast limit of the fold (Fig. 58.18).

Evidence for this fault comes partly from north of the map-area. Structure contours on any Paleozoic horizon or on the basement show a slight but persistent

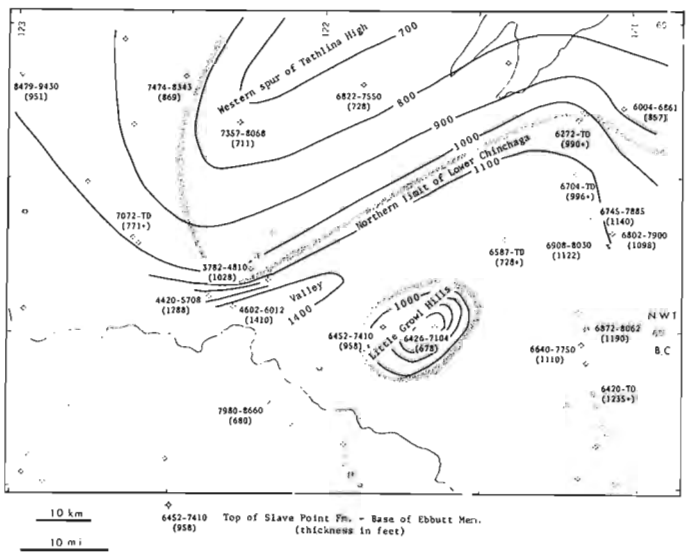

Figure 58.17. Pre-Devonian topography, Celibeta area. Isopach interval 100 feet.

jog, the 1000-foot contour on the east of Figure 58.16 is an example. This feature, which persists for a distance of about 80 km (50 miles) beyond the map-area, suggests a northeast-trending basement fault, northwest side up by a few tens of feet. The southern limb of the Celibeta fold lies on trend with this flexure. Some other features associated with this fault zone are: 1) the location and trend of a segment of the Slave Point carbonate front in the vicinity of Trout River (about 80 km (50 miles) northeast of the map-area); 2) the change in trend of the Bovie hinge line from nearly north-south within the map-area to south-southwest south of the map-area; and 3) roughly, the fault zone coincides with the eastern limit of lower Paleozoic or Proterozoic clastics; southeast of the fault zone Devonian rocks lie on crystalline basement.

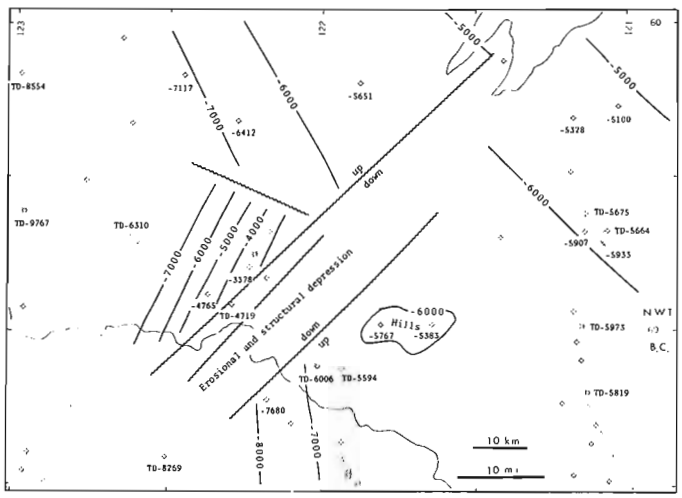

Figure 58.18. Structure contours, base of Devonian, Celibeta area. Contour interval 1000 feet.

Figure 58.17 summarizes what is known about pre-Devonian topography. The isopach interval, although the best available to illustrate topography, is far from satisfactory because: 1) the top of the Slave Point limestone almost certainly steps up- or down-section several tens of feet (aside from the main carbonate front); 2) there is some stratigraphic thinning within the Pine Point Group due to differential subsidence; and 3) the marker at the base of the interval is sometimes questionable; Chinchaga sandstone may be confused with lower Paleozoic or Proterozoic sandstone.

In spite of its weaknesses, Figure 58.17 suggests that there was considerable pre-Devonian topographic relief. The western spur of the Tathlina High was a broad upland, never covered by lowest Devonian sediments. Another high area, probably an isolated hill, lay to the south – the Little Growl Hills. The valley south of the Celibeta fold was at least 120 m (400 ft.) deep and had a steep northern bank. The combination of features – a northeast-trending basement fault and a pre-Devonian valley – is analogous to the Tathlina and Rabbit Lake fault zones. Although there is insufficient subsurface control to establish confidence, it is reasonable to assume that all three structures had a similar history. The Celibeta fold can be interpreted as a result of rejuvenation of an ancient, northeast-trending basement fault.

The determination of basement structure in the Celibeta area is hampered by uncertainty as to the age of the clastics at total depth in several wells – Devonian, lower Paleozoic or Proterozoic. The markers contoured in Figure 58.18 probably give a close approximation to Precambrian structure. The pattern shown is based on the Tathlina and Rabbit Lake models.

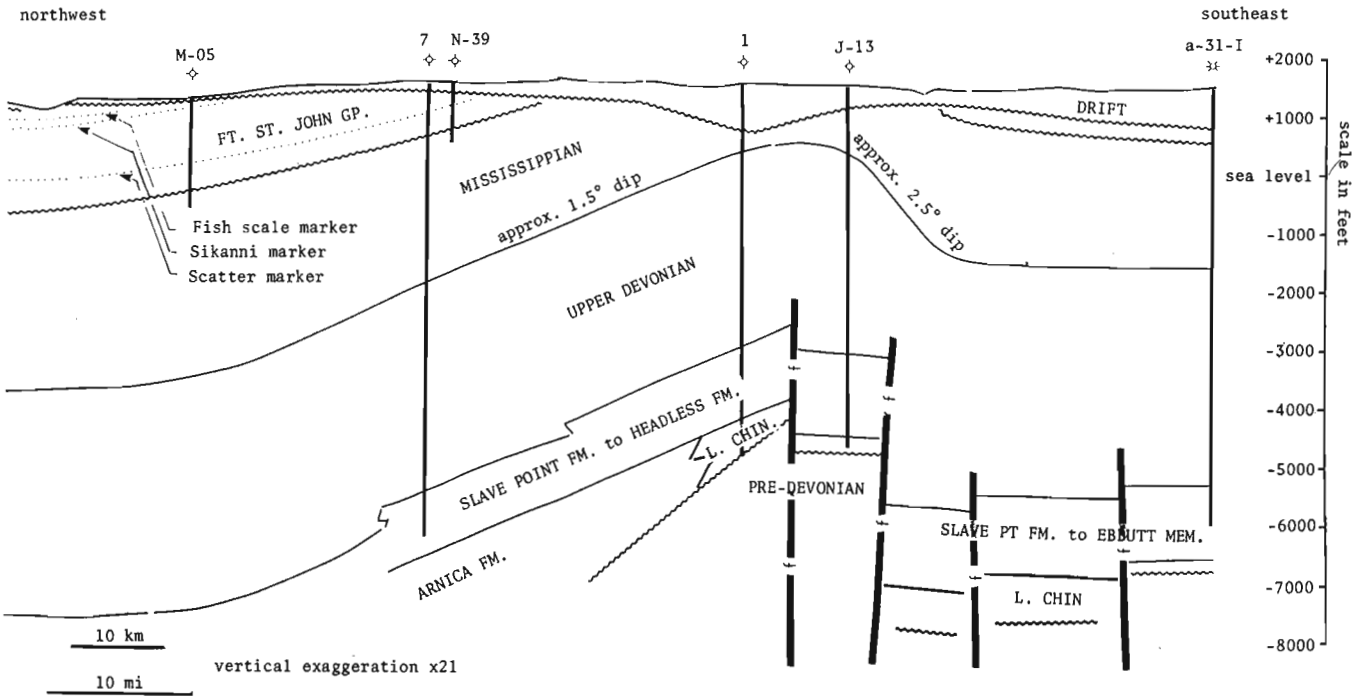

Figure 58.19. Cross-section, Celibeta area. Datum sea level. Line of section shown on Figure 58.12.

All evidence, sketchy though it is, indicates close structural conformity of all horizons (Figs. 58.12, 58.15, 58.16, 58.18, 58.19). The age of the structure is clearly post-Early Cretaceous. Probably it is a Laramide structure.

Summary

The Celibeta structure has been interpreted in such a way that it fits a model common to the Rabbit Lake, Tathlina and Pine Point fault zones; that is, a rejuvenated, ancient, basement fault zone which had, prior to Devonian deposition, been differentially eroded to produce a shallow depression. It must be emphasized that the Celibeta data were forced intentionally into this model. Alone, the data fit a variety of interpretations. It is to be hoped that someone who has access to geophysical data will be stimulated to confirm or reject this interpretation.

The Celibeta folding occurred after Early Cretaceous time – probably a Laramide event. If a common pattern of the four fault zones were to be confirmed, then a common time of rejuvenation would be a logical assumption. The second hypothesis of this paper – the influence of Laramide compression extended entirely across the Interior Plains – would then be elevated to respectability.

References

Belyea, H.R.
1971: Middle Devonian tectonic history of the Tathlina Uplift, southern District of Mackenzie and northern Alberta, Canada; Geol. Surv. Can., Paper 70-14.

Brown, I.C.
1950: Preliminary map, Fort Resolution, Northwest Territories; Geol. Surv. Can., Paper 50-28.

Burwash, R.A.
1957: Reconnaissance of subsurface Precambrian of Alberta; Bull. Am. Assoc. Pet. Geol., v. 41, p. 70-103.

Campbell, N.
1957: Stratigraphy and structure of Pine Point area, N.W.T. in Structural geology of Canadian ore deposits; 6th Commonwealth Mining Met. Congr., Canada, v. II, p. 161-174.

Department of Indian Affairs and Northern Development, Canada
1973: Schedule of wells, 1921-1971; Northern Economics Development Branch, Oil and Mineral Division, Oil and Gas Section, IAND Publ. QS-1214-000-EE-A-1.

de Wit, R., Gronberg, E.C., Richards, W.B., and Richmond, W.O.
1973: Tathlina area, District of Mackenzie in The future petroleum provinces of Canada, R.G. McCrossan, ed.; Can. Soc. Pet. Geol., Mem. 1, p. 187-212.

Douglas, R.J.W.
1959: Great Slave Lake and Trout River map-areas, Northwest Territories; Geol. Surv. Can., Paper 58-11.

1974: Trout River, District of Mackenzie; Geol. Surv. Can., Map 1371A.

Douglas, R.J.W. and Norris, D.K.
1959: Fort Liard and LaBiche map-areas, Northwest Territories and Yukon; Geol. Surv. Can., Paper 59-6.

National Energy Board, Canada
1974: Report to the Governor in Council in the matter of the application under the National Energy Board Act of Dome Petroleum Limited and Cochin Pine Lines Limited, January, 1974.

Norris, A.W.
1965: Stratigraphy of Middle Devonian and older Paleozoic rocks of the Great Slave Lake region, Northwest Territories; Geol. Surv. Can., Mem. 322.

Seismograph Service Corp. of Canada
1956: Report on a seismograph survey conducted in Northwest Territories, Canada; Northeast Tathlina Lake project; available at Dept. of Indian Affairs and Northern Development, Publ. 508-6-4-22; or from West Canadian Graphic Industries Ltd., Calgary, Publ. 261.

Sikabonyi, L.A. and Rodgers, W.J.
1959: Paleozoic tectonics and sedimentation in the northern half of the West Canadian Basin; J. Alberta Soc. Pet. Geol., v. 7, no. 9, p. 193-216.

Skall, H.
1975: The paleoenvironment of the Pine Point lead-zinc district; Econ. Geol., v. 70, no. 1, p. 22-45.

Sproule, J.C. and Associates
1955: Geological report, D. Todd Briggs project, N.W.T.; available at Dept. of Indian Affairs and Northern Development, Publ. 508-1-4-6; or from West Canadian Graphic Industries Ltd., Calgary, Publ. 252.

1956: Geological progress report, D. Todd Briggs project, N.W.T.; available at Dept. of Indian Affairs and Northern Development, Publ. 508-1-4-4; or from West Canadian Graphic Industries Ltd., Calgary, Publ. 250.

1957: Geological progress report, D. Todd Briggs project, N.W.T.; available at Dept. of Indian Affairs and Northern Development, Publ. 508-1-4-8; or from West Canadian Graphic Industries Ltd., Calgary, Publ. 253.

Taylor, G.D. and Stott, D.F.
1968: Maxhamish Lake, British Columbia; Geol. Surv. Can., Paper 68-12.

Project 730013

C.M. Cunningham[1] and W.W. Shilts
Terrain Sciences Division

Introduction

In 1976 Quaternary mapping in southern Keewatin was continued in the Baker Lake area (NTS 56 D, 66 A, 65 P) and portions of adjoining map-areas. The objectives of this mapping are: (1) to provide a map of surficial deposits suitable for input into environmental studies associated with the proposed eastern arctic gas pipeline; (2) to document and describe the complex ice flow directions associated with the migration of the Keewatin Ice Divide (Lee et al., 1957); (3) to describe the late-glacial relationship of the Tyrrell Sea to possible freshwater bodies dammed west of the ice divide in the Thelon-Dubawnt system; and (4) to describe the earlier Quaternary history as revealed by borehole data and the study of stratigraphic sections along Kazan, Thelon, Dubawnt, and other rivers.

Surficial Deposits

In the vicinity of the ice divide (Fig. 59.1), till is the main deposit. A zone of marine reworking extends up to altitudes ranging from 135 m to over 150 m a.s.l.

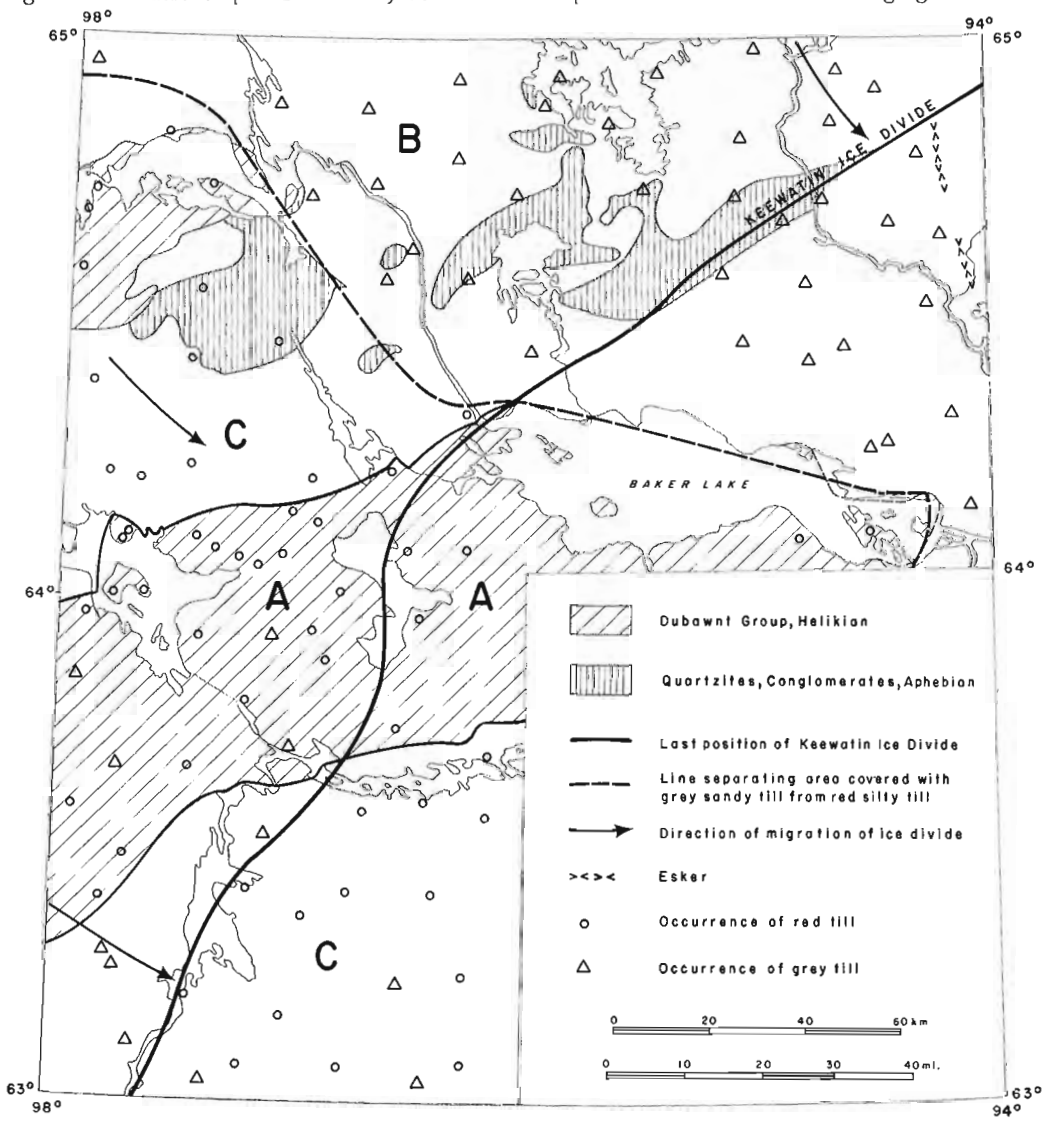

A — Area of gently rolling silty till plains with relatively few lakes; well developed marine beaches (below 150 m a.s.l.); active mudboils; relatively few outcrops; post-glacial streams deeply incised into bedrock; and no strongly oriented topographic grain.

B — Area of bouldery, grey-brown sandy till, many outcrops with felsenmeer, many lakes, sparse vegetation, with topographic grain strongly controlled by bedrock structure.

C — Area of red till cover on crystalline bedrock; outcrop frequency, number of lakes, and boulder frequency intermediate between areas A and B; topographic grain strongly lineated northwest-southeast by glacial erosion/-deposition.

Figure 59.1. Sketch map showing probable last position of Keewatin Ice Divide and distribution of red till derived from Dubawnt Group rocks, Baker Lake area.

[1]Department of Geology, University of Massachusetts, Amherst, Massachusetts

From: Report of Activities, Part B;
Geol. Surv. Can., Paper 77-1B (1977)

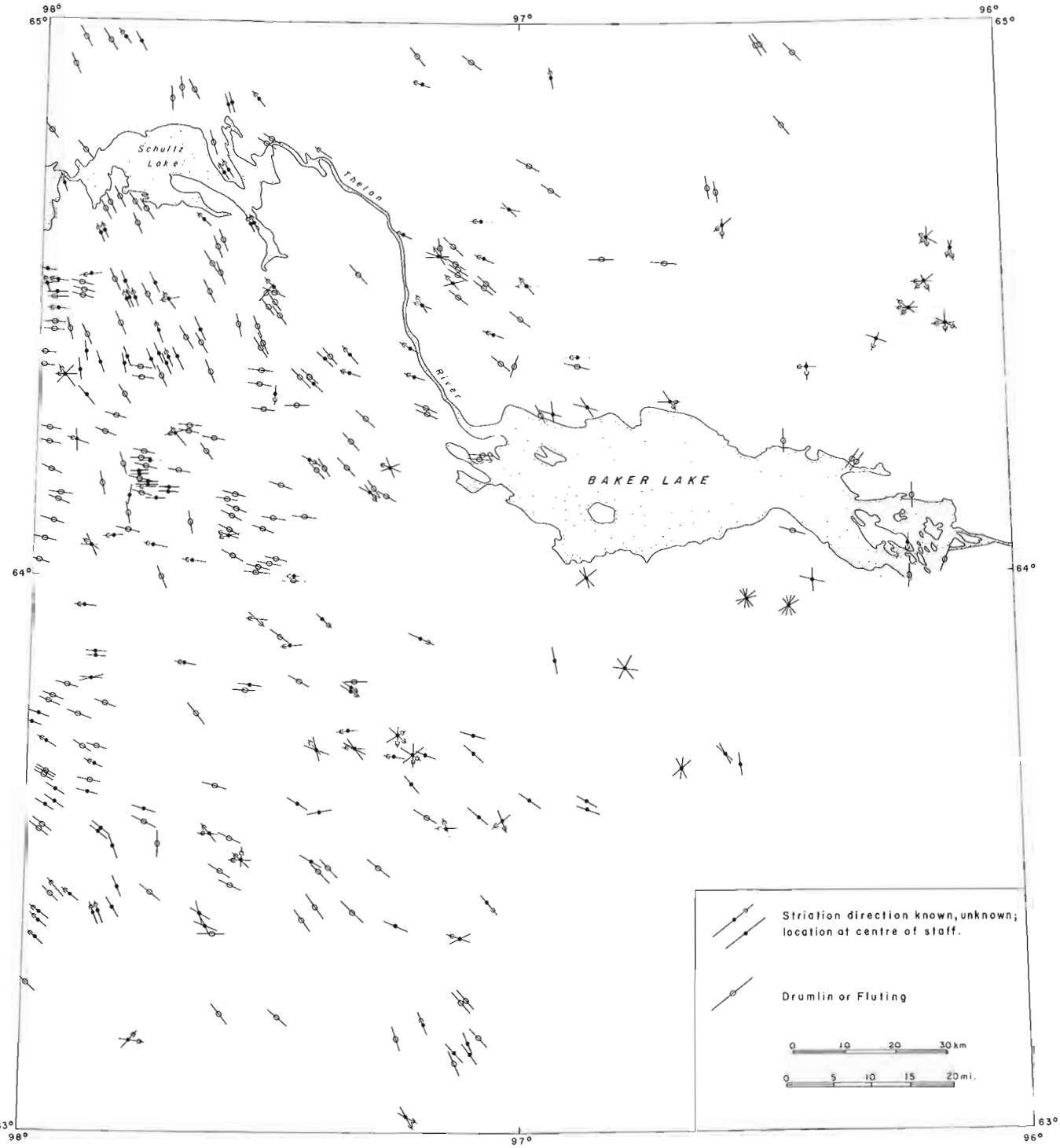

Figure 59.2. Ice flow directions generalized from striations and drumlins or fluting. Presence of quartzite erratics at Pitz Lake indicates southerly flow from at least as far north as Schultz Lake at some time.

Many streams, particularly those in the Pitz Lake basin, are flanked below 135 m a.s.l. by deltaic sand and fine gravel (informally called 'strip deltas') deposited by delta progradation as sea level fell at a relatively constant rate. Marine silty clays covered by thin sand form a persistent cover south of Thelon River between Pitz Lake and Baker Lake, but fine grained marine sediments are rare elsewhere. Beaches are particularly well developed on glacial sediments in areas underlain by Dubawnt Group rocks. Major areas of sandy deltaic deposits and spectacular flights of gravelly, sandy beaches are found at the northwest and northeast sides of Pitz Lake, respectively.

Within the area studied in 1976, no conclusions could be drawn regarding the relationship of the Tyrrell Sea to lakes in upper Thelon Valley. All shoreline features found in the map-area can be reasonably related to marine inundation. The northern limit of marine submergence is difficult to map because the bouldery terrain north of Baker-Schultz lakes was not suitable for beach formation.

Terrain underlain by late Precambrian (Helikian) rocks of the Dubawnt Group (Donaldson, 1965) (area A, Fig. 59.1) comprises a gently rolling surface of red till which is relatively rich in silt and clay derived largely from red beds of the Dubawnt Group. The till plain has few linear features related to ice flow, such as drumlins or fluting. Till surfaces generally are covered with active mudboils. The gently rolling terrain is broken in places by outcrops of resistant rocks such as the east-west trending ridges of intrusive and volcanic rocks north and south of Pitz Lake, by a major, northwest-trending diabase dyke that can be traced from Thirty Mile Lake to Schultz Lake along a line passing just west of Pitz Lake, and by hills of Aphebian age quartzites east and south of Schultz Lake.

North of Baker Lake, Thelon River, and Schultz Lake (area B, Fig. 59.1), the nature of the terrain changes dramatically. Vegetation is sparse in comparison to area A. The till plain is underlain by crystalline Archean bedrock that protrudes in numerous felsenmeer-covered outcrops with sharp local relief. A major ridge of Aphebian quartzite extends east-northeast from Whitehills Lake across Quoich River. Till is the major unconsolidated sediment, but in contrast to the red tills of areas A and C, it is generally grey-brown, sandy, and very bouldery. Most mudboils are relatively inactive and are surrounded by stone rings in the form of sorted circles. The number of lakes and control of topographic detail by bedrock structure is noticeably greater in this region than in the southern parts of the map-area.

Terrain underlain by crystalline Archean bedrock south of Thirty Mile Lake and between Schultz and Pitz-Princess Mary lakes (area C, Fig. 59.1) has local relief, density of lakes, and stoniness intermediate between areas underlain by Dubawnt Group rocks (area A) and areas underlain by the highly deformed and metamorphosed Archean-Aphebian rocks to the north (area B). Red till derived from red beds of the Dubawnt Group completely covers this area, forming dispersal trains that extend northward an undetermined distance past Schultz Lake and southeastward as a 75 km-wide, more than 200 km-long ribbon from the Pitz-Thirty Mile-Forde lakes area to Hudson Bay. Whereas the topographic grain is inherited largely from bedrock structures in the northern area (B), the orientation of topographic features of all scales and types in area C is closely related to erosion and deposition by southeastward or northeastward glacial flow.

Ice Divide – Ice Flow History

Figure 59.2 shows generalized ice flow directions measured in 1976. The directions of striations were determined by noting the trends of tails of uneroded rock protected in the lee of hard inclusions, such as pyrite grains, quartz grains or veins, etc. ('rat tail' striations). From Figure 59.2 it is evident that it is difficult to delimit the ice divide more precisely than it was defined by Lee (1959).

Erratics of quartzite of presumed Aphebian age are found at Pitz Lake and are interpreted to indicate a major period of southward transport from outcrops of these rocks at Schultz Lake. Despite the overwhelming evidence that late-glacial flow in this area was northwestward, this observation indicates that ice formerly flowed southward from a centre of outflow an unknown distance north of Schultz Lake. That the major flow event to affect the map area was related to a centre of outflow to the north is suggested further by southeastward trending geochemical dispersal trains in the southern part of the map area (R.A. Klassen, pers. comm., 1977) and old southward striations measured north of the ice divide in the Quoich River area. A preliminary interpretation of these observations could be that the Wisconsinan (or Late Wisconsinan) ice sheet grew with its centre of outflow in northern Keewatin and that the centre migrated to the south and east to the vicinity of Baker Lake in the final phases of glaciation. Such migration would have been controlled in a presently undefinable way by significant drawdowns caused by calving into lakes abutting the ice in the south and west and into the sea abutting the ice in the east and north.

The last recorded directions of glacier flow were generally westward or northwestward and southeastward from an arcuate zone extending through Forde, Pitz, and Whitehills lakes and thence northeastward across Quoich River about 15 to 25 km south of its junction with Tehert River. In a zone from Schultz Lake to Forde Lake, west of Pitz Lake, the direction of the last ice flow seems to have been due west. The westward flow apparently postdated flow that was north to northwest in the same zone. Southeastward migration of the ice divide is confirmed by the association of southeastward oriented striations with younger westward or northwestward striations in close proximity or on the same outcrops.

Meltwater channels and the distribution of ice-contact deposits indicate that the Pitz Lake basin was filled with a discrete ice mass to an altitude below the hills defining the basin shortly before flooding by marine waters. Thus, this would be the site of one of the last remnants of the continental glacier west of Hudson Bay. Remnant ice masses are also thought to have occupied other major lake basins near the divide.

Stratigraphy

At two sections along lower Kazan River and one section on a Thelon River tributary near Schultz Lake, boulder pavements separate two texturally and compositionally contrasting till units. At present it is thought that the lower of these units represents early ice flow from northern Keewatin and that the upper unit, although not necessarily correlative among all sections, may represent the period of significant shift in ice flow associated with the migration of the ice divide into Baker Lake region. The upper till, where observed, is 2 to 4 m thick and overlies more than 10 m of lower till. Except for wave reworked zones or thin marine sands or silts at the surface, no water laid sediments were found in the sections. Preliminary examination of samples made available by Polar Gas at the time of writing this report indicates that these two tills may be underlain by fluvial sands (interglacial?) which overlie an older till along Thelon River between Schultz and Baker lakes.

Acknowledgments

B.C. McDonald provided considerable unpublished data on eskers and marine limit in the Baker Lake region. R.A. Klassen provided logistical support and published and unpublished data, including detailed terrain observations gathered during extensive drift prospecting studies carried out in the centre of the area. Samples and stratigraphic records from overburden drilling have been graciously provided by EBA Engineering Consultants Ltd. by permission of Polar Gas. The report was critically read by R.N.W. DiLabio and R.J. Fulton.

References

Donaldson, J.A.
1965: The Dubawnt Group, Districts of Keewatin and Mackenzie; Geol. Surv. Can., Paper 64-20, 11 p.

Lee, H.A.
1959: Surficial geology of southern District of Keewatin and the Keewatin Ice Divide, Northwest Territories; Geol. Surv. Can., Bull. 51, 42 p.

Lee, H.A., Craig, B.G., and Fyles, J.G.
1957: Keewatin Ice Divide (abstr.); Geol. Soc. Am., Bull., v. 68, p. 1760-1761.

A BRIEF DESCRIPTION OF THE SURFICIAL MATERIALS OF NORTH-CENTRAL KEEWATIN, NORTHWEST TERRITORIES

Project 760012

R.D. Thomas
Terrain Sciences Division

Introduction

Reconnaissance terrain mapping was conducted in north-central Keewatin (NTS 56 E, F, K, L, M, and N) (Fig. 60.1) during summer 1976. This area lies between the areas mapped by Boydell et al. (1974, 1975) to the north and Cunningham and Shilts (1977) to the south and includes one of the proposed eastern arctic gas pipeline routes. Initially, Craig (1961) and Fyles (Wright, 1967) mapped the surficial geology and Wright (1967) and Heywood (1967) mapped the bedrock geology.

This project involved preliminary airphoto interpretation, field checking of the interpretation by helicopter traversing, and detailed ground investigation of preselected sites. In addition, shallow drilling in fine grained materials was conducted by J.J. Veillette and M. Nixon; the vegetation types were mapped by Edlund (1977); and the soils were mapped by Tarnocai (1977). Surficial geology maps at a scale of 1:125 000 are being prepared for open file release through the Geological Survey of Canada. The purpose of this report is to provide a brief description of the surficial materials of the area.

Materials

Till

The most extensive surficial deposit of the area is a sandy till, although a silty till occurs in the northern part of NTS map-area 56 N (Fig. 60.1).

The till surface generally is covered by an abundance of angular to subrounded boulders commonly more than 1 m in length. The boulders are concentrated on the surface from within the till by frost action. Usually the boulders are petrologically the same as the underlying bedrock; however, in one locality in northern map-area 56 K, the boulders are mainly gneissic in composition, with less than one per cent having been derived from the metavolcanic bedrock which outcrops in the vicinity. Generally the boulders cover from 30 to 50 per cent of the surface; however, where the till is thin, the concentrations are much higher. Of particular interest is one region in the east-central part of map-area 56 K where the ground surface is completely covered by boulders. The deposit is drumlinized, which implies a till genesis for the material. This interpretation is supported by the fact that even though most of the boulders were derived locally, some have been transported for considerable distances (M. Schau, pers. comm., 1977).

The thickness of the till varies from a veneer of less than 1 m to a blanket of several tens of metres. Where it occurs as a veneer, the surface topography conforms to the surface of the underlying bedrock. Where the till is thicker, it masks the detail of the underlying bedrock topography, commonly forming a gently rolling surface with an average relief of 20 to 30 m. Crag-and-tail

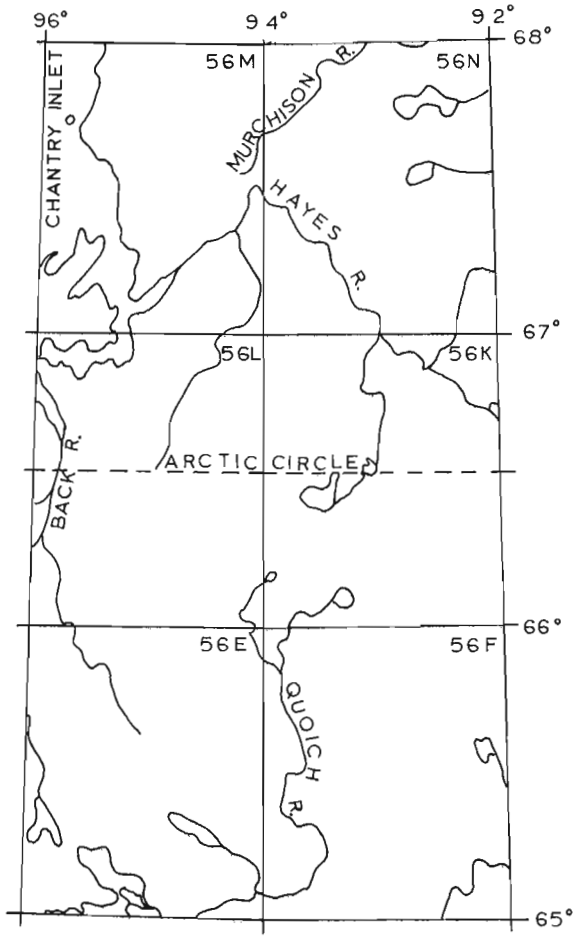

Figure 60.1. Location map.

landforms are common, whereas drumlins are rare. The direction of ice flow indicated by these features is generally northward, varying from northwest to northeast depending on the location within the area. Various types of moraines, both large and small, were encountered throughout the area.

The active layer in till averages from 50 to 100 cm thick (Tarnocai, 1977). Stripes, either as boulder stripes where boulders are abundant or as vegetation stripes where the vegetation mat is more continuous, commonly are formed on the tills. Sorted and nonsorted nets and circles occur in areas of low slope angle. The sorted circles average 1 m in diameter, although circles several metres across are common. At one site, circles several tens of metres across, having a fine grained centre 3 m in diameter and boulders up to 2 m long in the periphery, were observed. Nonsorted circles average 1 m across and commonly have turf ramparts around the perimeter.

From: Report of Activities, Part B; Geol. Surv. Can., Paper 77-1B (1977)

One till unit, which occurs throughout the area, is particularly evident on aerial photographs due to its well developed stripes. These stripes, formed by vegetation, are composed of wide light-toned bands and narrow dark-toned bands associated with rills. The underlying material was much sandier, yet relatively deficient in boulders, compared with the regional till. At two locations the stripes were found to occur only below proglacial lake strandlines. Moreover these units are common below marine limit. Other occurrences are all within possible proglacial lake basins. Thus it is concluded that these deposits are a veneer of either lacustrine or marine sand overlying till.

Stratified Drift

These deposits, including both glaciofluvial and ice-contact stratified drift, range in composition from silty sand to gravel, with the surface of some eskers being entirely covered by boulders. The cobbles and boulders are rounded to subrounded, are up to 1 m in length, and are gneissic or quartzitic in composition. These materials were recognized on aerial photographs, not only because of their morphology, but because the steeper slopes are light toned and the flatter tops are dark toned because of the dark green and black lichens (**Alectoria** sp.) that grow preferentially on them.

Eskers, either as single isolated ridges or as groups of ridges, commonly associated with terraced glaciofluvial deposits, are common throughout the area. They range in height from 2 m to over 30 m and have steep slopes and either flat or sharp crests. Aligned towards the north-northwest, single eskers cross the area, in places ending in or leading from steep-sided meltwater channels with boulder-covered floors cut in either till or bedrock.

Larger esker complexes occur in valleys 1 or 2 km wide where the meltwater has removed or reworked the previously deposited till to leave behind either bare rock with a lag concentration of cobbles and boulders or hummocky to transversely ridged sand and gravel. On either side of the esker complex, a veneer of sand was deposited over the till and bedrock.

Commonly, esker complexes grade into a valley fill of terraced glaciofluvial material, but some end in large deltas built into marine water. These deltas are flat topped and commonly are incised by channels. The backslopes are steep, whereas the foreslopes, although steep, usually have terraces cut into them.

The active layer in these materials may be up to 2 m thick. At one site where thermistor temperature measurements were taken, the sand was found to be below 0°C at a depth of 1 m even though visible ice was not observed to a depth of 2 m. Most of the flat-topped sand deposits have ice-wedge polygons, generally in a rectangular pattern up to 7 m across, developed on them; vegetation stripes or solifluction lobes were observed on the flanks. At one location in map-area 56 K, a possible pingo was found on a glaciofluvial terrace. It is 20 m high, 80 m in diameter, and is composed of the same material that occurs on the valley floor. The ice-wedge cracks on the valley floor run across the pingo and intersect at the summit. Although pingos in coarse material are not common, Pissart (1967) has described some pingos in sand and gravel on Prince Patrick Island, Northwest Territories.

Several lakes were found to have no surface outlet but to drain through the unfrozen bases of adjacent eskers as numerous springs or seeps. During the winter, at some locations this water spreads out over the ground surface forming icings or **aufeis**. In a number of cases the aufeis was still present in the middle of August. Obtaining large quantities of aggregate from the unfrozen sections of eskers around the seepage areas may be of possible economic significance.

Marine

Occurring mainly in the northern part of the area (map-areas 56 M and N), marine deposits are commonly a grey interbedded clay, silt, and sand unit overlain by brown sand. Fossils are very rare in this material, being found only at one location on a tributary to Murchison River. The sand commonly is covered by vegetation; however, the silts at the surface are mostly bare.

The thickness of marine deposits varies from less than 1 m, in which case it reflects the topography of the underlying bedrock or till, to over 50 m as a valley fill in Hayes and Murchison river valleys. In these latter localities the sand unit comprises the upper 10 to 20 m. Between these two extremes of thickness, the marine material forms a blanket deposit which masks the underlying topography and forms a gently rolling surface. Where relief is high, as along Hayes River, the deposits are incised up to 50 m by an intricate dendritic gully system.

Marine beaches are not prevalent, occurring well below marine limit. The highest elevation of marine silts found is 275 m in the southwest part of map-area 56 N.

The most common patterned ground feature developed on marine material is low-centred polygons which are especially abundant in the northern part of map-area 56 M. Other features, such as desiccation cracks and nonsorted nets and circles, only have limited occurrence.

Eolian

Along rivers and on adjacent terraces, eolian activity has transported fine sand and silt. In some places large areas of bare sand have formed, which are presently encroaching on adjacent vegetated areas. The largest of these areas is 20 km^2 and is composed of 60 cm of eolian sand overlying a well developed soil (C. Tarnocai, pers. comm., 1976). In a few localities blowout dunes, of the order of 20 m long and 1 m high, occur. These dunes, being vegetated, are not active today; however, they indicate the same northwest wind direction as the modern eolian features.

Most eskers in the area have patches of bare sand along their crests. These areas were probably much more extensive in the past, for on the eastern flanks of most eskers an accumulation of eolian sand exists. Where the slopes are steep, the sand formed solifluction lobes.

Acknowledgments

The author would like to acknowledge the scientific and logistic assistance, both in the office and in the field, provided by A.S. Dyke, R.J. Hawes, and J.J. Veillette.

Capable field assistance from D. Noakes, W. Peryouar, D. Johnson, D. Brown, A. Murdock, and L. Moyer was greatly appreciated. Stimulating discussions with C. Tarnocai and S.A. Edlund, both on traverse and in camp, were very helpful. Comments by A.S. Dyke, J.J. Veillette, D.M. Barnett, and L.A. Dredge concerning the manuscript were of much benefit.

References

Boydell, A.N., Drabinsky, K.A., and Netterville, J.A.
1974: Surficial geology and geomorphology, Boothia Peninsula; Geol. Surv. Can., Open File 285.

1975: Terrain inventory and land classification, Boothia Peninsula and northern Keewatin; in Report of Activities, Part A, Geol. Surv. Can., Paper 75-1A, p. 393-396.

Craig, B.G.
1961: Surficial geology of northern District of Keewatin, Northwest Territories; Geol. Surv. Can., Paper 61-5, 8 p.

Cunningham, C.M. and Shilts, W.W.
1977: Surficial geology of the Baker Lake area, District of Keewatin; in Report of Activities, Part B, Geol. Surv. Can., Paper 77-1B, rep. 59.

Edlund, S.A.
1977: Vegetation types of north-central District of Keewatin; in Report of Activities, Part A, Geol. Surv. Can., Paper 77-1A, p. 385-386.

Heywood, W.W.
1967: Geological notes, northeastern District of Keewatin and southern Melville Peninsula, District of Franklin, Northwest Territories; Geol. Surv. Can., Paper 66-40, 20 p.

Pissart, A.
1967: Les pingos de l'ile Prince-Patrick; Geogr. Bull., vol. 9, n° 3, p. 189-217.

Tarnocai, C.
1977: Soils of north-central Keewatin; in Report of Activities, Part A, Geol. Surv. Can., Paper 77-1A, p. 61-64.

Wright, G.M.
1967: Geology of the southeastern barren grounds, parts of the Districts of Mackenzie and Keewatin; Geol. Surv. Can., Mem. 350, 91 p.

61. MID-CENOZOIC PALEOGEOMORPHOLOGY AND TECTONIC SETTING OF THE ST. ELIAS MOUNTAINS, YUKON TERRITORY

Project 750013

G.H. Eisbacher and S.L. Hopkins
Regional and Economic Geology Division, Vancouver

Introduction

The St. Elias Mountains of southwestern Yukon Territory and the contiguous Alaska Range form a prominent topographic barrier between the northwest Pacific Ocean and the North American continent. The highest peaks in North America are within these mountain ranges. Mt. Logan, with an elevation of 5950 m, is the highest point in Canada and is in the Icefield Ranges of the St. Elias Mountains. Much of the elevated terrain of this region is covered with large icefields. Glaciers flow northeastward into winding low valleys or south towards the Pacific Ocean. The high peaks in the St. Elias Mountains are remnants of granitic batholiths sculptured by erosion from less resistant volcanic greenstone, phyllites, and carbonate rocks (Fig. 61.1). The evolution of the landscape is geologically young and resulted from collision of the Pacific crustal plate with the continental margin of North America (Plafker, 1969). As a consequence of regional compression the crust has thickened and its surface is rising. Earthquakes in the region attest to continuing crustal unrest in a broad zone at the continental margin (Tobin and Sykes, 1968; Gedney, 1970). In detail the Cenozoic evolution of the Cordilleran landscape can be read from the stratigraphy of Cenozoic rocks near the mountains. This report is mainly concerned with the Cenozoic record and structural history of the eastern St. Elias Mountains (Fig. 61.2). However, data from the literature on southern Alaska have been incorporated in order to establish a regional framework. Much of the information on the St. Elias Mountains was collected by G.H. Eisbacher during Operation St. Elias of the Geological Survey of Canada in 1974.

Figure 61.1. The young erosional landscape of the Icefield Ranges in the western St. Elias Mountains. Mt. Logan (5950 m), a granitic massif, rises above a low terrain underlain by phyllites, limestone, and greenstone.

Regional Geologic History

The stratigraphic and structural relationships in the Alaska Range, St. Elias Mountains, Gulf of Alaska, and Cook Inlet have been reviewed recently by MacKevett (1970, 1971), Richter and Jones (1973), Berg et al. (1972), Read and Monger (1975), Eisbacher (1976), Plafker (1971), Plafker et al. (1975), and Kirschner and Lyon (1973). A schematic composite stratigraphic column for the St. Elias region is shown in Figure 61.4.

The pre-Cenozoic history of the St. Elias Mountains is deduced from its sedimentary and volcanic stratigraphy and from its intrusive rocks. During Late Jurassic – Early Cretaceous time a thick succession of marine flysch was deposited in two extensive basins. One has been referred to as Gravina-Nutzotin Belt by Berg et al. (1972) and straddles the zone between the St. Elias and Coast mountains. It includes the Dezadeash Formation and the Nutzotin Mountains Sequence (Fig. 61.2). This flysch was derived from a plutonic-volcanic terrane to the southwest (Eisbacher, 1976). Another intensely deformed belt of Jurassic – Cretaceous flysch is preserved along the Gulf of Alaska and is referred to as Valdez – Yakutat Group (Fig. 61.2). In latest Cretaceous to earliest Tertiary time both clastic basins were tectonically foreshortened and their contained rocks underwent severe deformation. Closure of the inner eastern basin, the Gravina – Nutzotin Belt, was accompanied by metamorphism and thrust faulting along the western margin of the Coast Mountains, followed by the rise and cooling of discordant plutons of the Coast Plutonic Complex between 70 and 50 m.y. ago. In the Cook Inlet region this orogenic event is recognized in tightly folded Upper Cretaceous strata of Cenomanian, Turonian and Senonian age (Kirschner and Lyon, 1973). As a consequence of this deformation clastic deposition shifted southwestward into the Gulf of Alaska and the Cook Inlet. The oldest Tertiary record in the Gulf of Alaska Province is a Paleocene to Eocene (?) flysch derived from the east and deposited along trend with the base of the tectonically active continental margin. It was deformed shortly after deposition and intruded by acidic plutons ranging in age from 49 to 52 m.y. (Winkler, 1976). Farther to the west Paleocene-Eocene quartzose clastics, derived from the north and northwest were

From: Report of Activities, Part B; Geol. Surv. Can., Paper 77-1B (1977)

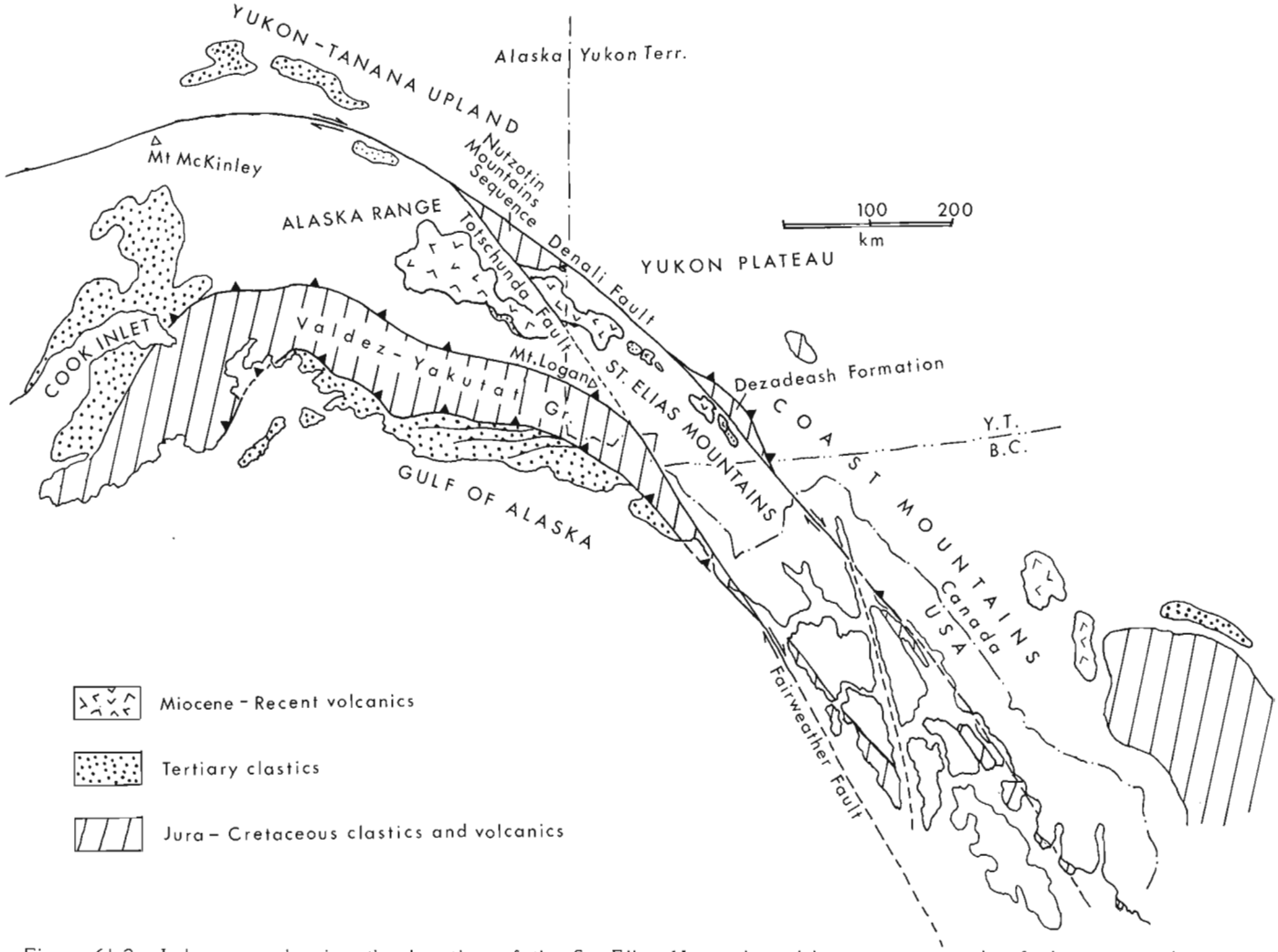

Figure 61.2. Index map showing the location of the St. Elias Mountains with respect to major fault zones and tectonostratigraphic units discussed in the text.

deposited into the actively subsiding Cook Inlet basin (Kirschner and Lyon, 1973). Right-lateral transcurrent movement of 300 km along the Denali Fault has disrupted the inner Jura-Cretaceous flysch belt into two distinct outcrop belts, the Dezadeash Formation and the Nutzotin Mountains Sequence (Eisbacher, 1976).

Prior to initiation of Oligocene – Miocene sedimentation a pulse of uplift and profound erosion affected all older deposits (Kirschner and Lyon, 1973; Plafker et al., 1975). The latest Eocene (?) – Oligocene is therefore an appropriate time interval at which to introduce an examination of the paleogeomorphology of the St. Elias region.

Faults and Oligocene Basins, Eastern St. Elias Mountains

The St. Elias Mountains are bounded on the east by the broad Shakwak Valley (Bostock, 1952), a young erosional trench which lies partly along the Denali Fault, and partly along an older (latest Cretaceous – earliest Tertiary) shear zone between biotite schists of the Yukon Crystalline Terrane and Jura-Cretaceous flysch. Northwest of Kluane Lake the Shakwak Valley follows the principal strand of the Denali Fault. Southeast of Kluane Lake the Denali Fault swings southward away from the Shakwak Valley but is still marked by a well defined topographic lineament. Southwest of the Denali Fault numerous fault strands break across the oldest sedimentary and volcanic rocks of the St. Elias Mountains (Fig. 61.3). They are high angle faults along which all rock units are shattered. These faults are significant in that they collected mid-Tertiary trunk streams localizing subsequent deposition of clastic material in small continental basins along them. Remnants of the continental clastics within fault bounded panels make up the Amphitheater Formation. The principal areas where the Amphitheater Formation is preserved are near Cement Creek, Amphitheater Mountain, Sheep Creek, and east of Bates Lake (Fig. 61.3).

Offset metamorphic rocks which yield K-Ar ages of about 50 m.y. indicate that large right-lateral transcurrent motion along the Canadian segment of the Denali Fault took place after 50 m.y. (Eisbacher, 1976). Slivers

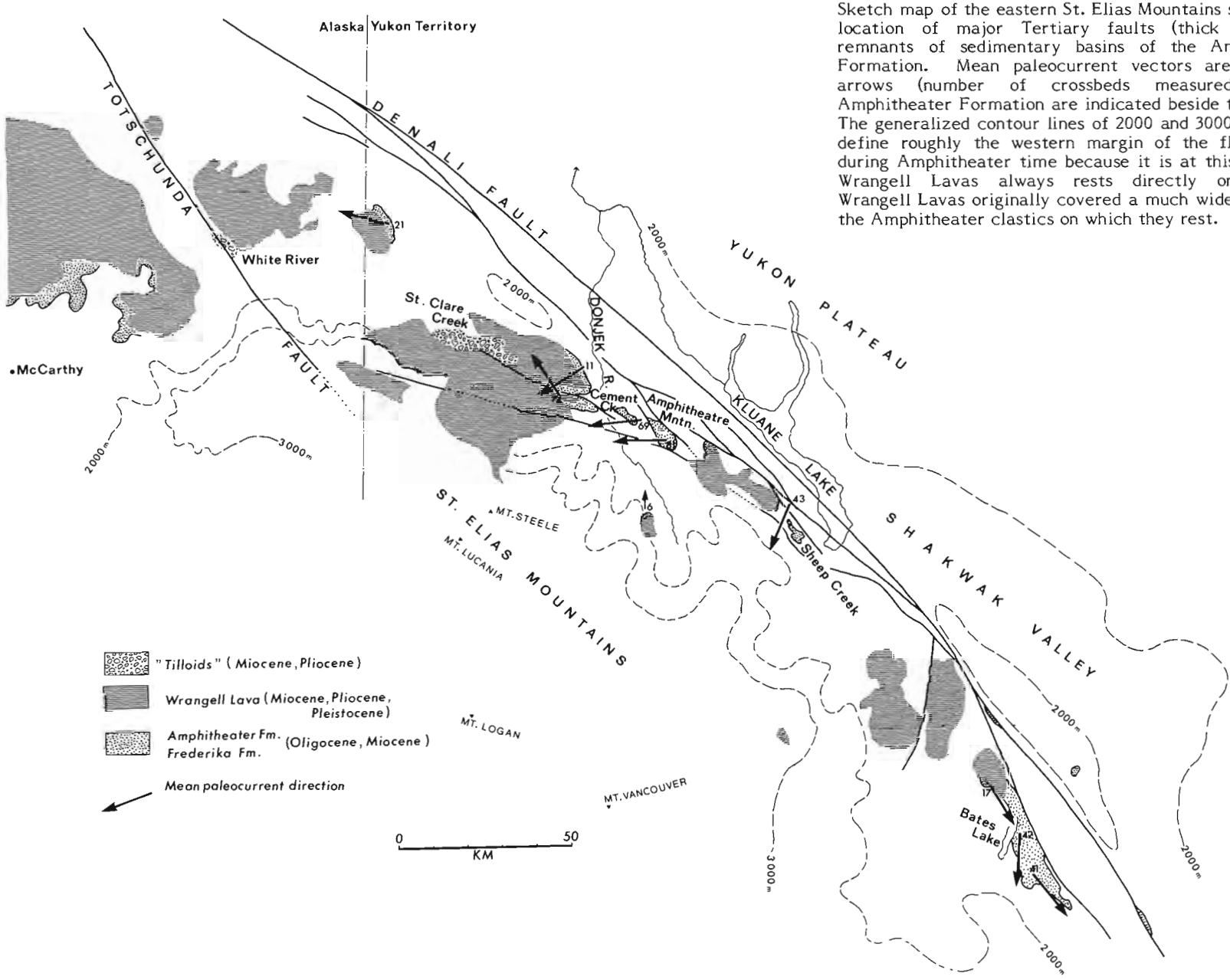

Figure 61.3.

Sketch map of the eastern St. Elias Mountains showing the location of major Tertiary faults (thick lines) and remnants of sedimentary basins of the Amphitheater Formation. Mean paleocurrent vectors are shown by arrows (number of crossbeds measured in the Amphitheater Formation are indicated beside the arrows). The generalized contour lines of 2000 and 3000 m seem to define roughly the western margin of the fluvial basin during Amphitheater time because it is at this level that Wrangell Lavas always rests directly on bedrock. Wrangell Lavas originally covered a much wider area than the Amphitheater clastics on which they rest.

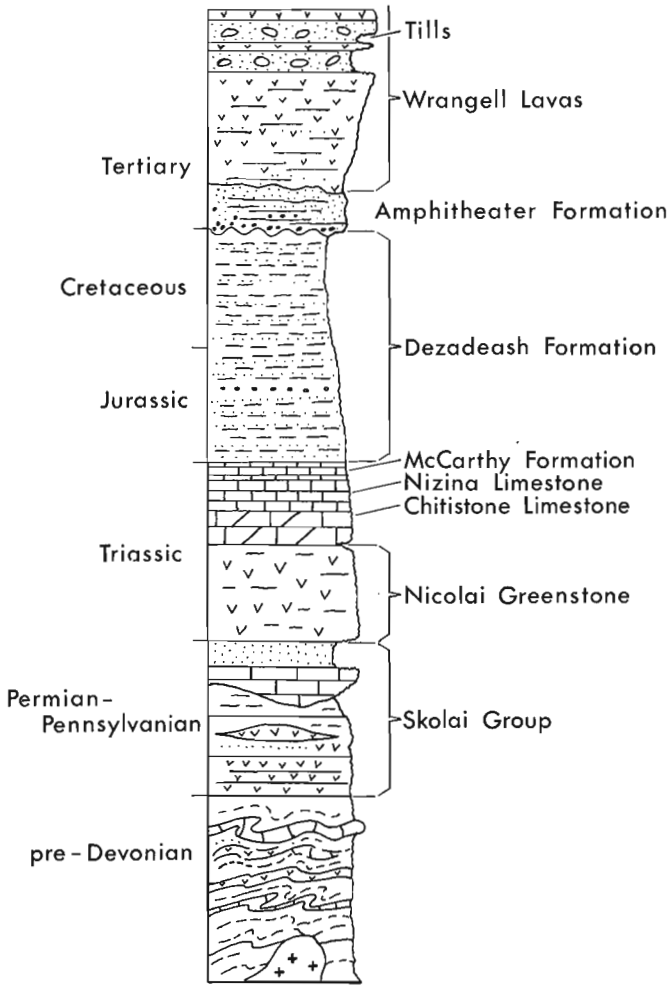

Figure 61.4. Schematic stratigraphic chart for the eastern St. Elias Mountains, Yukon Territory.

of Tertiary clastic rocks are tectonically involved along the fault, but the exact timing of the principal right-lateral fault movement of about 300 km is unknown. Data presented in the following sections show that subsidiary faults in the eastern St. Elias Mountains must have been particularly active towards the end of Oligocene. However, the main displacement could have taken place prior to the onset of clastic deposition coincident with the regional depositional hiatus between 50 and 40 m.y. ago.

Tertiary Stratigraphy

The mid-Tertiary clastics overlie older sedimentary and plutonic complexes of the St. Elias Mountains with profound unconformity. In Yukon Territory the basal sequence of conglomerate, sandstone, mudstone, and coal has been named the Amphitheater Formation (Muller, 1967). The name is derived from Amphitheater Mountain which displays the best exposed section of mid-Tertiary clastics in the area along its southern scarp (Badlands Creek). In adjacent Alaska roughly correlative strata are known as Frederika Formation (MacKevett, 1970 and 1971). Farther west in Alaska mid-Tertiary continental rocks comprise the Coal-Bearing Group (Wahrhaftig et al., 1969). The Amphitheater Formation is probably Oligocene (see below), the Frederika Formation seems to be mainly Miocene (MacKevett, 1970 and 1971), and the Coal-Bearing Group ranges in age from Oligocene to Miocene (Wahrhaftig et al., 1969).

In the St. Elias Mountains and eastern Alaska Range the clastic units are overlain by 300 to 2000 m of subaerial basaltic to andesitic flows and volcaniclastics. They have been named Wrangell Lavas in Alaska (Mendenhall, 1905; MacKevett, 1970) and this term has been used for coeval volcanics in the Yukon Territory by Souther and Stanciu (1975). K-Ar ages obtained from Wrangell Lavas and related high-level felsite intrusions in Canada range between 16 m.y. and 6 m.y. (J.G. Souther, pers. comm., 1976). However, locally the base of the Wrangell Lavas is probably older than 16 m.y. The youngest manifestation of volcanic activity is post-Pleistocene. Extensive ash-falls occur over large areas of

Figure 61.5.

The headwaters of Badlands Creek with outcrops of Amphitheater Formation. The dark resistant unit above the talus on the right is Wrangell Lavas. The glaciated peak of Mt. Hoge is in the background.

Table 61.1

Microflora from the Amphitheater Formation

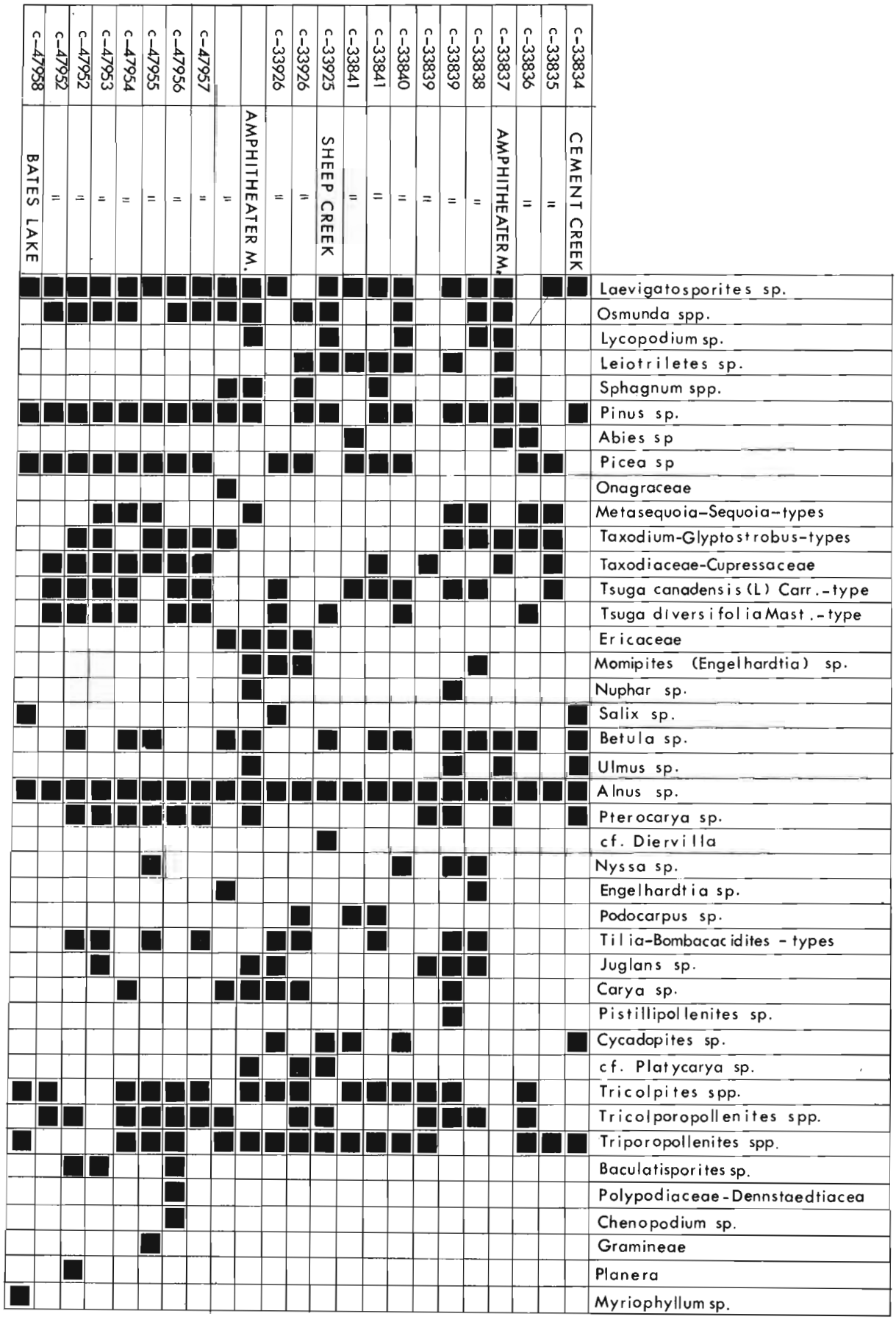

western Yukon Territory (Bostock, 1952; Lerbekmo and Campbell, 1969). Higher parts of the Wrangell Lavas are interstratified with till sheets and fluvioglacial deposits near the White River in Alaska and St. Clare Creek in Yukon Territory (Capps, 1916; Muller, 1967). The White River locality has been studied in detail by Denton and Armstrong (1969) who determined K-Ar ages as old as 9 to 10 m.y. for lavas interlayered with tillite sheets. Onset of glaciation in the St. Elias Mountains therefore began in middle or late Miocene. The tilloids at St. Clare Creek and White River (Fig. 61.3) are tilted tectonically and cut by faults (Denton and Armstrong, 1969; Souther and Stanciu, 1975).

Age of the Amphitheater Formation

Samples of shale and carbonaceous mudstone from the Amphitheater Formation have been analyzed for their spore and pollen content. The 23 samples were obtained from fine grained sediments at Cement Creek, Amphitheater Mountain, Sheep Creek and one sample from Bates Lake (Table 61.1). Preservation of the palynomorphs ranges from excellent to poor, apparently depending on the distance of the host rocks to overlying lavas or intruding felsites.

The age assignment of this composite assemblage is tenuous at best, largely because most of the contained taxa are abundant throughout the Cenozoic. Perhaps most significantly, no representatives of the family Compositae were encountered, and only one specimen each of the families Gramineae and Chenopodiaceae were found. These three families, if represented in any numbers, would strongly suggest a Neogene (Miocene-Pliocene) age for the sediments. Furthermore, one specimen of **Pistillipollenites** was found in a sample from Amphitheater Mountain. This genus has been recorded only in Eocene or Paleocene rocks. In addition, several questionably identified specimens of **Platycarya** were found, a genus essentially restricted to Eocene rocks in North America. Also, probably significant, are the presence of several specimens of cf. **Diervilla** and representatives of the family Onagraceae. To date, in British Columbia, these have been found only in Oligocene rocks. **Momipites**, which is present in four samples, is largely an Eocene form, but is also known to occur in Oligocene strata.

Generally, epoch/series boundaries within continental rocks of the Paleogene are difficult to define, partly because the European type sections are not clearly defined, and partly because correlation with North American sections are, to say the least, incomplete. Finally, Cenozoic palynological control, in northwestern North America is far from understood. However, on the basis of admittedly insufficient data we feel the microflora is most likely Oligocene, although an upper Eocene age is possible.

The microflora is dominated by ferns, alder and pine, and suggests a wet temperate climate, rather unlike the more subtropical climate which typically characterizes the coastal Eocene. The middle Oligocene appears, at least in North America, to be a time when comparatively abrupt climatic deterioration began (Wolfe, 1971) which may be partly related to the considerable tectonic uplift at the time (see also Hopkins et al., 1972). This raises the possibility that the flora from the Amphitheater Formation indicates the declining temperature side of the

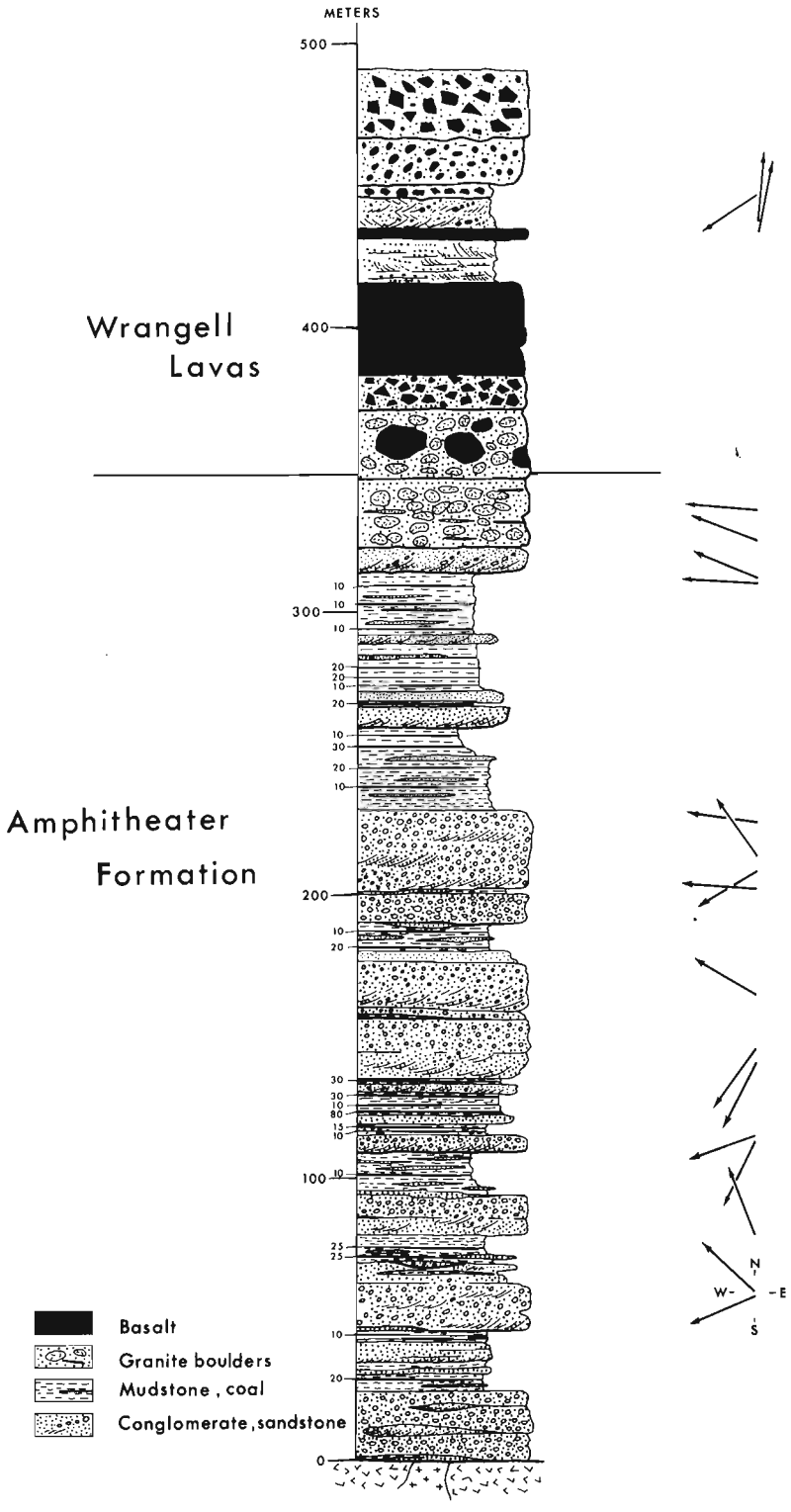

Figure 61.6. Type section of Amphitheater Formation measured south of Amphitheater Mountain along the headwaters of Badlands Creek. Arrows indicate direction of individual large foresets in crossbedded conglomeratic sandstones. Smaller numbers along the left side of the column give thickness (centimetres) of lignite seams. Top of the Amphitheater Formation is the first occurrence of basalt blocks in debris flow deposits (shown in black).

Oligocene, i.e. middle or upper Oligocene. However, until further data are available it is unprofitable to speculate farther.

Sedimentology of the Amphitheater Formation

The Oligocene Amphitheater Formation rests with profound unconformity on older Paleozoic and Mesozoic rocks. The basal surface is a sharp break between an erosional pediment and conglomerate of the Amphitheater Formation. In several places regolith or angular scree is preserved in topographic depressions of the bedrock. A reddish regolith is well developed along the greenstone pediment south of Amphitheater Mountain and at the basal contact in Cement Creek. The most spectacular scree deposits occur about 15 km south of Bates Lake, where unsorted and angular material near the bedrock grades vertically and laterally into crudely stratified material. Stratigraphic thickness varies tremendously between outcrops. Environment of deposition, paleocurrents and composition will therefore be discussed separately for the main outcrop areas shown in Figure 61.3.

Cement Creek

The sections exposed along and near Cement Creek are tilted and broken by faults. The bulk of the sediments are coarse grained lithic arenites and polymictic conglomerate. Their thickness is about 200 to 300 m near the axis of the outcrop belt and decreases to zero towards the north and south within a few kilometres. The conglomerate clasts are rounded to well-rounded, and include volcanics (30-50%), granitoids (20-40%), chert and volcanic tuffs (30-40%). Laterally and towards the top of the sections the fluvial succession grades into thinly bedded siltstones intercalated with delicately laminated calcareous bands. These are probably lacustrine sediments. Several seams of lignite less than 30 cm thick occur within the finer grained parts of the section.

Most of the conglomerate is loosely packed and sandy portions are commonly crossbedded. Crossbedding indicates westerly flowing paleocurrents (Fig. 61.3). Relatively fresh detrital biotites separated from lithic arenite exposed a few kilometres north of Cement Creek yielded a K-Ar age of 50 m.y. (GSC K-Ar 2459). This indicates a source area east of the Shakwak Valley where biotite schists of this age are exposed (Eisbacher, 1976; Tempelman-Kluit, 1974). The outcrops near Cement Creek are thus characterized by fluvial deposits intercalated with deposits of swamps and ephemeral lakes. The general paleocurrent flow was to the west.

Amphitheater Mountain

South of Amphitheater Mountain, the type area of the Amphitheater Formation, excellently exposed sections are encountered in erosional gullies and ridges near the headwaters of Badlands Creek (Fig. 61.5). The succession consists of polymictic conglomerate, sandstone, siltstone and numerous thin seams of lignite. The thickness of the type section as measured on the south side of Amphitheater Mountain is 350 m (Fig. 61.6). The conglomerate clasts are made up of basic and acidic volcanics, granitoids, foliated metasediments, chert or

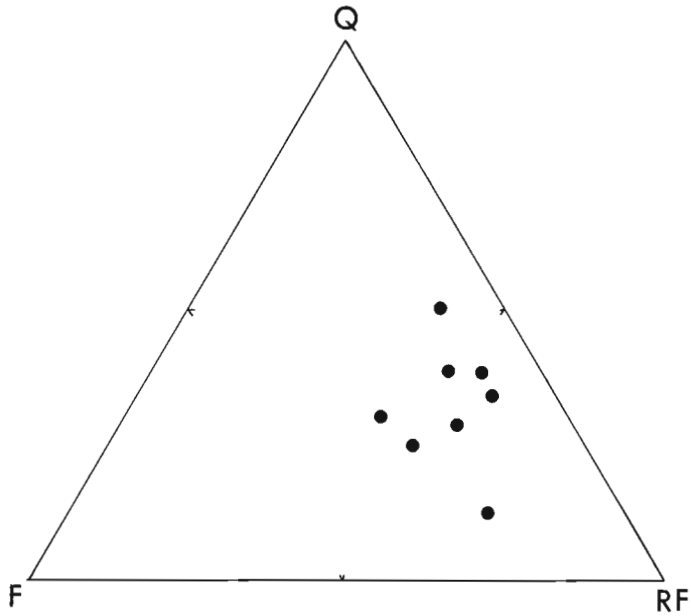

Figure 61.7. Modal composition of sandstone from the type locality of the Amphitheater Formation (Q=quartz, F=feldspar, RF=chert, volcanic and metasedimentary rock fragments).

tuff in about equal proportions. Modal counts show that the sandstones are lithic arenites (Fig. 61.7). As suggested by Muller (1967, p. 81) most of the conglomerate clasts, particularly the granitic constituents, point to source areas on the east side of the Shakwak Valley. Relatively fresh volcanic clasts of rhyolite-dacite composition collected from conglomerates of the Amphitheater Mountain section are similar to early Tertiary Mt. Nansen volcanics of the Yukon Plateau (D.J. Tempelman-Kluit, pers. comm., 1976).

Crossbedding and sporadic pebble imbrication indicate westerly flowing paleocurrents (Fig. 61.3), which agrees with the inferred easterly source area for the conglomerate clasts. About 20 km south of Amphitheater Mountain a small outcrop of angular boulder conglomerate made up of locally derived granite, sericite schist, and calcareous phyllite demonstrates that the principal westward directed drainage received subsidiary rivers from local uplands to the south as well.

The environment of deposition of the Amphitheater Formation can be inferred from the section illustrated in Figure 61.6. None of the simple models described from recent fluvial settings can be directly applied to the section or to outcrops on the nearby Burwash Uplands. It is therefore appropriate to discuss some of its characteristics in detail. Two basic types of deposits can be differentiated: one is a complex of conglomerate and sandstone, the other a mudstone-siltstone-lignite succession (Fig. 61.6).

The first type consists of an interlaced framework of lenticular conglomerate lenses, crossbedded pebbly sandstone, and flatbedded sandstones which commonly contain pieces of silicified wood (Fig. 61.8). These composite conglomerate-sandstone bodies range between 5 and 30 m in thickness. Foreset slopes of crossbeds are

as much as 3 m long, suggesting large migrating sand and gravel bars. Internal features are clearly indicative of channel erosion, channel filling, and channel abandonment with both progradation and lateral accretion of sedimentary material. Some of the conglomerate-sandstone complexes coarsen upward in grain size; others fine upwards. The upward-fining complexes are distinctly channelled into underlying mudstone or siltstone, whereas upward-coarsening complexes commonly start with planar crossbedded sandstones smoothly overlying a base of laminated strata of mudstone or siltstone. The upward-fining complexes are most likely the result of meandering,

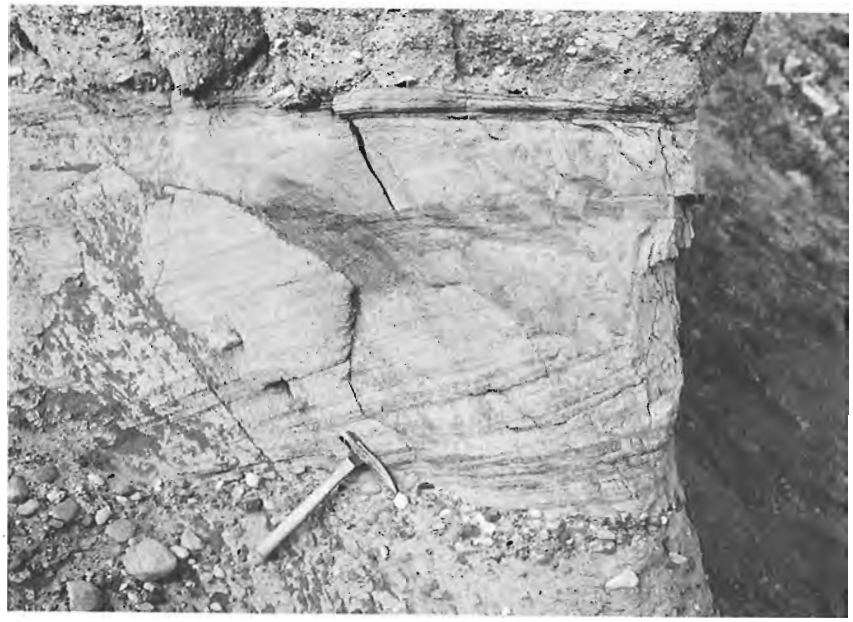

Figure 61.8.

Intricately crossbedded sandstone and massive conglomerate of Amphitheater Formation. The three photographs demonstrate that gradation from conglomerate to conglomeratic sandstone occurs on all scales.

Figure 61.9.

Granitic sharpstone conglomerate at the top of Amphitheater Formation at Amphitheater Mountain. In the centre of the picture a thin layer of lignitic coal demonstrates layering of this sedimentary deposit (pick for scale at bottom of picture).

high-gradient, river channels, the upward-coarsening complexes represent the gradual progradation of fluvial lobes into completely stagnant backwaters. The coarse grained clastics of the Amphitheater Formation thus represent the facies characteristic of strong meandering and braided channel systems (see Eynon and Walker, 1974; McGowen and Garner, 1970).

The second type of clastic deposit within the Amphitheater Formation are packets of siltstone, mudstone, and lignitic coal. The coal seams are numerous but thin (Fig. 61.6) and of limited extent. Coals and mudstones were probably deposited within temporary stagnant backwaters of the alluvial system. The rapid vertical alternation between coal bearing fine grained clastics and thick conglomerate complexes is an unusual feature. Buffler and Triplehorn (1976) have commented on the occurrence of this seemingly contradictory facies pair in the mid-Tertiary Coal-Bearing Group of Alaska as well. A possible explanation is that high tectonic relief favoured coexistence of temporary protected backwaters and high-gradient channels on the same alluvial plain. Progradation of one environment over the other would have occurred during dislocation of trunk streams by faulting.

Towards the top of the Amphitheater Mountain section a thick deposit of coarse boulder conglomerate consisting almost entirely of granitic debris overlies in sharp contact thinly laminated siltstone and lignite (Fig. 61.9). The massive debris-flow deposit was derived from granitic rocks which outcrop immediately east of Amphitheater Mountain. The debris flow deposit grades upwards into a chaotic boulder conglomerate containing blocks of both granite and Wrangell Lavas up to 7 m in diameter. This interval of coarse debris-flow channels has been interpreted by Muller (1967) as the base of a flat westward directed thrust fault, with 'crushed granodiorite' separating the cap of Wrangell Lavas from the Amphitheater Formation below (Muller, 1967, p. 100 and Plate 7). Stratification, imbrication and rounding of granitic clasts contradicts Muller's interpretation of the granite boulder conglomerate as a tectonic breccia. The size of the boulders indicates high flow gradients which were probably related to contemporaneous faulting.

Sheep Creek

The mid-Tertiary sequence of the Sheep Creek area is broken by high-angle faults making it difficult to determine stratigraphic relationships. However, a rough idea of the succession was obtained on the western side of the unnamed mountain between Fisher Creek and Sheep Creek (see Fig. 61.12). This outcrop area is shown in Figure 61.10. About 180 m of section are exposed. The lowest part consists of friable lithic arenite which dips gently to the southwest. These beds are overlain unconformably by siltstone, mudstone and lignite. The discordance at the unconformity is about 10 degrees. Above the lignite layers are 50 m of polymictic conglomerate. The conglomerate, in turn, is locally truncated erosionally, and the section is capped by coarse angular debris with blocks of gabbro, argillite, and calcareous siltstone. This debris is interpreted as a landslide deposit that caps the Tertiary clastics. Immediately west of the section shown in Figure 61.10 (i.e. west of Sheep Creek) the angular landslide rubble is incorporated in the sedimentary sequence of the Amphitheater Formation indicating that the landslide deposits are an integral part of the mid-Tertiary succession (Fig. 61.13). The slide probably had its source northeast of the debris lobe where rocks similar to the rubble in the landslide are part of the bedrock. West of Sheep Creek the highest beds of the Amphitheater Formation include large blocks of limestone and Wrangell Lavas derived from an adjacent bedrock ridge. Conglomerate in the Sheep Creek area is polymictic with abundant acid to intermediate volcanics, granitoids, vein quartz, and quartzite. Particularly the presence of quartzite clasts strongly suggests a source area east of the Shakwak Valley. Possibly, the source of these was the Nasina quartzite, an extensive bedrock unit underlying the Yukon Plateau (Tempelman-Kluit, 1974).

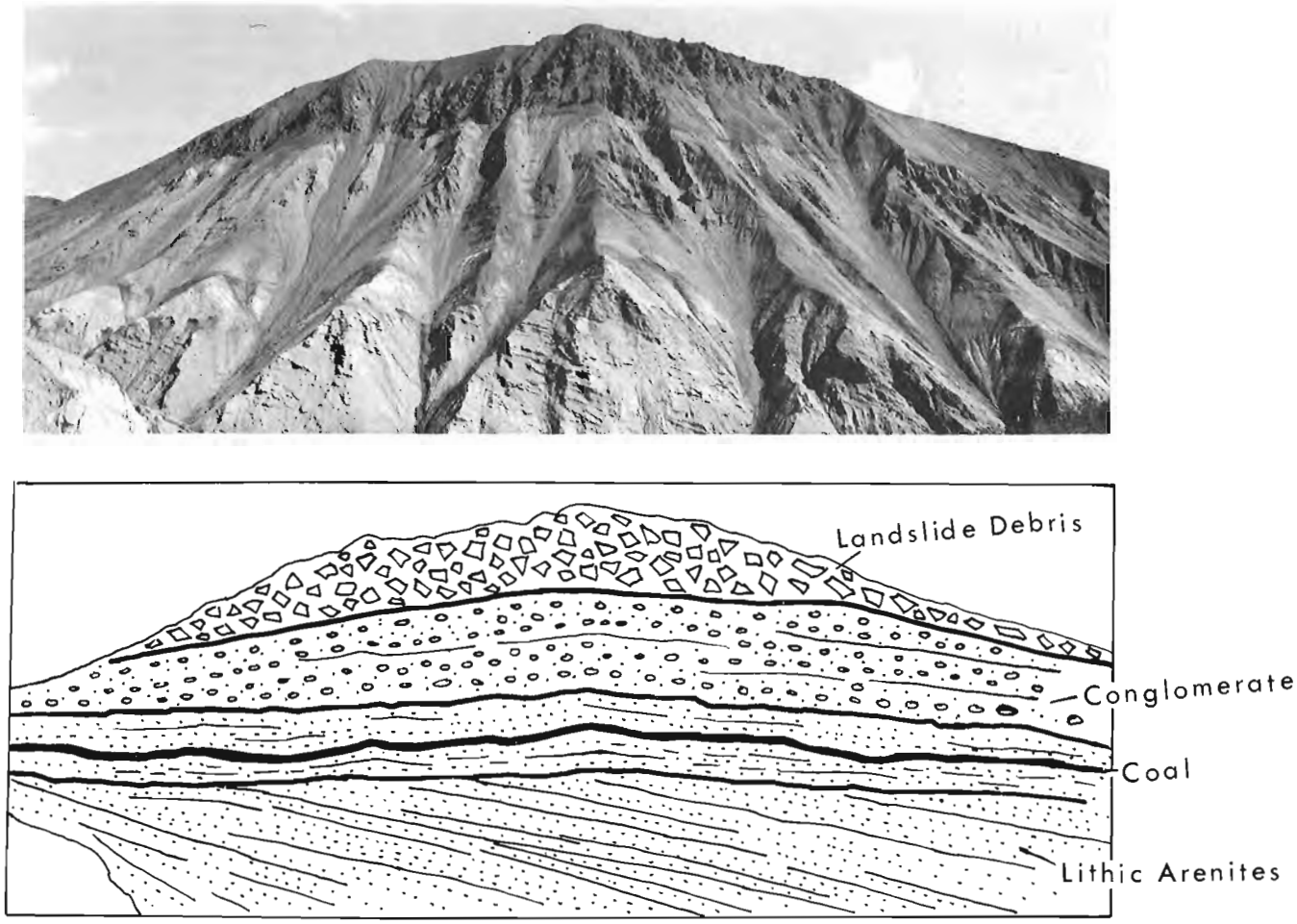

Figure 61.10. Photograph and generalized sketch of Amphitheater Formation east of Sheep Creek. A low-angle unconformity within the succession and landslide deposits above the conglomerate indicate synsedimentary tectonic activity.

Crossbedding in sandstone and imbrication in conglomerate indicate southwesterly flowing paleocurrents for the Sheep Creek area (Fig. 61.3).

A different interpretation of the Tertiary succession of the Sheep Creek was put forward by Muller (1967, p. 100, Fig. 5, and Plates 1, 2 and 9A) who proposed that the rubbly mass of gabbro and argillite above the Tertiary succession is a tectonic klippe emplaced by a regional thrust fault that dips gently eastward (Muller, 1967, Plate 1). Careful mapping east of the rubbly mass did not confirm the existence of a low-angle thrust fault. It is therefore inferred that the rubbly deposit capping the mid-Tertiary clastics was implaced as a debris stream or landslide, rather than as part of a low-angle thrust sheet.

Bates Lake

Mid-Tertiary clastic deposits near Bates Lake filled a one-sided graben bounded by a high-angle fault on the east. Along its western flank the basinal deposits overlap

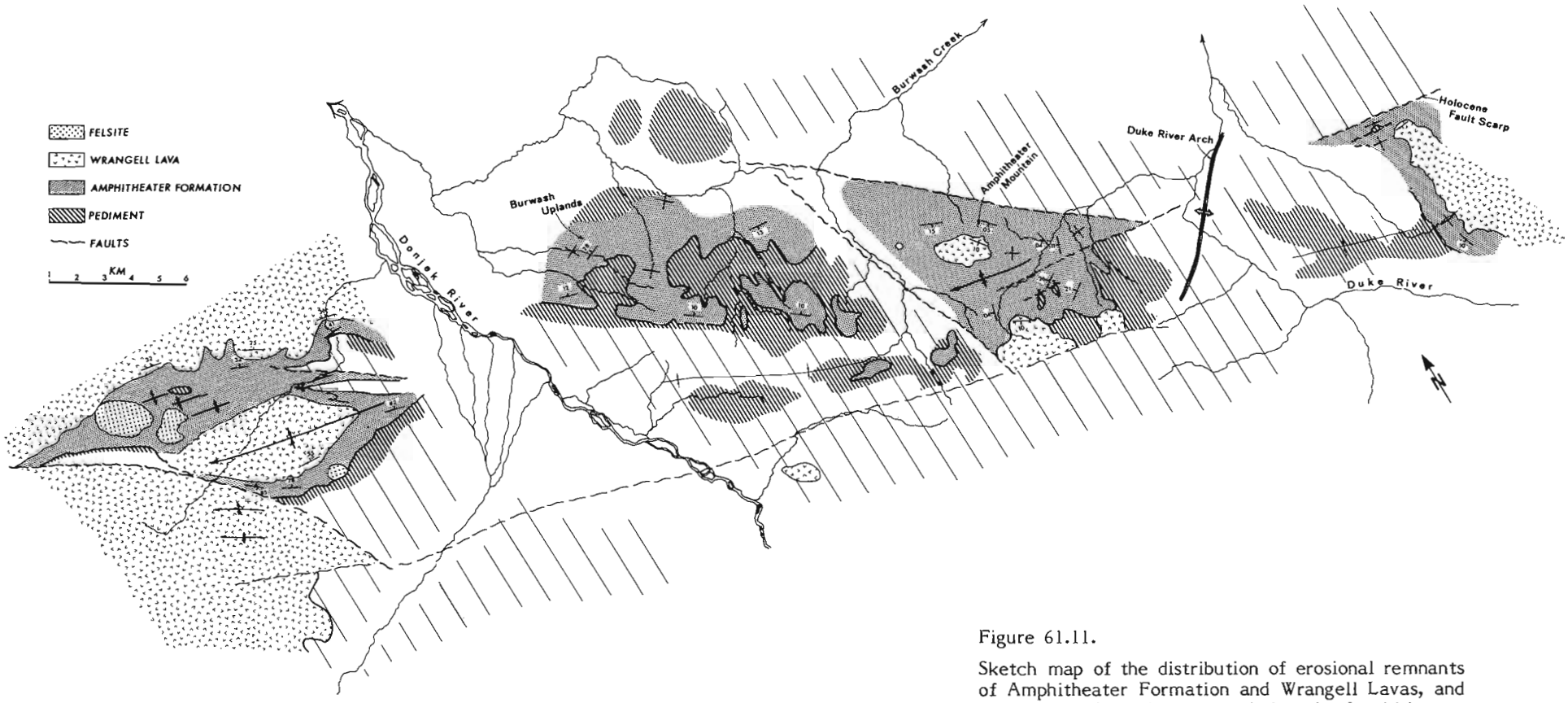

Figure 61.11.

Sketch map of the distribution of erosional remnants of Amphitheater Formation and Wrangell Lavas, and the partly exhumed pediment below the Amphitheater Formation near Amphitheater Mountain. Light ruling indicates exposures of pre-Tertiary rock formations.

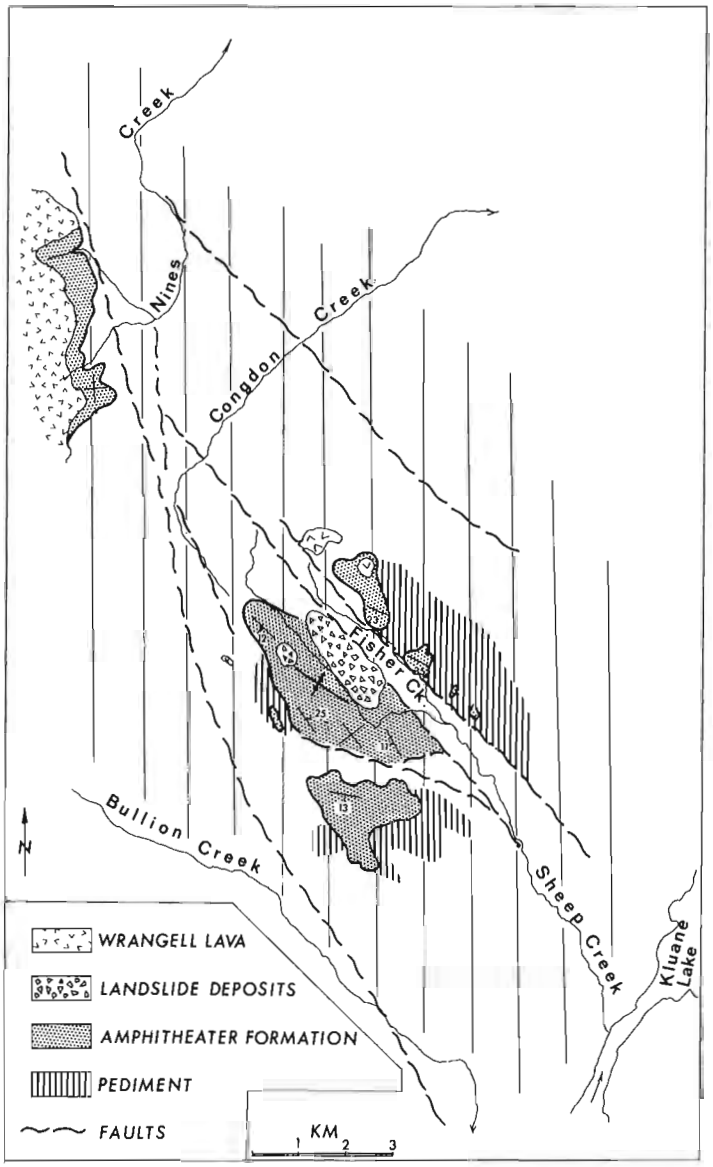

Figure 61.12.

Sketch map showing the distribution of Amphitheater Formation, mid-Tertiary landslide material, Wrangell Lavas, and exhumed pediment in the Sheep Creek area. Light ruling outlines exposures of pre-Tertiary rock formations.

Figure 61.13.

Angular debris reworked by running water from the mid-Tertiary landslide deposits shown at the top of Figure 61.10. Pollen from carbonaceous mudstones interstratified with these sharpstone channels are the same as those from lignite in adjacent Amphitheater Formation indicating that landslides occurred at the time the Amphitheater Formation was deposited.

and bury older bedrock topography. Angular scree deposits and boulder conglomerate up to 100 m thick are common along the southwest side of the basin. The composition of the blocky scree reflects the local bedrock geology of limestone, phyllite, and granite. Upwards and eastward the succession is progressively finer grained although most of the material is angular and poorly sorted. In contrast to the Amphitheater Mountain and Cement Creek sections coal or coaly mudstones are extremely rare. The total thickness of the exposed succession seems to range between 100 and 500 m (Kindle, 1953). The bulk of the sandstones is lithic arenite.

The sandstones and siltstones are predominantly flatbedded or parallel laminated with loosely defined pockets and lenses of angular pebbles scattered throughout the section. Crossbeds are rare but those that were measured (about 100) indicate southerly flowing paleocurrents (Fig. 61.3). The interpretation of the sedimentary setting, as based on the limited data presented, would favour clastic input from alluvial fans on the east and west with southward progradation along the axis of a high-gradient fluvial basin.

Paleogeomorphology and Tectonics

Paleogeomorphology

The paleogeomorphology of the region during deposition of the Oligocene Amphitheater Formation can be studied in two areas, which are illustrated in Figures 61.11 and 61.12. Although broken by faults and locally deformed the Amphitheater Formation commonly overlies a broadly planar bedrock pediment. In the Burwash Uplands the pediment is partly exhumed and dips to the northeast (Fig. 61.14). Patches of Amphitheater Formation are preserved as erosional remnants above a pediment of greenstone and granite. From the width of the outcrop belt it can be inferred that the width of the valley into which the Amphitheater Formation was deposited must have exceeded 16 km. The thickness of the Amphitheater Formation at Amphitheater Mountain (about 350 m) and the onlap of overlying Wrangell Lavas onto bedrock pediment immediately to the south suggests that towards the margin of this broad valley a local relief of up to 300 m could have existed. Because the fluvial system originated east of the Shakwak Valley (see above)

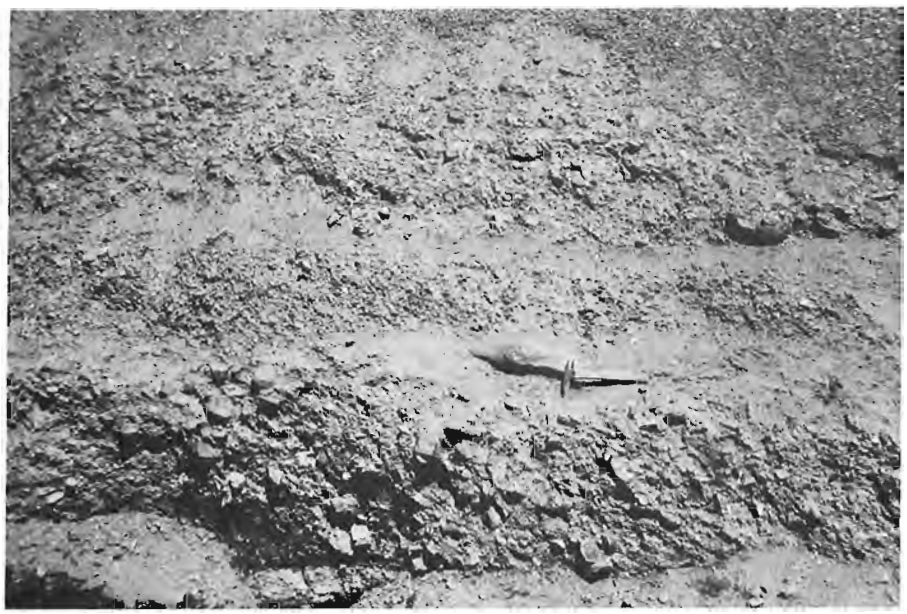

Figure 61.14.

View along the partly exhumed pediment of Burwash Uplands towards the southeast.

Figure 61.15.

Systematically fractured clasts from conglomerate in the Amphitheater formation. Although fractured and commonly sheared as well, clasts can be removed from their matrix in their entirety. Most of the fractures originate at points where the clasts were in contact with others (see Eisbacher, 1969).

it is likely that a broad pediment extended from the Burwash Uplands eastward onto the Yukon Plateau and the Coast Plutonic Complex. Bedrock hills and knolls must have projected above these valleys which were definitely broader than the ones in existence today. The Shakwak Valley near Kluane Lake is also mainly a post-Oligocene erosional feature.

In mid-Tertiary time the presently glaciated area of the central St. Elias Mountains (Icefield Ranges) was an upland region, dissected by rivers flowing northeast and southwest. The present topographic contour interval between 2000 and 3000 m can probably be taken as an indication of the margin of mid-Tertiary fluvial deposition because above this elevation Wrangell Lavas rests directly on bedrock (Fig. 61.3). The topographic surface of the Yukon Plateau above 2000 m and its extension southward into the Coast Mountains must also contain remnants of the Eocene-Oligocene pediment which was subsequently dissected by fluviatile erosion (Tempelman-Kluit, 1974). Towards the end of Amphitheater time much of the gently rolling topography laced by systems of open valleys was broken up by faults. Debris flows and landslides such as those of the Amphitheater Mountain and Sheep Creek sections probably blocked local drainage basins which were subsequently obliterated by

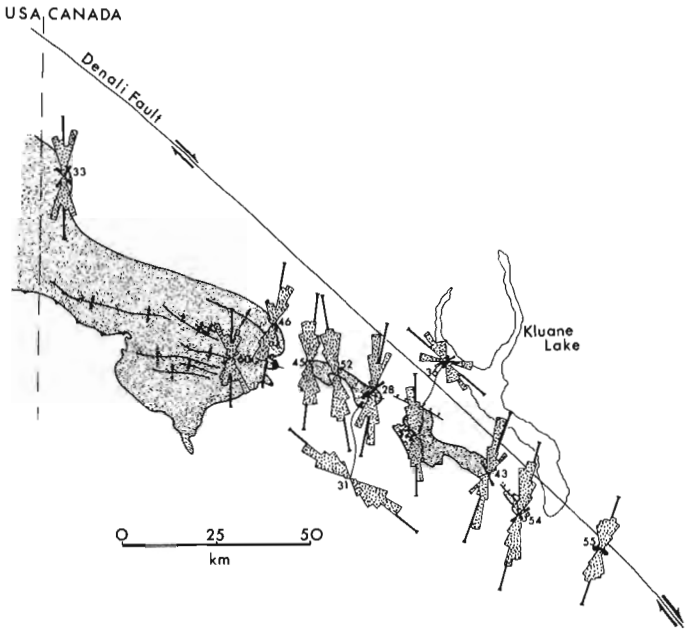

Figure 61.16. Regional distribution of localities where systematic fractures of conglomerate clasts within the Amphitheater Formation were measured. Number of fractures measured is indicated by the number beside each diagram.

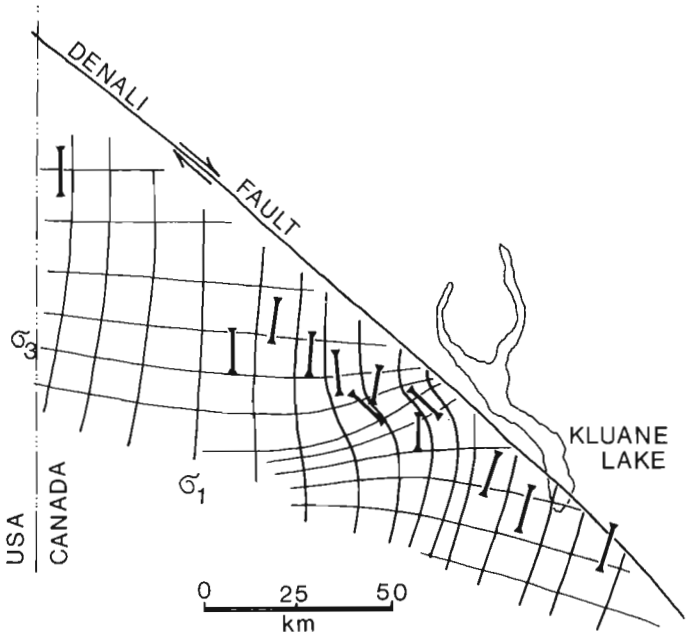

Figure 61.17. Regional compression axes derived from the orientation of fractures in conglomerate clasts and generalized stress trajectories deduced by drawing enveloping lines around compression axes.

thick blankets of Wrangell Lavas. The preservation of tillite interstratified with Wrangell Lavas near St. Clare Creek and White River (Fig. 61.3) suggests that in spite of the rapid rise of the St. Elias Mountains from mid-Miocene onward the tectonically controlled axis of the westerly trending valley system north of the high St. Elias Mountains might have occupied roughly the same position as in Oligocene time. In a regional sense the fluvial basins of the St. Elias region and others of the Yukon-Tanana Uplands probably contributed clastics to the Oligocene-Miocene Cook Inlet basin, until vigorous uplift of the Alaska Range (about 10 m.y. ago) disrupted the drainage pattern completely (Kirschner and Lyon, 1973).

Internal Deformation of the Amphitheater Formation

Much of the folding in the eastern St. Elias Mountains preceded the development of the extensive bedrock pediment and deposition of the Amphitheater Formation on it. A Late Cretaceous – earliest Tertiary phase of regional folding has been demonstrated in the eastern St. Elias Mountains (Eisbacher, 1976). This deformation coincided or preceded the rise of the Coast Plutonic Complex to the east and probably initiated westward directed river flow. However, brittle faulting coincided with and outlived deposition of the Amphitheater Formation. West of Donjek River all of the Tertiary formations are involved in west-northwest trending folds (Fig. 61.2). Most of the faults break across older structures below the bedrock pediment and folds within the Amphitheater Formation are commonly oblique to nearby faults. Along Duke River the pre-Oligocene pediment has been broadly folded into the northeast trending Duke River Arch which is almost perpendicular to folds below the pediment (Fig. 61.2). In the Sheep Creek area (Fig. 61.12) the pediment forms a broadly synclinal depression broken by longitudinal faults. The faults are possibly strands of the dextral Denali Fault System.

A curious effect of the regional deformation field upon the Amphitheater Formation is the development of a set of systematic fractures in well rounded conglomerate clasts (Fig. 61.15). The orientation of these fractures was measured at 12 sites along the outcrop belt of Amphitheater conglomerate. The statistical orientation of fractures at each site is plotted in Figure 61.16. Similar fractures have been described and measured by Ramsay (1964), Eisbacher (1969), and Brown and Helmstaedt (1970). The kinematic significance has been discussed in Ramsay (1964), Eisbacher (1969), and Tyler (1975). As in previous studies the regional pattern is very consistent and probably a fair approximation to the directional regional compression experienced by the conglomerate (Fig. 61.16). Due to the fact that small scale right-lateral and left-lateral offsets along the fractures within the clasts contribute equally to the overall pattern it can be assumed that the mean fracture orientation defines a local compression axis. These compression axes are plotted on a separate diagram (Fig. 16.17). An envelope of stress trajectories around the individual compression axes delimits the regional stress field. The largest principal compressive stress trends north to north-northeast. A major perturbation exists in the centre of the area (Fig. 61.17).

The stress field is compatible with dextral displacement along the Denali Fault. It is significant that the dykes which cut the Amphitheater Formation and feed the flows of the Wrangell Lavas generally trend northerly – as should be expected from the regional stress field. Older Eocene(?) dyke swarms of the Yukon Plateau also trend northerly (Muller, 1967; Tempelman-Kluit, 1974).

Figure 61.18

a) Holocene fault scarp northeast of Duke River (139°06'W, 61°16'30'N). View looking northwest towards the exhumed Tertiary pediment along Duke River Arch (for location see Figure 61.12).

b) Close-up of same Holocene fault scarp looking south; offset is about 1.5 m with west side uplifted relative to the east block.

The perturbation in the stress field referred to above is possibly due to regional buckling along the Denali Fault. It coincides with and may explain the northeasterly trending Duke River Arch (Fig. 61.11).

Systematic fractures in conglomerate clasts, dyke trends, and the sense of displacement on the Denali Fault thus are expressions of a regional north-south compression concomitant with slight east-west extension in Tertiary time. First-motion studies of earthquakes along the Denali Fault west of the Canadian-United States border indicate that north-south compression in the region is active up to the present (Gedney, 1970). In the eastern St. Elias Mountains only one active fault was found during field work. It is a short (6 km) Holocene scarp northeast of Duke River (Fig. 61.18) with 1 to 2 m of displacement. The Holocene fault follows an old break that separates volcanic bedrock from the Amphitheater Formation and the displacement is normal with the southwest side uplifted.

Regional Implications and Conclusions

The foregoing analysis of sedimentation, paleogeomorphology, and tectonics of the latest Eocene(?) – Oligocene Amphitheater Formation suggests that in mid-Tertiary time the St. Elias region was a rolling upland with wide shallow alluvial valleys and a temperate climate. The major rivers flowed westward from the Yukon Plateau – Coast Mountain terrain and deposited blankets of gravel, sand and coal. Subsequent faulting and folding accentuated local relief and triggered rockslides and debris flows. Extensive blankets of Miocene basalt

and andesite buried the area. By mid-Miocene the St. Elias Mountains had risen to an elevation which supported formation of thick ice sheets. These flowed away from the axis of the mountains northward into newly eroded valleys and southward into the tectonically active Gulf of Alaska where thick glacial marine diamictites accumulated along a steep coast (Plafker and Addicott, 1976). The rise of the present St. Elias Mountains and the sculpturing of its high granitic peaks commenced about 15 m.y. ago due to north-south crustal compression along the northern margin of the Pacific Ocean. One Holocene fault scarp encountered during field work attests to continuing uplift of the St. Elias Mountains.

Acknowledgments

The authors wish to acknowledge logistic support during Operation St. Elias and stimulating discussion with R.B. Campbell, Geological Survey of Canada. D.J. Tempelman-Kluit critically read the paper and suggested changes which improved the story.

References

Berg, H.C., Jones, D.L., and Richter, D.H.
1972: Gravina-Nutzotin Belt-tectonic significance of an Upper Mesozoic sedimentary and volcanic sequence in southern and southeastern Alaska; U.S. Geol. Surv., Prof. Paper 800-D, p. D1-D24.

Bostock, H.S.
1952: Geology of northwest Shakwak Valley, Yukon Territory; Geol. Surv. Can., Mem. 267, 54 p.

Brown, R.L. and Helmstaedt, H.
1970: Deformation history in part of the Lubec-Belleisle zone of southern New Brunswick; Can. J. Earth Sci., v. 7, p. 748-767.

Buffler, R.T. and Triplehorn, D.M.
1976: Depositional Environments of the Tertiary Coal-Bearing Group, central Alaska; in Recent and Ancient Sedimentary Environments in Alaska, T.P. Miller, ed.; Alaska Geol. Soc., H1-H10.

Capps, S.R.
1916: The Chisana-White River District, Alaska; U.S. Geol. Surv., Bull. 630, 130 p.

Denton, G.H. and Armstrong, R.L.
1969: Miocene-Pliocene glaciation in southern Alaska; Am. J. Sci., v. 267, p. 1121-1142.

Eisbacher, G.H.
1969: Displacement and stress field along part of the Cobequid Fault, Nova Scotia; Can. J. Earth Sci., v. 6, p. 1095-1104.

1976: Sedimentology of the Dezadeash flysch and its implications for strike-slip faulting along the Denali Fault, Yukon Territory and Alaska; Can. J. Earth Sci., v. 13, p. 1495-1513.

Eynon, G. and Walker, R.G.
1974: Facies relationships in Pleistocene outwash gravels, southern Ontario: a model for bar growth in braided rivers; Sedimentology, v. 21, p. 43-70.

Gedney, L.
1970: Tectonic stresses in southern Alaska in relationship to regional seismicity and the new global tectonics; Bull. Seismol. Soc. Am., v. 60, p. 1789-1802.

Hopkins, W.S., Rutter, N.W., and Rouse, G.E.
1972: Geology, paleoecology, and palynology of some Oligocene rocks in the Rocky Mountain Trench of British Columbia; Can. J. Earth Sci., v. 9, p. 460-470.

Kindle, E.D.
1953: Dezadeash map-area, Yukon Territory; Geol. Surv. Can., Mem. 268, p. 68.

Kirschner, C.E. and Lyon, C.A.
1973: Stratigraphic and tectonic development of Cook Inlet Petroleum Province; Am. Assoc. Petrol. Geol., Mem. 19, p. 396-407.

Lerbekmo, J.F. and Campbell, F.A.
1969: Distribution, composition, and source of the White River Ash, Yukon Territory; Can. J. Earth Sci., v. 6, p. 109-116.

MacKevett, E.M., Jr.
1970: Geology of the McCarthy B-4 Quadrangle, Alaska; U.S. Geol. Surv., Bull. 1333, 31 p.

1971: Stratigraphy and general geology of the McCarthy C-5 Quadrangle, Alaska; U.S. Geol. Surv., Bull. 1323, 35 p.

McGowen, J.H. and Garner, L.E.
1970: Physiographic features and stratification types of coarse-grained bars – Modern and ancient examples; Sedimentology, v. 14, p. 77-111.

Mendenhall, W.C.
1905: Geology of the central Copper River region: Alaska; U.S. Geol. Surv., Prof. Paper 41, 133 p.

Muller, J.E.
1967: Kluane Lake map-area, Yukon Territory; Geol. Surv. Can., Mem. 340, 137 p.

Plafker, G.
1969: Tectonics of the March 27, 1964, Alaska earthquake; U.S. Geol. Surv., Prof. Paper 543-1, 74 p.

1971: Pacific margin Tertiary basin; Am. Assoc. Petrol. Geol., Mem. 15, p. 120-135.

Plafker, G. and Addicott, W.O.
1976: Glaciomarine deposits of Miocene through Holocene age in the Yakataga Formation along the Gulf of Alaska margin, Alaska; in Recent and Ancient Sedimentary Environments in Alaska, T.P. Miller, ed.; Alaska Geol. Soc., p. Q1-Q23.

Plafker, G., Bruns, T.R., and Page, R.A.
1975: Petroleum potential and geologic hazards in the outer continental shelf of the Gulf of Alaska Tertiary Province; U.S. Geol. Surv. Open File 75-592, 74 p.

Ramsay, D.M.
1964: Deformation of pebbles in Lower Old Red Sandstone conglomerates adjacent to the Highland Boundary Fault; Geol. Mag., 101, p. 228-248.

Read, P.B. and Monger, J.W.H.
1975: Operation St. Elias, Yukon Territory: the Mush Lake Group and Permo-Triassic rocks in the Kluane Ranges; in Report of Activities, Part A, Geol. Surv. Can., Paper 75-1A, p. 55-59.

Richter, D.H. and Jones, D.L.
1973: Structure and stratigraphy of eastern Alaska Range, Alaska; in Arctic Geology, Am. Assoc. Petrol. Geol., Mem. 19, p. 408-420.

Souther, J.G. and Stanciu, C.
1975: Operation St. Elias, Yukon Territory: Tertiary volcanic rocks; in Report of Activities, Part A, Geol. Surv. Can., Paper 75-1A, p. 63-70.

Tempelman-Kluit, D.J.
1974: Reconnaissance geology of Aishihik Lake, Snag and part of Stewart River map-areas, west-central Yukon; Geol. Surv. Can., Paper 73-41, 97 p.

Tobin, D.G. and Sykes, L.R.
1968: Seismicity and tectonics of the Northeast Pacific Ocean; J. Geophys. Res., v. 73, p. 3821-3845.

Tyler, J.H.
1975: Fracture and rotation of brittle clasts in a ductile matrix; J. Geol., v. 82, p. 501-510.

Wahrhaftig, C., Wolfe, J.A., Leopold, E.B., and Lanphere, M.A.
1969: The Coal-Bearing Group in the Nenana Coal Field, Alaska; U.S. Geol. Surv., Bull. 1274-D, 30 p.

Winkler, G.R.
1976: Deep sea fan deposition of the lower Tertiary Orca Group, Eastern Prince William Sound, Alaska; in Recent and ancient sedimentary environments in Alaska; T.P. Miller, ed., Alaska Geol. Soc., R1-R20.

Wolfe, J.A.
1971: Tertiary climatic fluctuations and methods of analysis of Tertiary floras; Paleogeog., Paleoclimate, Paleoecol., v. 9, p. 27-57.

62. RADIOELEMENT DISTRIBUTION PATTERNS IN THE FRONTENAC AXIS, ONTARIO

Project 760045

B.W. Charbonneau
Resource Geophysics and Geochemistry Division

Introduction

Airborne gamma-ray spectrometric data covering some 38 000 km^2 in eastern Ontario between Ottawa to the east, Bancroft to the west, Pembroke to the north and Kingston to the south (map-sheet 31F, Geological Survey Open File 331 and map-sheet 31C, Geological Survey Open File 428) show the radioelement distribution pattern over a varied terrane of Precambrian rocks of the Grenville structural province, and the bordering Paleozoic rocks. Three areas of recent uranium exploration activity, Bancroft, and Palmerston and Huddersfield townships, lie within the surveyed block.

Figure 62.1 shows the 1, 2, and 3 ppm eU contours of average surface concentration from the airborne data as well as the area with eU/eTh ratio > 0.5. In addition simplified geology after Ayers et al. (1971) and Laurin (1969) is shown, and the known uranium occurrences after Robertson (1975) and Shaw (1958) are located on the map. This survey area, which basically constitutes a zone of Precambrian rock extending southeast into the Adirondacks of the United States, is generally known as the Frontenac axis.

General Discussion

The measurement from the air of the ground level uranium concentration provides the average surface concentration for an area under the aircraft at each point of measurement. The moving aircraft covers a swath on the ground. Within this swath there is overburden, vegetation, and variable amounts of water and some outcrop. For this reason the average surface concentration usually provides a minimum value in relation to the concentration in overburden. The relationship between average surface concentration and outcrop concentration is more variable, because outcrop usually constitutes only a small percentage of any area of measurement. In general the concentration in outcrop is higher than in associated overburden, but the reverse may be true. Charbonneau et al. (1976) investigated the relationship between average surface concentration (measured from the air) and ground level measurements, and found that generally average surface concentration values of 1 to 2 ppm eU correspond with outcrop concentrations of 4 to 5 ppm, average surface concentration values of 2 to 3 ppm eU correspond to outcrop concentrations of 7 to 8 ppm and average surface concentration values of 3 to 4 ppm eU correspond to 10 to 11 ppm eU in outcrop.

The uranium concentrations (Fig. 62.1) are not exceptionally high. Most of the area is below the 1 ppm eU a.s.c. contour, as is much of the Canadian Shield surveyed to date. However any area above 1 ppm eU merits some attention.

The process of compilation of contoured maps from reconnaissance surveys involves considerable smoothing of the data, which suppresses narrow anomalies that are possibly indicative of the presence of uranium mineralization. Narrow anomalies should be sought on the individual flight line profiles which should always be examined along with the contour maps. Even on profiles the expression of narrow zones of uranium enrichment may be suppressed by swamp and overburden cover, or the zones may occupy only a small fraction of the area analyzed in one airborne counting interval of 2.5 seconds (approximately 10^5 m^2), and thus their effects may be diminished significantly due to averaging with surrounding rock of lower radioelement abundance.

Interpretation

Much of the area of high eU (Fig. 62.1) is related to the distribution of granitoid rocks and associated pegmatites. The three areas where present uranium evaluation work is taking place are indicated on Figure 62.1: Huddersfield township, Quebec; the Bancroft area, and Palmerston township, Ontario. In all three areas prominent zones of uranium enrichment are indicated. North-south airborne profiles (Fig. 62.2) show the radiometric characteristics of the Huddersfield township area (H), the Bancroft zone (B), and the Palmerston township zone (P). The locations of the profiles are indicated on Figure 62.1. The marked subdivisions along the profiles correspond to miles. Profiles 11 and 31 relate to the northern map sheet (31F) between 45°N and 46°N and profiles 13 and 19 to the southern map sheet (31C) between 44°N and 45°N. The Huddersfield township radioactive zone is characterized by a prominent increase in eU and eTh, with no significant eU/eTh ratio increase. The Bancroft zone likewise is characterized by increases in eU and eTh with very little increase in ratio of eU/eTh. In contrast, the Palmerston township radioactive zone has several narrow anomalies in the eU profile and a broad, high eU/eTh ratio. This high eU/eTh ratio spreads out from the major radioactive body, which is a northeast trending band of granite about 50 km long and 10 km wide, terminating near Palmerston township. The anomaly lies over bordering marble and volcanic rocks as well. This indicates that these latter rocks may have been enriched in uranium. An elongate arm of granite, similar in dimension to the Palmerston granite, lies to the north of the Palmerston granite and terminates near Calabogie in the northeast. This granite is also enriched in uranium. The Bancroft syenite-granite which is distinctly above normal in uranium content has a northeast trend as well. Both the Palmerston and Calabogie granites have western portions that are distinctly low in uranium. Granite masses near Methuen (15 km south of Bancroft) and near Deloro (15 km southeast of Methuen) are higher in uranium than surrounding rocks. The Hurd Lake granite, a small granite body, 8 km northeast of the termination of the Calabogie granite, has pronounced marginal enrichment in uranium (Charbonneau and Jonasson, 1975). An uranium anomaly 45 km southeast of the Huddersfield anomaly in Quebec relates to the tailings pile of the Hilton iron mine and is due more to the effect of extensive exposure of the material than to a particularly high uranium content.

From: Report of Activities, Part B;
Geol. Surv.Can., Paper 77-1B (1977)

Figure 62.1. Airborne eU ppm map, geology and uranium occurrences in the Frontenac axis area, southeastern Ontario.

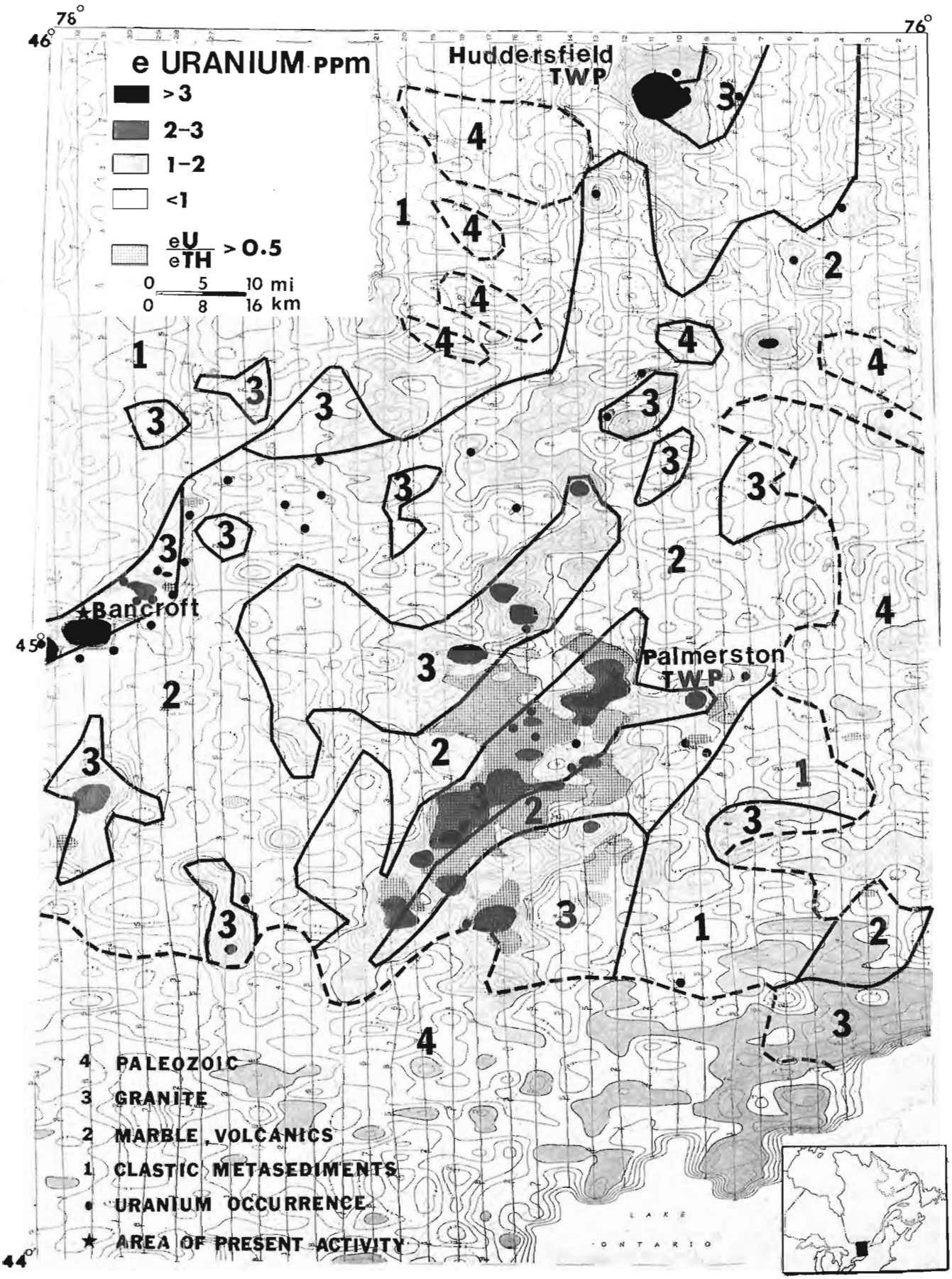

Figure 62.2. Profiles for airborne eU, eTh, eU/eTh intersections across Huddersfield township area (H), Quebec; Bancroft area (B), Ontario; Palmerston township area (P), Ontario.

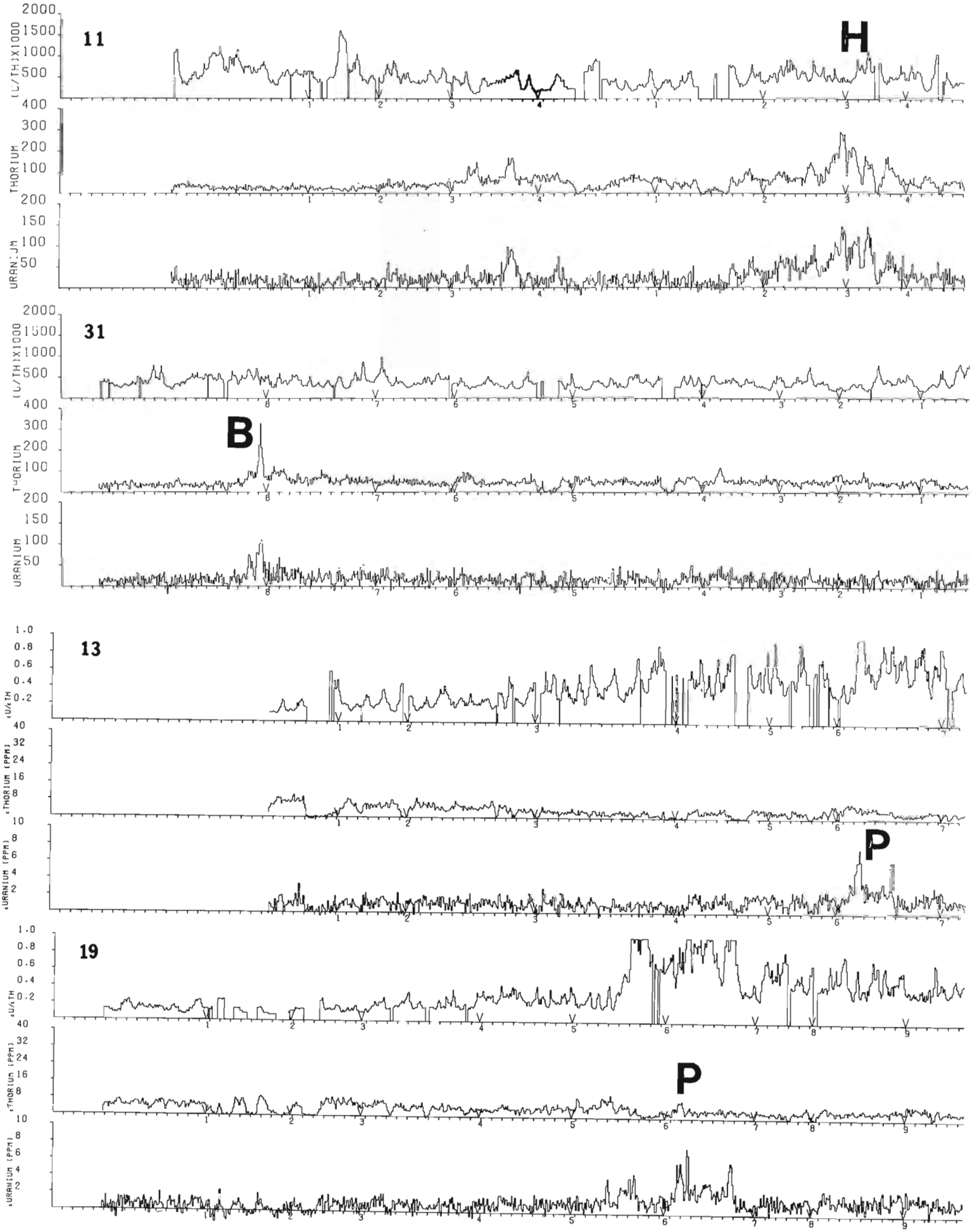

Uranium occurrences known in the area are plotted Figure 62.1. The distribution of these occurrences shows good relationship to the uranium distribution pattern. In Quebec, the Calumet Island occurrences 15 km southwest of the Huddersfield anomaly have an associated anomaly as do the occurrences near Wolfe Lake and Aldfield township 30 km southeast of the Huddersfield anomaly. In Ontario many occurrences are associated with the Bancroft anomaly, the Renfrew area (Hurd Lake) and farther south with the Calabogie and Palmerston anomalous zones. Minor areas of > 1 ppm eU occur over Paleozic rocks as well as the Precambrian. The Paleozoic rocks have been shown to be of economic interest for uranium. (Charbonneau et al. 1975a; Charbonneau et al., 1975b).

A general correlation of gold occurrences in the Palmerston area (Ontario Dept. of Mines Map 2053) with granites having high eU/eTh ratios is noted, and a similar correlation has been observed in the Yellowknife area (Geological Survey of Canada Open File 124) and in Nova Scotia (Geological Survey of Canada Open File 429).

Summary

The compilation of airborne gamma-ray spectrometer survey data in the Frontenac axis area clearly shows the three zones that are of economic interest at present: Huddersfield township, Bancroft, and Palmerston township areas. Palmerston township is clearly different from the previous two in that the ratio of uranium/thorium is high whereas the ratio only increases minimally in the Bancroft and Huddersfield areas. The Palmerston area lies well within the Grenville Group rocks (unit 2, Fig. 62.1) whereas the Bancroft and Huddersfield areas lie near the contact of these rocks with the underlying Aphebian metasediments (unit 1, Fig. 62.1). This may indicate that the Palmerston granite is at a higher structural level than the Bancroft material, and there may have been a greater degree of fractionation of the uranium from thorium resulting in the higher level of uranium/thorium ratio.

References

Ayres, L.D., Lumbers, S.B., Milne, V.G., and Robeson, D.W.
1971: Ontario Geological Map Southern Sheet – Map 2197 – Scale 1:1,000,000; Ontario Dept. of Mines and Northern Affairs.

Charbonneau, B.W. and Jonasson, I.R.
1975: Radioactive pegmatites in the Renfrew area, Ontario; in Report of Activities, Part-A, Geol. Surv. Can., Paper 75-1C p. 285-290.

Charbonneau, B.W., Jonasson, I.R., and Ford, K.L.
1975a: Cu-U mineralization in the March Formation Paleozoic rocks of the Ottawa St. Lawrence Lowlands; in Report of Activities, Part A, Geol. Surv. Can., Paper 75-1A, p. 229-233.

Charbonneau, B.W., Jonasson, I.R., Holman, P.B., and Ford, K.L.
1975b: Regional airborne gamma-ray spectrometry and stream sediment geochemistry, detailed ground gamma-ray spectrometry and soil geochemistry in an environment of stratabound Paleozoic U-Cu mineralization in the Ottawa-Arnprior area; Geol. Surv. Can. Open File Release 264, May 1975.

Charbonneau, B.W., Killeen, P.G., Carson, J.M., Cameron, G.W., and Richardson, K.A.
1976: Significance of radioelement concentration measurements made by airborne gamma-ray spectrometry over the Canadian Shield; IAEA Symposium on Exploration for Uranium Ore Deposits, Vienna, Austria, p. 35-53.

Laurin, A.F.
1969: Geological Map of Quebec – Scale 1:1,000,000; Quebec Dep. Mines.

Robertson, J.A.
1975: Uranium and thorium deposits of Ontario, Southern Sheet; Ontario Division of Mines, Prelim. Map P972, Mineral Deposits Series, Scale: 1 inch to 16 miles.

Shaw, D.M.
1958: Radioactive mineral occurrences of the Province of Quebec; Quebec Dep. Mines, Geol. Rep. 80.

63. URANIUM RESOURCES OF THE PERMO-CARBONIFEROUS BASIN, ATLANTIC CANADA

Project 760014

H.E. Dunsmore
Regional and Economic Geology Division

Introduction

As part of the uranium resource evaluation program of the Geological Survey of Canada, a two-man, geological reconnaissance of the Permo-Carboniferous sedimentary basin of Atlantic Canada was conducted during the 1976 field season. Parts of all four Atlantic provinces and the Magdalen Islands were visited. The short-term objectives of this survey were fourfold: (1) to examine all reported occurrences in Carboniferous strata; (2) to prospect for additional surface occurrences; (3) to formulate a preliminary classification system, and; (4) to assign priorities to future, more comprehensive research. The long-term objective of this project is to assess as accurately as possible the potential uranium resources of the area.

A number of previously unreported radioactive occurrences were discovered during the field season. None of the occurrences visited are in themselves economic, as is perhaps to be expected in an area with a long history of abundant rainfall and active groundwater flow systems. However, these crucial surface clues may point the way to economic grades and tonnages at depth.

Classification and Description of Uraniferous Occurrences

A preliminary classification of uranium enrichment in Permo-Carboniferous rocks is set out in Table 63.1. Three different types of mineralization are recognized, and one of these, the sandstone-type, consists of at least three different styles. The term style is used to denote relatively minor but distinctive differences within each group or class. Until relationships with the host rocks are more clearly understood, the various styles have been given geographical designations only.

The characteristics and geological settings of the various uraniferous showings are described. The distribution of individual occurrences, types and styles are shown in Figure 63.1. The exact locations of all occurrences visited are listed in Table 63.2.

Sandstone-Type – Magdalen Islands Style

Previously unreported concentrations of uranium were discovered at four separate localities in the Magdalen Islands. They are within very large, elongated pods of well-cemented, greenish grey, quartz-rich sandstones within thick sequences of poorly cemented, red-coloured sands. The uranium is directly associated with petroleum-derived hydrocarbons which fill fractures and impregnate interstitial porosity. Selected specimens of this material contain as much as 2.15% uranium.

The Magdalen Islands are underlain by great thicknesses of Mississippian, Windsor Group evaporites (Howie and Barss, 1975) and, indeed, appear to owe their existence to salt diapirism. Easterly to northeasterly trending salt-cored anticlines occur throughout the Islands

Table 63.1

Preliminary classification of uranium mineralization in Permo-Carboniferous basin, Atlantic Canada

TYPE	STYLE
SANDSTONE–TYPE	Magdalen Islands Style
	Prince Edward Island Style
	Pugwash–Tatamagouche Style
BITUMINOUS SHALE–TYPE	(Not Subdivided)
VOLCANOGENIC TYPE	(Not Subdivided)

(Sanschagrin, 1964), and similar salt structures are present to the east beneath the waters of the Gulf of St. Lawrence (Watts and Haworth, 1974). The cores of the anticlines consist of marine evaporites and associated rock types, and an intensively fractured basalt (Fig. 63.2). The latter appears to have been brought in with the evaporites. A large-scale operation to mine salt is currently in the final planning stage.

The red- and green-coloured sandstones of the Cap-aux-Meules Formation overlie the evaporites on the flanks of the anticlines. Their age is uncertain, but is believed to be Permo-Carboniferous (Sanschagrin, 1964). Similarly, the environment of deposition cannot be stated with certainty, but the presence of cross-beds as high as 7 m suggests eolian deposition. The uranium-bearing, greenish grey portions are found relatively near the evaporites (Fig. 63.2). They occur as elongated lenses up to 1 km long and at least 50 m thick. The long axes of these lenses are more or less parallel to the east-west trending anticlines. In marked contrast to the red-coloured sands, the greenish grey portions are highly indurated rocks (carbonate and silica cements) which form prominent hills, capes and headlands throughout the Islands. At the contacts examined by the writer, the red- and green-coloured sands are stratigraphically continuous, implying that the facies change is diagenetic rather than depositional in origin.

Numerous occurrences of petroleum-derived bitumen were observed throughout the pods of greenish grey sandstone. It is commonly present as a shiny, black material infilling interstitial porosity or fractures. At one locality, a substance with the appearance and consistency of machine grease was observed within a calcite-lined fracture. Many of these fractures also contain abundant pyrite. The presence of these bitumens, coupled with the close proximity of the grey sandstones to the impermeable evaporites, indicates that the sandstones must once have been structural petroleum traps on the flanks of the salt diapirs.

From: Report of Activities, Part B
Geol. Surv. Can., Paper 77-1B (1977).

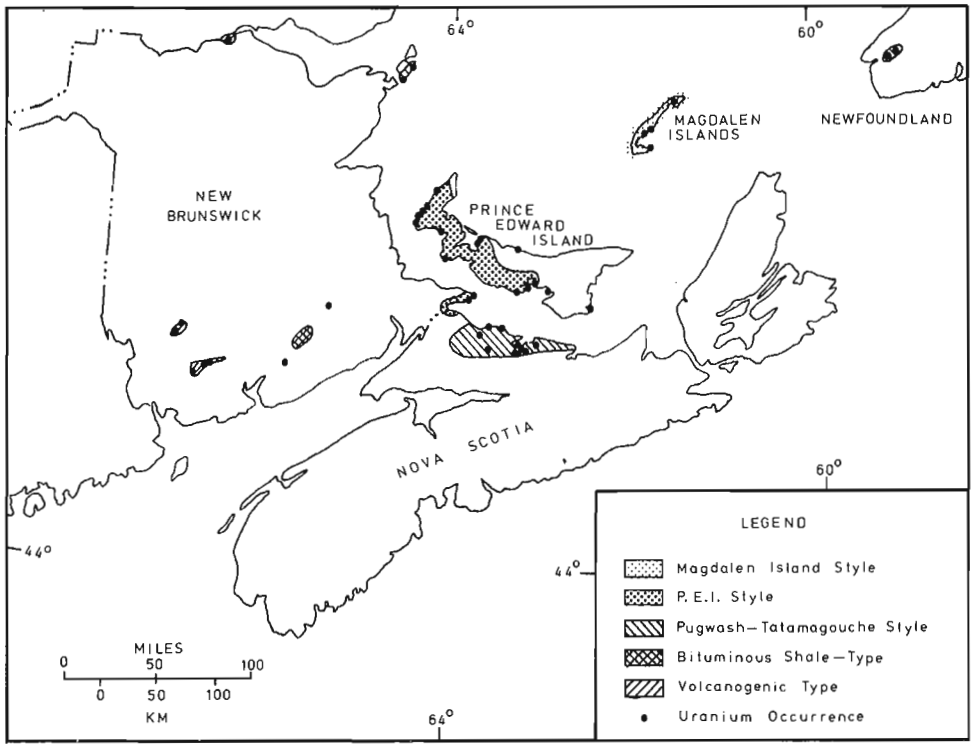

Figure 63.1. Regional distribution of types and styles of uranium mineralization, Permo-Carboniferous basin, Atlantic Canada.

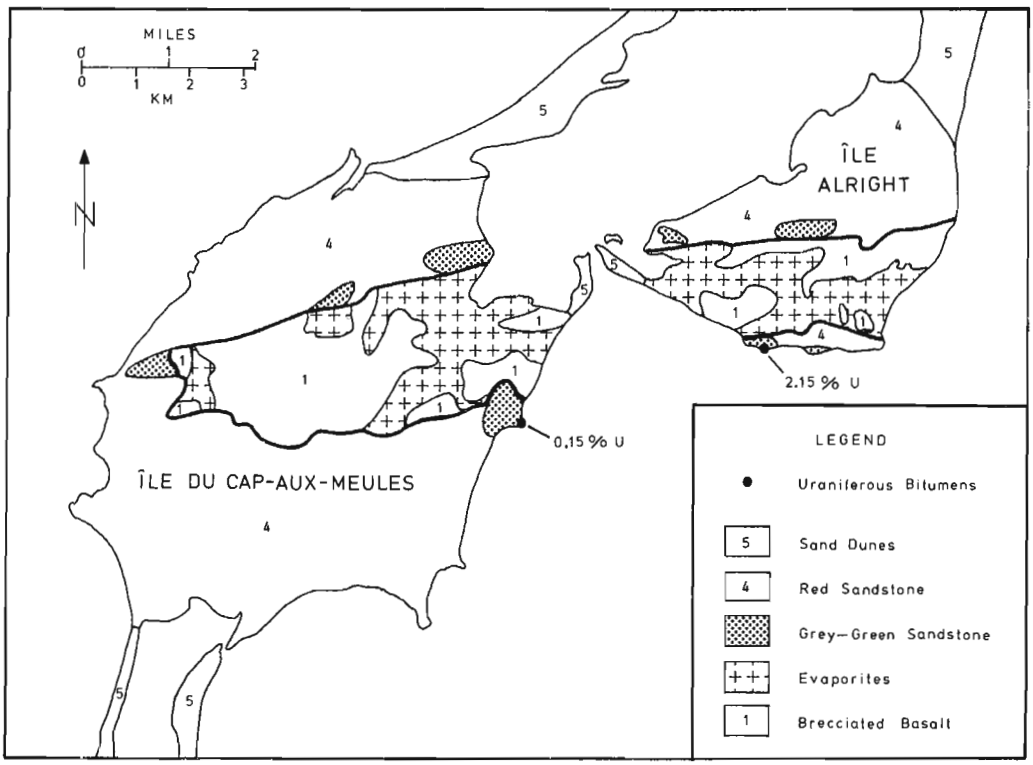

Figure 63.2. Geology and uranium occurrences of a portion of the Magdalen Islands archipelago, Quebec (geology after Sanschagrin, 1964).

Province	Map Sheet 1:50,000	U.T.M. Reference		Geographic Name	Type or Style	U Conc., ppm
		Easting	Northing			
Newfound-land	11 O/11	341600	5303800	Overfall Brook	Misc.	323.
	11 O/11	345600	5308200	Grand Codroy R.	P-T?	107.
	11 O/11	345100	5308950	Grand Codroy R.	P-T	30.6
	11 O/11	341950	5304650	Grand Codroy R.	P-T?	11.2
	11 O/11	339350	5303750	Grand Codroy R.	P-T?	13.1
Magdalen Islands, Quebec	11 N/12E	612600	5274250	Grosse Ile	MI	35.3
	11 N/5	590550	5249050	Pointe Basse	MI	21500.
	11 N/5	586200	5247550	Cap-aux-Meules	MI	1510.
	11 N/4	588350	5232200	Shea Point	MI	580.
Prince Edward Island	21 I/9W	391850	5168600	West Cape	PEI	28.5
	21 I/9W	392000	5170850	West Cape	PEI	150.
	21 I/9W	392050	5172300	West Cape	PEI	215.
	21 I/9W	392500	5173900	Cape Wolf	PEI	141.
	21 I/9W	394550	5176550	Seal Point	PEI	251.
	21 I/16W	400700	5183200	Campbellton	PEI	116.
	21 I/16W	399700	5182250	Campbellton	PEI	56.2
	21 I/16W	397400	5180000	Burton	PEI	88.8
	21 I/16E	410000	5198750	Waterford	PEI	99.7
	11 L/12E	444550	5154400	Malpeque Bay	PEI	42.4
	11 L/12E	447250	5155150	Darnley Basin	PEI	14.1
	11 L/12E	449600	5155050	Darnley Basin	PEI	17.2
	11 L/12E	448750	5157100	Cape Aylesbury	PEI	10.5
	11 L/6W	475150	5148600	Cavendish	PEI	98.5
	11 L/6W	474150	5149050	Cavendish	PEI	259.
	11 L/1W	541950	5095950	Murray Head	PEI ?	126.
	11 L/2W	502650	5108550	Gallas Point	P-T	62.4
	11 L/3W	477400	5110000	Canoe Cove	PEI	54.5
	11 L/3E	490000	5114900	Blockhouse Point	PEI	30.4
	11 L/3E	485500	5111600	Bacon Point	PEI	15.2
	11 L/3E	493000	5115550	Bellevue Cove	PEI	33.5
	21 I/8E	414750	5138850	Cape Egmont	PEI	25.9
	21 I/9E	410850	5161300	Brae Harbour	PEI	111.
Nova Scotia	11 E/11E	496050	5063500	Welsford	P-T	45.8
	11 E/11E	495850	5062900	Welsford	P-T	44.1
	11 E/11E	482250	5057500	Balfron	P-T	15.1
	11 E/11E	480600	5058250	———	P-T	150.
	11 E/11E	486800	5060000	Biz Brook	P-T	14.8
	11 E/11E	482300	5056400	Yellow Brook	P-T	12.5
	11 E/11E	483400	5057850	Black Brook	P-T	2520.
	11 E/11W	480500	5058250	———	P-T	N.D.
	11 E/11W	474700	5056200	Oliver	P-T	37.7
	11 E/11W	475650	5054500	Miller Brook	P-T	N.D.
	11 E/11W	474400	5064800	Blockhouse Point	P-T	48.0
	11 E/11W	473800	5064850	Blockhouse Point	P-T	N.D.
	11 E/11W	478150	5059950	Tatamagouche	P-T	841.
	11 E/12	457000	5059650	Wentworth	P-T	29.7
	11 E/13E	446900	5073850	Chisholm Brook	P-T	101.
	11 E/13E	447500	5074850	Pugwash River	P-T	10.7
	11 E/14W	464200	5080150	Cape Cliff	P-T	31.3
	11 E/14W	464750	5079750	Cape Cliff	P-T	212.
New Brunswick	21 I/3	321800	5103800	Ridge Brook	Misc.	82.7
	21 H/12W	281100	5050200	Hampton	B.S.	419.
	21 G/10E	684800	5046850	Shin Creek	V	54.5
	21 G/10E	688450	5049600	Pete Brook	V	21.3
	21 G/10E	689400	5050450	Oromocto River	V	N.D.
	21 G/7W	671150	5033300	Mount Pleasant	V	235.
	21 G/11E	648300	5058850	York Mills	V	179.
	21 G/11E	651250	5062900	Manners Sutton	V	177.
	21 P/15E	387250	5300550	Pigeon Hill	P-T	N.D.
	21 P/10E	377550	5287550	Chiasson	P-T	N.D.
	21 O/15E	———	———	Atholville	V	1080.
	11 L/4	437750	5103250	Cape Spear	PEI	55.3
	11 L/4	439000	5109100	Cape Tormentine	PEI	11.3
	11 L/4	440250	5105500	Indian Point	PEI	N.D.

TABLE 63.2

MI – Magdalen Islands Style

PEI – Prince Edward Island Style

P-T – Pugwash - Tatamagouche Style

BS – Bituminous Shale-Type

V – Volcanogenic Type

Misc – Miscellaneous Occurrence

N.D. – Not Determined

The chemically reducing environment associated with the hydrocarbons would provide a means of fixing the uranium. It would also account for the colour change and perhaps the high degree of cementation of the uranium-bearing sandstones. The presence of petroleum-derived bitumens also has important implications with regard to the oil and gas potential of similar salt structures beneath the waters of the Gulf of St. Lawrence.

The radioactive occurrences examined were very patchy, the largest, on Shea Point, Ile du Havre-Aubert, being only a few metres across. However, the precipitous nature of the headlands permitted only a small fraction of the exposures to be examined closely. Also, the base of the greenish grey lenses, assuming it represents a former oil-water contact, would perhaps be the most favourable horizon for uranium mineralization. Unfortunately, none of these are exposed.

In Atlantic Canada, the Magdalen Islands style of mineralization appears to be restricted to the Islands. There are apparent similarities, however, to the Rifle Creek deposit in the southwestern United States, one of the largest vanadium-uranium deposits in the Colorado Plateau region. There, ore is confined to "bleached" portions of a normally red-coloured, eolian sandstone (Fischer, 1960; Adler, 1974). The contacts between bleached and red sandstones are sharp and oblique to bedding, indicating an epigenetic rather than a syngenetic origin (Adler, 1974). The presence of solid hydrocarbons and late-stage pyrite suggests that the uranium host rock contained oil at one time (Adler, 1974).

Further exploration for uranium on the Magdalen Isands seems warranted.

Sandstone-Type — Prince Edward Island Style

The Prince Edward Island style of uranium mineralization appears to be potentially one of the most important in the whole of the Permo-Carboniferous basin.

The mineralized horizons, as exposed in outcrop along the west coast of the Island, display the following characteristics:

(1) they are concordant with bedding and are located at the base of fluviatile fining-upward cycles;

(2) they contain up to 250 ppm uranium;

(3) they are typically 5 to 30 cm thick, but can be in excess of 1 m;

(4) they can be traced laterally in outcrop for distances of several kilometres;

(5) at least five such zones are stacked one above the other, with a stratigraphic separation of 10 to 20 m.

The same style of mineralization was described by Prest et al. (1969) in a borehole core from central Prince Edward Island. A thin zone of mineralization, containing 290 ppm uranium oxide, was found at a depth of 716 feet (218 m) in a well at Kelly Cross, some 90 km southeast of the occurrences described above (Prest et al., 1969). There are numerous other surface showings, both on the Island and in the Cape Tormentine area of New Brunswick, which indicate that the mineralization is very widely distributed.

The host rocks are believed to be upper Pictou Group of late Pennsylvanian age (Barss et al., 1963). They consist of alternating sandstones and mudstones deposited by meandering rivers; the trough cross-bedded and ripple-marked sandstones represent the channel deposits, and the overlying mudstones and siltstones are the associated flood plain or overbank deposits. The flat-lying nature of the rocks in many areas permits individual fining-upward cycles to be traced for many kilometres along the coast. The paleoclimate was probably semi-arid to arid, as evidenced by the almost total absence of preserved plant debris and the extensive development of calcitic, caliche-like nodules or concretions near the top of many cycles. The absence of a quartz pebble conglomerate at the base indicates a distant source area and/or a low energy environment of deposition. However, a basal mud chip conglomerate is well developed locally, the result of erosion and scouring of the underlying mudstones and siltstones.

The rocks of Prince Edward Island are red except for a thin (typically 5 to 30 cm), laterally continuous, pale green horizon at the base of many fining-upward cycles. Radioactivity significantly above background was observed only in these green sands, but not all green sands are mineralized. The green coloration, no doubt due to a change in the valence state of iron, is most extensively developed in the sands, but extends for short distances into the underlying muds as well. It is highly concordant with bedding, often maintaining a uniform thickness along an undulating erosional surface. Green-coloured reaction rims were also observed around mud chips and lenses of mudstone within the overlying red sands. These zones of chemical reduction are clearly diagenetic rather than depositional in origin, but are too well defined and uniformly distributed to be due to the presence of carbonaceous material or sulphide minerals. Rather, it appears that some fundamental chemical process related to the abrupt physical-chemical interface between permeable sandstones above and impermeable mudstones below has produced and maintained a zone of chemical reduction. This, in turn, has resulted in the precipitation of uranium in some areas.

Some of the most enriched uranium occurrences of the Prince Edward Island style are to be found along the west coast of the Island, between the harbour at Seal Point and the small community of West Cape (Fig. 63.3). A study of these deposits proved most informative. The dips of the rocks in this area are sufficient to expose the bases of four fining-upward cycles, all of which are mineralized, within a distance of approximately 6 km. At least one other mineralized cycle is exposed a few kilometres along the coast to the northeast. The sample locations and uranium content of seven hand specimens from these horizons are shown in Figure 63.3, together with a generalized cross-section of the coastal exposures. The specimens selected in the field and subsequently analyzed are from the most radioactive portions of each zone, but are perhaps more representative than first thought; the analytical data reveal that the most radioactive portions of these laterally continuous radioactive horizons are not always the most uraniferous. The lateral persistence of the horizons is suggested by the fact that gentle synclinal folding has exposed one, and possibly two, of the uppermost zones at localities separated by 2 km and 4 km respectively (Fig. 63.3).

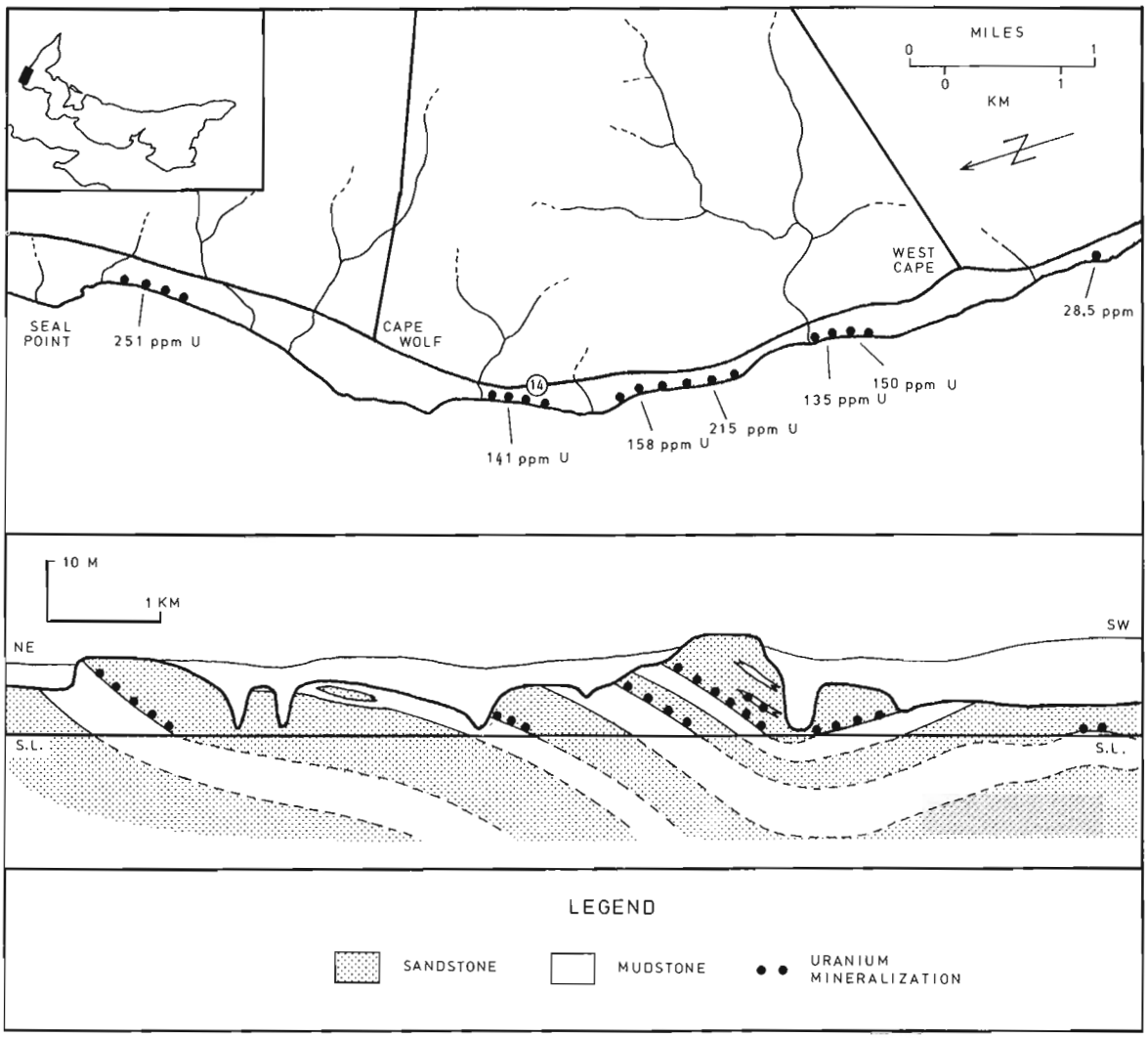

Figure 63.3. Locations of uranium occurrences in plan (upper) and cross-sectional (lower) views, western Prince Edward Island.

The mineralized specimens collected from these occurrences contain approximately 100 times more uranium than the 1.9 ppm found in normal, red-coloured sandstones on the Island. At these levels of concentration, they are two thirds of the way to high-grade, sandstone-type ore. The richest zones, at 250 ppm uranium, compare favourably with the 250 to 325 ppm contained by the richest portions of upper Cambrian, alum shales in Sweden (O.E.C.D. and I.A.E.A., 1976). There is no reason to suspect that the exposed occurrences are more highly or extensively mineralized than their subsurface equivalents; in fact, the opposite should be true. The presence of these significant uranium occurrences was not detected by a trace element reconnaissance survey throughout the area (Dyck et al., 1976). Twenty-seven samples of well water obtained last summer in the immediate vicinity of the west coast occurrences contained a mean value of only 0.7 ppb uranium (standard deviation, 1.0). Clearly, uranium is not being mobilized by present-day groundwaters. Thus, groundwaters issuing from many of the mineralized cliff faces have presumably long ago carried away any uranium that could be leached by such solutions.

Studies to determine the mineralogy and elemental associations of these occurrences have yet to be undertaken. However, data provided by Prest et al., (1969) suggest that they will be rich in vanadium and that the uraniferous minerals may be uranium vanadates. The existence of highly insoluble uranium vanadates might account for the relatively high concentrations of uranium observed in outcrop.

Other occurrences in the Prince Edward Island style were found along the western, southwestern and northern coasts of the Island, and on the shores of Cape Tormentine on the mainland. A minor variation occurs near Brae Harbour and Cape Egmont on the south coast of the Island. At these localities, uranium mineralization is associated with narrow lenses of channel sand deposits, rather than the more usual, laterally continuous sandstone units. Also, the geographic distribution of exposed mineralization is very much dependent on the dip of the rocks. Only where the strata are dipping to some extent, such as in the vicinity of the Hillsborough Bay salt dome near Charlottetown, are the bases of fining-upward cycles exposed. In many areas, subsurface data are required to supplement our knowledge.

The writer is optimistic that economic grades and tonnages of uranium will be found in the subsurface of Prince Edward Island.

Sandstone-Type – Pugwash-Tatamagouche Style

The third style of sandstone-type uranium mineralization also occurs in fluviatile red beds, at or near the base of fining-upward cycles. In this style, however, radioactivity is restricted to localized sites, and there is an obvious association with coalified plant debris and copper mineralization. Numerous uranium showings of this style occur in the basal Pictou Group of northern Nova Scotia, near Pugwash and Tatamagouche. A description of these occurrences and a model for their origin are presented in an accompanying paper (Dunsmore, 1977).

This style of mineralization was also found at scattered localities throughout the Permo-Carboniferous basin. For example, a single occurrence of uranium, copper and barite, directly associated with carbonaceous material, was found on Gallas Point, east of Charlottetown, Prince Edward Island. The rocks hosting the mineralization are Permian in age (Barss et al., 1963), and are on the east flank of the Hillsborough Bay salt diapir. A minor uranium-copper occurrence on Shippegan Island, northwestern New Brunswick, is also of the Pugwash-Tatamagouche style. In southwestern Newfoundland, several uranium-copper occurrences (Knight, 1976) on the banks of the Grand Codroy River are closely associated with megascopic plant debris; other radioactive occurrences in grey- and green-coloured, fluviatile sandstones in the immediate vicinity are not. The host rock is the North Branch Formation of the Codroy Group (Brown and Knight, Geology of Codroy map sheet, in prep.).

It should perhaps be stressed that none of the red bed, uranium-copper occurrences examined display any morphological resemblance to the much described roll-type deposits of the western United States. Radioactivity is restricted to tabular pods or lenses of a chemically reduced nature surrounding carbonaceous matter, typically in the form of coalified plant debris. The common association of uranium and copper suggests that both can be mobilized by the same aqueous solution.

Bituminous Shale-Type

The bituminous shale-type is defined on the basis of less supporting evidence than are the other types and styles. It is based on a single surface occurrence near Hampton, in southern New Brunswick, and on the presence of geochemical and geophysical anomalies in the vicinity of Sussex, northeast of Hampton.

The Lower Carboniferous Albert Formation of the Moncton-Sussex subbasin consists of grey to black shales, siltstones, sandstones and minor limestones, with salt occurring locally near the top (Gussow, 1953). The shales and siltstones are highly bituminous in places; albertite, a petroleum-derived solid hydrocarbon was once mined extensively at Albert Mines. There is a small exposure of Albert Formation, containing relatively thick zones of uranium-bearing solid hydrocarbon, along a major north-easterly trending fault, a few kilometres northeast of Hampton. The occurrence has been described in detail by Gross (1957). A specimen from the most radioactive portion contains 419 ppm uranium, which is in agreement with results obtained by Gross (1957).

A number of stream sediment, soil and groundwater uranium anomalies have been reported to the north and northeast of Sussex, some 30 to 50 km northeast of the Hampton occurrence (Dyck et al., 1976; Ball and Gemmell, 1975; Smith, 1968). The results of an airborne radiometric survey also provide encouragement (Geol. Surv. Can., Geophysical Series Map 35821G). The Albert Formation underlies the area in question, and it is possible that the observed geochemical and geophysical anomalies are due to the presence of uranium-bearing bituminous shales. Exploration in progress should soon confirm or disprove this hypothesis.

Samples of albertite from the dumps at Albert Mines, some 70 km northeast of the Sussex area, are not radioactive, although material of this type might be expected to retain its uranium. Thus, uranium mineralization within bituminous portions of the Albert Formation, if indeed it exists outside of the Hampton occurrence, may occur only locally.

Volcanogenic Type

A distinctly different type of uranium mineralization is associated with Mississippian volcanics in southwestern and northern New Brunswick (Fig. 63.1). Most of these occurrences have been described in some detail by Gross (1957), Ball and Gemmell (1975), Bell (1976) and Ruitenberg et al., (1976).

Uranium mineralization is found in a variety of volcanogenic rock types, including porphyritic rhyolites, foliated tuffs and volcanogenic clastics. There are, however, a number of common characteristics. The mineralization always appears to be associated with a permeable conduit of some sort, whether the origin be tectonic, sedimentary or a combination of both. The host rocks are invariably altered, extensively in the case of the volcanogenic clastics, indicating that the precipitation of uranium was but one of a series of reactions between the mineralizing fluids and the host rocks. A complex variety of different types of alteration was observed. These include chloritic, kaolinitic, sericitic, pyritic, hematitic, silicic and fluoritic alteration, although not all types are represented at all localities. One of the most significant features may be the presence of fluorite, a mineral which is invariably found in close association with the radioactivity. Bohse et al. (1974) have shown that during igneous crystallization, uranium can be strongly partitioned into acid melts rich in fluorine and chlorine. The persistent association of fluorite and radioactivity suggests that uranium was transported to the site of mineralization as fluoride complexes within highly reactive, magmatic fluids (Bohse et al., 1974). These fluids must have been expelled along fractures or through permeable, volcanogenic clastics during the final stages of magmatic differentiation.

The tungsten-molybdenum-bismuth-tin-fluorine deposits at Mount Pleasant occur within the same Mississippian volcanic complex as the scattered uranium occurrences just described. The same types of alteration have also been observed there (Parrish and Tully, 1973). Not surprisingly perhaps, surface samples from Mount Pleasant were found to contain as much as 235 ppm uranium. The vast amount of data that has been obtained during exploration at Mount Pleasant presents a unique opportunity to work out various elemental associations and to study relationships between uranium mineralization and rock alteration.

Subdivision of the volcanogenic type into various styles of mineralization must await a better understanding of these complex occurrences.

Miscellaneous Uranium Occurrences

Two other uranium occurrences, neither of which can yet be classified as to type, are of interest. One is in New Brunswick and the other in Newfoundland.

A previously unreported radioactive occurrence, up to 20 times background and containing as much as 82.7 ppm uranium, was discovered along Ridge Brook, a tributary of the Canaan River, some 48 km due west of Moncton. It is on the east bank of the stream about 4 km upstream (south) from its juncture with the Canaan River and 0.75 km upstream from the point where it flows beneath provincial highway 112. The poorly exposed host rock is a grey, iron-stained, laminated argillite. The zone of radioactivity extends for several tens of metres along the river bank and is a minimum of several metres in thickness. This uranium mineralization was not detected by stream sediment geochemistry (Smith, 1968). The host rock is believed to be pre-Carboniferous in age and to be positioned immediately beneath the pre-Carboniferous unconformity (Stewart, 1939). If these stratigraphic relationships are correct, this occurrence may represent a mineralized horizon which has perhaps not previously been recognized.

The most significant uranium mineralization observed within the Carboniferous rocks of southwestern Newfoundland is in the Overfall Brook Formation of the Barachois Group (Brown and Knight, Geology of Codroy map sheet, in prep.). This formation was designated as map unit 7 in a preliminary publication (Knight, 1976). The one known occurrence is located at the point where Overfall Brook enters the Grand Codroy River. Thin lenses (15 to 30 cm) of grey, carbonaceous sandstone within a massive, light-coloured, arkosic, micaceous, coarse sand and conglomerate contain as much as 323 ppm uranium. Unfortunately, time did not permit further field investigation of this promising style of mineralization. It is possible that the uranium-bearing, organic-rich facies is more extensively developed in adjacent areas.

Locations of Uranium Occurrences

The locations of all uranium occurrences visited are listed in Table 63.2 with reference to the Universal Transverse Mercator (U.T.M.) grid plotted on the various 1:50 000 topographic maps. Each location is believed to be accurate to within 100 m. For convenience, a geographic name has also been assigned to each of the occurrences. The uranium content of selected specimens, as determined by neutron activation analysis, is also given for a number of the more important sites of mineralization. It must be stressed that the specimens analyzed were usually from the most highly radioactive portions, and are not necessarily representative samples.

Conclusions

It is becoming apparent that portions of the crust within Atlantic Canada are enriched in uranium, and that this highly mobile element has been recycled and concentrated in a remarkable variety of ways. Within rocks of the Permo-Carboniferous basin, five different types and styles of mineralization are distinguished. However, the highly porous and permeable nature of many of the host rocks, coupled with a moist, temperate climate, probably dictate that economic grades and tonnages of ore will be found only at depth.

Presently known uraniferous occurrences are in rocks at the top and bottom of the Carboniferous succession (primarily Pictou and Horton groups respectively), but not in intervening strata. The stratigraphically higher occurrences are all of the sandstone-type; the lower occurrences consist of the volcanogenic and bituminous shale-types, but probably other types will eventually be recognized. It is tempting to speculate that Devonian granites and Mississippian acid volcanics were the source of the uranium which was subsequently recycled by sedimentary and diagentic processes. However, it should not necessarily be concluded that uranium resource potential diminishes with time elapsed since emplacement of the suspected source rock.

A knowledge of the uranium geology of the United States and Western Europe is a valuable tool for the exploration geologist who wishes to evaluate these styles of uranium mineralization.

The results obtained during the 1976 field season indicate that many areas of Atlantic Canada have not been thoroughly prospected. They also indicate that geochemical surveys and remote sensing techniques often fail to detect uranium mineralization which is easily discernible in outcrop. If this part of Canada is to contribute to the uranium resources of the nation, as the writer believes it will, genetic models with predictive capability will have to be developed. Such models will only be perceived and perfected as a result of careful geological studies.

References

Adler, H.H.
1974: Concepts of uranium-ore formation in reducing environments in sandstones and other sediments; Formation of Uranium Ore Deposits, Int. Atomic Energy Agency, Vienna, p. 141-168.

Ball, F.D. and Gemmell, D.E.
1975: Carboniferous compilation, Volume IV, Uranium and base metals; N.B. Dep. Natl. Resour., Topical Report 75-22, p. 1-28.

Barss, M.A., Hacquebard, P.A., and Howie, R.D.
1963: Palynology and stratigraphy of some Upper Pennsylvanian and Permian rocks of the Maritime Provinces; Geol. Surv. Can., Paper 63-3.

Bell, R.T.
1976: Geology of uranium in sandstones in Canada; in Report of Activities, Part A, Geol. Surv. Can., Paper 76-1A, p. 337-338.

Bohse, H., Rose-Hansen, J., Sørensen, H., Steenfelt, A., Løvborg, L., and Kunzendorf, H.
1974: On the behaviour of uranium during crystallization of magmas – with special emphasis on alkaline magmas; Formation of Uranium Ore Deposits, Int. Atomic Energy Agency, Vienna, p. 49-60.

Dunsmore, H.E.
1977: A new genetic model for uranium-copper mineralization, Permo-Carboniferous basin, northern Nova Scotia; in Report of Activities, Part B, Geol. Surv. Can., Paper 77-1B, rep. 45.

Dyck, W., Chatterjee, A.K., Gemmell, D.E., and Murricane, K.
1976: Well water trace element reconnaissance, eastern Maritime Canada; J. Geochem. Explor., v. 6, p. 139-162.

Fischer, R.P.
1960: Vanadium-uranium deposits of the Rifle Creek area, Garfield County, Colorado; U.S. Geol. Surv., Bull. 1101.

Gross, G.A.
1957: Uranium deposits in Gaspe, New Brunswick, and Nova Scotia; Geol. Surv. Can., Paper 57-2.

Gussow, W.C.
1953: Carboniferous stratigraphy and structural geology of New Brunswick, Canada; Bull. Am. Assoc. Pet. Geol., v. 37, p. 1713-1816.

Howie, R.D. and Barss, M.S.
1975: Upper Paleozoic rocks of the Atlantic provinces, Gulf of St. Lawrence, and adjacent continental shelf; Geol. Surv. Can., Paper 74-30, v. 2, p. 35-50.

Knight, I.
1976: Geology of the Carboniferous of the Codroy Valley and northern Anguille Mountains; Nfld. Dep. Mines Energy, Rep. 76-1, p. 10-18.

O.E.C.D. and I.A.E.A.
1976: Uranium-resources, production and demand; Joint Rep. by O.E.C.D. Nuclear Energy Agency and Int. Atomic Energy Agency, Paris, p. 55.

Parrish, I.S. and Tully, J.V.
1973: Molybdenum, tungsten and bismuth mineralization at Brunswick Tin Mines Ltd.; Guidebook to Geology of New Brunswick, New England Intercoll. Geol. Conf., N. Rast, ed., p. 99-114.

Prest, V.K., Steacy, H.R. and Bottrill, T.J.
1969: Occurrences of uranium and vanadium in Prince Edward Island; Geol. Surv. Can., Paper 68-74.

Ruitenberg, A.A., Ramachandra, B.L., and Watters, S.E.
1976: Uraniferous volcanogenic sedimentary rocks in the West Mill Settlement area; N.B. Dep. Natl. Resour., Topical Report 76-1.

Sanschagrin, R.
1964: Magdalen Islands; Que. Dep. Natl. Resour., Geol. Rept. 106.

Smith, A.Y.
1968: Uranium in stream sediments in southeastern New Brunswick; N.B. Dep. Natl. Resour., Information Circ. 68-3.

Stewart, J.S.
1939: Alward Brook; Geol. Surv. Can., Map 605A.

Watts, A.B. and Haworth, R.T.
1974: Geological interpretation of Bouguer anomaly and magnetic anomaly maps east of the Magdalen Islands, southern Gulf of St. Lawrence; Geol. Surv. Can., Paper 74-55.

Erratum

1976 Report of Activities, Part B

Geol. Surv. Can., Paper 76-1B

Paper 76-1B, p. 170, Fig. 35.2: A number of extraneous black marks appear on the published version of the figure which give a false impression of the Fraser Delta slope relief. Corrected versions of the map can be obtained from J.L. Luternauer, Geological Survey of Canada, 3rd Floor, 100 West Pender Street, Vancouver, B.C. V6B 1R8.

AUTHOR INDEX

	Page
Abbey, S. (21)	107
Amos, C.L. (7)	47
Annan, A.P. (5)	33
(9)	55
(10)	59
(11)	63
(12)	67
(14)	75
(24)	117
Ayres, L.D. (3)	25
(4)	29
Balkwill, H.R. (35)	181
Barendregt, R.W. (50)	271
Barrett, D.L. (26)	129
Battrum, D. (57)	295
Berdan, J.M. (2)	15
Blake, W., Jr. (53)	281
Bolton, T.E. (1)	1
Bornhold, B.D. (48)	265
Charbonneau, B.W. (22)	109
(62)	337
Christie, R.L. (42)	217
Chute, M.E. (4)	29
Copeland, M.J. (1)	1
(2)	15
Craw, D. (30)	145
Cunningham, C.M. (55)	291
(59)	311
Davis, J.L. (5)	33
(11)	63
(12)	67
(13)	69
(14)	75
(24)	117
Dawson, K.R. (27)	133
Dunsmore, H.E. (45)	247
(63)	341
Eisbacher, G.H. (61)	319
Falconer, R.K.H. (25)	125
(46)	255
Findlay, D.J. (3)	25
Ford, K.L. (22)	109
Foster, J.H. (50)	271
Fransham, P. (57)	295
Gibson, D.W. (40)	203
Goodfellow, W.D. (6)	37
Graham, P.S. (40)	203
Grasty, R.L. (16)	81
Gunther, P.R. (40)	203
Hardy, I.A. (18)	93
Heffler, D.E. (26)	129
Hopkins, S.L. (61)	319
Hopkins, W.S., Jr. (35)	181
(36)	185
Jerzykiewicz, T. (31)	149
Jonasson, I.R. (6)	37
(22)	109
Katsube, T.J. (56)	293
Keen, C.E. (26)	129
Klapper, G. (43)	227
Kurfurst, P.J. (52)	277
Lichti-Federovich, S. (54)	287
Linden, R. (49)	269
Long, B.F.N. (17)	85
Mackay, J. Ross (51)	273
MacLean, B. (25)	125
McLean, J.R. (31)	149
Miller, A.R. (23)	113
Mitchell, W.S. (28)	137
(29)	141
Pedder, A.E.H. (34)	173
(43)	227
Prasad, N. (39)	199
Price, R.A. (47)	261
Pringle, G.J. (23)	113
Rahmani, R.A. (32)	157
(36)	185
Rast, N. (8)	49
Reinson, G.E. (20)	99
Rimsaite, J. (44)	235
Schwarz, E.J. (38)	197
Sears, J.W. (47)	261
Shilts, W.W. (55)	291
(59)	311
Stalker, A. MacS. (50)	271
Swan, D. (49)	269
Taylor, K.A. (28)	137
(29)	141
Taylor, P.F. (29)	141
Thomas, R.D. (60)	315
Topp, G.C. (5)	33
Trzcienski, W.E., Jr. (15)	77
Umpleby, D.C. (18)	93
Uyeno, T.T. (41)	211
van Helden, B.G.T. (33)	163
Wagner, F.J.E. (19)	97
Wall, J.H. (35)	181
Williams, G.K. (37)	191
(58)	301
Zentilli, M. (28)	137
(29)	141